NATO Science for Peace and Security Series - C:
Environmental Security

Sol-Gel Methods for Materials Processing

Focusing on Materials for Pollution Control, Water Purification, and Soil Remediation

Edited by
Plinio Innocenzi
Yuriy L. Zub,
Vadim G. Kessler

Springer

NATO OTAN

This publication is supported by: The NATO Science for Peace and Security Programme

Sol-Gel Methods for Materials Processing

NATO Science for Peace and Security Series

This Series presents the results of scientific meetings supported under the NATO Programme: Science for Peace and Security (SPS).

The NATO SPS Programme supports meetings in the following Key Priority areas: (1) Defence Against Terrorism; (2) Countering other Threats to Security and (3) NATO, Partner and Mediterranean Dialogue Country Priorities. The types of meeting supported are generally "Advanced Study Institutes" and "Advanced Research Workshops". The NATO SPS Series collects together the results of these meetings. The meetings are co-organized by scientists from NATO countries and scientists from NATO's "Partner" or "Mediterranean Dialogue" countries. The observations and recommendations made at the meetings, as well as the contents of the volumes in the Series, reflect those of participants and contributors only; they should not necessarily be regarded as reflecting NATO views or policy.

Advanced Study Institutes (ASI) are high-level tutorial courses intended to convey the latest developments in a subject to an advanced-level audience

Advanced Research Workshops (ARW) are expert meetings where an intense but informal exchange of views at the frontiers of a subject aims at identifying directions for future action

Following a transformation of the programme in 2006 the Series has been re-named and re-organised. Recent volumes on topics not related to security, which result from meetings supported under the programme earlier, may be found in the NATO Science Series.

The Series is published by IOS Press, Amsterdam, and Springer, Dordrecht, in conjunction with the NATO Public Diplomacy Division.

Sub-Series

A.	Chemistry and Biology	Springer
B.	Physics and Biophysics	Springer
C.	Environmental Security	Springer
D.	Information and Communication Security	IOS Press
E.	Human and Societal Dynamics	IOS Press

http://www.nato.int/science
http://www.springer.com
http://www.iospress.nl

Series C: Environmental Security

Sol-Gel Methods for Materials Processing

Focusing on Materials for Pollution Control, Water Purification, and Soil Remediation

edited by

Plinio Innocenzi
University of Sassari,
Italy

Yuriy L. Zub
Ukraine Academy of Sciences,
Kiev, Ukraine

and

Vadim G. Kessler
Swedish Life Science University (SLU),
Uppsala, Sweden

Published in cooperation with NATO Public Diplomacy Division

Proceedings of the NATO Advanced Research Workshop on
Sol-Gel Approaches to Materials for Pollution Control, Water Purification
and Soil Remediation
Kyiv, Ukraine
25–27 October 2007

Library of Congress Control Number: 2008929546

ISBN 978-1-4020-8522-2 (PB)
ISBN 978-1-4020-8521-5 (HB)
ISBN 978-1-4020-8514-7 (e-book)

Published by Springer,
P.O. Box 17, 3300 AA Dordrecht, The Netherlands.

www.springer.com

Printed on acid-free paper

CONTENTS

PREFACE

The present Volume of NATO series contains the proceedings of the NATO ADVANCED RESEARCH WORKHOP dedicated to "Sol-Gel approaches to Materials for Pollution Control, Water Purification and Soil Remediation". The meeting has been held in Kiev, Ukraine on 25–27 October 2007 and has seen the participation of 15 invited speakers and more than 50 participants from NATO, associated and partner countries. The meeting has represented an important opportunity to gather leading scientists from former USSR and NATO countries and to discuss about an important topic with a big impact on the society, pollution control and remediation. The possibilities related with the application in this field of advanced functional materials, such as sol-gel processed materials is clearly emerged during the meeting. Future directions of research have been widely discussed and envisaged for a future scenario in this area.

The NATO Science Committee is gratefully acknowledged for the financial support given to the organization of the Workshop.

Plinio Innocenzi
Yuriy L. Zub
Vadim G. Kessler

DESIGN OF FUNCTIONALIZED POLYSILOXANE ADSORBENTS AND THEIR ENVIRONMENTAL APPLICATIONS

YURIY L. ZUB*
O.O. Chuiko Institute of Surface Chemistry, National Academy of Sciences of Ukraine, 17 General Naumov Str., Kyiv 03164 Ukraine

Abstract. Here we consider the routes of synthesis (which is performed by use of sol-gel method) of a new class of sorbents, namely: polysiloxane xerogels functionalized with nitrogen-, oxygen-, phosphorus- and sulfur content ligand groups. Applying a number of physical methods (SEM, TEM, AFM, IR and Raman spectroscopy, ^{1}H, ^{13}C, ^{29}Si and ^{31}P CP/MAS NMR, EPR spectroscopy, ERS, thermal analysis) we established the structure of both: the xerogels and their surface. An influence of some factors on the structural-adsorption characteristics of such xerogels and their sorption properties is analyzed.

Keywords: Sol-gel method, functionalized polysiloxane xerogels, synthesis, structure, sorption properties.

1. Introduction

Modification of silicas surface by trifunctional silanes, R_3SiR' (R – Cl or AlkO; R′ – functional group)[1–4]; realization of hydrolytic polycondensation of alkoxysilanes[5–9] (the sol-gel method[10]); accomplishment of hydrolytic polycondensation of alkoxysilanes in the presence of surfactants (the tamplate method)[11] – these are the most widly used approaches which are applied for synthesis of polysiloxane adsorbents that contain functional groups in their surface layer.

Here we consider the sol-gel method which recently had received wide practice. Usually, the most applied one is its variation which is based on reaction of joint hydrolytic polycondensation of alkoxysilanes (Scheme 1). Introduction of water and catalyst (e.g., H^+, OH^-, F^-) in the initial system leads to hydrolysis of alkoxysilanes with a formation of silanol groups, ≡Si–OH.

*To whom correspondence should be addressed: Dr. Yu.L. Zub, Head of Surface Chemistry of Hybrid Materials Department, O.O. Chuiko Institute of Surface Chemistry, NAS of Ukraine, 17 General Naumov Str., Kyiv 03164 Ukraine; e-mail: yuriyzub@voliacable.com

P. Innocenzi, Y. L. Zub and V. Kessler (eds.), *Sol-Gel Methods for Materials Processing*.

$$x\mathrm{Si(OAlk)_4} + y(\mathrm{AlkO})_3\mathrm{SiR'} + z(\mathrm{AlkO})_3\mathrm{SiR''} \xrightarrow[-\mathrm{AlkOH}]{+\,\mathrm{H_2O}\ (\mathrm{Solv}),\ \mathrm{catalyst}} (\mathrm{SiO_{4/2}})_x \cdot (\mathrm{O_{3/2}SiR'})_y \cdot (\mathrm{O_{3/2}SiR''})_z$$

Scheme 1

These groups start to interact with each other(or with alkoxysilyl groups, AlkO–Si≡) immediately, which leads to a creation of siloxane bounds (≡Si–O–Si≡), causing occurrence of oligomers. The results of further condensation of these oligomers are the occurrence of polymers of a various structure. The growth of polymers conducts to occurrence of colloidal particles which consequently leads to occurrence of sol. The further integration of these particles and creation of aggregates causes transaction of sol into gel. The following treatment of formed gel (its ageing, washing, drying, etc.) results in a xerogel. The presence of trifunctional silanes $(\mathrm{AlkO})_3\mathrm{SiR'}$ (functionalizing agents) in abovementioned systems allows one to obtain xerogels (adsorbents) which contain necessary functional groups in their surface layer. Most of alkoxysilanes are liquids, which are mixed up together, however, nonaqueous solvents often are used during synthesis – as with the purpose to avoid the occurrence of interface phases during the gel formation, and with the purpose of rendering influence on porous structure parameters of the final products.

Application of the sol–gel method to synthesising functionalized polysiloxane adsorbents (FPA) offers a number of advantages over other methods. The main one of these advantages lies in the possibility of application of multicomponent systems. Firstly, it is possible to vary both nature and concentration of the structure-forming agent.[12] Tetraethoxysilane, $\mathrm{Si(OC_2H_5)_4}$ (TEOS) is most often used as one. However, it is possible to use bis(trialkoxy)silanes, $(\mathrm{AlkO})_3\mathrm{Si\text{-}B\text{-}Si(OAlk)_3}$ (B – organic bridges)[13–15] and more complicated alkoxysilanes as structure-forming agents.[16] The combinations of structure-forming agents also can be used, including alkoxycompounds of other elements.[17] Secondly, it is possible to vary both composition and ratio of functionalizing agents.[18] In this case the application of one-stage process allows to prepare polysiloxane adsorbents which would contain simultaneously several functional groups with different nature.

It is meant, that character of these groups and the range of their ratios can be sufficiently wide. However, it is necessary to remember, that both nature and geometrical sizes of functional groups (R' и R") have, as a rule, an essential influence on a route of hydrolytic polycondensation reaction. As a result in such systems one can not observe gels' formation, or the formed gels would not be homogeneous, etc. It is noted, that the content of functional groups in xerogels can reach 6.0 mmol/g, which is about an order of magnitude greater than that attained in the situation with modified silicas.[1–4] It is noted also, that a wide

range in the choice of conditions which are acceptable for effecting the hydrolytic polycondensation reaction allows one to obtain final products – xerogels – with imperative properties. The above-stated relates, in the first place, to their structural-adsorption characteristics. Taking into account an existence of huge number of alkoxysilanes derivatives, it is possible to assert about the presence of significant prospect in search of new materials with unique properties. Therefore the fact of fast development of this chemistry area (especially last 10–15 years) does not cause surprise. The cycle of Slinyakova team's papers, which was devoted to research of organosilicon adsorbents (xerogels) with alkyl and aryl radicals in their surface layer,[19] was the base of such progress. Else in 1977 this team together with Voronkov's team also described a preparation of a xerogel with the use of hydrolityc polycondensation reaction of mercaptomethyltrimetoxysilane.[20,21] It was the start of papers series which concern S-containing silicon-organic sorption materials.[22,23] It is meant, that the nature of functional groups R′ in the initial trialkoxysilanes $(AlkO)_3SiR'$ may be rather different. This short review was intended to consider the methods of synthesis, structure and sorption properties of xerogels containing complexing groups as functional one's.

2. Synthesis of Functionalized Polysiloxane Adsorbents

Else in 1966 3-aminopropyltrietoxysilane $(C_2H_5O)_3Si(CH_2)_2NH_2$ (APTES) was offered for producing of an aminocontaining xerogel.[24] Later such xerogels were obtained repeatedly and they are studied in details. The aim of numerous works[25,26] was to synthesis an adsorbent with a high content of amine groups. However, the influence of TEOS/APTES and other conditions on structural-adsorption characteristics of the final producers the ratio was not yet established. As it is known these characteristics have direct relation with functional groups accessibility. This gap was filled in.[27–29] Reaction of a concurrent hydrolytic polycondensation of TEOS and APTES at their molar ratio of 2:1 is used for synthesis of such xerogel; the alkaline medium was created after addition of water. Some synthesis were carried out by the use of nonaqueous solvents. The procedure made it possible to prepare xerogels with reproducible main characteristics and a content of $[(SiO)_{2.6}(O_{3/2}Si(CH_2)_3NH_2)\cdot H_2O]$.[27–29] Depending on the synthesis conditions the content of amine groups varied in the interval from 2.8 to 4.2 mmol/g. The obtained xerogels have high hydrolytic and thermal stability, for example, the decomposition of their surface layer begins beyond 275°C.[25,30] The above-considered approach involved application of ethanol, which often allowed to avoid appearance of two phases during formation of gels and was employed for producing xerogels with such functional groups as $\equiv Si(CH_2)_3NHCH_3$, $\equiv Si(CH_2)_3NH(CH_2)_2NH_2$, $\equiv Si(CH_2)_3NC_3H_5N$ (imidazolyl), $[\equiv Si(CH_2)_3]_2NH$.[18,30]

In the last case the formation of so-called "arched structures" ≡Si$(CH_2)_3$–NH–$(CH_2)_3$Si≡ expexted, that obviously should have a high hydrolityc stability. The authors[31–33] described a synthesis of xerogels with ethylenediamine groups (and an additional vinyl groups[33]). These synthesis did not involve any solvent. The ratios of alkoxysilanes TEOS/$(CH_3O)_3Si(CH_2)_3NH(CH_2)_2NH_2$/$(C_2H_5O)_3$ $SiCH{=}CH_2$ in the initial solutions were 1:1:1 and 4:1:1; a content of aminogroups in the final products was 1.8–2.8 mmol/g. However, no parameters of the xerogel porous structure of were presented. In[6] it was shown when the ratio of alkoxysilanes of TEOS/$(CH_3O)_3Si(CH_2)_3NH(CH_2)_2NH_2$ = 2:1 the formed xerogel was practically nonporous. This agrees with the data of Silva and Airoldi.[34]

Synthesis of xerogels with aniline group (or its derivatives) were presented in[35–38] (catalyst – HF, solvent – ethanol). Obtaining low-density xerogels that contain aminogroups of various nature was analyzed in,[39] and obtained mono-dispersed colloid particles which contain aminogroups were considered in.[40] Obtaining xerogel-anion-exchanger with functional group of ≡Si$(CH_2)_3$ $N(CH_3)_3$ $^+Cl^-$ composition was described in[26,41] (acid medium, solvent – alcohol), with 3-n-propyl-1-azonia-4-azabicyclo[2.2.2]octanechloride – in.[42]

Monocomponent systems were used to obtain xerogels that contain cyclam.[43] It was shown that parameters of their porous structure depend on a nature of catalyst, solvent, composition of hydrolysing groups [Si$(OEt)_3$ or SiH_3] and a temperature of gel treatment. It is interesting, that hydrolytic polycondensation of the monomers with a ligand group –NHC(=NH)NH_2 was completed only in 70 h at 100°C, and in the situation of its symmetric analogue the corresponding polyalkylsilsesquioxane could not be obtained by this method. Therefore the hydrolytic co-polycondensation of that monomers with TEOS[23] was used.

The authors[18,30,44] described a synthesis of porous xerogels with a bifunctional surface layer composed of ≡Si$(CH_2)_3NH_2$/CH_3 (or C_6H_5). The ingredient ratio in the initial solution was 1:1:1. It allowed to keep relatively high content of 3-aminopropylgroups in the final products (3.0–3.7 mmol/g). A refusal to use of ethanol during synthesis of such xerogels leads to form two phases during gels formation.[29] Earlier[41] it was shown that an introduction of methyl groups increases mechanical strength of spheres of xerogels (0.2–1.5 mm) with amine groups.

Aminocontaining xerogels were obtained by $(C_2H_5O)_3Si(CH_2)_2Si(OC_2H_5)_3$ (BTESE), $(C_2H_5O)_3Si(CH)_2Si(OC_2H_5)_3$ (BTEST) and $(C_2H_5O)_3SiC_6H_4Si$ $(OC_2H_5)_3$ (BTESB)[13,14] as structure-forming agents. The authors[15] studied the particularities which were observed in the case of the synthesis of xerogels with 3-aminopropyl groups and showed that in order to avoid nonhomogeneous gelation it was necessary to use ethanol, to effect a preliminary hydrolysis of structure-forming agent (with F^- as a catalyst), and to enlarge the time for gel ageing with the purpose to increase of polycondensation degree. The content of ligand groups in

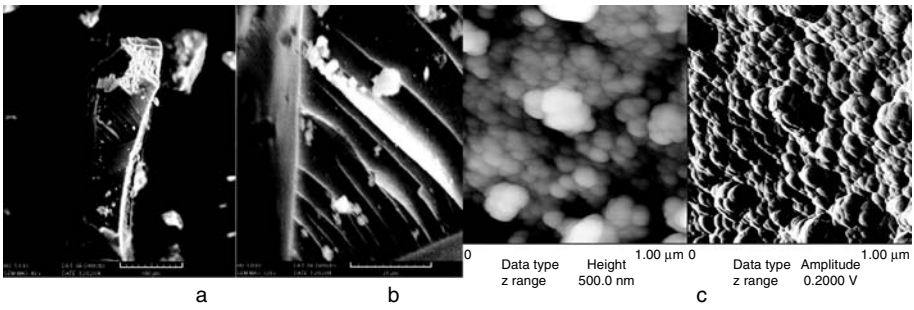

Figure 1. SEM (a – 480x; b – 3,200x) and AFM[14] micrographs of aminocontaining xerogel.

the prepared xerogels ranged from 1.0 to 2.6 mmol/g. According to SEM microphotographs (Figure 1a, b) the lamellar structure is characteristic feature for these xerogels. Their AFM micrographs are presented in Figure 1c. It is brought about by the existence of aggregates of primary particles (globules). Their size amounts to 30–65 nm.

Parish and co-workers[32] proposed several approaches to obtain xerogels which would contain $\equiv Si(CH_2)_2$ or $_3PPh_2$ groups (catalyst – $(n\text{-}Bu)_2Sn(CH_3COO)_2$, solvent – ethanol or toluene). Later these syntheses were reproduced in methanol.[45] The xerogels that contain additional groups (amine or thiol) were also described. Partial oxidation of P(III) atom was observed in all cases.[45] Obtaining xerogels with phosphine ligands was considered in details by Lindner.[46]

The systems with two and three components were used for synthesis of xerogels with (thio)urea groups (TEOS was a structure-forming agent; ethanol as a solvent; $F^-/Si \sim 1/100$). The alkoxysilanes $(C_2H_5O)_3Si(CH_2)_3NHC(S(O))\,NHR'''$, where $R''' = -C_2H_5$, $н\text{-}C_3H_7$; $-C_6H_5$; $-CNSC_6H_4$; $-(CH_2)_3Si(OC_2H_5)_3$, were involved as functionalizing agents.[47] Also the precursors forming arched structures are used.[48] When the TEOS/trifunctional silane ratio is 2:1 the surface of formed xerogels possessed hydrophobic properties, and the xerogel did not have porosity, while at a ratio of 4:1 (or 8:1) they showed hydrophilic properties and porous structure. The xerogel surface acquired hydrophilic properties also in the case of introduction of additional amine groups. The content of functional groups was 0.9–3.3 mmol/g. For xerogels with arched structure the first exoeffect was observed in the range 380–430°C.[47,48] Synthesis of xerogels with malonamide ligands were considered in.[40]

Unger and coworker[50] described the synthesis of xerogels using 1,2-epoxy-3-propoxypropyltriethoxysilane. Initially, polyethoxysiloxane was prepared from TEOS by acid hydrolysis. Homogeneity of the reaction medium in the second stage was maintained by adding of sodium or ammonium hydroxide, therefore the final product contained either 1,2-dihydroxyl-3-propoxypropyl or hydroxylamine functional groups.

Synthesis of xerogels with groups ≡Si$(CH_2)_3$SH is usually performed by applying such catalysts as $(n\text{-Bu})_2Sn(CH_3COO)_2$[25,26] or HCl.[51,52] However, according to the NMR spectroscopy data[26,53] the polysiloxane skeleton of these xerogels does not have any effective cross-linking. Besides that, the polymeric matrix composition includes tin.[25] Moreover, these systems are noted to have two phases, and the formed xerogel is practically non-porous.[54] These drawbacks could be avoided by using methanol as a solvent and F^- as a catalyst.[54] The xerogel obtained at TEOS/MPTMS = 2:1 possessed an extended porous structure (the content of HS groups was equal to 4.5 mmol g^{-1}).

The vary of alkoxysilanes ratio in the range of 5:1–1:1 allowed to obtain xerogels with thiol groups content from 1.9 to 5.3 mmol/g.[55] In the last case the sample consists of partly stick together particles of the spheric form (their size is 2.5–3.0 mkm, Figure 2). It is not typical for xerogels of this class. The xerogels which contain 3-mercaptopropl groups were synthesized with the use of BTESE and BTESB as structure-forming agents; the content of functional groups was 1.0–2.7 mmol/g.[14,56]

Obtainance of xerogel with a ligand group that contained sulphide, amine and thiol centers was considered in.[57] A comparative characteristic of sorbents with SH-groups is given in.[52,58]

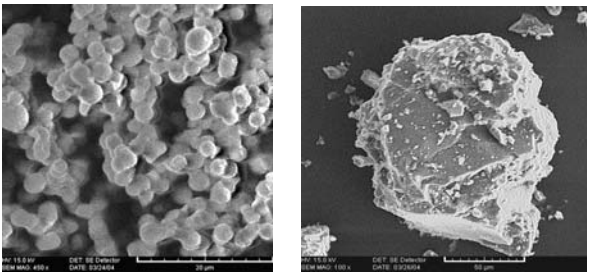

a b

Figure 2. SEM microphotographs of HS-containing xerogels (TEOS/MPTMS = 1:1 (a) and 3:1 (b)).[55]

The authors [18,54] described also preparation of xerogels which contained a bifunctional surface layer of the SH/NH_2 type (the structure-forming agent was TEOS). MPTMS/APTES ratio in an initial solution (3.0, 1.0 and 0.33 mol) determined the ratio of functional groups in the final products. Earlier synthesis of xerogels with thiol and amino groups were considered in.[51] Most of amino-groups in the obtained xerogel are protonated. The exception is a sample obtained at the ratio of TEOS/MPTMS//$(CH_3O)_3Si(CH_2)_3NH(CH_2)_2NH_2$ = 4:1:3. The authors[51] suppose that most of aminogroups form hydrogen bond with thiol groups. This hinders their protonation in the acid medium. It is interesting that the treatment of these xerogels by 0.11 M HCl gives only 1–2% mass loss, during that time

when the same treatment of aminocontaining xerogels gives mass loss of 8–10%.[26]

The xerogels with an analogous surface layer were obtained using BTESE as a structure-forming agent.[59] MPTMS/APTES ratio in an initial solution was 1:1. The synthesis of xerogel that contain simultaneously CH_3– and $HSCH_2$– groups in its surface firstly was described in.[60] Co-polycondensation of these two alkoxysilanes in aceton leads to polymers that as the authors suppose[60] has the following structure of its chain:

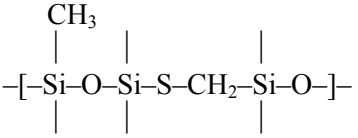

The surface of this polymer has weaker acidic properties than the surface of xerogel which was synthesized using only $(CH_3O)_3SiCH_2SH$.[17] Polysiloxane xerogels which contain 3-mercaptopropyl and methyl groups in the surface layer were obtained with ethanol used as a solvent and F^- used as a catalyst.[61] The ratio of trifunctional silanes is varied from 1:2 to 2:1, and the ratio of TEOS/(mix of trifunctional silanes) was 1:1 and 2:1. The content of HS groups in the xerogels obtained was 1.2–4.7 mmol/g. According to AFM these xerogels are composed of spheric particles. The mean size of these particles is close to 35–45 nm. The xerogels that contain *n*-propyl group instead methyl were synthesized in analogous conditions.[62] The content of HS groups in these xerogels was 1.2–3.5 mmol/g.

For the first time the xerogel with groups $\equiv Si(CH_2)_2COOH$ was synthesized in 1964[63] by the acid hydrolysis of $(C_2H_5O)_3Si(CH_2)_3CN$ with following addition of TEOS. Obtained white product sorbed well the $NHEt_2$ and Py. Later on this approach was considered in detail by the authors.[64,65] One of the salient features of the synthesized xerogels was that the content of carboxyl groups (according to the potentiometric titration data) was always lower than the content calculated from the element analysis data for carbon (1.8–3.7 mmol/g). Therefore, these groups may be partly incorporated in the polysiloxane matrix, or some part of them forms complex ethers. Synthesis of xerogels with ligand – EDTA analogue was described in.[66]

The hydrolytic polycondensation of $(C_2H_5O)_3Si(CH_2)_2P(O)(OC_2H_5)_2$ in boiling HCl (conc.) gives a fragile substance with a composition of $[O_{3/2}Si(CH_2)_2P(O)(OH)_2]_x$.[67] The xerogels contained (thio)phosphineoxide groups were also prepared using $(S,O=)P[C_6H_4Si(OPr^i)_3]_3$.[68] In this case the hydrolytic polycondensation was held in THF together with the presence of an excess of water, the catalyst was *n*-toluenesulfonic acid or HCl. In the last case the process resulted in formation of highly porous xerogels.

The system with two components TEOS/$(C_2H_5O)_3Si(CH_2)_2P(O)(OC_2H_5)_2$ (DFTS) was used to obtain xerogels with P=O-groups (the ratio of components was 2:1–10:1; ethanol used as a solvent; F^-/Si = 1/100 (mol)). [69] The content of functional groups in the obtained xerogels was 1.2–1.4 mmol/g. The samples which were synthesized at the alkoxysilanes' ratios of 6:1–10:1 had porosity.[69] At the same time the analogous xerogels which had HCl acid as the catalyst[70] were porous only at the ratios of alkoxysilanes equal 10:1. The acidic treatment of nonporous xerogels leads to formation of porous samples with $\equiv Si(CH_2)_2P(O)(OH)_2$ functional group.[71] Its content was 2.6–3.5 mmol/g.

Also bis(trialkoxy)silanes $(RO)_3Si\text{-}B\text{-}Si(OR)_3$ used for synthesizing P=O-containing xerogels.[70] However, in the case of B = $-(CH_2)_2-$ (at a content of 80 mol%) and HCl as a catalyst these xerogels turned to be practically non-porous, and porous samples were obtained only in the case of conversion $-P(O)(OEt)_2 \rightarrow -P(O)(OH)_2$. In[72] it was shown that gelation of alkoxysilane $(EtO)_3SiCH_2CH\,[PO(OEt)_2]CH_2CH_2Si(OEt)_3$ in the medium of 1 M HCl (with THF as a solvent) for 11 days led to the transparation of monolithic sample whose boiling in concentrated HCl yielded a xerogel with $-P(O)(OH)_2$ groups. Xerogels which contained amide derivatives of phosphonic and thiophosphonic acids, $\equiv Si(CH_2)_3NHP(O,S)(OC_2H_5)_2$ were obtained by application three components systems (TEOS was a structure-forming agent).[73] 3-mercaptopropyl and 3-aminopropyl groups were used in addition to P=O-groups. The general content of functional groups were reaching 3.6 mmol/g.

Ethoxysilyl derivatives[74] of α- and β-cyclodextrines were used for preparing xerogels with these macrocyclic molecules (DMF (or DMF/water) used as a solvent, F^-/Si = 1/100 (mol)).[75] The content of functional groups was 0.1, 0.5 and 1.0 mmol/g.

3. Structure of Functionalized Polysiloxane Adsorbents

The research of the FPA structure have some difficulties as FPA are the amorphous compounds. Therefore it is necessary to apply a number of physical methods which allow to obtain the reliable information about FPA's structure on the globular and molecular levels. There is also difficulties in the studying of the composition and structure of FPA surface layer, particularly, when this layer is polyfunctional. In this chapter the authors consider the possibilities which some physical methods give.

3.1. VIBRATIONAL SPECTROSCOPY

The vibrational spectroscopy, especially IR spectroscopy, is known to be a traditional technique used for FPA investigation. Its wide application makes it

possible to ascertain that the obtained adsorptive materials contain (a) siloxane bonds and introduced functional groups (and/or products of their transformation during the course of synthesis), (b) silanol groups (and/or alkoxysilane groups), (c) water and/or nonaqueous solvents used during synthesis. Finally, the vibrational spectroscopy data often gives possibility to make conclusions about the participation of functional groups in hydrogen bond formation.

Here we considered IR spectra of some xerogels which are typical for functionalized polysiloxane adsorbents. Thus, the most intensive adsorption band with a high-frequency shoulder is observed in the region 1,000–1,200 cm^{-1} of IR spectra of the xerogels with $\equiv Si(CH_2)_3SH/\equiv Si(CH_2)_3NH_2$ bifunctional surface layer[54] (Figure 3) consistent with the presence of a three-dimensional siloxane framework (≡Si-O-Si≡). The presence of propyl chains in the IR spectra is indicated by a group of adsorption bands of weak intensity in the region 1,300–1,500 cm^{-1} and two (sometimes – three) adsorption bands of medium intensity in the region 2,800–3,000 cm^{-1}. Last one is characterized by stretching vibrations of $\nu_{s,as}(CH)$. In the IR spectrum of xerogel with thiol groups (Figure 3B) at 2,565 cm^{-1} is legibly fixed the adsorption band which refers to ν(SH). The reduction of part of MPTMS in a starting solution results into the decrease of its intensity and which becomes invisible in the IR spectra of xerogels C and D (Figure 3). However, Raman spectra of these xerogels[6] have the line in 2,570–2,580 cm^{-1} region, assigned to ν(SH),[76] irrespectively to a ratio in surface layer of thiol and amino groups. Besides in Raman spectra of samples C and D at higher than 3,250 cm^{-1} weak lines are observed and assigned to $\nu_{s,as}(NH)$ vibrations of amino groups. As all the samples contain water, the adsorption band of medium intensity is observed in the region 1,625–1,640 cm^{-1} , and it correspond to vibrations of $\delta(H_2O)$. Other wide intensive band is presented at higher 3,100 cm^{-1} in all IR spectra, assigned to ν(OH) of adsorbed water. On its background for samples C, D, E and F at ~3,300 and ~3,370 cm^{-1} there are two additional low intensive adsorption bands which can be referred to $\nu_{s,as}(NH)$ of amino groups (Figure 3). Besides in the IR spectra of samples C-F there are weak adsorption bands at 1,585–1,595 and 1,540–1,555 cm^{-1} which intensity increases from the sample C to F, that is at increasing of amino groups in surface layer. Such bands are absent in the IR spectrum of xerogel B. Occurrence of these bands is caused by deformation vibrations of amino group $\delta(NH_2)$.

Considering the different nature of –SH and $–NH_2$ groups, it is possible to assume the protonation of amino groups. In other words, in such xerogels the surface layer can have salt character of type $[\equiv Si(CH_2)_3NH_3]^+[\equiv Si(CH_2)_3S]^-$. However the line correspond to ν(SH) in Raman spectrum is conserved even at dominating quantity of amino groups in surface layer (sample E).[76] Moreover the adsorption bands which correspond to stretching vibrations of $\nu_{s,as}(NH)$ and deformation vibrations $\delta(NH_2)$ of unprotonated amino groups are observed in the

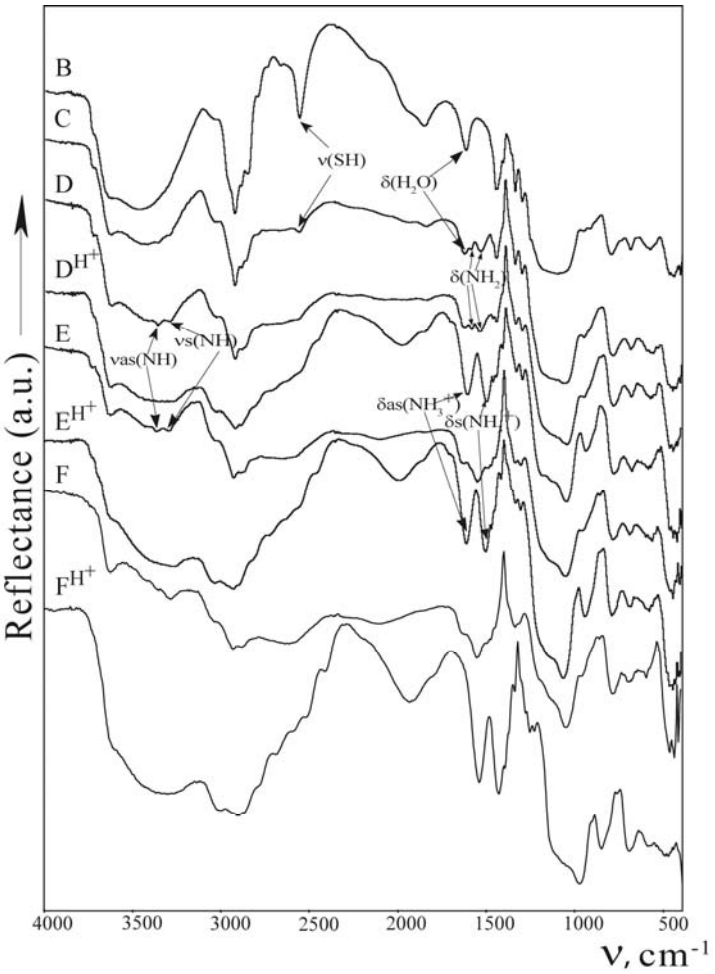

Figure 3. IR reflection spectra of xerogels containing HS–group (B); bifunctional surface layer with the ratio of $-SH/-NH_2 = 3.2$ (C), 1.1 (D) and 0.4 (E); amino group (F); the xerogels treated by 0.1 M HCl solution (D^{H+}, E^{H+} and F^{H+}).

IR spectra of xerogels C and D (Figure 3) (Worth mentioning that these figures have excess of thiol groups in relation to amino groups in thier surface layer). The similar situation was observed for the polymers which were obtained by reaction of hydrolytic polycondensation of mixtures MPTMS/APTES at the ratios 1:1 and 4:1.[77] If the alkylamonium cation was formed in samples B–D, several typical adsorption bands would have been observed in their IR spectra in the region 2,500–2,800 cm^{-1} and the band of medium intensity at ~2,000 cm^{-1}.[76] However these adsorption bands are not registered in the IR spectra for these samples (Figure 3). They are observed in the IR spectra of

samples D, E and F only after their treatment by 0.1 M HCl solution (Figure 3). Moreover two intensive adsorption bands at ~1,500 and ~1,610 cm^{-1} which are referred to $\delta_s(NH_3^+)$ и $\delta_{as}(NH_3^+)$ correspondingly (last adsorption band is masked by less intensive adsorption band of $\delta(H_2O)$ located in the same region) appear in the IR spectra of such samples (Figure 3). Similar adsorption bands were observed in the IR spectra of intercalate APTES/$Zr(HPO_4)_2$ which contained protonated products of the APTES condensation.[78] Thus, the amino groups in the surface layer of the initial FPA are non-protonated but are involved in the hydrogen bond formation. The weak adsorption band $\delta(NH_2)$ at 1,600 $cm^{-1}$is recorded in the IR spectrum of individual APTES. This band was assigned to a hydrogen bond between amino groups.[6] In the IR spectra of xerogels C–F there is low intensive adsorption band in this region (see above) which often splitted in two components and shifted in low-frequency area on 7–69 cm^{-1} (Figure 3). This fact may indicate the formation in xerogels of hydrogen bond of different nature than in APTES. Probably, the mentioned hydrogen bonds differ a little in nature. Similar observations have been made for bifunctional xerogels which were synthesized using BTESE as a structure forming agent.[59]

The application of IR spectroscopy aiming to study xerogels which synthesis involved participation of bis(trialkoxysilanes)[13–15] enabled one to reveal the presence of ≡Si–B–Si≡ bridges, noncondensed silanol groups of two types (their absorption bands ν(OH) are observed at ~3,730 and ~3,650 cm^{-1}) and some nonhydrolyzed ≡Si–OC_2H_5 groups. This provides evidence for particularities of a polymeric skeleton structure of such sorbents.

If in a surface layer of xerogels appear functional groups that are more complex in their composition (for instance, ≡Si$(CH_2)_2$NHC(O,S)NHR‴ or ≡Si$(CH_2)_2$P(O)$(OC_2H_5)_2$), the IR spectra of the xerogels also becomes more complex. However, the presence of typical absorption intensive bands in the region 1,400–1,700 cm^{-1} (one in the case of thiourea groups and two in the case of urea groups) allows one to detect easily the presence of –NH–C(O or S)–NH– fragments in the xerogel surface layer.[47] In the case of IR spectra of xerogels which contained ≡Si$(CH_2)_2$P(O)$(OC_2H_5)_2$ groups, the most intense absorption band exhibits the second shoulder at ~1,210 cm^{-1} corresponding to ν(P=O) This band is observed at 1,241 cm^{-1} for individual DFTS. Hence, the shift of this band in a low frequency region testifies to the presence of phosphoryl groups in the hydrogen bond formation.[69] The same situation is observed in the case of xerogels with such groups as ≡Si$(CH_2)_2$NHP(O)$(OC_2H_5)_2$.[73]

The absence of absorption bands ν(C≡N) in the region 2,200–2,300 cm^{-1} of the IR spectra for carboxyl-containing xerogels gives evidence for the complete saponification of nitrile groups.[79] At the same time in these spectra an intense band of absorption appears in the region 1,720–1,730 cm^{-1}. This is a typical

feature of COOH groups which are connected with OH groups by hydrogen bonds.[76] Moreover, another band appears at ~1,645 cm^{-1}, which provides evidence to formation of some carboxyl groups of ester bonds. This process is due to the interaction of carboxyl group with either silanol groups[4] or with ethanol.

3.2. SOLID-STATE NMR SPECTROSCOPY

It is noted that ^{13}C CP/MAS NMR spectroscopy is used to study mostly FPA, but its results have as a rule qualitative character. Here is considered spectra of some xerogels with mono (–SH or $–NH_2$) and bifunctional (–SH/$–NH_2$) surface layer (Figure 4). Assignment of signals which are observed in those solid-state NMR spectra are represented in Table 1. This fact supports in.[51]

The peculiarity of these spectra is a signal overlap of the central carbon atom of propyl chains and the C atom which is connected with SH-group of the same chain.[26,51] It is known that the chemical's shift value of the central carbon atom of propyl radical ≡Si-C[CH_2]C-NH_2 in the ^{13}C CP/MAS NMR spectrum points out the status of amino groups. Thus, this resonance line is present at ~28 ppm in the ^{13}C CP/MAS NMR spectrum for individual APTES which have a hydrogen bond between amino groups while in the case of protonation of 3-aminopropyl groups grafted to SiO_2 surface this line shifted into the strong field region and is seen at 21–22 ppm.[80]

Considering a signal location of the central carbon atom of 3-aminopropyl chain in the ^{13}C CP/MAS NMR spectrum of sample D (Figure 4 and Table 1), it is necessary to make a conclusion about protoning NH_2-groups of this xerogel. Thus the protoning of NH_2-groups can be as a result of interaction of this group either with a proton of thiol group or with a proton of silanol group. However it contradicts with the conclusions which were made on the basis of vibration spectroscopy data. Therefore, if the 3-aminoprpyl group is not protonated in xerogel D then it takes part in a hydrogen bond. This is due to shift in signal of the central carbon atom of propyl chains in the region of stronger fields (20–23 ppm). Thus, there is resonance at ~28 ppm of individual APTES in the ^{13}C CP/MAS NMR spectrum while at protoning of graft 3-aminopropyl groups to surface SiO_2 it is moved in the region of stronger fields (21–22 ppm). It is clear that the hydrogen bond characters in the sample D differs from the one which is realized in initial APTES. It is evident that 3-aminopropyl group in a surface of the sample D (and also C and E) forms hydrogen bond with a silanol group. Water molecules which are located in the surface layer of these xerogels[54] also form hydrogen bond, for example, like this type [≡Si(CH_2)$_3$$H_2$N ¨ H_2O ¨ HOSi≡]. Therefore, a signal from the central carbon atom of propyl chains will be located in the same region (20–23 ppm) of ^{13}C CP/MAS NMR spectrum – as well as in the case of protonation of the aminogroup, which is found in the xerogel surface

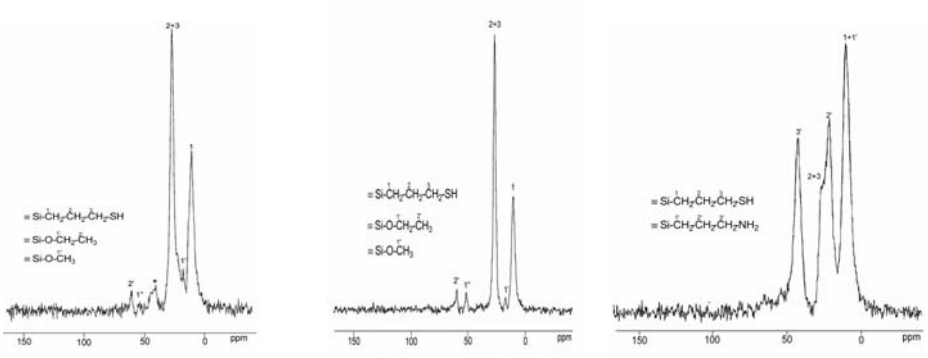

a b c

Figure 4. ^{13}C CP/MAS NMR spectra of samples A, B and D.

TABLE 1. Summary of ^{13}C CP/MAS NMR data for A, B , D and F xerogels.

Signals assignment	Chemical shifts (ppm)			
	Sample A	Sample B	Sample D	Sample E[81]
≡Si$\underline{C}$H$_2$CH$_2$CH$_2$(SH or NH$_2$)	10.9	10.8	10.0	10.4
≡SiO$\underline{C}$H$_2$CH$_3$	17.7	17.7	–	–
≡SiCH$_2\underline{C}$H$_2$CH$_2$NH$_2$	–	–	21.2	22.1; 25.5 (sh)
≡SiCH$_2\underline{C}$H$_2\underline{C}$H$_2$SH	27.2	27.1	27.0	–
≡SiCH$_2$CH$_2\underline{C}$H$_2$NH$_2$	–	–	41.9	42.9
≡SiO$\underline{C}$H$_3$	~52	51.4	–	–
≡SiOCH$_2\underline{C}$H$_3$	60.4	59.7	–	–

layer, and same is in the case of its formation of hydrogen bond with a silanol group (with participation of water molecule).

The suggested hypothesis about surface layer structure in such bifunctional xerogels correlates and is supported by the results of studying ^{13}C CP/MAS NMR and ^{1}H MAS NMR spectra of sample F.[13] Thus, a signal from the central carbon atom of propyl chains is found in the same region (21–23 ppm) in ^{13}C CP/MAS NMR spectrum of this sample obtained before and after its treatment by HCl solution (Figure 5). This signal is moved to weak fields in the ^{13}C CP/MAS NMR spectrum when the initial xerogel are heated in a oven (Figure 5). This is in that region where the signal from the central carbon atom of individual APTES is located. In other words, removing of water from surface layer during the heating of the sample results into removing of a bridge between amino and silanol groups, the role of which carried out water molecule, and to form a new hydrogen bond between only amino groups.

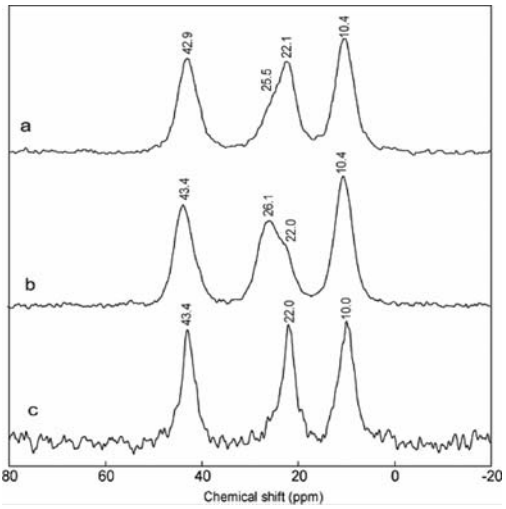

Figure 5. ^{13}C CP/MAS NMR spectra of initial xerogel E (a), dried in oven (b) and treated by 0.1M HCl (c).

Otherwise, there is a reorganization of surface layer in the xerogel. Therefore, the state of surface layer in such xerogels depends on a drying condition of the samples. This conclusion is supported by the results of works[26,52,82] for which long drying of xerogels in vacuum is characterised: according to ^{13}C CP/MAS NMP spectroscopy data amino groups in the surface layer of these samples take part at hydrogen bond the character of which is similar to one in individual APTES.

The use of ^{31}P CP/MAS NMR spectroscopy allowed to reveal transformation of $\equiv Si(CH_2)_2P(O)(OC_2H_5)_2$ functional groups in the surface layer of xerogels after they were treated by boiling conc. HCl.[69,83] Thus, ^{31}P CP/MAS NMR spectrum of the initial xerogel contains a single intense symmetric signal within the region from 10 to 40 pmm (Figure 6a). The location of this signal is close to the one of phosphorus atom signal of the initial DFTS (32.9[84] or 34.5 ppm[70]). The appearance of an additional signal at 23–24 ppm in the ^{31}P CP/MAS NMR spectrum was observed after the treatment of the initial xerogel by conc. HCl and its drying in vacuum (Figure 6b). This signal gives evidence to the formation of $\equiv Si(CH_2)_2P(O)(OH)–OSi\equiv$ product during the drying in vacuum at 120°C. The difference between the two signals is ~9 pmm, therefore, two types of functional groups are presented on the surface: those which take part in the hydrogen bonds formation, $\equiv Si(CH_2)_2P(O)(OH)_2$, and those which are involved in the $\equiv Si–O–P(O)(OH)–$ bond formation.[69,83] The appearance of an additional signal in the ^{31}P CP/MAS NMR spectra of bifunctional xerogels most likely is due to formation of similar bridges, $\equiv Si(CH_2)_2P(O)(OC_2H_5)–OSi\equiv$, by the part of phosphorus containing groups.[73]

Solid-state NMR spectroscopy was found very useful for studying xerogels with complex functional groups, for instance, cyclodextrines (CD).[75] In ^{13}C CP/MAS NMR spectrum of the xerogel which were functionalized by α-CD with ethoxysilyl groups are presented by signals on CD fragment as $\equiv Si(CH_2)_3$ NHC(O)O– spacer.

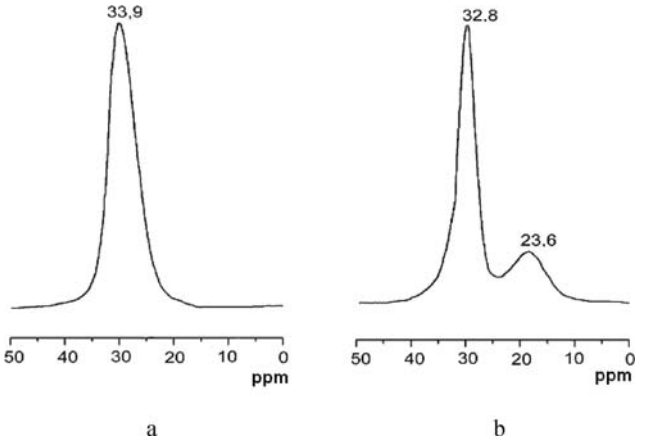

Figure 6. ^{31}P CP/MAS NMR spectra of the xerogels containing $\equiv Si(CH_2)_2P(O)(OC_2H_5)_2$ groups: before (a) and after (b) the treatment of conc. HCl.

^{29}Si CP/MAS NMR spectra can furnish valuable information about local surroundings of the silicon atoms. These spectra of functionalized polysiloxane xerogels contain, as a rule, two sets of resonance signals in the spectrum interval from −110 to −50 ppm relating to different structural units (Figure 7). In the first region there are three signals at about −110, −100, and −90 ppm that are related to $(\equiv SiO)_4\underline{Si}$ (Q^4), $(\equiv SiO)_3\underline{Si}(OAlk)$ (Q^3) and $(\equiv SiO)_2\underline{Si}(OAlk)_2$ (Q^2), respectively (Alk = H, Me or Et).[85] The second region also contains one signal at −66 ppm with a shoulder at −57 ppm, that are related to the structural units $(\equiv SiO)_3\underline{Si}R'$ (T^3) and $(\equiv SiO)_2(AlkO)\underline{Si}R'$ (T^2). ^{29}Si CP/MAS NMR spectra of xerogels which contain 3-mercaptopropyl and methyl groups in their surface layer presented in Figure 7 as example.[61] The absence of signals from structural units T^0, T^1 and Q^0, Q^1 type in the considered spectra testifies about a high degree of course of hydrolytic polycondensation reaction. The analysis of ^{29}Si DP/MAS NMR spectra of these xerogels showed that, in all samples, the content of structural units of T^3 type [$(\equiv SiO)_3SiCH_3$ and $(\equiv SiO)_3Si(CH_2)_3SH$] is significantly higher than structural units of T^2 type [$(\equiv SiO)_2Si(OR)CH_3$ и $(\equiv SiO)_2Si(OR)(CH_2)_3SH$, R = H, CH_3 or C_2H_5]. Thus, the T^3/T^2 ratio for sample **2TMM** equals to 4.8. Therefore, these xerogels should be characterized by a sufficiently high hydrolytic stability of the surface layer. Note that the use of

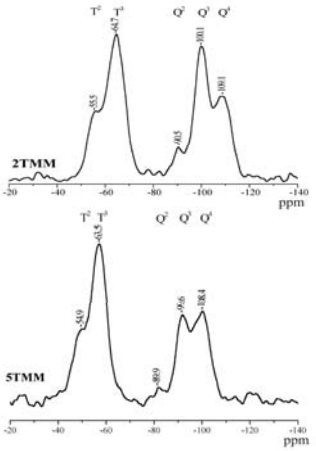

Figure 7. ^{29}Si CP/MAS NMR spectra of xerogels with HS–groups: TEOS/MPTMS/MTES ratio was equal to 4:1:1 (**2TMM**) and 2:1:1 (**5TMM**).[61]

other catalysts[53] for preparing xeroges with thiol groups results in the formation of a significant number of structural units of T^2 type in their surface layer.

Introduction of *n*-propyl groups instead of methyl groups are conduct to occurrence easy hydrolyzed structural units of T^1 type in ^{29}Si CP/MAS NMR spectra of these samples, i.e. structural units, which are connected with polysiloxane framework by only one siloxane bond. Moreover, if in a content of the xerogel with methyl groups structural units of T^3 type prevail appreciably above T^2, then in a content of the xerogel with propyl groups their contents are about identical. Therefore, the significant degree of incompleteness of the polycondensation process is typical for the last-mentioned xerogel due to influence of the geometrical size of functional group on this process. It is interesting, that replacement of amino group in the xerogel with $\equiv Si(CH_2)_2P(O)(OC_2H_5)_2$/ $\equiv Si(CH_2)_3NH_2$ in surface layer of thiol group also conducts to occurrence of a signal from structural units of T^1 type[73] in ^{29}Si CP/MAS NMR spectrum. Apparently, it reflects the influence of pH from environment on a degree of polycondensation in such xerogels.

The analysis of the ^{29}Si CP/MAS NMR spectra of xerogels which were obtained by the use of BTESE/APTES/MPTMS system (Figure 8) leads to the conclusion that in alkoxysilanes during the reaction of hydrolytic polycondensation the ≡Si–C bond is stabile.[59] The absence of any signals in the region of –90 to –110 ppm confirms such statement. Secondly, only one wide and asymmetric resonance signal is present in the range of –43 to –75 ppm in the ^{29}Si CP/MAS NMR spectra of these xerogels (Figure 8). A deconvolution of this signal gives five components that corresponds with T^1, T^2 and T^3 structural

units. For BTESE these signals correspond with the following products of its hydrolysis and condensation: $(\equiv SiO)_2(RO)SiC_2H_4-$ (–55.7 ppm; T^2) and $(\equiv SiO)_3SiC_2H_4-$ (–64.1 ppm; T^3), where R is C_2H_5 or OH [20]. From the last three signals the first one (at –46.6 ppm) has been attributed to the T^1 structural unit of MPTMS, and the rest of two (at –60.0 and –69.5 ppm) has been attributed consecutively to the T^2 and T^3 structural units of APTES and MPTMS. [6,53] Therefore, solid-state NMR spectroscopy application allows to make identification of the nature of functional groups in the surface layer of xerogels. It also reveals the transformation of these groups during the course of xerogels synthesis and allows to establish structural units' type, which form both xerogels and their surface layer. This spectroscopy application allows to fix the participation of functional groups in hydrogen bond formation and other interactions.

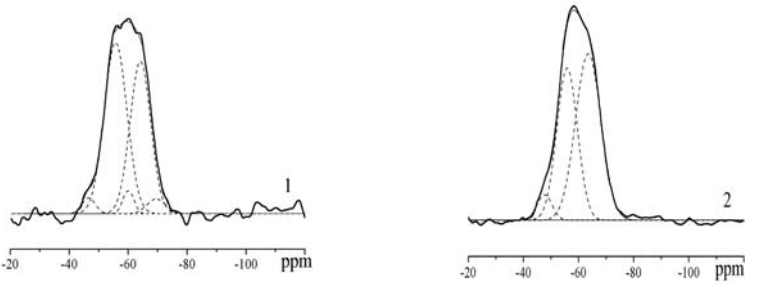

a b

Figure 8. ^{29}Si CP/MAS NMR spectrum of the xerogel obtained with the use of BTESE/APTES/MPTMS systems (4:1:1 and 8:1:1 (mol)).[59]

3.3. METAL MICROPROBE TECHNIQUE

The topography of FPA surface presents un undoubtful interest. For its establishment the authors[86–88] employed the metal microprobe technique: composition and structure of complexes coordination bundle, which forms during sorption of copper(II) ions by amine-containing xerogels from acetonitrile solutions, were identified by electron reflection spectroscopy (ERS) and EPR spectroscopy. It was found that irrespective of degree of surface coverage by the metal on the surface there is the proceeded formation of complexes of one and the same composition (CuO_2N_2) only. That means that at the equatorial plane of a coordination polyhedron of copper (II) there were two nitrogen atoms. However, the increase of copper(II) content on the surface of xerogels often leads to reduction, firstly, of geometry uniformity of formed complexes and, secondly,

to reduction of a number of the isolated paramagnetic centers, for which the superfine structure is typical. It encounters on an idea that the surface in such xerogels has quite complex character. The similar conclusion also has been made during the study of copper(II) complexes by ERS and EPR spectroscopy. This complexes are formed on the surface of bifunctional xerogels (-SH/-NH_2) during the sorption of copper(II) ions from their acidified water solutions.[89] The signals form and the calculated values of spectra parameters[89] are typical for tetragonal complexes of copper(II) with a coordination environment [2N, 2O].[90] The analysis of ERS and EPR spectroscopy data which was received during the study of Cu^{2+} ions complexation with aminogroups on the surface of FBPS[91] also results in a conclusion that complexes form coordination bundle with [CuO_2N_2].

The comparison of EPR spectra parameters for copper(II) complexes, which are formed on the surface of aminocontaining xerogels, leads to following conclusion: two nitrogen atoms are always included in the coordination sphere of copper(II) ion – irrelevant to the nature of structuring agents, to the nature of amine groupings, to functionality of the surface layer, to structural-adsorption characteristics of the sorbent as well as to the nature of the solvent which was used for the sorption. Moreover, all of the Cu(II) complexes, which were identified on the surface of different aminocontaining silicas,[6] have the same composition of a coordination polyhedron, CuN_2O_2. All these was determined from the analis EPR spectra parameters.[6] It gave grounds to conclude about a specific and, probably, similar distribution of complexing groups in the surface layer of those silicas. One can not exclude that this is due to exist in that layer – at least, in the case of xerogels – oligomers with the aminopropyl groupings.

4. Adsorption Properties of Functionalized Polysiloxane Xerogels

4.1. SOME FACTORS CONTRIBUTING TO STRUCTURAL-ADSORPTION CHARACTERISTICS OF FUNCTIONALIZED POLYSILOXANE XEROGELS

Early in[6] on the example of amine-containing xerogels, which were obtained using of two-component system of TEOS/APTES, it was shown that (1) all of the obtained samples are classified as mesoporous adsorbents (for the majority of them their values of S_{sp}, sorption volume V_s, and size d fall within the interval 92–315 $m^2\ g^{-1}$, 0.12–1.38 $cm^3\ g^{-1}$, 3.7–17.7 nm, respectively); (2) in all cases the introduction of a nonaqueous solvent results in a decrease of S_{sp} and V_s and an increase of d; (3) with decrease of TEOS/APTES ratio the porosity of samples decreases substantially (at a ratio of 1:1 the xerogel becomes practically nonporous); (4) a similar effect is exerted by a decrease in the amount

of water taken for the hydrolysis; (5) drying of liogels at atmospheric pressure leads to large-pored sorbents; (6) washing of xerogels with water (before repeated vacuum drying) results in a fine-pored adsorbents while washing with abundant amounts of water considerably increases sizes of pores. Relative increase of geometric sizes of the functional group leads to practically nonporous xerogels.

These conclusions were confirmed and expanded in future by studying xerogels with functional groups of other nature. Thus, the increase of TEOS's loading in an initial solution caused the increase in S_{sp} of the xerogels which contained (thio)urea,[47] thiol,[61] phosphoryl[69] and propionic acid[6,65] groups. However, it should be mentioned that formation of porous structures was observed only for the systems with TEOS/trifunctional silane molar ratio which was higher than 1:1 in case of the HS-groups,[61] 2:1 in case of –NHC(O,S)NHR‴ groups[47,48] or 4:1 in case of the $–P(O)(OC_2H_5)_2$ groups.[69] Geometric sizes of the mentioned functional groups increases with the same sequence. An influence of the contain of functional groups on structural-adsorption characteristics is clearly seen on samples of xerogels with calixarene or cyclodextrine groups.[75,92]

It was shown by the example of TEOS/(MPTMS + MTES) system that the change in molar ratio of trifunctional silanes in the initial solution from 2:1 to 1:2 leads to the formation of xerogels with the developed porous structure. Thus, at TEOS/trifunctional silanes ratio of 2:1 S_{sp} raised from 408 to 678 m^2/g and at the molar ratio of 1:1 it raised from 44 to 394 m^2/g. Simultaneously, the tendency to the increase of other parameters, namely V_s and d, was observed.[55] Similar tendencies were defined also for the xerogels with a bifunctional surface layer of NH_2/CH_3 (or C_6H_5) composition.[28,29] By the example of amine-containing xerogels[6] it was shown with using of TEM that such distinctions were determined by sizes of globules and their packed structure.

In the case of the bridged polysilsesquioxane xerogels which were functionalized by amine and thiol groups, their high values of S_{sp} attract attention, namely from 510 to 840 m^2/g for xerogels with ethylene bridges and from 650 to 970 m^2/g for xerogels with phenylene bridges.[13–15] The type of isotherms of these xerogels depends, on the first place, from the nature of functional groups (amine or thiol groups). In the first case the isotherms for xerogels with ethylene bridges are S-shaped and have a distinct hysteresis loop (in contrast to xerogels with phenylene bridges) while isotherms in the second case are more likely to be Langmuir isotherms (Figure 9). This difference is brought about by the nature of a medium that is created by these groups during the synthesis. It was shown[13–15] that the parameters of the porous structure of such xerogels were substantially affected by the nature of a spacer, relative size of the functional group, ratio of reacting alkoxysilanes, and gel ageing time.

Thus, taking into account the mentioned above factors, it is possible to obtain polysiloxane xerogels with controlled porosity, surface layer composition and loading of functional groups.

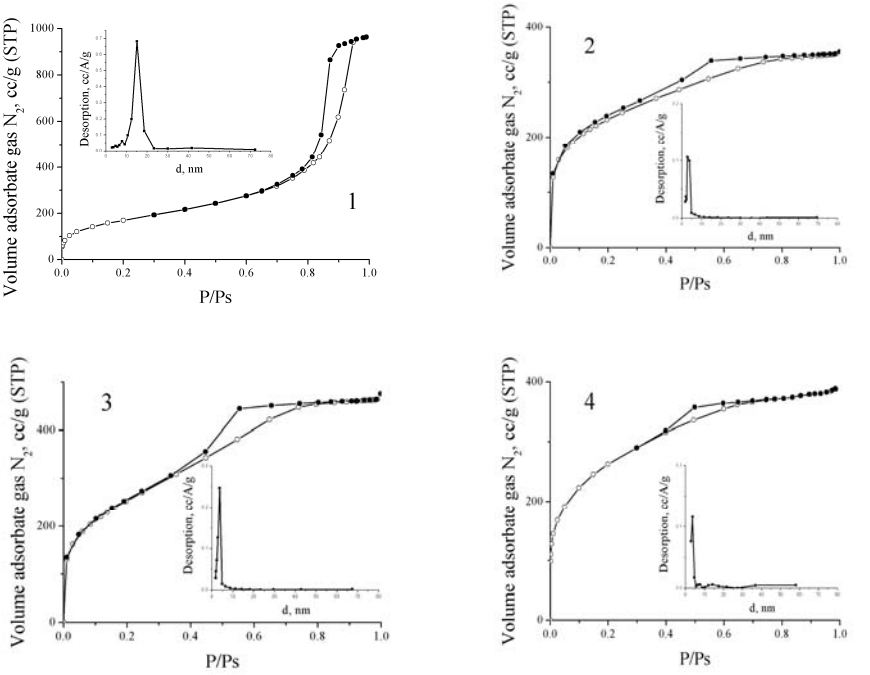

Figure 9. Isotherms of N_2 adsorption/desorption and PSDs for the xerogels synthesized using the following systems: (1) -C_2H_4-/-NH_2=4:1; (2) -C_2H_4-/-SH=4:1; (3) -C_6H_4-/-NH_2=4:1; (4) -C_6H_4-/-NH_2=4:1.[13–15]

4.2. ADSORPTION PROPERTIES OF FPA

Parish and co-workers[25] studying in 1989 adsorption of Ni(II), Co(II), Cu(II) and Zn(II) by aminocontaining xerogels showed that an equilibrium in such systems is reached at least in 15 h. Xerogels with PPh_2 groups[32] absorb metal ions (Co and Ni(II)) from their ethanol solution slowlier. It is noted that time of equilibrium attainment depends on particle sizes. The other authors[35] pointed out that the equilibrium attainment at absorption of metal ions during 20–30 min. However even at optimal sorption conditions a part of xerogels' functional groups does not take part in complex formation.[25,32,33,93] This data is confirmed by HCl acid adsorption by aminocontaining xerogels.[94] However, as it was shown for the Cu(II) adsorption from the acetonitrile solutions, that almost all the amino-groups are accessible for metal ions (adsorption time was 48 h).[86,88] In acid medium these xerogels absorb copper ions best of all that is in agreement with data.[95]

It was shown that a separation of Ni(II) and Cu(II) is possible for xerogels with bifunctional surface layer (ethylenediamine and vinyl groups).[33] In[96] attention has been given to sorption of microquantities of Au(III) from acidic solutions by xerogels which surface layers contain thiourea and thiourea/amine groups. It has been found that the maximum degree of extraction of Au(III) is typical for the sorbent with a bifunctional surface layer. It is interesting that an increase of solution temperature (up to 50°C) causes the significant decreases in the time of an attainment of sorption equilibrium (up to 5 min) and at the same time increases the degree of gold extraction. The xerogels with thiourea- and aminogroups in their surface layer also have a high efficiency in sorbing mercury(II) from acidic solutions.[97]

Hg(II) ions could be effectively extracted from their acidic solutions by xerogels with monofunctional surface layer containing thiol groups.[98] Good extraction of mentioned ions from their acidic solutions (pH ~ 2) was achieved also for the xerogels that contain 3-mercaptopropyl and alkyl groups. The influence of surface layer's composition and pore structures' parameters of such xerogels on their complexing properties towards Hg(II) was studied in details.[99] Using the model of chemical reactions,[100] it was possible to calculate the constants of stability for the complexes which are formed on the surface of considered xerogels. The analysis of obtained data shows, that complexes stability decreases at the increasing of surface concentration of 3-mercaptopropyl groups in these xerogels. Moreover, the bordered concentration of functional groups was revealed. The complexes with compositions 1:1 and 1:2 are formed above this concentration. In conclusion, the authors considered the values of static sorption capacity (SSC) for such adsorbents. One can assume, that gradual increase of 3-mercaptopropyl groups concentration should lead to systematic increase of xerogels SSC. However, this dependence has the maximum for the xerogels with thiol groups concentration near 3.0–3.8 mmol/g (Figure 10). Further increase of 3-mercaptopropyl groups concentration leads to SSC decrease. This fact is due to complexes' formation with composition 1:2 in the surface of these sorbents. It should be pointed out, that highest SSC (620 mg Hg^{2+}/g), which was achieved, is comparable with SSC for the best organic cation-exchangers which are used for the Hg(II) extraction.[101] Hence, presented results give evidence, that synthesized xerogels with 3-mercaptopropyl groups could be used for the extraction of Hg(II) from aqueous solutions.

In this case the surface concentration of thiol groups strongly influences on both: stability and composition of the complexes which are formed on the surface of such polysiloxane sorbents. Since the surface concentration of functional groups is determined as a ratio of functional groups quantity to adsorbent surface area, then porous structure parameters of xerogels strongly influences their sorption properties.

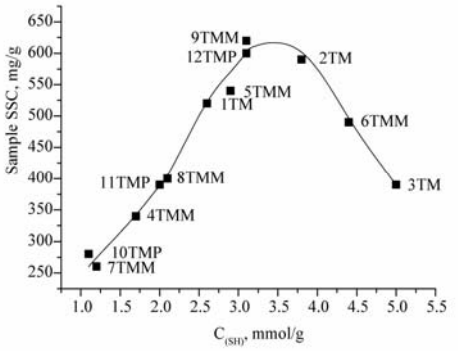

Figure 10. Dependence of SSC sorbents from 3-mercaptopropyl groups concentration.[99]

It was found that FBPS xerogels which were functionalized by 3-mercaptopropyl groups have a high efficiency in sorbing Ag(I) ions.[102] It should be mentioned that functionalized xerogels were used mostly to study sorption of 3d-metals.[35,57,95] However recently a range of investigated metals has been extended such as: (Hg(II)[52,58,95,103]; Ca(II)[66]; Zn(II)[66]; Cd(II)[52,66]; Pb(II)[52]; Pd(II)[66]; UO_2(II)[104]; Ln(III),[105] Am(III), Pu(IV)[49,105]). It was shown,[92] that xerogels with calixarene groups could adsorb Cs(I) ions from acidic aqueous solutions (1 M HNO_3). The adsorption equilibrium in the system is reached less than in 1 h. It was determined that the increase of functional groups' contain leads to the increase of Cs(I) sorption degree. However, no more then 10–40% of functional groups takes part in Cs(I) extraction process.[92]

Finally it should be noted that sol-gel method has a great potential at synthesis of sorbents "with memory" for metal ions[106] or for their analytical determination.[107,108]

5. Conclusions

In this paper we have discussed the preparation routes of polysiloxane xerogels which contain functional groups of different nature in their surface layer and which are capable to complexation. Significant influence on structural-adsorption characteristics of formed xerogels with a monofunctional surface layer has the nature and the geometrical sizes of functional groups, the nature of structure-forming agent as well as the synthetic conditions.

The preparation paths of polysiloxane xerogels with a bifunctionalized surface layer has also been discussed. In this case the ratio of alkoxysilanes and nature of additional functional groups influence significantly on surface hydrophobicity degree of such materials as well as their porosity.

Physical method data testify about presence of structural units with the same nature on the surface of functionalized polysiloxane xerogels and about the similar character of surface structure.

Taking into account the presented results on sorption of metal ions as well as the results obtained by other authors,[22,23,106–109] it as possible to assert the significant perspectives of the usage of functionalized polysiloxane xerogels in sorptive technology.

Acknowledgment

The author would like to acknowledge the partial financial support of NATO for this work (Grant SfP–978006) and also to thank Professor A. Dabrowsky, Dr. B. Alonso and Dr. M. Barchak for NMR spectra and productive discussion.

References

1. V.A. Tertykh, L.A. Belyakova, *Chemical Reactions Involving Silica Surface* (Naukova Dumka, Kiev, 1991) (in Russian).
2. E.F. Vansant, P. van der Voort, K.C. Vrancken, *Characterization and Chemical Modification of the Silica Surface* (Elsevier, Amsterdam, 1995).
3. V.N. Zaitsev, *Complexing Silicas: Synthesis, Structure of Bonded Layer and Surface Chemistry* (Folio, Kharkiv, 1997) (in Russian).
4. *Chemistry of Surface Grafted Compounds*, edited by L.G. Lisichkin (Fizmatlit, Moscow, 2003) (in Russian).
5. Yu.L. Zub, R.V. Parish, Functionalized polysiloxane sorbent: preparation, structure, properties and use, *Stud. Surf. Sci. Catal.* 99, 285–299 (1996).
6. Yu.L. Zub, A.A. Chuiko, Salient features of synthesis and structure of surface of functionalized polysiloxane serogels, in: *Colloidal Silica: Fundamentals and Applications*, edited by H.E. Bergna and W.O. Roberts (Taylor & Francis, Washington, DC, 2005), pp. 397–424.
7. Yu.L. Zub, A.A. Chuiko, Synthesis, Structure and Adsorption Properties of Functionalized Polysiloxane Materials, in: *NATO ARW* "*Combined and Hybrid Adsorbents*", edited by J.M. Loureiro and M.T. Kartel (Springer, Dordrecht, The Netherlands 2006), pp. 3–21.
8. *Handbook of Sol-Gel Science and Technology: Processing, Characterization, and Applications*, edited by S. Sakka (Kluwer, Dordrecht, The Netherlands, Vol. 1–3, 2005).
9. *Functional Hybrid Materials*, edited by P.Gomez-Romero and C.Sanchez (Wiley-VCH, Weinheim, 2004), pp. 1–417.
10. C.J. Brinker, G.W. Scherer, *Sol-Gel Science: The Physics and Chemistry of Sol-Gel Processing* (Academic, San Diego, CA, 1990).
11. J. Liu, X. Feng, G.E. Fryxell, L.-Q. Wang, A.Y. Kim, M. Gong, Hybrid mesoporous materials with functionalized monolayers, *Adv. Mater.* 10, 161–165 (1998).
12. Yu.L. Zub, M. Ya. Gorochovatskaya, A.A. Chuiko, A.M. Nesterenko, Polysiloxane matrices with functional groups as a basis of new sorbents, *Ext. Abstract Fourth International Conference on Fundamentals of Adsorption* (Kyoto, 1992), pp. 461–463.

13. Yu.L. Zub, A.A. Chuiko, N.V. Stolyarchuk, I.V. Mel'nyk, A. Dabrowski, New amine-containing adsorbents on the basis of bridged polysilsesquioxanes, *Dopov. NAN Ukrainy* 2, 117–122 (2005) (in Russian).
14. A. Dabrowski, M. Barczak, N.V. Stolyarchuk (Shvaykovska), I.V. Melnyk, Yu.L. Zub, Bridged polysilsesquioxane xerogels functionalizated by amine– and thiol–groups: synthesis, structure, adsorption properties, *Adsorption* 11, 501–517 (2005).
15. N.V. Shvaikovska, I.V. Mel'nyk, G.R. Yurchenko, O.K. Matkovski, Yu.L. Zub, Synthesis and structure–adsorption characteristics of bridged polysilsesquioxanes with aminopropyl groups, *Chem. Phys. Technol. Surf.* 10, 80–84 (2004) (in Russian).
16. *Tailor-Made Silicon-Oxygen Compounds*, edited by R. Corriu and P. Jutzi (Vieweg, Wiesbaden, 1996).
17. O.V. Stechenko, Yu.L. Zub, R.V. Parish, Polyaminosiloxane adsorbents: preparation and properties, *Proceedings of 3rd International Symposium "Effects of Surf. Heterogeeneity in Adsorp. and Catal. on Solids"* (Torun, Poland, 1998), pp. 231–232.
18. Yu.L. Zub, L.S. Drozd, A.A. Chuiko, Factors influencing the porous structure of poly-organosiloxanes, *Abstract of IUPAC Symposium on the Characterization of Porous Solids* (Marseille, France, 1993), 95 pp.
19. I.B. Slinyakova, T.I. Denisova, *Organo-silicon Adsorbents: Production, Properties, and Application* (Naukova Dumka, Kyiv, 1988) (in Russian).
20. L.P. Finn, I.B. Slinyakova, M.G. Voronkov, N.N. Vlasova, F.P. Kletsko, A.I. Kirillov, T.V. Shklyar, Structure and properties of polymercaptomethylsilsesquioxane xerogel, *Dokl. AN SSSR* 235(6), 1426–1429 (1977) (in Russian).
21. L.P. Finn, I.B. Slinyakova, M.G. Voronkov, N.N. Vlasova, F.P. Kletsko, *Certificate of Authorship No. 2322972* (1976) (in Russian).
22. M.G. Voronkov, N.N. Vlasova, Yu.N. Pozhidaev, Organosilicon ion-exchange and complexing adsorbents, *J. Appl. Chem.* 69, 705–718 (1996) (in Russian).
23. M.G. Voronkov, N.N. Vlasova, Yu.N. Pozhidaev, Organosilicon ion-exchange and complexing adsorbents, *Appl. Organometal. Chem.* 14, 287–303 (2000).
24. A.A. Chuiko, G.Ye. Pavlik, G.B. Budkevich, I.Ye. Neimark, A method of preparation of silica gels containing aminoalkyl groups, *USSR Certificate of Authorship No. 182719* (1966) (in Russian).
25. I.S. Khatib, R.V. Parish, Insoluble ligands and their applications I. A comparison of silica-immobilized ligands and functionalized polysiloxane, *J. Organomet. Chem.* 369, 9–16 (1989).
26. J.J. Yang, I.M. El-Nahhal, G.E. Maciel, Synthesis and solid-state NMR structural characterization of some functionalized polysiloxanes, *J. Non-Crystal. Solids.* 204, 105–117 (1996).
27. O.V. Stechenko, Synthesis, structure and structural-adsorption characteristics of polyamino-siloxane adsorbents, *Synopsis of Thesis for Ph.D. Degree* (ISC of NAS of Ukraine, Kyiv, 2002) (in Ukrain).
28. O.V. Stechenko, G.R. Yurchenko, O.K. Matkovskii, Yu.L. Zub, Adsorption properties of some polyaminosiloxanes, *Naukovyi Visnyk Uzhgor. Univer., Series 'Khimiya'* 5, 107–112 (2000) (in Ukrain).
29. O.K. Matkovskii, G.R. Yurchenko, O.V. Stechenko, Yu.L. Zub, Influence of solvent nature on structure-adsorption characteristics of poly(3-aminopropyl)siloxane, *Naukovi Zapysky Ternopil's kogo Derzhav. Pedagog. Univer., Series 'Khimiya'* 4, 40–45 (2000) (in Ukrain).
30. Yu.L. Zub, A.A. Chuiko, O.V. Stechenko, Synthesis, structure and structure-adsorption characteristics of some polyamonisiloxanes, *Doklady NAN Ukrainy* 4, 150–155 (2002) (in Russian).
31. J.J. Yang, I.M. El-Nahhal, I.-S. Chuang, G.E. Maciel, Synthesis and solid-state NMR structural characterization pf polysiloxane-immobilized amine ligands and their metal complexes, *J. Non-Crystal. Solids* 209, 19–39 (1997).

32. R.V. Parish, D. Habibi, V. Mohammadi, Insoluble ligands and their applications II. Polysiloxane-phosphine ligands, their complexes, and hydrogenation catalysts, *J. Organomet. Chem.* 369, 17–28 (1989).
33. I.M. El-Nahhal, R.V. Parish, Insoluble ligands and their applications III. Polysiloxane diaminoethane derivatives, *J. Organometal. Chem.* 452, 19–22 (1993).
34. C.R. Silva, C. Airoldi, Acid and base catalysts in the hybrid silica sol-gei process, *J. Colloid Interf. Sci.* 195, 381–387 (1997).
35. F.A. Pavan, I.S. Lima, E.V. Benvenutti, Y. Gushikem, C. Airoldi, Hybrid aniline/silica xerogel cation adsorption and thermodynamics of interaction, *J. Colloid Interf. Sci.* 275, 386–391 (2004).
36. F.A. Pavan, W.F. de Mahalhaes, M.A. de Luca, C.C. Moro, T.M.H. Costa, E.V. Benvenutti, A characterization study of xerogel silicapropylaniline powders, *J. Non-Crystal. Solids* 311, 54–60 (2002).
37. F.A. Pavan, L. Franken, C.A. Moreira, T.M.H. Costa, E.V. Benvenutti, Y. Gushikem, Synthesis of a thermal stable silica/p-anisidine sol-gel powdered material, *J. Colloid Interf. Sci.* 241, 413–416 (2001).
38. D.R. Azolin, C.C. Moro, T.M.H. Costa, E.V. Benvenutti, Effects of organic content and H_2O/TEOS molar ratio on the porosity and pore size distribution of hybrid naphthalene-amineпropylsilica xerogel, *J. Non-Cryst. Solids* 337, 201–206 (2004).
39. C. Alie, F. Ferauche, R. Pirard, A.J. Lecloux, J.-P. Pirard, preparation of low-density xerogels by incorporation of additives during synthesis, *Micropor. Mesopor. Mat.* 70, 57–62 (2004).
40. V. van Blaaderen, A. Vru, Synthesis and characterization of monodisperse colloidal organo-silica Shperes, *J. Colloid Interf. Sci.* 156, 1–18 (1993).
41. E. Yacoub-George, E. Bratz, H. Tiltscher, Preparation of functionalized polyorganosiloxane spheres for the immobilization of catalytically active compounds, *J. Non-Cryst. Solid*s 167, 9–15 (1994).
42. L.T. Arenas, T.A.S. Aguire, A. Langaro, Y. Gushikem, E.V. Benvenutti, T.M.H. Costa, 3-n-propyl-1-azonia-4-azabicyclo[2.2.2]octanechloride/silica hybrid polymer. A morphologic study in relation to the organic content, *Polymer* 44, 5521–5525 (2003).
43. G. Dubois, R.J.P. Corriu, C. Reye, S. Brandes, F. Denat, R. Guilard, First organic-inorganic hybrid materials with controlled porosity incorporating cyclam units, *Chem. Commun.* 2283–2284 (1999).
44. I.V. Melnyk, Synthesis and investigation of polyorganosiloxanes with bi- and trifunctional surface layer, *Synopsis of Thesis for Ph.D. Degree* (ISC of NAS of Ukraine, Kyiv, 2002) (in Ukrain).
45. J.J. Yang, I.M. El-Nahhal, I.-S. Chuang, G.E. Maciel, Synthesis and solid-state NMR structural characterization of polysiloxane-immobilized phosphine, phosphine-amine and phosphine-thiol ligand systems, *J. Non-Cryst. Solids* 212, 281–291 (1997).
46. Z. Lu, E. Lindner, H.A. Mayer, Applications of sol-gel-processed interphase catalysts, *Chem. Rev*. 102, 3543–3578 (2002).
47. Yu.L. Zub, I.V. Melnyk, A.A. Chuiko, D. Cauzzi, G. Predieri, Design of functionalized polysiloxanes: synthesis and investigation of sulfur-containing xerogels with mono- and bifunctional surface layer, *Chemistry, Physics and Technology of Surface* 7, 35–45 (2002).
48. I.V. Melnyk, N.V. Stolyarchuk, Yu.L. Zub, A. Dabrowski, Polysiloxane xerogel containing arch-fixed urea groups, *J. Appl. Chem.* 79, 992–997 (2006) (in Russian).
49. J.-C. Broudic, O. Conocar, J.J.E. Moreau, D. Meyer, M.W.C. Man, New hybrid silica based materials for the solid-liquid extraction of actinides, *J. Mater. Chem*. 9, 2283–2285 (1999).
50. N. Becker, K. Unger, Synthesis and properties of chemical modified dihydroxy-, hydroxyamino- and amino-functional silica packings in adsorption chromatography, *Fresenius Z. Anal. Chem.* 304, 374–381 (1980).

51. I.M. El-Nahhal, J.J. Yang, I.-S. Chuang, G.E.Maciel, Synthesis and solid-state NMR structural characterization of polysiloxane-immobilized thiol and thiol-amine ligands, *J. Non-Cryst. Solids* 208, 105–118 (1996).
52. J.S. Lee, S. Gomes-Salazar, L.L. Tavlarides, Synthesis of thiol functionalized organo-ceramic adsorbent by sol-gel technology, *React. Funct. Polym.* 49, 159–172 (2001).
53. G.E. Maciel, NMR characterization of functionalized polysiloxanes, in: *Solid State NMR of Polymers*, edited by I. Ando and T.Asakura (Elsevier, Amsterdam, 1998), pp. 923–984.
54. I.V. Melnyk (Seredyuk), Yu.L. Zub, A.A. Chuiko, Van Der P. Voort, Novel polyorgano-siloxane xerogels with a bifunctional $\equiv Si(CH_2)_3SH/\equiv Si(CH_2)_3NH_2$ surface layer, *Chemistry, Physics and Technology of Surface* 8, 125–133 (2002).
55. H.I. Dobryanska, I.V. Melnyk, Yu.L. Zub, A.A. Chuiko, M. Barchak, A. Dabrowski, The influence of the $Si(OC_2H_5)_4/(CH_3O)_3Si(CH_2)_3SH$ ration on the structure-adsorption characteristics of xerogels formed and accessibility of functional groups in thier surface layers, *J. Phys. Chem.* 80, 939–944 (2006) (in Russian).
56. Yu.L. Zub, N.V. Stolyarchuk, I.V. Melnyk, A.A. Chuiko, A. Dabrowski, M. Barczak. New adsorbents based on bridged polysilsesquioxanes containing 3-mercaptopropyl functional groups, *Mendeleev Commun.* 15(4), 168–170 (2005).
57. C. Airoldi, L.N.H. Arakaki, Immobilization of ethylenesulfide on silica surface through sol-gel process and some thermodynamic data of divalent cation interaction, *Polyhedron* 20, 929–936 (2001).
58. H.-J. Im, C.E. Barnes, S. Dai, Z. Xue, Functionalized sol–gels for mercury(II) separation: a comparison of mesoporous materials prepared with and without surfactant templates, *Micropor. Mesopor. Mat.* 70, 57–62 (2004).
59. N.V. Stolyarchuk, I.V. Melnyk, Yu.L. Zub, M. Barchak, A. Dabrovski, *Colloid J.* (2008) (in press) (in Russian).
60. L.P. Finn, I.B. Slinyakova, M.G. Voronkov, N.N. Vlasova, Study of structure and adsorption properties of sulfur-containing polyorganosiloxane xerogels, *Adsorbtsiya i Adsorbenty* 8, 98–102 (1980) (in Russian).
61. G.I. Dobryanskaya, Yu.L. Zub, M. Barczak, A. Dabrowski, Synthesis and structure-related adsorption characteristics of bifunctional polysiloxane xerogels with methyl and 3-mercaptopropyl groups, *Colloid J.* 68, 548–557 (2006) (in Russian).
62. G.I. Dobryanskaya, I.V. Melnyk, Yu.L. Zub, A. Dabrowski, SPorous xerogels with bi-functional surface layer of $\equiv Si(CH_2)_3SH/\equiv Si(CH_2)_2CH_3$ composition, *J. Phys. Chem.* 81, 410–417 (2007) (in Russian).
63. A.A. Chuiko, G.Ye. Pavlik, I.Ye. Neimark, Method of preparation of organosilica gel, *USSR Certificate of Authorship No. 164680* (1964).
64. N.A. Prybora, L.S. Dzyubenko, Yu.L. Zub, M. Jaroniec, Synthes of the polysiloxane containing butyric acid residue on its surface layer, *Khimichni Nauky. Collected Sci. Papers of Nat. Training M.P. Dragomanov's Univ.* 41–47 (1999) (in Ukrain).
65. N.A. Prybora, Yu.L. Zub, A.A. Chuiko, M. Jaroniec, Synthesis and properties of some polycarboxylsiloxane sorbents, *Abstract of 2nd International Conference on Silica Science and Technology* (Mulhouse, France, 2001), 171 pp.
66. P. Tien, L.-K. Chau, Novel sol-gel-derived material for separation and optical sensing of metal ions: propyl-ethylenediamine triacetate functionalized silica, *Chem. Mater.* 11, 2141–2147 (1999).
67. G.H. Barnes Jr., M.P. David, Synthesis and hydrolityc stability of some organosilicon phophonate esters, *J. Org. Chem*. 25, 1191–1194 (1960).
68. J.-P. Bezombes, C. Chuit, R.J.P. Corriu, C. Reye, Preparation and characterization of new organic-inorganic hybrid materials incorporating phosphorus centers, *J. Mater. Chem.* 8, 1749–1759 (1998).

69. O.A. Dudarko, I.V. Mel'nyk, Yu.L. Zub, A.A. Chuiko, A. Dabrowski, Synthesis of polysiloxane xerogels using teraethoxysilane/(diethylphosphoneethyl)triethoxysilane system, *Colloid J.* 67, 753–758 (2005) (in Russian).
70. A. Aliev, D.L. Ou, B. Ormsby, A.C. Sullivan, Porous silica and polysilsesquioxane linked phosphonates and phosphonic acids, *J. Mater. Chem*. 10, 2758–2764 (2000).
71. A. Dabrowski, M. Barczak, O.A. Dudarko, Yu.L. Zub, Preparation and characterization characterization of polysiloxane xerogels having covalently attached phosphonic groups, *Polish J. Chem.* 81, 475–483 (2007).
72. M. Jurado-Gonzalez, D.L. Ou, A.C. Sullivan, J.R.H. Wilson, Synthesis, characterization and catalytic activity of porous vanadyl phosphonate-modified silicas, *J. Mater. Chem.* 12, 3605–3609 (2002).
73. O.A. Dudarko, Yu.L. Zub, A. Dabrowski, M. Barczak, Polysiloxane xerogels with a bi-functional surface layer containing O/N, O/S, S/N and S/S donor centres, *J. Appl. Chem.* (2007) (in press) (in Russian).
74. C. Liu, J.B. Lambert, L. Fu, Simple surfactant-free route to mesoporous organic-inorganic hybrid silicas containing covalently bound cyclodextrins, *J. Org. Chem.* 69, 2213–2216 (2004).
75. O.V. Kuchma, Yu.L. Zub, S.V. Ryabov, L.V. Kobrina, Hybrid organic-inorganic materials on a base of α- and β-cyclodextrins derivatives obtaining sol-gel method, *Polym. J.* 28, 147–154 (2006).
76. D. Lin-Vien, N.B. Colthup, W.G. Fateley, J.G. Grasselly, *The Handbook of Infrared and Raman Characteristic Frequencies of Organic Molecules* (Academic, San Diego, CA, 1991).
77. H. Okabayashi, K. Izawa, T. Yamamoto, H. Masuda, E. Nishio, C.J. O'Connor, Surface structure of silica gel reacted with 3-mercaptopropyltriethoxysilane and 3-aminopropyltriethoxysilane: formation of the S-S bridge structure and its characterization by raman scattering and diffuse reflectance fourier transform spectroscopic studies, *Colloid Polym. Sci.* 280, 135–145 (2002).
78. L. Li, X. Liu, Y. Ge, L. Li, J. Klinowski, Interaction and pillaring of zirconium bis(monohydrogenphosphate) with $NH_2(CH_2)_3Si(OC_2H_5)_3$, *J. Phys. Chem.* 95, 5910–5914 (1991).
79. Yu.L. Zub, I.V. Melnuk, N.V. Stolyarchuk et al., Synthesis of functionalized polysiloxane xerogels, structure of their surface layer and sorption properties, *Chemistry, Physics and Technology of Surfaces* 11–12, 165–203 (2006).
80. Yu.L. Zub, I.V. Seredyuk, A.A. Chuiko, M. Jaroniec, M.O. Jones, R.V. Parish, S. Mann, Polyfunctionalised surfactant-templated adsorbents with high specific surface areas, *Mendeleev Commun.* 11, 238–240 (2001).
81. Yu.L. Zub, I.V. Melnyk, M.G. White, B. Alonso, Structure peculiarities of the surface layer of bifunctional polysiloxane xerogels containing 3-aminopropyl and 3-mercaptopropyl groups, *Ads. Sci. Technol.* (2008) (in press).
82. J.J. Yang, I.M. El-Nahhal, I.-S. Chuang, G.E. Maciel , Synthesis and solid-state NMR structural characterization of polysiloxane-immobilized amine ligands and their metal complexes, *J. Non-Cryst. Solids.* 209, 19-39 (1997).
83. O.A. Dudarko, I.V. Mel'nyk, Yu.L. Zub, A.A. Chuiko, A. Dabrowski, Template synthesis of mesoporous silicas containing phosphonic acid derivatives in their surface layer, *Inorg. Mater.* 42, 413–420 (2006) (in Russian).
84. A. Cardenas, N. Hovnanian, M. Smaihi, Sol-Gel formation of heteropolysiloxanes from diethylphosphatoethyltriethoxysilane and tetraethoxysilane, *J. Appl. Polym. Sci.* 60, 2279–2288 (1996).
85. G. Engelhardt, D. Michel, *High-Resolution Solid-State NMR of Silicates and Zeolites* (Wiley, Chichester, 1987).
86. O.V. Stechenko, T.N. Yakubovich, V.V. Teslenko, Yu.L. Zub, A.A.Chuiko, Study of copper(II) absorbtion by some polyaminosiloxanes from the acetonitrile solutions, *Chemistry, Physics and Technology of Surface* 2, 62–67 (1997) (in Ukrain).

87. Ye.V. Stechenko, T.N. Yakubovich, V.V. Teslenko, B.K. Veisov, Yu.L. Zub, A.A. Chuiko, Copper(II) adsorption from acetonitrile solutions by nitrogencontaining polysiloxanes, *Chemistry, Physics and Technology of Surface* 3, 46–50 (1999) (in Russian).
88. O.V. Stechenko, T.N. Yakubovich, V.V. Teslenko, Yu.L. Zub, A.A. Chuiko. Copper(II) ions adsorption from acetonitrile solutions by polyaminosiloxane xerogel with bifunctional surface layer, *Ukr. Khim. Zh*. 69, 19–24 (2003) (in Russian).
89. A.K. Trofimchuk, V.A. Kuzovenko, I.V. Melnyk, Yu.L. Zub, Comparation of complexing ability of bifunctional polisiloxane xerogels and chemical modified silica gels, *J. Applied Chem.* 79, 230–236 (2006) (in Russian).
90. B.J. Hathway, A.A.G. Tomlinson, Copper (II) ammonia complexes, *Coord. Chem. Rev.* 5, 1–43 (1970).
91. N.V. Stolyarchuk, I.V. Melnyk, Yu.L. Zub, N.V. Kozak, Copper(II) adsorption from acetonitryl solutions by aminocontaining bridged polysilsesquioxane xerogels, *Visnyk donest'kogo universytetu* A, 283–288 (2006) (in Ukrain).
92. O.V. Kuchma, Yu.L. Zub, Experimental approach to the synthesis of hybrid adsorbents on the basis of polysiloxane xerogels functionalized with calix[4]arenes and their derivatives, in: *ARW NATO "Combined and Hybrid Adsorbents: Fundamental and Applications"*, edited by J.M. Loureiro and M.T. Kartel (Springer, Dordrecht, The Netherlands, 2006), pp. 49–54.
93. I. Ahmed, R.V. Parish, Insoluble ligands and their applications IV. Polysiloxane-bis(2-aminoethyl)amine ligands and some derivatives, *J. Organomet. Chem.* 452, 23–28 (1993).
94. I.M. El Nahhal, M.M. Chehimi, C. Cordier, G. Dodin, XPS, NMR and FTIR structural characterization of polysiloxane-immobilized amine ligand system, *J. Non-Cryst. Solids* 275, 142–146 (2000).
95. A.R. Cestari, E.F.S. Vieira, J. de A. Simoni, C. Airoldi, Thermochemical investigation on the adsorption of some divalent cations on modified silicas obtained from sol-gel process, *Thermochim. Acta* 348, 25–31 (2000).
96. I.V. Melnyk, V.Ya. Demchenko, Yu.L. Zub, A.A. Chuiko, Sorption of aurum(III) using polysiloxane xerogels functionalized with thiourea groups, *Chemistry, Physics, and Technology of Surface* 9, 31–36 (2003) (in Ukrain.).
97. Yu.L. Zub, Surface chemistry of new hybrid organic-inorganic materials, *Synopsis of Thesis for a Doctor's Degree* (ISC, NAS of Ukraine, Kyiv, 2002) (in Ukrain).
98. H.I. Dobryanska, V.P. Honcharyk, L.I. Kozhara, Yu.L. Zub, A. Dabrowski, Sorption of mercury(II) by polysiloxane xerogels functionalized with $\equiv Si(CH_2)_3SH$ groups, *4th International Conference on Sol-Gel Materials* (Kliczkow Castle, Poland, 2006), 40 pp.
99. H.I. Dobryanska, V.P. Honcharyk, L.I. Kozhara, Yu.L. Zub, A. Dabrowski, Complexation with participation of Hg(II) on the surface polysiloxane xerogels functionalized by 3-mercapropropyl groups, *Coord. Chem.* 2008 (in press) (in Russian).
100. Yu.V. Kholin, *Quantitative Physico-Chemical Analysis of Complexation in Solutions and on the Surface of Chemical Modified Silicas* (Folio, Karkiv, 2000).
101. G. Zuo, M. Mohammed, Selective binding of mercury yo thiourea-based coordinating resins, *React. Funct. Polym.* 27, 187–198 (1995).
102. N.V. Stolyarchuk, I.V. Melnyk, Yu.L. Zub, Ag(I) cations sorption by thiolcontaining bridged polysilsesquioxane xerogels, *Proceedings of X International Conference on "Theoretical problems of surface chemistry, adorption and chromatography"* (Klyaz'ma, Moscow, 2006), pp. 236–241.
103. K.H. Nam, S. Gomez-Salazar, L.L. Tavlarides, Mercury(II) adsorption from wastewaters using a thiol functional adsorbent, *Ind. Eng. Chem. Res.* 42, 1955–1964 (2003).
104. F. Caprasse, D. Leroy, L. Martinot, J.P. Pirard, J. Guillaume, C. Jerome, R. Jerome, New silica based polymeric systems designed for the solid-liquid extraction of uranyl ions, *J. Mater. Chem.* 12, 137–142 (2002).

105. S. Bourg, J.-C. Broudic, O. Conocar, J.J.E. Moreau, D. Meyer, M.W.C. Man, Tailoring of organically modified silicas for the solid-liquid extraction of actinides, *Chem. Mater.* 13, 491–499 (2001).
106. S. Dai, Hierarchically imprinted sorbents, *Chem. Eur. J.* 7, 763–768 (2001).
107. M.M. Collinson, Analytical applications of organically modified silicates, *Mikrochim. Acta* 129, 149–165 (1998).
108. D. Avnir, L.C. Klein, D. Levy, U. Schubert, A.B. Wojcik, in: *The Chemistry of Organic Silicon Compounds*, edited by Z. Rappoport and Y. Apeloig (Wiley, Chichester, Vol. 2, 1998), pp. 2317–2362.
109. Yu.N. Pozhidaev, Carbofunctional polyalkylsilsesquioxanes with ion-exchange and complexing properties, *Synopsis of Thesis for a Doctor's Degree* (IrIC, SB of RAN, Irkutsk, 2004) (in Russian).

NUCLEAR MAGNETIC RESONANCE AS INVESTIGATION TOOL FOR POLLUTANT/SORBENT INTERACTIONS

NIKI BACCILE[1,2,3], FLORENCE BABONNEAU[1,2*]
[1]*UPMC University of Paris 06, LCMCP, 4 Place Jussieu, Paris, France*
[2]*CNRS, LCMCP, 4 Place Jussieu, Paris, France*
[3]*Present address: Max-Planck Institute for Colloids and Interfaces, Golm, Germany*

Abstract. This chapter will illustrate how solid-state NMR techniques can provide extremely valuable information on the interactions between pollutant and adsorbent in depollution-related systems. In a first sub-chapter, NMR techniques based on dipolar coupling and well-adapted to probe spatial proximities between species, will be briefly introduced. The second sub-chapter deals with the role of solid-state NMR technique in two fields: (1) accidental dispersion of pollutant in soil matter and (2) volunteer adsorption within specially conceived hybrid organic/inorganic materials for depollution applications. Experimental data will be given to illustrate this last point.

Keywords: Nuclear Magnetic Resonance, pollutant adsorption, silica, interactions.

1. NMR Techniques for Pollutant/Sorbent Interactions

1.1. INTRODUCTION

Recent developments in solid state Nuclear Magnetic Resonance (NMR) offer appealing perspectives for the detailed characterization of interactions between organic molecules and inorganic surfaces.[1,2] This spectroscopic technique, which is a *local* probe in nature, can establish dialogs between nuclear spins for typical lengths of several Å. In that sense, solid state NMR is a perfect tool of

* To whom correspondence should be addressed: Florence Babonneau, Université Pierre et Marie Curie, LCMCP, CC 174, 4 Place Jussieu, 75005 Paris, France; e-mail: fb@ccr.jussieu.fr

P. Innocenzi, Y. L. Zub and V. G. Kessler (eds.), *Sol-Gel Methods for Materials Processing*.

investigation for a better understanding of the interactions between pollutant and sorbent in depollution-related systems.

The versatility of the NMR approach relies on the fact that it is possible to "play" with several interactions, namely the chemical shift (δ), the scalar coupling (*J*) and the dipolar (*D*) and quadrupolar (Q, I > 1/2) interactions. Each one can provide specific structural information: local environment of a given site for δ and Q, bond connectivity for *J* or spatial proximities for *D*. This last interaction relies on the through-space dipolar interaction between two nuclear spins. It is proportional to $1/r^3$ where *r* stands for the internuclear distance and will be effective for distances shorter than 1 nm. This makes it extremely well suited to explore the relative location of atoms with respect to each other. The intensity of the dipolar interaction will not only depend from the internuclear distance but also from the magnetogyric ratios γ of the coupled nuclei. The higher the γ is, the larger the dipolar coupling, which makes the ^{1}H spins, the most suitable to apply NMR techniques based on *D* couplings.

All these arguments show clearly that solid state NMR experiments involving ^{1}H nuclei will play a key role to investigate interactions between organic molecules and inorganic surfaces. To retrieve the maximum of information, it is essential to reach the highest resolution. Needless to say that all the experiments are performed under Magic Angle Spinning (MAS), which average out the anisotropic part of most interactions to obtain high resolution spectra. In the next paragraph, the problems to reach high resolution in ^{1}H MAS NMR spectra will be discussed. Then the various NMR sequences involving heteronuclear ^{1}H-X as well as homonuclear ^{1}H-^{1}H dipolar couplings will be presented.

1.2. NMR METHODS

1.2.1. *^{1}H high Resolution Solid State NMR*

In contrast with high resolution ^{1}H NMR spectra that can be easily recorded in solution, the ^{1}H NMR spectra recorded on solids usually strongly suffer from a lack of resolution. ^{1}H nuclei are mainly subjected to the homogeneous homonuclear ^{1}H-^{1}H dipolar interaction. Standard Magic Angle Spinning (MAS) experiments with spinning rates ≤15 kHz are generally unable to achieve reasonable resolution. Resolution has been greatly improved during the last few years based on the development of homonuclear decoupling techniques,[3] multiple pulses experiments[4] and tailored pulse schemes.[5] Another alternative for high resolution ^{1}H NMR is to use fast MAS, and combination with high magnetic field is even better. The spectacular gain in resolution at very high magnetic field (B_0 = 7.6 T) and under fast MAS (33 kHz) is demonstrated in Figure 1. Here, thymine is taken as a reference. When compared to standard MAS experiment

(14 kHz, B_0 = 7.0 T, Figure 1a), three *distinct* resonances are now observed at very high field and rotation frequency (Figure 1b) that can be safely assigned to the C<u>H</u>$_3$ (2.0 ppm), C<u>H</u> (7.4 ppm) and N<u>H</u> (11.4 ppm) resonances, respectively. Similar resolution can be reached with lower magnetic field (11.7 T), but under ultra-fast MAS conditions (67 kHz, 1.3 mm rotor) (Figure 1c). The relative integration of the lines gives ~3:1:2, as expected.

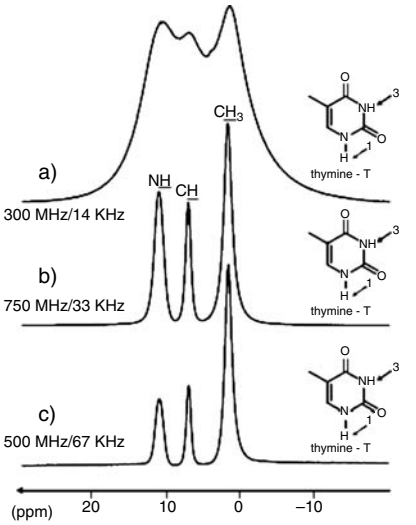

Figure 1. ^{1}H MAS NMR spectra recorded on thymine and thymine-derivatives using one-pulse experiment: effect of MAS rate and magnetic field.

1.2.2. *NMR Experiments Based on Heteronuclear Dipolar Coupling*

The most common NMR experiment based on heteronuclear ^{1}H-X dipolar coupling is the well known CP (Cross Polarization) experiment.[6] It establishes contacts between dipolarly coupled spins and results in a magnetization transfer between the two spin systems, whose efficiency will be directly proportional to the strength of the dipolar interaction that is proportional to $1/r^3$ where r stands for the internuclear distance. The magnetization transfer occurs during a time called contact time, whose value can be adjusted. A variation of contact time allows exploring a range of internuclear distances. The CP approach is therefore a method of choice for the characterization of interfaces through HETCOR experiments (HETeronuclear CORrelation). The resulting two-dimensional spectra present correlation peaks that correspond to ^{1}H and X nuclei, which are dipolarly coupled; they consequently provide direct evidence for spatial proximities between sites.

Relevant examples can be found in the field of long-range ordered silica obtained through the self-assembly of a variety of amphiphilic templating agents with an inorganic phase generated through sol-gel process.[7] Silica-surfactant interactions in mesostructured materials have been investigated using ^{1}H-^{29}Si HETCOR experiments. The sample was prepared under basic conditions with cetyltrimethylammonium bromide as structuring agent. The HETCOR spectrum recorded at short contact time (Figure 2a) shows only interactions between the positively charged polar head groups of the surfactant and the $Si\text{-}O^{-}$ surface sites (Q_3). By increasing contact times (Figure 2b), new correlations are now present between the protons of the surfactant (polar head group but also chain), and not only the Q_3 sites, but also the fully condensed Q_4 sites. From this analysis, a schematic model for the surfactant/silica interface has been proposed (Figure 2c).

The CP process is strongly modulated by molecular motions and can become rather inefficient for highly mobile sites. In that case, it could be interesting to lower the temperature to decrease mobility, and to recover at least partially CP efficiency.

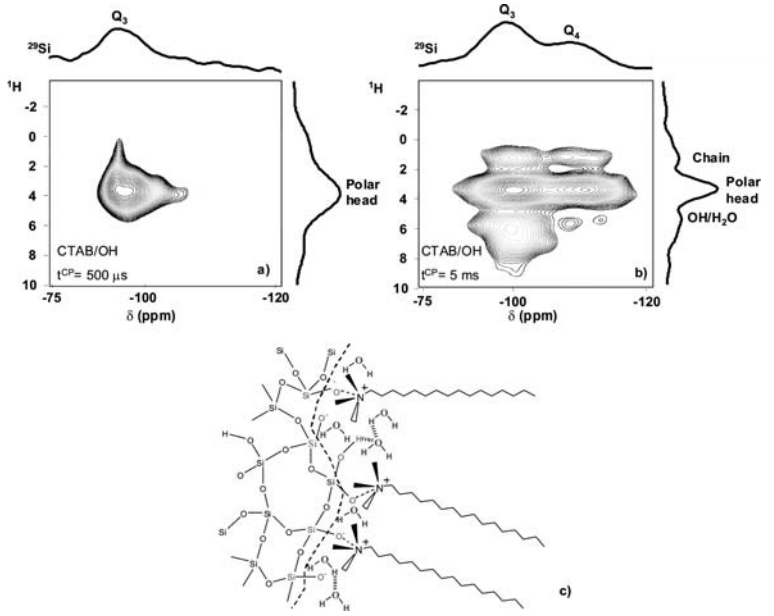

Figure 2. Two dimensional HETCOR $^{29}Si\{^{1}H\}$ spectra recorded on surfactant/silica mesostructured sample with contact time of 500 µs (a) and 5 ms (b), and the corresponding schematic model for the interface.

1.2.3. *NMR Experiments Based on Homonuclear Dipolar Coupling*

The strong ^{1}H-^{1}H dipolar interaction can also be used for the description of proton spatial connectivities and H-bonded networks. The most sensitive experiment to probe such homonuclear dipolar couplings in solids is the double quanta (DQ) NMR experiment combined with fast MAS.[8] It leads to a two-dimensional spectrum in which the dipolarly coupled spin pairs can be directly identified. For ^{1}H DQ spectroscopy, the BABA or BAck to BAck[9] sequence is often used (Figure 3). For example, this sequence was used to investigate templated silicas functionalized with vinyl groups in order to characterize the location of the vinyl groups in the silica framework with respect to the polar head groups of the surfactant molecules (CTA+). In the ^{1}H DQ experiment, coherences between the vinyl protons and the $N(CH_3)_3^+$- head-group of CTA^+ molecules are observed, which clearly indicates that most of the vinyl groups are located at the surface. Reference[10] is an excellent review dealing with ^{1}H DQ spectroscopy in the context of macromolecular and supramolecular systems.

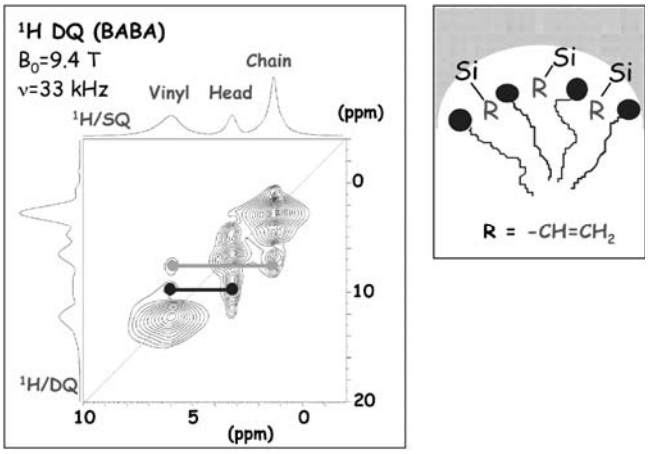

Figure 3. ^{1}H Double Quanta experiment recorded on a surfactant templated silica sample functionalized with vinyl groups.

2. Application of Solid-State NMR to Characterize Pollutant/Sorbent Interactions

This chapter deals with the role that solid-state NMR technique may play for the characterization of (organic) pollutant/sorbent interactions in two fields:

- Accidental dispersion of pollutant in soil matter
- Volunteer adsorption within specially conceived hybrid organic/inorganic materials for depollution applications.

2.1. ADSORPTION BY SOIL MATTER

The fate of pollutant molecules in the environment is a general concern due to the number of unknowns still existing about interactions occurring between dispersed molecules and soil matter. In fact, the chemical nature of the polluting agent may go under severe changes after coming in contact with humic material and track of both original molecules and by-products becomes somewhat difficult to pursue and, in most cases, it is completely lost. Interest was then directed towards NMR technique, which can potentially elucidate such a matter. The following paragraphs will try to highlight positive as well as some negative aspects of solid state NMR techniques applied to the study of pollutant/soil interaction.

Application of NMR to the study of interactions between pollutant and inorganic matrices in the domain of soil science is a topic in continuous development and has inspired a recent review paper.[11] Initially, liquid state NMR was used to study possible interactions between pollutant and soil after dispersion but this approach needs a previous and generally quite laborious treatment of the soil matter before recovering an analyzable liquid solution. More information on soil treatment for analytical purposes can be found in the literature.[12] Scientists are most generally concerned about the pollutant fate at the moment of its adsorption; thus, post-treatment of soil matter to obtain a liquid sample is quite a limiting factor to fully understand the pollutant/soil interactions. The passage from liquid to solid-state measurements was thus obvious. Study of soil matter alone[13] and soil matter in presence of pollutant at the moment of the adsorption and degradation processes becomes of widespread interest. Unfortunately, NMR technique imposes some important constraints to any *in-situ* study of humic matter:

- Natural presence of paramagnetic species, like iron, in soils strongly contributes to poor spectral resolution. Special treatment of soil matter to reduce its quantity is generally needed.[14]
- Richness of soil composition in organic matter results in quite complicated ^{1}H, ^{13}C or ^{15}N spectra, leading to difficulties in identification and quantification.
- NMR sensibility is generally low for most nuclei; hence concentration of species of interest may be too low to be detected in reasonable time or within an amount of time where pollutant does not go under any change.
- When ^{1}H NMR spectra are recorded, presence of high quantities of water may hide contributions from other protonated species existing at much smaller quantities.

For these reasons, interesting model studies have been performed under laboratory conditions on sample clays in presence of polluting molecules. The idea of such approach is to follow the pollutant molecules and their trans-formation products in a controlled environment.

1. *Choice of model soil samples with known structure and composition*. For instance, mobility behaviours of 4-chloro-2-methylphenoxyacetic acid was followed by ^{1}H high resolution MAS-NMR inside a synthetic layered double hydroxide.[15]
2. *Use of pollutants with specific, easy detectable, nuclei*. For instance, ^{19}F solid-state NMR was used to observe a dual-mode sorption uptake of hexafluorobenzene by two peat samples.[16]
3. *Selective isotopical enrichment of one or more positions within the polluting molecule or the sorbent*. For instance, Knicker used ^{13}C-enriched sorbent (plant organic matter) as well as ^{15}N-enriched 2,4,6-trinitrotoluene (TNT) to demonstrate covalent binding between TNT transformation products and the sorbent.[17]

Once major intrinsic problems related to the technique itself have been resolved or overcome in some way, NMR reveals to be one of the most powerful and reliable technique to provide information about direct interactions between two chemical species close in space as illustrated by the last example from Knicker.[17]

When interest is shifted towards the problem of retaining persistent pollutants by mean of advanced functional materials specially designed for this task, we will show in the next paragraphs how, even in this case, advanced solid-state NMR experiences may help in the characterization of pollutant/material interface.

2.2. ADSORPTION BY SYNTHETIC HYBRID ORGANIC-INORGANIC FUNCTIONAL MATERIALS

Soil adsorption of pollutants is simply a phenomenon that should be prevented. Natural or synthetic filtering materials that retain polluting agents have thus to be developed. Indeed, this research field is as old as mankind since, e.g., activated carbon is used since ancient times to accomplish this task. Nevertheless, advances in material science during the last century have opened the way to synthetic materials whose performances give better retention capacities than activated carbon. The word “better” hides a double meaning of quantity and specificity, in the sense that the same material should be able to adsorb all classes of pollutants (e.g., organic molecules, toxic metals) in high quantities and to allow facile regeneration of the matrix. The next sub-chapter will summarize the state-of-the-art

on a particular class of hybrid organic/inorganic materials that are potentially good candidates in the field of pollutant adsorption.

Long-range ordered mesoporous silica powders have been at the centre of interest within the material science community for the past 15 years. Their structural characteristics (high surface area; tunable geometry of the porous network; narrow pore size distribution) combined with the possibility to process them in various shapes (calibrated spherical powders, thin films, membranes, monoliths) make them extremely attractive for a wide range of applications in the fields of catalysis, chromatography, drug release, sensing or electronics. Recent review articles will help the reader to find more detailed pieces of information from the historical to the applicative point of view.[18,19] One main interesting point for these material is undoubtedly the possibility for modification of surface properties by introduction of a large variety of organic pendant groups.[20,21]

As far as applications in the depollution field are concerned, mesoporous (mainly silica based) materials where tested in three major domains:

1. Materials for VOC (Volatile Organic Compounds) adsorption
2. Materials for POP (Persistant Organic Pollutant) adsorption
3. Materials for toxic metal adsorption.

One examples regarding VOCs was given by X.S. Zhao et al.[22] who showed that a long range ordered mesoporous silica matrix (MCM-41) was more efficient than activated carbon, zeolite T and silicalite-1 materials with respect to benzene, carbon tetrachloride and n-hexane adsorption. Adsorption of POPs in water was performed, among others, by H. Zhao et al.[23] who studied tri- and tetrachloroethylene adsorption in water using calcined MCM-41 with various amounts of structural aluminium sites. As far as toxic metal adsorption is concerned, material surface needs, in most cases, to be chemically modified in order to favour metal-ligand interaction and enhance adsorption properties. In general, Fe^{3+}, Co^{2+}, Ni^{2+} and Cu^{2+} ions are trapped by amino-functionalized silica surfaces while Hg^{2+} species are adsorbed by thiol-modified surfaces.[24]

Little attention is generally addressed towards the fate of the pollutant after its adsorption. In some cases[25,26], its degradation is performed by introduction of a photocatalytic TiO_2 phase within the mesoporous silica host via the sol-gel process. One could also consider to recover the pollutant by washing and thus to regenerate the absorbent.[27] In that case, it is of prime importance to characterize the interactions that the pollutant may develop with the surface sites, in order to evaluate the possibility of later pollutant recovering and adsorbent recycling. Until now, almost no characterization has been performed to better understand the pollutant/surface interactions. Inumaru et al.[28] concluded from

IR data that alkyl-anilines are strongly hydrogen-bonded to silanol groups on the inorganic pore walls. However, this type of analysis cannot be extended to any type of pollutants and in the same paper authors mention that no similar spectroscopic evidence could be obtained for nonylphenol.

This lack of knowledge regarding pollutant/silica surface interactions prompted us to prepare long-range ordered silicas whose surface is chemically modified with alkyl groups of increasing chain length. High-resolution solid-state NMR techniques are used to investigate the physical state of the organic pollutant in the various confined environments as well as the interactions it may develop with the modified silica surface. Results are given below while experimental details can be found elsewhere.[29]

2.3. ADSORPTION OF ORGANIC POLLUTANTS IN HYBRID ORGANIC/ INORGANIC SILICAS

Adsorption of POP's was tested by a number of research groups on three categories of (mainly) ordered silica-based materials:

- Class A: As synthesized surfactant-containing silicas
- Class B: Calcined porous silicas
- Class C: Organo-modified surfactant-extracted silicas.

Table 1 shows some examples of class A, B or C materials that have been tested so far in literature to adsorb organic pollutants. Though we have classify the materials in three main classes, each sample presents its own features (porous structure, overall synthesis conditions) and we suggest the reader to check the relative references for more information about the synthesis procedure and adsorption conditions. Adsorbed quantities are comparable but the range of equilibrium compositions for which experiments have been performed, may be very broad among the various studies. To this regard, we reported either the lowest or the highest readable equilibrium concentration value at which adsorption took place.

It is important to point out that materials having the highest specific available surface (as high as 1,000 m^2/g) belong to class B, for which the templating agent is removed by a calcination step. Nevertheless, materials from class B systematically show lower specific adsorption values of polluting agent within pores. On one side, this behaviour seems a bit puzzling if one does not take into account the existence of interactions between organic pollutant and silica surface. In the case of class A or C, hydrophobic interactions seem to increase pollutant adsorption within pores, though a smaller porous volume is available. To this regard, Figure 4 compares adsorption results when a modified chlorophenol molecule is adsorbed on calcined silica sample (SiO_2, specific surface

TABLE 1. Adsorption capacities of class A to C materials towards some common POP's.

Class of material	Pollutant	Adsorbed amount ($mmol \cdot g^{-1}$)[a]	Concentration at equilibrium ($mmol \cdot L^{-1}$)[b]	Reference
A	Dichlorophenol	0.6	<<1	30
A	Trichlorophenol	0.5	<<1	30
A	Chlorophenol	0.2	<<1	30
A	Pentachlorophenol	>0.1	<<1	30
A	Phenol	0.6	<<1	30
A	Dichlorophenol	~1	<<20	31
A	Phenol, chlorophenol	~0.4	<<20	31
A – swollen pores	Dichlorophenol	~0.9	<<10	31
A – swollen pores	Phenol, chlorophenol	~0.5	<<10	31
A	Trichloroethylene	$1.1 \cdot 10^{-2}$	~0.2	31
A	Tetrachloroethylene	$9.0 \cdot 10^{-2}$	$\sim 3.6 \cdot 10^{-2}$	31
B	Chloro-2-methoxyphenol	$5.0 \cdot 10^{-5}$	1.0	29
B	Trichloroethylene	$3.2 \cdot 10^{-3}$	$\sim 9.0 \cdot 10^{-2}$	23
B	Tetrachloroethylene	$4.5 \cdot 10^{-3}$	$\sim 6.0 \cdot 10^{-2}$	23
C – Si/Al network	4-nonylphenol	0.8	$4.0 \cdot 10^{-3}$	28
C – Si/Al network	4-*t*-amylphenol	<0.1	$4.0 \cdot 10^{-3}$	28
C – Si/Al network	4-*n*-heptylphenol	0.7	$4.0 \cdot 10^{-3}$	28
C – Si/Al network	4-*n*-heptylaniline	1.2	$4.0 \cdot 10^{-3}$	28
C – Si/Al network	*p*-toluidine	<0.1	$4.0 \cdot 10^{-3}$	28
C – propyl grafted	Chloro-2-methoxyphenol	$\sim 1.5 \cdot 10^{-4}$	1.0	29
C – hexyl grafted	Chloro-2-methoxyphenol	$>2.5 \cdot 10^{-4}$	1.0	29
C – phenyl grafted	Chloro-2-methoxyphenol	$\sim 2.0 \cdot 10^{-4}$	1.0	29
C – hexadecyl grafted	Chloro-2-methoxyphenol	<0.1	1.0	29

[a]Quantity of pollutant per mass of powder. [b]Quantity of residual pollutant in solution at equilibrium after adsorption per volume of solution.

area, ssa ~1,100 m^2/g) and a sample modified with hexyl chains (Hexyl-SiO_2, ssa ~300 m^2/g). It is clear that large difference with regard to adsorption properties exists between the two materials even if hexyl-modified silica has a much less developed specific surface area.

2.4. CHARACTERIZATION OF POLLUTANT/SILICA INTERFACE BY SOLID - STATE MAS NMR EXPERIMENTS

The singular and interesting behaviour revealing apparent discrepancies in pollutant adsorption between high-surface SiO_2 (Class B) and Hexyl-SiO_2 (Class C)

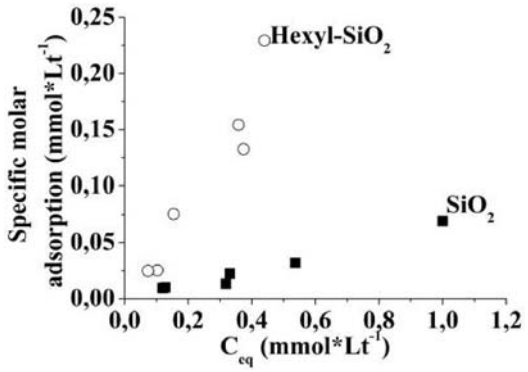

Figure 4. Adsorption isotherms of 4-chloro-2-methoxyphenol in water using calcined (SiO_2) and hexyl-modified (Hexyl-SiO_2) mesoporous silicas as sorbents.[29]

mesoporous powders was investigated by advanced solid-state NMR experiments. The following sub-chapters will illustrate how NMR techniques can be combined to provide complementary pieces of information about silica/sorbate interactions. Details of NMR acquisition parameters for all experiments and specific referencing can be found in ref.[29]

2.4.1. *Mobility of Pollutant: ^{13}C NMR Experiments*

A series of ^{13}C NMR experiments (Figures 5 and 6) has been performed at room temperature to obtain information concerning pollutant mobility within the two powders. In single pulse experiments (Figures 5a and 6a), all carbon sites are detected: the region between 160 and 100 ppm are due to the aromatic carbons of the pollutant and the peak at 56.5 ppm to the methoxy OCH_3 groups. All the other peaks belong to grafted ethoxy groups due to the surfactant removal procedure, to residues from the templating agent and to carbons from the grafted hexyl chains in Hexyl-SiO_2.

CP and INEPT sequences are respectively based on *through-space* and *through-bond* magnetization transfers from ^1H to ^{13}C. They are known to be sensitive to rigid and mobile groups, respectively.[32] If one concentrates on the pollutant signals observed in CP spectra (Figures 5b and 6b), it is clear that they are hardly detected while the same peaks gain in intensity when INEPT sequence is used (Figures 5c and 6c). These spectroscopic responses suggests a high mobility of the pollutant in both SiO_2 and Hexyl-SiO_2 samples, even if one would expect that, due to hydrophobic interactions, pollutant would have a lower mobility in Hexyl-SiO_2. Next section hence will show variable temperature experiments recorded to verify such unexpected behaviour.

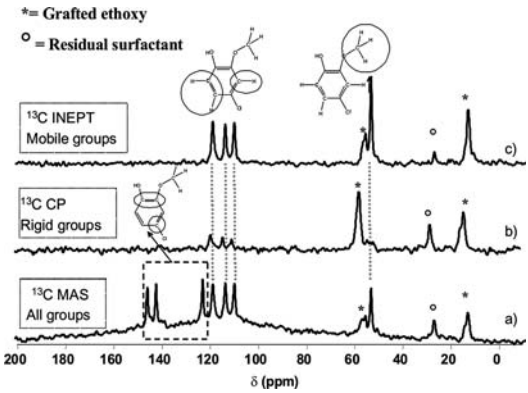

Figure 5. ^{13}C MAS NMR experiments performed at room temperature on pollutant adsorbed on calcined mesoporous silica powder (SiO_2). (a) Single pulse spectrum (ν_{MAS}=5 kHz); (b) CP (t^{CP} =3 ms, ν_{MAS} =5 kHz) and (c) INEPT (ν_{MAS} =14 kHz).

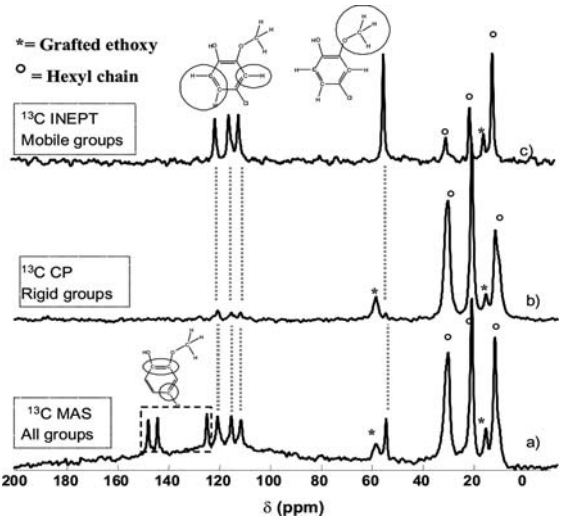

Figure 6. ^{13}C MAS NMR experiments performed at room temperature on pollutant adsorbed on mesoporous silica powders functionalized with hexyl chains (Hexyl-SiO_2). (a) Single pulse spectrum (ν_{MAS}= 5 kHz); (b) CP (t^{CP} = 3 ms, ν_{MAS} = 5 kHz) and (c) INEPT (ν_{MAS} = 14 kHz).

2.4.2. *Mobility of Pollutant: ^{1}H NMR Experiments as a Function of Temperature*

^{1}H MAS-NMR variable-temperature experiments are directly sensitive to the mobility behaviour of the adsorbed pollutant molecule: the broader the peak

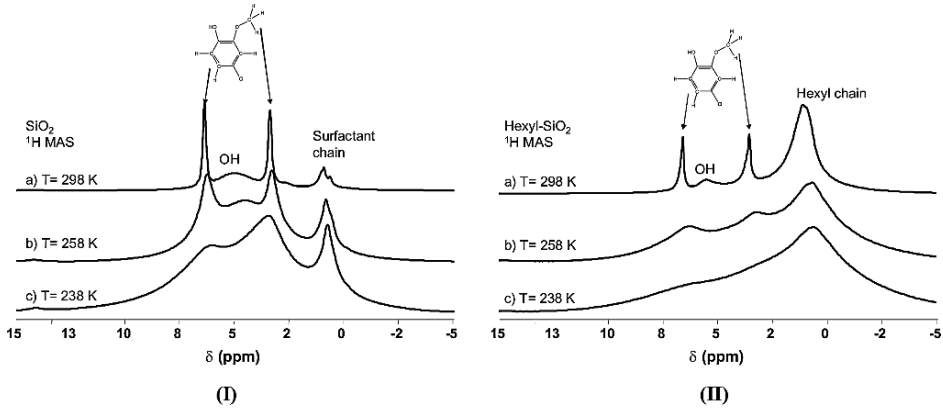

Figure 7. ^{1}H MAS NMR experiments as a function of temperature for pollutant adsorbed on SiO_2 (I) and Hexyl-SiO_2 (II) mesoporous silica powders. (a) 298 K, (b) 258 K and (c) 238 K.

linewidth, the lower the molecular mobility (Figure 7). The peak assignments are schematically indicated in the figure.

Broad signals are recorded at 238 K while peak resolution increases with T up to 298 K. At this temperature, peaks due to aromatic and methoxy protons from pollutant are fairly narrow in both samples confirming that at room temperature, though higher affinity between organic pollutant and hexyl chains are expected, hydrophobic interactions are not strong enough to prevent high molecular mobility. At low temperature, on the other hand, broader peaks are detected in Hexyl-SiO_2 indicating that under these conditions, affinity between hexyl chains and pollutant molecules may increase. ^{13}C CP MAS spectra recorded at the same temperatures have confirmed the same trends[29] and have shown that increase in peak linewidth only depends on mobility issues and not on distribution of chemical shift values, due to distribution of local atomic environments.

2.4.3. *Interactions at Pollutant/silica interface: ^{1}H-^{13}C HETCOR Experiments*

Heteronuclear correlation (HETCOR) experiments based on CP sequence are very useful (see §1.2.2) to probe through-space proximities between molecular species via dipolar coupling. Here, a two-dimensional ^{1}H-^{13}C experience was performed with the goal of establishing, if any, correlations between pollutant sites and hexyl-grafted surface sites existing at room temperature. All correlations, which are observed in the 2D spectrum (Figure 8) can be sorted out in five major domains: each cross-peak correlates a proton site to a carbon site, which are dipolarly coupled. C_i, D_i and E_i signals are due to intra- and intermolecular correlations between CH_2 and CH_3 groups in, respectively, ethoxy

groups (C, D) and grafted hexyl chains (E). The A and B cross-peaks are due to intra-molecular interactions within, respectively, the aromatic ring and the methoxy groups of pollutant. No correlation peaks between sites from the pollutant molecules and the silica surface species are detected. It suggests either the lack of strong interactions because of excessive mobility of the adsorbed molecules and/or long distances between the adsorbed pollutant molecules and the hexyl-modified silica surface. This behaviour is however very interesting since it could be possible to integrate a recycling step of the final adsorbent material after a washing extraction procedure of the pollutant.

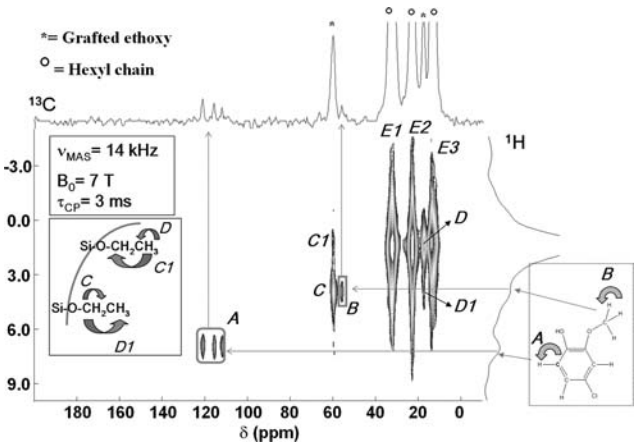

Figure 8. 2D ^{1}H-^{13}C CP HETCOR experiment recorded on pollutant in Hexyl-SiO_2 mesoporous silica (ν_{MAS} = 14 kHz; t^{CP} = 3 ms).

3. Conclusions

Solid-state NMR experiments have been performed on a methoxy-modified chlorophenol adsorbed on mesoporous silicas with various surface sites. They have revealed high mobility of the pollutant molecules within pores at room temperature, whatever the surface sites. These results seem to be in contrast with the general assumption that hydrophobic interactions between organic molecules and long chain groups at silica surface should bring both species in close proximity and lead to a reduction in mobility of the adsorbed molecules. Indeed, some questioning about the way the pollutant is adsorbed and is located with respect to the grafted functions may arise. Lack of complementary fundamental work done on adsorption of organic molecules in confined environment prevents us from proposing a model able to explain the high mobility of pollutant molecules observed by the different solid-state NMR techniques.

References

1 F. Babonneau, C. Bonhomme, C. Gervais and J. Maquet, Advances in characterization methods for sol-gel derived materials: high resolution solid state Nuclear Magnetic Reso-nance. J. Sol-Gel Sci. Technol. 31, 9–17 (2004).

2 C. Bonhomme, C. Coelho, N. Baccile, C. Gervais, T. Azaïs and F. Babonneau, Advanced solid state NMR techniques for the characterization of sol-gel derived materials. Acc. Chem. Res. 40, 738–746 (2007).

3 B.J. Van Rossum, C.P. De Groot, V. Ladizhansky, S. Vega and H.J.M. De Groot, A method for measuring heteronuclear (1H-13C) distances in high speed MAS NMR. J. Am. Chem. Soc. 122, 3465–3472 (2000).

4 B.C. Gerstein, R.G. Pembleton and R.C. Wilson, High resolution NMR in randomly oriented solids with homonuclear dipolar broadening: combined multiple pulse NMR and Magic Angle Spinning. J. Chem. Phys. 66, 361–362 (1977).

5 B. Elena, G. De Paëpe and L. Emsley, Direct spectral optimisation of proton-proton homonuclear dipolar decoupling in solid-state NMR. Chem. Phys. Lett. 398, 532–538 (2004).

6 A. Pines, M.G. Gibby and J.S. Waugh, Proton-enhanced NMR of dilute spins in solids. J. Chem. Phys. 59, 569–590 (1973).

7 N. Baccile, G. Laurent, C. Bonhomme, P. Innocenzi and F. Babonneau, Solid state NMR characterization of the surfactant/silica interface in templated silicas: acidic versus basic conditions. Chem. Mater. 19, 1343–1354 (2007).

8 I. Schnell and H.W. Spiess, High-resolution 1H NMR spectroscopy in the solid state: very fast sample rotation and multiple-quantum coherences. J. Magn. Reson. 151, 153–227 (2001).

9 M. Feike, D.E. Demco, R. Graf, J. Gottwald, S. Hafner and H.W. Spiess, Broadband multiple-quantum NMR spectroscopy. J. Magn. Reson. A 122, 214–221 (1996).

10 S.P. Brown and H.W. Spiess, Advanced solid-state NMR methods for the elucidation of structure and dynamics of molecular, macromolecular, and supramolecular systems. Chem. Rev. 101, 4125–4157 (2001).

11 A.-M. Delort, B. Combourieu and N. Haroune, Nuclear magnetic resonance studies of interactions between organic pollutants and soil components, a review. Environ. Chem. Lett. 1, 209 (2004).

12 I. Kögel-Knaber, Analytical approaches for characterizing soil organic matter. Org. Geochem. 31, 609 (2000).

13 E.W. Randall, N. Mahieu and G.I. Ivanova. NMR studies of soil, soil organic matter and nutrients: spectroscopy and imaging. Geoderma 80, 307 (1997).

14 M. Schilling and W.T. Cooper, Effects of chemical treatments on the quality and quantitative reliability of solid-state 13C NMR spectroscopy of mineral soils. Anal. Chim. Acta 508, 207 (2004).

15 B. Combourieu, J. Inacio, A.-M. Delort and C. Forano, Differentiation of mobile and immobile pesticides on anionic clays by 1H HR MAS NMR spectroscopy. Chem. Commun. 2214 (2001).

16 S.D. Kohl, P.J. Toscano, W. Hou and J.A. Rice, Solid-state 19F NMR investigation of hexafluorobenzene sorption to soil organic matter. Environ. Sci. Technol. 34, 204 (2000).

17 H. Knicker, Incorporation of 15N-TNT transformation products into humifying plant organic matter as revealed by one- and two-dimensional solid-state NMR spectroscopy. Sci. Total. Environ. 308, 211 (2003).

18 G.J. de Soler-Illia, C. Sanchez, B. Lebeau and J. Patarin, Chemical strategies to design textured materials: from microporous and mesoporous oxides to nanonetworks and hierarchical structures. Chem. Rev. 102, 4093 (2002).

19 Y. Wan and D.Y. Zhao, On the controllable soft-templating approach to mesoporous silicates. Chem. Rev. 107, 2821 (2007).

20 S.L. Burkett, S.D. Sims and S. Mann, Synthesis of hybrid organic-inorganic mesoporous silica by co-condensation of siloxane and organosiloxane precursors. Chem. Commun. 1367 (1996).
21 D.J. Macquarrie, Direct preparation of organically modified MCM-type materials. Preparation and characterization of aminopropyl-MCM and 2-cyanoethyl-MCM. Chem. Commun. 1961 (1996).
22 X.S. Zhao, Q. Ma and G.Q. Lu, VOC removal: comparison of MCM-41 with hydrophobic zeolites and activated carbon. Energ. Fuels 12, 1051 (1998).
23 H. Zhao, K.L. Nagy, J.S. Waples and G.F. Vance, Surfactant templated mesoporous silicate materials as sorbents for organic pollutants in water. Environ. Sci. Technol. 34, 4822 (2000)
24 A.M. Liu, K. Hidajat, S. Kawi and D.Y. Zhao, A new class of hybrid mesoporous materials with functionalised organic monolayers for selective adsorption of heavy metal ions, Chem. Commun. 1145 (2000).
25 E.P. Reddy, B. Sun and P.G. Smirniotis, Transition metal modified TiO^2-loaded MCM-41 catalysis for visible- and UV-light driven photodegradation of aqueous organic pollutants. J. Phys. Chem. B 108, 17198 (2004).
26 T. Kasahara, K. Inumaru and S. Yamanaka, Enhanced photocatalytic decomposition of nonylphenol polyethoxylate by alkyl-grafted TiO^2-MCM-41 organic-inorganic nanostructure. Micro. Meso. Mater. 76, 123 (2004).
27 A. Yamaguchi, T. Awano, K. Oyaizu and M. Yuasa, Surface modified mesoporous silica as recyclable adsorbents of an endocrine disrupter, bisphenol A. J. Nanosci. Nanotech. 6, 1689 (2006).
28 K. Inumaru, Y. Inoue, S. Kakii, T. Nakano and S. Yamanaka, Molecular selective adsorption of dilute alkylphenols and alkylanilines from water by alkyl-grafted MCM-41: tenability of the cooperative organic-inorganic function in the nanostructure. Phys. Chem. Chem. Phys. 6, 3133 (2004).
29 N. Baccile and F. Babonneau, Organo-modified mesoporous silicas for organic pollutant removal in water: solid-state NMR study of the organic/silica interactions. Micro. Meso. Mater. (in press), doi: 10.1016/j.micromeso.2007.06.056 (2007).
30 K. Hanna, R. Denoyel, I. Beurroies and J.P. Dubès, Solubilization of pentachlorophenol in micelles and confined surfactant phases. Coll. Surf. A: Physicochem. Eng. Aspects 254, 231 (2005).
31 K. Hanna, I. Beurroies, R. Denoyel, D. Desplantier-Giscard, A. Galarneau and F. Di Renzo, Sorption of hydrophobic molecules by organic/inorganic mesostructures. J. Coll. Interf. Sci. 252, 276 (2002).
32 B. Alonso and D. Massiot, Multi-scale NMR characterization of mesostructured materials using 1H-13C through bond polarisation transfer, fast MAS, and 1H spin diffusion. J. Magn. Reson. 163, 347 (2003).

SOL-GEL APPROACHES IN THE SYNTHESIS OF MEMBRANE MATERIALS FOR NANOFILTRATION AND PERVAPORATION

BEN C. BONEKAMP, ROBERT KREITER, JAAP F. VENTE*
Energy Research Centre of the Netherlands, Box 1, 1755 ZG Petten, The Netherlands

Abstract. Molecular separation using membranes is widely considered as an energy-efficient alternative for conventional industrial separation techniques. For the preparation of such membranes sol-gel technology is highly suitable. Using sol-gel techniques thin (50–100 nm) amorphous nanoporous layers having pore sizes in the micropore (<2 nm) or fine mesoporous (<5 nm) region can be prepared on a porous substrate. These layered porous systems, usually in tubular form, can be used for nanofiltration, pervaporation and gas separation applications. The application window is dependent on the material properties, such as the pore size and pore size distribution, the interfacial properties of the pores, and the defect density. The success of this technology in actual industrial applications strongly depends on reproducible large scale production of the sol-gel membranes and on a sufficient stability of the membranes with respect to flux and selectivity. In addition the production cost of the full membrane system is an important aspect. Here, we will focus on the more chemical aspects in the membrane preparation. Main topics are synthesis and properties of the sols, the preparation of microporous thin films, and the search for membrane materials that have a high hydrothermal stability.

Keywords: Membrane technology, microporous thin films, porous layers, silica sols, metal oxide sols.

1. Introduction

Molecular separation processes have great influence on the total use of energy in industry, chemical production costs and the price of products for the consumer. As an example, about 40% of final energy use in the Dutch (petro)chemical industry, an estimated 190 PJ/year, is applied to separation processes alone. The most commonly used technology is distillation, which has a very low intrinsic

*To whom correspondence should be addressed: Jaap F. Vente; e-mail: vente@ecn.nl

P. Innocenzi, Y. L. Zub and V. G. Kessler (eds.), *Sol-Gel Methods for Materials Processing*.

exergetic efficiency of 10%. Membrane technology has been widely recognized as one of the most promising energy-efficient alternatives. Demands of flux, selectivity and lifetime, set on the membranves performances lead to the use of thin microporous layers. In practice this means layers as thin as 50–100 nm, a pore diameter of less than 2 nm and a very high porosity.[1,2] These layers are too thin to be self supporting and a dedicated support has to be used (supported thin films shown in Figure 1). As the selectivity depends on the pore characteristics and defect density, strict control over the parameters of support manufacturing and sol synthesis and coating is essential for obtaining high quality membranes.[3] Proper characterization techniques, such as dynamic light scattering and perm-porometry, are important for effective membrane development and production.

One of our main goals is the development of methods for the reproducible preparation of microporous membrane layers (see Figure 1) on tubular mesoporous substrates of up to 1 m long. We have selected sol-gel technology as a prime tool for achieving this. The sol-gel membranes were successfully used for gas separation experiments, e.g. hydrogen/methane and hydrogen/carbon dioxide separation.[4] These thin films are an alternative for crystalline zeolite membranes despite the broader intrinsic pore size distribution.[5] We also discovered that such microporous films are very suitable for dewatering of organic liquids by pervaporation.[6]

As sol-gel membranes have a very thin and often amorphous structure in combination with a very high specific surface area, there is a significant driving force towards states having a lower energy. In practice, this means that the sol-gel film has a tendency to reorganize to a lower surface area or even crystallize. Active operation of sol-gel membranes seems to accelerate this transformation. Therefore, the challenge is to reduce the kinetics of this process to obtain membranes with sufficient lifetime for industrial applications. Especially the hydrothermal stability is an issue. In a dry atmosphere, these inorganic membranes can function up to temperatures of ~300°C. In the presence of small amounts of water the stability decreases very rapidly.

Nanofiltration membranes demand pore size control in the region of 1–3 nm to achieve molecular mass cut-off values in the region of 1,000–5,000 Da.

The materials should have a very low acid solubility for a number of important commercial applications.

In this paper, we present a brief overview of sol-gel technology for the preparation of porous membrane layers suitable for molecular separations. The preparation of the mesoporous support layers made from alumina or titania is also included. Furthermore, a historical path of the development of microporous selective layers is followed, starting from pure silica (SiO_2), via organic end groups towards bridging organic groups in the silica structure. As alternatives metal oxide membranes based on titania and zirconia are discussed. The focus

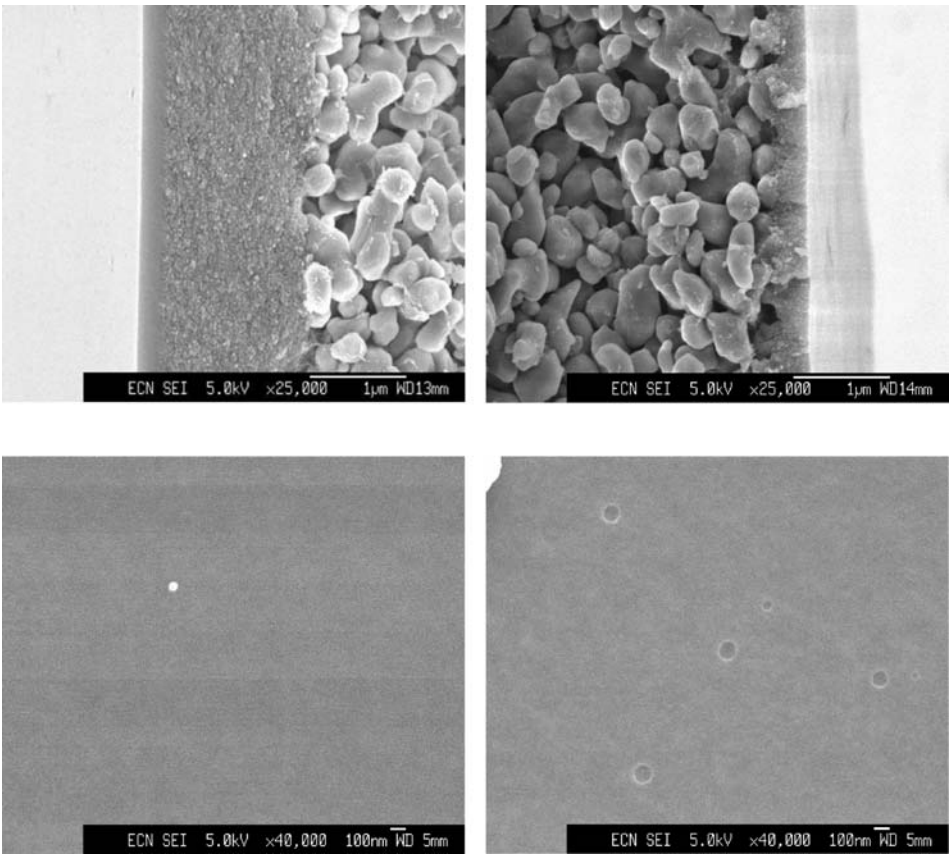

Figure 1. SEM pictures of a. fracture surface of a microporous silica sol-gel film on a mesoporous γ-alumina substrate; b. mesoporous titania sol-gel film on a macroporous α-alumina substrate; c. surface of a microporous methylated silica thin film; d. methylated silica thin film (~50 nm).

is on sol preparation and the resulting properties of thin film coatings that are suitable for large scale production of membrane tubes.

2. Sols and Thin-Films

The transition of sol species into a gel state is an important step in the formation of a porous structure. This transition is followed by a consolidation step consisting of drying and calcining at an appropriate temperature. For the sake of the current discussion, we consider a sol-gel process as a route to inorganic or inorganic-organic hybrid materials via intermediate individual sol and gel states.

2.1. SOL PREPARATION

Microporous thin films for molecular separation purposes can be obtained from various sol types. The type of sol needed depends on the mechanism of pore formation during the deposition of the thin films.[7] Microporous films can be prepared with and without the deliberate addition of pore templates. In the former case it is difficult to obtain pores below 2 nm. In general, this method is more suitable for obtaining porosity in the small mesoporous region. In contrast, for the formation of crystalline microporous structures such as zeolites pore directing agents are commonly used, even for the smallest pore sizes.[8]

The preparation of sols for membrane preparation is in general a two step process. Starting from alkoxide precursors, oxides are obtained via hydrolysis and condensation steps. For silicon-based precursors it is generally accepted that these two processes occur consecutively, whereas for metal alkoxides these two processes cannot be distinguished, due to the faster kinetics. Hydrolysis and condensation can be represented by the following equations:

$$M(OR)_z + H_2O \rightarrow M(OH)(OR)_{z-1} + ROH$$

$$\text{-M-OH} + \text{M-OR} \rightarrow \text{-M-O-M-} + ROH$$

The sol species formed can either consist of fractal-like or polymeric particles or of dense and possibly crystalline structures. The nature of these building blocks can be tailored by appropriate selection of the reaction conditions. For example, in the case of silicon alkoxides, the use of a base catalyst leads to dense particles whereas an acid catalyst leads to open polymeric species.[9] During the gelation stage, controlled particle packing without agglomeration is important, especially for dense particles. For polymeric sol particles interpenetration plays a crucial role. For both cases the sol-gel transition occurring during the drying of supported thin films is different from that occurring in bulk sols. The formation of microporous silica thin films requires sols that consist of relatively linear species with limited branching. The interpenetration of such species can be given by:

$$M_{1,2} \propto r_c^{D1+D2-3},^{10}$$

where $M_{1,2}$ is the number of intersections, r_c the species radius and D1 and D2 are the fractal dimension of the respective species. So when the fractal dimension of the sol species is <1.5 interpenetration is almost not restricted and small pores can form during the drying process.

In contrast, condensation of titanium and zirconium alkoxides gives rise to dense particles originating from a nucleation and growth mechanism. Apart

from the differences in sol particles, the reaction kinetics are much faster compared to those of silica-based sols.[11] One of the main issues in preparing these sols is to slow down the kinetics and to limit the particle growth to 5–10 nm. In addition, metal oxides have a tendency to crystallize during heat treatment or during membrane application.[12]

For the characterization of sol species in a liquid medium Small Angle X-ray Scattering (SAXS) and Dynamic Light Scattering (DLS) can be used. SAXS can be applied to determine particle size and fractal dimensions of sol species. Unfortunately, SAXS equipment (often at a synchrotron facility) is not routinely accessible. DLS is a much more convenient alternative for a sol-gel laboratory as a first tool for the determination of the particle size distribution.[13]

2.2. FORMATION OF A THIN FILM AND THE SOL-GEL TRANSITION

Dip-coating (Figure 2) is a suitable and well-known method for preparing thin film coatings from sols. This method can be used for coating of sols on macroporous and mesoporous substrate tubes. The physical processes that occur during film formation were extensively studied by Brinker et al.[14] During evaporation of the solvent the water concentration strongly increases and influences the ongoing reactions. At the same time, gelation starts to occur. When menisci are formed in the network (the second drying stage) the network collapses due to capillary forces until the network strength prevents further collapse. At this stage the pore structure is formed. Polymeric sol networks are consolidated by further condensation reactions. Solvent molecules may function as a pore template. The pore size can also be controlled by adding pore directing agents on purpose.[15,16]

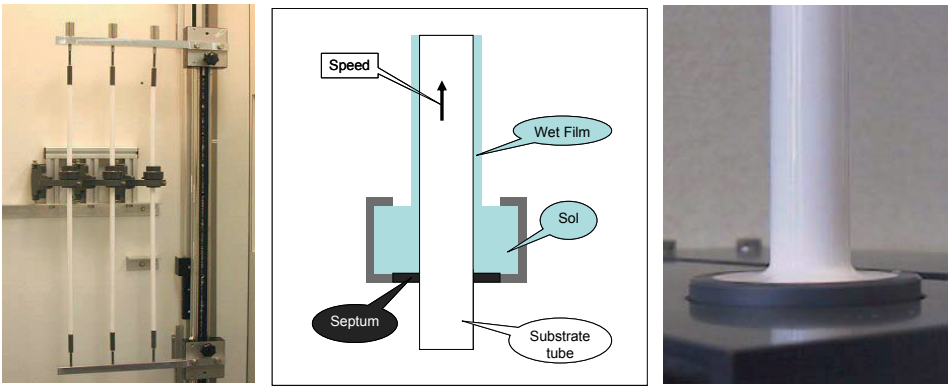

Figure 2. Dip-coating of membrane tubes.

As stated earlier, control over the defect density is of eminent importance to reach molecular separation with an acceptable selectivity. However, repairing defects in calcined thin films by application of second sol-gel coating often leads to unsatisfactory results. This can be ascribed to dewetting phenomena reminiscent to those occurring in thin polymer films.[17] Occasionally, this is also observed in single-layer coatings of sol-gel films (Figure 1d). The relation between the dewetting phenomenon and specific interactions of substrate and the coating liquid is not fully understood. This effect decreases the membrane yield in production and may also affect the adherence of the thin film after calcining. Therefore, applying a single sol-gel layer of sufficient thickness is to be preferred over multi-coating approaches. To achieve this, suitable sols and substrates having a low defect density are crucial.

3. Structure of Porous Supports

3.1. DEFECTS

For defect free films the intrinsic micropore characteristics, such as pore size distribution, tortuosity, and connectivity are the determining factors for the separation performance. In addition, the performance is influenced by the physico-chemical properties of the pore interfaces, such as wettability, presence of adsorption sites etc. The selectivity decreases when channels are present that are much larger than the intrinsic pore size. These so-called defect pores can be formed during the dip-coating process, due to asperities, larger voids, and dust particles (Figure 3). Alternatively, shrinkage and interaction with the substrate during the drying/consolidating stage can lead to microcrack formation. Defects in the top-layer can also originate from the larger pores present in the support.

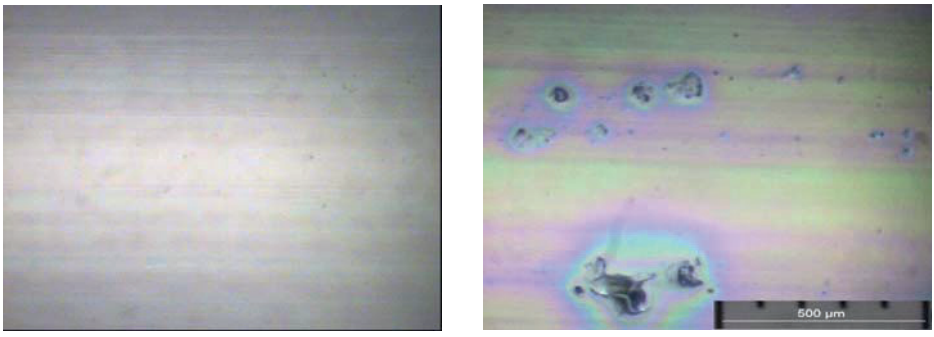

Figure 3. Optical micrographs of the surface of a microporous zirconia thin film having a high defect density (left) and a defect poor microporous methylated silica thin film (right).

The use of clean rooms during the coating procedure reduces the influence of dust particles and enhances the quality of the film.[18] Other important steps are the pretreatment of the substrates and sol filtration prior to coating. The support structure must be smooth, flawless and homogeneous to obtain defect free sol-gel membranes. This can only be achieved through the application of a multilayer support system.[19]

3.2. MESOPOROUS SOL-GEL LAYERS: γ-ALUMINA AND TITANIA

Mesoporous γ-alumina obtained from boehmite sols (γ-AlO(OH), Yoldas[20]) were developed by Leenaars.[21] The pore size is determined by the plate-like structure of the primary particles in the boehmite sols consisting of ellipsoidal aggregates of these platelets. The aggregates are restructuring during drying and calcining of a coating. However, remnants of the aggregates after the sol-gel transition in a coating may cause larger intra-aggregate pores. Such larger pores (i.e. >20 nm) can be observed by bubble number porometry but are hard to observe with a Scanning Electron Microscope. The plate-like structure facilitates stress relaxation during drying stages. If required, further stress relaxation can be obtaining by adding suitable polymers to the coating sol. Stress relaxation is much more difficult in sol-gel coatings from sols with spherical particles, such as titania sols. Here, polymer additives are a prerequisite for obtaining crack free films.[12] Based on previous work by Sekulic et al. and Van Gestel et al.,[22,23] we succeeded in making crack free anatase titania mesoporous coatings on tubes that are suitable as substrates for microporous sol-gel films. The critical layer thickness of these mesoporous titania films before cracking is about 600 nm. This value is much lower than that observed for the boehmite films (~3 μm).

4. Membranes Prepared from Silica-Based Sols

4.1. PURE SILICA

Polymeric silica sols are suitable for the preparation of microporous pure silica films on a mesoporous substrate if the interpenetration of the species during the drying phase of a dip-coating process is sufficient.[24] The preparation of suitable sols from tetraethylorthosilicate (TEOS) by acid catalyzed hydrolysis in ethanol is relatively straightforward. To obtain reproducible sol properties, fresh precursors and well-defined synthesis parameters are required. A suitable formulation is: TEOS/EtOH/H_2O/HNO_3 = 1/3.8/6.4/0.085.[18] These recipes were first

developed at the university of Twente by Uhlhorn,[25] followed by further developments by De Lange,[24] and De Vos.[26] To obtain reproducible sols, it is essential to keep the reaction mixture below 0°C during mixing of the reactants. Subsequently, the reaction mixture is quickly heated up to 60°C, and keep it at this temperature for 3 h (Scheme 1).

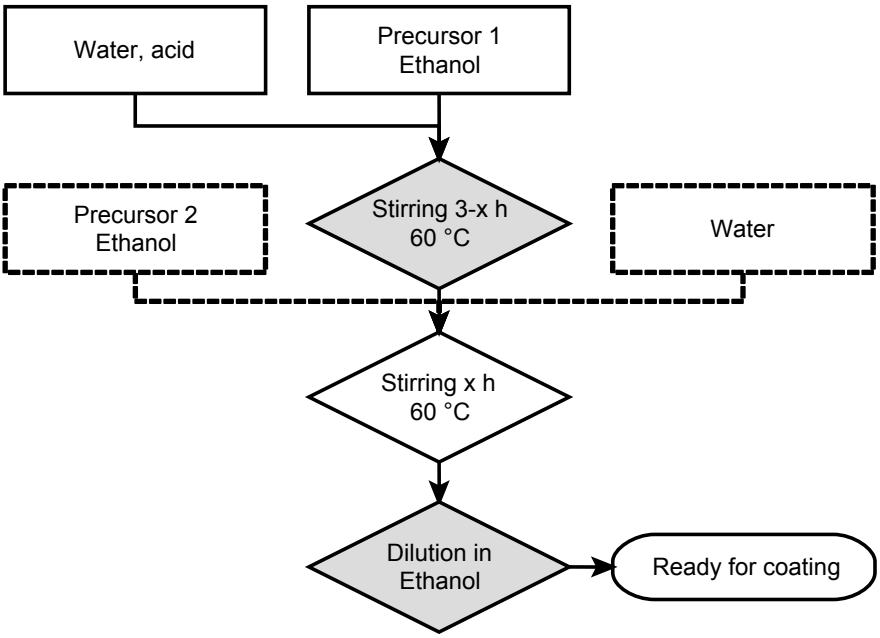

Scheme 1. General synthesis scheme for silica-based sols; dashed steps are optional.

Directly after synthesis, the sol is diluted with ethanol, filtered and used in the dip-coating process. Aging of the sol leads to larger pores in the final membrane because of increased branching of the sol species. Using these sols it is possible to obtain microporous silica membranes by a single layer coating on a preconditioned mesoporous γ-Al_2O_3 substrate. In related work by Brinker et al.[27] first a larger pore size silica layer was coated on the support, followed by coating of a second microporous layer.

The silica concentration in the sol and the coating speed determine the thickness of the layer formed after dip-coating to a large extent. The critical layer thickness for pure microporous silica layers is about 200 nm. Above this thickness microcracks occur during drying and/or calcining. The average pore size of pure silica thin film determined by gas permeation of several gases was about 0.4 nm.[24] SAXS measurements showed that the fractal dimension of the

silica species in these sols is about 1.4 to 1.5, which points to with weakly branched linear species. The radius of gyration was found to be about 2 nm. The hydrothermal stability of pure silica membranes is very limited, resulting in a maximum application temperature in pervaporation applications of ~70°C (Figure 6).[28]

4.2. METHYLATED SILICA

The first approach to increase the hydrothermal stability of the pure silica membrane was by incorporating terminal Si-methyl groups. The reasoning was that by replacing silanol-groups, the surface would become less susceptible to hydrolytic attack. De Vos was the first to develop such a membrane.[29]

In the original recipe,[29] the sol preparation starts with a hydrolysis step similar to that in the pure silica synthesis. After reacting at 60°C for 165 min methyltriethoxysilane (MTES, Figure 5) in ethanol is added, leading to final molar ratios of: MTES/TEOS/EtOH/H_2O/HNO_3 = 1/1/7.6/6.4/0.085. The reaction mixture is cooled down to room temperature 15 min after the addition of MTES, and subsequently diluted with ethanol. The dip-coatings are performed immediately thereafter.

Molecular masses of sol species were investigated by Gel Permeation Chromatography (GPC). The GPC particle size of the methylated silica sol is similar to that of the pure silica sols. The distribution is polydisperse with a maximum molecular mass of 4 kg/mol. Besides the one-step acid hydrolysis described above, also a two-step acid hydrolysis procedure was developed to prepare methylated silica sols with varying methyl content.[30] These two step sols have a much smaller GPC particle size distribution with a maximum of ~1 kg/mol, which has been ascribed to the higher methyl content of the species. Coatings of these sols on mesoporous γ-Al_2O_3 and TiO_2 could be prepared and the results were very reproducible. The layer thickness can be varied between 50–150 nm by adjusting the sol concentration and coating speed. The defect density was found to be related to the layer thickness, and increases with decreasing layer thickness (Figure 1d). The calcination of dried films in air at 250°C results in membranes with a satisfactory pervaporation performance. The pore size distributions for individual sol and membrane preparations estimated from the uncorrected Kelvin equation using water permporometry[31] were quite reproducible (Figure 4). The average pore diameter d50 of about 0.6 nm, is somewhat larger than that of pure silica films. The pervaporation performance of these methylated silica membranes is excellent up to temperatures of 95°C (Figure 6).[30] Above this temperature rapid degradation of the membrane takes place.

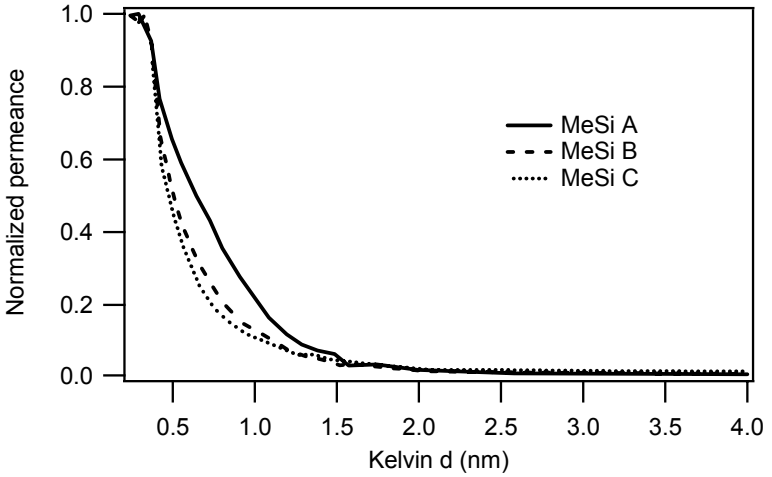

Figure 4. Normalized pore size distributions of methylated silica (MeSi) membranes. A, B and C represent individual sol and membrane preparations on mesoporous γ-alumina substrate tubes; d50 ≈ 0.6 nm.

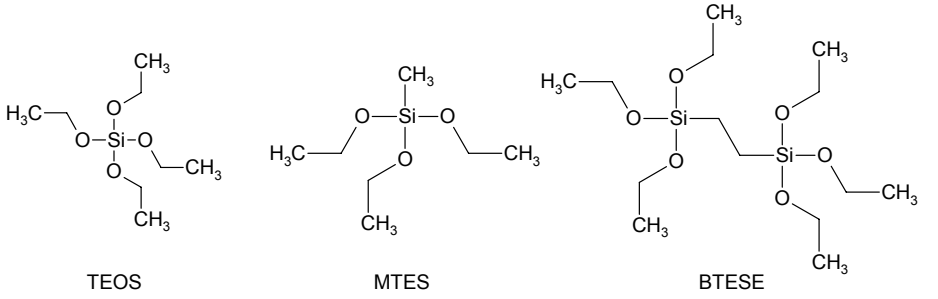

Figure 5. Precursors used for the preparation of silica (TEOS), methylated silica (MTES), and hybrid silica (BTESE) membranes.

4.3. HYBRID SILICA

A dramatic increase in hydrothermal stability can be achieved when part of the siloxane bonds (Si-O-Si) are replaced by organic bridges (Si-CH_2-CH_2-Si). As a result a truly organic-inorganic hybrid material is formed.[32] This hybrid silica material can be obtained through the application of bisfunctional precursors, such as 1,2-bis(triethoxysilyl)ethane (BTESE, Figure 5). The synthesis of sols for such membrane layers was developed by Sah et al.[33,34] This synthesis consists of a two step acid hydrolysis of BTESE/MTES mixtures. MTES is added to prevent the formation of unreactive cyclic species[35] and it reduces the speed

of gel formation. The two step addition of the acid/water mixture suppresses multiple hydrolysis and therefore promotes the formation of linear and weakly branched sol species. The structure of sol species can be controlled further by the BTESE/MTES ratio, pH, hydrolysis ratio, and reflux time. Based on a screening of acid and water concentrations and the precursor ratio the following composition was selected for membrane preparations: BTESE/MTES/H_2O/HNO_3 = 1/1/2/0.05.The average hydrodynamic diameter of these sols ranges from 3–10 nm[36] and the fractal dimension of the species as obtained from SAXS is about 1.1.[33] Based on these data, good particle interpenetration during drying and the formation of micropores is expected. In general, the pore size distributions of the hybrid thin films were broader than those of methylated silica membranes. The average pore diameter estimated from permporometry is also slightly larger (d50 = 0.6–0.9 nm). A striking feature of the hybrid films is the unusually large critical layer thickness of about 1 μm. Presumably, this is a consequence of the presence of the bridging alkyl groups which decrease the elasticity modulus of the film, i.e. enhancing the possibilities for viscous relaxation.

Above, we have shown that the maximum application temperature of pure and methylated silica in the pervaporation of *n*-butanol/water is limited to a maximum value of 95°C.[30] The hybrid silica membranes show remarkably stable performance at temperatures as high as 150°C. These membranes have excellent water fluxes and selectivity and maintain this performance up to at least 600 days of total running time (Figure 6).[33] We believe that several factors play a critical role in the differences in stability between silica, methylated silica, and

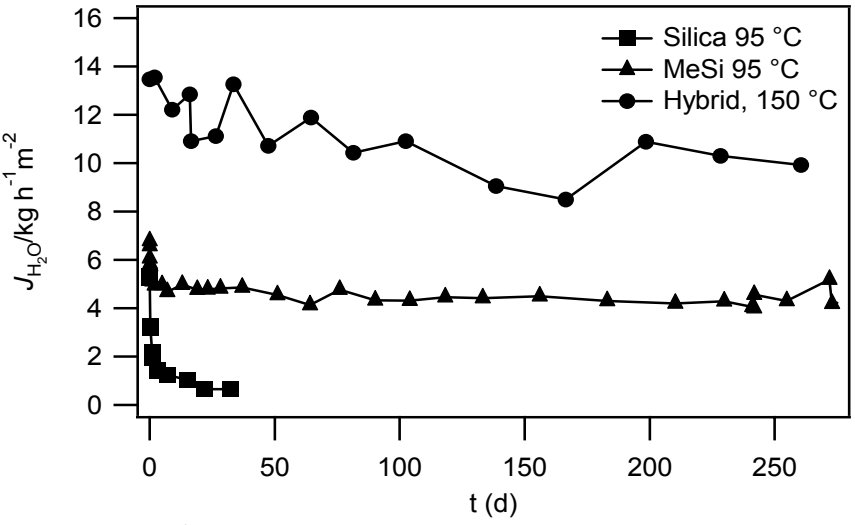

Figure 6. Long-term performance of silica-based membranes in pervaporation.

hybrid silica membranes. The presence of organic groups in the structure leads to a more hydrophobic character and the silicon atoms are partly shielded from attack by water. In addition, the network in this hybrid silica is partly formed by silicon-carbon bonds that do not hydrolyze. Furthermore, the bridging momomers are connected via six siloxane groups compared to four or three in TEOS and MTES respectively. This characteristic of bisfunctional precursors lowers the probability of full hydrolysis and subsequent removal of monomers from the membrane film.

In addition to the above, we believe that mechanical factors are of importance. Pure silica sols obtained by acid hydrolysis contain a relatively large content of three and four membered strained siloxane rings.[37] The content of these strained rings may even increase during the dip-coating process and the subsequent drying and calcining. It has been suggested that especially these strained bonds are susceptible to hydrolysis followed by a restructuring to a more favorable relaxed structure.[38] This transforms microporous silica in dense silica with some remaining mesoporosity.

The incorporation of (non-binding) methyl groups probably retards the restructuring of the silica network, which explains the increased stability of methylated silica. This effect is exponentially larger in the presence of bridging -Si-CH_2-CH_2-Si groups. The formation of three-membered rings is much more unlikely using the bridging precursors. Tensile film stresses increase the sensitivity for water attack similar to the presence of strained three membered rings.[39] We think the possibilities for stress relaxation in the hybrid membrane films are larger hence decreasing the reactivity for water. In addition, recent studies on the use of such materials as insulators for microelectronic devices have shown that crack propagation is retarded by the incorporation of organic bridging groups in the silica network.[40]

5. Membranes Prepared from Metal Oxide Sols

As an alternative to silica-based materials we have investigated metal oxides, such as titania and zirconia. These metal oxides are known for their stability in aqueous environment in a wide pH range.[23,41] A number of different routes have been employed for the sol-gel synthesis of metal oxide particles. Most of these aim at the limitation of reaction kinetics involved in the sol-synthesis based on alkoxide precursors. Two main approaches can be distinguished. One approach uses ligands to stabilize the precursor (Scheme 2),[42–46] the other is based on stabilization of nanoparticles before they aggregate (Scheme 3).[47] For the first approach, ligands such as amino-alcohols or β-diketones are used, of which acetylaceton (acac) is the best-known example. Aggregation of nanoparticles

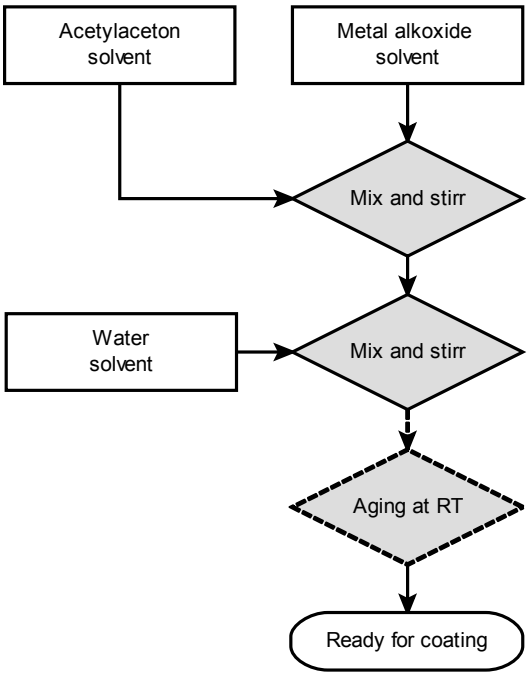

Scheme 2. General route for ligand-based metal oxide sol preparation.

can be prevented by the introduction of an acid dispersant or by using a sub-stoichiometric amount of water. We have used both approaches for the preparation of titania and zirconia thin films.

5.1. TITANIA

Titania sols were prepared by premixing acac and titanium isopropoxide in isopropanol (IPA) in a molar ratio of 1:1 (sol Ti-1). To this mixture a solution of water in IPA was added slowly, leading to a final molar ratio H_2O/Ti of 2:1. Using this approach, sol particles with an average hydrodynamic diameter of 2 nm were obtained. Coatings on γ-alumina support tubes resulted in very thin layers that appeared to be defect-free by microscopy techniques. However, pore size analysis by permporometry indicated the presence of smaller mesopores. This is an indication that no complete coverage of the mesoporous support was achieved. We presume that the small particle size obtained by this route leads to sol infiltration into the support rather than the formation of a porous layer on top of the support.

In a second approach the aim was to prevent aggregation of particles during sol synthesis. This time a mixture of water, concentrated HNO_3, and IPA was added dropwise to titanium *iso*-propoxide in IPA.[47] We used water to titanium ratios of 1.4:1 (sol Ti-2) and 2:1 (sol Ti-3). After addition of the water mixture, the sols were heated to reflux for 10 min and aged for 1 day before coating. The average particle size of sol Ti-2, prepared with lower amount of water, was smaller than that of sol Ti-3, prepared with a stoichiometric water content. In addition, the size distribution is somewhat broader for sol Ti-2. Sol Ti-C has a narrow size distribution with an average hydrodynamic diameter of 10 nm (Figure 7). The particle size distribution of sols Ti-2 and Ti-3 did not change over time for at least 1 week.

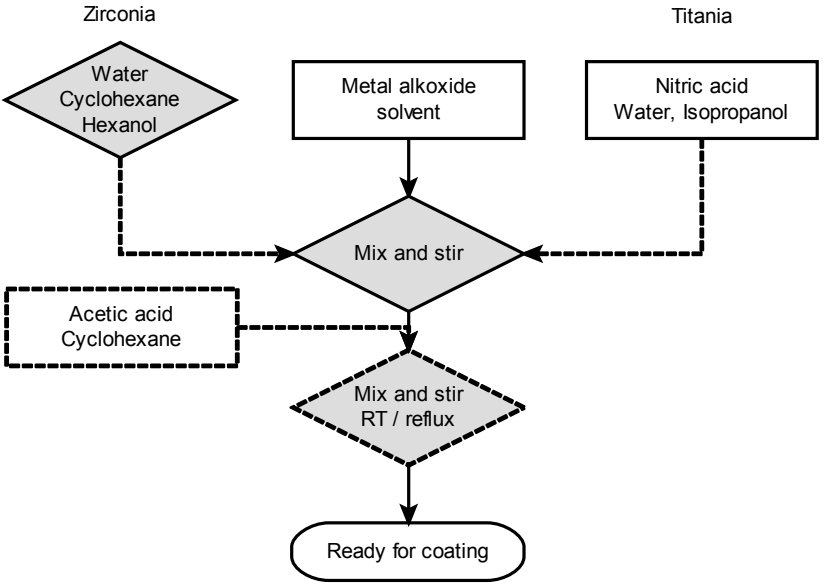

Scheme 3. General preparation of metal oxide sols using acid (used for zirconia) or a sub-stoichiometric amount of water (used for titania).

5.2. ZIRCONIA

A ligand-based zirconia sol was prepared using acac as modifying ligand (Sol Zr-1). Similar to the titania sol, a solution of zirconium *n*-propoxide in *n*-propanol was mixed with a solution of acac in *n*-propanol in a ratio of 1:1. To this modified precursor a solution of water in *n*-propanol was added drop-wise Different from our work on titania, a second type of zirconia sol was based on a approach inspired by microemulsions.[48] First a mixture water, hexanol, and cyclohexane was stirred vigorously. This mixture was added drop-wise to a

solution of zirconium *n*-propoxide in cyclohexane in a molar ratio H_2O/Zr of 3:1. Subsequently, the resulting sol was stirred for 15 min and acetic acid in cyclohexane was added in one portion. After this the sol was ready for further use (sol Zr-2).

The dynamic light scattering experiments for zirconia sols based on the second approach indicate that the hydrodynamic diameters are in the nanosize range and that the size distributions are quite narrow. The average hydro-dynamic diameters of these sols are around 5–7 nm (Figure 7). Interestingly, when the same sol preparation was repeated and the sols were aged for different periods of time, the size distributions found with DLS are very similar. Clearly, the sol preparation using a microemulsion is highly reproducible and the sols are highly stable against particle growth.

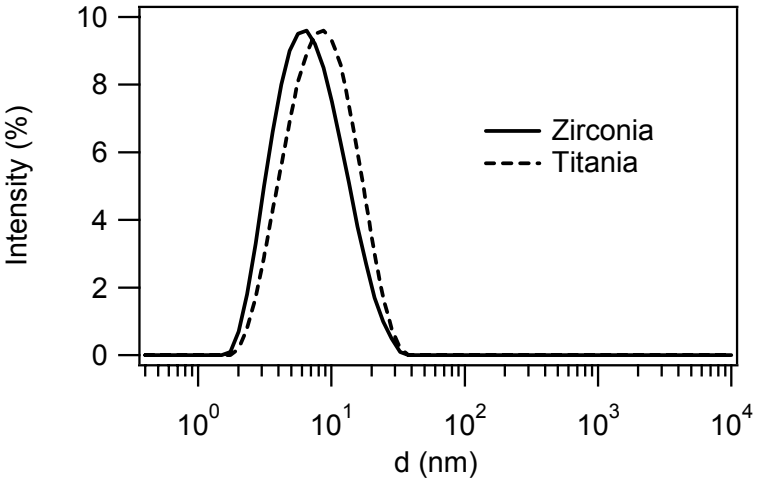

Figure 7. Dynamic light scattering results showing the hydrodynamic diameter of titania (sol Ti-3) and zirconia (sol Zr-2) sols.

Based on these measurements the membranes based on titania sols Ti-3 and zirconia sol Zr-2 were selected for further investigation. Pervaporation measurements were carried out at 95°C using a mixture of *n*-butanol and water (95/5 wt%). The zirconia membrane has an initial water flux of around 5 kg/m^2 h, which decreases during the first 20 days of operation. After 20 days, the membrane performance is stable up to at least 120 days. The measurement was terminated after 123 days. The water content of the permeate stream initially is quite low, but after about 20 days an acceptable 90% water is reached. This increases to the required 95% after 40 days.

The titania membrane also has an initial water flux of over 5 kg/m^2 h. Also in this case, the flux decreases rapidly during the first 20 days of operation. In addition, the water content in the permeate stream starts at a disappointing 75%, rises to 95%, after which the water content drops dramatically. This is a clear indication for breakdown of the membrane after about 15 days.

The titania membrane based on sol Ti-2 was selected for nanofiltration experiments in supercritical CO_2. Microporous membranes, such as silica membranes and the titania membrane described here are very effective in retaining a fluorinated phosphine complex, a modified version of Wilkinsons complex.[49]

Based on our data it seems that the zirconia membranes, and more heavily the titania membranes, suffer from densification and crystallization effects. It has to be noted that the actual process conditions for pervaporation resemble many of the hydrothermal treatments done to prepare crystalline nanoparticles. Therefore, the conditions of the separation process could easily provide the energy to transform the material to its thermodynamically favorable state.

6. Outlook

In this chapter we have presented a brief overview of the use of different sol-gel approaches for the formation of microporous membranes. The examples indicate that such membranes are highly suitable for molecular separations. Still, the issue of long-term stability in media that contain water, or in addition are highly acidic or basic needs to be addressed. The sol tailoring we and others have done shows that particle morphology and size can be directed by choosing the right precursors, reaction conditions, and stabilizing agents.

The remarkable stability of the first generation of microporous hybrid membranes indicates that much can be gained by including organic groups in the network structure. We feel that the field of membrane science would benefit from additional studies into the nature of this stabilizing effect. The potential of hybrid materials for membrane applications poses a great challenge for sol-scientists, because of the vast amount of possible variations.

The limited life-time of membranes based on titania and zirconia sols suggest that the use of (partly) amorphous mono-metal oxide sol species does not lead to membranes that have long-term stability. In our view, the development of sols for membrane preparation should either focus on stabilization of amorphous structures by, e.g. dopants, or on the use of crystalline nano-particle sols. As an additional advantage, the surface of crystalline nanoparticle can be tailored to the application, as was nicely demonstrated by the group of Niederberger.[50,51] Recent work on mixed metal precursors by Spijksma et al. opens the way for amorphous mixed oxide membranes.[52] The use of these mixed metal oxides for

membrane applications could improve stability by preventing the phase changes commonly observed for titania and zirconia.

Over the years, the field of sol-gel science has had a large influence on the development of membranes that have to survive under industrial, often corrosive conditions. Based on the described recent developments in the field of sol-gel membranes, we conclude that membrane science still is a challenging topic for sol-gel scientists.

References

1. M. Asaeda, Sol-gel derived ceramic membranes for separation of molecular mixtures, *Porous. Ceram. Mater., Conf. Proc.* (2005).
2. J. F. Vente, H. M. van Veen, and P. P. A. C. Pex, Microporous sol-gel membranes for molecular separations, *Ann. Chim. Sci. Mat.* 32(2), 231–244 (2007).
3. B. C. Bonekamp, A. van Horssen, L. A. Correia, J. F. Vente, and W. G. Haije, Macroporous support coatings for molecular separation membranes having a minimum defect density, *J. Membr. Sci.* 278(1–2), 349–356 (2006).
4. P. P. A. C. Pex and Y. C. van Delft, in: *Carbon dioxide capture for storage in deep geological formations*, 1 ed., edited by D. C. Thomas, and S. M. Benson (Elsevier, Amsterdam, 2005), pp. 307–319.
5. C. J. Brinker, Porous inorganic materials, *Curr. Opin. Solid State Mater. Sci.* 1, 798–805 (1996).
6. H. M. van Veen, Y. C. van Delft, C. W. R. Engelen, and P. P. A. C. Pex, Dewatering of organics by pervaporation with silica membranes, *Separ. Purif. Technol.* 22–23, 361–366 (2001).
7. C. J. Brinker, R. Sehgal, S. L. Hietala, R. Deshpande, D. M. Smith, D. A. Loy, and C. S. Ashley, Sol-gel strategies for controlled porosity inorganic materials, *J. Membr. Sci.* 94, 85–102 (1994).
8. A. W. Burton and S. I. Zones, in: *Introduction to zeolite science and practice*, edited by J. Cejka, H. van Bekkum, A. Corma, and F. Schüth (Elsevier, Amsterdam, 2007), pp. 137–179.
9. C. J. Brinker and G. W. Scherer, *Sol-gel science – the physics and chemistry of sol-gel processing* (Academic, New York, 1990).
10. C. J. Brinker, N. K. Raman, M. N. Logan, R. Sehgal, R. A. Assink, D.-W. Hua, and T. L. Ward, Structure-property relations in thin films and membranes, *J. Sol-gel Sci. Technol.* 4, 117–133 (1995).
11. A. C. Pierre, *Introduction to sol-gel processing* (Kluwer, Dordrecht, The Netherlands, 1998).
12. A. J. Burggraaf, in: *Fundamentals of inorganic membrane science and technology*, edited by A. J. Burggraaf, and L. Cot (Elsevier, Amsterdam, 1996).
13. A. Rawle, The importance of particle sizing to the coatings industry Part 1: particle size measurement, *Adv. Col. Sci. Technol.* 5(1), 1–12 (2002).
14. C. J. Brinker, Review of sol-gel thin film formation, *J. Non-cryst. Solids* 147/148, 424–436 (1992).
15. A. J. Hurd and L. Steinberg, The physics of evaporation-induced assembly of sol-gel materials, *Granul Matter* 3(1–2), 19–21 (2001).
16. C. Nguyen, K. R. Carter, C. J. Hawker, R. L. Jaffe, R. D. Miller, J. F. Remenar, H.-W. Rhee, P. M. Rice, M. F. Toney, M. Trollsås, and D. Y. Yoon, Low-dielectric nanoporous organo-

silicate films prepared via inorganic/organic polymer hybrid templates, *Chem. Mater.* 11, 3080–3085 (1999).
17. G. Reiter, Dewetting of thin polymer films, *Phys. Rev. Lett.* 68, 75–82 (1992).
18. R. M. de Vos and H. Verweij, High-selectivity, high-flux silica membranes for gas separation, *Science* 279, 1710–1711 (1998).
19. B. C. Bonekamp, in: *Fundamentals of inorganic membrane science and technology*, *Volume 4*, edited by A. J. Burggraaf and L. Cot (Elsevier, Amsterdam, 1996).
20. B. E. Yoldas, Alumina gels that form porous transparent Al_2O_3, *J. Mater. Sci.* 10, 1856–1860 (1975).
21. A. F. M. Leenaars, K. Keizer, and A. J. Burggraaf, The preparation and characterization of alumina membranes with ultra-fine pores, Part 1. Microstructural investigations on non supported membranes, *J. Mater. Sci.* 19, 1077 (1984).
22. J. Sekulić, A. Magraso, J. E. ten Elshof, and D. H. A. Blank, Influence of ZrO_2 addition on microstructure and liquid permeability of mesoporous TiO_2 membranes, *Micropor. Mesopor. Mater.* 72, 49–57 (2004).
23. T. van Gestel, C. Vandecasteele, A. Buekenhoudt, C. Dotremont, J. Luyten, R. Leysen, B. van de Bruggen, and G. Maes, Alumina and titania multilayer membranes for nanofiltration: preparation, characterization and chemical stability, *J. Membr. Sci.* 207, 73–89 (2002).
24. R. S. A. de Lange, K. Keizer, and A. J. Burggraaf, Aging and stability of microporous sol-gel-modified ceramic membranes, *Ind. Eng. Chem. Res.* 34, 3838–3847 (1995).
25. R. J. Uhlhorn, Ceramic membranes for gas separation. Ph.D. thesis, University of Twente (1990).
26. R. M. de Vos and H. Verweij, Improved performance of silica membranes for gas separation. *J. Membr. Sci.*143, 37–51 (1998).
27. C. J. Brinker, C. Y. Tsai, and Y. Lu, Inorganic dual-layer microporous supported membranes. US Patent 6,536,604 (2003).
28. T. A. Peters, J. Fontalvo, M. A. G. Vorstman, N. E. Benes, R. A. van Dam, Z. A. E. P. Vroon, E. L. J. van Soest-Vercammen, and J. T. F. Keurentjes, Hollow fiber microporous silica membranes for gas separation and pervaporation. Synthesis, performance and stability, *J. Membr. Sci.* 248, 73–80 (2004).
29. R. M. de Vos, W. F. Maier, and H. Verweij, Hydrophobic silica membranes for gas separation. *J. Membr. Sci.* 158(1–2), 277–288 (1999).
30. J. Campaniello, C. W. R. Engelen, W. G. Haije, P. P. A. C. Pex, J. F. Vente, Long-term pervaporation performance of microporous methylated silica membranes, *Chem. Commun.* 834–835 (2004).
31. T. Tsuru, T. Hino, T. Yoshioka, and M. Asaeda, Permporometry characterisation of microporous ceramic membranes, *J. Membr. Sci.*, 186(2), 257–265 (2001).
32. K. J. Shea and D. A. Loy, Bridged polysilsesquioxanes, molecular-engineered hybrid organic-inorganic materials, *Chem. Mater.*, *13*, 3306–3319 (2001).
33. H. L. Castricum, A. Sah, R. Kreiter, D. H. A. Blank, J. F. Vente, and J. E. ten Elshof, Hybrid organosilica membranes: molecular separation under hydrothermal conditions. (submitted) (2007).
34. A. Sah, Chemically modified ceramic membranes – study of structural and transport properties. Ph.D. thesis, University of Twente (2006).
35. D. A. Loy, J. P. Carpenter, T. M. Alam, R. Shaltout, P. K. Dorhout, J. Greaves, J. H. Small, and K. J. Shea, Cyclization phenomena in the sol-gel polymerization of α,ω-bis(triethoxysilyl)alkanes and incorporation of the cyclic structures into network silsesquioxane polymers, *J. Am. Chem. Soc.*, 121, 5413–5425 (1999).
36. H. L. Castricum, R. Kreiter, J. F. Vente, and J. E. ten Elshof, to be published.
37. C. J. Brinker, W. L. Warren, and S. Wallace, in: *Structure and imperfections in amorphous and crystalline silicon dioxide*, edited by R. A. B. Devine, J.-P. Duraud, and E. Dooryhée (Wiley, Chichester, 2000), pp. 475–493.

38. R. M. van Ginhoven, H. Jónsson, B. Park, and L. R. Corrales, Cleavage and recovery of molecular water in silica, *J. Phys. Chem. B*, 109(21), 10936–10945 (2005).
39. T. A. Michalske and B. C. A. Bunker, Chemical kinetics model for glass fracture, *J. Am. Ceram. Soc.*, 76, 2613–2618 (1993).
40. G. Dubois, W. Volksen, T. Magbitang, R. D. Miller, D. M. Gage, and R. H. Dauskardt, Molecular network reinforcement of sol–gel glasses, *Adv. Mater.*, doi: 10.1002/adma.200701193 (2007).
41. G. I. Spijksma, Modification of zirconium and hafnium alkoxides – the effect of molecular structure on derived materials. Ph.D. thesis, University of Twente (2006).
42. G. A. Seisenbaeva, S. Gohil, and V. G. Kessler, Influence of heteroligands on the composition, structure and properties of homo- an heteremetallic ziconium alkoxides. Decisive role of thermodynamic factors in their self-assembly, *J. Mater. Chem.*, 21, 3177–3190 (2004).
43. G. A. Seisenbaeva, S. Gohil, and V. G. Kessler, Molecular design approach to a highly soluble and volatile bimetallic alkoxide of late transition metal and zirconium. Synthesis, X-ray single crystal and mass-spectral study of $NiZr_2(acac)(OiPr)_9$, *Inorg. Chem. Commun.*, 10, 94–96 (2007).
44. G. I. Spijksma, H. J. M. Bouwmeester, D. H. A. Blank, and V. G. Kessler, Stabilization and destabilization of zirconium propoxide precursor by acetylacetone, *Chem. Commun.*, 1874–1875 (2004).
45. L. Armelao, C. Eisenmenger-Sittner, M. Groenewolt, S. Gross, C. Sada, U. Schubert, E. Tondello, and A. Zattin, Zirconium and hafnium oxoclusters as molecular building blocks for highly dispersed ZrO_2 or HfO_2 nanoparticles in silica thin films, *J. Mater. Chem.*, 15, 1838–1848 (2005).
46. U. Schubert, Organofunctional metal oxide clusters as building blocks for inorganic-organic hybrid materials, *J. Sol-Gel Sci. Technol.*, 31, 19–24 (2004).
47. J. Sekulić, J. E. ten Elshof, and D. H. A. Blank, A microporous titania membrane for nanofiltration and pervaporation, *Adv. Mater.*, 16(17), 1546–1550 (2004).
48. S. E. Friberg and J. Sjöblom, in: *Industrial applications of microemulsions*, edited by C. Solans and H. Kunieda (Marcel Dekker, New York, 1997), pp. 267–277.
49. E. L. V. Goetheer, A. W. Verkerk, L. J. P. van den Broeke, E. de Wolf, B.-J. Deelman, G. van Koten, and J. T. F. Keurentjes, Membrane reactor for homogeneous catalysis in super-critical carbon dioxide, *J. Catal.*, 219, 126–133 (2003).
50. G. Garnweitner and M. Niederberger, Nonaqueous and surfactant-free synthesis routes to metal oxide nanoparticles, *J. Am. Ceram. Soc.*, 89(6), 1801–1808 (2006).
51. M. Niederberger, G. Garnweiter, F. Krumeich, R. Nesper, H. Cölfen, and M. Antonietti, Tailoring the surface and solubility properties of nanocrystalline titania by a nonaqueous in situ functionalization process, *Chem. Mater.*, 16, 1202–1208 (2005).
52. G. I. Spijksma, C. Huiskes, N. E. Benes, H. Kruidhof, D. H. A. Blank, V. G. Kessler, H. J. M. Bouwmeester, Microporous zirconia-titania composite membranes derived from diethanolamine-modified precursors, *Adv. Mater.*, 18, 2165–2168 (2006).

SOL-GEL SYNTHESIS OF NANOSTRUCTURED TiO_2 FILMS FOR WATER PURIFICATION

YONGJUN CHEN, DIONYSIOS D. DIONYSIOU*
Department of Civil and Environmental Engineering, 765 Baldwin Hall, University of Cincinnati, Cincinnati, OH 45221-0071, USA

Abstract. Sol gel method is an important technology for the synthesis of TiO_2 films for water treatment. In this chapter, we will discuss the critical issues on the sol gel synthesis of TiO_2 films with high photocatalytic activity and good long-term mechanical stability. The aspects will mainly include the following: (1) design of film structure for increasing the number of electron-hole pairs generated and number of hydroxyl radicals produced, (2) tailor-design of the film pore structure for increasing adsorption of treated contaminants and enhancing mass transfer between the contaminants and catalyst active sites, and (3) improvements in the long-term mechanical stability of the TiO_2 films by achieving good adhesion of immobilized TiO_2 films on the support (substrate). Important achievements of our research works related to sol gel synthesis of TiO_2 films and membranes and the application of these TiO_2 photocatalysts in promising photocatalytic reactors are summarized. Current challenges and future directions on the sol gel synthesis of TiO_2 films for water purification are also discussed.

Keywords: Sol-gel method, titanium dioxide, photocatalysis, immobilized TiO_2 films, water purification.

1. Introduction

During the last few years, serious water pollution problems stimulated a dramatic increase in research activities dealing with the development of high performance TiO_2 films for water purification.[1–6] Because of many advantages in the use of sol gel methods to synthesize nanostructured TiO_2 films, many scientists and engineers have focused on the development of novel sol gel methods for the synthesis of immobilized TiO_2 films.[2–12] In this chapter, we will not review

* To whom correspondence should be addressed: Dionysios D. Dionysiou; e-mail: dionysios.d.dionysiou@uc.edu

P. Innocenzi, Y. L. Zub and V. G. Kessler (eds.), *Sol-Gel Methods for Materials Processing*.

general aspects of TiO_2 photocatalysis and sol gel chemistry, which have been reviewed by other researchers. Instead, we will discuss critical issues associated with the design of TiO_2 film structural properties for improving film photocatalytic activity and long-term mechanical stability.

Promising sol gel methods developed in our group and relevant photocatalytic reactors are summarized in this chapter. Current challenges and future directions on sol gel synthesis of TiO_2 films for water purification will be discussed.

2. Background: The Importance for Preparing TiO_2 Photocatalytic Films for Water Purification

Dramatic increase in human population, urbanization, limited water resources especially in arid climates, development of a variety of new products that find their ways into our water supplies, intense agricultural activities, booming of industrial activities in several developing countries with dense populations, unavailability of even simple processes to provide basic water sanitation in several developing countries, and several other reasons are causing serious water pollution threats in both developed and developing countries around the world.[13]

Along with a variety of other water pollutants such as pathogenic microorganisms and toxic inorganic chemicals, numerous harmful organic contaminants, such as pesticides, herbicides and other synthetic or naturally occurring organic chemicals can cause serious adverse health effects when present, even at small concentrations, in potable water.[14–20] Therefore, the need for eliminating toxic organic contaminants in water becomes a vital priority. Since certain toxic and non-biodegradable organic pollutants in contaminated water cannot be effectively eliminated by conventional technologies such as biological processes, the development of more powerful and effective technologies for water decontamination becomes especially important.

TiO_2 is a ceramic semiconductor material and is characterized by a void energy region between its valence (VB) and conduction (CB) bands, which is called the band gap. The band gaps of anatase and rutile crystal phases are 3.0 and 3.2 eV, respectively.[21] When the TiO_2 catalyst receives sufficient energy (i.e., UV radiation equal to or above the band-gap energy), there is excitation of an electron from the valance band to the conduction band. As a result, electrons and holes are generated in the semiconductor. Electrons and holes can induce redox reactions at the surface of TiO_2 photocatalyst. Superoxide radical anion ($O_2^{-\bullet}$) can be formed due to interaction of the oxygen adsorbed at catalytic sites and photogenerated electron, while hydroxyl radicals ($^{\bullet}OH$) can be formed at the surface of TiO_2 photocatalyst due to the interaction of holes and adsorbed hydroxyl groups.[21–23] Hydroxyl radical is a strong and non-selective oxidizing

species, which can decompose organic contaminants into CO_2, H_2O and other mineral species (i.e., a process known as mineralization).

Since the pioneering discovery of the photocatalytic properties of TiO_2[24] and the demonstration of its effectiveness to generate hydroxyl radicals when illuminated by UV light along with its environmentally benign properties (i.e., non-toxicity, absence of dissolution in water, photostability), and relatively low cost, TiO_2 photocatalyst has been considered a key material in the destruction of recalcitrant organic pollutants in water,[21,25] as well as for killing pathogenic microorganisms.[26] TiO_2 photocatalysis, one of the so-called advanced oxidation technologies/processes (AOTs, AOPs) based on hydroxyl radicals, has been considered an emerging technology with great potential to completely destroy harmful non-biodegradable and biocidal organic contaminants in water.[21] More importantly, TiO_2 photocatalysis can utilize solar light, which is plentiful. As a result, the process has unique advantages over other catalytic technologies, especially for the elimination of toxic and bioresistant contaminants in water.[21,27]

Traditionally, two types of photocatalytic reactors were used in studies concerning water treatment. Those that utilize powder type TiO_2 photocatalysts in suspension and those that utilize film type TiO_2 photocatalysts immobilized on a support. Although characterized by larger catalytic surface area and absence of mass transfer limitations, systems with suspended TiO_2 nanocatalyst impose the requirement for filtering the effluent to remove TiO_2 particles of nanoscale dimensions.[28] This filtration process is tedious and costly. Furthermore, it requires several other unit operations and separation processes and does not guarantee complete removal of the ultrafine particles. Therefore, most current research activities are centered on the area of photocatalysis using immobilized catalyst.[1–12]

Considering the fact that TiO_2 photocatalytic film is the key component in immobilized-type photocatalytic reactors, it is especially important to design and synthesize high performance photocatalytic films with good long-term mechanical stability, which is a critical requirement in the development of large-scale photocatalytic reactors in large-scale industrial installations.

3. Sol-gel Method: A Promising Approach for the Synthesis of Immobilized TiO_2 Films

The term "sol-gel" refers to the first stage of material transformation from a "liquid-like" sol to a "solid-like" gel. Sol-gel preparation method is essentially a room temperature wet chemistry-based formation of solid inorganic materials from molecular precursors. Sol-gel processes for the synthesis of TiO_2 films involve a series of processing steps: (1) formulation of a sol containing either colloidal TiO_2 precursor or Ti $(OR)_4$ precursors;(2) aging and deposition of the

sol on appropriate supports; (3) evaporation of the solvent and other volatile compounds for gel formation and film solidification; (4) heat treatment for the pyrolysis of residual organics, densification of the film, and crystallization of the Ti-O-Ti inorganic network for obtaining the desired crystalline TiO_2 phase. A typical first step of the sol-gel process from the titanium alkoxide precursor can be illustrated as follows[29]:

$$Ti(OR)_4 + (2 + x)\ H_2O \longrightarrow TiO_2\ x\ H_2O \text{ (oxide nanoparticle)} + 4ROH$$

$Ti(OR)_4$ is titanium alkoxide and R is a short aliphatic group.

Compared with many preparation methods for the synthesis of immobilized TiO_2 films, such as chemical vapor deposition (CVD), impregnation, and thermal oxidation of Ti metal, the sol gel method has many unique advantages because it requires relatively simple process equipment[11] and it is suitable for coating the films on supports of various shapes. Moreover, in the formation of the films, sol-gel processes are flexible in adjusting various preparation conditions,[3,30] which is beneficial to the improvement in the physicochemical properties of the final TiO_2 films. The controllable preparation conditions in such a wet chemistry method include the type and concentration of precursor (i.e., $Ti(OR)_4$), pH, water content, solvent, size and type of templating agents, aging conditions, sintering temperature, and presence and size of solid particles in the sol.

4. Sol gel Synthesis of Immobilized TiO_2 Films for Water Purification

There are two important issues to be addressed before immobilized TiO_2 films can be used in large-scale ultraviolet or solar-based photocatalytic reactors for water treatment applications. One is good photocatalytic activity; another is good and long-term mechanical stability. In order to prepare high performance immobilized TiO_2 films with long-term mechanical stability, it is important to understand what type of film properties could significantly affect their photocatalytic activity and long-term mechanical stability. Catalytic activity of TiO_2 photocatalysts can be measured by quantum yield,[22] which is determined by the charge transfer rate and the electron-hole recombination rate in both bulk and surface of TiO_2 photocatalyst.[22] It is well known that the anatase phase is, in general, the most desirable active crystalline phase for obtaining high photocatalytic activity.[21,22,27] In addition, many other film properties can also affect the photocatalytic activity of such films. These film properties mainly include the amount of crystalline materials immobilized on the support, film thickness, particle size, BET surface area, pore volume/porosity, pore structure, surface morphology (surface roughness), and surface chemical composition.[7,9] No matter what type of film property is improved, increase in photocatalytic activity is

essentially achieved by (1) increasing the number of "effective" electro-hole pairs on the surface of the photocatalyst,[21,22,31] which are generated after the photoexcitation event, and/or (2) improving adsorption and/or mass transfer of the treated contaminants on the active sizes.[8,32] On the other hand, the long-term mechanical stability of sol gel derived TiO_2 films is determined by film hardness and adhesion, which have been proven to greatly depend on the heat treatment temperature during calcination.[7,33] In addition, good structural integrity is desirable for maintaining film mechanical robustness. As a consequence, improving the above film properties has become an important strategy for the preparation of highly active TiO_2 film with good long-term mechanical stability. Many efforts have been devoted to the sol gel synthesis of TiO_2 films with improved film properties for water treatment.[2–12,34] From one prospective, the current sol gel methods can be categorized as "conventional sol gel methods without the use of template" and "template-associated sol gel methods." Sol gel methods often involve the use of relatively high heat treatment temperatures during film calcination[7,35] to eliminate organic solvents and precursors, crystallize the coated gel to the desirable crystal form, and form strong chemical bonds between the film and the substrate for good adhesion.[7,33] As a result, the TiO_2 films prepared by conventional sol gel methods often present low catalyst activity due to several reasons induced by the high calcination temperature, such as low BET surface area, low porosity, and smaller than optimum pore size.[5] Considering the fact that template-associated sol gel methods can overcome the above shortcomings due to the formation of tailor designed crystalline frameworks with high BET surface area and optimum pore structure formed after the decomposition of the supramolecular template at higher calcination temperatures,[35] template-associated sol gel methods are in general considered more promising technologies among the sol gel methods associated with an afterwards heat treatment process.

Based on the scientific and technological importance on the sol gel synthesis of robust nanostructured TiO_2 photocatalytic films for the development of efficient water purification systems for advanced life support in long-duration space missions of NASA as well as in long-term terrestrial applications, during the last few years, we have developed various novel sol gel methods to synthesize nanostructured TiO_2 films and membranes, so as to develop highly efficient reactors and membrane systems for water purification. The supramolecular templates we have employed mainly included polymers (i.e., polyethylene glycol) and surfactants (i.e., Tween 20), which are also considered to be two types of popular pore directing agents in the sol gel synthesis of porous TiO_2 films by other researchers.[11,29,36] Based on the research results in our group, using surfactant Tween series as templates can present some unique advantages on the synthesis of TiO_2 films[4,37] and TiO_2 membranes[4,38,39] because Tween surfactants

have the following properties: (1) they are environmentally friendly, (2) they are highly viscous, which is beneficial to the improvement in film thickness, and (3) they can induce the formation of mesoporous film structure with high BET surface area (i.e., above 100 m^2/g). However, our research results also demonstrated that the photocatalytic activities of porous TiO_2 films synthesized by template associated sol gel methods may not be optimum because of some problems, such as (i) relatively small amount of crystalline material at each dip coating cycle, (ii) poor UV absorbance due to small film thickness and (iii) possible mass transfer limitations between the treated contaminants and active sites in the inner layers due to non-optimized pore structure.[40] On the other hand, former research results showed that incorporating highly active Degussa P25 nanoparticles into alkoxide precursor sol (without templates) could improve film thickness/film weight and obtain good mechanical stability of the films.[6,9,41] However, our research results show that increasing P25 loading can lead to crack formation,[9] which in fact has a detrimental effect on the long-term mechanical stability of the films. Enlightened by the advantages of both template-associated sol gel methods and P25 powder modified sol gel methods, we have recently developed promising template-assisted Degussa P25 TiO_2 powder modified sol gel methods. Such approaches are the combined sol gel processes using Degussa P25 nanoparticles as fillers with a relatively low loading (i.e., 10 g/l in the sol), which is beneficial to the improvement in film thickness and avoid crack formation in the films, and using environmental friendly templates such as polyethylene glycol (PEG 2000) or polyoxyethylene (20) sorbitan monolaurate (Tween 20) as pore directing agent. Moreover, by employing such nanotechnological template-associated sol gel methods, P25 associated larger pores (i.e., macropores or larger mesopores) can be formed, which is beneficial to the increase of mass transfer of the treated contaminants in the larger pore channels. As a result, the enhancement in photocatalytic activity induced by low loading P25 is high. By using these methods, almost all physicochemical properties of the films can be improved, which is beneficial for improving the photocatalytic activity and long-term mechanical stability of the films. After optimizing the preparation conditions (i.e., calcination temperature and template loading), the final TiO_2 films possess high BET surface area, large pore volume, bimodal pore size distribution, enhanced film thickness, good UV light utilization, large amount of crystalline materials (enhanced number of active sites) on the support by one dip coating cycle, robust crystal structure, good structural integrity, and good adhesion on the substrate. Our research results proved that the final films exhibit high photocatalytic activity in the degradation of model organic contaminants such as 4-chlorobenzoic acid (4-CBA) and creatinine in water.[8,40] Therefore, the as-prepared "thick" films have great potential to be used for the development of large-scale photocatalytic reactors for water purification.

5. Summary and Future Directions

Based on the above analysis and discussion, it can be concluded that combined sol gel synthesis route associated with the coupling of nanoparticles as filler and a template as a pore directing agent seems to be a promising approach for the synthesis of high performance TiO_2 films for water purification because almost all film properties can be simultaneously improved, which is beneficial to achieve significant improvement in photocatalytic activity and enhancement in mechanical stability of the films. On the other hand, considering that surfactant self-assembling sol gel methods (without P25 nanoparticles) can provide an effective way to synthesize TiO_2 films with periodic surface structures,[42] which allows the orientation of the treated chemical molecules in the pores to improve photocatalytic activity and selectivity,[42] surfactant self-assembling sol gel methods are still considered to be an important approach especially for the synthesis of porous TiO_2 films/TiO_2 membranes with high selectivity and/or high permeability. Our research work showed that the as-prepared porous TiO_2 films with increased photocatalytic activity, good structural integrity and adhesion have great potential to be used for the fabrication of tubular reactors with UV (254 nm) radiation (mainly) for the continuous-mode purification and disinfection of wastewater in space and terrestrial applications. In such continuous-mode tubular reactors, destruction of organic contaminants and breakdown of microbial debris can be achieved by both TiO_2-photocatalysis (UV, 254 nm) and UV (254 nm) radiation (photolysis). In addition, although many studies on sol gel synthesis of high performance TiO_2 membranes are still underway in our group, the photocatalytic membranes with excellent multifunctional properties are believed to have great potential to be used for larger integrated disinfection-photocatalytic-membrane reactors for the long-term continuous-mode disinfection, treatment and purification of wastewater contaminated with pathogenic microorganisms (i.e., *Escherichia coli*, *Cryptosporidium parvum*), organic contaminants (phenol, chlorinated aromatics, etc.), and other inorganic species (arsenic) as well as for wastewater from hand washing (i.e., containing surfactants) and human urine. Another issue is related to solar TiO_2 photocatalysis, which is somewhat limited due to the fact that the solar light contains only a small percentage of ultraviolet light with wavelength less than 380 nm (3–5%).[43] Therefore, sol gel synthesis of high performance TiO_2 films with visible light response is an important issue in the field of TiO_2 photocatalysis for water treatment. Such related studies are also underway in our group.

Acknowledgements

We appreciated financial support from the National Science Foundation (CAREER award to D. D. Dionysiou, BES 0448117) and the Office of Biological and

Physical Research of the National Aeronautics and Space Administration (NASA) (NRA Grant number: NAG 9-01475) to support our research studies on sol gel synthesis of nanostructured TiO_2 films and membranes for water purification.

References

1. B. -G. Julián, F. -I. Pilar and M. -R. Sixto. *J. Solar Energy Eng.*, 129, 4 (2007).
2. M. Langlet, S. Permpoon, D. Riassetto, G. Berthomé, E. Pernot and J. C. Joud. *J. Photochem. Photobiol. A: Chem*., 181, 203 (2006).
3. M. H. Habibi and M. N. Esfahani. *Dyes Pigments*, 75, 714 (2007).
4. H. Choi, E. Stathatos and D. D. Dionysiou. *Appl. Catal. B: Environ.*, 63, 60 (2006).
5. Y. J. Chen and D. D. Dionysiou. *Appl. Catal. B: Environ*., 69, 24 (2006).
6. G. Balasubramanian, D. D. Dionysiou, M. T. Suidan, I. Baudin and J.-M. Laîné. *Appl. Catal. B: Environ.*, 47, 73 (2004).
7. Y. J. Chen and D. D. Dionysiou. *J. Mol. Catal. A: Chem.*, 244, 73 (2006).
8. Y. J. Chen and D. D. Dionysiou. *Appl. Catal. A: General*, 317, 129 (2007).
9. Y. J. Chen and D. D. Dionysiou. *Appl. Catal. B: Environ.*, 62, 255 (2006).
10. M. G. Antoniou, U. Nambiar and D. D. Dionysiou. *Catal. Today*, 30, 215 (2007).
11. J. C. Yu, J. G. Yu and J. C. Zhao. *Appl. Catal. B: Environ.*, 36, 31 (2002).
12. M. -K. Yeo and M. Kang. *Water Res.*, 40, 1906 (2006).
13. http://www.choike.org/nuevo_eng/informes/730.html
14. J. F. Davis. *Wat. Environ. Res.*, 71, 1070 (1999).
15. U.S. EPA, Office of Ground Water and Drinking Water, MTBE in Drinking Water. http://www.epa.gov/safewater/mtbe.html (March 2001).
16. AWWA. Water Quality and Treatment, A Handbook of Community Water Supplies, 5th Edition, McGraw-Hill, New York.
17. D. Lince, L. R. Wilson and G. A. Carlson. *Bull Environ. Contamin. Toxicol.*, 61, 484 (1998).
18. U.S. EPA, Office of Ground Water and Drinking Water, MTBE in Drinking Water. http://www.epa.gov/safewater/mtbe.html (March 2001).
19. M. Berg, H. C. Tran, T. C. Nguyen, H. V. Pham, R. Schertenleib and W. Giger. *Environ. Sci. Technol.*, 35, 2621 (2001).
20. R. Nickson, J. McArthur, W. Burgess, K. M. Ahmed, Ravenscroft and M. Rahman. *Nature*, 365, 338 (1998).
21. M. R. Hoffmann, S. T. Martin, W. Choi and D. W. Bahnemann, *Chem. Rev.*, 95, 69 (1995).
22. A. L. Linsebigler, G. Q. Lu and J. T. Yates, *Chem. Rev.*, 95, 735 (1995).
23. D. F. Ollis, E. Pelizzetti and N. Serpone, *Environ. Sci. Technol.*, 25, 1522 (1991).
24. A. Fujishima and K. Honda, *Nature*, 238, 37 (1972).
25. R. Molinari, M. Mungari, E. Drioli, A. Di, V. Loddo, L. Palmisano and M. Schiavello. *Catal. Today*, 55, 71 (2000).
26. C. Wei, W. -Y. Lin, Z. Zainal, N. E Williams, K. Zhu, A. Kruzic, R. L. Smith and K. Rajeshwar. *Environ. Sci. Technol.*, 28, 934 (1994).
27. A. Fujishima, K. Hashimoto and T. Watanabe. TiO_2 Photocatalysis—Fundamentals and Applications, BKC, Tokyo, Japan (1999).
28. M. Bideau, B. Claudel, C. Dubien, L. Faure and H. Kazouan. *J. Photochem. Photobiol. A: Chem.*, 91, 137 (1995).

29. V. G. Kessler, G. I. Spijksma, G. A. Seisenbaeva, S. Håkansson, D. H. A. Blank and H. J. M. Bouwmeester. *J. Sol-Gel Sci. Tech.*, 40, 163 (2006).
30. G. J. Soler-Illia, C. Sanchez, B. Lebeau and J. Patarin. *Chem. Rev.*, 102, 4093 (2002).
31. I. Parkin and R. G. Palgrave. *J. Mater. Chem.*, 15, 1689 (2005).
32. X. C. Wang, J. C. Yu, C. M. Ho, Y. D. Hou and X. Z. Fu. *Langmuir*, 21, 2552 (2005).
33. M. Keshmiri, M. Mohseni and T. Troczynski. *Appl. Catal. B: Environ.*, 53, 209 (2004).
34. B. Guo, Z. l. Liu, L. Hong and H. X. Jiang. *Surf. Coat. Technol.*, 198, 24 (2005).
35. K. H. Qi, W. A. Daoud, J. H. Xin, C. L. Mak, W. Tang and W. Cheung. *J. Mater. Chem.*, 16, 4567 (2006).
36. M. C. Fuertes and G. J. A. A. Soler-Illia. *Chem. Mater.*, 18, 2109 (2006).
37. Y. J. Chen, E. Stathatos and D. D. Dionysiou. *Surf. and Coatings Technol.* 2008 (in press). Corrected Proof. Available online 30 August 2007.
38. H. Choi, M. G. Antoniou, A. A. de la Cruz, E. Stathatos and D. D. Dionysiou. *Desalination*, 207, 395 (2007).
39. H. Choi, A. C. Sofranko and D. D. Dionysiou. *Adv. Func. Mater.*, 16, 1067 (2006).
40. Y. J. Chen and D. D. Dionysiou. *Appl. Catal. B: Environ.* 2008 (in press). Accepted manuscript. Available online 22 November 2007.
41. G. Balasubramanian, D. D. Dionysiou, M. T. Suidan, V. Subramanian, I. Baudin and J. -M. Laîné. *J. Mat. Sci.*, 38, 823 (2003).
42. D. G. Shchukin and D. V. Sviridov. *J. Photochem. Photobiol. C: Photochem. Rev.*, 7, 23 (2006).
43. A. Fujishima, X. T. Zhang and D. A. Tryk. Intern. *J. Hydrogen Energy*, 32, 2664 (2007).

APPLICATION OF GEL SYSTEMS WITH VARIOUS BIOCATALYSTS DETOXIFYING NEUROTOXIC AGENTS FOR POLLUTION CONTROL, WATER PURIFICATION, AND SELF-DEFENSE

ELENA EFREMENKO*, ILYA LYAGIN, OLGA SENKO,
DENIS GUDKOV, SEGEY VARFOLOMEYEV
The M.V. Lomonosov Moscow State University, Lenin's Hills, 1/3, 119991, Moscow, Russia

Abstract. The development and potential application of various biosystems based on enzymes and living cells of microorganisms, immobilized into gel-containing carriers and capable of detoxifying neurotoxic agents such as organophosphorous pesticides and chemical warfare agents as well as products of their destruction are discussed.

Keywords: Immobilized biocatalysts, organophosphorus hydrolase, polyhistidine sequence, organophosphorous pesticides, chemical warfare agents, poly(vinyl alcohol) cryogel, cross-linked sulphate chitosan gel, polyacrylamide cryogel.

1. Introduction

The organophosphorous pesticides are extensively applied in agriculture despite their mammalian neurotoxicity. The world market analysts gave the following prognosis: the e turnover of the market sector will grow per 11.7% annually and reach the $210 billion up to 2007 year. The abundant application of organophosphate compounds (OPC) along with their low water solubility results in the accumulation of the compounds in soil, ground and river waters. All OPC possess acute or delayed neurotoxicity, but the cumulative mutagenic effect of low OPC quantities appeared to be even more dangerous than neurotoxic one. The comprehension of real OPC threat for human health starts to be absolutely clear when someone take into account that OPC penetrate into the human body

*To whom correspondence should be addressed: Elena Efremenko, Chemical Enzymology Department, Chemistry Faculty, The M.V. Moscow State University, Lenin's Hills, 1/3, Moscow, 119991, Russia

P. Innocenzi, Y. L. Zub and V. G. Kessler (eds.), *Sol-Gel Methods for Materials Processing*.

via skin, inhalation and with water and foods. Today, the costumers widely used the OPC as domestic insecticides to treat their farmlands, backyards and pets without appropriate control compose the largest group of people who risk their health every day.[1] The diagnosis of cancerous or chronic diseases as result of OPC poisoning became reality of our days especially for those who participates in the production of pesticides or works in contact with OPC.[2,3]

According to Chemical Weapons Convention, 1,000 t of stored organophosphorous warfare agents (Vx, sarin, soman) should be destroyed in various countries during next several years. The technologies accepted for the destruction of chemical warfare agents (CWA) have various disadvantages (non-destructed residual amounts of toxic CWA, corrosive or flammable wastes, etc.) and all means enabling their elimination are of high scientific and practical importance.

Thus, the development of effective, user-friendly and economically appropriate biocatalytic systems that can prevent or reduce the threat of toxic influence of OPC used for the indoor and agricultural purposes as well as stored in depots is one of the main tasks of up-to-date biotechnology.

Organophosphorus hydrolase (OPH, EC 3.1.8.1) being a key enzyme in the detoxification of mentioned compounds catalyses the hydrolysis of a rather broad spectrum of OP neurotoxins and can be used for "Green solution" of the problem.[4]

The immobilization of OPH and whole cells containing OPH into gel systems appeared to be the most effective ways in the obtaining of biocatalysts with high catalytic activity, long shelf life and half-life time in the operating systems that could be used for pollution control, water purification, and self-defense. The examples illustrating this point of view are present in this review.

2. Gel Biocatalysts for Pollution Control in the Processes of Detoxification of Neurotoxic Organophosphorous Compounds

2.1. ENZYMATIC BIOCATALYSTS IN THE GEL-CONTAINING CARRIERS FOR CONTROL OF DETOXIFICATION OF NEUROTOXINES

The use of the enzyme as an active part of biosensors for discriminative OPC determination stimulates the development of its forms stabilized via immobilization in gel systems.[5,6] The attachment of OPH to various gel carriers (silica gel, poly(vinyl alcohol cryogel)) via multiple covalent bounds,[5,7] was successfully applied in the development of biocatalysts for detection of various OPC concentrations.

The direct control of efficiency of OPC detoxification was realized owing to combination of OPC hydrolysis with accumulation of hydrolytic products with acidic pH values. So, potentiometric analysis was accomplished by using a flow-through bioassay system with Corning glass pH-microelectrode.

Owing to immobilization, the stability of OPH in the solutions with acidic pH values was considerably higher as compared to its free form. The covalent immobilization of OPH[8] being a part of non-covalent complex, formed by enzyme with 1,5-dimethyl-1,5-diazaundecamethyene polymethobromide (polybrene), provided five-fold increase in stability of biocatalyst in 15% (v/v) ethanol solution as compared to soluble enzyme.[9] Immobilized biocatalyst, prepared with an addition of polybrene, retained a half of its initial activity in 50% (v/v) aqueous ethanol solution, 90% of activity during 10 working cycles at pH 6.5–7.5, when the optimum of enzyme action was 8.0–9.0.

The discriminative detection of OPC in various mixtures with carbamates was demonstrated, when combined biosensor containing both immobilized OPH and acetylcholinesterase was used. The detection ranges of this integrated biosensor was 10^{-9} to 10^{-5} M for paraoxon or diisopropyl fluorophosphate. The elimination of organophosphorous neurotoxins from different multi-component inhibitor combinations via sample pretreatment with immobilized forms of OPH was shown to be possible. Since then, the inhibiting influence of non-OPC on the acetylcholinesterase could be separated and its true value might be determined by this approach.

2.2. TEST-SYSTEMS BASED ON APPLICATION OF LIVING CELLS

A biosensor for direct detection of OPC was developed using recombinant *Escherichia coli* cells with OPH activity, immobilized into cryogel of poly (vinyl alcohol).[10] The same potentiometric approach to determination of OPC concentrations as in case of immobilized OPH was utilized here. The linear detection range for paraoxon detection was 0.25–250 ppm (0.001–1 mM), the response times were 10 and 20 min in the batch and flow-through reactors, respectively. It was possible to use same sample of immobilized biocatalyst repetitively for 25 analyses with a 10 min intermediate washing of granules with cells, required for reestablishing starting conditions.

Recently, another one immobilized biocatalyst for the detection of various OPC was developed on the basis of *Photobacterium phosphoreum* cells. It is known, that photobacteria are commonly used test-biosystem allowing revealing of various types of ecological toxins.[11] However, their use in suspended state is limited by several disadvantages: low enough stability of biolumine-scent signal

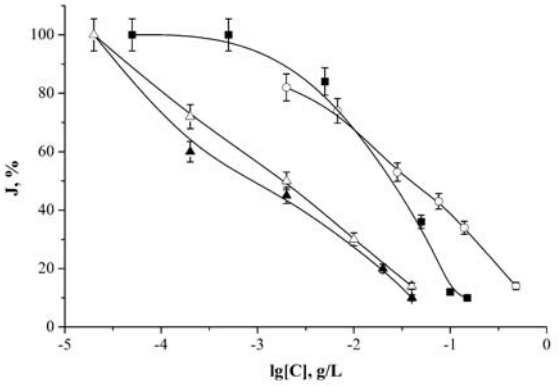

Figure 1. Decrease in bioluminescence of immobilized photobacteria under the inhibiting action of following organophosphorous compounds: ● – methylphosphonic acid, ▲ – malathion, ■ – coumaphos, △ – parathion.

at temperatures over 28°C, storage only in lyophilized form, etc. The cryogel of poly(vinyl alcohol) (PVA)[12] was used as a carrier for photo-bacteria in our work.

It was shown that immobilization of cells did not decrease the light emission and considerably stabilized the level of registered bioluminescence. The storage time of immobilized cells without reduction of initial level of luminescence was 1 month at –20°C and 6 month (as minimum) at –80°C. The concentrations of various compounds inhibiting bioluminescence of immobilized photobacteria were established (Figure 1).

The ranges of concentrations detected for various OPC by immobilized cells were following: 5–150 ppm coumaphos, 0.02–6 ppm parathion, 0.02–40 ppm malathion. The possible determination of concentrations of methylphosphonic acid (MPA) being product of hydrolysis of all known organophosphorous chemical warfare agents (scheme 1) was demonstrated for immobilized photobacteria for the first time. The range of detected concentrations for MPA was 2–500 ppm.

Thus, it was established, that it is possible to use the photobacteria immobilized into PVA cryogel for quantitative determination of neurotoxins.

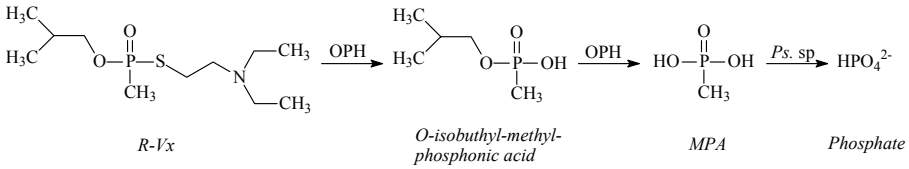

Scheme 1. Biological hydrolysis of R-Vx.

3. Biocatalysts Immobilized in Gel-Containing Carriers for Detoxification of Neurotoxic Organophosphorous Compounds

3.1. BIOCATALYSTS BASED ON IMMOBILIZED LIVING CELLS-PRODUCERS OF ENZYMES CATALYSING OPC HYDROLYSIS

Recently, a new line of enzymes decontaminating various toxins was developed by Genencor Int. in partnership with U.S. Army's Edgewood Chemical Biological Center (Table 1). Genencor plans to spread these new products selling them to military and civilian fire departments and hazardous material team as well as to apply the products for the bioremediation of industrial and agricultural waste sites. The stabilized enzymatic preparations with general name DEFENZ can be used in immobilized state being introduced into the content of the fire foam.[13]

TABLE 1. Commercial products for OPC destruction.

Company/product	Objects for treatment	References
Genencor Int.		
DEFENZ^{TM} 120 BG	Flat surfaces,	www.genencor.com
DEFENZ^{TM} 130 BG	ground	
Reactive Surfaces, Ltd.	Paints,	www.reactivesurfaces.com
OPDtox^{TM}	coatings	

Another one commercial product (OPDtox^{TM}) for OPC detoxification was developed by Reactive Surfaces, Ltd. as an additive for various environmentally friendly paints and latex coatings. This additive contains a dried whole-cell powder of *E. coli* DH5α cells with OPH activity.[14]

Thus, the commercial immobilized biocatalysts based on enzyme and whole cells with detoxifying activity against neurotoxic organophosphorous compounds are already known. Nevertheless, new variants of effective biocatalysts for OPC destruction are continued to be developed.

It was established that immobilization of whole cells capable of degrading OPC into porous structure of poly(vinyl alcohol) cryogel guaranteed the simple biotechnological procedure and a high viability of entrapped cells during their long-term use for OPC detoxification[15,16] as well as long-term storage.

3.2. BIOCATALYSTS BASED ON IMMOBILIZED ENZYMES WITH ACTIVITY OF ORGANOPHOSPHORUS HYDROLASE

To develop effective biocatalysts with OPH-activity suitable for flow systems, various approaches to enzyme immobilization have been applied.[5,15] The use of

various amino acid sequences genetically introduced into OPH structure as ligands for enzyme immobilization appeared to be advanced and very effective method for biocatalyst production.[15] The use of specific amino acid sequences allowed to combine the isolation, purification and immobilization of the target protein in one step.[17]

Macroporous hydrogel, so called cryogel produced by cross-linking radical polymerization of acrylamide[18] and modified by metal-chelating ligands charged by divalent metal ions, was used as a carrier. Polymer structuring or polymerization of monomers at sub-zero temperatures results in the formation of cryogels in solidified state. The freezing of the solutions of polymers or monomers with the addition of cross-linking agents allows to synthesize the monolith with three-dimensional structure containing numerous pores of 10–100 μm size. At the same time the carrier is the integral monolith allowing to get a notable decrease in diffusional limitations when it is used in a column reactor. The large size of pores allows for liquid to flow through the cryogel monolith with high enough flow rates while sizeable pore surface provides a sufficient area for its modification by metal-chelating ligands and further effective enzyme immobilization.[17] The large size of pores in the cryogel structure enables the use of cell extracts containing the target proteins for their direct loading onto the carrier without additional purification steps and with no risk of blocking the pores by cell debris.

New immobilized biocatalysts based on polypeptides containing polyhistidine (polyHis-) sequences at the N- or C-terminus of protein molecules and possessing activity of organophosphorus hydrolase were developed[19] and investigated for detoxification of organophosphorous neurotoxic compounds in the flow systems.[15,20,21,22]

The catalytic characteristics of the biocatalysts (catalytic constants, temperature and pH-optima) were very similar to each other, independently on genetic modification of OPH used for their production. The biocatalysts had high enough usage and storage stability. It was established that tried biocatalysts could be multiply regenerated by elution of inactive enzyme from the carrier with chelating agent and repeatedly loaded by active polyHis-tagged OPH. It was possible to carry out 10–15 reloading procedure.

The influence of the carrier composition on the catalytic characteristics of the immobilized biocatalysts was studied. Modification of the carrier was carried out via variations of co-monomer groups (allyl glycidyl ether) containing residue of iminodiacetic acid. The increase in ether portion guaranteed increase in amount of polyHis-tagged OPH bonded with the carrier (Figure 2). At the same time, there was no significant difference in the catalytic characteristics between biocatalysts based on carriers with different chemical content (Figure 3).

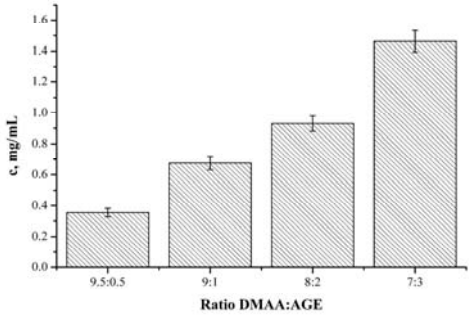

Figure 2. Influence of the monomer composition on the protein concentration immobilized onto the carrier. DMAA – *N,N'*-dimethyl-acrylamide, AGE – allyl glycidyl ether.

It was shown that some samples of gel-based biocatalysts could be dryed-reswollen with more than 90%-retaining of initial enzyme activity. These biocatalysts with immobilized OPH derivatives were successfully tried for OPC detoxification in the flow water systems. It was revealed, that volume of samples of immobilized biocatalysts can be varied from 5 up to 50 ml with retention of all catalytic characteristics. The regular velocity of flow of OPC solutions passed through the samples of immobilized biocatalysts was close to 120 ml/h.

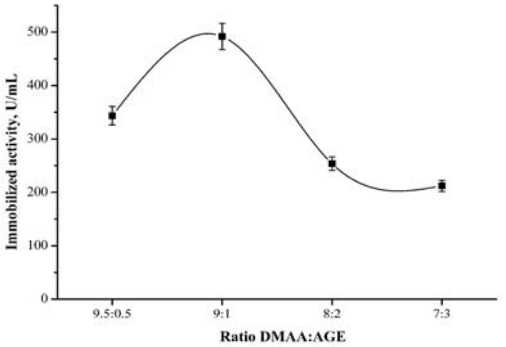

Figure 3. The dependence of specific activity of immobilized biocatalyst with His_6-OPH on the monomer composition: DMAA – *N,N'*-dimethyl-acrylamide, AGE – allyl glycidyl ether.

3.3. CELLS OF MICROORGANISMS IMMOBILIZED INTO CRYOGEL OF POLY(VINYL ALCOGOL) FOR DESTRUCTION OF HYDROLYTIC PRODUCTS OF ORGANOPHOSPHOROUS NEUROTOXINS

The reactions of degradation of organophosphorous chemical warfare agents usually results in accumulation of certain neurotoxic ethers of MPA (O-isopropyl-methylphosphonate, O-isobutyl-methylphosphonate, O-pinacolyl-methylphosphonate).[23] The further destruction of MPA is a significant problem

since C-P bond possesses high resistance to chemical hydrolysis. The disruption of C-P bond present in the chemical structures of three main organo-phosphorous chemical warfare agents (Vx, sarin, soman) is considered as irreversible conversion of the substances (Scheme 1). Until the bond is not destructed it is possible to use the MPA as precursor for restored synthesis of the neurotoxins. It is know, that only microbial conversion of MPA is effective, since microbial cells needed in source of phosphorus in nutrition media could catalyze the disruption of C-P bond.

Recently, new cryogel PVA-immobilized biocatalyst was developed on the basis of *Pseudomonas sp.* capable of destructing MPA.[24] It was revealed, that immobilized cells did not need in long-term adaptation to the toxic substrates like MPA or its ethers.

The immobilized cells were characterized by considerably improved stability to high concentrations of MPA (up to 0.5 g/l) as compared to suspended bacterial cells. The multiple applications of immobilized cells *Pseudomonas sp.* in the process of MPA degradation was demonstrated (Figure 4). The velocity of MPA destruction under batch conditions was actually the same in several working cycles of immobilized biocatalyst (6.6 mg/l/h or 158 mg MPA per one working cycle).

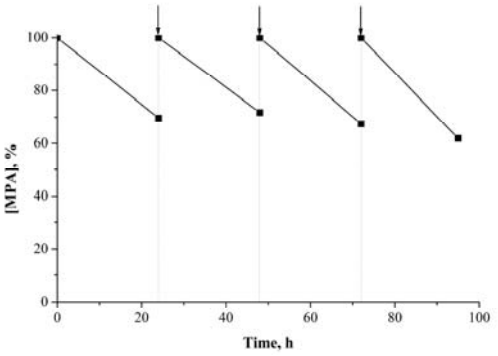

Figure 4. The degradation of methylphosphonic acid in cultural medium during multiple use of immobilized biocatalyst based on *Pseudomonas sp*. Arrows show the replacement of spent cultural medium by fresh one.

The possible reutilization of biocatalyst for MPA degradation was demonstrated (Table 2, Figure 5). To reveal that, the granules of immobilized biocatalyst used for 70 h in the process of MPA degradation were washed with tap water and thawed at 108°C for 20 min.

The obtained PVA solution contained residual concentrations of protein being a part of cell debris. The solution was used to form new portion of granules with immobilized cells. The analysis of mechanical and catalytic characteristics of fresh and reutilized biocatalysts revealed their similarity.

TABLE 2. Characteristics of initial and reutilized samples of immobilized biocatalyst based on *Pseudomonas sp.* cells and PVA cryogel.

Characteristics	Immobilized biocatalyst	
	Initial sample	Reutilized sample
ATP, mol/g biocatalyst	2.01×10^{-9}	1.01×10^{-9}
Protein, mg/g biocatalyst	2.0	4.3
Modulus of elasticity, kPa	65.3 ± 3.8	62.8 ± 4.1

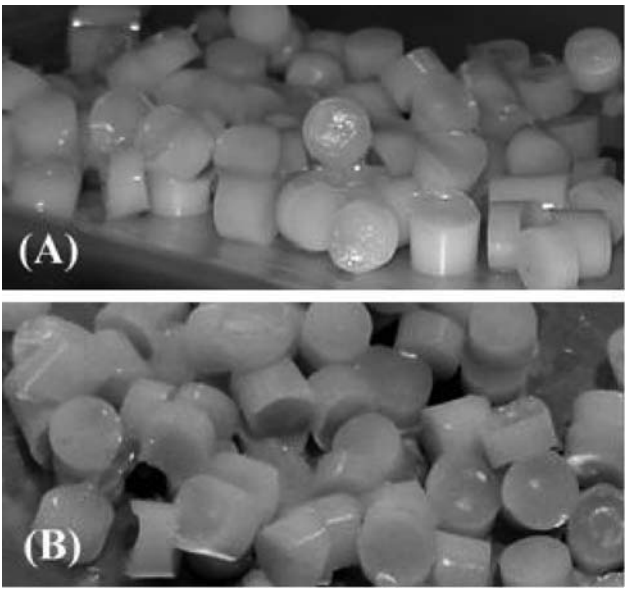

Figure 5. The view of granules of immobilized biocatalyst with *Pseudomonas sp.* cells, immobilized into PVA cryogel: A – initial sample, B – reutilized sample.

TABLE 3. Modulus of elasticity of granules of immobilized biocatalyst formed during the growth of filamentous *Aspergillus niger* cells.

Time (h)	0	24	48	72	96
Modulus of elasticity, kPa	56.5 ± 3.1	68.7 ± 5.3	79.6 ± 8.0	79.6 ± 8.0	78.6 ± 3.2

Another one biocatalyst was recently developed for the degradation of such a product of chlorpyrifos degradation as 3,5,6-trichloro-2-pyridinol (TCP). This compound possesses the toxic properties of both chloride- and organophosphorous compounds and should be destructed. The cells of filamentous

fungi *Aspergillus niger* entrapped into PVA cryogel appeared to be effective catalyst in their application for TCP biodegradation.

To obtain active immobilized biocatalyst, the fungus spores were initially immobilized into polymer structure. Then the granules were exposed in nutritional medium to germinate the spores and form active mycelium filling the inner free volume of porous PVA cryogel matrix. The process of formation of active biocatalyst was followed by control of mechanical characteristics of granules (Table 3). It was shown that filamentous fungus cells increased the solidity of biocatalyst granules and reinforced the polymer matrix.

The investigation of surface of biocatalyst granules with well-developed immobilized mycelium by SEM (Figure 6) confirmed that polymer matrix was completely penetrated by fungus cells. The prepared biocatalyst was successfully applied for degradation of TCP, obtained as a product of enzymatic hydrolysis of chlorpyrifos, and it was established that it can destruct 0.1 mM TCP per 24 h. The possible multiple use of the immobilized biocatalyst in the process of TCP degradation under batch conditions also was revealed in experiments.

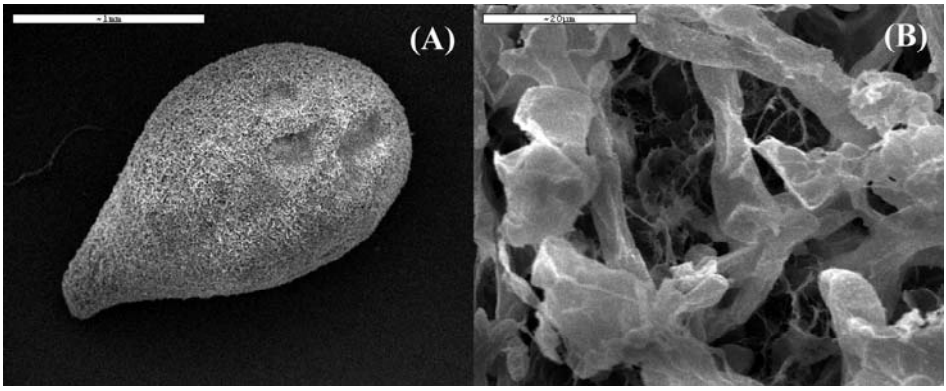

Figure 6. SEM of surface of biocatalyst granules with immobilized filamentous *A. niger* cells.

4. Biocatalytic Gel-Based Systems for Self-Defense

Enzyme His_6-OPH[25] was introduced into the gel system that was applied as a part of self-decontaminating defense material, containing three main layers, providing isolation of neurotoxic agents, detoxification the toxic compounds in case of their penetration into the inner parts of material and playing a role of hygienic barrier. Such complex material patented this year in Russia[26] allowed to considerably increase the defense degree against the CWA action and to get

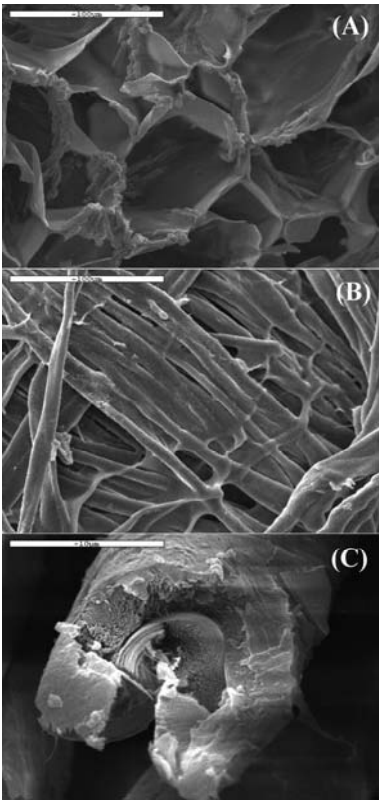

Figure 7. SEM of section of 7% sulphate chitosane gel highly cross-linked by glutaric aldehyde (A), coarse calico surface modified by sulphate chitosane gel composition (B) and section of cellulose fibers covered with protein-polymer composition (C).

as minimum 12-fold-prolongation of the material working time as compared to samples currently used in practice. It appeared that the catalytic system can be further activated by introduction of amines[27] into the sample of immobilized enzyme.

Immobilized biocatalyst based on OPH and porous fabric materials impregnated with chemically cross-linked sulphate gels was developed (Figure 7).

The fabric matrix possessed high sorption and water-retaining capacity, storage stability for at least 2 months and could effectively catalyze the hydrolysis of a wide spectrum of OPC. The immobilized enzymatic biocatalyst appeared to be very suitable form in the removal of OPC pollutions from various surfaces including skin.

Acknowledgements

Present results were partially supported by the Federal Agency of science and innovations of Russian Federation (Contract No. 02.515.11.5002).

References

1. Obendorf, S. K., Lemley, A. T., Hedge, A., Kline, A. A., Tan, K., Dokechayeva, T., Distribution of pesticides within homes in central New York state. *Arch. Environ. Con. Tox.*, 50, 31–44 (2006).
2. Alavanja, M. C., Hoppin, J. A., Kamel, F., Health effects of chronic pesticide exposure: cancer and neurotoxicity. *Annu. Rev. Public Health*, 25, 155–197 (2004).
3. Rothlein, J., Rohlman, D., Lasarev, M., Phillips, J., Muniz, J., McCauley, L., Organophosphate pesticide exposure and neurobehavioural performance in agricultural and nonagricultural hispanic workers. *Environ. Health Persp.*, 114, 691–696 (2006).
4. Efremenko, E., Sergeeva V., Organophosphate hydrolase – an enzyme catalyzing degradation of phosphorous-containing toxins and pesticides. *Rus. Chem. Bull., Int. Ed.*, 50, 1826–1832 (2001).
5. Efremenko, E. N., Lozinsky, V. I., Sergeeva, V. S., Plieva, F. M., Makhlis, T. A., Kazankkov, G. M., Gladilin, A. K., Varfolomeyev, S. D., Addition of polybrene improves stability of organophosphate hydrolase immobilized in poly(vinyl alcohol) cryogel carrier. *J. Biochem. Bioph. Meth.*, 51, 195–201 (2002).
6. Varfolomeyev, S., Kurochkin, I., Eremenko, A., Efremenko, E., Chemical and biological safety-biosensors and nanotechnological methods for the detection and monitoring of chemical and biological agents. *Pure Appl. Chem.*, 74, 2311–2316 (2002).
7. Simonian, A. L., Efremenko, E. N., Wild, J. R., Discriminative detection of neurotoxins in multi-component samples. *Anal. Chim. Acta*, 444, 179–186 (2001).
8. RU Patent 2,232,807, 2004, Recombinant plasmid DNA pTrcTE-OPH and producer of organophosphorus hydrolase.
9. Sergeeva, V. S., Efremenko, E. N., Kazankov, G. M., Gladilin, A. K., Varfolomeyev, S. D., Kinetic behavior of phosphotriesterase and its non-covalent complexes with polyelectrolyte in systems with polar and non-polar organic solvents. *Biotechnol. Tech.*, 13, 479–483 (1999).
10. Rainina, R. I., Efremenko, E. N., Varfolomeyev, S. D., Simonian, A. L., Wild, J. R., The development of a biosensor based on recombinant E.coli for the direct detection of organophosphorus neurotoxins. *Biosens. Bioelectron.*, 11, 991–1000 (1996).
11. Ribo, J. M., Kaiser, K. L. E., *Photobacterium phosphoreum* toxicity bioassay. I. Test procedures and applications. *Environ. Toxicol.*, 2, 305–323 (2006).
12. Lozinsky, V. I., Plieva, F. M., Poly(vinyl alcohol) cryogels employed as matrices for cell immobilization. 3. Overview of recent researches and developments. *Enzyme Microbiol. Technol.*, 23, 227–242 (1998).
13. Russell, A. J., Berberich, J. A., Drevon, G. F., Koepsel, R. R., Biomaterials for mediation of chemical and biological warfare agents. *Annu. Rev. Biomed. Eng.*, 5, 1–27 (2003).
14. McDaniel, C. S., McDaniel, J., Wales, M. E., Wild, J. R., Enzyme-based additives for paints and coatings.*Prog. Org. Coat.*, 55, 182–188 (2006).

15. Efremenko, E., Lyagin, I., Gudkov, D., Varfolomeyev, S., Immobilized biocatalysts for detoxification of neurotoxic organophosphorus compounds. *Biocatal. Biotransfor.*, 25, 359–364 (2007).
16. Efremenko, E. N., Tatarinova, N. Yu., The effect of long-term preservation of bacterial cells immobilized in poly(vinyl alcohol) cryogel on their viability and biosynthesis of target metabolites. *Microbiology*, 76, 336–341 (2007).
17. Efremenko, E., Votchitseva, Y., Plieva, F., Galaev, I., Mattiasson, B., Purification of His6-organophosphate hydrolase using monolithic supermacroporous polyacrylamide cryogels developed for immobilized metal affinity chromatography. *Appl. Microb. Biotech.*, 70, 558–563 (2006).
18. Lozinsky, V. I., Galaev, I. Yu., Plieva, F. M., Savina, I. N., Jungvid, H., Mattiasson, B., Polymeric cryogels as promising materials of biotechnological interest. *Trends Biotechol.*, 21, 445–451 (2003).
19. RU Patent Proposal 2,006,121,781, 2006, Method of immobilized biocatalyst production and the immobilized biocatalyst for detoxification of organophosphorus neurotoxic compounds in the flow systems.
20. Gudkov, D. A., Votchitseva, Yu. A., Efremenko, E. N., Hydrolysis of paraoxon catalyzed by organophosphorus hydrolase containing polyhistidine sequence at the C-terminus of protein molecule. *Moscow Univ. Chem. Bull.*, 61, 1–6 (2006).
21. Efremenko, E. N., Votchitseva, Yu. A., Aliev, T. K., Varfolomeyev, S. D., Expression of recombinant organophosphorus hydrolase in active form, in: *Biocatalytic technology and nanotechnology*, edited by G. E. Zaikov (Nova Science Publisher Inc, 2004), pp. 65–71.
22. Votchitseva, Yu. A., Efremenko, E. N., Aliev, T. K., Varfolomeyev, S. D., Properties of hexahistidine-tagged organophosphate hydrolase. *Biochemistry (Moscow*), 71, 167–172 (2006).
23. RU Patent 2,296,164, 2007, Method of the enzymohydrolysis of the organophosphorus combat poisonous substances.
24. RU Patent Proposal 2,007,136,007, 2007, Biocatalyst on the basis of immobilized cells of bacteria for degradation of methylphosphonic acid and its ethers.
25. RU Patent 2,255,975, 2005, Recombinant plasmid DNA pTES-His-OPH and producer of oligohistidine-containing organophosphate hydrolase.
26. RU Patent Proposal 2,007,102,061, 2007, Absorbing and self-decontaminating material as a mean for personal defense against the action of organophosphorous compounds.
27. Sergeeva, V. S., Efremenko, E. N., Kazankov, G. M., Varfolomeyev, S. D., Double effect of organic amines (activation and inhibition) on the phosphotriesterase. *J. Molec. Catal. B- Enzym.*, 10, 571–576 (2000).

DESIGN OF INORGANIC AND INORGANIC-ORGANIC HYBRID MATERIALS BY SOL-GEL PROCESSING – FROM NANOSTRUCTURES TO HIERARCHICAL NETWORKS

NICOLA HÜSING*
Inorganic Chemistry I, Ulm University,
Albert-Einstein-Allee 11, 89081 Ulm, Germany

Abstract. The preparation of porous hierarchical architectures that have structural features spanning from the nanometer to micrometer and even larger dimensions which in addition exhibit defined functionalities is one of today's challenges in materials chemistry. Sol-gel chemistry is a versatile tool for the formation of inorganic as well as inorganic-organic hybrid materials. Controlled hydrolysis and condensation reactions of (organo)alkoxysilanes allow the combination with organic entities and even their deliberate positioning in an inorganic network on the nanometer level. Moreover, not only the chemical composition, but also the structure of the final material is easily controlled on different length scales from the nanometer level up to the macroscopic morphology. In the present paper, opportunities from the application of novel diol-modified silanes are discussed for the synthesis of hierarchically organized inorganic, but also inorganic-organic porous monoliths. In addition, strategies for macroscopic shaping of hybrid materials with hierarchical porosity as well as exotemplating approaches are presented. In addition, strategies for macroscopic shaping of hybrid materials with hierarchical porosity as well as exotemplating approaches are presented.

Keywords: Mesostructured materials, aerogels, inorganic-organic hybrid materials, sol-gel processing.

* To whom correspondence should be addressed: Nicola Hüsing; e-mail: nicola.huesing@uni-uln.de

P. Innocenzi, Y. L. Zub and V. G. Kessler (eds.), *Sol-Gel Methods for Materials Processing*.

1. Porous Inorganic Materials

1.1. SOL-GEL PROCESSING AND A DELIBERATE DESIGN OF POROSITY

Despite the enormous progress in the synthesis of porous inorganic and inorganic-organic hybrid materials with control of pore sizes from Ångstrom to micrometers, the preparation of materials with simultaneous tailoring of morphology (monoliths, fibres, etc.) and pore structures on different length scales still remains a challenging task. Maximum control of the porous structure of oxidic materials can be obtained by combining different synthetic strategies such as templating approaches and sol-gel processing.

Discussing the different templating strategies that can be combined with hydrolysis and condensation reactions of alkoxysilanes (sol-gel processing), e.g. molecular templating is well known from the synthesis of the highly organized channel structures of zeolites.[1] In addition to single molecules as templates, also supramolecular arrays of molecules such as lyotropic phases of amphiphilic surfactants or block copolymers can be used as structure-directing agents in the presence of alkoxysilanes for a deliberate design of pore systems in the mesoscopic regime.[1–3] Other approaches utilize latex spheres for periodically arranged macropores,[4,5] microemulsion droplets,[6] or other macromolecules such as bacterial threads to name only a few of the possibilities.[7]

1.1.1. *Alkoxysilanes and Hierarchical Porosity*

There is a considerable interest in the manufacturing of porous materials that exhibit a bi- or even multi-modal pore size distribution. Such materials benefit from the combined advantages provided by the different pore size regimes: that is on one hand selectivity and large specific surface area from pores in the micro- and mesoscopic range. On the other hand, a high accessibility and rapid mass transport contributed from the macropores can be achieved. Sol-gel processing – thus, network formation via hydrolysis and condensation reactions of metal alkoxides – very often plays the key role in the synthesis of these porous materials since it provides an exceptional control over the composition and morphology of the final material by adjusting a large variety of parameters such as precursor concentration, pH-value, temperature, solvent, etc., to deliberately tailor the final network built-up and pore structure (from polymeric to particulate, large or small particles, etc.).

Different approaches have been published for the synthesis of hierarchically organized porous materials – not only based on silica, but also on hybrid inorganic-organic networks or even other metal oxides, carbon etc.[8–10] Chemical routes are often based on phase separation strategies in combination with sol-gel processing e.g. the preparation of monolithic materials for chromatography

purposes. Nakanishi and coworkers published a series of papers in which they reported the use of water-soluble organic polymers such as poly(ethylene oxide) (PEO), to control macroscopic phase separation parallel to the sol-gel transition.[8,9] Lindén and Nakanishi extended this approach by applying the macroscopic, (PEO) polymer-controlled phase separation of silica particles in combination with an ionic or non-ionic surfactant as structure-directing agent in the nanometer regime.[10] The material they obtained exhibited interconnected porosity on several length scales, for which the macropore diameter is controlled via PEO-nanoparticle interactions, and the mesopore diameter by the presence of the surfactant e.g. cetyltrimethylammonium bromide or a poly(ethylene oxide)-based polymer. A different approach was published by Lev et al.[11] Here, methyltrimethoxysilane was condensed in the presence of hydrogen peroxide resulting in a truly inorganic-organic hybrid material containing micro- and macropores and showing an excellent mechanical stability.

1.1.2. *Glycolated Silanes and Hierarchical Porosity*

The reaction of silanes with diols/polyols was already reported in the 1950s to 1960s, however, the hydrolytic instability of these compounds was considered as a big disadvantage for many applications in comparison to other commercially available precursors. Only at the end of the last century – in the nineties – polyol esters of silicates and siloxanes were identified as ideal precursor candidates in the synthesis of functional silica-based materials for several reasons, e.g. biocompatibility, fast autohydrolysis, compatibility with LC surfactant phases, etc.[12,13]

Since then several groups started to use diol/polyol modified silanes for various applications, e.g. Brook and Brennan described the use of diglyceryl-silane as well as sugar-and polysaccharide-derived silanes as precursors for silica monoliths with reduced shrinkage levels during drying and as biocompatible precursors for the entrapment of enzymes into sol-gel derived silica,[14] Shchipunov applied tetrakis(2-hydroxyethyl)orthosilicate as water soluble precursor in sol-gel processes[15] and our group reported the use of tetrakis(2-hydroxyethyl)orthosilicate and its glycerol- and 1,2-propanediol derivatives in the synthesis of porous monoliths with hierarchical network architecture.[16] Figure 1 shows some of the diol/polyol precursor molecules that have been applied by the different groups. However, one should keep in mind that the schematic drawing does not represent truly isolated molecular structures, but gives only an indication of the molar composition (silicon to diol/polyol). In most cases, an equilibrium between bridging and chelating species is present and sometimes even hypervalent silicon species have been reported.

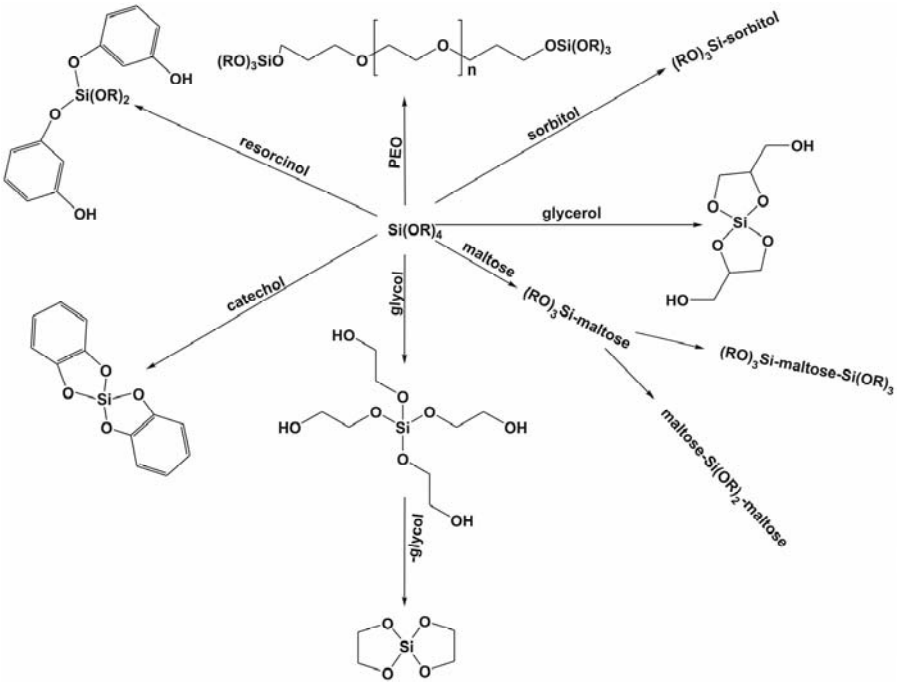

Figure 1. Schematic representation of diol- or polyol-modified silanes used in the syntheses of functional silica-based materials.[12–16]

Processing of these diol- or polyol-modified silanes in the presence of a structure-directing agent such as an amphiphilic block copolymer (as shown in Figure 2) result in the formation of a monolithic body. The network exhibits a bi-modal pore size distribution with macropores between 500 nm up to 2 mm and periodically arranged mesopores of about 7 nm.

1.2. POROUS HYBRID MATERIALS FROM GLYCOLATED SILANES

For silica based systems, the inner surface of the meso- and macroporous hosts contains pendant silanol groups that are unfavorable for many applications but at the same time enable easy modification of the surface properties. The challenge in modifying porous silica-based materials by organic groups is to improve the spectrum of properties without deteriorating the existing positive property profile, e.g. the porosity, the periodic ordering, large surface area, etc. Several pathways have been reported for the functionalization of porous silica-based systems: *Postfunctionalization* of a preformed calcined porous host via adsorption from the gas or liquid phase or *in-situ modification* directly during the synthesis by co-condensation of different silanes, respectively.

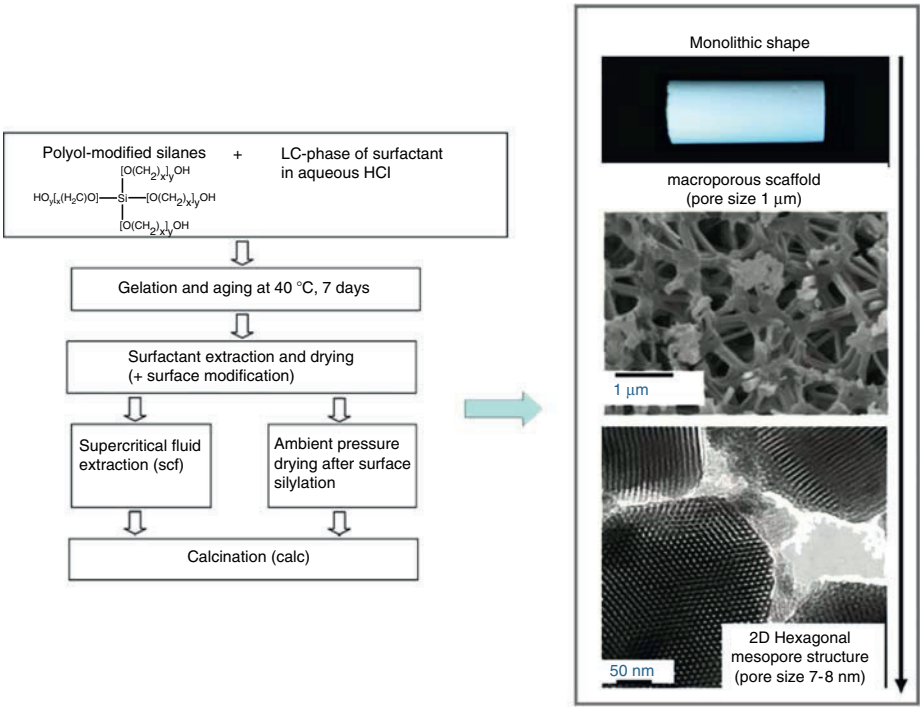

Figure 2. General scheme for templating of a preformed lyotropic liquid crystalline surfactant phase with a diol/polyol-modified silane precursor (left) and the hierarchically organized, porous silica-based monolith (right).

1.2.1. *Postsynthesis Treatment*

In principle, a postsynthesis treatment of a gel body can be performed prior or after drying of the gel. To minimize the processing steps, this type of modification is often done with the wet gel. This approach has previously also been published as an alternative approach to ease drying of monolithic gels without cracking and for extraction of surfactant phases from templated silica powders.[17,18] As the driving force for this reaction the replacement of electrostatic interactions at the inorganic-organic interface by covalent siloxane bonds, that is the formation of Si-O-SiR_3, was named. The same approach was used for the drying of large hierarchically organized wet silica gels (see Figure 2: typically these highly porous gels are dried supercritically (left path); surface silylation corresponds to the right path).[19] Upon treatment of the wet gel with trimethylchlorosilane in petroleum ether, a surface silylation occurs, completely reversing the surface polarity. The whole gel is turned from a hydrophilic, water containing system to a non-polar, hydrophobic one, thus resulting in an almost complete extraction of the non-ionic block copolymer (P123) that was used as a

structure directing agent. In addition, this process allows drying without any crack formation and with complete structural integrity of the network by simply heating the gels to 150°C. The surface chemistry of the gels can be deliberately tailored by this approach resulting in hydrophobic gels after drying (Figure 3). The most intriguing feature of this silylation procedure are a minimized number of processing steps along with a dramatic reduction of the time required for the production of these hierarchically organized monolithic gels drastically. Moreover, this very general approach can be applied to almost any functional organosilane that is available.

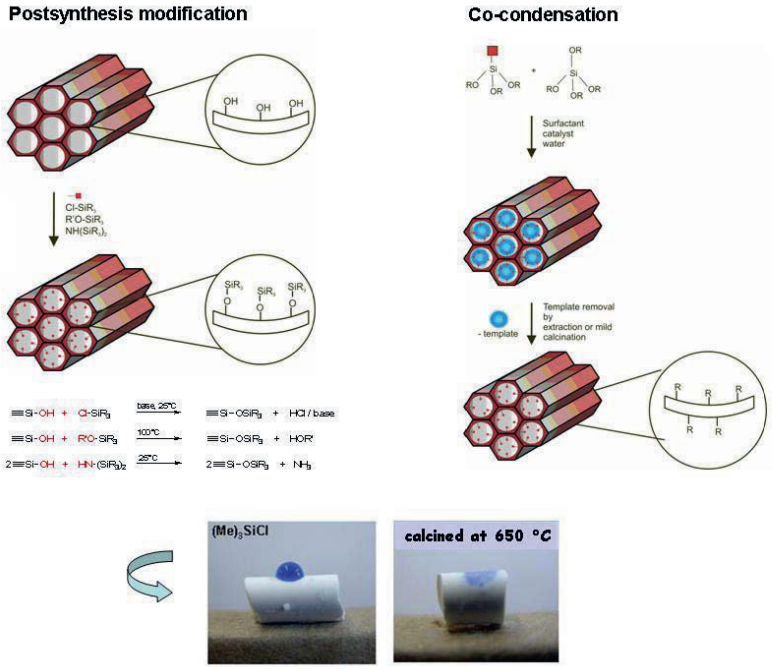

Figure 3. Schematic representation of the two different possibilities in the formation of hybrid porous materials (top); Hierarchically structured gels that were treated postsynthetically with trimethylchlorosilanes, thus inverting the polarity of the network to hydrophobic. Calcination at 650°C allows to change the polarity back to hydrophilic without structural changes (bottom).

1.2.2. *Co-condensation Approach*

An alternative approach towards hybrid inorganic-organic silica-based materials is based on the co-condensation between tetra- and organotrialkoxysilanes, the latter carrying an organic (functional) group connected via a hydrolytically stable silicon-carbon bond (a large variety of triethoxy- or trimethoxy- pre-cursor molecules is already commercially available). Many functional materials, e.g. as

coatings, have been prepared by just mixing these different silanes. However, it should be kept in mind that the structure of the final material is strongly influenced not only by the ratio of tetra- to trialkoxysilane, but also by the nature of the organo (functional) group and the relative reaction rates of the two precursors. By substituting the glycol-modified silane (e.g. tetrakis (2-hydroxyethyl)orthosilicate, EGMS) by glycol-modified organo(functional) silanes such as the methyl derivatives tris(2-hydroxyethoxy)methylsilane (MeGMS), organic groups can be introduced into the silica gel network.20 The major impact of the increasingly nonpolar starting composition on the structure of the final gel can be observed in the SEM images in Figure 4. Starting from a cellular network structure, the morphology of the structure is changed dramatically with increasing content of the methyl-substituted silane. The periodic ordering of the mesopores is maintained up to 30% substitution, however, higher concentrations of the methyl-modified silane result in disordered mesoporous networks.

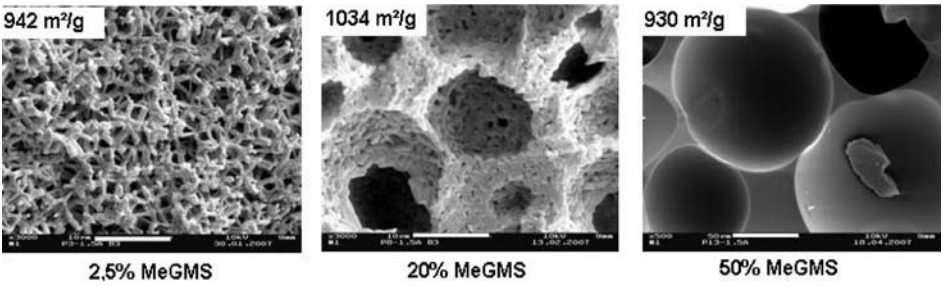

Figure 4. SEM images of MeGMS modified silica gels prepared via co-condensation. The amount of MeGMS is increased from left (2.5 mol% substitution) to right (50 mol% substitution). In the top left corner the corresponding specific surface areas (measured by N_2-sorption) are given. The scale bars correspond to 10 μm (left and middle image) and 50 μm (right image).

Only very few studies report on the formation of highly porous monoliths from pure silsesquioxanes e.g. methyltrialkoxysilanes.[21,22] This can probably led back to the lower degree of crosslinking that is expected when precursors are used with only three potential reaction sites (resulting in long gelation times) as well as the mechanical instability of the resulting gels due to the lower connectivity. In addition, phase separation phenomena of oligomeric or polymeric silsesquioxanes due to the polarity differences within the precursor molecule also can occur. As one of the most remarkable features of the modification of silanes with diols it was shown that tris(2-hydroxyethoxy)methylsilane and other organosilanes allow for the formation of gels of very low density composed of 100% methylsilsesquioxane (organosilsesquioxane) over a wide pH-range and even in a purely aqueous environment.

1.2.3. *Bridged Polysilsesquioxanes*

The use of bridged silsesquioxanes [$(R'O)_3Si–R–Si(OR')_3$ R'= $-CH_3$ or $-CH_2CH_3$] to synthesize periodic mesoporous organosilicas (PMO's) is an approach that has gained much attention in recent years.[23–26] The possibility to deliberately tailor framework and surface functionality on the molecular level of periodic mesoporous materials in addition to their unique features such as tunable pore size, narrow pore size distribution, high surface area, and controlled morphology, significantly increases their potential of application in e.g. catalysis, (bio-) immobilisation and separation, adsorption, sensing, and optoelectronics. Phenylene-bridged materials synthesized with cationic surfactants revealed molecular scale periodicity along the pore-channels with a lamellar scaffold of hydrophobic phenylene layers and hydrophilic silica layers, whereas the molecular scale ordering was very low when non-ionic surfactants were applied, and could only be observed by TEM.[27] However, all synthesis protocols reported so far describe only the fabrication of PMO powders or films, and not of monolithic materials, although the ability to mold porous materials into any desired shape and size increases their range of applications significantly. In particular the synthesis of monolithic materials with hierarchical pore structure is under extensive investigation, as the combination of different pore size regimes within one material leads to multiple benefits arising from each regime. Only recently, the first reports on monolithic organosilica materials with hierarchical architecture were published by us and Nakanishi.[28,29] Again, diol-modified pre-cursors allow for an easy access towards phase separated silica monoliths with a hierarchical build-up of highly ordered mesopores and interconnected, uniform macropores (Figure 5).

Starting from an ethylene glycol modified bridged silsesquioxane precursor molecule, 1,4-bis[tris-(2-hydroxyethoxy)silyl]benzene, which was obtained by simple transesterification reaction of the corresponding ethoxy-derivative with ethylene glycol in a molar ratio of 1:6, hydrolysis and condensation were induced by addition to a preformed lyotropic LC phase of P123 in aqueous hydrochloric acid (as depicted in Figure 2). Large, low density (0.240 g cm^{-1}) phenylene-bridged silica monoliths were obtained (Figure 5). Interestingly, this is the first report on stacking of the phenylene units to give semicrystalline pore walls in a mesostructured matrix that was templated by a non-ionic amphiphile. The macrostructure can easily be tuned by the ratio of the precursor compounds from a particulate network structure to a cellular one and the final material now shows four levels of hierarchy: monolithic structure (photograph), exhibiting an interconnected, uniform macroporous network (SEM image) built from particles or cellular strands, with a highly organized hexagonal mesopore system (TEM, SAXS) in addition to molecular scale periodicity of the phenylene groups in the pore wall.

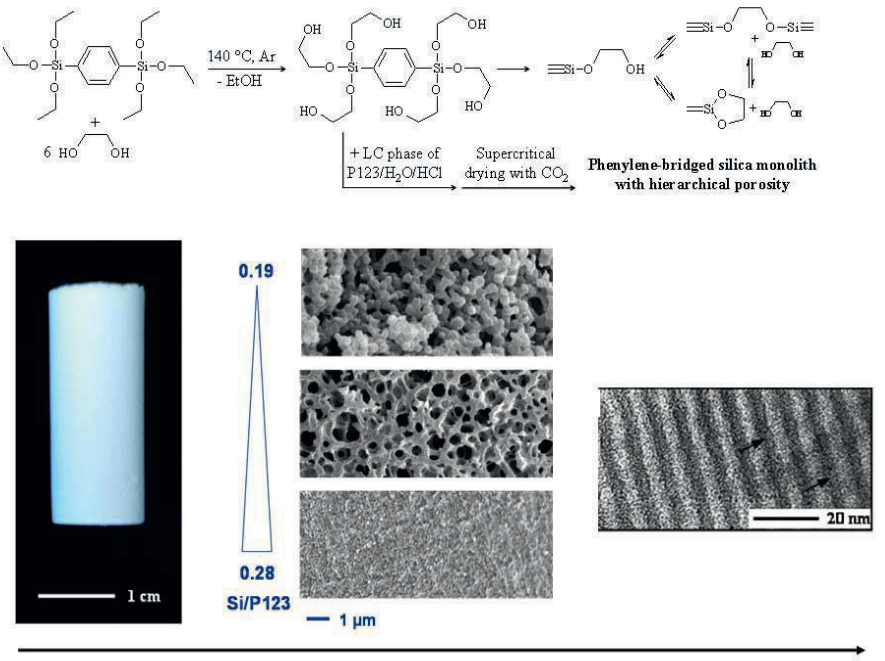

Figure 5. Synthesis scheme of a phenylene-bridged polysilsesquioxane material that exhibits hierarchy on multiple levels.

2. Macroscopic Shaping

For several applications it is desired to built-up more complex three-dimensional shapes and in principle, sol-gel processing is the ideal approach to do so. The liquid precursor solution can be casted due to its liquid nature in any desired mold and on the other hand a huge variety of organic molds is available that can be applied. The mold material has to fulfill two prerequisites: First it should be easily removable after sol-gel processing, second it should be possible to shape it in any desired form. For purely oxidic networks these requirements present no limit and it has been shown that shaping of various structures is possible. Only if inorganic-organic hybrid materials are prepared it becomes more difficult to remove the mold, since thermal degradation of the organic polymer can not be applied anymore without destruction of the organic functionalities in the network. For several applications it is strongly desirable to shape hybrid materials with a hierarchical porosity and therefore, alternative ways towards controlled molding into three-dimensional complex forms have to be developed.

One possibility lies in the development of photocurable resins, from organo-soluble polymers that (a) are stable in an aqueous environment, (b) can easily be processed in any desired form and (c) are soluble in organic solvents. As a possible route for shaping the polymer stereolithography is a useful tool. N, N-diisobutylacrylamide (DIBA) was used as a base monomer, because of its high reactivity and good mechanical properties of the homopolymer. Methacrylic acid anhydride was selected as suitable cross-linker for the polymer to avoid swelling of the polymer during the rapid prototyping process. Cleavage of the crosslinker and thus degradation of the polymer network during dissolution can be achieved using n-butylamine (NBA). By careful adjustment of the amount of base monomer, cross-linker, filler and photoinitiator cellular organosoluble 3D molds as shown in Figure 6 can be built.[30]

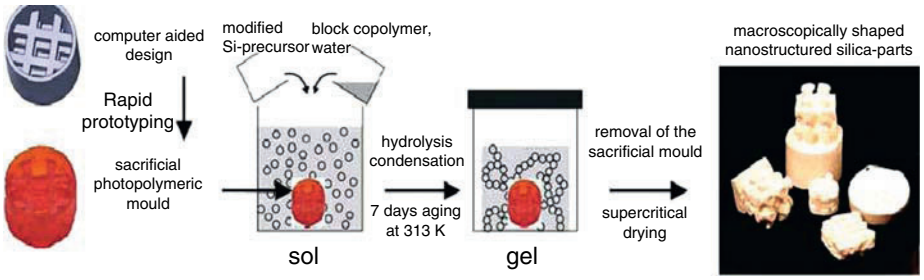

Figure 6. Casting of a hierarchically organized porous network in an organo-soluble mold.

Casting of the sol (see also Figure 2) into these molds, followed by subsequent condensation and gelation, allowed to obtain wet monolithic gels as the negative of the sacrificial organosoluble photopolymer. Prior to drying of the inorganic gel, the polymer can be dissolved in tetrahydrofuran/NBA within 30 minutes.[30] As the next step, drying can then be performed either via supercritical extraction or by surface silylation followed by thermal treatment. The structure in the dried silica gel is similar to the hierarchical network built-up that has been shown previously in Figure 2. Using sacrificial organosoluble photopolymers is a very attractive approach since it allows to combine more complex three-dimensionally shapes with hybrid inorganic-organic porous materials.

3. Chemical Transformation by Nanocasting

Synthesis pathways towards porous materials by sol-gel processing developed rapidly over the last 15 years. However, the wet-chemical synthesis protocols (sol-gel processing) are mainly useful for oxides, hybrid materials and only rare examples of other compositions can be found. With the increasingly better

control over pore structures and assemblies, another strategy towards mesoporous materials came up: nanocasting. This approach is especially useful for carbon-based materials, since porous carbons are not only very interesting for technical applications, but more difficult to obtain by liquid precursor-based route. Porous monoliths and periodically arranged mesoporous powders have been prepared from liquid precursors by sol-gel processing, but hierarchically organized materials have not yet been reported.[1] The nanocasting strategy is based on infiltration of a preformed mesoporous mold (the exotemplate) with a liquid precursor that can be polymerized in the mold material. With respect to the process it is very similar to that already depicted in Figure 6, however, here the structures to be replicated and infiltrated are interconnected channel systems in the nanoscopic regime.[1,31–35]

Hierarchically organized silica monoliths prepared from ethylene glycol-modified silanes are very interesting exotemplates, because they combine their porous structures with a monolithic shape. Infiltration of this structure with a furfuryl alcohol, oxalic acid and mesitylene mixture, followed by polymerization of the monomers to give an organic polymer resulted in a hierarchically organized inorganic-organic hybrid material. Subsequent carbonization at 900°C in inert gas atmosphere yielded the corresponding silica/carbon composite that was converted to pure carbon by treatment with hydrofluoric acid. This material is characterized by a hierarchical network built-up (Figure 7) and very high surface areas up to 1,800 m^2/g.

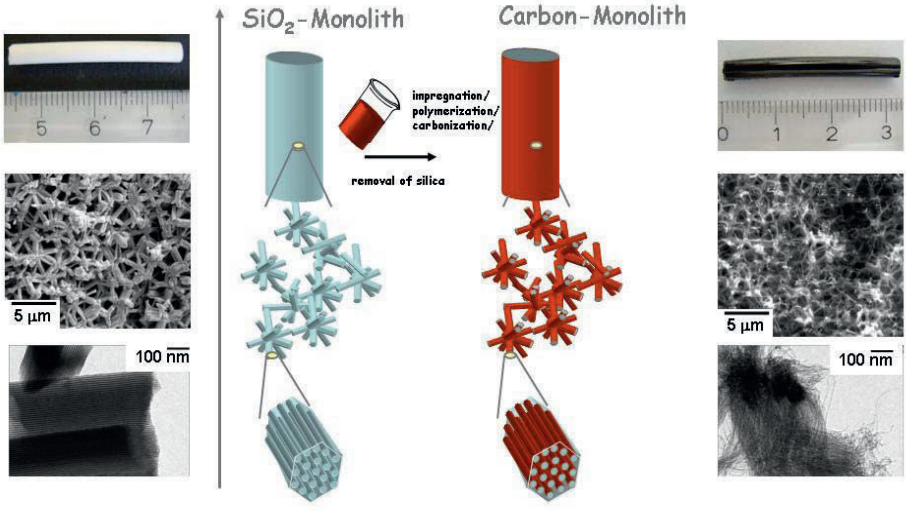

Figure 7. Schematic representation of the nanocasting approach towards carbon monoliths.

4. Conclusions and Future Perspectives

The greatest appeal but probably also the major challenge of sol-gel chemistry is the flexibility not only in the design of the final network structure and morphology, but also in the choice of the precursors. Already a simple variation of an alcoholic leaving group from ethanol to ethylene glycol opens completely new opportunities for the later materials properties and applications. Diol- and polyol-modified silanes have proven to be very attractive precursor candidates for the synthesis of silica gels, since they cannot only be processed in purely aqueous conditions without the need of an acid or base catalyst, but the diol released upon hydrolysis shows a higher compatibility with lyotropic LC phases of surfactants or amphiphilic block copolymers. Thereby, access to a large variety of novel hierarchically organized silica architectures is gained by performing the hydrolysis and condensation reactions in the presence of structure-directing amphiphiles. The few examples presented here give just a few glimpses of the changes for a deliberate materials design. For the systems described, the further development of the chemical modification of the pore walls as well as the possibilities of impregnation with functional moieties such as biological entities, e.g. proteins, living cells, etc., will broaden the potential applications of these hierarchically porous materials. The large variety of functional silanes in combination with the huge amount of different diols/polyols that are available allows for the formation of many different functional hybrid porous architectures. One of the biggest prospects of diol-modified organosilanes lies in the possibility to process them as the sole precursor in the formation of monolithic silsesquioxane gels in reasonable fast gelation times, thereby resulting in 100% substitution with organic moieties.

In addition to these advantages of sol-gel processing of glycol-modified silanes, the combination with other methods of preparations, e.g. processing in sacrificial organosoluble molds or application as exotemplates in nanocasting strategies even opens the way to completely different fascinating materials combining periodic nanostructures with several levels of hierarchy of almost any desired composition.

Especially with respect to applications in sensing, separation and even absorption of molecules, e.g. for soil remediation applications, these hierarchical matrices show a high potential. Nevertheless, much room is left for innovative preparation strategies to materials with an even higher level of organization and functionality.

References

1. F. Schüth, K.S.W. Sing, J. Weitkamp, *Handbook of Porous Solids*, (Wiley-VCH: Weinheim, Germany, 2001).
2. J.S. Beck, J.C. Vartuli, W.J. Roth, M.E. Leonowicz, C.T. Kresge, K.D. Schmitt, C.T.W. Chu, D.H. Olson, E.W. Sheppard, S.B. McCullen, J.B. Higgins, J.L. Schlenker, *J. Am. Chem. Soc.* 114, 10834–10843 (1992).
3. D. Zhao, J. Feng, Q. Huo, N. Melosh, G.H. Frederickson, B.F. Chmelka, G.D. Stucky, *Science* 279, 548–552 (1998).
4. B.T. Holland, C.F. Blanford, A. Stein, *Science* 281, 538–540 (1998).
5. S.H. Park, D. Qin, Y. Xia, *Adv. Mater.* 10, 1045–1048 (1998).
6. A. Imhof, D.J. Pine, *Nature* 389, 948–951 (1997).
7. S.A. Davis, S.L. Burkett, N.H. Mendelson, S. Mann, *Nature* 385, 420–423 (1997).
8. K. Nakanishi, *Bull Chem. Soc. Jpn.* 79, 673–691 (2006).
9. K. Nakanishi, *J. Porous Mater.* 4, 67–112 (1997).
10. J.H. Smått, S. Schunk, M. Lindén, *Chem. Mater.* 15, 2354–2361 (2003).
11. J. Gun, O. Lev, O. Regev, S. Pevzner, A. Kucernak, *J. Sol-Gel Sci. Technol.* 13, 189–193 (1998).
12. I. Gill, A. Ballesteros, *J. Am. Chem. Soc.* 120, 8587–8598 (1998).
13. K. Sattler, H. Hoffmann, *Progr. Colloid Polym. Sci.*, 112, 40–44 (1999); M. Meyer, A. Fischer, H. Hoffmann, *J. Phys. Chem. B* 106, 1528–1533 (2002).
14. M.A. Brook, Y. Chen, K. Guo, Z. Zhang, J.D. Brennan, *J. Mater. Chem.* 14, 1469–1479 (2004).
15. A. Mitra, T. Imae, Y.A. Shchipunov, *J. Sol-Gel Sci. Technol. 34*, 127–130 (2005).
16. N. Hüsing, C. Raab, V. Torma, A. Roig, H. Peterlik, *Chem. Mater.* 15, 2690–2692 (2003); D. Brandhuber, V. Torma, C. Raab, H. Peterlik, A. Kulak, N. Huesing, *Chem. Mater.* 17, 4262–4271 (2005); S. Hartmann, D. Brandhuber, N. Hüsing, *Acc. Chem. Res.* 40, 885–894 (2007).
17. D.M. Smith, G.W. Scherer, J.M. Anderson, *J. Non-Cryst. Solids* 188, 191–206 (1995).
18. V. Antochshuk, M. Jaroniec, *Chem. Mater.* 12, 2496–2501 (2000).
19. D. Brandhuber, N. Hüsing, H. Peterlik, *J. Mater. Chem.* 15, 3896–3902 (2005); N. Hüsing, C. Raab, V. Torma, D. Brandhuber, H. Peterlik, *J. Mater. Chem.* 15, 1801–1806 (2005).
20. D. Brandhuber, P. Kaiser, N. Hüsing, *J. Sol-Gel Sci. Technol.* 40, 131–139 (2006).
21. K. Nakanishi, K. Kanamori, *J. Mater. Chem.* 14, 3776–3786 (2005).
22. H. Dong, J.D. Brennan, J.D. *Chem. Mater.* 18, 4176–4182 (2006).
23. D.A. Loy, K.J. Shea, *Chem. Rev.* 95, 1431–1442 (1995).
24. B.J. Melde, B.T. Holland, C.F. Blanford, A. Stein, *Chem. Mater.* 11, 3302–3308 (1999).
25. S. Inagaki, S. Guan, Y. Fukushima, T. Ohsuna, O. Terasaki, *J. Am. Chem. Soc.* 121, 9611–9614 (1999).
26. T. Asefa, M.J. MacLachlan, N. Coobs, G.A. Ozin, *Nature* 402, 867–871 (1999).
27. S. Inagaki, S. Guan, T. Ohsuna, O. Terasaki, *Nature* 416, 304–307 (2002).
28. K. Nakanishi, Y. Kobayashi, T. Amatani, K. Hirao, T. Kodaira, *Chem. Mater.* 16, 3652–3658 (2004).
29. D. Brandhuber, H. Peterlik, N. Huesing, *Small* 2, 503–506 (2006).

30. R. Inführ, R. Liska, H. Lichtenegger, C. Fritscher, J. Stampfl, N. Huesing, *RadTech Europe 05: Conference Proceedings*, Vol. 2, pp. 489–494 (2005).
31. R. Ryoo, S.H. Joo, S. Jun, *J. Phys. Chem. B* 103, 7743–7746 (1999).
32. J. Lee, S. Yoon, T. Hyeon, S.M. Oh, K.B. Kim, *Chem. Commun.* 2177–2178 (1999).
33. J.H. Knox, B. Kaur, G.R. Millward, *J. Chromatogr.* 352, 3–25 (1986).
34. M. Kruk, M. Jaroniec, R. Ryoo, S.H. Joo, *J. Phys. Chem. B* 104 7960–7968 (2000).
35. S. Polartz, M. Antonietti, *Chem. Commun.* 2593–2604 (2002).

MESOPOROUS THIN FILMS: PROPERTIES AND APPLICATIONS

PLINIO INNOCENZI*, STEFANO COSTACURTA,
TONGJIT KIDCHOB, LUCA MALFATTI
Laboratorio di Scienza dei Materiali e Nanotecnologie,
Università di Sassari, Nanoworld Institute and CR-INSTM,
Palazzo del Pou Salit, Piazza Duomo 6, 07041 Alghero, Italy

PAOLO FALCARO
Associazione CIVEN – Nano Fabrication Facility,
Via delle Industrie 9, 30175 Marghera, Venezia, Italy

GALO SOLER-ILLIA
Gerencia de Quimica, CNEA, Av. Gral Paz 1499 B1650KNA,
San Martín, Buenos Aires, Argentina., CONICET,
Av. Rivadavia 1917, C1033AAV, Buenos Aires, Argentina

Abstract. Mesoporous films are a fine example of a self-assembled nanosystem, containing ordered porosity in the 2–50 nm range. A great number of characteristics, including framework nature (composition, crystallinity), high surface area, pore dimension, shape, surface, accessibility and pore array symmetry and interconnection can be tuned using green chemistry synthetic techniques. These materials present potentials in several fields where a large functional interfacial area contained in a robust framework is required. The capability of changing in a separate way the characteristics of the inorganic framework and the pore surface leads to an amazing potential in tuning functional properties, due to the combined properties of a thoroughly tailored pore system and the inherent features of thin films. These properties can be tailored to respond to changes in the environment, such as relative humidity, making mesoporous hybrid thin films an exciting prospect for several nanotechnology applications (e.g. sensors, actuators, separation devices). Here we present some basic concepts revolving around mesoporous films. We will first comment on the synthetic approach in the fabrication of these materials. Second, we will discuss the aspects regarding template organization and surface functionalization. Third, we will review some applications illustrating the potentialities of theses self-assembled nanomaterials.

* To whom correspondence should be addressed: Plinio Innocenzi; e-mail: plinio@uniss.it

P. Innocenzi, Y. L. Zub and V. G. Kessler (eds.), *Sol-Gel Methods for Materials Processing.*

Keywords: Mesoporous, thin-films, self-assembly, sol-gel.

1. Sol-Gel Chemistry, Self-Assembly and Mesoporous Thin Films

1.1. INTRODUCTION

Sol-gel processing is a low temperature synthesis route that is particularly suitable for the deposition of thin films from a liquid phase.[1] The high versatility of the technique has allowed a wide diffusion in different fields of applications and several products are now on the market.[2] The soft chemistry approach of sol-gel has known a renewed interest because of the recent boom of nano-science; sol-gel processing has emerged as one of the most interesting routes to bottom-up preparation of nanomaterials, nanoparticles and surface functionalization of nanostructures.

Two main different approaches to sol-gel nanochemistry can be envisaged. In the first one sol-gel reactions are used to obtain interconnected structures through polycondensation of the precursors, which is the typical bottom-up route for thin and ultra-thin film preparation. In the second one the final material is obtained through an intermediate step by using sol-gel chemistry for the synthesis of nano-objects, such as nanoparticles or nano-building blocks (NBBs).[3] Sol-gel chemistry can be, however, also combined with more sophisticated nanosynthesis techniques to get ordered and hierarchical structures. Controlled porosity in a material can be achieved, for instance, by templates that are removed after the preparation; templates of different dimensions can give hierarchical porous materials.[4] Porosity in the nano-scale is an important property of a material that should find its field of applications in nanotechnologies.

Micro- (<2 nm), meso- (2–50 nm) and macro-porosity (>50 nm)[5] can be used to entrap organic functional molecules, to create nanoreactors or as host for nanoparticles.[6] The properties of porous materials can be greatly enhanced if an organized and interconnected porous "structure" is obtained, in this case diffusion, adsorption and entrapping of functional molecules are favored and the material can reach a high level of sophistication. Mesoporous ordered materials are an important example of this type of nano-engineered materials whose synthesis is achieved through a combination of sol-gel and supramolecular chemistry.[7,8] The formation of an organized array of pores, whose topology, size and distribution is controlled by the processing parameters, is obtained through a self-assembly process. Amphiphilic molecules, such as ionic surfactants and block copolymers, are used to generate organic micelles that serve as the templates; removal of the micelles leaves ordered pores (Figure 1).

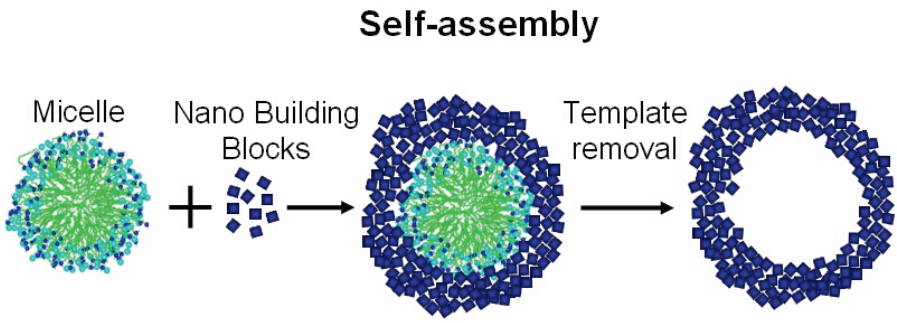

Figure 1. Schematic picture of the condensation of the nanobuilding blocks on the micelle surface.

The micelle formation and their organization is driven by solvent evaporation, and in the particular case of thin mesoporous films this process is specifically indicated as evaporation-induced self-assembly (EISA).[9,10] Even if several details of self-organization need to be studied, the overall process of self-assembly is quite well understood. The control of the kinetics of the different reactions and processes involved in EISA plays the main role. Several parallel processes are involved in EISA: film formation upon solvent removal, template-NBB self assembly and inorganic condensation. Controlling of the mutual interactions and kinetics is very important to avoid phase separation and to obtain an organized templated mesostructure. The variables that affect self-assembly are different from those used in the preparation of mesoporous pow-ders and monoliths, such as MCM-41, the first one to be synthesised by Mobil researchers.[11,12] Many parameters such as withdrawal rate, relative humidity and temperature in the deposition room, must be controlled very carefully. By this technique it is possible to fabricate different types of mesoporous ordered thin films, the most common are silica, transition metal oxides, hybrid inorganic-organic oxides, phosphates or carbon mesoporous films.

Due to their properties, mesoporous materials have found important applications in several emerging fields: the high specific surface area, composed of well-ordered tunable porosity within the 2–50 nm range, and the possibility to functionalize this large surface is an important feature of mesoporous organized thin films; they can be used for immobilizing guest molecules, such as biomolecules and functional organic molecules.[13–14] The pores can be also used as nano-reactors for the in situ growth of nanosized objects,[15,16] or as preferential adsorption sites in catalytic and sensing applications. The large number of publications and patents in different fields such as microelectronics, photonics, optoelectronics, electrochemistry and biosensing are witnessing the potentialities of these materials.

1.2. SELF-ASSEMBLY IN MESOPOROUS THIN FILMS

Self-assembly of mesoporous thin films could appear a quite simple process if we look only to the preparation protocol. A typical synthesis is based on sol containing an alkoxide or an inorganic salt as inorganic precursors, and a surfactant or an amphiphilic block copolymer as the structure-directing agent. Self-assembly is, however, achieved through a delicate balancing of the different processes: the polycondensation reactions of the precursors that will form the species condensing at the micelle surface, the micelle formation and the formation of a hybrid interface. Solvent evaporation pushes the micelle formation and their organization, leading to the formation of an organized array of templating micelles into a periodic mesophase. At the same time, the sol-gel reactions give rise to the formation of an interconnected network that contains the organic ordered mesophase. The organic template is then removed either by thermal decomposition or by chemical extraction, and leaves an ordered array of pores which reproduces the micelle arrangement in their size, shape and relative spatial location. Post-treatments on mesoporous films are used for chemically grafting of functional molecules or to enhance the stability of the film.[17]

The sol-gel chemistry plays its major role to form the chemical species that will self-assemble and finally condense on the micelle surface. A cluster of condensed species of nano-dimension, which is obtained by controlling the polycondensation of inorganic molecular precursors in mild temperature conditions is, in general, the product of the sol-gel synthesis.[18,19] The choice of the organic solvents, the pH and the amount of water directly affect the process. The choice of the pH value is a critical parameter because if the polycondensation reactions are too fast with respect to the micelle formation and assembly, the global self-organization process will fail. In silica-based systems, the pH is generally set near the isoelectric point ($pH_{iep} \approx 2$): in this way, the inorganic colloids in the solution do not aggregate and the solution can be stable even for several months. In general, both hydrolysis and condensation have to be controlled and optimised, to obtain small hydrophilic silica-derived nano-objects.[13] For transition-metal oxide precursors, hydrolysis and condensation are fast, and extended condensation is avoided only in highly acidic media, lower than $pH < 1$. In these conditions, using small hydrophilic clusters as NBBs results in good ordering.[20,21]

The "*race towards order*" gives organised structures only if the kinetic constants of the process are in this order:

$$k_{inter} > k_{org} > k_{inorg}$$

with k_{inter}, k_{org} and k_{inorg} the relative rates of interface formation, organic array assembly and inorganic polycondensation, respectively. The condensation of

the inorganic clusters must be slowed down enough, in order to avoid that an extended polycondensation before the appearance of an interface and formation of the micelles stop self-assembly.

The overall self-assembly process to obtain an organized mesoporous film is based therefore, on co-assembly of inorganic clusters to form an interconnected framework (the pore walls) with the template in an adequate balance of the different kinetics. An important point is that the framework and the template are in contact along the "hybrid interface", which in the case of a mesoporous material reaches as much as several hundreds of square meters per gram.[22] An important fraction of the energy towards stabilization of a mesostructured material arises from favorable interactions of NBBs at the hybrid interface. Figure 2 shows an ideal representation of the Evaporation-Induced Self-Assembly that is observed during the deposition of thin films via dip-coating. It should be underlined that self-assembly is also observed if the films are deposited via spin-coating, spraying or casting. In the dip-coating, the substrate is immersed and withdrawn from a precursor solution containing the alkoxide, water, the solvent, the catalyst and the surfactant at concentrations lower than critical

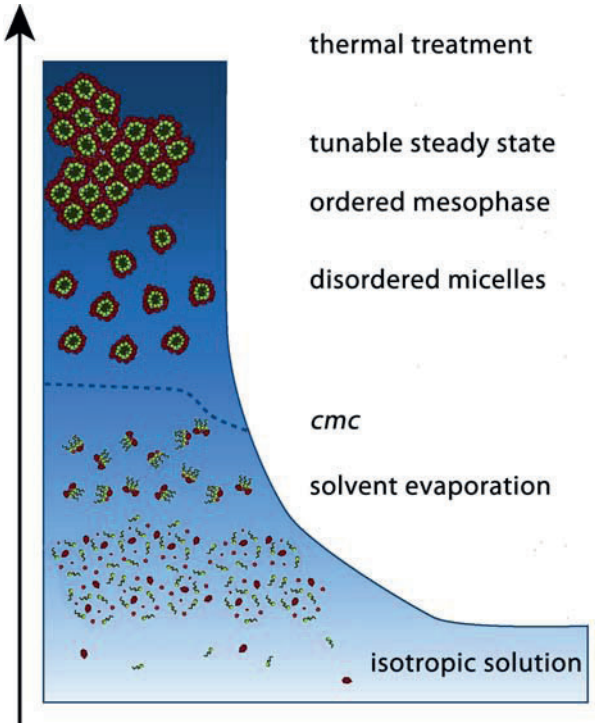

Figure 2. Self-assembly of mesoporous thin films during dip-coating.

micelle concentration, *cmc*.[23] Evaporation of the solvent (typically an alcohol such as ethanol) and water leaves a film that is enriched in nonvolatile species (inorganic and template). As soon as *cmc* is reached, the isolated surfactant molecules form disordered micelles within the film and in a second stage an ordered array. The organization of the micelles represents a templated order in the film, which can be disposed in several possible phases. Just as an example, several different ordered phases such as 2d-hexagonal,[24] cubic,[25] orthorhombic,[26] bicontinuous[27] and tetragonal[28] have been observed in silica films. A post-deposition thermal treatment is necessary to stabilize the structure, this is a delicate point because thermal induced shrinkage can change the mesophase (see Figure 3) and the pore shape, which typically shows an elliptical form upon shrinkage.[29]

Mesoporous thin films also exhibit a very peculiar property, *tunable steady state*, which can be defined as a particular metastable stage during which it is still possible to change the mesophase by intervention from the external environment.[30] The ordered arrays of the micelles is changed by variations of the relative humidity that induces a controlled swelling of the micelles. The ordered mesophase can be also disrupted and restored by X-rays, reversible order-disorder transitions have been observed in hafnia films.[31]

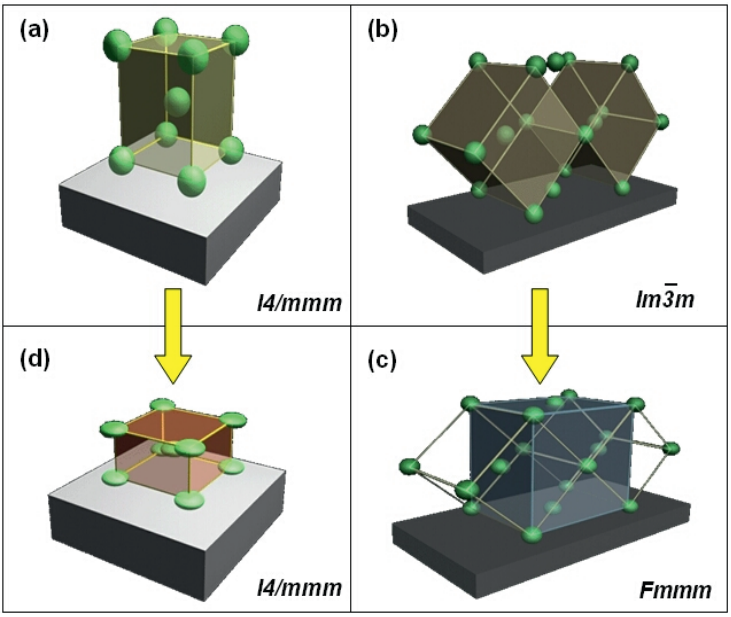

Figure 3. Changes in the mesophase induced by thermal shrinkage.

2. Morphology and Functionalization of the Pore Surface

2.1. ORDER-DISORDER IN MESOPOROUS FILMS

Another fascinating aspect of self-assembled mesoporous films is associated to order and disorder. As we have seen, the "race towards order" that governs the self-assembly process is driven by the solvent evaporation. The final material, after film deposition, is a system in which an ordered array of micelles is entrapped in an interconnected backbone. The consolidation of the framework and the removal of the template leave a porous ordered mesostructure, where the order is in the porous phase. The possibility to observe order in the pore walls, i.e. crystalline structures, depends on composition and processing conditions. Silica films give only amorphous pore walls; it seems impossible, at least at the moment, to obtain crystalline silica structures of any phase in the pore walls of mesoporous films. Other oxides, such as titania or hafnia, at the proper temperature of treatment form nano-crystals in the pore walls, in general, at temperatures that are low enough to avoid collapse of the mesostructure.[32,33] It should be underlined that in any case these mesoporous films show a surprising stability at high processing temperatures. Mixed oxide mesoporous films, such as perovskite have been also obtained, by using templates with enhanced solubility difference among their hydrophilic and hydrophobic regions.[34]

In mesoporous films we have, therefore, two possible degrees of order, one is correlated with the porosity and the other with the framework that forms the pore walls. The first case is represented by an ordered mesoporous film with amorphous pore wall, which is actually the case of silica or other oxides if the processing temperature is not high enough to produce a crystalline phase. The case of silica is, however, very intriguing and the reason why we could not yet be able to get an ordered phase with crystalline walls is challenging several researchers in the field.[35] The particular processing conditions that are used for self-assembly of silica films (the low pH) can produce, however, an intrinsic formation of middle range ordered nano-structures, such as four-fold and three-fold rings at least. This case has been well documented by several researcher and is an intermediate case of order-disorder in silica mesoporous films, the pores are ordered, the pore walls are amorphous but a medium range order (the silica rings) is observed. This is not just an "academic" classification because it has been demonstrated that the presence of silica rings in the pore walls strongly influences the mechanical properties, such as the elastic modulus.[36] The third case is represented by ordered porous films whose pore walls are crystalline. In this case nanocrystalline domains of different orientations form the material framework. The last case is also peculiar of mesoporous materials, even

if not yet reproduced in films, which is the formation of an ordered hybrid organic-inorganic structure in the backbone. This has been reported by Inagaki and coworkers for mesoporous powders and can be observed if the organically modified alkoxide precursor is a bridged silsesquioxane.[37]

2.2. MONOCRYSTALS – POLYCRYSTALS

The organization of the pores within a mesoporous films is achieved through self-assembly and the mesostructure that is formed is governed by the chemical-physical parameters of the process. We have seen that the concept of order is very important in mesoporous films and that several types of ordered nano-structures can be found. In general, the ordered arrays of micelles, or, after template removal, the ordered porous structures that are observed, can be described using crystallographic tools in terms of a "crystal-like" phase.

There is a good correspondence between the phases that can be indexed by small angle X-ray scattering (SAXS) and TEM and the crystalline structures of the phase group. The variation of the electronic density that is measured by SAXS allows indexing the mesostructure such as a crystalline-like phase. In general, detailed SAXS measurements in grazing and normal conditions determine that there is a polycrystalline distribution of mesoporous domains, which are well oriented along the substrate (i.e., the *z* direction), but present all possible orientations in the *x-y* plane (Figure 4). This feature is commonly known as *planar disorder*.

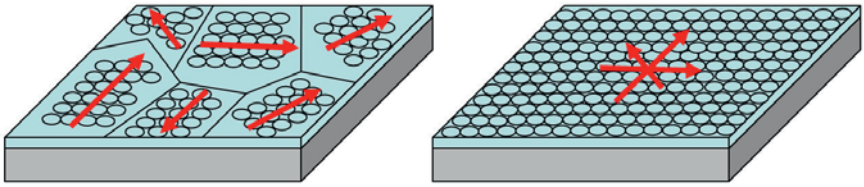

Figure 4. "Polycrystal"- and "monocrystal"-like porous structures.

Detailed TEM analysis shows grain boundaries at the mesoscale.[38] The preparation of a "monocrystal", in which the order is extended on the whole film, or at least on a longer scale (mm to cm) can be carried out by depositing the mesoporous thin film on a polymeric substrate which has been pre-patterned by rubbing.[39] This perfection is however hard to achieve. Another point is the quality of the ordered phase that can be obtained. Some studies have shown that defects, similar to those observed in metallic crystalline structures can be

formed, such as stacking faults and dislocations.[40] Controlling the order and the defects is however possible, as shown by some researchers that obtained "mono-crystals" like films and "defect" free mesoporous films.[41] It is, however, important to be aware that in most cases it is quite difficult to control defects in the porous phase and to obtain an extended organization (from a micron scale up to centimeters).

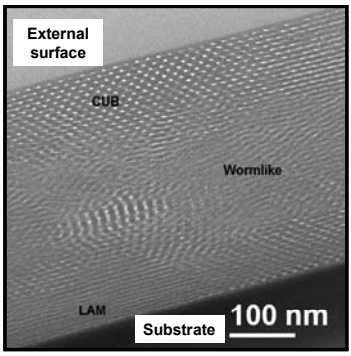

Figure 5. TEM image of a section of a mesoporous silica film, different mesophases can be identified.

The TEM image in Figure 5 shows a cross-section of a mesoporous silica film, the light regions of the sample are the pores. Specific domains of different phases are observed in this sample; in particular, a lamellar phase is formed at the bottom of the film, closer to the substrate, worm-like disordered domains can also be identified in the middle of the films and a cubic ordered phase is located close to the external surface.

2.3. PORE SURFACE FUNCTIONALIZATION

The large reactive surface area is one of the most interesting features of mesoporous films. Silica mesoporous films show a high silanol coverage of the pore surface even after a mild thermal treatment to stabilize the mesostructure.[42] The presence of silanols on the mesopore surface can be used to graft organic functional molecules to add specific properties such as the capability of adsorbing heavy metals or sensing species.[43,44]

Surface functionalization can be achieved mainly by two different routes that are generally indicated as "one pot" and post functionalization. In the first case an alkoxide (or a metal salt) is co-reacted with an organically modified alkoxide to add the functional species. By this type of approach the functional group will reside on the external surface of the pores, with the exception of

the synthesis that employs a type of organically modified alkoxides, bridged silsesquioxanes (Figure 6).[37] In this case the organic groups will be part of an interconnected hybrid organic-inorganic network that forms the backbone of the mesoporous films. Post grafting is another viable route, after deposition the film is functionalized by immersing in a solution (a typical example is 3-aminopropyltriethoxysilane in toluene) containing the organically-modified alkoxide.[14] Functionalization is, however, not a trivial process and a full control and reproducibility, especially in the case of post grafting, is still quite difficult to achieve.

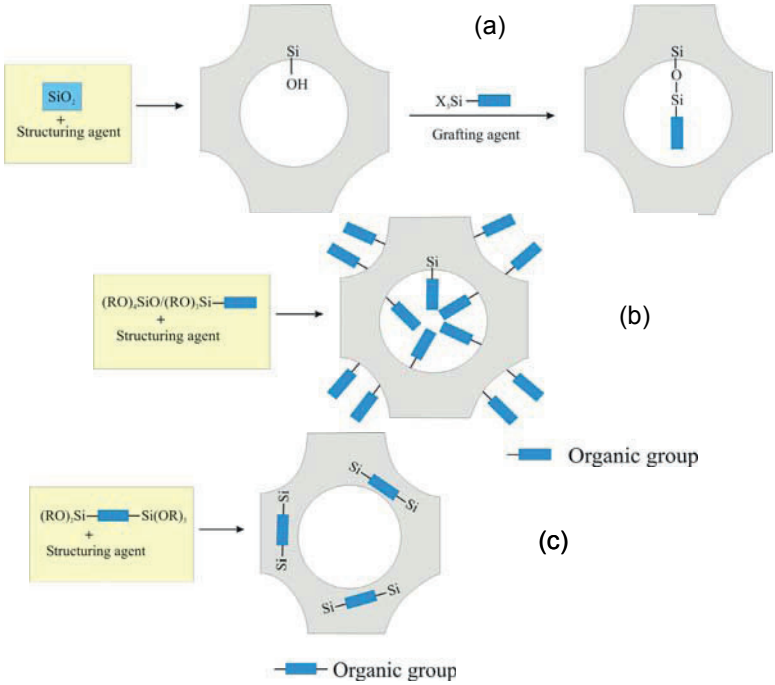

Figure 6. Pore surface functionalization: (a) post grafting; (b) "one pot" route; (c) "one pot" with bridged silsesquioxanes.

3. Applications of Mesoporous Films

3.1. HUMIDITY SENSORS BASED ON MESOPOROUS SILICA THIN FILMS

The importance of pore surface and the presence of silanols (in silica based mesoporous films) or -OH groups in other materials is shown by the properties of the films that are achieved by controlling the pore surface. An interesting example

is the response of silica mesoporous films to changes of relative humidity in the external environment.[45] Humidity and alcohol vapor sensor devices are fabricated using mesoporous silica thin film as sensitive membranes. The films have shown a very different sensitive response with respect to non-mesoporous silica sol–gel thin films used as reference in testing measurements. In general, silica dense films do not show any electrical response and are not used for sensing applications, but in the case of mesoporous silica the high silanol coverage allows activating a protonic conducting mechanism of the "Grotthus" type and work well as simple humidity sensors (Figure 7).

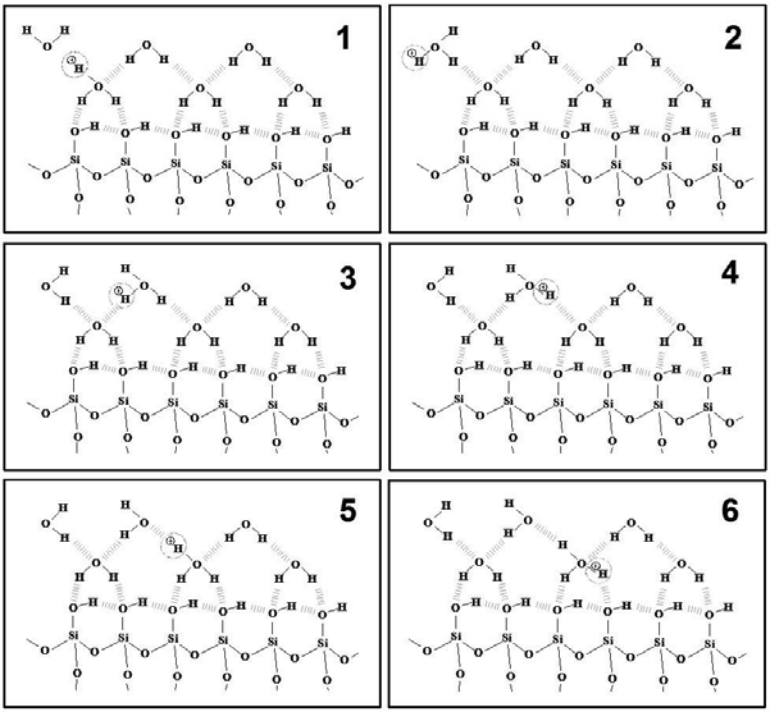

Figure 7. Schematic drawing of a the "Grotthus" model applied to mesoporous silica films.

The mesophase is easily accessible by the external environment and increases the performances for sensing applications. A strong response has been observed in continuous current in mesoporous silica films that have been treated to 350°C; this temperature is high enough to remove the template and stabilize the mesostructure. The films deposited on an interdigited circuit have shown a fast and reproducible electrical response whilst dense sol-gel silica films did not exhibit

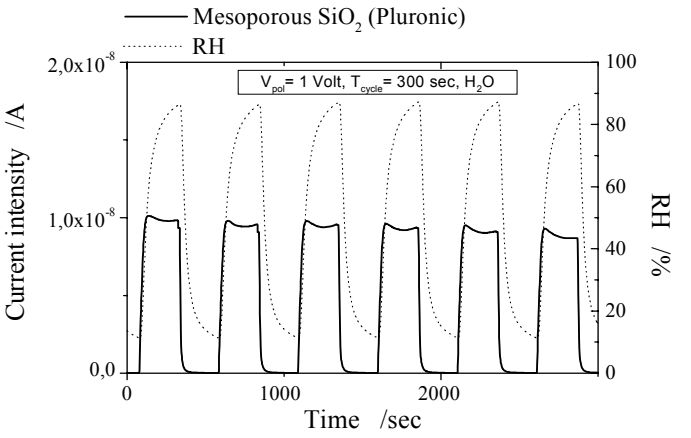

Figure 8. Electrical response of a mesoporous thin films to cyclic changes of relative humidity from the external environment.

any change (Figure 8). A good reproducibility of the electrical response and a different response as function of the surfactant used as templating agent have been observed.

3.2. MESOPOROUS TITANIA FILMS FOR DYE-SENSITIZED SOLAR CELLS

Mesoporous titania materials have important applications in photocatalysis, electrochemical sensors and photovoltaic devices. Mesoporous films prepared by wide-band gap semiconductor oxides, such titania, niobia or tantalia and formed by interconnected nanocrystalline particles allow, in fact, an efficient charge carrier transport. The interface between the organic dye and the surface of the titania mesoporous walls forms a heterojunction where photo-induced charge transfer separation is observed. By filling the mesopores with a proper liquid hole conductor (usually a solution containing the redox couple I^-/I^{3-}), a heterojunction with a very large contact area will be formed. If the formation of an interconnected network of oxide nanocrystals is crucial for electronic conduction, oxide porous films with a large surface area and controlled pore organization are expected to add a significant improvement to the overall performances of a dye-sensitized solar cell (DSSC) device. The presence of an organized porosity within the films can, in fact, allow the formation of highly controlled morphology that facilitates the electronic conduction. Mesoporous channels organized with a preferential orientation that is normal to the substrate will give, therefore, one of the best configurations for DSSC materials.

Since the discovery of organic-sensitized photovoltaic devices, the utilization of nanocrystalline anatase electrodes is a standard in the Grätzel-type solar cells.[46,47] The DSSC combines the high light absorption of a specifically designed organic dye with the electronic conductivity of a nanocrystalline anatase network. Several papers have reported systematic studies about the optimal conditions to prepare thick titania layers by screen-printed (or doctor-bladed) colloidal solutions;[48,49] using this technique, the typical thickness of nano-crystalline anatase electrode is 1–10 μm. The control of the synthesis parameters in the EISA technique allows obtaining thick films via multiple dip-coating, this process does not disrupt the organization of the pores in the single layers and the structure of the porous phase is maintained even after removal of the organic template. Controlled crystallization of the amorphous titania pore walls into crystalline anatase, whose crystallite dimensions can be adjusted within a certain degree as a function of the processing conditions, is attained through thermal calcination. Thermal treatments at temperatures between 400°C and 600°C give a high surface area mesoporous nano-anatase coating presenting channel-voids very interesting for dye-sensitized solar cells.

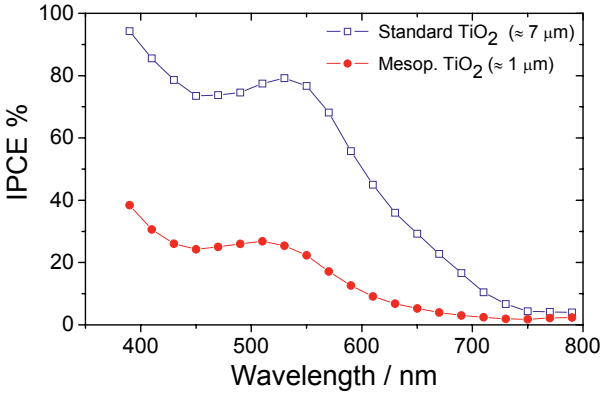

Figure 9. Photoaction spectra of a 1 μm thick mesostructured titania film (calcined at 350°C) compared with a 7 μm thick TiO_2 reference electrode. The incident photon current conversion efficiency is shown as a function of the wavelength. The two samples are both sensitized by N3.

In order to improve the control of morphology of TiO_2 electrodes for DSSC applications, mesostructured titania films have been prepared by EISA.[50] These films are composed of a continuous TiO_2 network of organized porosity that is partially crystallized. TiO_2 thick films, impregnated with a ruthenium dye, have been used to fabricate a DSSC device whose photoactivity have been tested.[51] The measurement of the incident-photon-to-current-efficiency (IPCE) of proto-typed solar cell based on titania mesostructured films (Figure 9) showed

that this mesostructured material can be efficiently used, upon optimization of the thickness and processing conditions, as electrode in dye-sensitized solar cells.

3.3. X-RAY PATTERNING OF MESOPOROUS FILMS

The integration of bottom-up synthesized materials in devices requires a top-down processing.[52,53] Self-assembled mesoporous thin films are no exception, because specific patterning of mesoporous films in order to obtain circuits or dot arrays cannot be fulfilled by coating a substrate with the sol-gel film, without further processing.[54] In particular, the bottom-up route needs coupling with top-down processing such as substrate pre-patterning or film lithography.[55,56] In this way, hierarchically-structured materials can be obtained where organization resides on multiple length scales. The ordered mesopores are an ideal host for functional organic molecules or nanoparticles and the patterns, from the nano- to the micro-scale, allow designing devices for different types of advanced applications,[57] for example in DNA nanoarrays or lab-on-a-chip devices.

The possibility to pattern mesoporous films was first demonstrated by Brinker and coworkers, who employed a wide range of different several lithographic techniques. These were based either on mesophase change or on mesostructure disruption occurring upon irradiation with UV light. Alternatively, dip-pen nanolithography, ink-jet printing using a "self-assembling ink" and selective de-wetting were used to obtain patterned mesoporous arrays and microfluidic devices.

The possibility to pattern of mesoporous films was first demonstrated by Brinker and coworkers, who applied several lithographic techniques to fabricate patterned mesoporous films.[58,59] These techniques were based either on mesophase change or on mesostructure disruption occurring upon irradiation with deep UV light (wavelength 256 nm). Thin (max thickness 360 nm) films were patterned with a lateral resolution of 10 μm. Using an excimer laser (wavelength 248 nm) coupled with a phase mask, a resolution of around 560 nm could be reached. However, the use of a phase mask is restricted to the patterning periodical objects and is not suited for the fabrication of non-periodical structures. Alternatively, dip-pen nanolithography or ink-jet printing using a "self-assembling ink", dip-coating and selective de-wetting were used to obtain patterned mesoporous arrays with high resolution (150 nm) and micro-fluidic devices.[60]

Photopatternable cyclic silsesquioxane compositions containing a photoacid generator were prepared, with the goal of achieving a photoresist-free porous low-dielectric constant precursor.[61] The films were patterned with a standard UV lamp (wavelength 350 nm), reaching a pattern lateral resolution on the micrometre scale (≈2 μm) with the possibility of patterning thick (1.3 μm) films.

A spatially-directed impingement of UV light (wavelength 187–254 nm) was demonstrated to be effective in selectively removing surfactant molecules from mesostructured thin films, generating patterns as small as 3 μm.[62] However, only thin (300 nm) films could be obtained, Immersion in a NaOH solution preferentially and completely etched the mesostructured material from the surface, leaving patterned mesoporous islands. This process was studied using optical microscopy, spatially resolved FTIR and spatially resolved ellipsometry.

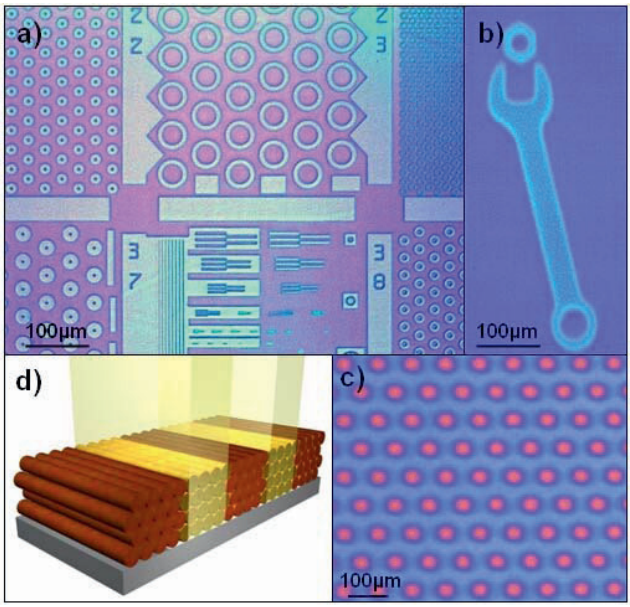

Figure 10. Optical micrograph of a patterned mesostructured silica film. The patterned objects can be discerned by their color, due to the difference in refractive index between the masked and the unmasked regions (a–c). Illustration of a mesostructured film subjected to DXRL (d).

Deep X-ray lithography (DXRL) can be used to pattern mesostructured silica thin films. DXRL is a manufacturing process by which a material that is exposed to high-resolution, high-intensity and extremely collimated synchrotron radiation through an X-ray mask changes its dissolution rate in a liquid solvent (developer). By this lithographic method, the mask pattern is, therefore, transferred to the material (Figure 10).[63]

This lithographic approach is based on selective template removal and silica polycondensation induced by synchrotron radiation. The areas of the film that are not exposed to radiation can be selectively etched due to a lower cross-linking degree of the inorganic network. An important advantage of this method

is the possibility to simultaneously remove the surfactant and to induce condensation of the silica network in a single-step process.

Mesoporous pillars fabricated by DXRL were specifically functionalized by means of a dip-pen technique using the cantilever tip of an atomic force microscope (AFM). In a proof-of-concept experiment, the cantilever tip was used as a dip pen using rhodamine 6G as the ink in order to functionalize selected mesoporous pillars. The AFM cantilever tip was dipped into the rhodamine solution to take up a drop of solution, then it was approached to its destination pillar. When the tip landed on the pillar and the solution came into contact with the film, capillary forces drove the solution from the cantilever tip into the pillar, so that the mesopores became filled with the rhodamine solution. The results of this controlled writing process demonstrate that, using this method, it is possible to fabricate highly fluorescent mesoporous microstructures by the functionalization of micrometric mesoporous objects with different guest molecules (for example, oligonucleotide strands can be attached to the pillars in the fabrication of microarrays for DNA spotting). The lateral feature size of the patterned pillars corresponds to the conditions for microarray deposition, which are typically around 30 μm.[64] The lateral resolution of AFM enables functionalization of sub-micron mesoporous objects using small amounts of analytes; in addition, the patterned mesoporous support maximizes adsorption of guest molecules due to the high specific surface area of mesoporosity. Further-more, hexagonal p6 m mesostructures associated with cylindrical pores allow accessibility of the material from the outside and diffusion of analytical species into the material, opening the route for efficient immobilization of biological species in analytical applications.

4. Conclusions

Mesoporous thin films are an important class of bottom-up fabricated nanostructured materials. Evaporation-induced self-assembly allows preparing materials containing controlled ordered pores in the 2–50 nm range and with a number of functional properties. The high flexibility of the low-temperature and self-assembling route is a big advantage in designing materials with complex geometries and applications in advanced materials. Several applications have been demonstrated in different fields and high capability to integrate in the current technologies for photonics, sensors and electronics. The development of complex systems, such multifunctional hierarchical materials, based on mesoporous thin films is one of the main future directions of research in this field.

References

1. C. J. Brinker and G. W. Scherer, *Sol-gel science* (Academic, San Diego, CA, 1992).
2. *Handbook of sol-gel science and technology*, edited by S. Sakka (Kluwer AP, Dordrecht, 2004).
3. G. A. Ozin and A. C. Arsenault, *Nanochemistry: a chemical approach to nanomaterials* (The Royal Society of Chemistry, Cambridge, 1995).
4. D. Kuang, T. Brezesinski, and B. Smarsly, *J. Am. Chem. Soc.* 126, 10534 (2004).
5. J. Roquerol, D. Avnir, C. W. Fairbridge, D. H. Everett, J. H. Haynes, N. Pernicone, J. D. F. Ramsay, K. S. W. Sing, and K. K. Unger, *Pure and Appl. Chem.* 66, 1739 (1994).
6. M. Antonietti and G. A. Ozin. *Chem. Eur. J.* 10, 28 (2004)
7. G. Soler-Illia, C. Sanchez, B. Lebeau, and J. Patarin, J. *Chem Rev.* 102, 4093 (2002).
8. G. Soler-Illia, E. L. Crepaldi, D. Grosso, and C. Sanchez, *Curr. Opin. Colloid Interf. Sci.* 8, 109 (2003).
9. C. J. Brinker, Y. Lu, A. Sellinger, and H. Fan, *Adv. Mater.* 11, 579 (1999).
10. C. J. Brinker, *MRS Bull.* 29(9), 631 (2004).
11. C. T. Kresge, M. E. Leonowicz, W. J. Roth, J. C. Vartuli, and J. S. Beck, *Nature* 359, 710 (1992).
12. J. S. Beck, J. C. Vartuli, W. J. Roth, M. E. Leonowicz, C. T. Kresge, K. D. Schmitt, C. T.-W. Chu, D. H. Olson, E. W. Sheppard, S. B. McCullen, J. B. Higgins, and J. L. Schlenker, *J. Am Chem. Soc.* 114, 10834 (1992).
13. G. Soler-Illia and P. Innocenzi, *Chem. Eur. J.* 12, 4478 (2006).
14. L. Nicole, C. Boissiere, D. Grosso, A. Quach, and C. Sanchez, *J. Mater. Chem.* 15, 3598 (2005).
15. S. Besson, T. Gacoin, C. Ricolleau, C. Jacquiod, and J. P. Boilot, *Nano Lett.* 2, 409 (2002).
16. M. D. Pérez, E. Otal, S. Aldabe-Bilmes, G. Soler-Illia, E. L. Crepaldi, D. Grosso, and C. Sanchez, *Langmuir* 20, 6879 (2004).
17. P. C. Angelomé and G. Soler Illia, *Chem. Mater.* 17, 322 (2005).
18. D. Grosso, F. Babonneau, P.-A. Albouy, H. Amenitsch, A. R. Balkenende, A. Brunet-Bruneau, and J. Rivory. *Chem. Mater.* 14, 931 (2002).
19. M. Klotz, A. Ayral, C. Guizard, L. Cot, *J. Mater. Chem.* 10, 663 (2000).
20. G. Soler-Illia, E. Scolan, A. Louis, P. -A. Albouy, and C. Sanchez, *New J. Chem.* 25 156 (2001).
21. E. L. Crepaldi, G. Soler-Illia, D. Grosso, F. Ribot, F. Cagnol and C. Sanchez, *J. Am. Chem. Soc*. 125, 9770 (2003).
22. D. M. Antonelli, *Microp. Mesop. Mater.* 30, 315 (1999).
23. J. N. Israelachvili, *Intermolecular and surface forces* (Academic, London, 1998).
24. (a) M. Ogawa and N. Masukawa, *Microp. Mesop. Mater.* 38, 35 (2000). (b) D. A. Doshi, A. Gibaud, V. Goletto, M. C. Lu, H. Gerung, B. Ocko, S. M. Han, and C. J. Brinker, *J. Am. Chem. Soc.* 125, 11646 (2003).
25. Y. F. Lu, R. Ganguli, C. A. Drewien, M. T. Anderson, C. J. Brinker, W. L. Gong, Y. X. Guo, H. Soyez, B. Dunn, M. H. Huang, and J. I. Zink, *Nature* 389, 364 (1997).
26. P. Falcaro, D. Grosso, H. Amenitsch, and P. Innocenzi, *J. Phys. Chem. B* 108, 10942 (2004).
27. R. C. Hayward, P. C. A. Alberius, E. J. Kramer, and B. F. Chmelka, *Langmuir* 20, 5998 (2004).
28. P. Falcaro, S. Costacurta, G. Mattei, H. Amenitsch, A. Marcelli, M. Cestelli Guidi, M. Piccinini, A. Nucara, L. Malfatti, T. Kidchob, and P. Innocenzi, *J. Am. Chem. Soc.* 127, 3838 (2005).
29. P. Innocenzi, L. Malfatti, T. Kidchob, P. Falcaro, S. Costacurta, M. Guglielmi, G. Mattei, V. Bello, and H. Amenitsch, *J. Sync. Rad.* 12, 734 (2005).

30. F. Cagnol, D. Grosso, G. Soler-Illia, E. L. Crepaldi, F. Babonneau, H. Amenitsch, and C. Sanchez, *J. Mater. Chem.* 13, 61 (2003).
31. L. Malfatti, T. Kidchob, S. Costacurta, P. Falcaro, P. Schiavuta, H. Amenitsch, and P. Innocenzi, *Chem. Mater.* 18, 4553 (2006),
32. D. Grosso, G. Soler-Illia, E. L. Crepaldi, F. Cagnol, C. Sinturel, A. Bourgeios, A. Brunet-Bruneau, H. Amenitsch, P. -A. Albouy, and C. Sanchez, *Chem. Mater.* 15, 4562 (2003).
33. T. Brezesinski, B. Smarsly, K. Iimura, D. Grosso, C. Boissière, H. Amenitsch, M. Antonietti, and C. Sanchez, *Small* 1, 889 (2005).
34. D. Grosso, C. Boissière, B. Smarsly, T. Brezesinski, N. Pinna, P.-A. Albouy, H. Amenitsch, M. Antonietti, and C. Sanchez, *Nature Mater.* 3, 787 (2004).
35. N. Hedin, R. Graf, S. C. Christiansen, C. Gervais, R. C. Hayward, J. Eckert, and B. F. Chmelka, *J. Am. Chem. Soc.* 126, 9425 (2004).
36. H. Y. Fan, C. Hartshorn, T. Buchheit, D. Tallant, R. Assink, R. Simpson, D. J. Kisse, D. J. Lacks, S. Torquato, and C. J. Brinker, *Nature Mater.* 6, 418 (2007).
37. S. Inagaki, S. Guan, T. Ohsuna, and O. Terasaki, *Nature* 416, 304 (2002).
38. M. Klotz, P. A. Albouy, A. Ayral, C. Menager, D. Grosso, A. Vander Lee, V. Cabuil, F. Babonneau, and C. Guizard, *Chem. Mater.* 12, 1721 (2000).
39. H. Miyata, T. Suzuki, A. Fukuoka, T. Sawada, M. Watanabe, T. Noma, K. Takada, T. Mukaide, and K. Kuroda, *Nature Mater.* 3, 651 (2004).
40. X. Wu, K. Yu, C. J. Brinker, and J. C. Ripmeester, *Langmuir* 19, 7289 (2003).
41. P. Falcaro, S. Costacurta, G. Mattei, H. Amenitsch, A. Marcelli, M. Cestelli Guidi, M. Piccinini, A. Nucara, L. Malfatti, T. Kidchob, Tongjit, and P. Innocenzi, *J. Am. Chem. Soc.* 127, 3838 (2005).
42. P. Innocenzi, P. Falcaro, D. Grosso, and F. Babonneau, *J. Phys. Chem. B* 107, 4711 (2003).
43. L. Nicole, C. Boissière, D. Grosso, P. Hesemann, J. Moreau, and C. Sanchez, *Chem. Commun.* 2312 (2002).
44. (a) N. Liu, R. A. Assink, B. Smarsly, and C. J. Brinker, *Chem. Commun.* 1143 (2003). (b) N. Liu, R. A. Assink, and C. J. Brinker, *Chem. Commun.* 370 (2003).
45. A. Bearzotti, J. Mio Bertolo, P. Innocenzi, P. Falcaro, and E. Traversa, *Sens. Act. B: Chem.* 95, 107 (2003).
46. B. O'Regan and M. Grätzel, *Nature* 353, 737 (1991).
47. M. Grätzel, *Nature Mater.* 421, 586 (2003).
48. C. J. Barbè, F. Arendse, P. Comte, M. Jirousek, F. Lenzmann, V. Shklover, M. Grätzel, *J. Am. Ceram. Soc.* 80, 3157 (1997).
49. S. Burnside, V. Shklover, C. J. Barbe`, P. Comte, F. Arendse, K. Brooks, M. Grätzel, *Chem. Mater.* 10, 2419 (1998).
50. E. Lancelle-Beltran, P. Prené, C. Boscher, P. Belleville, P. Buvat, S. Lambert, F. Guillet, C. Boissiére, D. Grosso, C. Sanchez, *Chem. Mater.* 18, 6152 (2006).
51. L. Malfatti, P. Falcaro, H. Amenitsch, S. Caramori, R. Argazzi, C. A. Bignozzi, S. Enzo, M. Maggini, P. Innocenzi, *Microp. Mesop. Mater.* 88, 304 (2006).
52. C. J. Brinker and D. R. Dunphy, *Curr. Opin. Coll. Inter. Sci.* 11, 126 (2006).
53. J. Y. Cheng, C. A. Ross, H. I. Smith, and E. L. Thomas. *Adv. Mater.* 18, 2505 (2006).
54. H. Yang, N. Coombs, and G. A. Ozin, *Adv. Mater.* 9, 811 (1997).
55. D. Grosso, F. Cagnol, G. Soler-Illia, E. L. Crepaldi, H. Amenitsch, A. Brunet-Bruneau, A. Bourgeois, and C. Sanchez, *Adv. Funct. Mater.* 14, 309 (2004).
56. G. Soler-Illia, C. Sanchez, B. Lebeau, and J. Patarin, *Chem. Rev.* 102, 4093 (2002).
57. B. J. Scott, G. Wirnsberger, M. D. McGehee, B. F. Chmelka, and G. D. Stucky, *Adv. Mater.* 13, 1231 (2001).

58. D. A. Doshi, N. Huesing, M. Lu, H. Fan, Y. Lu, K. Simmons-Potter, B. G. Potter Jr., A. J. Hurd, and C. J. Brinker, *Science* 290, 107 (2000).
59. H. Fan, Y. Lu, A. Stump, S. T. Reed, T. Baer, R. Schunk, V. Perez-Luna, G. P. Lopez, and C. J. Brinker, *Nature* 405, 56 (2000).
60. Y. Lu, Y. Yang, A. Sellinger, M. Lu, J. Huang, H. Fan, R. Haddad, G. Lopez, A. R. Burns, D. Y. Sasaki, J. Shelnutt, and C. J. Brinker, *Nature* 410, 913 (2001).
61. Y. Y. Lyu, J. H. Yim, Y. Byun, J. M. Kim, and J. K. Jeon, *Thin Solid Films* 496, 526 (2006).
62. A. M. Dattelbaum, M. L. Amweg, L. E. Ecke, C. K. Yee, A. P. Shreve, and A. N. Parikh, *Nano Lett.* 3, 719 (2003).
63. E. W. Becker, W. Ehrfeld, P. Hagmann, A. Maner, and D. Munchmeyer, *Microelectron. Eng.* 4, 35 (1986).
64. M. Schena, *Microarray analysis* (Wiley-Liss, New York, 2003).

ACTIVE SOL-GEL MATERIALS

MAREK JASIORSKI*, BEATA BORAK, ANNA ŁUKOWIAK, AGNIESZKA BASZCZUK
Wroclaw University of Technology, Institute of Materials Science and Applied Mechanics, Smoluchowskiego 25, 50-370 Wroclaw, Poland

Abstract. Sol-gel technology has attracted considerable attention due to possibility of obtaining submicron and nano-sized materials. The method of silica and titania nanopowders and thin films obtaining will be presented. Also properties and prospective application of these materials will be express. Additionally, methods of obtaining nanomaterials with different grains shape and specific properties (submicron spherical silica powders, titania nanofibers) will be showed. One of the main advantages of the sol-gel technique is the easiness of doping of the obtained materials with various substances (inorganic, organic, biological). Materials activated this way possess several useful properties. For example, silica spherical matrices with metallic nano-islands on their surface will be presented. Such silver-doped silica powders display anti-microbial capabilities and can be used to obtain doped thin-film coatings e.g. for the production of bacteriostatic textiles. Moreover, materials obtained by the sol-gel method have found wide application in the area of sensors. Examples of optical sensors based on sol-gel derived thin films and optical fiber or planar wave-guide will be also presented.

Keywords: Sol-gel method, thin films, nanoparticles, nanofibers, biological properties of sol-gel materials, sensors.

* To whom correspondence should be addressed: M. Jasiorski, Wroclaw University of Technology, Institute of Materials Science and Applied Mechanics, Smoluchowskiego 25, 50-370 Wroclaw, Poland; e-mail: marek.jasiorski@pwr.wroc.pl

P. Innocenzi, Y. L. Zub and V. G. Kessler (eds.), *Sol-Gel Methods for Materials Processing*.

1. Introduction

The sol-gel process is a versatile solution process for making ceramic and glass materials. In general, the sol-gel process involves the transition of a system from a liquid "sol" (mostly colloidal) into a solid "gel" phase. The precursors are usually organosilicates (e.g. TEOS – tetraethoxysilane) yielding silicate sol-gel materials. However, the method is not restricted to the silicon compounds – for example compounds of zirconium, vanadium, titanium etc. can be used as precursors leading to materials possessing different physico-chemical properties. Furthermore, it is possible to obtain modified organosilicate precursors with direct Si-C bonds (which do not undergo hydrolysis) and possessing terminal functional groups (e.g. $-NH_2$, $-SH_2$ etc.). Such precursors, either pure or mixed with the conventional ones, yield inorganic-organic materials with mechanical (e.g. elasticity) and physico-chemical properties (e.g. wetability) modified by the organic components of the inorganic polymer network. The functional groups can be also used for covalent binding of various chemicals (including biomolecules) giving specifically modified glassy materials.[1] Since the early steps of the sol-gel process occur in liquid phase, it is possible to add basically any substance (as solutions or suspensions) at this stage. Simple mixing provides uniform distribution of the dopant within the liquid host phase. After the gelation the guest molecules become physically entrapped within the solid host

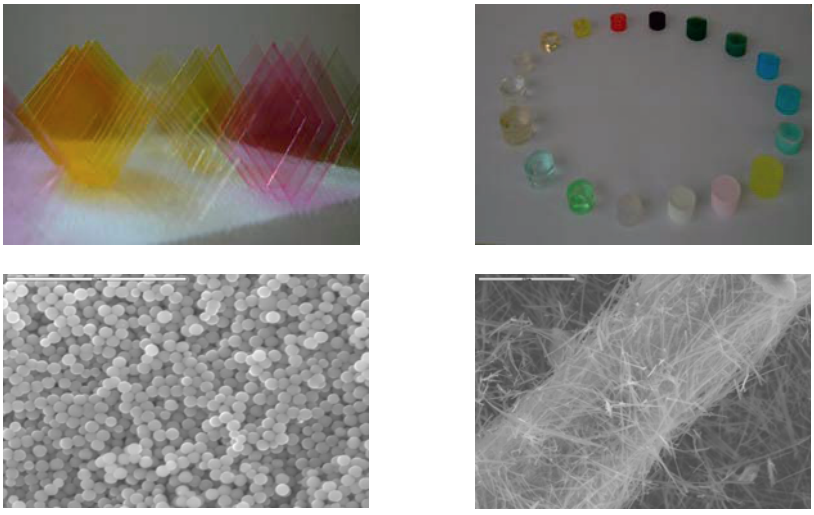

Figure 1. Wide range of sol-gel materials forms.

matrix. Furthermore, the hydrolysis, doping and gelation occur usually at ambient temperatures – allowing entrapment of even such delicate molecules as proteins without their decomposition. Sol-gel doped matrices, obtained in the above described manner, are of the form of xerogels and possess a network of internal pores and cavities enabling the entrapped molecules to interact with the surrounding medium. Furthermore, the doped matrices usually possess good optical characteristics (transparency and high refractive indexes). Those features are of key importance for production of optical sensors (optodes). Another convenient feature of this technology is the fact that applying the sol-gel process it is possible to fabricate materials of high purity and homogeneity in a wide variety of forms: ultra-fine or spherical shaped powders, thin film coatings, ceramic fibers, microporous inorganic membranes, monolithic ceramics and glasses, or porous aerogel materials (Figure 1).

Many specific applications of sol-gel materials include optics, protective and porous films, optical coatings, window insulators, dielectric and electronic coatings, high temperature superconductors, reinforcement fibers, fillers, and catalysts. A brief overview of the sol-gel process conducted in our Sol-Gel Laboratory is presented in this paper.

2. Sol-Gel Optical Sensors (optodes)

The idea behind the sol-gel optical sensors (optodes) is based on changes of optical parameters of active (sensing) molecules physically entrapped in (or, in some cases, covalently bound to) porous sol-gel thin films. Changing external physico-chemical parameters such as temperature, hydrostatic pressure or presence of analyte molecules or, for example, bacteria induces those changes.[2]

There are several kinds of optical signals, which could be used as analytical response of such optodes. In general, one can observe changes of: (a) intensity of light absorbed or emitted by the sensing molecules, (b) time of decay of the sensing molecules luminescence, (c) changes in vibrational spectra (bands intensity and frequency) of the sensing molecules and (d) polarization properties of the sensing molecules.

Electronic spectroscopy in the visible region offers several advantages stemming from molecules possesses electronic transitions in the VIS range. This fact lowers the possibility of optical interference with the sensing molecules coming from unwanted molecules (in most cases organic), which might diffuse into the matrix pores or adhere to the optode surface. Furthermore, spectral bands corresponding to such transitions are usually broad in condensed phases and

even in gases. This property makes them easier to detect. Simple colorimetric measurements of acidity supply an example of this analytical method. In this case changes in pH result in changes of absorption patterns (color) of organic indicator dyes such as, for example, henolophtaleine, bromocresol blue, rosolic acid etc.[3]

Sol-gel optodes for ammonia based on pH depended color changes of rosolic acid have been made using the sol-gel method. Figure 2 presents absorption spectra of rosolic acid entrapped in silicate thin films obtained via the sol gel method and coated onto a glass planar support (A) and onto an unclad fragment of a commercial optical fiber (B). In the latter case the light passing through the fiber interacts with the dye molecules immobilized in the sol-gel film on its surface via the so-called "evanescent wave" effect.[4] Signal from this optodes informs about base or acid pollutions presented around sensor. The process is fully reversible, replacing the ammonia solution with clean water results in a return to the original spectrum of the dye (Figure 2C). The gaseous optode may be used even for detection of ammonia traces.

Next example of sensor is gamma radiation optode. Changes in absorption spectrum of Safranine O entrapped in bulk silica matrices caused by gamma radiation are presented on Figure 3.

The samples were exposed to ^{60}Co radiation source at a dose rate of 15.8 Gy/min. The Safranin O in silica has maximum absorption at 519 nm. Intensity of absorption decreases as a function of increasing irradiation dose. As a reference Safranin O in DMF solution was measured. The absorption changes at 519 nm, characterized by linear relation versus intensity of radiation in very wide range from 0 to 40 kGy, are presented in Figure 3b.

Similar effect was observed for magnesium (II) phthalocyanine entrapped in silica matrix. The intensity of dye absorption (observed at e.g. 750 nm) decreases as a function of increasing irradiation dose (Figure 4). The dyes in DMF solution were also measured as references. The decrease of absorption intensity was very fast for dyes in DMF solutions and much slower for molecules in silica matrices. For selected Mgpc concentration, color of the sample with DMF disappears at radiation dose of about 10 kGy, while the color of silica sample disappears at doses higher than 1 MGy.

This experiment provides that silica matrix protects entrapped molecules from gamma radiation. Silica matrix has good mechanical and optical (it is transparent) properties and can be used in dosymetry. Choice of dye and concentration of molecules allows measuring wide range of gamma radiation intensity.[5]

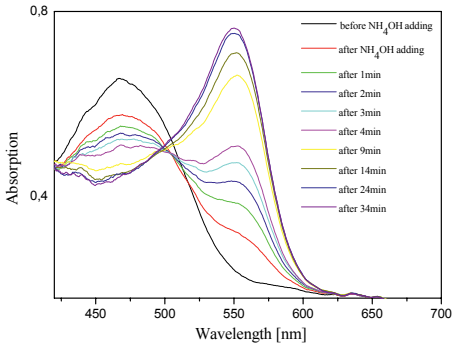

A)

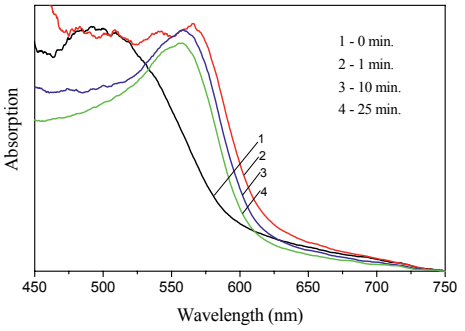

B)

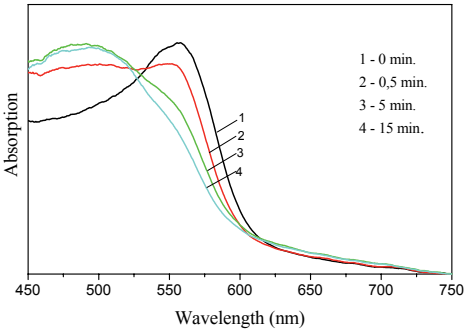

C)

Figure 2. Absorption spectra of rosolic acid entrapped in silicate thin films obtained via the sol gel method and coated onto a glass planar support (A) and onto an unclad fragment of a commercial optical fiber (B and C).

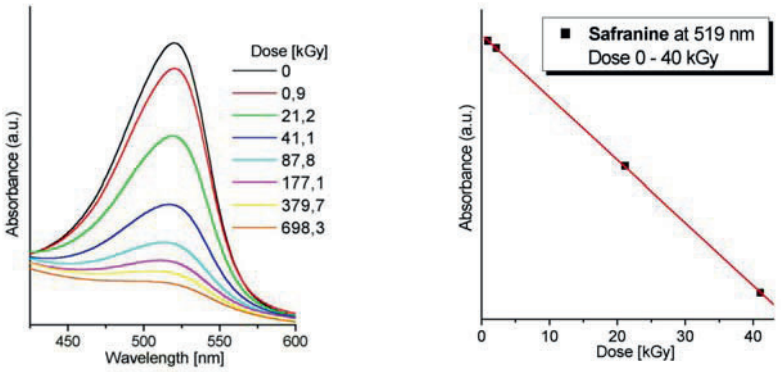

a) b)

Figure 3. Changes in absorption spectrum of Safranin O in sol-gel-derived silica matrix caused by gamma radiation.

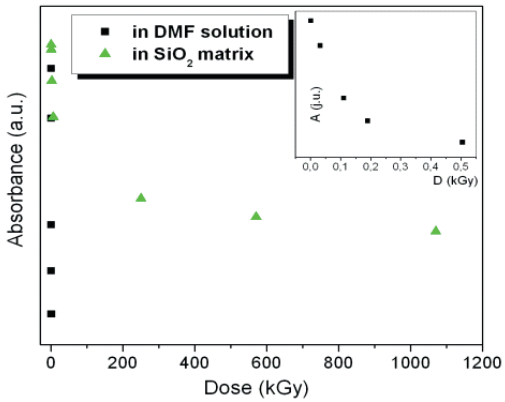

Figure 4. Changes in absorption spectrum of Mgpc in DMF solution (A 670) and silica matrix (A 750).

2. Sol-Gel Nanopowders

Nanostructured materials possess unique mechanical, chemical and optical properties.[6] Nanometer-sized metal and semiconductor particles have been attracting much attention due to their novel properties significantly different from those *-*-of corresponding bulk materials, such as quantum-size effect, nonlinear optical properties and unusual luminescence.[7,8,9]

The sol-gel method can be employed to produce powder materials. One of the most interesting aspects of this approach is possibility of uniform submicron-sized silica particles production. Modifications of the original Stöber method[10]

have yielded[11,12] nanopowders consisting of silica spheres having virtually identical diameters. It has to be stressed that these syntheses are carried out at room temperature in water solutions of the precursors. SEM and AFM studies have revealed that shape of silica particles was evidently regular and spherical, with diameter of 60 or 500 nm depending on type of substrates (silica precursors, type of solvent). Because of very small diameter of the silica spheres, close-packed thin layer of particles on the glass support was observed. In the case of smaller particles with 60 nm diameters, larger tendency to aggregates and creation clusters was observed. Figure 5 presents SEM micrograph of silica submicron-sized spheres.

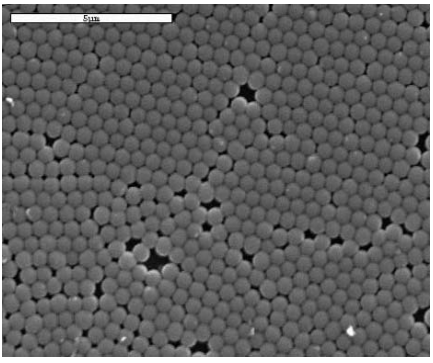

Figure 5. SEM micrograph of silica submicron-sized spheres.

The sol-gel method can be successfully used to obtain well separated metallic nanoparticles. The effective method for prevention of aggregation of nanoparticles is placement of metal ions on the surface of uniform separated silica spheres. For this purpose silica submicron powders presented on Figure 5 were impregnated in solution of silver nitrate. The impregnated silica powders were reduced to transform cationic form of silver Ag^+ to metallic silver. Reduction was conducted using formaldehyde, $NaBH_4$ or H_2. On Figure 6 SEM micrograph of the silica spheres with silver nanoislands is presented.

It is well known that in certain cases adsorption of organic molecules on silver or gold electrodes resulted in significant increase in intensity of Raman scattering of the adsorbed molecules. This phenomenon is known as Surface Enhanced Raman Scattering (SERS).[13] Such enhancement has been also observed for molecules adsorbed on aqueous Ag sols,[14] on silver nanoparticles embedded in a cellulose film[15] or on Ag evaporated onto SiO_2 nanoparticles.[16] In order to establish if the SERS effect would work also for organometallic molecules possessing D_3 symmetry adsorbed on silver nanoclusters, the SiO_2-Ag^0 powders

were soaked in $Ru(bpy)_3^{2+}$ ethanol solutions. Subsequently, the powders were filtered, washed, dried and their Raman spectra were obtained. Figure 7b presents the FT-Raman spectra of the Ag^0-doped submicron silica powders after impregnation in solutions of tris(bipirydyne)ruthenium(II) with the complex concentrations of: 5.2×10^{-7} M/l (Trace A), 7.81×10^{-6} M/l (Trace B) and 7.81×10^{-5}

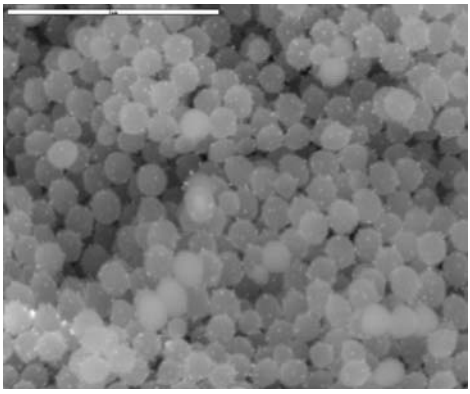

Figure 6. SEM micrograph of silica submicron-sized spheres with silver nanoislands on the grains surfaces.

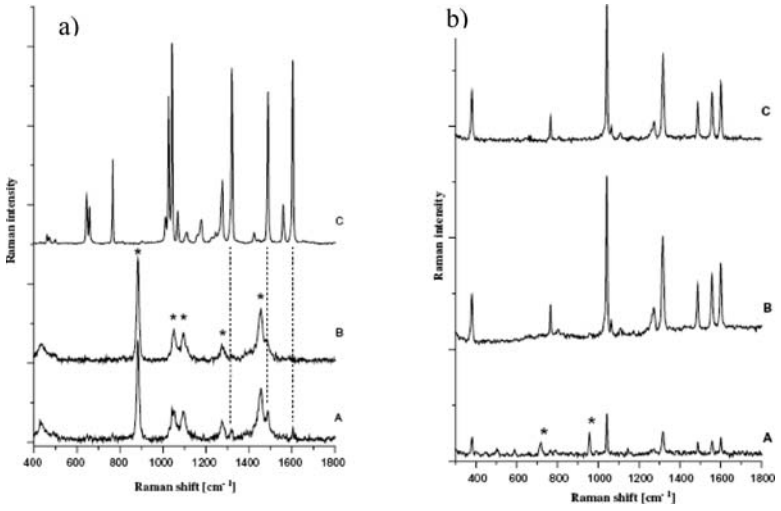

Figure 7. (a) FT-Raman spectra of the ethanol solutions of the ruthenium complex and of the pure solid (C). The solution concentrations are: 1.6×10^{-2} M/l (A) and 2.6×10^{-3} M/l (B). The asterisk denotes ethanol bands; (b) FT-Raman spectra of the Ag^0-doped submicron silica powders impregnated in solutions of tris(bipirydyne)ruthenium(II) with the complex concentrations of: 5.2×10^{-7} M/l (A), 7.81×10^{-6} M/l (B) and 7.81×10^{-5} M/l (C). The asterisk denotes ethanol bands.

M/l. As it can be seen, the $Ru(bpy)_3^{2+}$ Raman spectrum can easily be observed even for its concentrations as low as ca. 5×10^{-7} M/l. Comparison with the results obtained for aqueous solutions of the ruthenium complex (Figure 7a) reveals that using the Ag^0-doped silica powders for the SERS measurements allows to lower the $Ru(bpy)_3^{2+}$ detection limit by approximately four orders of magnitude (in this experimental set-up). It is important to note that in the case of silica powders without silver nanoclusters no Raman signal was observed upon their impregnation even in the concentrated $Ru(bpy)_3^{2+}$ solutions.

Thus, such materials could be used for improving analytical methods employed in, for example, medicine (detection of drugs or important metabolites), crime prevention (detection of chemical or biological weapons) or environmental

Bacteriostatic properties of silver have been known for centuries.[17,18,19] The antimicrobial activity of silica particles with nanosilver on the surface (presented on the Figure 6) against *Staphylococcus aureus*, *Klebsiella pneumoniae* and *Escherichia coli* as a model of Gram-negative and Gram-positive bacteria was observed. Thinking about future applications the best way of using nanosilver-silica powder was their connection to everyday used textile materials. First step was to prepare thermo-polymeric paste consisting of good dispersed silica powders with silver nanoislands. Figure 8 presents SEM micrographs of thin (20–40 μm) polymeric coats on the surface of textiles. This membrane, prepared by Institute of Textile Materials Engineering (from Łódź) led by Prof S. Brzeziński has important properties such as: letting in the steam, water-resistant, good mechanical properties (resistance to washing) – significant in application aspect of this materials.

Figure 9 presents silica silver particles incorporated into porous polymeric coat on textile. Unfortunately, aggregates of spherical particles, which are the result of membrane creation process, are clearly seen (Figure 9a). After modification of synthesis process and creation of stable polymeric paste with good

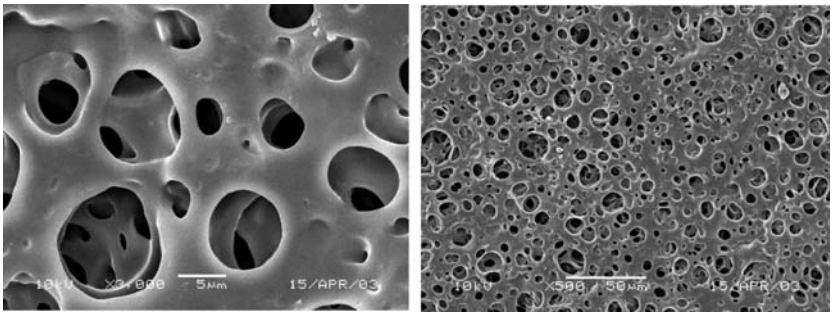

Figure 8. SEM micrographs of thin (20–40 μm) polymeric coats on the surface of textiles.

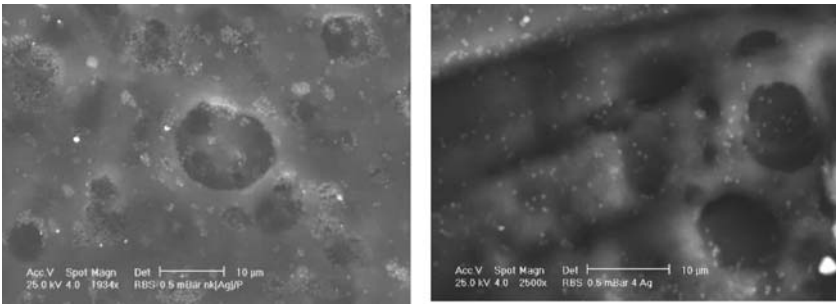

Figure 9. SEM micrographs of thin polymeric coats consisting of aggregates (a) and good dispersed silica powders with silver nanoislands (b) on the surface of textiles.

distribution of active silica particles, homogenic layer with uniformly distributed silver dopant (Figure 9b) was obtained.

The antimicrobial activity of textile samples with silver-doped silica materials against *Staphylococcus aureus*, *Klebsiella pneumoniae* and *Escherichia coli* were investigated. All biological measurements were conducted basing on international standard: ISO: Textile fabrics Determination of antibacterial activity. Agar diffusion plate test ISO/DIS 20645:2002. As a reference: pure textile material without dopants and textile material with silica but without silver islands were used. Additionally all textile materials were washed ten times to check their biological activity after that. It was found that, the lowest concentration of silica-silver dopant in dry polymeric substance, which created good bacteriostatic properties, is about 2%. After washing slight decrease of bacteriostatic effect (induced by leaching active silver) was observed. Summarizing, these hybrid active powders could be used as a novel bacteriostatic agent. They can have a wide field of application in sport and recreational clothes production, shoes insertions, hospital and nursing bed-sheets and protective uniforms for personnel, clothes for newborn, surgical and dressing materials.[20]

Other interesting material with photocatalitical, biological and bacteriostatic properties is titania dioxide. Titania dioxide exists in four forms: amorphous and three crystallic forms: anatase, brukite and rutile. It was shown, that the mixture of anatase/rutile in proper ratio has the best photocatalitic properties for the oxidation of organic materials in the wastewater treatment.[21,22] For this reason extremely important is to understand and control the most critical para-meter of anatase/rutile transition. There are several factors such as: type of precursor, type of solvent, catalyst, aging time, water-alkokside molar ratio which have influence on titania dioxide crystal structure. Very important parameter for physicochemical properties is specific surface area of material. Good way to increase active

surface of titania dioxide powder is transformation of crystalline anatase into the nanofiber/nanowires form using hydrothermal method. Titania nanowires have large specific surface area available for the absorption of photons compared to bulk material and they also provide channels for enhanced electron transfer, thereby are helping to increase the efficiencies for solar cells, electrolysis, and photocatalysis.[23,24] Also, the TiO_2-derived nanotubes such as sodium titanate and hydrogen titanate have useful optical and magnetic properties.[25]

TiO_2 anatase nanoparticles obtained by the sol-gel method and used as a precursor in hydrothermal synthesis and well isolated nanowires successfully obtained after the synthesis are presented on Figure 10. The as-prepared materials have diameter of about 50 nm and several micrometers in length.

Figure 11 shows XRD profiles of starting anatase and nanowires synthesized in hydrothermal process and annealed at different temperatures.

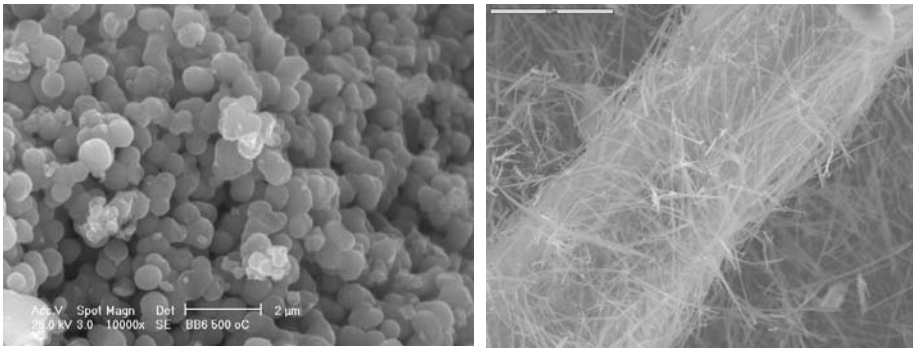

Figure 10. SEM micrographs of TiO_2 anatase nanoparticles obtained by the sol-gel method (a) and well isolated nanowires obtained after the hydrothermal synthesis (b).

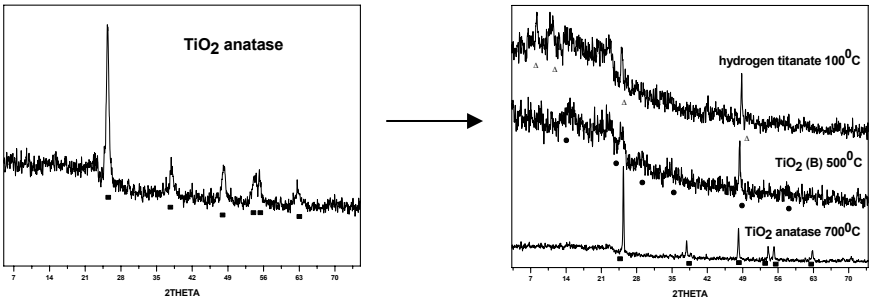

Figure 11. The XRD profiles of starting form of titania (anatase) and hydrothermal synthesized TiO_2 nanowires.

In contrast to the starting TiO_2 powder consisted of pure anatase the as-synthesized nanowires powder has a different crystal structure. Diffraction pattern of powder annealed at 100°C can be assigned to trititanate $H_2Ti_3O_7$ as it was proposed by authors,[26] but more preferably expressed as $H_2Ti_3O_7 * n H_2O$.[27] There are two low-angle area diffraction peaks at about 10.82 and 8.20 2theta. They correspond to hydrogen titanate and water containing derivatives, respectively. By subsequent heat treatment (300–500°C) hydrogen titanates were converted to TiO_2 (B) metastable polymorph phase. After annealing at 600°C anatase form is obtained but sample still retain the nanowire shape.

3. Conclusions

Presented in this paper sol-gel materials are only small part of researchers which are done in our Laboratory. It was a short review about synthesis, creation of different shape, structure transformation and possibility application of silica and titania particles and thin films. Prepared materials can be modified by doping active molecules what provides to creation of new optical, biological, mechanical properties. Showed materials are in nano and submicro-size which are easer to incorporate into textile, paper and other useful materials changing its properties and area of application. This review presents interdisciplinary character of measurements and cooperation between different groups of scientist, which is important in creation and application of new active nanomaterials.

References

1. C.J. Brinker and G.W. Scherer, Sol-Gel Science: The Physics and Chemistry of Sol-Gel Processing (Academic, New York, 1990).
2. H. Dislich, Thin films from the sol-gel process, [in:] L.C. Klein (Ed.) Sol-Gel Technology for Thin Films, Fibers, Performs, Electronics, Specialty Shapes (Noyes Publications, Park Ridge, NJ, 1988).
3. K. Maruszewski, W. Stręk, M. Jasiorski, A. Ucyk, Technology and applications of sol-gel materials, *Radiation Effects and Defects in Solids* 158, 439–450 (2003).
4. Fiber Optical Sensors and Biosensors, edited by O.S. Wolfbeis (CRC Press, Boca Raton, FL, 1991).
5. A. Łukowiak, E. Łukowiak, M. Jasiorski, K. Maruszewski, W. Stręk, Influence of gamma radiation on neodymium bisphthalocyanine, *Optical Materials* 26, 163–166 (2004).
6. H. Gleiter, Nanostructured materials: basic concepts and microstructure, *Acta Materialia* 48, 1–29 (2000).
7. A.J. Bard, Photoelectrochemistry, *Science* 207, 139–144 (1980).
8. A.J. Bard, Design of semiconductor photoelectrochemical systems for solar energy conversion, *Journal of Physical Chemistry* 86, 172–177 (1982).

9. E. Joselevich, I. Willner, Photosensitization of quantum-size TiO_2 particles in water-in-oil microemulsions, *Journal of Physical Chemistry* 98, 7628–7635 (1994).
10. W. Stöber, A. Fink, E. Bohn, Controlled growth of monodisperse silica spheres in the micron size range, *Journal of Colloid and Interface Science* 26, 62–69 (1968).
11. M. Jasiorski, K. Maruszewski, W. Strek, Optical behavior of sol-gel derived photonic structures formed by submicron silica spheres, *Materials Science* 20, 51–56 (2002).
12. K. Maruszewski, M. Jasiorski, D. Hreniak, W. Stręk, K. Hermanowicz, K. Heiman, Raman spectra of molecules adsorbed on Ag centers in sol-gel matrices, *Journal of Sol-Gel Science and Technology* 26, 83–88 (2003).
13. A. Campion, S. Kambhampati, Surface-enhanced Raman scattering, *Chemical Society Reviews* 4, 241–250 (1998).
14. X.Y. Li, V.I. Petrov, D. Chen, N.T. Yu, Surface-enhanced resonance Raman spectroscopy of water-insoluble Ni(II) porphine adsorbed on aqueous silver sol: suppression of anti-symmetric scattering, antiresonance effect and higher order scattering, *Journal of Raman Spectroscopy* 32, 503–519 (2001).
15. Y. Kurokava, Y. Imai, Y. Tamai, Surface-enhanced Raman scattering observations on bipyridine, phthalimide, phenylethylamine and theobromine by using a fine silver particle-doped cellulose gel film, *Analyst* 122, 941–944 (1997).
16. M. Litorja, C.L. Haynes, A.J. Haes, T.R. Jensen, R.P. Van Duyne, Surface-enhanced Raman scattering detected temperature programmed desorption: optical properties, nanostructure, and stability of silver film over SiO_2 nanosphere surfaces, *Journal of Physical Chemistry B* 105 , 6907–6915 (2001).
17. S. Silver, Bacterial silver resistance: molecular biology and uses and misuses of silver compounds, *FEMS Microbiology Reviews* 27, 341–353 (2003).
18. J.M. Schierholz, L.J. Lucas, A. Rump, G. Pulverer, Early onset pneumonia in neurosurgical intensive care unit patients, *Journal of Hospital Infection* 40, 275–280 (1998).
19. R. Kumar, H. Munstedt, Silver ion release from antimicrobial polyamide/silver composites, *Biomaterials* 26, 2081–2088 (2005).
20. S. Brzeziński, K. Maruszewski, M. Jasiorski, M. Ornat, G. Malinowska, B. Borak, I. Karbownik, Bacteriostatic textile-polymeric coat materials modified with nanoparticles, *POLIMERY* 52, 362–366 (2007).
21. T. Ohno, D. Haga, K. Fujihara, K. Kaizaki, M. Matsumara, Experimental absolute cross-sections for the reaction F + D2 at collision energies 90-240 meV, *Journal of Physical Chemistry B* 101, 6415–6428 (1997).
22. R.J. Berry, M.R. Mulle, Photocatalytic decomposition of crude oil slicks using TiO_2 on a floating substrate, *Microchemical Journal* 50, 28–32 (1994).
23. J. Cao, J.Z. Sun, H.Y. Li, J. Hong, M. Wang, A facile room-temperature chemical reduction method to TiO_2@CdS core/sheath heterostructure nanowires, *Journal of Materials Chemistry* 14, 1203–1206 (2004).
24. W. Wang, O. Varghese, O. Paulose, C. Grimes, A study on the growth and structure of titania nanotubes, *Journal of Materials Research* 19, 417–422 (2004).
25. X. Sun, Y. Li, Synthesis and Characterization of Ion-Exchangeable Titanate Nanotubes, *Chemistry – A European Journal* 9, 2229–2238 (2003).
26. Ch. Quing, Z. Wuzong, D. Gaohui, P. Lian-Mao, Protonated titanates and TiO_2 nanostructured materials: synthesis, properties, and applications, *Advanced Materials* 18, 2807–2824 (2006).
27. S. Zhang, Q. Chen, L.-M. Peng, Structure and formation of $H_2Ti_3O_7$ nanotubes in an alkali environment, *Journal of Physical Chemistry B* 71, 014104–014119 (2005).

NEW INSIGHT INTO MECHANISMS OF SOL-GEL PROCESS AND NEW MATERIALS AND OPPORTUNITIES FOR BIOENCAPSULA-TION AND BIODELIVERY

VADIM G. KESSLER*, GULAIM A. SEISENBAEVA
Department of Chemistry, SLU, Box 7015, 75007 Uppsala, Sweden

Abstract. The review considers principal mechanisms in solution transformations, hydrolysis and condensation of alkoxysilanes and metal alkoxide complexes and the pathways of further transformations of the thus formed colloid systems. The versatility of silica sol-gel is provided by the possibility to direct the kinetically controlled process towards either polymeric or micellar colloids. The hydrolysis of metal alkoxides is kinetically unhindered and results in formation of Micelles Templated by Self-Assembly of Ligands (MTSALs) under the local equilibrium conditions. The morphology, reactivity, long term stability and biocompatibility of MTSALs can be efficiently controlled by the choice of metal cations, ligands and the conditions of hydrolysis. Application of the MTSAL concept for the synthesis of hierarchically porous materials and the prospects of their use in bio-encapsulation and biodelivery for water and soil remediation processes are discussed.

Keywords: Chemical modification, functional ligands, micelles templated by self-assembly of ligands (MTSAL) mechanism, drug delivery, controlled release, biocontrol applications, soil and water remediation.

1. Introduction

The growing interest in water and soil remediation strategies based on environmentally friendly approaches in combination with the need in monitoring the biologically significant concentrations of potentially hazardous pollutants has urged during the last decade a search for directly biological means for solution

*To whom correspondence should be addressed: Vadim G. Kessler; e-mail: vadim.Kessler@kemi.slu.se

P. Innocenzi, Y. L. Zub and V. G. Kessler (eds.), *Sol-Gel Methods for Materials Processing*.

of these problems. An especially attractive possibility is provided by the use of naturally immobilized organisms such as marine algae for water remediation. The species of a very common Porphyra family have been shown, for example, to be able to decrease strongly the nitrogen content in waters deteriorated by common agricultural fertilizers, permitting a quick and efficient restoring of the biodiversity.[1] Application of bacterial and bacteria-fungi co-cultures can significantly broaden the spectrum of environmental problems that can be solved using biological tools. There has been reported in particular a successful removal of uranium from groundwater by iron-reducing Geobacter species stimulated by acetate amendment[2] and remediation of soils highly polluted by polycyclic aromatic hydrocarbons using a co-culture of Aspergillus terreus and Penicillum species.[3] A brief overview of the enormously broad field of the use of bacteria in bioremediation has been recently provided by Saier in.[4]

Efficient application of microorganisms for biosensing and bioremediation requires their immobilization in biocompatible matrices able to support their survival and useful activity during a long time. The quest for immobilization becomes ultimate for the application of biomolecules for these purposes. Immobilization and, more specifically, encapsulation for the microorganisms and solid grafting for biomolecules are also indispensable for preventing the leakage of the non-inherent biological material into the environment. The research in development of materials for bioencapsulation has originally been focused almost exclusively on organic and, in the first hand, biodegradable polymers such as starch,[5] guar gum[6] and calcium alginate,[7,8] being directed primarily on the delivery of probiotics into human organism. The focus on biosensing and bioremediation applications urged then interest for the systems able to host living microorganisms while at the same time preventing their proliferation.[9] Capsules of this kind had to be highly resistant to biodegradation and the approach to their preparation was sought in the inorganic sol-gel technology.[10] The aim of this review is to demonstrate how the fundamental mechanisms of sol-gel processing can be exploited for the preparation of different types of bioencapsulation materials with controlled porosity, biocompatibility, stability and chemical reactivity.

2. Sol-Gel Synthesis of Silica

Silica along with calcium carbonate and calcium hydroxide phosphate, apatite, belongs to the most widespread natural mineral components in the skeletal tissues, which made it an attractive and the historically first candidate for the role of the sol-gel bioencapsulation matrix.

2.1. HYDROLYSIS OF ALKOXYSILANES

The most important feature of the alkoxide derivatives of silicon – alkoxysilanes, $Si(OR)_4$, and alkylalkoxysilanes, $R_nSi(OR)_{4-n}$, where n = 1–3, lies in the character of the chemical bonding in these species. Silicon is a non-metal with a pronounced trend to formation of high energy Si···O bonds with increased multiplicity due to pπ-dπ interactions. The latter compensate for the relatively electropositive character of the silicon atom (Pauling electronagativity 1.8) in the σ-bonds, which results in anomalously low polarity of the silicon-oxygen bonds.[11–13] The calculated partial charge at the silicon atom equals approximately +0.32.[14] It is even possible to draw an analogy between the conjugation in the tetrahedral ensemble of the Si···O bonds in $Si(OR)_4$ with that in the carboxylic ester groups C=O(OR) (see Figure 1).[13]

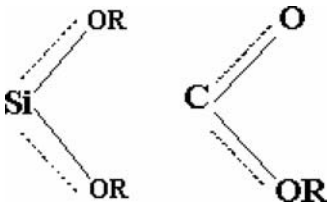

Figure 1. Bond conjugation in silica and carboxyl esters.

Due to the low polarity of bonds, the alkoxysilanes display a complex of properties typical for the esters (fats) as a class of compounds: they are well soluble in organic solvents, but practically insoluble in water and, due to their extremely low acidity and basicity by Lewis, are rather stable to hydrolysis. The latter can be facilitated using protolytic catalysts, acids or bases, i.e. by the same approaches as the hydrolysis of carboxylic esters. The analogous reaction mechanisms belonging to the nucleophylic substitution type have been originally proposed for these processes by Bradley, Mehrotra and Gaur.[15] It can be noticed that in analogy with the organic esters, where the increase in the size of the alkyl group in the alcohol residue and, to a smaller extent, in the size of the carboxylic acid residue are hindering the kinetics of hydrolysis, the speed of hydrolysis decreases in the series Me > Et > ^{n}Pr > ^{i}Pr ≈ ^{n}Bu and is slightly lower for alkylalkoxysilanes compared to unsubstituted $Si(OR)_4$.

2.1.1. *Basic Catalysis in Hydrolysis of Alkoxysilanes*

The hydrolysis of alkoxysilanes in solution in water-alcohol medium can be accelerated by addition of basic reagents, usually ammonia or alkylamines. The reaction mechanism involves nucleophylic attack of the hydroxide group on the positively charged silicon atom with formation of an intermediate penta-

coordinate anion (S_N2-type process, see Figure 2). The alkoxide anion is a bad leaving group and the process results in the further proton transfer to it from the more acidic Si-OH group with formation of an alcohol. The hydrolyzed species is initially negatively charged and can loose this charge through hydrolysis equilibrium with the excess of water. The decreased spatial hindering and lower inductive effect of the proton replacing the alkyl group makes the partially hydrolyzed species more prone to further hydrolysis, while the negative charge obtained through their deprotonation is a considerable hinder for the condensation. The practically complete loss of alkoxide groups with formation of initially mainly monomeric species is a matter of minutes at room temperature.[16, 17]

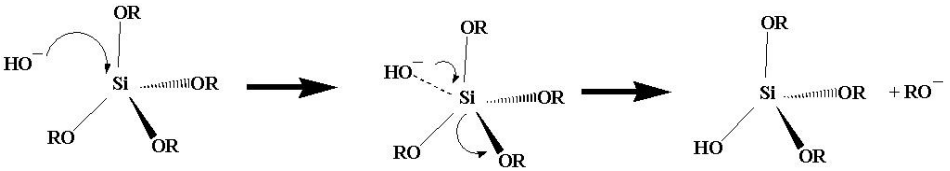

Figure 2. Basic catalysis in hydrolysis of alkoxysilanes.

2.1.2. *Acidic Catalysis in Hydrolysis of Alkoxysilanes*

The hydrolysis of alkoxysilanes in the presence of acids becomes a really facile reaction. The mechanism[15,17] involves at the beginning the protonation of an oxygen atom of the alkoxide ligand and passes through a tetra-coordinate alkoxide cation (proton-assisted S_N1 reaction, see Figure 3).

This indicates that the Lewis basicity dominates over Lewis acidity for the alkoxysilane compounds. The intermediate species formed in the acid-catalyzed hydrolysis is uncharged and its acidic dissociation is hindered by the low pH in the solution, which opens the ways for condensation reactions.

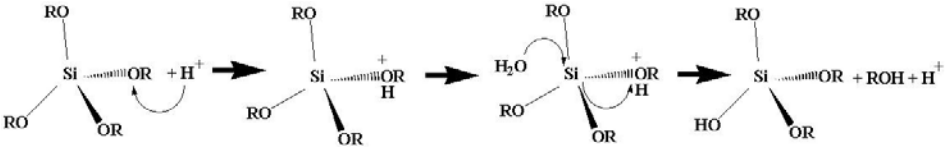

Figure 3. Acidic catalysis in hydrolysis of alkoxysilanes.

2.1.3. *Polycondensation Reactions in Formation of Silica*

The covalent character of bonding in the silicon-based species makes the reactions of hydrolysis and condensation/polycondensation kinetically independent. Moreover, two different kinetically independent pathways, oxolation and alkoxolation (see Figure 4) have been discussed in literature, but the occurrence of the latter one is strongly questionable at least in the basic media.[16]

The rheology and structure of the resulting colloids is very strongly dependent upon the conditions of their preparation: application of basic catalysis leads to formation of monomers that are transformed further into smaller cross-linked aggregates with micellar type rheology (weak interactions between micelles). The acidic catalysis results initially in less cross-linked long chain polymer molecules. Such colloids display well-pronounced aging behavior, starting with low viscosity but soon becoming highly viscous and then turning into transparent monoliths[16–18] (see Figure 5). Addition of an excess of acid (achieving pH below 1.0) results, however in peptization of gels with formation of positively charged highly internally cross-linked micelles.

The application for bioencapsulation purposes requires normally presynthesis of a sol (colloid solution) and mixing it with a solution of biological components (biomolecules, organelles, microorganisms) buffered at neutral pH. The achievement of the gelation point is most commonly assisted by drying. The alternative approach to biocompatible silica is provided by the use of the soda glass – the water-soluble sodium silicate. Its solution with appropriate concentration is simply mixed with a buffered solution of the biological samples and the condensation occurs in analogy with that for the alkoxysilanes hydrolyzed in the basic media through formation of loosely connected aggregates.

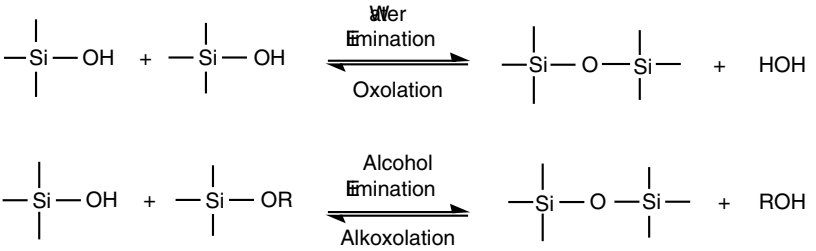

Figure 4. Condensation reactions of silicon-based species.

Figure 5. The structure of typical silica colloids obtained via polycondensation in acidic (upper image) and basic media (below) respectively.

2.1.4. *Activation of Silicon Alkoxides Through Complexation with Chelating Ligands*

The studies of silicon alkoxide complexes with chelating ligands have started as purely fundamental structural research in the early 1980s. It appeared intriguing to be able to approach the "hypervalent", highly coordinated, derivatives of silicon. The first and rather fascinating result of these works was that the ligand-induced deviation of the O-Si-O angle from the ideal tetrahedral values causes directly the weakening of the Si-O bonds through elimination of the pπ-dπ component. Thus if the Si-O bond length in the ideally tetrahedral $Si(O^iPr)_4$ is 1.615 Å[19] and in the symmetric octamethoxy-octasiloxane, $[CH_3OSiO_{3/2}]_8$, even shorter 1.592–1.605 Å,[20] the bond length within the SiO_4 tetrahedron formed by two chelating ligands in the silicon pinacolate-monomethyl-diethanolaminate varies already in the interval 1.644–1.671 Å.[21] The increase in bond lengths in combination with unchanged coordination number gives a strong indication of enhanced charge distribution. In the structures of pentacoordinated glycolato-silicate alkoxides (see Figure 6) the bond lengths within the chelating cycles are approximately in the same range or even slightly elongated compared to the tetracoordinate chelates, 1.663–1.762 Å.[22,23]

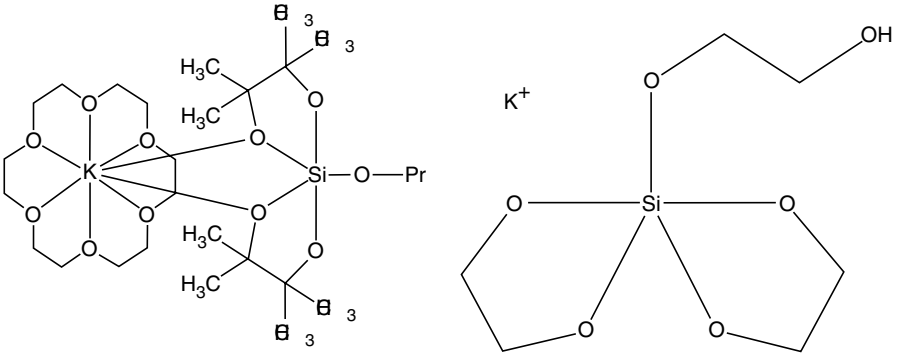

Figure 6. Structure diagrams for the pentacoordinated glycolato-silicate alkoxides.[22,23]

The most indicative is that the length of the Si-O bond to the fifth – alkoxide (!) – ligand is in these species also increased to 1.654–1.679 Å, independently of the sterical demands of the chelating ligands, being practically identical for both pinacolate and glycolate complexes. This means that introduction of the chelating ligands is generally associated for the alkoxysilane species with appreciably increased polarity of bonds. The anionic pentacoordinate chelate complexes of silicon with glycolate ligands are rather stable and can in fact be obtained through facile dissolution of silica in glycol in the presence of alkali hydroxides.[23] It has been noticed already at the end of 1990s that pentacoordinate silicon complexes

with chelating glycolate ligands are demonstrating much higher reactivity in the reactions of ligand exchange in comparison with tetracoordinate homoleptic alkoxysilanes. In analogy with metal alkoxides (see below) they are readily exchanging the alkoxide ligands with the alcohol solvent without need in prolonged reflux to shift the equilibrium.[24] It has also been noticed that both the pentacoordinate glycolate alkoxide and also the recently studied hexacoordinate β-diketonato-alkoxide complexes of silicon[25] are hydrolyzed already in contact with atmospheric moisture, without any need in a protic catalyst. This increased reactivity can only be attributed to strongly increased Lewis basicity of these species, originating from the efficiently increased charge distribution, and permitting to exploit the proton-assisted S_N1 pathway.

2.2. BIOENCAPSULATION IN THE SILICA MATRICES

The development of silica-based bioencapsulates has a long and successful story. Already in the mid 1990s the classic sol-gel approaches based on hydrolysis of alkoxysilanes and alkylalkoxysilanes have been applied for the efficient immobilization of proteins and whole cells in chemically and mechanically resistant inorganic matrices.[26–28] As it was summarized in 1998 by Gill and Ballesteros[29] an impressive success had been achieved, just to mention some examples, in using silica immobilized enzymes, catalytic antibodies, noncatalytic proteins, (poly)nucleic acids and microbial, plant, and animal cells for the preparation of biocatalysts,[27,30–36] biosensors,[37–41] immunodiagnostic kits,[42–45] bio-optical devices,[46–49] bioimplants and artificial organs,[50,51] adsorbents for the removal of enzymes[52] etc. The use of alkoxysilanes, however, was envisaged to import a number of considerable drawbacks, decreasing the possible biocompatibility and viability/long term biological stability of encapsulates obtained from them. The major difficulties turned to be associated with liberation of alcohols and the need in a co-solvent and catalysts for the carrying out of hydrolysis. A principal innovation proposed by Gill and Ballesteros lied in application of silica esters of polyols.[29] The products of pre-hydrolysis of $Si(OMe)_4$ together with polymethylsilicate were subjected to transesterification with glycerol offering water-soluble and biocompatible polyglycerolsilicate, providing an approach to a silica matrix under pH-neutral and alcohol-free conditions. Broad variety of enzymes have been encapsulated in thus obtained matrix revealing stable high longtem activity. The results of this work have been summarized in[53] and developed further towards preparation of hybrid polymers in combination with conjugated polydiacetylenes as copolymers possessing useful optical properties. The hybrids have been successfully used then as optical immunosensors.[54] The idea of employing a hybrid matrix in encapsulation of enzymes had been developed further by the group of Livage towards com-bination of the

most biocompatible organic matrix – calcium alginate – with a silica-based inorganic one. Both coating of alginate capsules with a silica layer[55] and coating of a mesoporous silica beads with a calcium alginate layer[56] have been reported. Further search for improved biocompatibility has attracted attention of many researchers to creation of truly biomimetic conditions, urging application of the biosynthetic pathways offered by the metabolism of micro-organisms possessing a silica skeleton. Transformation of amorphous silica with the aid of silaffin polypeptides from diatoms permitted to obtain at pH-neutral conditions and at ambient temperature and pressure the silica spheres loaded with enzymes demonstrating unreduced long-term activity.[57]

The polycondensation of sodium silicate in a buffered solution of living cells provided an approach to immobilization of the living cells in a silica matrix.[10] This approach has failed, however, in achieving the conditions of true encapsulation: the immobilized cells (E-coli bacteria) displayed unhindered proliferation when spread on the cultivation plates. The practical solution for the application of the thus immobilized bacteria has been sought in placing the prepared silica matrix into a specially designed filter constructed using a small-pore polyester membrane[58] (see Figure 7).

The biological application of silica-based sol-gel materials have been recently reviewed in.[59]

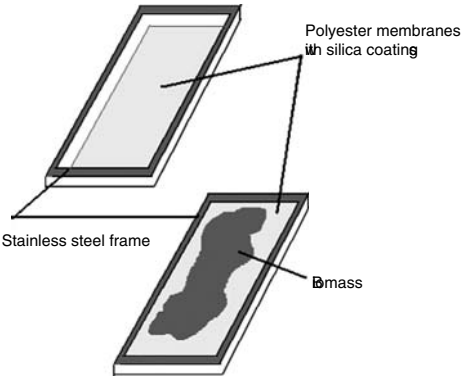

Figure 7. Experimental scaffold for enclosure of silica-immobilized biomass.[58]

3. Sol-Gel Synthesis of Metal Oxides

While metal oxides are actually not found as skeletal materials in the living beings, many of them are present as mineral components in natural biosystems and display high chemical and biological inertness and excellent biocompatibility. As the best studied examples one can mention titanium dioxide and iron(III)

oxide. Titanium dioxide is even classified as an internationally accepted food additive (E171) and is used as a component in toothpaste, drug formulations (tablets) and, as a pigment, in food, for example, mayonnaise. The application of metal oxides as matrices in bioencapsulation is only uprising and we will discuss below the particular features of their formation in sol-gel approaches.

3.1. HYDROLYSIS OF METAL ALKOXIDES

Metal alkoxides are compounds resembling the alkoxysilanes in some of their physicochemical characteristics, such as solubility in organic solvents, in many cases – volatility, and last, but far not the least, in a possibility to convert them into oxides through hydrolytic treatment, constituting the basis of the sol-gel technology. This resemblance, however, is just illusory. The theoretical analysis of the chemical bonding in metal alkoxides demonstrates clearly that the nature of the alkoxide ligand as a weak σ- and a strong π-donor favors the predominantly electrostatic interactions for the metal cations incomparable with silicon in the ability to charge-compensation via pπ-dπ interactions. Metal alkoxides can be described as ionic salts not only for the derivatives of the most electropositive metals, such as alkali or alkaline earth ones. The theoretical studies indicate domination of the electrostatic interactions even for the derivatives of Mo(VI) and W(VI),[60] and Nb(V) and Re(V,VI).[61] The partial charge distribution in the structures of the known titanium alkoxides turns out to be very closely analogous to that in the polymorphs of crystalline TiO_2 – typical ionic close-packed structures.[62] It is necessary to keep in mind that metal alkoxides are salts of alcohols – extremely weak and often volatile acids, which makes them to behave as strong Brønsted bases as they involve the corresponding bases of these protolyte solvents as ligands. The ability of metal alkoxides to react immediately with acidic ligands was first reported by Wengrovius et al. in 1986.[63] Another important combination of properties – extremely weak Lewis acidity and high Lewis basicity has been noticed by Bradley et al. already in the early 1960s: metal alkoxides form eagerly aggregates, using alkoxide ligands for bridging. Formation of solvates is possible only if the solvating ligand can form a hydrogen bond to an alkoxide ligand, i.e. acts as a Brønsted acid.[64,65] The solvates are naturally common for the alkoxides of the most electropositive metals – alkaline, alkaline earth and rare earth ones, but are extremely scarce or non-existent for high-valent metals, e.g. Nb(V), Mo(VI), W(VI), where the Lewis basicity is decreased by the increased charge of the cation. The Lewis acidity of the metal centers themselves is apparently insufficient to influence reactivity of the species. A plethora of structural confirmations of this fact has recently been produced by Schubert et al.[66]

3.1.1. *Mechanism of Ligand Exchange Reactions in Metal Alkoxides*

One of the most important consequences of the electrostatic character of bonding in metal alkoxides lies in low activation energies of the ligand exchange processes. According to the experimental kinetic measurements carried out for the alkoxides of aluminium in 1986 by Wengrovius et al.[63] and recently for Ti(IV) by Brown et al.[67] their values normally do not exceed 30–40 kJ/mol. The reaction starts with the protonation of the highly basic alkoxide ligand with the formation of the intermediate alkoxide cation as the speed-limiting step followed by addition of the corresponding base of the new ligand with simultaneous elimination of alcohol,[67] i.e. follows the proton-assisted S_N1-type transformation (see Figure 8).

The S_N2 mechanism sometimes earlier argued for the ligand exchange in metal alkoxides (see, for example,[14]) is contradicting to the experimental kinetic data and should be, according to the theoretical calculations reported in,[68] associated with activation energies of about 600 kJ/mol, i.e. about 20 (!) times higher than those observed experimentally.

The low activation energies in the ligand exchange reactions in combination with extremely facile rearrangement of the metal-oxygen cores convert microhydrolysis and condensation for metal alkoxides into one single process leading to equilibrium oxoalkoxide products.[69,70] Introduction of the chelating ligands has recently been demonstrated to additionally accelerate the hydrolysis-condensation process through increased charge distribution, decreased sterical protection of the metal centers and high mobility of the chelating ligands enhanced additionally on application of polar and protic solvents such as alcohols.[71] The molecular species isolated in microhydrolysis display often the fraction of chelating ligands considerably different from that observed for the non-hydrolyzed species in solution.[72]

It should thus be concluded that the sol-gel transition in metal oxide colloids produced from metal alkoxides could impossibly be due to the hydrolysis-condensation reaction. The latter is tremendously quick and results in self-assembled micellar particles formed under the conditions of local equilibrium. The ligands attached to the hydrolyzed metal hydroxide units are concentrated

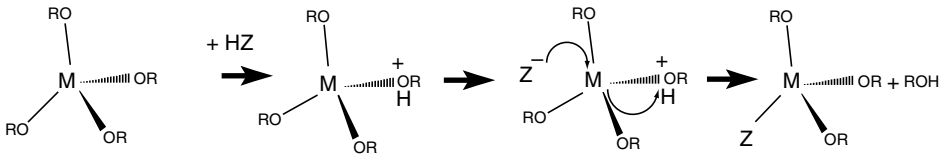

Figure 8. Proton-assisted S^N1-type mechanism for ligand exchange in metal alkoxides.

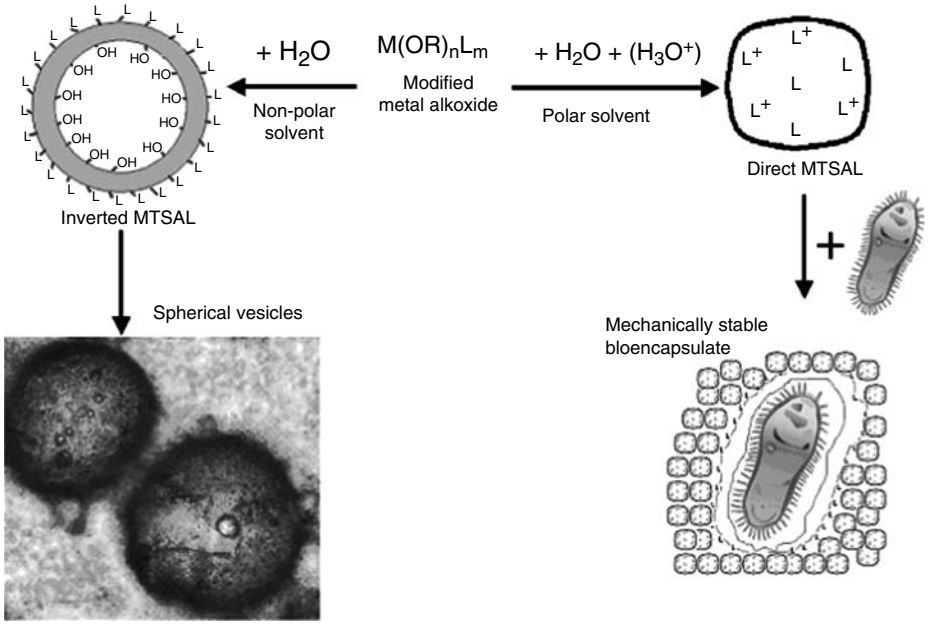

Figure 9. Formation of Micelles Templated by Self-Assembly of Ligands (MTSALs) on hydrolysis-condensation of metal alkoxides.

on the surface of the thus formed aggregates and act as surfactants stabilizing the resulting micelles (see Figure 9). We have proposed to designate these particles by a term Micelles Templated by Self-Assembly of Ligands (MTSALs).[71]

3.2. ENCAPSULATION PROSPECTS IN THE METAL OXIDE MATRICES

The inverted micellar systems are formed when a solution in a polar solvent, most often water, is introduced into a non-polar medium with controlled viscosity (solvent or oil) and stabilized by a surfactant. As the modified alkoxide produces units, acting as surfactant on hydrolysis, we investigated the formation of vesicles on introduction of water-based solutions of inorganic and organic dyes into hydrocarbon (hexane) solution of modified zirconium and titanium alkoxides on vigorous shaking. This procedure resulted in formation of spherical capsules with an approximate size of about 100 μm. The optical properties of the capsules indicated that they had dense walls: the color of the dyes was lighter in reflected and darker in transient light. That demonstrated the occurrence of the complete inner reflection phenomenon requiring the ideal mirror properties of the inner surface of the shell walls.

We wanted also to apply a sensitive marker to demonstrate that the hydrocarbon solvent does not diffuse efficiently inside the inverted micelles. As a marker, we have chosen the whole blood cells. The solution of erythrocytes was prepared by diluting 0.2 ml of fresh blood with 20 ml of isotonic NaCl solution. 0.5 ml of this bright red solution, containing undestroyed erythrocytes according to microscopic observation, were added by syringe on vigorous shaking to the of solution of $Zr(O^nPr)_3(thd)$ in 5 ml dry hexane. The water phase was immediately transformed into tiny light brick-red spheres hardly distinguishable by a bare eye. The solution above them remained completely clear for at least 1 h, when light opalescence started to appear. The spheres were stable on shaking in the hexane solution but were destroyed by putting a cover glass over them. The immediate observation of the water phase released then into paraffin oil (about 3 h after encapsulation) showed a fraction of undestroyed erythrocytes (which are highly sensitive and destroyed rather quickly on contact with hexane).

The amphiphylic nature of the walls of the prepared vesicles was additionally demonstrated by encapsulation of a water suspension of green fluorescing 2.2 μm polystyrene microspheres (Duke Scientific Corp., Palo Alto, CA, USA). These suspensions are commonly used in the microbiological studies and are stable in water. Polystyrene, however, is a weakly hydrophobic material, which meant it should have been extracted into the amphiphylic shell in the process of encapsulation. The microscopic observations were completely in accordance with the expectations – the microspheres have not escaped from the droplets into hexane solution as the formation of the shells is a quick process, but turned to be located inside the shells and not in the volume of the droplets.

The stability of these latter thin-walled shells was evaluated in the presence of humidity and shear forces via drying of a colloid solution, containing "hollow" (water solution filled) spheres on carbon grids, followed by investigation by Scanning Electron Microscopy (SEM). This treatment (see Figure 10) resulted in formation of dense films incorporating spherical cavities – potential hosts for encapsulation of a target aqueous medium. This deep transformation of the original spherical shells indicates that the mobility of ligands is actually very high even after the formation of the capsules. Films with random distribution of closed spherical cavities filled with a hydrophilic component are a new and interesting type of material.

A series of experiments on encapsulation of microorganisms and of plant seeds applying direct micelles prepared from titanium and zirconium alkoxides has also been carried out, demonstrating biocompatibility of the produced encapsulates and also their high mechanical stability. The details of this work have been protected by a Patent[73] and will be reported in a near future.

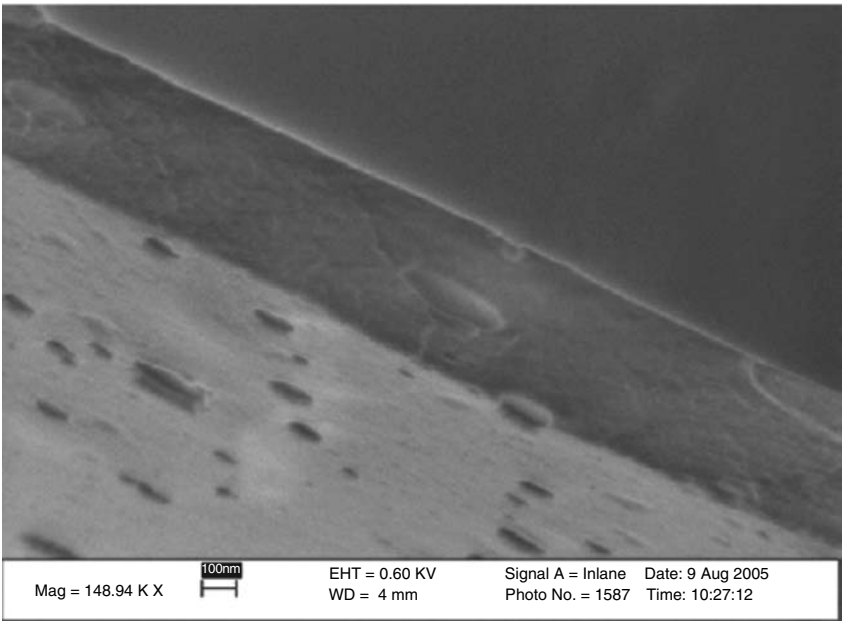

Figure 10. Films prepared on carbon grids from the colloids containing hollow spheres.[71]

References

1. J.K. Kim, G.P. Kraemer, C.D. Neefus, I.K. Chung, C. Yarish, *J. Appl. Phycol.* 19, 431 (2007).
2. S.B. Yabusaki, Y. Fang, P.E. Long, C.T. Resch, A.D. Peacock, J. Komlos, P.R. Jaffe, S.J. Morrison, R.D. Dayvault, D.C. White, R.T. Anderson, *J. Contaminant Hydrol.* 93, 216 (2007).
3. J.D. Kim, C.G. Lee, *Biotechnol. Bioproc. Eng.* 12, 410 (2007).
4. M.H. Saier, *Water Air Soil Pollut.* 184, 1 (2007).
5. T. Jankowski, M. Zielinska, A. Wysakowska, *Biotechnol. Tech.* 11, 31 (1997).
6. T.B. Hammill, R.L. Crawford, *Canadian J. Microbiol.* 43, 1091 (1997).
7. K.E. Stormo, R.L. Crawford, *Appl. Environ. Microb.* 58, 727 (1992).
8. C. Bienaime, J.N. Barbotin, J.E. Nava-Saucedo, *J. Biomed. Mater. Res.* 67A, 376 (2003).
9. J.R. Premkumar, R. Rosen, S. Belkin, O. Lev, *Anal. Chim. Acta* 462, 11 (2002).
10. N. Nassif, O. Bouvet, M.N. Rager, C. Roux, T. Coradin, J. Livage, *Nat. Mater.* 1, 42 (2002).
11. I.A. Brytov, Y.N. Romashenko, B.F. Shchegolev, *J. Struct. Chem*. 20, 190 (1979).
12. L.N. Pankratova, V.V. Zhakhovskii, G.S. Kharitonova, A.Y. Rabkina, B.G. Zavin, *Russ. Chem. Bull.* 37, 1573 (1988).
13. A.N. Egorochkin, *Russ. Chem. Rev.* 54, 786 (1985).
14. J. Livage, C. Sanchez, *J. Non-Cryst. Solids* 145, 11 (1992).
15. D.C. Bradley, R.C. Mehrotra, D. Gaur, *Metal Alkoxides* (Academic, London) (1978).

16. C.J. Brinker, G.W. Sherer, *J. Non-Cryst. Solids* 70, 301 (1985).
17. C.J. Brinker, *J. Non-Cryst. Solids* 100, 31 (1991).
18. C.J. Brinker, K.D. Keefer, D.W. Chaefer, R.A. Assink, B.D. Kay, C.S. Ashley, *J. Non-Cryst. Solids* 63, 45 (1984).
19. N.W. Mitzel, A.J. Blake, D.W.H. Rankin, *J. Am. Chem. Soc*. 119, 4143 (1997).
20. V.W. Day, W.G. Klemperer, V.V. Mainz, D.M. Millar, *J. Am. Chem. Soc*. 107, 8282 (1985).
21. A.A. Kemme, Y.Y. Bleidelis, I.P. Urtane, G.I. Zelchan, E. Dukevits, *J. Struct. Chem.* 25, 165 (1984).
22. K.C.K. Swamy, V. Chandrasekhar, J.J. Harland, J.M. Holmes, R.O. Day, R.R. Holmes, *J. Am. Chem. Soc.* 112, 2341 (1990).
23. K.Y. Blohowiak, D.R. Treadwell, B.L. Mueller, M.L. Hoppe, S. Jouppi, P. Karsal, K.W. Chew, C.L.S. Scotto, F. Babonneau, J. Kampf, R.M. Laine, *Chem. Mater.* 6, 2177 (1994).
24. W. Donharl, I. Elhofer, P. Wiede, U. Schubert, *J. Chem. Soc., Dalton Trans.* 15, 2445 (1998).
25. C. Xu, T.H. Baum, A.L. Rheingold, *Inorg. Chem.* 43, 1568 (2004).
26. D. Avnir, *Acc. Chem. Res*. 28, 328 (1995).
27. D. Avnir, S. Braun, *Biochemical Aspects of Sol-Gel Science and Technology* (Kluwer, Hingham, MA) (1996).
28. L.M. Ellerby, C.R. Nishida, F. Nishida, F.A. Yamanaka, B. Dunn, J.B. Valentine, J.I. Zink, *Science* 255, 1113 (1992).
29. I. Gill, A. Ballesteros, *J. Am. Chem. Soc.* 120, 8587 (1998).
30. D. Avnir, S. Braun, O. Lev, M. Ottolenghi, *Sol-Gel Optics* (Klein L., Ed., Kluwer, Berlin) (1994).
31. D. Avnir, S. Braun, O. Lev, M. Ottolenghi, *Chem. Mater.* 6, 1605 (1994).
32. R. Armon, C. Dosoretz, J. Starosvetsky, F. Orshansky, I. Saadi, *J. Biotechnol.* 51, 279 (1996).
33. S. Shtelzer, S. Rappoport, D. Avnir, M. Ottolenghi, S. Braun, *Biotechnol. Appl. Biochem.* 15, 227 (1992).
34. M.T. Reetz, A. Zonta, J. Simplekamp, *Angew. Chem., Int. Ed.* 34, 301 (1995).
35. O. Heichal-Segal, S. Rappoport, S. Braun, *Biotechnology* 13, 798 (1995).
36. M.T. Reetz, A. Zonta, J. Simplekamp, W. Koenen, *Chem. Commun.* 1397 (1996).
37. B.C. Dave, B. Dunn, J.S. Valentine, J.I. Zink, *Anal. Chem.* 66, 1120A (1994).
38. J. Lin, C.W. Brown, *Trends Anal. Chem.* 16, 200 (1997).
39. S. Barreau, J.N. Miller, *Anal. Commun.* 33, 5H (1996).
40. B.D. MacCraith, C.M. McDonagh, G. O'Keefe, A.K. McEnvoy, T. Butler, F.R. Sheridan, *Sens. Actuators* B29, 51 (1995).
41. I. Pankratov, O. Lev, *J. Electroanal. Chem*. 393, 35 (1995).
42. J.Y. Barreau, J.M. Da Costa, I. Desportes, J. Livage, M. Monjour, M. Gentilini, *Compt. Rend. Acad. Sci., Ser. III* 317, 653 (1994).
43. J. Livage, J.Y. Barreau, J.M. Da Costa, I. Desportes, *SPIE Proc*. 2228, 493 (1994).
44. J. Livage, C. Roux, J.M. Da Costa, I. Desportes, J.F. Quinson, *J. Sol-Gel Sci. Tech.* 7, 45 (1996).
45. R. Wang, U. Narang, P.N. Prasad, F.V. Bright, *Anal. Chem.* 65, 2671 (1993).
46. H.H. Weetall, *Biosens. Bioelectr.* 11, 327 (1996).
47. S. Wu, L.M. Ellerby, J.S. Cohan, B. Dunn, M.A. El-Sayed, J.S. Valentine, J.I. Zink, *Chem. Mater.* 5, 115 (1993).
48. Z. Chen, L.A. Samuelson, J. Akkara, D.L. Kaplan, H. Gao, J. Kumar, K.A. Marx, S.K. Tripathy, *Chem. Mater.* 7, 1779 (1995).
49. Z. Chen, D.L. Kaplan, K. Yang, J. Kumar, K.A. Marx, S.K. Tripathy, *J. Sol-Gel Sci. Tech.* 7, 99 (1996).

50. E.J.A. Pope, K. Braun, C.M. Peterson, *J. Sol-Gel Sci. Tech.* 8, 635 (1997).
51. E.J.A. Pope, *Ceram. Trans.* 63, 17 (1996).
52. U. Narang, M.H. Rahman, J.H. Wang, P.N. Prasad, F.V. Bright, *Anal. Chem.* 67, 1935 (1995).
53. I. Gill, *Chem. Mater.* 13, 3404 (2001).
54. I. Gill, A. Ballesteros, *Angew. Chem., Int. Ed.* 42, 3264 (2003).
55. T. Coradin, E. Marcey, L. Lisnard, J. Livage, *Chem. Commun.* 2496 (2001).
56. T. Coradin, J. Livage, *Compt. Rend. Chim.* 6, 147 (2003).
57. H.R. Luckarift, J.C. Spain, R.R. Naik, M.O. Stone, *Nature Biotechnol.* 22, 211 (2004).
58. R. Pedrazzani, G. Bertanza, C. Maffezzoni, M. Gelmi, N. Manca, L.E. Depero, *Water Res.* 39, 2056 (2005).
59. D. Avnir, T. Coradin, O. Lev, J. Livage, *J. Mater. Chem.* 16, 1013 (2006).
60. G.A. Seisenbaeva, P. Werndrup, L. Kloo, V.G. Kessler, *Inorg. Chem.* 40, 3815 (2001).
61. G.A. Seisenbaeva, A.I. Baranov, P.A. Shcheglov, V.G. Kessler, *Inorg. Chim. Acta* 357, 468 (2004).
62. K. Gigant, A. Rommel, M. Henry, *J. Am. Chem. Soc.* 123, 11632 (2001).
63. J.H. Wengrovius, M.F. Garbauskas, E.A. Williams, R.C. Going, P.E. Donahue, J.F. Smith, *J. Am. Chem. Soc.* 982, 108 (1986).
64. M.S. Bains, D.C. Bradley, *Can. J. Chem.* 40, 2218 (1962).
65. M.S. Bains, D.C. Bradley, *Can. J. Chem.* 44, 534 (1966).
66. H. Fric, M. Puchberger, U. Schubert, *J. Sol-Gel Sci. Tech.* 40, 155 (2006).
67. K.C. Fortner, J.P. Bigi, S.N. Brown, *Inorg. Chem.* 44, 2803 (2005).
68. A. Senouci, M. Yaakoub, C. Huguenard, M. Henry, *J. Mater. Chem.* 14, 3215 (2004).
69. G. Westin, U. Bemm, R. Norrestam, M. Nygren, *J. Sol-Gel Sci. Tech.* 8, 23 (1997).
70. G.A. Seisenbaeva, S. Gohil, V.G. Kessler, *J. Mater. Chem.* 14, 3177 (2004).
71. V.G. Kessler, G.I. Spijksma, G.A. Seisenbaeva, S. Håkansson, D.H.A. Blank, H.J.M. Bouwmeester, *J. Sol-Gel Sci. Tech.* 40, 163 (2006).
72. G.I. Spijksma, H.J.M. Bouwmeester, D.H.A. Blank, A. Fischer, M. Henry, V.G. Kessler, *Inorg. Chem.* 44, 9938 (2006).
73. V.G. Kessler, G.A. Seisenbaeva, S. Håkansson, M. Unell, Patent WO 07145573 A1, priority date June 12, 2006.

SELECTED CONTEMPORARY TOPICS IN SOL-GEL ELECTRO-CHEMISTRY

SERGEY SLADKEVICH, SHAUL MIZRAHI, JENNY GUN, PETR PRIKHODCHENKO, DAN RIZKOV, RIMMA SHELKOV, NILAR KYI, VITALY GUTKIN AND OVADIA LEV*

The Casali Institute, The Institute of Chemistry, The Hebrew University of Jerusalem, Jerusalem, 91904, Israel

Abstract. This review provides an overview of some exciting, new as well as somewhat older, directions in sol-gel electrochemical applications of silicates and composite silicate electrodes. Rather than provide an exhaustive account of all the many papers that have been published on sol-gel electrochemistry and composite sol-gel electrodes, we prefer to illustrate the versatility of sol-gel chemistry by a few select examples which on the one hand illustrate the power entailed in sol-gel technology for electrochemical applications, and on the other hand point to hot electrochemical fields in which more research is due and exciting developments are to be expected. We start this review with a brief historical perspective. The inorganic sol-gel and silicone electrochemistry fields are both rather old though never extensively dealt with particularly when it comes to sensing applications. In contrast, the sol-gel electrochemistry of inorganic-organic hybrids is a relatively young field whose importance was recognized only in the last 30 years, and despite, or maybe even owing to the late recognition it is being very extensively studied nowadays. The use of composite electrodes for sensing and other applications is emphasized in this review, and the fast evolving electrodriven deposition techniques are reviewed.

Keywords: Silica, silicate, ormocer, doped sol-gel, polymer, redox, graphite, CCE.

1. Introduction with Some Historical Perspective

Sol-gel electrochemistry is by now a mature technology that is used regularly for diverse applications in practically all fields of electrochemistry with a special appeal for electrosensing applications.[1–7] Silicates are by far the most useful non

* To whom correspondence should be addressed: O. Lev; e-mail: Ovadia@vms.huji.ac.il

P. Innocenzi, Y. L. Zub and V. G. Kessler (eds.), *Sol-Gel Methods for Materials Processing*.

transition element oxide for sensing applications, partly owing to the redox inertness of the silicates and partly to their inherent rigidity. Indeed for many applications – some of which reviewed here – these two properties are even too constrictive for practical applications and are therefore delicately interfered with by appropriate precursor selection, choice of processing conditions, and more relevant to the current review, by incorporation of a second phase into the silicate network.

This review has the following general structure: It starts with an historical perspective describing in chronological order milestones in the evolution of sol-gel electrochemistry. The second chapter is devoted to a description of some major general advantages entailed in the use of composite materials in sol-gel electrochemistry with extensive referencing and test case demonstrations. The third chapter is devoted to a review of some of the activities in sol-gel electrochemistry of carbon ceramic electrodes with emphasize on their versatile biosensing applications. The fifth chapter describes a recent offspring of the carbon ceramic electrodes – namely the nanoparticle and ATO modified clay – silicate electrodes. Biosensing applications of CCEs are then used to demonstrate the versatility of these composites. The last section is devoted to a brief outline of the fast growing ceramic electrodeposition techniques.

1.1. EARLY STEPS IN THE EVOLUTION OF SOL-GEL ELECTROCHEMISTRY

For centuries the technology of silicon compounds was governed by high temperature processing, limited therefore, to the production of inorganic ceramics. The modern era of silicon chemistry can be traced to the discoverer of silicon. Brezelius used potassium for the reduction of potassium fluosilicate to receive solid silicon and potassium fluoride. Moreover, he soon prepared one of the most important sol-gel precursors, tetrachlorosilane by oxidation of silicon with chlorine.

$$4K + K_2SiF_6 \rightarrow Si + 6KF \tag{1}$$

$$Si + 2Cl_2 \rightarrow SiCl_4 \tag{2}$$

The first record of sol-gel chemistry of silicates is attributed to the French engineer, Jacques Joseph Ebelmen. Looking for a way to prepare tetraethoxysilane from tetrachlorosilane and ethanol, he discovered that the material hydrolyzed slowly to give solid monoliths.[8] Ebelmen's experiment is also a remarkable example of the importance of catalysis in sol-gel processing. Ebelmen did not catalyze the gelation process, and it took 2 years to form the silicate monolith. The experiment that is generally regarded to be the first record of sol-gel processing deserves therefore also a patience award.

$$SiCl_4 + 4C_2H_5OH \rightarrow Si(OCH_2CH_3)_4 + 4HCl \quad (3)$$

The first production of tetraethoxysilane, Ebelmen's original synthesis goal, had to await Mendeleev's time. In 1918 Walter A. Patrick from the John Hopkins University patented the use of silica gel absorbents and licensed it to Grace Davison who continues to manufacture silica gel absorbents up to these days. This development paved the road for the production of chromatographic and other separation media.

Surprisingly, none of the contemporary activities in sol-gel electrochemistry can be traced to the pre-eighties time. The electrochemical applications of silicates did not materialize until the production of NASICONs by sol-gel processing in the early eighties of the last century. NASICON, an acronym for sodium (Na^+) super ion conductor, is a useful class of material exhibiting selective and fast transport of sodium ions.[9] NASICONS have many potential applications in sodium-sulfur batteries and electrochromic displays as well as sodium and carbon dioxide sensing. Until 1980, NASICONs, $Na_{1+x}Zr_2Si_xP_{3-x}O_{12}$ were prepared by high temperature treatment of different mixtures of metal oxides and carbonates. However, at elevated temperatures segregation of a zirconia phase takes place, which interferes with the formation of the NASICON phase. The intimate mixing provided by sol-gel processing allowed reduction of the operating temperature down to 750°C.[10]

The development of organic silicon materials occurred within approximately the same time frame, the most pronounced milestone being the synthesis of tetraethylsilane by Charles Friedel & James Mason Crafts in 1863.

$$SiCl_4 + 2Zn(C_2H_5)_2 \rightarrow (C_2H_5)_4Si + 2ZnCl_2 \quad (4)$$

It took an additional century until the Rochow-Muller copper catalyzed synthesis of dimethylsiloxanes materialized and gave birth to the silicone revolution.

$$SiO_2 + 2C + 2CH_4 + Cl_2 \xrightarrow{Cu} Me_2SiCl_2 + 2HCl + 2CO \quad (5)$$

$$nCl_2(CH_3)_2Si + (n+1)H_2O \rightarrow OH[Si(CH_3)_2O]_nH + 2nCl^- + 2nH^+ \quad (6)$$

The methylsilicones became, almost immediately after the discovery of their industrial synthesis technology in 1940, a center of immense technological activity, and methods to control the molecular size and reactivity of the monomers and for crosslinking of polymers were devised. Compatible pigments, reinforcement agents and additives were developed to extend the range of physical properties attainable by silicones and silicone composites. This effort yielded commercial oils, adhesives, sealants, paints, insulating resins, and many

other useful, widely used products.[11] However, the electrochemical manifestation of this discovery was slow to follow. Early, pre-1980 electrochemical applications were almost exclusively restricted to liquid paste electrodes (made of a mixture of silicone oil and graphite powder), to applications based on RTV binding material (a vulcanized form of dimethylsiloxane), and to gas permeable membranes, such as the oxygen permeable membrane of the Clark type oxygen electrode.

In the early seventies of the last century the field of modified electrodes started to dominate electrochemical sciences. The research was largely driven by the understanding that it is possible to modify electrode properties by polymer or monolayer coatings. Indeed, the first recognition of the importance of organic silicon chemistry for electrochemists came with the emergence of the polymer modified electrodes. Murray and co-workers[12–15] were the first to apply redox modified siloxane films on silicon, platinum, and other metal electrodes. Monolayers and thin films based on trichloro- or trimethoxy-aminosilanes were first coated on electrodes, and redox species were then anchored onto the pre-prepared layers. Although the original intention was to apply a monolayer of redox modifiers, a thin cross-linked polymer coating was often observed. Later, Wrighton and co-workers applied chloro- or ethoxy-silylferrocene modifiers on inert metals and n-type semiconductors.[16,17] These studies can be regarded as the earliest electrochemical investigations of sol-gel derived materials, though the terminology "sol-gel" was never mentioned in these studies. However, even at this point, electrochemists failed to recognize the importance of reconciliation of sol-gel inorganic chemistry and silicone (organic) chemistry in order to make the most of the two fields through the formation of inorganic-organic sol-gel derived hybrids. This situation was radically changed with two scientific developments that took place in the early eighties.

Schmidt and coworkers from the Fraunhofer-Institute fur Silicatforschung in Wurzburg exploited the fact that Si-C bonds are stable and do not hydrolyze during sol-gel processing in order to develop and nickname the organically modified ceramic (Ormocers) and silicate (Ormosil) materials, using organo-functional silane precursors such as methyltrimethoxysilane.[18] This class of materials, in which the organic moiety is covalently attached to the siloxane backbone, is now classified as class I inorganic – organic hybrids.

David Avnir, Renata Reisfeld and their doctoral student, David Levy[19] introduced yet another way to form inorganic-organic hybrids by the so called sol-gel doping process. They introduced different dye compounds into the silicate during sol-gel polymerization. Some of the organic hybrids could then be retained within the silicate for prolonged periods without dye leaching and loss. David Avnir and Michael Ottolenghi from the Institute of Chemistry of the Hebrew University collaborated with Sergey Braun from the Life Science Institute of the same

university to initiate another major scientific breakthrough.[20,21] They encapsulated various enzymes in sol-gel silicates by mixing the biomolecules with sol-gel precursors. Surprisingly, the enzymes withstood the harsh conditions of the inorganic polycondensation. They were not completely denatured by the alcohol solvent and remained active and encapsulated in the silicate network even after shrinkage of the porous structure during the drying stage.

These two methods for obtaining organic-inorganic hybrids were not merely an addition to the repertoire of the already reported organic and biochemical adsorption and impregnation. The new methods showed higher stability and low or nil leaching, and active organic-inorganic hybrids could be attained by relatively simple processing. The two technologies thus opened new avenues to combine the superior physical properties of inorganic materials with the large variety of organic compounds. The availability and the power of the new inorganic – organic hybrids, the versatility provided by this set of materials, and the facile sol-gel processing techniques especially when it came to film formation proved irresistible to the electrochemical community. Today, sol-gel processing finds applications in numerous electrochemical fields including corrosion protection, battery solid electrolytes, membrane and electrodes, electrochromic windows, fuel cell membranes and electrodes as well as sensors and biosensors – the primary subject of this report. Of particular contemporary importance is the use of sol-gel composites – integrating a second phase of organic, inorganic or biochemical moiety within the sol-gel porous matrix. In the following sections we shall briefly review recent landmarks in the evolution of these materials.

2. Electrochemical Properties of Composites

Blends and composites based on sol-gel technology are used in order to improve stiffness, strength, toughness, and to a certain extent also to gain temperature and corrosion resistance.[22] The advantages entailed in composite electrode materials are completely different, and they are detailed below.

2.1. FUNDAMENTAL BACKGROUND: WAYS TO ENHANCE SENSORS' SIGNAL TO NOISE

The signal and sensor sensitivity of electrochemical cells is determined by the flux of analytes and their electrochemical products to and from the electrode conductive surface. Examination of the undimensional, diffusion-limited current through a porous film of thickness l to an electrode with surface area A is given by (7).

$$i/A = F\frac{DC}{l} \tag{7}$$

F is the Faraday constant, and D is the effective diffusion coefficient of a key analyte in the film. Another, equally simplified equation which is relevant to our discussion is the differential capacitance of electrodes during potential scan at a scan rate, *v* (usually expressed in V/sec). The current density in (8), i/A is the background current observed during cyclic voltammetry, which can be taken to represent the background current or noise level in many other electrochemical methods as well.

$$i/A = c_{dl}v \tag{8}$$

c_{dl} stands for the double layer capacitance of the electrode. Equations (7) & (8) show that there are several facile ways to increase the current density of the Faradaic reaction while retaining low background current. The first is to increase the concentration of the analyte at the gel side, very near the liquid-gel interface. The concentration at the gel phase, C is determined by a partition coefficient, K times the concentration of the analyte in the liquid phase, c, Now, since the concentration in the liquid side is an external constraint which is beyond the control variables of the experimentalist, the most important adjustable parameter that determines the flux to the electrode surface under a given analyte concentration is the affinity of the analyte to the gel.

Under usual conditions, except for very low pH (pH < 2), silica gels are negatively charged in aqueous solutions due to the deprotonation of the surface silanol groups (≡SiO^-), which endows large surface area silica gels with cation exchange properties. Thus, unmodified silica gel films exhibit large partition coefficients for positively charged species. Indeed, inorganic silicate modified electrodes show larger selectivity for cationic species (e.g., ruthenium(II) tris(bipyridine)), while the flux of anionic redox species such as ferricyanide/ferrocyanide is significantly hindered.[23] This permselectivity is reversed by incorporation of cationic functional groups such 3-aminopropyl-methyl-diethoxysilane into the starting sol-gel solution. Thus, the first mode by which composites can increase the current density is by the incorporation of another phase with high affinity to analytes, which increases the effective concentration of the analyte in the film. This is the most important reason for incorporation of Nafion and amine containing polymers (e.g. the natural positively charged polymer, chitosan) within sol-gel materials, though the entailed premselectivity by hindrance of the mobility of negatively charged ions is often of the same or even higher importance, as discussed below.

Equation (7) also reveals the importance of the effective diffusion coefficient for efficient current generation. The effective diffusion parameter can be expressed as the product of the pore diffusion coefficient and the void fraction – thus, the larger the void fraction the larger the flux to the electrode and the resulting current signal. Thin silicate films that are produced by virtually all conventional sol-gel film casting protocols (with the possible exception of mesoporous silicate films) are more compact than monoliths that are formed under similar pH conditions, and thus possess a very small void fraction. This limits the diffusion rate inside the porous network, which in turn reduces the attainable current and the response time in amperometric applications. Incorporation of a guest phase may improve the diffusion in the composite electrode by several ways.

Incorporation of a second phase and leaching out of the guest phase vacates large voids in sol-gel films and monoliths. This concept was indeed used for sol-gel thin layer chromatographic plates[24] and monolithic columns.[25] A remarkable example, which is not connected to the electrochemistry of silicates, is the incorporation of poly(ethylene oxide), a water soluble polymer which undergoes phase separation during sol-gel processing of monoliths. This technique was used by Nakanishi and coworkers to form monolithic chromatography columns with exceptionally high accessibility.[25] The chromatographic monoliths are marketed by the trade name Chromlith. Template formation by introduction of porogens or surfactants is another attractive and popular way to form ordered mesostructured materials and thus increase the void fraction in sol-gel silicates.[26] This method has been gaining immense popularity among electrochemical practitioners over the last few years.[27]

Another approach to increase the current is to introduce solid guest fillers into the sol-gel film. Enhanced diffusion takes place along the grain boundaries and along the volume of the silicate film adjacent to the interfacial area. Despite the increased tortuosity of the analyte diffusion pathway between the electrolyte and conductive electrode interfaces, the observed diffusion is accelerated. It is plausible that fast polymerization of the silicate creates a third phase of macroporous voids or less dense film through which accelerated diffusion takes place. Another possibility is that the segregated phases do not wet each other efficiently, and a third phase with different properties is formed near the interface between the phases. Enhanced diffusion can then take place through this phase. The large nanostructured metal-silicate and graphite powder-silicate interface is probably one of the reasons for the favorable electrochemical characteristics of carbon and metal-doped silicates[28] as discussed below.

A large charge-preferred permeability is obtained by incorporation of negatively charged polymers that facilitate H^+ and other cations' (e.g., methylviologen) transport.[29,30] By far, the most useful anionic polymers are the perfluorosulfonic acid polymers and particularly Nafion (Du Pont). Similarly,

amine containing polymers, such as the natural chitosan[31] or the synthetic poly(ethyleneimine) are used to enhance the transport of small anionic species.

Another important parameter in (7) is the effective film thickness l, or to put it another way, the average distance between the outer gel – liquid interface and the interface on which charge transfer can take place. For a unidimensional homogeneous film, l is indeed the film thickness, but for a heterogeneous electrode incorporating, for example, graphite powder, l is of the order of magnitude of the average pore diameter, much lower than the thickness of the film. Incorporation of heterogeneity by introduction of grains of a second phase can therefore provide alternative routes to increase the current in composite electrodes.

Equation (8) shows that the signal to noise of the electrode can be enhanced by the formation of a partially blocked electrode configuration. Incorporation of an intercalated conductive phase (such as those formed in carbon ceramic (CCE) or metal silicate electrodes) in hydrophobic silicate exposes only the surface of the conductive phase to the outer electrolyte and prevents the wetting of the bulk of the composite by the electrolyte. Figure 1 shows that for an ensemble of microelectrodes configuration (such as those obtained for hydrophobic CCEs), only the array of microelectrodes at the outer surface of the CCEs is exposed to the electrolyte, whereas the remaining surface is isolated from the electrolyte by the surface hydrophobicity. Since the background current in electrochemistry is proportional to the exposed conductive surface of the electrode (A in (8)) and the sensing signal is determined by the diffusion of the analytes to the geometric cross section of the electrode, the ensemble of microelectrodes configuration such as that formed by hydrophobic CCEs provides an ideal balance between low background and high accessibility of solutes. The ratio of the Faradaic signal to the background current of carbon black CCEs is several orders of magnitude superior to the response of glassy carbon electrodes as can be observed in Figure 2 (from G. Gun et al.[32]).

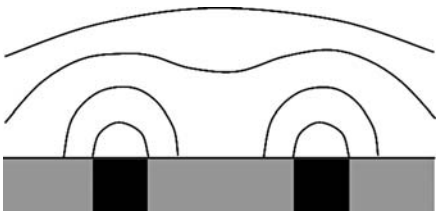

Figure 1. A scheme of the equiconcentration lines in the vicinity of partially blocked electrode, such as the hydrophobic carbon ceramic electrodes. (From ref.[32])

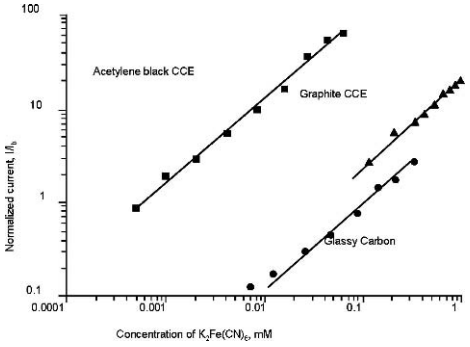

Figure 2. A comparison of the signal to background (current density divided by the background current density, I/I_b) obtained for CCE (made of small grain acetylene black graphite, large grain graphite, and glassy carbon electrodes). The signal to noise is considerably enhanced by the formation of the ensemble of microelectrodes configuration. (From ref.[32])

2.2. ADDITIONAL ELECTROCHEMICAL BENEFITS OF COMPOSITES

In addition to the significant advantages entailed in composites, sol-gel processing provides efficient ways to obtain favorable structures and other electrode material attributes. The most important examples of such benefits follow.

2.2.1. *Size Exclusion by Composite Electrodes*

The silicate network can act as an efficient size exclusion membrane. The pore size distribution can be controlled, at least to some extent, by incorporation of water soluble polymers such as poly(ethyleneglycol) or by pH changes.[33] Carefully tailored silicate membranes, using low pH synthesis exhibit Knudsen flow, thus facilitating the separation of air components.[34] Incorporation of zeolites, surfactants, templated mesoporous silicates, and leaving template materials can be used to generate tailored size excluding films.[5]

2.2.2. *Specific Recognition*

Silicates have low specific affinity to organic compounds, and although deprotonated surface silanols attract positively charged groups, the uptake is not selective. Incorporation of an organofunctional group or addition of a chemical or biochemical can be used to concentrate with high specificity desirable compounds. The most striking example of specific recognition is through the encapsulation of enzymes, antibodies and oligonuclides,[20,35] but specific recognition can be achieved also by doping the silicates with low molecular weight complexation agents[36,37] or by molecular imprinting as discussed above.

2.2.3. *Adhesion to the conductive support*

Composite sol-gel silicate – organic compounds can be tailored to have very good adhesion to oxide substrates due the **≡Si-O-M≡** bonding (where M is a metal atom). For example, polyaniline/silica composite coatings have much higher operational stability compared to polyaniline films.[38] It is difficult to construct sol-gel films thicker than *ca.* 10 μm. The high surface tension that builds up in partially filled pores during the drying stage fractures sol-gel matrices and limits their usefulness. The inherent heterogeneity of composite electrodes provides routes for stress relaxation and prevents fractures. Indeed, thick polymer/silicate and carbon/silicate films can be easily deposited on solid substrates.

2.2.4. *Tailored Design of the Porous Structure of the Sol-Del Films by Templating Approaches*

The design of porous films attracts considerable attention in contemporary sol-gel science, though this activity is still only partly reflected in sol-gel electrochemistry. Two central approaches dominate the main thrust of scientific activity in this field: (a) Formation of porous materials with narrow pore size distribution. (b) Design of artificial enzymes, receptors exhibiting a key-hole recognition capability. Although the final products are conceptually different, both approaches rely on the introduction of a foreign pore forming agent during gelation and subsequent removal of the guest after cross-linking.

2.2.5. *Formation of Ordered Mesoporous Materials*

The successful production of mesoporous silicate molecular sieves by Mobile Corporation scientists[26] by addition of surfactants and by introduction of linear polymers during sol-gel synthesis[39] introduced several efficient ways to design porous silicates. A similar procedure yields thin mesostructured films by dip coating.[40] Indeed, the surfactant template process was already used to fabricate thiol grafted mesoporous electrochemical sensors for stripping electroanalysis of lead (II) ions[41] and to control the porosity of silicate-carbon paste composite electrodes.[42] Recently Walcarius and his team advanced this technology considerably by attaining mesoporous materials by electrochemical deposition. A review of mesoporous sol-gel electrode was recently published.

Porous structures were also obtained by introduction of micron dimension particles such as latex beads[2] or bacteria cells,[44] though the latter has not been used for electrochemical applications yet.

A third templating approach involves block polymerization of two precursors followed by the selective removal of one. This class of templating is rather

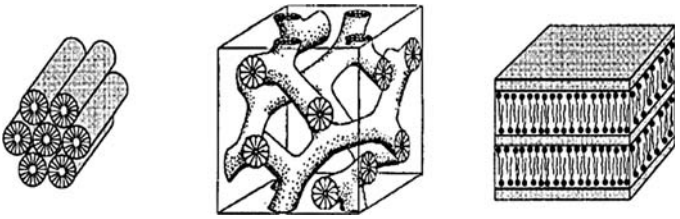

Figure 3. Typical forms of hexagonal (right), cubic (center) and bicontinuous mesoporous material. (From Raman et al.[43])

wide, encompassing a range of affinities between the different mono-mers. An example is the macroporous materials which – as mentioned above – were produced by Nakanishi et al.[45] by copolymerization of polyols (e.g., PVA or PEO) and tetraethoxysilane. Polymerization induced phase separation, and thermal removal of the segregated organic phase resulted in the formation of macroporous materials with narrow pore size distributions. In a related approach, Tsionsky et al.[24] used bromocresol as a template former in Ormosils. In this case, bromocresol aggregates were formed during sol-gel polymerization and their alcohol extraction from the cross-linked silicate induced macroporosity.

2.2.6. *Molecular Imprinting and Artificial Enzyme Formation*

Molecular imprinting is a related technique in which a guest molecule or a hydrolyzable leaving group is incorporated into the silicate film.[46] The guest molecule is usually of asymmetric geometry with two or more different functionalities. Each functionality interacts with a complementing functional group on the walls of the encapsulating pore. Removal of the guest molecular imprint after gel formation leaves a vacant hole with specific affinity to compounds of the same size, shape and functionalities of the imprint. Mandatory requirements for successful imprinted polymers were summarized by Srebnik and Lev.[47] (1) The polymerization process should be a soft one as to avoid deformation of the imprinting molecule. (2) The polymer should contain intimately mixed different attractive functionalities that will complement their matching groups on the imprinting molecule. (3) The polymer should be sufficiently rigid so that it will retain the shape of the imprint long after its removal. (4) The polymer should be porous in order to allow evacuation of the imprinting molecule and interaction with the target molecules in the surrounding. (5) Thin film formation capability is a mandatory requirement for accessibility. Sol-gel technology fulfills all of these requirements.

Today, there are two generic methods for the introduction of template agents into cross-linked silicates. The most common involves polymerization and cross-linking in the presence of non-covalently bonded templates that are removed after gelation. Small molecules such as methyl orange,[48] dopamine,[1] propranolol[49,50]

and phenanthroline – iron complexes[51] were used as molecular imprints. A second approach involves polycondensation, where the pendant group induces a pore distribution. Hunnius et al.[52] used bornyloxytriethoxysilane and methyltriethoxysilane sol-gel precursors, where the borneol acts as a pore forming agent. Boury et al. 1999[53] used a similar approach for the preparation of inorganic porous silicate networks by removal of an organic bridge from organic silsesquioxanes of the general structure $(OCH_3)_3Si$ (R)Si $(OCH_3)_3$ (where R, the removable bridge, is for example an ethylene group) using a mild ammonium fluoride treatment. Only very few successful electrochemical applications of molecular imprinting were reported so far, but those reported are exciting and stimulating.[1,2,7,49–51]

In a remarkable demonstration of this technology, Makote and Collinson[54] presented a highly selective sensor for catechol amine (dopamine). The sol-gel precursors were phenyltrimethoxysilane, methyltrimethoxysilane and tetramethoxysilane with ethoxyethanol as solvent. Every one of these ingredients was crucial for specific molecular recognition. The phenyl group was selected because it had a high affinity to the aryl group of the catechol. Ethoxyethanol was selected due to its affinity for polar as well as apolar molecules. Methyltrimethoxysilane contributed hydrophobicity and increased the adhesion to the support. The electrode showed high accessibility for dopamine (see Figure 4 after[54]), rather low accessibility for positively charged interferences such as norepinephrine and epinephrine, and practically zero interference of negatively charged species.

The complex multicomponent starting sol-gel solution explains why there are still so few successful electrochemical manifestations of this approach. A notable exception is the successful imprinting of iron complexes and the pesticide paraoxon which was demonstrated by the groups of Mandler and Marx.[51]

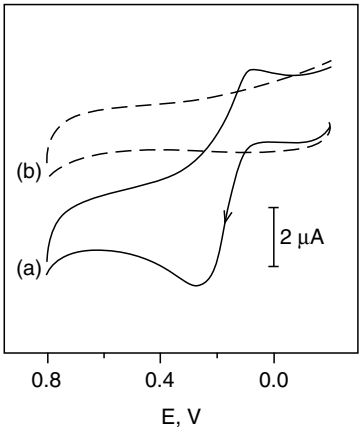

Figure 4. Selective detection of Dopamine by template film compared with a blank film lacking dopamine recognition capability. (From Makote and Collinson[54].)

2.2.7. *Biocompatibility*

Improvement of protein stability in sol-gel materials is perhaps one of the most innovative and rapidly developing areas of research in the field of sol-gel electrosensing. Braun and his coworkers,[21] the pioneers of the current wave of sol-gel biochemical encapsulation were also the first to report that sol-gel encapsulation endows increased protein stability and protects the biochemicals against heat denaturation. A dramatic increase of stability was noted by a number of other researchers for a wide range of biochemicals.[35,36,55–58] Heller reported a 200-fold stability increase of glucose oxidase by encapsulation in monolithic silica.[56] However, unlike monoliths and powders the encapsulation of proteins in silicate films is more demanding. Only a few authors reported successful immobilization of proteins within thin sol-gel silicate films; for the most part this was unsuccessful due to physical constraints imposed by the silicate networks. Successful encapsulations protocols of active biochemicals were reported for composite films or for sandwich like materials where the biomolecules are entrapped in the interface between a solid support and a sol-gel membrane. The incorporation of second, less crosslinked, organic polymer phase provides modes for stress relaxation and reduces the physical constraints on the encapsulated proteins, probably by creation of flexible microdomains within the silicate matrix. Additionally, it seems that the adsorption of the proteins onto solid grains within the silicate films stabilize the globular 3-D structure of the biochemicals. These two mechanisms are probably responsible for the success of guest fillers such as glycerol,[59] polymers,[50,51,56] graphite,[28,52–54] metallic particles[55] and nanoparticles,[56–58] and even inorganic additives such as Prussian blue[59,70] in enzyme preservation within silicate composite films.

2.2.8. *Ionic Conductivity*

Ionic conduction in silicate sensors and biosensors is important in order to decrease the Ohmic drops in Amperometric applications. The conductivity of silicate networks is dependent on the imbedded salts, and it is amply discussed in references within the context of ionic membranes.[71,72] Conductivity of silicates can be improved by surface modification so as to increase the concentration of the surface charges within the porous network or by incorporation of cationic or anionic polymers such as Nafion[61,73] and poly(ethyleneoxide)–phosphotungstic[74] as mentioned above.

2.2.9. *Electric and Redox Conductivity*

Electrochemistry involves electric charge transport in an electron conductor and ionic conductivity in an adjacent phase – the silicate film. For practically all the amperometric applications and for most of the potentiometric ones, it is beneficial to increase the interfacial area between the ionic and electronic conductors

and to minimize the mass transport barrier in the ionic conductor. A way to accomplish that is to minimize the length of the diffusion pathway of the analyte by very thin silicate films (i.e. decreasing l in (7)). However, the thin layer configuration implies low capacity for encapsulated reagents and catalysts in the silicate film. A way to approach thin layer configuration and still benefit from large encapsulation capacity is to minimize the pathlength from the reaction center or the liquid sensor interface to the electronically conductive phase by incorporation of an additional conductive phase within the silicate. This, in a way, can be viewed as a combination of increasing the surface area A in (7) and decreasing the pathlength l in the same equation. This can be done by coating of a porous conductive network (e.g. reticulated vitreous carbon cylinder) with silicate film[75–77] or by the incorporation of a second, electron conductive phase made of interconnected particles or conducting polymer. The catalyst or biocatalyst can then be imbedded in the three dimensional silicate structure.[28,78] Sol-gel electrochemical applications based on this approach include carbon ceramic[28] and metal ceramic,[65,66,79] sensors and biosensors, in which a network of metallic particles provides large surface area and long range electron percolation. Similar approaches using electrically conductive organic polymers such as polyaniline and polypyrrole instead, or in addition to the conductive metal phase.[80,81] Electric conduction can also be carried out by a hopping mechanism between adjacent redox sites. This mode of self exchange charge transfer within a silicate composite was exploited by the incorporation of redox polymers such as osmium redox polymer, [Os(bpy)(2)(PVP)(10)Cl]Cl[82] in the silicate backbone. A similar approach based on the creation of redox silicate polymers was also demonstrated, and it is discussed in application section.

3. Preparation of Hybrid Materials

The preparation of four types of hybrids are described in this section: Nanoporous Composite Materials – Polymer–Silicate Composite Electrodes; Carbon ceramic electrodes; Metal ceramic electrodes; and conductive clay modified electrodes.

3.1. NANOPOROUS COMPOSITE MATERIALS – POLYMER–SILICATE COMPOSITE ELECTRODES

This mode of hybrid synthesis involves the formation of a domain containing organic polymer or inorganic amorphous material. The guest polymer partly interpenetrates the porous inorganic silicate. The guest polymer can be either of inorganic nature such as Prussian blue[69] or polyoxometalates[83] or more often

organic polymer. The guest polymer can be either grafted, doped or electrochemically deposited. Polymer science makes a distinction between polymer blends and interpenetrating polymers. The distinction is based on the formation of segregated phases in interpenetrating polymers, which are often distinguished from molecularly mixed materials by some opacity due to light scattering by the interfacial area. For optical materials segregation should be avoided because it leads to optical losses and lower material strength. However, for most electrochemical applications, segregation on an appropriate, 50–500 nm scale is favorable since it provides enhanced diffusion, and the segregated composites can provide soft, accommodating nanodomains for biochemical guests as well as a tough network to prevent matrix deformation under flow conditions. For most electrochemical applications the loss of material strength due to the incorporation of the organic phases can be compensated by the toughness of the conductive electrode support.

Four methods to prepare polymer – silicate composites were reported and employed in demonstrative electrochemical applications.

3.1.1. *Polymer Doping*

Sol-gel polymerization of the silicate network in the presence of a preprepared guest polymer yields an inorganic-organic hybrid copolymer. Both synthetic (PVA, polysiloxane) and natural (chitosan, starch) polymers were used for electro and biosensing. In all these cases the polymer should be sufficiently bulky to prevent leakage from the inorganic-organic film.

3.1.2. *Polymer Grafting*

Sol-gel polymerization of the silicate network takes place in the presence of a preprepared guest polymer that can link to the silicate network. Although the preparation conditions are identical to the previous protocol, here, the covalent linkage provides stronger attachment, which is important when linear polymers or thin film configuration are involved. The covalent bond between the two polymers is often created by condensation reactions between the silane monomer and the alcohol groups on the polymer. This is indeed the case in the formation of PVA/polyvinylpyridine (PVA-g-PVP) and polyethylene glycol and dextran sulfate – silica sol composite which was used for hydrogen peroxide or glucose electrosensing.[60,84] Another synthesis procedure involves linear polymers containing reactive end-groups such as hydroxyl terminated poly(dimethyl siloxane), $[OH\ [Si(CH_2)_2\ O]_n\ Si(CH_2)_2\ OH]$.[85]

3.1.3. *Polymerization of Organic Polymers within a Preformed Silicate Films*

The silicate film is first deposited on the solid substrate and then monomers of the guest polymer are impregnated into a preformed porous silicate film, then

polymerization of the guest polymer is initiated either by ultra violet irradiation (e.g. for monomers containing epoxide groups) or by chemical oxidation (for example by peroxodisulfate for aniline and thiophene based polymers).

3.1.4. *Electropolymerization of Organic Polymers within a Preformed Silicate Film*

A related method that is specific for electrochemical applications is the polymerization of conductive polymer within a preformed silicate film.[80,81] Polyaniline, polypyrrole, and polythiophene are popular conductive polymers, widely used by electrochemists, and they all can be easily polymerized by electrooxidation within interconnected pores of silicate films. This mode guarantees electroconductivity by the conductive polymer material, material strength which is donated by the silicate and good adhesion due to surface silanols. This technique was reported this year for the electrodeposition of Prussian blue in ATO/Clay/silicate[86] and CCE.[70]

3.2. CARBON CERAMIC ELECTRODES (CCES)

Carbon-ceramic composite electrodes (CCEs) and the closely related metal – silicate electrodes are comprised of carbon or metal dispersion in sol-gel derived silicates or Ormocers. In this construction the silicate serves as a binder for the conductive dispersion. The conductive component is added as powders, nanoparticles, ATO coated clays, or carbon nanotubes. The improved conductivity by the interconnected conductive powder, as well as other favorable attributes of composites, including improved catalytic reactivity, biological compatibility, and control of the thickness of the wetted section of the electrodes in aqueous electrolyte attract practitioners. Since the metal silicate electrodes call for different preparation protocols they are addressed separately.

The carbon ceramic electrodes are prepared by mixing different forms of graphitic materials with the sol-gel reactants.[28] A porous brittle composite matrix is formed after gelation and drying. The composite electrodes benefit from the mechanical properties of the silicate backbone, from electron percolation conductivity through the interconnected carbon grains and from the ability to manipulate the physicochemical characteristics of the matrix by incorporation of suitable guest moieties including monomer precursors or sol-gel dopants.

The preparation protocols of CCEs allow wide flexibility in choosing the starting carbon type as well as with the choice of the inorganic binder. Graphite, carbon black, glassy carbon particles and carbon nanotubes were all successfully incorporated in CCEs. Like different Ormosil binders as well as a large variety of inorganic oxides such as titanium, zirconium and ruthenium oxides[78,28] were used for CCE preparation. Ormosils are usually preferred over

pure inorganic networks for several reasons. It is possible to control the exposed surface area of the electrode in aqueous electrolytes by tuning the hydrophobicity of the Ormosil binder. Appropriate organofunctional groups are useful anchors for subsequent covalent modification of the electrodes with desirable functionality. Popall has shown that for some applications such as the lithium ion batteries it is useful to use an aprotic binder which can be easily accommodated by sol-gel technology.[77] As discussed earlier, aminopropyl functionalities provide a useful anchor for aldehyde and carboxylate reagents.[12] Finally, the silane monomer can contain organofunctional ligands, charge mediators, electrocatalysts or redox groups which can participate in desirable electroanalytical tasks. Several applications demonstrating these capabilities will be briefly addressed below.

The choice of carbon powder affects significantly the properties of the CCEs.[32] The conductivity percolation threshold ranges between a few weight percent for carbon black up to approx. 30% for 40 μm, graphite powders (Figure 5). The type of carbon used also affects the maximum attainable carbon loading which ranges between *ca.* 15% (w) for carbon black electrodes and up to *ca.* 90% for 40 μmr graphite particles. The pore size distribution of CCEs can be influenced by changes of the water:silicon ratio used for preparation of the CCEs and by pH tuning.[87] It is possible to cast CCEs in a wide range of electrode configurations including supported and unsupported thick films, rods and disks. Since large grain carbon powder CCEs do not shrink during gelation and they adhere very well to metal oxide supports it is possible to cast electrodes and microelectrodes in glass tubes.

It is possible to control the configuration of the wetted section of CCEs in aqueous electrolytes by manipulation of the hydrophobicity of the graphitic filler and the organofunctionality of the Ormocer binder. Methyltrimethoxysilane

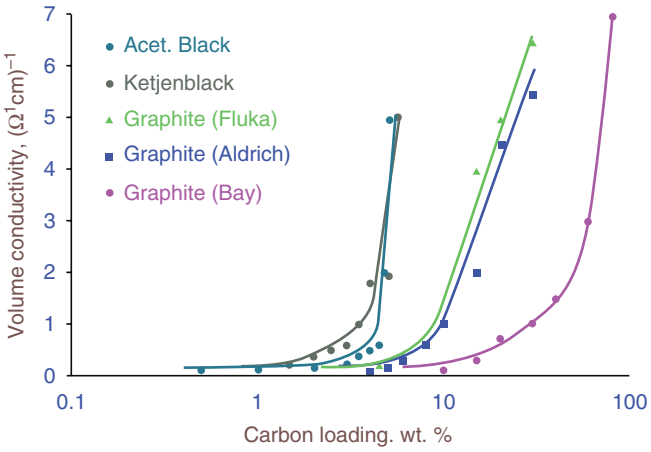

Figure 5. Conductivity – graphite loading relationship for various methylsilicate CCEs.

or phenyltrimethoxysilane based binders reject water leaving only segregated islands of carbon at the outer surface exposed to the electrolyte. Hydrophilic starting monomers (e.g. tetraalkoxysilane or aminoalkyltrimethoxysilane) yield completely wetted electrodes. A controlled wet porous section of CCEs, ranging between some 50 and 1,000 μm was demonstrated. The active section of the CCEs does not clog upon repeated polishing due to the brittleness of the sol-gel silicate backbone, and thus the electrode active section can be renewed by mechanical polish after each – or several – measurements. The reported relative standard deviations of renewal repeatability[28,88,89] or sensor-to-sensor reproducibility by screen printing are usually only several percents.[28]

An important variant of the CCEs was introduced by Gavalas et al.[90] In this electrode material carbon nanotubes replaced the carbon grains. Carbon nanotubes were introduced into the electrochemical arena by the Crooks group,[91] and they acquired large popularity owing to their favorable characteristics: large aspect ratio, low double layer capacitance, fast charge transfer rate, and high selectivity for certain classes of compounds. Additionally, as a CCE filler the large anisotropy of this material ensures electric percolation threshold at relatively low carbon concentrations. Figure 6 (from Gavalas et al.[90]) shows a comparison between the CV of a CNT-methyl-silicate composite electrode and a conventional CCE. In this particular example it can be seen that the CV peaks of the CNT-CCE are more pronounced compared to regular CCEs. The CNT–CCEs have already been used for the construction of ethanol biosensors by Nim Choi et al.[92]

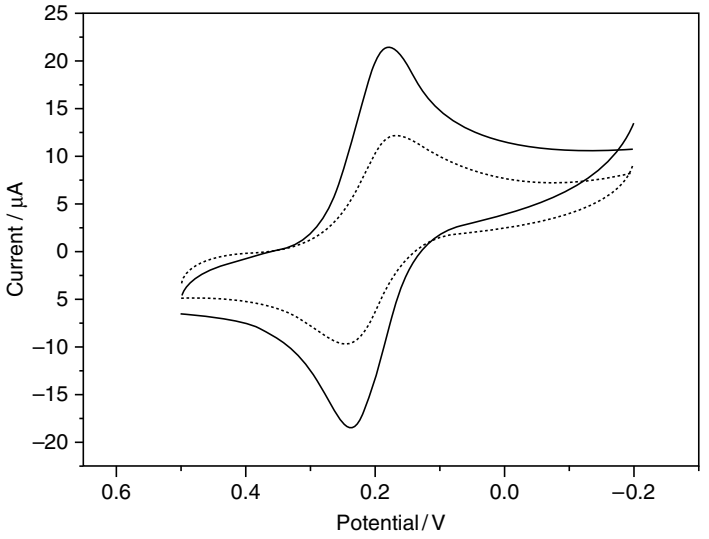

Figure 6. A comparison of the cyclic voltammograms of 1 mM ferricyanide at CNT-CCE (solid) and regular CCE. (dotted) Scan rate 50 mV. (From Gavalas et al.[90])

3.3. METAL-CERAMIC COMPOSITE ELECTRODES (METAL CCES)

Gold and other metals can be used instead of graphite as the conductive network in CCEs. The main difference between the metal and graphite fillers stems from the larger density of the latter. The specific density of gold is about 20, thus while 15–20 wt% of carbon is sufficient for electron percolation, over 80% of the metal CCE should be comprised of gold in order to exceed the percolation threshold. This limits the practical application of the metal ceramic electrodes to thin films and microelectrodes. On the other hand, metal ceramic electrodes have several advantages compared to graphite CCEs. Metals provide better electrocatalysis, and it is easier to prepare metal nanoparticles of controlled dimension and to functionalize their surface.

Procedures for the preparation of metal ceramic electrodes range from simple mixing of a fine metal powder with the silicate precursors to elaborate techniques which involve preprepared metallic nanoparticles. Wang and Pamidi[65] used 0.5 μm gold microparticles, tetramethoxysilane, and glucose oxidase to cast a sol-gel composite glucose biosensor. Aminosilane stabilized gold nanoparticles (*ca* 3–10 nm) were prepared in a one pot procedure by reduction of gold

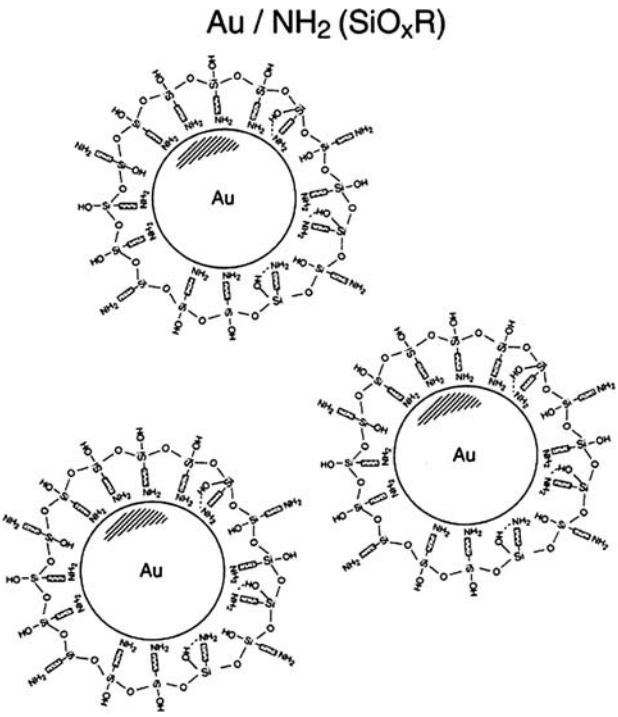

Figure 7. Aminosilicate-stabilized gold particles. (From Fishelson et al.[79].)

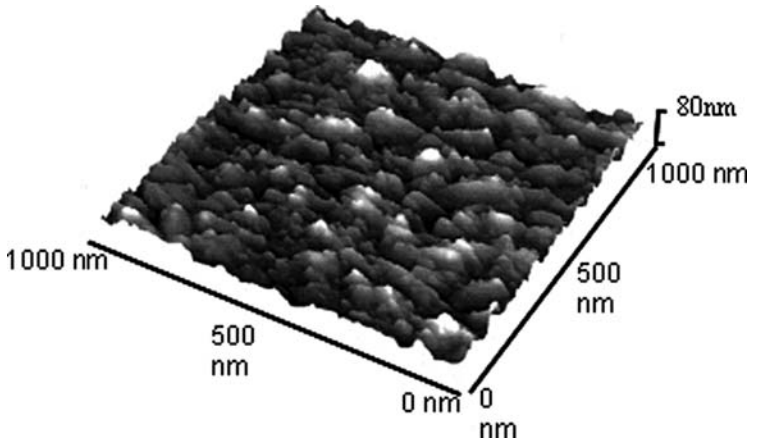

Figure 8. AFM microscope image of electropolymerized gold nanoparticles – aminosilicate. (From ref. [94].)

tetrachloride in aminopropyltrimethoxysilane solution (Figure 7). The sol was used to dip-coat electrodes with a thin gold-silicate composite film.[66] One of the major limitations of carbon CCEs is the lack of transparency, prohibiting optical analysis. The metal nanoparticle – silicate films provide sufficient transparency and overcome this problem. We used a similar protocol to prepare glucose biosensors after mixing glucose oxidase with the gold sol. However, in this construction the active concentration of gold particles in the film was rather low (<2%). Electropolymerization using potential driving force helped us to increase the active gold nanoparticle concentration in the film and even to exceed the gold percolation threshold by electrochemical deposition of the gold sol on conductive substrates as described schematically in Figure 9.[67] The aminosilicate capped sol of Figure 7 was first deposited on an ITO or metal electrode by dip-coating. Then the nanoparticles were partly electrooxidized, a procedure that desorbed the organic moieties from the gold surface and prepared the film for another round of dip-coating and for the attachment of yet another layer of nanoparticles. The process could be repeated giving eventually a conductive film of sub-micrometer thickness.[67,68] Interestingly, the electrodeposition took place only above about 0.7 V *vs*. Ag/AgCl which shows that both electrophoretic mobility and oxidation of the surface of the nanoparticles were essential for efficient electropolymerization. A combination of XPS and direct quantification of the gold surface by gold oxide formation showed that approx. 25% of the theoretically calculated surface of the gold nanoparticles in the film could participate in charge transfer reactions and is therefore in direct contact with the solution as well as electrically connected to the electrode.

Moreover, the Au:Si ratio in the film is about 100 fold higher than the ratio between these atoms in the precursors solution. The same procedure was later used by Nagomi and Bharathi to prepare fast responding glucose biosensors.[93]

More recently Mandler and coworkers[96] demonstrated that it is possible to deposit by a single electrochemical step, copper and silicate on electrodes using

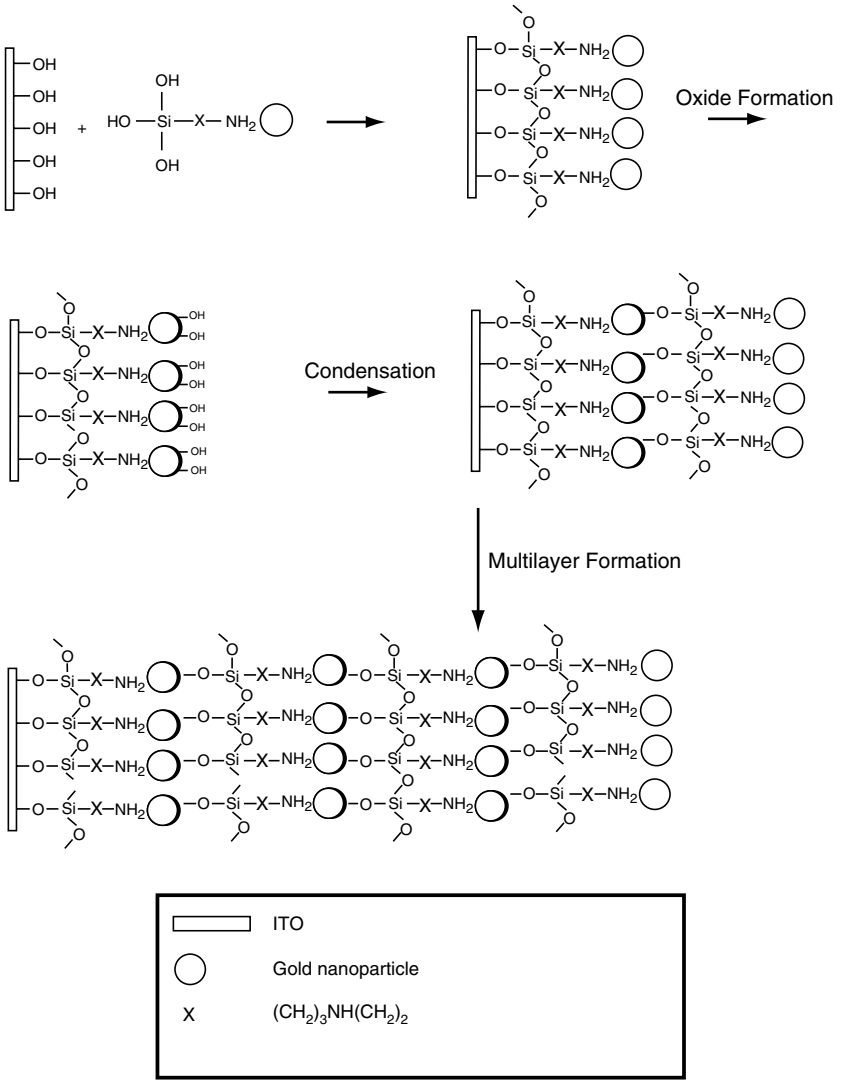

Figure 9. Multilayer deposition of aminosilane doped gold nanoparticles on a conductive ITO substrate. (From Bharathi et al. [95].)

cathodic bias. The deposition mechanism involves two important steps, a pH increase in the vicinity of the electrode surface, which accelerates the electropolymerization of the silicate, and reduction of the metal ions.

3.4. ATO COATED CLAY SILICATE POROUS AND CONDUCTIVE ELECTRODES

The research on conductive CCEs is in a way frustrating, since it involves silicate research without benefiting from one of the most attractive features of silicates – optical transparency. In fact, there is a real need for a transparent conductive and porous electrode material. Every combination of two of these three

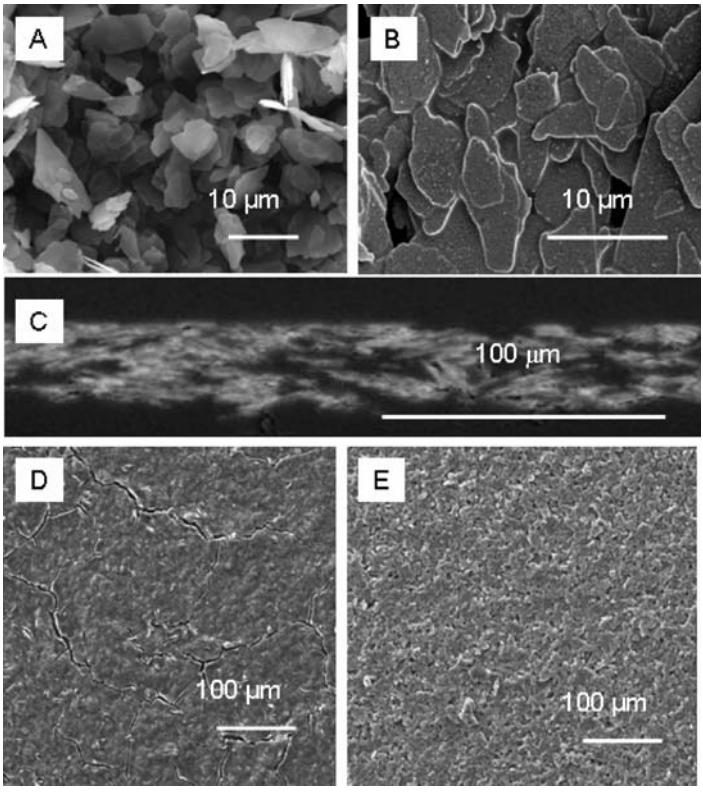

Figure 10. ATO/mica clay silicate composites. (A) ATO modified clay powder- lack of order is apparent; (B) 40% ATO modified mica platelets in methyl silicate film deposited on a glass slide; (C) cross section of a film of the same composition as of B, but this film was deposited on PET and covered by epoxy resin. Alignment of the mica platelets in parallel to the glass substrate is apparent. (D) 40% ATO modified mica platelets in silicate. E) 40% ATO modified mica platelets in methyl silicate matrix. (From Sadeh et al.[86])

attributes can easily accomplished, but it is difficult to achieve all three features together. A new form of conductive, porous and transparent composite electrode was introduced by our group very recently.[86] The electrode material is comprised of antimony-doped tin oxide (ATO) coated mica platelets imbedded in a sol-gel derived silicate or methyl-silicate network. The platelet clays self align in a layered structure within the silicate film, an anisotropic construction which minimizes the ATO loading required to achieve electric percolation. Figure 10 from Sadeh et al.[86] shows that the ATO coated Moskovite clays predominantly self align in the direction of the substrate providing the aniso-tropy that is needed for reduction of the electric percolation threshold. Typical values of 100 kΩ/sq. sheet resistance and 1.5 OD for a 20 μm thick film were reported. The transparency is lower as compared to sputtered ATO glasses (or for sol-gel derived ATO–GLYMO coatings[97]), but this is apparently the best method for low temperature preparation of transparent, porous, and electrically conductive electrode material. Permselectivity induced by the silicate and clay ingredients was demonstrated by the fast permeation of positively charged Methyl viologen compared to hindered transport of the negatively charged ferricyanide. Prussian blue modified ATO coated platelets dispersed in sol-gel derived silicate were prepared in several alternative ways and used to demonstrate the feasibility of a transparent and electrically conductive.

4. Bioapplications of CCEs

The versatility in configuring composite sol-gel electrodes in the molecular and the macrodomain levels is reflected in the large number of different applications that were proposed for these composites within a fairly short period of time. Rather than to attempt a comprehensive description of all these applications, a description that is bound to be outdated before this chapter is published, we address here only a single application, which illustrates the most important property of sol-gel electrochemistry – its versatility.

We shall take a simple example – glucose sensing – and follow ways by which sol-gel technology can accommodate different ways to produce electrochemical biosensors. The overall chemistry of glucose sensing is rather simple. Glucose is oxidized to gluconolactone by the flavin prosthetic group imbedded in the glucose oxidase (GOD), a 160 KD enzyme.

This reaction is a favorite case study for the analytical community due to the high stability and low cost of GOD. The flavin is then regenerated by chemical oxidation; in nature it is done by dioxygen which is converted to give hydrogen peroxide as a byproduct.

$$Glucose + [G.O.D. - (FAD)] \rightarrow [G.O.D. - (FADH_2)] + Gluconolactone \quad (9)$$

$$[G.O.D. - (FADH_2)] + O_2 \rightarrow [G.O.D. - (FAD)] + H_2O_2 \quad (10)$$

Translation of this technology to sol-gel electrochemical sensing faced two challenges. First it was not simple to produce thin silicate films without enzyme denaturation. Two ways were devised to solve this problem. The first involved encapsulation of the enzymes in the interface between a solid electrode support and the sol-gel film, a configuration that is sometimes referred to as sandwich type electrodes. The second involved the production of composite materials such as carbon CCEs and metal CCEs or by incorporation of latex beads or inorganic or organic polymers in silica, alumina, titania or other metal oxides. The second challenge was to generate an electrochemical signal from reactions 9 and 10. The simplest way to do so is by oxidation of the hydrogen peroxide to oxygen on the electrode surface. The selectivity of most electrochemical biosensors is determined by the specificity of the electrode charge transfer rather than by the enzymatic specificity. The overvoltage for the oxidation of hydrogen peroxide on graphite is larger than 0.5 V which makes the blank CCE sensors susceptible to interferences from reducing agents such as ascorbic acid and acetaminophen.

Several ways were devised in order to reduce this high overvoltage.

4.1. INCORPORATION OF INERT METAL CATALYSTS

Electrocatalysis of hydrogen peroxide conversion was used to reduce the sensing potential. Several groups incorporated metal and metal oxide catalysts such as palladium, rhodium and ruthenium in CCE biosensors.[63–65]

4.2. INCORPORATION OF CHARGE MEDIATOR DOPANT

Another way to lower the overpotential of the glucose sensor was to introduce charge mediators that will replace the oxygen, oxidize and regenerate the prosthetic group of the enzyme and will be regenerated by the Faradaic reaction. Several different mediators (e.g. ferrocene (Fc) or other ferrocenyl compounds and tetrathiafulvalene) were incorporated in glucose biosensors.[62,64] Glucose sensing is then described by (9), (11) and (12).

$$[G.O.D. - (FADH_2)] + Fc^+ \rightarrow [G.O.D. - (FAD)] + Fc \quad (11)$$

$$Fc \rightarrow Fc^+ + e^- \quad (12)$$

However, slow leaching of the free mediator was encountered when small mediators were used. At least four different methods were used in order to prevent leaching of the mediators from CCEs. Similar approaches were used for other polymer-silicate biosensors.

4.3. ENCAPSULATION OF MEDIATOR MODIFIED GOD IN CCE[64]

In this construction, ferrocenyl functionalities were first covalently bonded to lysine groups on the GOD. After purification, the redox labeled proteins were encapsulated in the sol-gel – graphite matrix. Thus, electron transfer from the active center of the enzyme to the carbon network was accomplished by mediation through the immobilized ferrocenyl groups.

4.4. D. IMMOBILIZATION OF ENZYMES IN REDOX MEDIATOR COATED GRAPHITE CCE[98]

The graphite surface was coated by the ferrocenyl functionalities. First the graphite was coated by a gold layer. Then cystamine was self assembled on the gold. An alkyl diamine spacer was subsequently attached by glutaraldehyde linkage; finally a ferrocenyl group was attached to the pending amine, and the ferrocenyl modified grains were impregnated with GOD. The modified graphite was then used for CCE production. The charge transfer mechanism involves oxidation of the flavin group by the immobilized ferrocinium, which is then reduced back by a charge transfer step.

4.5. ENCAPSULATION OF ENZYMES IN REDOX MODIFIED CCE[99]

The electrode material was comprised of a dispersion of GOD. impregnated graphite powder in ferrocenyl-, and methyl-modified silicate. The siloxane polymer provided for a highly crosslinked and rigid backbone, and the ferrocenyl was responsible for the signal transduction from the active center of the enzyme to the interconnected graphite network by an electron hopping mechanism.

There are other methods to use leaching-free glucose CCEs including the use of redox polymer dopants[82]; the use of Prussian Blue doped mediator[70]; the use of consortium of two enzymes for catalytic utilization of the hydrogen peroxide product[100] but the few examples described here are sufficient for our purpose – demonstration of the versatility and capabilities of composite sol-gel electrodes.

5. Electropolymerization of Sol-Gel Silicate and other Films

The last section of this chapter describes briefly milestones in the evolution of an exciting new development in sol-gel electrochemistry, namely the electropolymerization/electrodeposition of silicates and composite silicate materials. Despite the fact that theoretically silicates lack redox properties, the electrodeposition of silicates is well known. Electrophoretic deposition of inorganic polymers and silicates is an established procedure to induce concentration change near the electrode which may yield deposition by increased concentration or precipitation on the conductive electrode.

The simplest and most well known approach is to deposit the silicate by electrophoretic driving force.[101] We have used the approach for the deposition of 2-chloro-3-[[2-(dimethyl(3-(trimethoxynaphthoquinonetrimethoxysilyl)-propyl-ammonio)ethyl]amino]-1,4-naphthoquinone bromide (NPQ) and electrodeposited it on a glassy carbon electrode. Another method which was mentioned in this short overview involved the polymerization of aminosilicate capped gold nanoparticles. The first technique involved a straightforward electrophoretic mechanism whereas the second, the nanoparticle deposition technique, is more intricate and involves a two step mechanism: electrophoretic attraction of the aminosilicate capped gold and an electrochemical oxidation step to remove the capping agent and oxidize the gold to allow gradual build up of additional layers of gold-silicate on the electrode material. A third attractive electrodeposition technique involves a Faradaic reaction that converts a silicate electroactive and soluble species into an uncharged precipitate. The precipitate can then crosslink and form the gel directly on the electrode surface. The technique was successfully used by Leventis and Chen[102] to deposit methylene blue appended with trimethoxysilane on electrode surfaces.

Recently the groups of Avnir and Mandler from the Hebrew university proposed an interesting variant of the electrochemically driven deposition. Faradaic current was used to increase the pH near the electrode surface and thus catalyze the gelation process.[103] The process was successfully adapted by others[7] and perhaps the most remarkable demonstration of its versatility is the ability to produce ordered mesoporous materials as demonstrated by Walcarius[104] and the ability to deposit active enzymes by this process.[105]

The electrophoretic deposition and for that matter all other electrochemical depositions offer substantial advantages for sol-gel practitioners: first the process is controlled, and an exact amount of deposit can be accumulated on the electrode. Secondly the polymerization and sol-gel coating is confined to the electrochemically active material, and the insulator remains bare of sol-gel coating. Third, the electropolymerized layer contains a substantially different concentration of the active ingredients – different from the composition of the sol.

The electropolymerization technique is a mild deposition technique that does not involve harsh conditions. Electrodeposition also usually results in denser more uniform films. Finally electrodeposition is very suitable for coating of complex configuration and high aspect ratio cervices and patterns which are not readily deposited by spray coating or dip coating techniques.

Acknowledgement

This work was sponsored by the Scientific Infrastructure Program of the Ministry of Science, Culture, and Sport. J. G thanks the Alexander von Humboldt Foundation for financial support.

References

1. M. M. Collinson, and A. R. Howells, Sol-gels and electrochemistry: research at the intersection, *Anal. Chem.* 72, 702A–709A (2000).
2. M. M. Collinson, Recent trends in analytical applications of organically modified silicate materials, *TrAC, Trends Anal. Chem.* 21(1), 31–39 (2002).
3. O. Lev, Z. Wu, S. Bharathi, V. Glezer, A. Modestov, J. Gun, L. Rabinovich, and S. Sampath, Sol-gel materials in electrochemistry, *Chem. Mater.* 9(11), 2354–2375 (1997).
4. A. Walcarius, Electrochemical applications of silica-based organic-inorganic hybrid materials, *Chem. Mater.* 13(10), 3351–3372 (2001).
5. A. Walcarius, Electroanalysis with pure, chemically modified, and sol-gel-derived silica-based materials, *Electroanalysis* 13(8–9), 701–718 (2001).
6. J. Wang, and P. V. A. Pamidi, Sol-gel-derived gold composite electrodes, *Anal. Chem.* 69(21), 4490–4494 (1997).
7. M. M. Collinson, Electrochemistry: an important tool to study and create new sol-gel-derived materials, *Acc. Chem. Res.* 40, 777–783 (2007).
8. J. J. Ebelmen, Sur les éthers siliciques, *C. R. Acad. Sci.* 19, 398–400 (1844).
9. H. Y. -P. Hong, Crystal structures and crystal chemistry in the system $Na_{1+x}Zr_2Si_xP_{3-x}O_{12}$, *Mater. Res. Bull.* 11(2), 173–182 (1976).
10. D. H. H. Quon, T. A. Wheat, and W. Nesbitt, Synthesis, characterization and fabrication of $Na_{1+x}Zr_2Si_xP_{3-x}O_{12}$, *Mater. Res. Bull.* 15(11), 1533–1539 (1980).
11. E. P. Plueddemann, *Silane Coupling Agents* (Plenum Press, New York, 2nd ed., 1991).
12. J. R. Lenhard, and R. W. Murray, Chemically modified electrodes. 13. Monolayer/multilayer coverage, decay kinetics, and solvent and interaction effects for ferrocenes covalently linked to platinum electrodes, *J. Am. Chem. Soc.* 100(25), 7870–7875 (1978).
13. J. R. Lenhard, and R. W. Murray, Chemically modified electrodes: part VII. Covalent bonding of a reversible electrode reactant to Pt electrodes using an organosilane reagent, *J. Electroanal. Chem.*78(1), 195–201 (1977).
14. K. -N. Kuo, P. R. Moses, J. R. Lenhard, D. C. Green, and R. W. Murray, Immobilization, electrochemistry, and surface interactions of tetrathiafulvalene on chemically modified ruthenium and platinum oxide electrodes, *Anal. Chem.* 51(6), 745–748 (1979).

15. R. W. Murray, Chemically modified electrodes, *Acc. Chem. Res.* 13(5), 135–141 (1980).
16. M. S. Wrighton, R. G. Austin, A. B. Bocarsly, J. M. Bolts, O. Haas, K. D. Legg, L. Nadjo, and M. C. Palazzotto, A chemically derivatized platinum electrode: persistent attachment of an electroactive ferrocene derivative, *J. Electroanal. Chem.* 87(3), 429–433 (1978).
17. D. C. Bookbinder, and M. S. Wrighton, Thermodynamically uphill reduction of a surface-confined N,N'-dialkyl-4,4'-bipyridinium derivative on illuminated p-type silicon surfaces, *J. Am. Chem. Soc.* 102(15), 5123–5125 (1980).
18. G. Philipp, and H. Schmidt, New materials for contact lenses prepared from Si- and Ti-alkoxides by the sol-gel process, *J. Non-Cryst. Solids* 63(1–2), 283–292 (1984).
19. D. Avnir, D. Levy, and R. Reisfeld, The nature of the silica cage as reflected by spectral changes and enhanced photostability of trapped Rhodamine 6G, *J. Phys. Chem.* 88(24), 5956–5959 (1984).
20. S. Braun, S. Rappoport, R. Zusman, D. Avnir, and M. Ottolenghi, Biochemically active sol-gel glasses: the trapping of enzymes, *Mater. Lett.* 10(1–2), 1–5 (1990).
21. S. Braun, S. Rappoport, R. Zusman, S. Shteltzer, S. Drukman, D. Avnir, and M. Ottolenghi, in: *Biotechnology: Bridging Research and Applications*, edited by D. Kamely, A. Chakrabarty, and S. E. Kornguth (Kluwer, Amsterdam, 1991).
22. Y. S. Lipatov, Polymer blends and interpenetrating polymer networks at the interface with solids, *Prog. Polym. Sci.* 27(9), 1721–1801 (2002).
23. M. M. Collinson, C. G. Rausch, and A. Voigt, Electroactivity of redox probes encapsulated within sol-gel-derived silicate films, *Langmuir* 13(26), 7245–7251 (1997).
24. M. Tsionsky, A. Vanger, and O. Lev, Macroporous thin films for planar chromatography, *J. Sol-Gel Sci. Technol.* 2(1–3), 595–599 (1994).
25. H. Minakuchi, K. Nakanishi, N. Soga, N. Ishizuka, and N. Tanaka, Octadecylsilylated porous silica rods as separation media for reversed-phase liquid chromatography, *Anal. Chem.* 68(19), 3498–3501 (1996).
26. C. T. Kresge, M. E. Leonowicz, W. J. Roth, J. C. Vartuli, and J. S. Beck, Ordered mesoporous molecular sieves synthesized by a liquid-crystal template mechanism, *Nature* 359(6397), 710–712 (1992).
27. M. Etienne, A. Quach, D. Grosso, L. Nicole, C. Sanchez, and A. Walcarius, Molecular transport into mesostructured silica thin films: electrochemical monitoring and comparison between *p*6*m*, $P6_3/mmc$, and P*m*3*n* structures, *Chem. Mater.*19(4), 844–856 (2007).
28. L. Rabinovich, and O. Lev, Sol-gel derived composite ceramic carbon electrodes, *Electroanalysis* 13(4), 265–275 (2001).
29. R. A. Zoppi, and S. P. Nunes, Electrochemical impedance studies of hybrids of perfluorosulfonic acid ionomer and silicon oxide by sol-gel reaction from solution, *J. Electroanal. Chem.* 445(1–2), 39–45 (1998).
30. B. Barroso-Fernandez, M. T. Lee-Alvarez, C. J. Seliskar, and W. R. Heineman, Electrochemical behavior of methyl viologen at graphite electrodes modified with Nafion sol-gel composite, *Anal. Chim. Acta* 370(2–3), 221–230 (1998).
31. C. -Z. Zhao, N. Egashira, Y. Kurauchi, and K. Ohga, Electrochemiluminescence sensor having a Pt electrode coated with a $Ru(bpy)_3^{2+}$-modified chitosan/silica gel membrane, *Anal. Sci.* 14(2), 439–441 (1998).
32. G. Gun, M. Tsionsky, and O. Lev, Preparation and characterization of carbon ceramic electrodes, in: *Better Ceramics Through Chemistry VI*, edited by C. Sanchez, M. L. Mecartney, C. J. Brinker, and A. K. Cheetham (Materials Research Society, Pittsburgh, PA, 1994), pp. 1011–1017.
33. C. J. Brinker, and G. W. Scherer, *Sol-Gel Science* (Academic, San-Diego, CA, 1989).

34. C. J. Brinker, T. L. Ward, R. Sehgal, N. K. Raman, S. L. Hietala, D. M. Smith, D. -W. Hua, and T. J. Headley "Ultramicroporous" silica-based supported inorganic membranes, *J. Membr. Sci.* 77(2–3), 165–179 (1993).
35. D. Avnir, T. Coradin, O. Lev, and J. Livage, Recent bio-applications of sol-gel materials, *J. Mater. Chem.* 16(11), 1013–1030 (2006).
36. D. Avnir, Organic chemistry within ceramic matrices: doped sol-gel materials, *Acc. Chem. Res.* 28(8), 328–334 (1995).
37. O. Lev, Diagnostic applications of organically doped sol-gel porous glass, *Analusis* 20(9), 543–553 (1992).
38. Y. Wei, J. -M. Yeh, D. Jin, X. Jia, J. Wang, G.-W. Jang, C. Chen, and R. W. Gumbs, Composites of electronically conductive polyaniline with polycrylate-silica hybrid sol-gel materials. *Chem. Mater.* 7(5), 969–974 (1995).
39. D. Y. Zhao, J. L. Feng, Q. S. Huo, N. Melosh, G. H. Fredrickson, B. F. Chmelka, and G. D. Stucky, Triblock copolymer syntheses of mesoporous silica with periodic 50 to 300 angstrom pores, *Science* 279(5350), 548–552 (1998).
40. Y. Lu, R. Ganguli, C. A. Drewien, M. T. Anderson, C. J. Brinker, W. Gong, Y. Guo, H. Soyez, B. Dunn, M. H. Huang, and J. I. Zink, Continuous formation of supported cubic and hexagonal mesoporous films by sol-gel dip-coating, *Nature* 389(6649), 364–368 (1997).
41. W. Yantasee, Y. Lin, X. Li, G. E. Fryxell, T. S. Zemanian, and V. V. Viswanathan, Nanoengineered electrochemical sensor based on mesoporous silica thin-film functionalized with thiol-terminated monolayer, *Analyst* 128(7), 899–904 (2003).
42. S. Sayen, M. Etienne, J. Bessiere, and A. Walcarius, Tuning the sensitivity of electrodes modified with an organic-inorganic hybrid by tailoring the structures of the nanocomposite material, *Electroanalysis* 14(21), 1521–1525 (2002).
43. N. K. Raman, M. T. Anderson, and C. J. Brinker, Template-based approaches to the preparation of amorphous, nanoporous silicas, *Chem. Mater.* 8(8), 1682–1701 (1996).
44. S. Chia, J. Urano, F. Tamanoi, B. Dunn, and J. I. Zink, Patterned hexagonal arrays of living cells in sol-gel silica film, *J. Am. Chem. Soc.* 122(27), 6488–6489 (2000).
45. K. Nakanishi, H. Komura, R. Takahashi, and N. Soga, Phase separation in silica sol-gel system containing poly(ethylene oxide). I. Phase relation and gel morphology, *Bull. Chem. Soc. Jpn.* 67(5), 1327–1335 (1994).
46. K. Haupt, and K. Mosbach, Molecularly imprinted polymers and their use in biomimetic sensors, *Chem. Rev.* 100(7), 2495–2504 (2000).
47. S. Srebnik, and O. Lev, Theoretical investigation of imprinted crosslinked silicates, *J. Sol-Gel Sci. Technol.* 26(1–3), 107–113 (2003).
48. F. H. Dickey, The preparation of specific adsorbents, *Proc. Nat. Acad. Sci. U.S.A.* 35, 227–229 (1949).
49. S. Marx, and Z. Liron, Molecular imprinting in thin films of organic-inorganic hybrid sol-gel and acrylic polymers, *Chem. Mater.* 13(10), 3624–3630 (2001).
50. S. Marx, and D. Avnir, The induction of chirality in sol-gel materials, *Acc. Chem. Res.* 40(9), 768–776 (2007).
51. G. Shustak, S. Mark, I. Turyan, and D. Mandler, Application of sol-gel technology for electroanalytical sensing, *Electroanalysis* 15(5–6), 398–408 (2003).
52. M. Hunnius, A. Rufinska, and W. F. Maier, Selective surface adsorption versus imprinting in amorphous microporous silicas, *Microp. Mesop. Mater.* 29(3), 389–403 (1999).
53. B. Boury, R. J. P. Corriu, V. Le Strat, and P. Delord, Generation of porosity in a hybrid organic-inorganic xerogel by chemical treatment, *New J. Chem.* 23(5), 531–538 (1999).
54. R. Makote, and M. M. Collinson, Template recognition in inorganic-organic hybrid films prepared by the sol-gel process, *Chem. Mater.* 10(9), 2440–2445 (1998).

55. S. Shtelzer, S. Rappoport, D. Avnir, M. Ottolenghi, and S. Braun, Properties of trypsin and of acid-phosphatase immobilized in sol-gel glass matrices, *Biotechnol. Appl. Biochem.* 15(3), 227–235 (1992).
56. J. Heller, and A. Heller, Loss of activity or gain in stability of oxidases upon their immobilization in hydrated silica: significance of the electrostatic interactions of surface arginine residues at the entrances of the reaction channels, *J. Am. Chem. Soc.* 120(19), 4586–4590 (1998).
57. M. T. Reetz, A. Zonta, and J. Simpelkamp, Efficient heterogeneous biocatalysts by entrapment of lipases in hydrophobic sol-gel materials, *Angew. Chem. Int. Ed.* 34(3), 301–303 (1995).
58. D. T. Nguyen, M. Smit, B. Dunn, and J. I. Zink, Stabilization of creatine kinase encapsulated in silica sol-gel materials and unusual temperature effects on its activity, *Chem. Mater.* 14(10), 4300–4306 (2002).
59. I. Gill, and A. Ballesteros, Encapsulation of biologicals within silicate, siloxane, and hybrid sol-gel polymers: an efficient and generic approach, *J. Am. Chem. Soc.* 120(34), 8587–8598 (1998).
60. Q. Chen, G. L. Kenausis, and A. Heller, Stability of oxidases immobilized in silica gels, *J. Am. Chem. Soc.* 120(19), 4582–4585 (1998).
61. M. A. Kim, and W. -Y. Lee, Amperometric phenol biosensor based on sol-gel silicate/Nafion composite film, *Anal. Chim. Acta* 479(2), 143–150 (2003).
62. I. Pankratov, and O. Lev, Sol-gel derived renewable-surface biosensors, *J. Electroanal. Chem.* 393(1–2), 35–41 (1995).
63. S. Sampath, and O. Lev, Inert metal-modified, composite ceramic-carbon, amperometric biosensors: renewable, controlled reactive layer, *Anal. Chem.* 68(13), 2015–2021 (1996).
64. S. Sampath, and O. Lev, Renewable, reagentless glucose sensor based on a redox modified enzyme and carbon-silica composite, *Electroanalysis* 8(12), 1112–1116 (1996).
65. J. Wang, P. V. A. Pamidi, and D. S. Park, Sol-gel-derived metal-dispersed carbon composite amperometric biosensors, *Electroanalysis* 9(1), 52–55 (1997).
66. S. Bharathi, and O. Lev, Sol-gel-derived nanocrystalline gold-silicate composite biosensor, *Anal. Commun.* 35(1), 29–31 (1998).
67. S. Bharathi, J. Joseph, and O. Lev, Electrodeposition of thin gold films from an aminosilicate stabilized gold sol, *Electrochem. Solid-State Lett.* 2(6), 284–287 (1999).
68. S. Bharathi, M. Nogami, and O. Lev, Electrochemical organization of gold nanoclusters in three dimensions as thin films from an aminosilicate-stabilized gold sol and their characterization, *Langmuir* 17(9), 2602–2609 (2001).
69. S. Bharathi, and O. Lev, Sol-gel-derived prussian blue-silicate amperometric glucose biosensor, *Appl. Biochem. Biotechnol.* 89(2–3), 209–216 (2000).
70. B. Haghighi, N. Shams, and L. Gorton, Effect of various deposition techniques, electrode materials and posttreatment with tetrabutylammonium and tetrabutylphosphonium salts on the electrochemical behavior and stability of various Prussian blue modified electrodes, *Electroanalysis* 19(18), 1921–1932 (2007).
71. H. Wakamatsu, S. P. Szu, L. C. Klein, and M. Greenblatt, Effect of lithium-salts on the ionic conductivity of lithium silicate gels, *J. Non-Cryst. Solids* 147, 668–671 (1992).
72. I. Gautier-Luneau, A. Denoyelle, J. Y. Sanchez, and C. Poinsignon, Organic-iorganic protonic polymer electrolytes as membrane for low-temperature fuel cell, *Electrochim. Acta* 37(9), 1615–1618 (1992).
73. N. Miyake, J. S. Wainright, and R. F. Savinell, Evaluation of a sol-gel derived Nafion/silica hybrid membrane for proton electrolyte membrane fuel cell applications: I. Proton conductivity and water content, *J. Electrochem. Soc.* 148(8), A898–A904 (2001).

74. I. Honma, Y. Takeda, and J. M. Bae, Protonic conducting properties of sol-gel derived organic/inorganic nanocomposite membranes doped with acidic functional molecules, *Solid State Ionics* 120(1–4), 255–264 (1999).
75. K. Ramanathan, B. R. Jönsson, and B. Danielsson, Sol-gel based thermal biosensor for glucose, *Anal. Chim. Acta* 427(1), 1–10 (2001).
76. M. E. Tess, and J. A. Cox, Chemical and biochemical sensors based on advances in materials chemistry, *J. Pharm. Biomed. Anal.* 19(1–2), 55–68 (1999).
77. M. Popall, M. Andrei, J. Kappel, J. Kron, K. Olma, and B. Olsowski, ORMOCERs as inorganic-organic electrolytes for new solid state lithium batteries and supercapacitors, *Electrochim. Acta* 43(10–11), 1155–1161 (1998).
78. M. Tsionsky, G. Gun, V. Glezer, and O. Lev, Sol-gel-derived ceramic-carbon composite electrodes: introduction and scope of applications, *Anal. Chem.* 66(10), 1747–1753 (1994).
79. S. Bharathi, N. Fishelson, and O. Lev, Direct synthesis and characterization of gold and other noble metal nanodispersions in sol-gel-derived organically modified silicates, *Langmuir* 15(6), 1929–1937 (1999).
80. J. Widera, and J. A. Cox, Electrochemical oxidation of aniline in a silica sol-gel matrix, *Electrochem. Commun.* 4(2), 118–122 (2002).
81. M. M. Verghese, K. Ramanathan, S. M. Ashraf, M. N. Kamalasanan, and B. D. Malhotra, Electrochemical growth of polyaniline in porous sol-gel films, *Chem. Mater.* 8(4), 822–824 (1996).
82. T. -M. Park, E. I. Iwuoha, M. R. Smyth, R. Freaney, and A. J. McShane, Sol-gel based amperometric biosensor incorporating an osmium redox polymer as mediator for detection of L-lactate, *Talanta* 44(6), 973–978 (1997).
83. W. Song, Y. Liu, N. Lu, H. Xu, and C. Sun, Application of the sol-gel technique to polyoxometalates: towards a new chemically modified electrode, *Electrochim. Acta* 45(10), 1639–1644 (2000).
84. A. Kros, M. Gerritsen, V. S. I. Sprakel, N. A. J. M. Sommerdijk, J. A. Jansen, and R. J. M. Nolte, Silica-based hybrid materials as biocompatible coatings for glucose sensors, *Sens. Actuators, B* 81(1), 68–75 (2001).
85. Z. Gao, J. S. Nahrup, J. E. Mark, A. Sakr, Poly(dimethylsiloxane) coatings for controlled drug release. I. Preparation and characterization of pharmaceutically acceptable materials, *J. Appl. Polym. Sci.* 90(3), 658–666 (2003).
86. A. Sadeh, S. Sladkevich, F. Gelman, P. Prikodchenko, I. Baumberg, O. Berezin, and O. Lev, Sol–gel-derived composite antimony-doped, tin oxide-coated clay-silicate semitransparent and conductive electrodes, *Anal. Chem.* 79(14), 5188–5195 (2007).
87. J. Wang, D. S. Park, and P. V. A. Pamidi, Tailoring the macroporosity and performance of sol-gel derived carbon composite glucose sensors, *J. Electroanal. Chem.* 434(1–2), 185–189 (1997).
88. J. Li, L. S. Chia, N. K. Goh, and S. N. Tan, Renewable silica sol-gel derived carbon composite based glucose biosensor, *J. Electroanal. Chem.* 460(1–2), 234–241 (1999).
89. J. Gun, and O. Lev, Wiring of glucose oxidase to carbon matrices via sol-gel derived redox modified silicate, *Anal. Lett.* 29(11), 1933–1938 (1996).
90. V. G. Gavalas, R. Andrews, D. Bhattacharyya, and L. G. Bachas, Carbon nanotube sol-gel composite materials, *Nano Lett.* 1(12), 719–721 (2001).
91. J. K. Campell, L. Sun, and R. M. Crooks, Electrochemistry using single carbon nanotubes, *J. Am. Chem. Soc.* 121(15), 3779–3780 (1999).
92. H. N. Choi, Y. -K. Lyu, J. H. Han, and W. -Y. Lee, Amperometric ethanol biosensor based on carbon nanotubes dispersed in sol-gel-derived titania-Nafion composite film, *Electroanalysis* 19(14), 1524–1530 (2007).

93. S. Bharathi, and M. Nogami, A glucose biosensor based on electrodeposited biocomposites of gold nanoparticles and glucose oxidase enzyme, *Analyst* 126(11), 1919–1922 (2001).
94. S. Bharathi, J. Joseph, and O. Lev, Electrodeposition of thin gold films from an aminosilicate stabilized gold sol, *Electrochem. Solid-State Lett.* 2(6), 284–287 (1999).
95. S. Bharathi, M. Nogami, and O. Lev, Electrochemical organization of gold nanoclusters in three dimensions as thin films from an aminosilicate-stabilized gold sol and their characterization, *Langmuir* 17(9), 2602–2609 (2001).
96. D. Mandler, Private communication, 2007.
97. N. Al-Dahoudi, and M. A. Aegerter, Comparative study of transparent conductive In_2O_3:Sn (ITO) coatings made using a sol and a nanoparticle suspension, *Thin Solid Films* 502(1–2), 193–197 (2006).
98. S. Sampath, and O. Lev, 3D organized self-assembled monolayer electrodes: a novel biosensor configuration, *Adv. Mater.* 9(5), 410–413 (1997).
99. J. Gun, and O. Lev, Sol-gel derived, ferrocenyl-modified silicate-graphite composite electrode: wiring of glucose oxidase, *Anal. Chim. Acta* 336(1–3), 95–106 (1996).
100. L. Coche-Guérente, S. Cosnier, and P. Labbé, Sol-gel derived composite materials for the construction of oxidase/peroxidase mediatorless biosensors, *Chem. Mater.* 9(6), 1348–1352 (1997).
101. A. Sussman, and T. J. Ward, Ceramic coatings on metal substrates by electrophoretic deposition, *J. Electrochem. Soc.* 129, C324–C324 (1982).
102. N. Leventis, and M. Chen, Electrochemically assisted sol-gel process for the synthesis of polysiloxane films incorporating phenothiazine dyes analogous to methylene blue. Structure and ion-transport properties of the films via spectroscopic and electrochemical characterization, *Chem. Mater.* 9(11), 2621–2631 (1997).
103. R. Shacham, D. Avnir, and D. Mandler, Electrodeposition of methylated sol-gel films on conducting surfaces, *Adv. Mater.* 11(5), 384–388 (1999).
104. A. Walcarius, E. Sibottier, M. Etienne, and J. Ghanbaja, Electrochemically assisted self-assembly of mesoporous silica thin films, *Nat. Mater.* 6(8), 602–608 (2007).
105. W. -Z. Jia, K. Wang, Z. -J. Zhu, H. -T. Song, X. -H. Xia, One-step immobilization of glucose oxidase in a silica matrix on a Pt electrode by an electrochemically induced sol-gel process, *Langmuir* 23(23), 11896–11900, 2007.

SYNTHESIS OF SOL-GEL AND GEL-BASED MATERIALS AND THEIR USE FOR ADSORPTION OF ORGANICS

DUNCAN J. MACQUARRIE*, WENBIN HU
Centre of Excellence in Green Chemistry University of York, Heslington, York YO10 5DD, UK; Green Chemistry Research Institute, Zhongkai University of Agriculture and Technology, Guangzhou 510225, PR China

Abstract. The development of mesoporous silicas containing organic functionality via templated sol-gel methodology has led to a great deal of interest, primarily as catalysts, but also in applications such as adsorbency.

It is possible to prepare materials with a mechanically stable silica backbone, with mesopores having narrow pore size distribution, and which can be coated with a wide range of functionality. They are promising adsorbents due to their controllable surface chemistry and their significant pore volumes.

We have also demonstrated that starch can be expanded to give a gel, which can be converted to a novel range of mesoporous carbons, with tuneable surface functionality, high surface area and good pore volume.

They display remarkable catalytic activity (for example, they can completely esterify succinic acid in *aqueous* environments). We believe that this unusual behaviour can be related to their adsorbency properties.

We present details of the properties of these materials, as well as preliminary results on their ability to adsorb a range of compounds.

Keywords: Mesoporous silicas, starch, starbon, mesoporous carbon, surface chemistry, adsorbency, organics.

1. Introduction

The synthesis of silicas with controlled regular porosity, high surface area has led to an explosion of interest in their use, primarily as catalysts, but also in many other applications such as sensors and as hosts for nanoparticles.[1]

It is well known that the rate of catalysis of liquid phase reactions with solid catalysts such as mesoporous silicas can depend not only on the intrinsic

*To whom correspondence should be addressed: Duncan J. Macquarrie; e-mail: djm@york.ac.uk

P. Innocenzi, Y. L. Zub and V. G. Kessler (eds.), *Sol-Gel Methods for Materials Processing*.

reaction step(s) but also on adsorption/desorption of reactants and products to/from the active site. Therefore, it is not only important to provide the silica with catalytically active sites, but also with the appropriate surface properties for the reaction. These may include modification of the polarity of the surface to improve adsorption/desorption processes, by the inclusion of second "spectator" groups, which are themselves devoid of catalytic activity. Given that such processes can deliver significant (order of magnitude in some cases) improvements in catalytic activity,[2] it seems reasonable that the same materials and the same approach might be used to adsorb organic species from solution.

2. Experimental

Materials were prepared by standard procedures.[6,7,9] Adsorbency experiments were carried out by stirring the adsorbent with the desired compound in distilled water at 298 K for 16 h, unless stated otherwise. The quantities adsorbed were determined by centrifugation and UV-vis analysis of the supernatant.

3. Results and Discussions

3.1. SYNTHESIS OF ORGANICALLY MODIFIED SILICAS

The basic templated synthesis of silicas, involving $(EtO)_4Si$ (TEOS), a micelle forming system such as a long chain amine, a quaternary ammonium salt or a block copolymer, and water can be carried out to give the micelle templated silica. This can be functionalised with a range of silanes to give surface organic groups (Figure 1a).

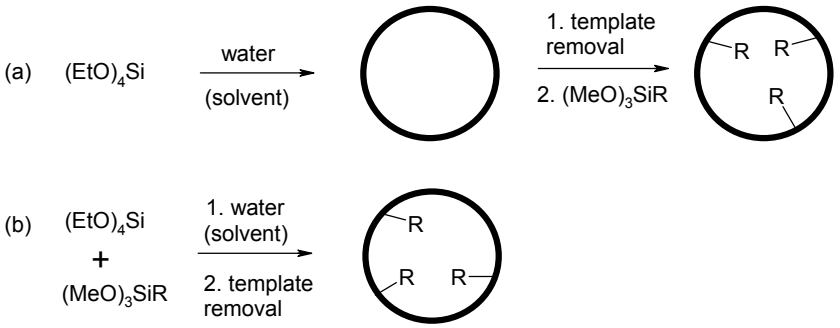

Figure 1. The two major routes for the preparation of organically modified micelle templated silicas. In route (b) it is possible to add more than one functional silane.

A shorter alternative incorporates the functional silane directly in the synthesis. This leads to organically functionalised silicas in one stage. (Figure 1b) The loading of groups is controlled by variation in the ratio of TEOS: organosilane; up to ca. 10–20% is possible, while preserving the templated structure, depending on the silane. Higher loadings (up to ca. 3.8 mmol g^{-1}) are possible but lead to amorphous materials.

It should be noted that the materials prepared from each of these two routes are not necessarily the same. Differences in behaviour have been noted, which have been ascribed to different distributions of silanes (in-pore vs. external[3]; clustering on hydrophobic patches[4] as opposed to evenly distributed; occluded within walls vs. on the surface[5]).

Template removal is an important consideration, not just from the point of view of green chemistry (recovery and reuse of template) but also because a considerable amount of chemistry can take place in the washing stage. We have found that solvent extraction of template (in our case 1-aminododecane, leading to the HMS series of mesoporous silicas) is successful where the solvent has a significant H-bonding capacity. This disrupts H-bonding interactions between the template head group and the silanols on the surface and allows the template to be removed and reused.[6] Alcohols, acetone and acetic acid are all effective. Importantly, alcohols react with the silanols, possibly catalysed by the amine template, to generate surface SiOR species (Figure 2). Thus, template removal with methanol leads to 3.2 mmol g^{-1} loading of SiOMe, with larger alcohols (up to C_8) still giving >2 mmol g^{-1}. Thermal stability is good – those which can readily eliminate alkenes (e.g. 2-propyl) being lower (ca. 400°C) than those with less stabilised alkene products (e.g. linear alkyl) which decompose at ca. 500°C. Methanol begins to decompose around 700°C via a different mechanism, possibly by elimination of HCHO. Hydrolytic stability of small R groups is relatively low, but larger groups such as hexyl or benzyl give materials of pronounced hydrophobicity, and are water stable, at least at lower temperatures.

A further opportunity to modify the surface of silica materials comes from the possibility of removing template by reaction of the as-synthesised material with a silane. This can migrate into the template-filled pore, cap the silanol and thus disrupt the H-bonding interaction with the template, which can then be readily removed by non-polar solvents such as toluene under conditions where the template would otherwise remain in pore. Functional silanes (i.e. $(MeO)_3SiR$) can be added to attach a second silane to the surface, as can Me_3Si groups to improve hydrophobicity and lower polarity.

In particular, we have recently found that the incorporation of CF_3SiMe_3 directly into the synthesis mixture provides material with exceptional hydrophobicity, far more than more conventional silylating agents such as Me_3SiCl

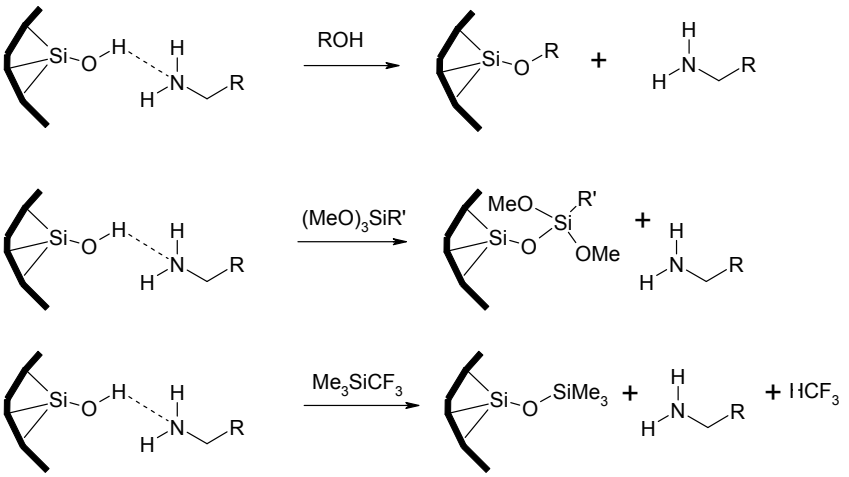

Figure 2. Strategies for reactive template removal.

or $Me_3SiNHSiMe_3$.[7] Thus, it is possible to produce extremely hydrophobic materials directly from an aqueous synthesis gel, without the need for subsequent treatment. Thermal analysis indicates that no water is present on the surface after template extraction (weight loss $\leq$150°C is <0.2%)

We have utilised these strategies for the preparation of a series of silica materials with differing surface chemistries, and have applied them to the adsorption of small molecules from water.

The adsorption of phenols from water is a system often studied for adsorption processes.[8] We studied the adsorption of phenol from water at 25°C (initial concentration of phenol 1,000 ppm). After 16 h, samples were centrifuged and the supernatant analysed for phenol. The results are given in Figure 3.

The more polar materials are poor adsorbents of phenol, with no adsorption for silica itself or for HMS-Et, which has limited stability in water, and is likely to lose Et groups rapidly. The benzyl system, the most hydrophobic of the alcohol-extracted systems works very well, and surprisingly, the acetone extracted system has some activity. However, the CF_3SiMe_3 system displays excellent activity, adsorbing more than its own mass. Clearly, the best systems allow very effective removal of phenol from aqueous environments into the non-polar pore system.

The more polar benzoic acid was also investigated, and the trend obtained was the opposite, with the more polar materials adsorbing the acid much better than the more hydrophobic systems. It should be noted that the quantities adsorbed were significantly lower in all cases (Figure 4).

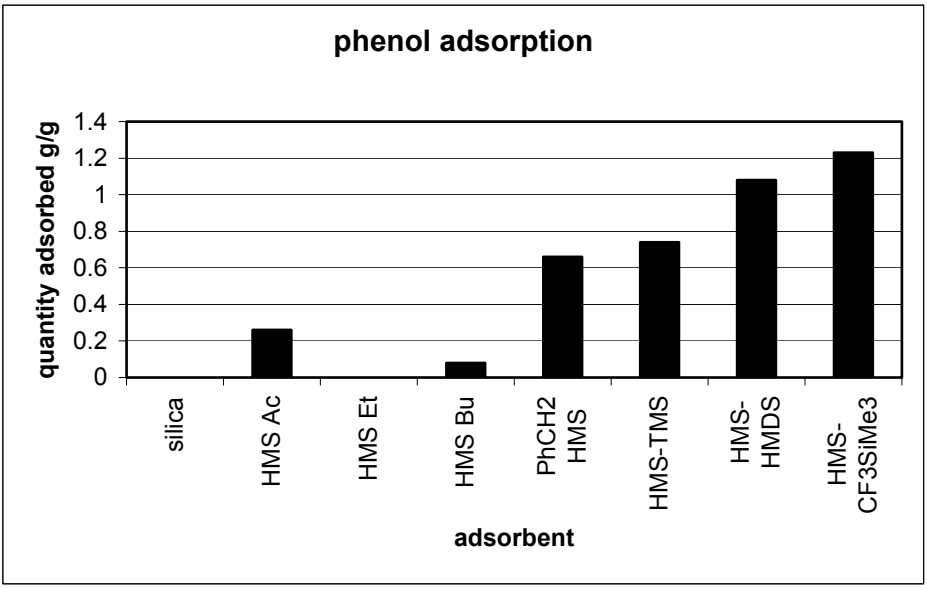

Figure 3. Phenol adsorption over a range of silicas. HMS-Ac – acetone extracted micelle templated silica (no surface functionalisation; HMS-Et (EtOH extracted, 2.4 mmol/g loading of SiOEt); HMS Bu (toluene/1-BuOH extracted, 2.2 mmol/g loading of SiOBu; $PhCH_2HMS$ – micelle templated silica extracted with toluene/$PhCH_2OH$, 2.1 mmol/g loading. The three to the right were synthesised by variations of the bottom route in Figure 2 using Me_3SiCl (TMS), $Me_3SiNHSiMe_3$ (HMDS) and CF_3SiMe_3 respectively.

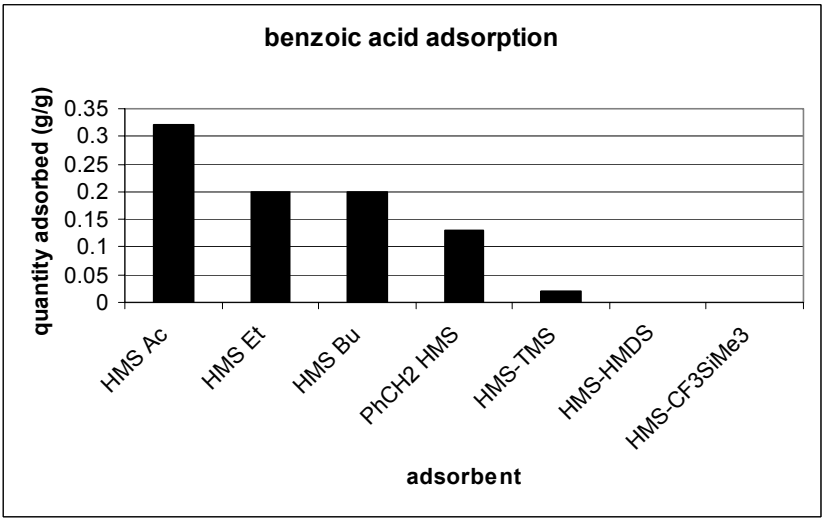

Figure 4. Adsorption of benzoic acid from water with modified silicas.

3.2. STARBONS

Starbons[9] are prepared from starch by expansion and acid catalysed carbonisation. Carbonisation can take place from 200°C to 1,000°C. As this temperature increases the materials are converted from a hydrophilic hydroxylic polysaccharide to a partly carbonised material with carbonyl functionality as well as hydroxylic, through to more aromatic-rich materials. Throughout this process, surface area remains broadly constant at ca. 100–130 $m^2\ g^{-1}$ and the pore diameter is also relatively constant at ca. 10 nm.

We have used these materials, in a sulfonated form, as solid acid catalysts for esterifications.[10] Remarkably, they catalyse esterifications in water. Diethyl succinate can be formed from succinic acid and ethanol in water in almost 100% yield. This is invaluable in the valorisation of fermentation-derived feedstocks, where isolation from the broth is expensive and difficult. Organic transformations (especially to water-insoluble products) in situ is an important short-cut to key products.

We believe that the key to this activity is its ability to partition acids (and alcohols) into the pores, to the (partial) exclusion of water, so that catalysis actually occurs in a low-water environment.

Thus, we have looked at the adsorption of acids from water onto starbon. (Figures 5, 6). Since there is a marked dependence of reaction rate on preparation temperature, and since the optimum preparation temperature for succinic acid esterification is 400°C (the materials is designated starbon 400), we studied the adsorbency using 400°C starbon.

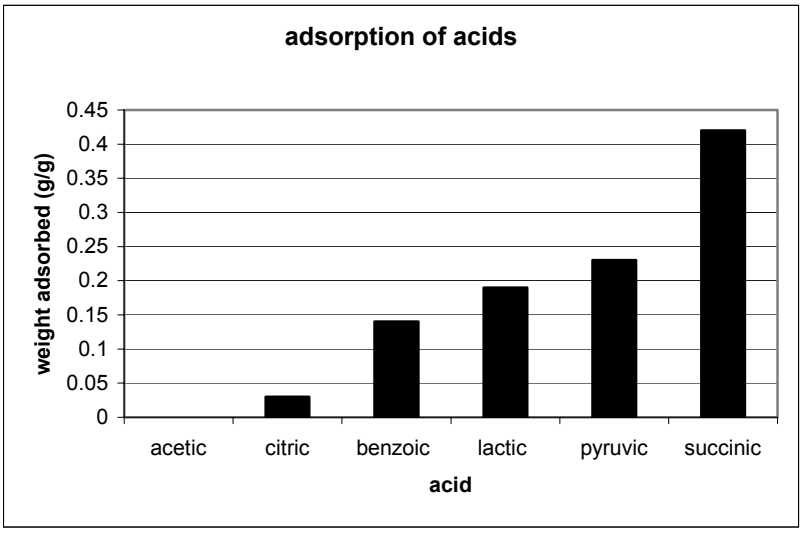

Figure 5. Adsorption of acids from water onto Starbon 400.

Figure 5 shows that succinic acid is adsorbed onto the material more than the others. Succinic acid appears to be less well adsorbed onto other starbons, consistent with the theory that adsorption is a key step in catalysis.

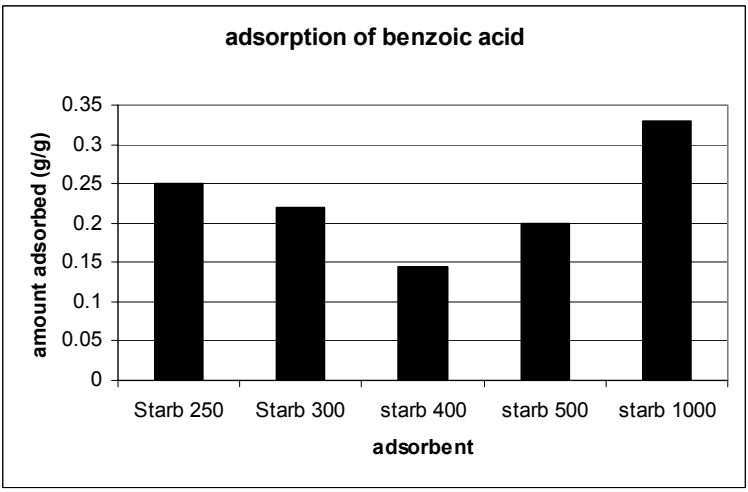

Figure 6. Adsorption of benzoic acid on starbons.

4. Conclusions

Control over surface chemistry can be readily achieved in micelle templated silicas by a combination of in situ synthetic strategies during the sol-gel synthesis of the materials, and appropriate template removal strategies. Materials can be designed to have optimum activity by a combination of appropriate active sites and surface polarity and hydrophobicity modification. Likewise mesoporous carbons can be prepared from expanded starch and thermal treatment, which allows excellent of control over surface chemistry.

Initial results on adsorbency, have shown that appropriately modified materials can display interesting adsorbency effects on simple systems.

Acknowledgements

WH thanks the China Scholarship Council (No.2004836011), and the Education Foundation of Jiangxi Province (Project 2005(95) for financial support.

References

1. (a) J. H. Clark, D. J. Macquarrie, S. J. Tavener, The application of modified mesoporous silicas in liquid phase catalysis, Dalton Trans., 2006, 4297; (b) A. Stein, B. J. Melde, R. C. Schroden, Hybrid inorganic-organic mesoporous silicates: nanoscopic reactors coming of age, Adv. Mater., 12, 1403 (2000).
2. (a) D. J. Macquarrie, S. J. Tavener, M. A. Harmer, Novel mesoporous silica-perfluorosulfonic acids as strong Bronsted acid catalysts, Chem. Commun. 2363 (2005); (b) I. Diaz, C. Marques-Alvarez, F. Mohino, J. Perez-Pariente, E. Sastre, Combined alkyl and acid functionalised of MCM-41 silicas. Part 1 synthesis and characterisation and Part 2 Esterification of fatty acids with glycerol, J. Catal., 193, 283 and 295 (2000); (c) Y. Wan, J. Chen, D. Zhang, H. Li, Ullmann coupling reaction in aqueous conditions over the Ph-MCM-41 supported Pd catalyst, J. Mol. Catal., A, 258, 89 (2006).
3. M. H. Lim, A. Stein, Comparative studies of grafting and direct synthesis of inorganic-organic hybrid mesoporous materials, Chem. Mater., 11, 3285 (1999).
4. D. Brunel, A. Cauvel, F. di Renzo, F. Fajula, B. Fubini, B. Onida, E. Garrone, Preferential grafting of alkoxysilane coupling agents on the hydrophobic portion of the surface of micelle templated silica, New J. Chem., 24, 807 (2000).
5. T. Yokoi, H. Yoshitake, T. Tatsumi, Synthesis of amino-functionalised MCM-41 via direct co-condensation and post-synthetic grafting methods using mono-, di-, and triamino-organoalkoyssilanes, J. Mater. Chem., 14, 951 (2004).
6. D. J. Macquarrie, D. B. Jackson, B. L. King, A. Watson, Preparation of novel organic-inorganic hybrid micelle templated silicas. Comparison of different routes for preparation, Stud. Surf. Sci., Catal., 142, 1125 (2002).
7. W. Hu and D. J. Macquarrie, manuscript in preparation.
8. B. C. Pan, W. Du, W. M. Zhang, X. Zhang, Q. R. Zhang, B. J. Pan, L. Lv, Q. X. Zhang, J. L. Chen, Improved adsorption of 4-nitrophenol onto a novel hyper cross-linked polymer, Environ. Sci. Technol., 41, 5057 (2007).
9. V. Budarin, J. H. Clark, J. J. E. Hardy, R. Luque, K. Milkowski, S. J. Tavener, A. J. Wilson, Starbons: new starch-derived mesoporous carbonaceous materials with tunable properties, Angew. Chem. Int. Ed., 45, 3782 (2006).
10. (a) V. L. Budarin, J. H. Clark, R. Luque, D. J. Macquarrie, Versatile mesoporous carbonaceous materials for acid catalysis, Chem. Comm., 634 (2007); (b) V. L. Budarin, J. H. Clark, R. A. Luque, D. J. Macquarrie, A. Koutinas, C. Webb, Tuneable mesoporous materials optimised for aqueous phase esterifications, Green Chem., 9, 992 (2007).

CHARACTERIZATION OF GELS AND NETWORKS USING NEW CALORIMETRIC TECHNIQUES

JEAN-MARIE NEDELEC[1*], MOHAMED BABA[2]
[1]*Laboratoire des Matériaux Inorganiques, CNRS UMR 6002*
[2]*Laboratoire de Thermodynamique des Solutions et des Polymères, CNRS UMR 6003*
Université Blaise Pascal & ENSCCF, 24 Avenue des Landais, 63177 Aubière, France

Abstract. Recent developments of calorimetric techniques for the characterization of porous materials and gels are presented. In particular thermoporosimetry is introduced along with recent applications to soft materials like gels and polymers. In a second part, photo-DSC technique is presented with the new developments for the study of gels networks and photo-ageing of polymers. An overview of the potential of the two techniques towards sol-gel materials is finally given.

Keywords: Sol-gel, calorimetry, photo-DSC, gels, networks, crosslinking, porous materials, polymers, hybrid organic-inorganic materials, confinement effects.

1. Introduction

Porous materials are solids made up of interconnected networks of pores delimited by solid walls. These materials are omnipresent in nature and find various industrial applications. Numerous biological processes also involve such porous materials making them the object of abundant studies. The characterization of porosity is therefore a crucial issue.

[*]To whom correspondence should be addressed: Dr. J.-M. Nedelec, TransChiMiC, Laboratoire des Matériaux Inorganiques, CNRS UMR 6002, Université Blaise Pascal & ENSCCF, 24 Avenue des Landais, 63177 Aubière, France; e-mail: j-marie.nedelec@univ-bpclermont.fr

P. Innocenzi, Y. L. Zub and V. G. Kessler (eds.), *Sol-Gel Methods for Materials Processing*.

The control of 3D organization is also a major challenge in soft matter like polymers and gels. In this case, the function of the material is controlled by the cross-linking level and chains arrangement. As far as polymers are concerned, the reticulation level is strongly dependant on the history of the material, from processing to ageing. This cross-linking level greatly affects the mechanical properties of the material and knowledge of its evolution is therefore crucial for long term durability prediction. Numerous experimental techniques have been used for the study of spatial organization in polymers and gels. In most cases, the information is derived at a molecular or macroscopic level. In this paper, we would like to present new applications of calorimetric techniques to study porous materials and soft matter organization directly on the mesoscopic scale. Two original techniques, namely thermoporosimetry (TPM) and photo-Differential Scanning Calorimetry (Photo-DSC) will be presented and recent applications will be given.

2. Thermoporosimetry

2.1. EFFECT OF CONFINEMENT ON THERMAL TRANSITIONS

If one considers the thermodynamical equilibrium between the three phases (solid, liquid, gas) of a pure compound, three volumic phases and two inter-phases, liquid/solid (ls) and solid/gas (sg) considered as surfacic phases have to be taken into account.

On each side of the interfaces, there is equality of both chemical potentials and variations of these potentials. These variations can be expressed using the first principle of thermodynamics[1]:

$$du_i = \delta q_i + \delta w_i = T_i ds_i - P_i dv_i \tag{1}$$

$$d\mu_i = dh_i - T_i ds_i - s_i dT_i \tag{2}$$

$$dh_i = du_i + P_i dv_i + v_i dP_i \tag{3}$$

Combining (1), (2) and (3), the variation of the potential can be written:

$$d\mu_i = v_i dP_i - s_i dT_i \tag{4}$$

Subscript i refers to the phase in which the compound is (i = l, s or g).

For a multiphasic system, the thermodynamical equilibrium implies temperature homogeneity but not pressures equality. If the interfaces are not planar, the pressure on the concave side is superior to the one on the convex side. The difference of pressure between the two sides is given by Laplace law:

$$P_i - P_j = \gamma_{ij} \frac{dA_{ij}}{dV_j} \tag{5}$$

At the liquid-solid interface one can write:

$$d\mu_s = d\mu_l \quad \Leftrightarrow \quad -s_s dT_s + v_s dP_s = -s_l dT_l + v_l dP$$

But according to Laplace formula,

$$dP_s - dP_l = d(\gamma_{sl} \frac{dA_{sl}}{dV_s})$$

If one considers the thermal equilibrium, and one can write:

$$dP_s = dT \frac{(s_s - s_l)}{(v_s - v_l)} - \frac{v_l}{(v_s - v_l)} d\left(\gamma_{sl} \frac{dA_{sl}}{dV_l} \right) \tag{6}$$

Similar consideration at the solid-gas interface allows writing:

$$dP_s = dT \frac{(s_s - s_g)}{(v_s - v_g)} + \frac{v_g}{(v_s - v_g)} d\left(\gamma_{gs} \frac{dA_{gs}}{dV_s} \right) \tag{7}$$

Neglecting the molar volume of condensed phases in front of the one of gas phase, combination of (6) and (7) yields:

$$dT = \frac{v_s - v_l}{(s_s - s_g)} d\left(\gamma_{gs} \frac{dA_{gs}}{dV_s} \right) + \frac{v_l}{(s_s - s_l)} d\left(\gamma_{sl} \frac{dA_{sl}}{dV_l} \right) \tag{8}$$

According to (8), the thermodynamical equilibrium temperature, called the triple point temperature, is not a constant. The variation of the triple point temperature depends on the curvatures of both interfaces solid-liquid and solid-gas. These curvatures are controlled by the geometry of the volumes confining the solvent. In the general case solving of (8) is difficult.

If one considers the thermodynamical equilibrium between gas, liquid and solid phases in a cylindrical pore, combination of Clausius-Clapeyron and Kelvin equations yields:

$$\ln \frac{T_p}{T_0} = \frac{2V_m \gamma_{sl}}{\Delta H_m r} \tag{9}$$

Relating the melting temperature inside the pore T_p to T_0 the normal melting temperature and to 1/r. ΔH_m is the enthalpy of melting, V_m the molar volume, and γ_{sl} the interfacial energy.

Writing $\Delta T = T_p - T_0$, a serial development of (9) at the first order yields:

$$\Delta T = T_p - T_0 = \frac{2T_0 V_m \gamma_{sl}}{\Delta H_m r} \tag{10}$$

Equation (10) is known as the Gibbs-Thomson[1] equation and is classically used experimentally to calculate r from the measurement of ΔT. In the case of a cylindrical pore of radius r_p, (10) can be written:

$$\Delta T = T_p - T_0 = \frac{2T_0 V_m \gamma_{sl} \cos\theta}{\Delta H_m r_p} \tag{11}$$

Where θ is the contact angle between the liquid and the solid usually taken to be 0°.

In general, the creation of an adsorbed layer of non freezing solvent of thickness t is assumed on the surface of the pores (Figure 1). In this case, the measured r_p corresponds to $(R_p - t)$, R_p being the real radius of the pore.

This thickness t is usually found lower than 2 nm (usually a few molecular layers) and gives the lower limit of measurable pore size. This layer must be taken into account for precise derivation of R_p through ΔT measurement.

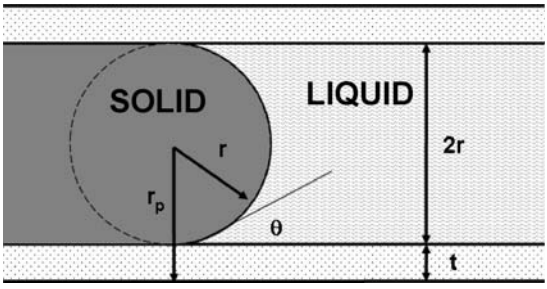

Figure 1. Scheme of liquid-solid equilibrium in a cylindrical pore of radius R_p considering the creation of an adsorbed layer t.

2.2. APPLICATION OF THERMOPOROSIMETRY FOR THE CHARACTERIZATION OF POROUS SOLIDS

Equation (11) gives a direct relation between the depression of the melting point of a given confined solvent and the radius of the pores in which it is confined. Measurement of ΔT can then give access to the pore size. In the 1950s Kuhn et al.[2] proposed to use Differential Scanning Calorimetry (DSC) to measure ΔT and invented the so called thermoporosimetry technique (TPM). This technique has been further described by Fagerlund[3] and popularized and developed by Brun.[4] It is now a recognized technique even if gas sorption remains the gold standard for porosity measurements in solids.

In a thermoporosimetry experiment, not only the average pore size can be determined but also the full pore size distribution (PSD) by considering the whole DSC curve. Using (11) the PSD can be derived as follows:

$$\frac{d(V_p)}{d(R_p)} = \frac{dQ(T)}{dt}\frac{dt}{d(\Delta T)}\frac{d(\Delta T)}{d(R_p)}\frac{1}{W_a(T)} \tag{12}$$

where V_p ($cm^3\ g^{-1}$) is the pore volume, $dQ(T)/dt$ ($W\ g^{-1}$) is the heat flow per gram of the dry porous sample given by the ordinate of DSC thermogram, $dt/d(\Delta T)$ ($s\ K^{-1}$) is the reverse of the cooling rate, $d(\Delta T)/d(Rp)$ ($K\ nm^{-1}$) is derived from the empirical relationship corresponding to (11) and $W_a(T)$ ($J\ cm^{-3}$) is the apparent energy as defined by Brun. However, the specific energy of crystallization is temperature dependent and, in addition, all the solvent does not take part in the thermal transition since, as stated before, a layer of the solvent remains adsorbed on the internal wall of the pores. Only an apparent energy (W_a) can be calculated, dividing the total heat, released by the thermal transition, by the total volume or mass of the confined solvent.

In order to reach the PSD calculation, it is necessary to establish the temperature dependence of both R_p and W_a. This is obviously a severe drawback for thermoporosimetry as a precise calibration procedure is requested. The extraordinary progress in the preparation of porous materials with well controlled pore sizes during the last 20 years is now circumventing this problem. Comparison of PSD derived from gas sorption, TPM and NMR cryoporometry[5,6] clearly demonstrated the validity of TPM for the study of nanoporous materials.

Various solvents have been calibrated providing data for TPM measurements. The first studies dealt essentially with water and benzene. In the 1990s Jackson and McKenna published data for n-heptane, cis- and trans-decaline, cyclohexane, naphthalene, and chlorobenzene.[7]

In recent years, numerous solvents have been calibrated for thermoporosimetry including acetonitrile,[8] CCl_4,[9,10] xylenes, various substituted benzenes,[11] linear alkanes,[12,13] cyclohexane,[14] dioxane[15] and acetone.[16]

Thanks to the calibration curves proposed in the literature for various solvents, thermoporosimetry has become a functional technique. TPM also addresses some major fundamental issues concerning melting/freezing in confined geometries and the underlying energetic and thermodynamics. In the following section we will show how TPM can also be used very efficiently to study less rigid materials like polymers and gels.

2.3. APPLICATION OF THERMOPOROSIMETRY FOR THE CHARACTERIZATION OF SOFT MATERIALS

In the 1950s Kuhn already observed the peculiar behavior of liquids swelling polymeric gels.[2] Indeed a strong analogy can be proposed between solvent trapped inside the pores of a rigid material and the solvent swelling the chains of a polymeric network. In the case of polymer swelling, the network limits the mobility of the solvent molecules inducing a confinement effect. As observed for nanoporous materials, the trapped solvent exhibits a shift of its melting/freezing temperature directly related to the size of the confinement domain. The shift ΔT can be associated with the size of the meshes defining the 3D network between successive reticulation knots.

The use of TPM on swollen polymers can give access to Mesh Size Distribution (MSD) in the swollen state. The ability of the polymer to swell depends on the reticulation level which in turn can vary a lot during polymer ageing.

In the following some examples will illustrate the use of TPM to characterize soft materials.

2.3.1. *Elastomers*

Since the pioneering work of Kuhn, the solvent freezing point depression observed in swollen cross linked rubbers has been the subject of many works. In 1991, Jackson and McKenna[17] studied both the freezing and melting of solvent crystals in crosslinked and uncrosslinked natural rubber swollen in benzene. More recently, the authors[18] proposed a detailed study of natural rubber containing fillers. This possibility offered by TPM to work on formulated polymers makes it a very unique technique.

In 2006, McKenna and coworkers reviewed recent work devoted to the use of TPM to study polymer heterogeneity.[19] In this work, uncrosslinked and crosslinked polyisoprene was studied with benzene and hexadecane as swelling solvents. It was shown that for uncrosslinked sample, an excess shift ΔT is measured compared to Flory Huggins theory.[20,21] This is interpreted in terms of nanoheterogeneities in the uncrosslinked polymer.

Photo-oxidation of various elastomers has been studied by TPM in recent years.[13–14] The effect of photo-ageing is clearly observed with an important shift of the mean mesh size towards low sizes upon ageing and also a narrowing of the MSD (Figure 2). The MSD is clearly a good indicator of the evolution of the polymer network upon ageing. Its measurement by TPM gives a very efficient tool for the follow up of the ageing.

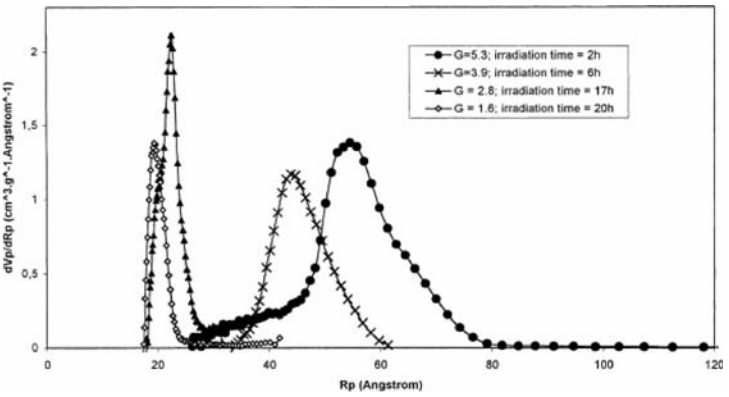

Figure 2. Mesh Size Distributions determined by n-heptane TPM for EPDM samples crosslinked during various irradiation times. Reproduced from,[13] © 2003. With permission from Elsevier.

2.3.2 *Other Polymers*

In 2000, Iza et al.[22] described a TPM study of hydrogels. In the meanwhile, TPM has become a popular tool for measuring pore size distribution in polymer membranes as illustrated by recent reviews.[23,24] Cellulosic membranes were also studied by water TPM.[25,26] In 2005 TPM was used to measure pore size distributions in porous polymers networks.[27]

Recently we studied polyolefin samples presenting various degree of cross-linking by TPM with xylenes.[28] Upon increasing irradiation dose, a correlative decrease of G and of the maximum of the MSD (R_{Max}) measured by TPM is observed (Figure 3). These observations are in agreement with the subsequent cross linking increase upon irradiation making TPM a valuable technique to discuss the evolution of the polymeric network.

TPM appears to be a unique technique to study soft matter organization on a nanoscopic level. TPM can also be very valuable for the study of hybrid organic-inorganic materials associating a rigid inorganic part (that can be porous)

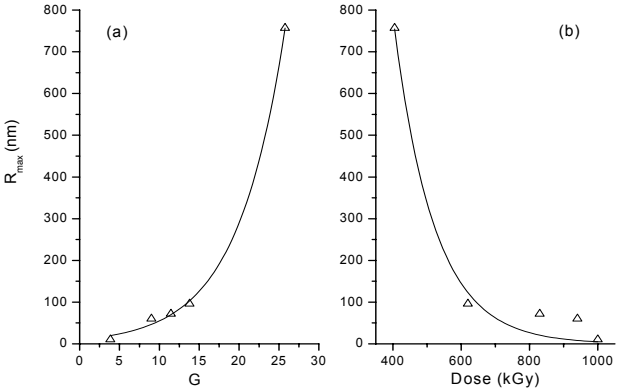

Figure 3. Evolution of the maximum of the Mesh Size Distribution (R_{max}) as a function of the swelling ratio (a) and the irradiation dose (b) for p-xylene.

and a more flexible organic counterpart. In this sense, TPM appears to be a universal technique directly associated to the physics of confinement. The intense development of porous samples with very well controlled pore size distribution allows determining calibrations curves for numerous solvents. The simplicity and the low cost associated with TPM are further arguments for extended use of this technique.

4. Photo-DSC: A Powerful Tool for the *In Situ* Study of Photo Initiated Reactions

4.1. PHOTO-DSC: THE STATE OF THE ART

Photo-DSC, or Photo-Calorimetry, combines in a single equipment light irradiation and classical DSC measurement. Irradiation conditions (wavelength, intensity, duration,…) can be chosen in a wide range. It is also possible to easily control the temperature (–150°C to 500°C) and the nature of the atmosphere (inert, reactive, oxidative,…) making Photo-DSC a very useful and versatile device.

Until very recently Photo-DSC was essentially used for the study of photocuring and photopolymerization reactions. A well documented review has been recently dedicated to the curing of composites by ultraviolet radiation.[29] Two main curing mechanisms are reported: radical polymerization for acrylic-based

resins and cationic polymerization for epoxies and vinyl ether. In both cases the properties of the photocured matrix are determined by its crosslinking density. Khudyakov and his co-workers[30,31] combined Photo-DSC with the curing monitoring and Time-Resolved Electron Paramagnetic Resonance to follow the course of the photopolymerization of a variety of acrylates. Photo-polymerization has also been studied by Photo-DSC in solution. The study of HEMA/DEGDMA hydrogel provides a nice illustration.[32]

4.2. ACCELERATED AGEING OF POLYMER MATERIALS: APPLICATION OF PHOTO-DSC

Photo-oxidation is the most common cause of polymer degradation in outdoor conditions. Light-polymer interactions lead to drastic changes in the physical and chemical properties of the material. Many studies have been devoted to the comprehension[33,34] and the prediction of complex phenomena occurring upon the photo-ageing of polymers. Several accelerated photo-oxidation devices have been proposed.[35,36] In these devices the irradiation step mimicking the aging of the materials is performed independently from the analysis usually performed afterwards by non destructive methods such as FTIR spectroscopy.

We recently proposed to use photo-DSC to study polymer photo-ageing. Indeed, the ability of a semi-crystalline polymer to crystallize is greatly affected by its photo-ageing. Notably, crosslinking and chain scissions, by altering the macromolecular chain mobility, decreases the “crystallizability” of the polymer. Photo-DSC, by following the change of the temperature and the heat of crystallization, is a good tool to study semi-crystalline polymers photo-ageing. In the following, we will illustrate the great potential of Photo-DSC through two selected examples

4.3. CROSS LINKING OF POLYCYCLO-OCTENE

The effects of ageing conditions (irradiation time, light intensity and atmosphere) of polycyclo-octene have been studied.[37]

Photoageing has been performed in situ followed by a crystallization step and then a melting step. Both the area and the maximum of the crystallization peak decrease when the light intensity increases.

The same polycyclo-octene sample was subjected repeatedly to the same program with time increment of 10 min. Upon increasing irradiation time the peak of crystallization shifts towards low temperatures while the released heat decreases as shown in Figure 4.

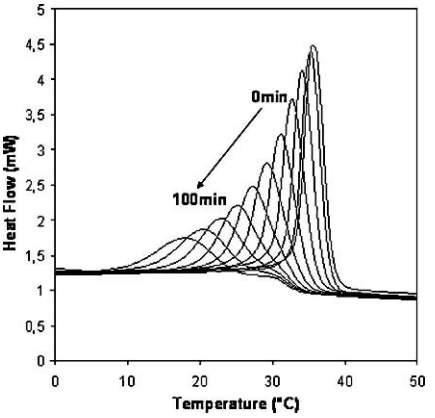

Figure 4. DSC traces of the crystallization of polycylo octene irradiated at 35°C with Xe/Hg lamp having a light intensity of 6.5 mW/cm^2 for irradiation times ranging from 0 to 100 min. The cooling rate was 10°C/min.

The composition of the atmosphere surrounding the polymeric sample can be controlled. The experiments previously described were repeated under nitrogen, air and oxygen atmospheres. No significant modification is noticed under N_2 atmosphere while pure O_2 seems to accelerate the decrease of the crystallization temperature of the material. These results confirm that the changes observed in the polymer aptitude to crystallize can be attributed to an oxidative process.

Photo-oxidation can be classically monitored by FTIR spectroscopy by following the vibration bands corresponding to carbonyl functions at ~1,700 cm^{-1}. To investigate the relation between the accumulation of the oxygenated photo-products and the change in the crystallinity of polycyclo-octene, the decrease of the heat of crystallization was compared with the rise of this vibration band (Figure 5). The enthalpy of crystallization falls at early stages of irradiation before significant accumulation of the carbonyl. Assuming that the decrease of the polymer crystallizability is related to the network densification, polycyclo-octene seems to predominantly undergo the cross linking reactions before a noticeable formation of oxygenated photo-products. This behaviour is observed for the first time in this system thanks to the use of Photo-DSC as it was also the case for other dienic elastomers like polybutadiene[38] and ethylene-propylene-diene-monomer (EPDM).[39]

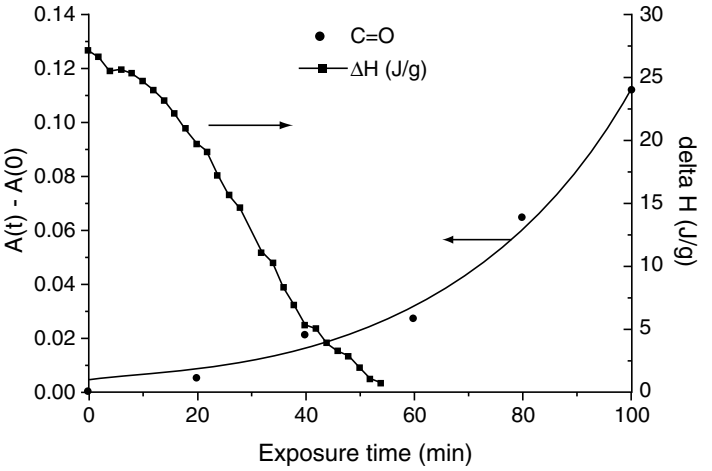

Figure 5. Polycyclo octene irradiated in PhotoDSC system at 35°C and under air. (●, left ordinate): IR kinetic evolution of carbonyl band (1,721 cm^{-1}). (■, right ordinate): change in crystallization heat. (Reproduced from,[38] © 2005. With permission from Elsevier.)

4.4. KINETICS OF CHAIN SCISSIONS DURING ACCELERATED AGEING OF POLY(ETHYLENE-OXIDE)

PEO is a semi-crystalline water-soluble polymer, with a crystallinity which is very sensitive to the thermal history of the samples, making this property interesting as an indicator of degradation. Because it is biodegradable and biocompatible, PEO is a good candidate for environmental and medical applications.[40–42] The mechanisms of thermo and photooxidation of PEO have already been investigated[43,44] on the basis of IR identifications of the oxidation products. The chain scissions predicted by this chemical mechanism have been observed by IR spectroscopy. Photo-DSC, provides a direct mean to observe the transition temperature shift and the change in the heat of crystallization/fusion upon chain scissions as demonstrated recently.[45]

Here, we would like to report another study concerning isothermal crystallization kinetics study of PEO ageing.[46]

Isothermal crystallization thermograms of thermally and photo-oxidized PEO have been subjected to Avrami analysis formalism.[47–49] Fundamental Avrami equation can be expressed as:

$$\alpha(t) = 1 - \exp(-k_a t^n) \tag{13}$$

where k_a is Avrami rate constant and n Avrami exponent. $\alpha(t)$ is the relative crystallinity defined as follows:

$$\alpha(t) = \frac{\Delta H(t)}{\Delta H_\infty} \tag{14}$$

$\Delta H(t)$ is the enthalpy of isothermal crystallization at t and ΔH_∞ its value after complete crystallization.

The value of Avrami exponent ranges from 1 to 4 depending on the geometric characteristics of nuclei: n = 1 being ascribed to a rod, 2 to pellets and 3 or 4 to three-dimensional structure.

To calculate k_a and n, a log-log graphic representation is classically used:

$$\log(-\ln(1-\alpha(t)) = \log(k_a) + n\log(t) \tag{15}$$

Thus, if the experimental data follow Avrami's theory, the plot of $\log(-\ln(1-\alpha(t))$ as a function of $\log(t)$ should be linear yielding $\log(k_a)$ as intercept and n as slope.

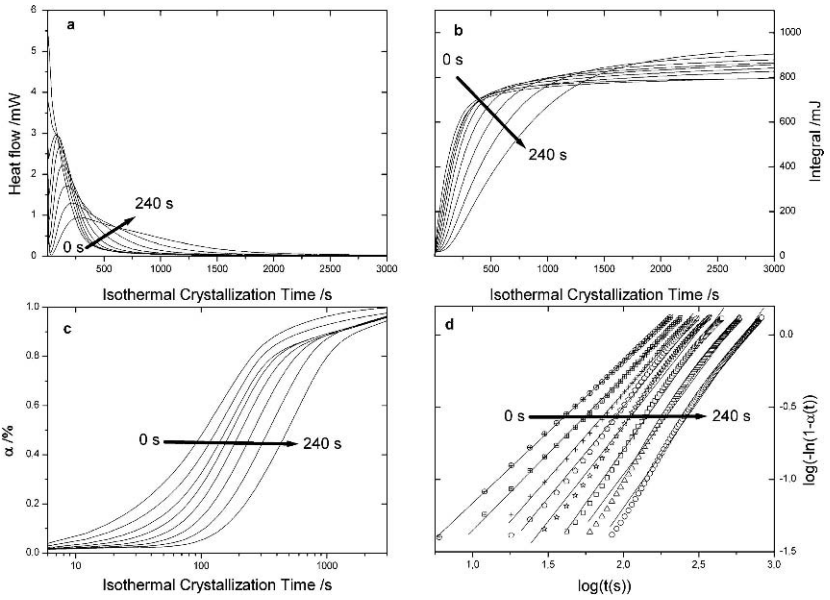

Figure 6. Isothermal crystallization of PEO photo-aged at 15°C for the ageing times ranging between 0 and 240 sec and under 100 mW/cm^2 as selected light intensity. (**a**) DSC exotherms of isothermal crystallization at 55°C. (**b**) Integrations from the exotherms of isothermal crystallization. (**c**) Relative crystallinity ($\alpha(t)$) as a function of isothermal crystallization time after varying ageing times. (**d**) Avrami analysis of the isothermal crystallization data. (Reproduced from,[46] © 2007. With permission from Royal Society of Chemistry.)

Figure 6 shows, thermograms of isothermal crystallization, the corresponding integrals, the relative crystallinity and Avrami plots related to photo-aged PEO at 15°C. These plots were drawn for $\alpha(t)$ ranging between 0.1 and 0.56. It was found that isothermal crystallization of Photo-DSC aged PEO follows Avrami's model. Indeed the crystallization half-time ($t_{0.5}$), defined as the time required for the relative crystallinity ($\alpha(t)$) to reach 0.5, was calculated from the knowledge of k_a and n and compared with its experimental value. A good agreement was observed between the two sets of data.

The half-time crystallization can be converted into the rate of crystallization as follows:

$$G_{cal} = \frac{1}{t_{0.5cal}} = \frac{1}{(\frac{\ln 2}{k_a})^{\frac{1}{n}}} \tag{16}$$

where $t_{0.5cal}$ is the calculated half-time crystallization and G_{cal} the calculated crystallization rate.

Figure 7 shows a comparison between the experimental and calculated crystallization rate of PEO submitted to the photo and thermal ageing at various temperatures. It is clearly evidenced that the light irradiation increases drastically the fall of the crystallizability of the polymeric material and that the

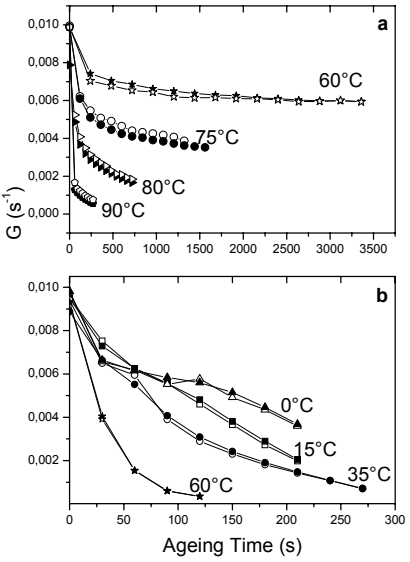

Figure 7. Isothermal crystallization rate G (empty symbols for G_{cal} and the filled ones for G_{exp}) of PEO as a function of exposure time (a) thermoaging at 60°C, 75°C, 80°C and 90°C, (b) photo-aging at 0°C, 15°C, 35°C and 60°C. The isothermal crystallization temperature (Tc) was 55°C.

PhotoDSC constitutes a good alternative, in the accelerated ageing field of materials, to the traditional, sequential and time consuming techniques.

5. Conclusions

Two techniques based upon calorimetric measurements have been presented for the structural characterization of soft matter and porous materials.

New developments of thermoporosimetry are presented. In particular TPM application in polymers is an emerging field full of promises. The simplicity and the low cost of the technique make TPM a very valuable characterization tool for soft materials.

On the other hand, new applications of Photo-DSC have been presented. This technique was mainly intended to be used to study photo-polymerisation or photo-curing reactions by measuring the heat of reaction. We proposed to use this powerful technique to study polymer photo-ageing, using the Photo-DSC as an accelerated ageing device and coupled *in-situ* analysis of the modification of the morphology of the materials. In this case, the crystallisability of the polymer is used as an indicator of the structural modifications. It has been shown that kinetics studies can also be performed bringing information on the crystallization process in particular in confined geometry.

These two techniques offer new tools for the study of porous materials including polymers and hybrid organic-inorganic materials and should, in our opinion, receive much attention in the coming years.

Acknowledgment

The authors would like to thank ANR for funding under project Nanothermomécanique ACI Nanosciences 108.

References

1. J. Gibbs, Collected works, New Haven, CT : Yale University Press (1928).
2. W. Kunh, E. Peterli and H. Majer, Freezing point depression of gels produced by high polymer network, *J. Polymer Sci.*, 16, 539 (1955).
3. G. Fagerlund, Determination of pore-size distribution from freezing-point depression, *Mater. Struct.*, 6(3), 215 (1973).
4. M. Brun, A. Lallemand, J.-F. Quinson and C. Eyraud, A new method for the simultaneous determination of the size and shape of pores: the thermoporometry, *Thermochim. Acta*, 21, 59 (1977).

5. P. Gane, C. Ridgway, E. Lehtinen, R. Valiullin, I. Furo, J. Schoelkopf, H. Paulapuro and J. Daicic, Comparison of NMR cryoporometry, Mercury intrusion porosimetry, and DSC thermoporosimetry in characterizing pore size distributions of compressed finely ground calcium carbonate structures, *Ind. Eng. Chem. Res.*, 43, 7920 (2004).
6. E. Robens, B. Benzler and K.K. Unger, Comparison of sorptometric and thermoporometric measurements on porous glass and some others, *J. Therm. Anal. Calorim.*, 56, 323 (1999).
7. C.L. Jackson and G.B. McKenna, The melting behavior of organic materials confined in porous solids, *J. Chem. Phys.*, 93(12), 9002 (1990).
8. M. Wulff, Pore size determination by thermoporometry using acetonitrile, *Thermochim. Acta*, 419, 291 (2004).
9. T. Takei, Y. Ooda, M. Fuji, T. Watanabe and M. Chikazawa, Anomalous phase transition behavior of carbon tetrachloride in silica pores, *Thermochim. Acta*, 199, 352–353 (2000).
10. B. Husár, S. Commereuc, L. Lukáč, S. Chmela, J.M. Nedelec and M. Baba, Carbon tetrachloride as a thermoporometry liquid probe to study the cross-linking of styrene copolymer networks, *J. Phys. Chem. B*, 110, 5315 (2006).
11. N. Billamboz, M. Baba, M. Grivet and J.M. Nedelec, A general law for predictive use of thermoporosimetry as a tool for the determination of textural properties of divided media, *J. Phys. Chem. B*, 108, 12032 (2004).
12. N. Bahloul, M. Baba and J.M. Nedelec, Universal behavior of linear alkanes in a confined medium: toward a calibrationless use of thermoporometry, *J. Phys. Chem. B*, 109, 16227 (2005).
13. M. Baba, J.M. Nedelec, J. Lacoste, J.L. Gardette and M. Morel, Crosslinking of elastomers resulting from ageing: use of thermoporosimetry to characterise the polymeric network with n-heptane as condensate, *Polym. Degrad. Stabil.*, 80(2), 305 (2003).
14. M. Baba, J.M. Nedelec, J. Lacoste and J.L. Gardette, Calibration of cyclohexane solid–solid phase transition thermoporosimetry and application to the study of crosslinking of elastomers upon aging, *J. Non-Cryst. Solids*, 315, 228 (2003).
15. M. Baba, J.M. Nedelec et al., unpublished results.
16. J.M. Nedelec, J.P.E. Grolier and M. Baba, Thermoporosimetry: a powerful tool to study the cross-linking in gels networks, *J. Sol-Gel Sci. Tech.*, 40, 191 (2006).
17. C.L. Jackson and G.B. McKenna, On the anomalous freezing and melting of solvent crystals in swollen gels of natural rubber, *Rubber Chem. Technol.*, 64(5), 760 (1991).
18. J.M. Nedelec and M. Baba, On the use of monolithic sol-gel derived mesoporous silica for the calibration of thermoporisemetry using various solvents, *J. Sol-Gel Sci. Tech.*, 31, 169 (2004).
19. Q. Qin and G.B. McKenna, Melting of solvents nanoconfined by polymers and networks, *J. Polym. Sci. B*, 44, 3475 (2006).
20. P.J. Flory, Thermodynamics of high polymer solutions, *J. Chem. Phys.*, 10, 51 (1942).
21. M.L. Huggins, Theory of solutions of high polymers, *J. Am. Chem. Soc.*, 64, 1712 (1942).
22. M. Iza, S. Woerly, C. Damnumah, S. Kaliaguine and M. Bousmina, Determination of pore size distribution for mesoporous materials and polymeric gels by means of DSC measurements: thermoporometry, *Polymer*, 41, 5885 (2000).
23. S.I. Nakao, Determination of pore size and pore size distribution : 3. Filtration membranes, *J. Membr. Sci.*, 96, 131 (1994).
24. K.J. Kim, A.G. Fane, R.B. Aim, M.G. Liu, G. Jonsson, I.C. Tessaro, A.P. Broek and D. Bargeman, A comparative study of techniques used for porous membranes characterization – pore characterization, *J. Membr. Sci*., 87, 35 (1994).
25. J.N. Hay and P.R. Laity, Observations of water migration during thermoporometry studies of cellulose films, *Polymer*, 41, 6171 (2000).

26. A. Ksiqzczak, A. Radomski and T. Zielenkiewicz, Nitrocellulose porosity – thermoporometry, *J. Therm. Anal. Calorim.*, 74, 559 (2003).
27. G. Rohman, D. Grande, F. Lauprêtre, S. Boileau and P. Guérin, Design of porous polymeric materials from Interpenetrating Polymer Networks (IPNs): poly(DL-lactide)/poly(methyl methacrylate)-based semi-IPN systems, *Macromolecules*, 38, 7274 (2005).
28. N. Billamboz, J.M. Nedelec, M. Grivet and M. Baba, Cross-linking of polyolefins : a study by thermoporosimetry with benzene derivatives swelling solvents, *Chem. Phys. Chem.*, 6 (6), 1126 (2005).
29. A. Endruweit, M.S. Johnson and A.C. Long, Curing of composite components by ultraviolet radiation: a review, *Polym. Composite.*, 27(2), 119 (2006).
30. R.M. Williams, I.V. Khudyakov, M.B. Purvis, B.J. Overton and N.J. Turro, Direct and sensitized photolysis of phosphine oxide polymerization photoinitiators in the presence and absence of a model acrylate monomer: a time resolved EPR, cure monitor, and PhotoDSC study, *J. Phys. Chem. B*, 104, 10437 (2000).
31. I.V. Khudyakov, W.S. Fox and M.B. Purvis, Photopolymerization of vinyl acrylate studied by PhotoDSC, *Ind. Eng. Chem. Res.*, 40, 3092 (2001).
32. V. Narayanan and A.B. Scranton, Photopolymerization of composites, *Trends Polym. Sci.*, 5, 415 (1997).
33. I.V. Khudyakov, J.C. Legg, M.B. Purvis and B.J. Overton, Kinetics of photopolymerization of acrylates with functionality of 1-6, *Ind. Eng. Chem. Res.*, 38, 3353 (1999).
34. N. Grassie and G. Scott, *Polymer degradation and stability*, Cambridge: Cambridge University Press (1985).
35. B. Mattson and B. Stenberg, Thermo-oxidative degradation and stabilisation of rubber materials, *Progr. Rubber. Plastic. Tech.*, 9, 1 (1985).
36. J. Lemaire, Predicting polymer durability, *Chemtec*, 10, 42 (1996).
37. N.S. Allen, M. Edge, A. Ortega, G. Sandoval, C. M. Liauw, J. Verran, J. Stratton and R.B. McIntyre, Degradation and stabilisation of polymers and coatings: nano versus pigmentary titania particles, *Polym. Degrad. Stabil.*, 85, 927 (2004).
38. M. Morel, J. Lacoste and M. Baba, Photo-DSC I: a new tool to study the semi-crystalline polymer accelerated photo-ageing, *Polymer*, 46, 9274 (2005).
39. P.-O. Bussiere, M. Baba, J.-L. Gardette and J. Lacoste. Characterization of photodegradation of polybutadiene and polyisoprene: chronology of crosslinking and chain-scission, *Polym. Degrad. Stabil.*, 88, 182 (2005).
40. J.M. Harris, Poly*(ethylene glycol) chemistry: biotechnical an biomedical application*, New York: Plenum (1992).
41. J.-M. Blin, A. Léonard, Z-Y. Yuan, L. Gigot, A. Vantomme, A.K. Cheetham and B.L. Su, Hierarchically mesoporous/macroporous metal oxides templated from polyethylene oxide surfactant assemblies, *Angew. Chem. Int. Ed*, 42, 2872 (2003).
42. S.M. Rele, W. Cui, L. Wang, S. Hou, G. Barr-Zarse, D. Tatton, Y. Gnanou, J.D. Esko and E.L. Chaikof, Dendrimer-like PEO glycopolymers exhibit anti-inflammatory properties, *J. Am. Chem. Soc.*, 127(29), 10132 (2005).
43. S. Morlat and J.-L. Gardette, Phototransformation of water-soluble polymers. I: photo- and thermooxidation of poly(ethylene oxide) in solid state, *Polymer*, 42, 6071 (2001).
44. C. Wilhem and J.-L. Gardette, Infrared analysis of the photochemical behaviour of segmented polyurethanes: aliphatic poly(ether-urethane)s, *Polymer*, 39, 5973 (1998).
45. F. Fraisse, S. Morlat-Thérias, J.-L. Gardette, J.-M. Nedelec and M. Baba, In situ study of the accelerated ageing of poly(ethylene oxide), *J. Phys. Chem. B*, 110, 14678 (2006).

46. F. Fraisse, J.-M. Nedelec, J.-P. E. Grolier and M. Baba, Isothermal crystallization kinetics of in situ photo and thermo aged poly(ethylene oxide) using PhotoDSC, *Phys. Chem. Chem. Phys.*, 9, 2137 (2007).
47. M. Avrami, Kinetics of phase change. I. General theory, *J. Chem. Phys.*, 7, 1103 (1939).
48. M. Avrami, Kinetics of phase change. II. Transformation-time relations for random distribution of nuclei, *J. Chem. Phys.*, 8, 212 (1940).
49. M. Avrami, Granulation, phase change, and microstructure kinetics of phase change. III, *J. Chem. Phys.*, 9, 177 (1941).

ORGANIC-INORGANIC HYBRID NANOMATERIALS WITH OPTICAL PROPERTIES FOR USE IN MEDICAL APPLICATIONS

STEPHANE PAROLA*
Laboratoire des Multimatériaux et interfaces UMR CNRS 5615
University Claude Bernard Lyon 1

Abstract. The tremendous developments of materials with fine tuning of the composition, shape, size and chemical functionalities at the nanometre scale has opened a wide range of applications in medicine. An overview of hybrid nanomaterials for applications in biological environment will be presented. The use of functional particles for medical imaging and therapy will be especially discussed. These functional systems usually require combination of different properties such as luminescence (imaging) or molecular recognition (targeting) and non-linear optical properties (therapy), together with size/shape control and biocompatibility (cells diffusion, solubility, biochemical stability). For example series of hybrid metal or oxide nanoparticles can be prepared for medical imaging. Some of them are already commercially available. The most recent work in this field will be presented and the future developments will be discussed. For example one can expect to combine several imaging techniques (multimodal contrast agents) or imaging and therapy in the same nanocomposite. The use of hybrid systems combining inorganic (metal or oxide) with their organic counterparts shows the most promising routes towards such applications in biological environment. New trends in the field of phototherapy will be discussed.

Keywords: Nanoparticles, hybrid, sol-gel, luminescence, phototherapy, imaging, non-linear absorption.

1. Introdu1ction

Hybrid materials for biology have been intensively studied for the past 15 years. Most of them are dealing with encapsulation of biomolecules (proteins, enzymes,

* To whom correspondence should be addressed: Stephane Parola; e-mail: stephane.parola@univ-lyon1.fr

P. Innocenzi, Y. L. Zub and V. G. Kessler (eds.), *Sol-Gel Methods for Materials Processing*.

antibodies, cells) in sol-gel matrices. Even if the first work concerning enzyme encapsulation was already published in the 1950s by F.H Dickeys[1] and a second paper by Johnson and Watheley[2] appeared some 15 years later on the immobilization of Tripsin, the real breakthrough happened in the early 1990s with the work of D. Avnir and co-workers on the protein entrapment in sol-gel silica glasses.[3] From this point, several papers dealing with encapsulation of biomolecules were published, with for instance the work from Zink and co-workers[4] on the retention of the O_2 binding ability of myoglobine entrapped in sol-gel silicate, or the work from Livage et al. on the entrapment of living cells in silicate.[5] Several reviews are reporting on these materials.[6–8]

More recently systems organized at the nanolevel, combining inorganic nanoparticles or capsules with organic based functionalities were investigated for medical applications in imaging (fluorescence or magnetism) or therapy (PDT, trafficking, targeting). Typically such multifunctional systems are expected to provide wide range of advantages compared to conventional approaches, from biocompatibility and targeting to optical properties (luminescence, non linear optics…). One of the most important targets are the cancer cells. The general idea is to provide highly sensitive systems which can be excited under irradiation. The response should then be as efficient as possible in order to gain in sensitivity, contrast and resolution and eventually penetration depth when considering photodynamic therapy. In any case the size and surface of the particles play an important role in the blood dissemination through the body and the targeting of the tumor cells. The materials should possess sizes in the range 2–100 nm. The surface of the particles can also be of importance in the site recognition and trafficking of the particles. Finally some properties might be influenced by the morphology of the particles but very few papers are dealing with this final aspect. The synthesis of hybrid materials involves several approaches depending on the morphology of the final material (films, bulk and particles) and the expected organization and structure. This was fully reported previously in particular by C. Sanchez and co-workers.[9] In this paper we will focus essentially on the most recent nanohybrid systems with optical properties prepared for imaging of cells or for therapy (photodynamic and photothermal therapies).

2. Hybrid Nanoparticles for Medical Imaging

2.1. HYBRID PARTICLES FOR FLUORESCENCE IMAGING

Organic-inorganic hybrid materials are potential probes in biomedical applications. The use of dye-doped nanoparticles for medical imaging can provide high photostability to the system (stabilization of dye molecules in a protective

matrix), amplification of the fluorescent signal (for example through high dye-incorporation capabilities of silica NPs) and biocompatibility. Several approaches have been explored to prepare dye-doped nanomaterials. Silica based materials have been one of the most extensively studied materials. For instance one can functionalize mesoporous silica with luminescent dye. Corriu and co-workers have prepared SBA_n type silica post-functionalized with Eu(III) complexes with cyclane ligands attached to the silica walls (Figure 1).[10] Following a different approach, L. Sun et al. have prepared similar materials using phenantroline based Europium complex.[11] Hybrid materials prepared from MCM-41 mesoporous silica combined with Ln(III) complexes were also reported for similar purposes.[12,13]

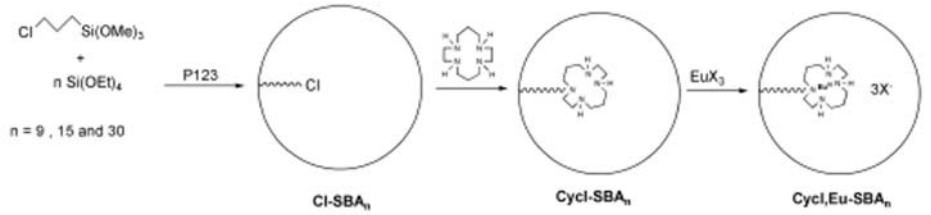

Figure 1. Example of SBA_n porous silica functionalized with luminescent dye. ([10]Reproduced by permission of The Royal Society of Chemistry (RSC) on behalf of the Centre National de la Recherche Scientifique (CNRS)).

The synthesis of functional nanoparticles remains the most interesting approach for bio-imaging because of the size compatibility with the blood vessels for easy trafficking in the body and the cells penetration mechanisms. The surface of the particles, which are at the moment essentially spherical, can play an important role in the way the material will diffuse in the organs and the cells. In vivo studies on the effect of the surface charge on the distribution of the particles have shown for example important changes in the behavior of the particles in the body depending on the surface modification.[14] In this work, the luminescent particles were prepared in the system $Ca_{0.2}Zn_{0.9}Mg_{0.9}Si_2O_6$ doped with Eu^{2+}, Dy^{3+} or Mn^{2+}. The NPs surface charge modification was achieved through functionalization by positive amino groups, negative carboxylates or neutral PEG (Figure 2). The authors showed that positive surface led to lung retention (1st highly vascularized organ encountered by NPs (iv injection)). This was attributed to either aggregation (increase of the size of the particles) or to electrostatic interactions with the negative charges of the capillary endothelial cells. In the case of negative or neutral surface, the particles remain longer time in circulation. They are cleared from blood by liver with some accumulation in the case of neutral particles for time >30 min.

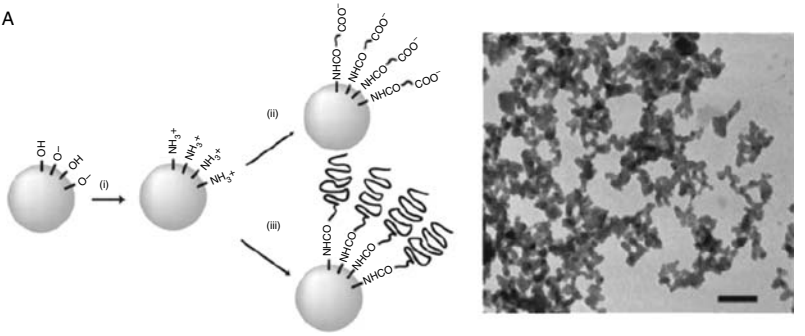

Figure 2. Modification of the surface charges of the particles. (From ref.[14] Copyright 2007 National Academy of Sciences, U.S.A.)

2.2. TOWARDS NEW MULTIMODAL CONTRAST AGENTS COMBINING FLUORESCENCE AND MAGNETISM FOR MEDICAL IMAGING (FI AND MRI)

Inorganic nanomaterials have been recently evaluated as potential probes for biomedical applications. Their specific properties obtained from nanoscale effects and their size fully compatible with biological systems has allowed for example sensitive detection of biomolecular targets. Quantum dots and fluorescent hybrid silica NPs have for instance been used as nanoprobes for optical imaging. Dye-doped silica NPs possess high photostability (stabilization of dye molecules in a protective silica environment), amplification of the fluorescent signal (high dye concentration in silica nanoparticles), and enhanced biocompatibility.

The need for new materials for use as contrast agents with other imaging techniques has recently emerged concomitantly with the development of luminescent NPs for bio-imaging. Because of its non-invasive nature, high spatial resolution and processes using non radioactive contrast agents, improving thus the comfort of the patient, magnetic resonance imaging (MRI) has emerged as one of the most interesting and powerful diagnostic technique in the field of medical imaging. In this sense, magnetic NPs can be used as high contrast agents that provide magnetic-resonance enhancement effects allowing MR imaging of cells, cancer. However, both resolution and sensitivity remain low when considering the MRI technique. Among the various contrast agents available for clinical use, a large majority are based on gadolinium and manganese coordination complexes. These complexes require high concentration in order to provide sufficient contrast images. Nanoparticles containing high payloads of contrast agents can be prepared and are susceptible to provide similar quality of imaging with lower concentration. Iron oxide NPs are for example currently

available. Until recently, most studies using optical or magnetic nanoparticles focused on monofunctional probes. But the combination of both potentialities for fluorescence imaging (FI) and magnetic resonance imaging (MRI) in the same material would be very convenient in order to gain in reliability for the medical diagnostics. The synthesis of multimodal contrast agents for *in vivo* imaging, in particular combining FI and MRI potentialities, is a research area of growing interest. Such nanosystems provide both the high sensitivity of the fluorescence and the high spatial resolution of MRI.

Several approaches were investigated for the preparation of bimodal probes. For example S. Roux and co-workers prepared hybrid gadolinium oxide nanoparticles.[15] The systems are built of magnetic Gd_2O_3 cores covered with hybrid silica shells doped with a common fluorescent organic dye such as fluoresceine or rhodamine and finally surrounded by a polyethylene glycol (PEG) layer. The PEG shells confer high solubility and permit dissemination through the body without accumulation in the liver and the lung, to the contrary of similar non Pegylated systems. Following the same idea, core-shell SiO_2 coated magnetic ferrite (Fe_3O_4) functionalized at the surface with Ln^{3+} complexes were also recently reported.[16]

Another approach is to prepare nanoparticles via a luminescent core coated with paramagnetic such as reported by Rieter et al. (Figure 3).[17]

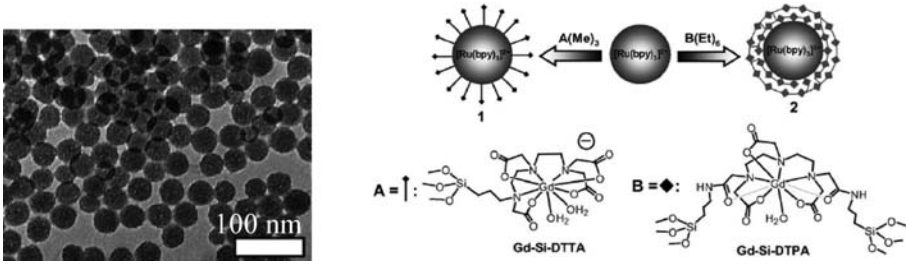

Figure 3. Example of hybrid silica nanoparticles with luminescent core and paramagnetic coating. ([17] Copyright Wiley-VCH Verlag GmbH & Co. KGaA. Reproduced with permission).

The luminescent part is provided by a Ruthenium complex entrapped in silica nanoparticles which are covered by a paramagnetic gadolinium complex providing high loading of magnetic centers. The authors have shown that the NPs were not toxic to monocyte cells using (MTS) cell-viability assays. The nanoparticles were used as multimodal contrast agents for in vitro imaging and they were able to run fluorescence and MR imaging of monocyte cells.

It is also possible to combine two types of nanoparticles as shown by J. H. Lee et al. (Figure 4).[18] The silica NPs are doped with Rhodamine and attached

to Fe_3O_4 NPs through a coupling agent which is in this case the sulfosuccinimidyl-(4-N-maleimidomethyl)cyclohexane-1-carboxylate. The authors have shown an interesting synergistic MR enhancement effect of $DySiO_2–(Fe_3O_4)_n$ compared to the single iron oxide particles.

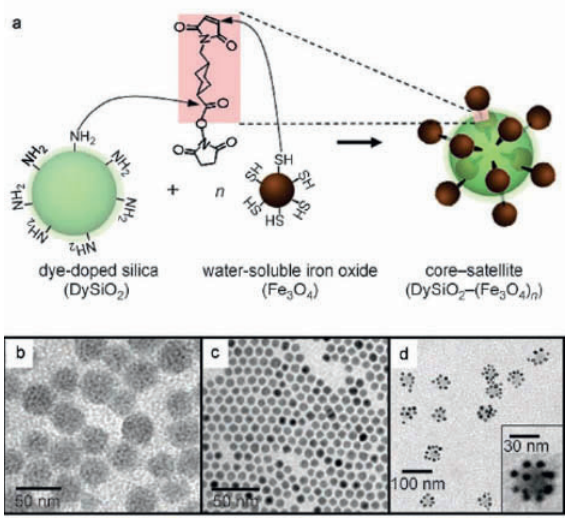

Figure 4. Dye-doped silica NPs coupled with Fe_3O_4 NPs.[18] (Copyright Wiley-VCH Verlag GmbH & Co. KGaA. Reproduced with permission.)

As shown in these examples, multimodal NPs are a growing field of research and one can expect strong enhancement of the properties of these systems in the near future.

3. Hybrid Nanoparticles for Phototherapy

The history of Phototherapy started in the early 1900 when Oscar Raab showed the cytotoxic effects f the combination of acridine and light on infusoria. Then, Niels Finsen received the Nobel Prize in 1903 for his work on phototherapy using light for the treatment of cutaneous tuberculosis for example. At the same period, H. von Tappeiner and A. Jesionek used white light to treat for the first time tumrs on the skin. In 1913, F. Meyer-Betz realized for the first time a Photodynamic experiment on his own hand using combination of haematopor-phyrin and light. However, it's only in the middle 1970s that Thomas Dougherty successfully treated skin cancer in patients and performed the first clinical studies in humans. Finally it's only in 1999 that the first PDT drug was approved in Canada. This was fully reviewed.[19–21]

The procedure involves the generation of cytotoxic singlet oxygen through interaction between light and a photosensitizer. Typically, the photosensitizer is excited trough absorption of photons from the light with tranfert to the triplet state of the chromophore. The excited molecule is then susceptible to interact with neighboring oxygen to generate radicals (singlet oxygen…). These species are strongly toxic and initiate cells death mechanisms (apoptosis, necrosis…). At the moment, PDT is based on one photon absorption mechanism, but we will see later on that the future might be in the utilization of multiphoton absorption processes in order to improve the efficiency of the treatment. Few photosensitizer are commercially available and have been approved in few countries. For instance the Photofrin (haematoporphyrin derivative), can be used for Cervical, endobroncheal, oesophageal and gastric cancers, brain tumors, (630 nm), the Metvix (5-aminolevulinic acid 5-methylesther) for basal-cell carcinoma, (635 nm) or the Foscan (metatetrahydroxyphenylchlorin) for head, neck, prostate and pancreatic tumors (652 nm). However the limitation of single-photon approach is mainly due to the fact that excitation occurs by excitation with visible light and photons in this spectral region do not penetrate deep enough.. Indeed, it is only possible to obtain a limited penetration depth due to the restrictive tissues absorption in the visible (tissues transparent spectral window is 700–1,100 nm). Another drawback is the limited resolution of the technique due to excitation of all the irradiated zone and thus destruction of adjacent healthy tissues. A recent idea was then to use multiphoton absorption process in order to gain in penetration depth and spatial resolution for both imaging and therapy.[22–30] The spatial probability of having a Two Photon Absorption (TPA) process is proportional to the square of the intensity of the laser light (cube for three photon absorption). This means that the probability is extremely high at the focal point of the laser and decreases rapidly out of this point. The ^{3}D spatial resolution becomes then much higher because excitation occurs essentially at the focal point (focal volume $\approx 1\ \mu m^3$) and healthy tissues can be preserved. Moreover, the working wavelength can be shifted to the NIR (800–1,000 nm) because of the simultaneous absorption of two photons. The utilization of higher wavelengths, out of the absorbing range of the human tissues, allows a much better penetration depth (>4 mm). Often the photosensitizers are toxic and require encapsulation into a neutral, hydrophilic matrix. For example polyacrilamide matrix incorporating porphyrin based photosensitizer (5,10,15,20-tetrakis(1-methyl 4-pyridinio) porphyrin tetra(ptoluenesulfonate)) was prepared by microemulsion approach, thus avoiding drug toxicity to cells.[31] The authors have shown that utilization of TPA-PDT combined with these safe NPs, is an efficient method for killing glioma cancer cells in vitro and are thus potential for application to deep tissue therapy.

For this purpose hybrid materials can also present several advantages compared to pure inorganic or organic materials. They can provide isolation of the photosensitizer from the medium, providing biocompatibility, lowering photobleaching effects (capsules, shells). NPs can be functionalized for site recognition and targeting. Interactions between metal nanosystems and the photosensitizer can provide electric field enhancement through surface plasmon resonance transfert towards the molecular system. Another interesting property of metal nanoparticles and in particular gold NPs is that they can be used for photothermal degradation of tumor cells (hyperthermia process).

P. N. Prasad and co-workers have proposed the encapsulation of a combination of organic photosensitizers (9,10-bis[4'-(4''- aminostyryl) styryl] anthracene (BDSA) + 2-devinyl-2-(1-hexyloxyethyl) pyropheophorbide (HPPH)) into ORMOCIL NPs obtained by co-precipitation in the presence of micelles (Figure 5).[32]

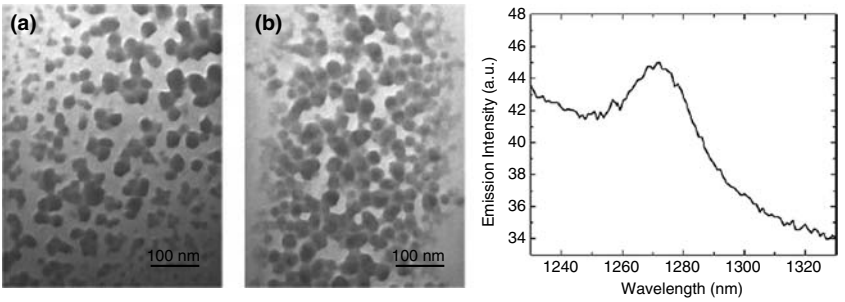

Figure 5. hybrid silica particles for two photon induced PDTand emission spectrum of singlet oxygen. (Reprinted from ref.[32] Copyright 2007 American Chemical Society. With permission).

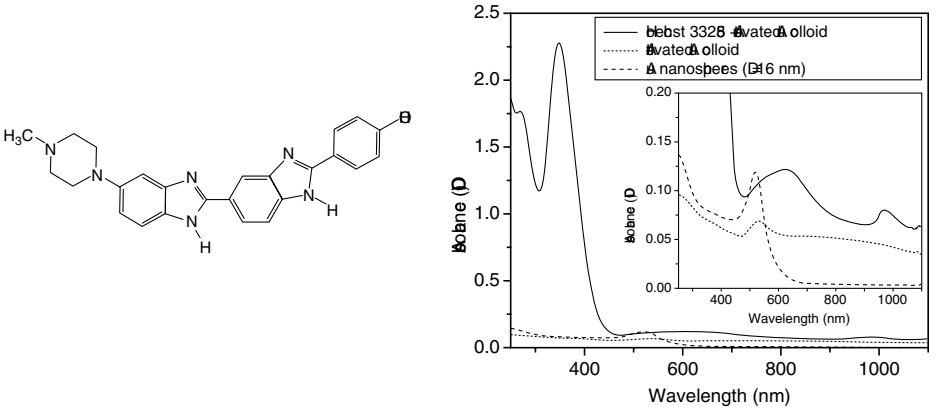

Figure 6. Example of Surface Plasmon Enhancement of Two Photon Absorption by a mixture of Hoechst 33 258 photosensitizer and gold NPs. (Reprinted from ref.[34] Copyright 2005 American Chemical Society. With permission).

The BDAS (energy donor) is used as TPA unit while the HPPH (energy acceptor) plays the role of photosensitizing. They reported in vitro fluorescence imaging of live tumor cells under two-photon excitation at 850 nm showing the efficiency of HPPH/BDSA co-encapsulating NPs. An intense fluorescence signal characteristic for HPPH emission is observed from the cells. This confirms that the intraparticular Fluorescence Resonance Energy Transfer (FRET) from the BDSA to the HPPH is operating as expected. They showed a FRET induced generation of singlet oxygen as shown by the typical emission of $^1O_2$ when excited at 532 (Figure 5). These hybrid NPs possess a good potential to induce cell necrosis.

Few years ago it was proposed by Kano and Kawata to use interaction between metal and the photosensitizer to induce electric field enhancement through surface plasmon resonance transfert from the metal to the molecular system.[33] They showed the possibility to enhance two-photon induced fluorescence by surface plasmon effect. With the same idea, Cohanoschi and Hernàndez used a two- and three- photon absorption photosensitizer (Hoechst 33 2587) mixed with gold nanoparticles prepared through the wet chemical method.[34,35]

The absorption spectrum of the dye remains approximately unchanged in the presence of the NPs (Figure 6). Looking closer to the surface plasmon resonance band of NPs in the presence of Hoechst 33 258, a shift can be

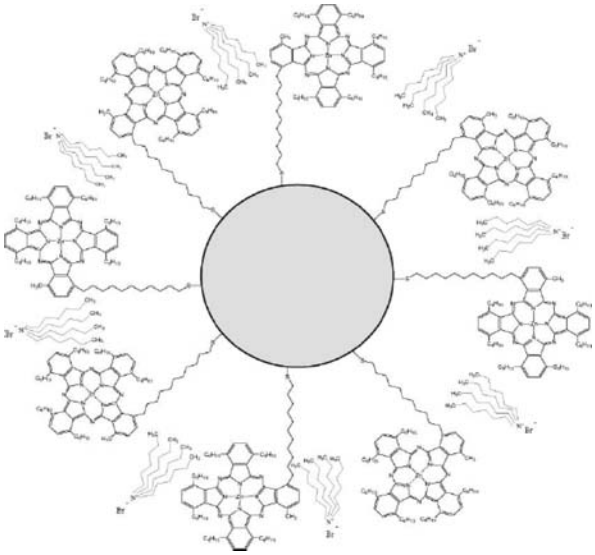

Figure 7. Phtalocyanine functionalized gold particle. (Reproduced from ref. [40] With permission of The Royal Society of Chemistry (RSC) on behalf of the European Society for Photobiology and the European Photochemistry Association).

observed indicating interaction between dye molecules and the particles. The 2nd and 3rd order absorption coefficients and cross-sections in the presence of activated gold NPs were found to be $\sigma_2' = (1{,}160 \pm 0.2) \times 10^{47}$ cm^4 s photon^{-1} and $\sigma_3' = (244 \pm 10) \times 10^{-78}$ cm^6 s^2 photon^{-2}. The presence of activated gold NPs enhanced by 480- and 30-fold the two- and three-photon absorptions cross sections of the chromophore. The change in TPA and 3PA absorption was assumed to be a consequence of the surface plasmon electric-field enhancement on Au NPs.

Another approach is to prepare functional hybrid NPs with photosensitizers attached to the surface of the particles. It is possible to easily attach functional organics or organometallics onto gold NPs surface using for example thiols, disulfides or phenantroline functional groups.[36–39] Example of system produced by Russel et al. is the Phtalocyanine-nanoparticle conjugates designed for the delivery of the photosensitizer for PDT of cancers (Figure 7).[40]

As previously mentioned, hybrid gold particles can also be used for photothermal therapy. Gold NPs can be, for example, interestingly functionnalized with viral vectors for a combination of hyperthermia and targeting.[41] This

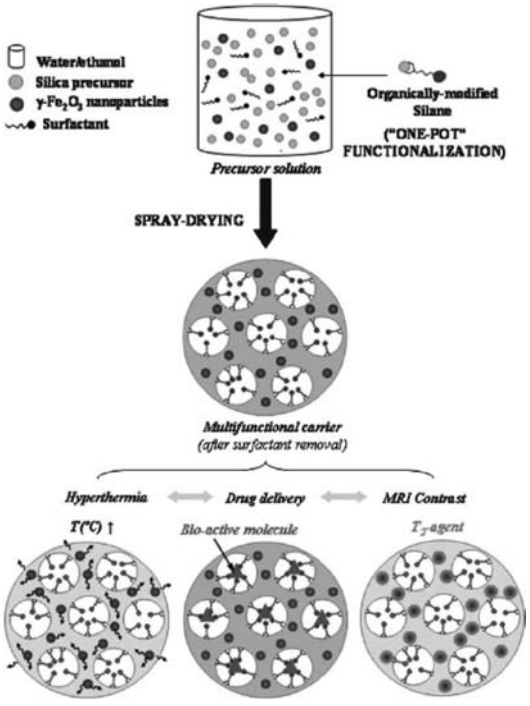

Figure 8. γ-Fe_2O_3–hybrid SiO_2 microspheres for biomedical applications. (Reproduced from ref. [42] With permission of The Royal Society of Chemistry).

should allow selective delivery of the gold nanoparticles to tumor cells, with the perspective to combine hyperthermia and gene therapy. Multifunctional hybrid platforms will probably take over conventional systems in the near future, allowing multimodal imaging combined with multitherapy approaches (Hyperthermia, PDT, gene therapy, MRI, FI…). A recent example published by Sanchez and co-workers reported a route to such multifunctional hybrid platform which can be used for either imaging, or therapy (hyperthermia) or drug delivery, or a combination of processes (Figure 8).[42]

4. Conclusion

The study of nanohybrid materials is a field of growing interest, especially for medical applications, even if very few is known at the moment concerning the real toxicity of such nanosized systems. As shown by the recent publications, one can expect interesting improvements of these materials in the near future. Among the possibilities one can quote the enhancement of the contrasts in imaging processes (MRI, FI) using potentialities of new dyes combined with stabilizing inorganic particles or organic-inorganic synergistic contributions, the improvement of the efficiency in phototherapy, or help with trafficking and targeting in the human body using surface modification with possible site recognition. Further researches on multifunctional hybrid nanomaterials combining at least two of the explored properties are ongoing and will probably represent most of the future developments in the multidisciplinary field of optical hybrid materials devoted to medicine. Finally one should probably also consider the morphology of the particles which can drastically change some of the properties (surface plasmon resonance…) of the material which should have a strong impact in the case of medical applications.

References

1. F. H. Dickey, *J. Phys. Chem*., 58, 695 (1955).
2. P. Johnson, T. L. Whateley, *J. Colloid Interface Sci.*, 37, 557 (1971).
3. S. Braun, S. Rappoport, R. Zusman, D. Avnir, M.Ottolenghi, *Mater. Lett*., 10, 1 (1990).
4. J. I. Zink, J. S. Valentine, B. Dunn, *New J. Chem*., 18, 1109 (1994).
5. J. Livage, *C. R. Acad. Sci*. (Paris IIb), 322, 417 (1996).
6. D. Avnir, T. Coradin, O. Lev, J. Livage, *J. Mater. Chem*., 16, 1013 (2006).
7. J. Livage, T. Coradin, C. Roux, *J. Phys.: Condens. Matter*., 13, R673 (2001).
8. W. Jin, J. D. Brennan, *Anal. Chim. Acta*, 461, 1 (2002).
9. C. Sanchez, B. Julian, P. Belleville, M. Popall, *J. Mater. Chem*., 3559 (2005).

10. R. J. P. Corriu, A. Mehdi, C. Reyé, C. Thieuleux, A. Frenkel, A. Gibaud, *New. J. Chem.*, 28, 156 (2004).
11. C. Peng, H. Zhang, Q. Meng, H. Li, J. Yu, J. Guo, L. Sun, *Inorg. Chem. Commun*., 8, 443 (2005).
12. X. Guo, L. Fu, H. Zhang, L. D. Carlos, C. Peng, J. Guo, J. Yu, R. Deng, L. Sun, *New J. Chem*., 29, 1351 (2005).
13. L.-N. Sun, J.-B. Yu, H.-J. Zhang, Q.-G. Meng, E. Ma, C.-Y. Peng, Q. Y. Yang, *Micropor. Mesopor. Mater*., 98, 156 (2007).
14. Q. le Masne de Chermont, C. Chaneac, J. Seguin, F. Pelle, S. Maîtrejean, J.-P. Jolivet, D. Gourier, M. Bessodes, D. Scherman, *PNAS*, 104, 22, 9266 (2007).
15. J. -L. Bridot, A.-C. Faure, S. Laurent, C. Riviere, C. Billotey, B. Hiba, M. Janier, V. Josserand, J. -L. Coll, L. Vander Elst, R. Muller, S. Roux, P. Perriat, O. Tillement, *J. Am. Chem. Soc*., 129, 5076 (2007).
16. J. Choi, J. C. Kim, Y. B. Lee, I. S. Kim, Y. K. Park, N. H. Hur, *Chem. Commun*., 1644 (2007).
17. W. J. Rieter, J. S. Kim, K. M. L. Taylor, H. An, W. Lin, T. Tarrant, W. Lin, *Angew. Chem. Int. Ed.*, 46, 3680 (2007).
18. J. -H. Lee, Y. -W. Jun, S.-I. Yeon, J.-S. Shin, J. Cheon, *Angew. Chem. Int. Ed*., 45, 8160 (2006).
19. D. E. J. G. J. Dolmans, D. Fukumura, R. K. Jain, *Nature*, 3, 380 (2003).
20. A. P. Castano, P. Mroz, M. R. Hamblin, *Nat. Rev. Cancer*, 6, 535 (2006).
21. S. B. Brown, E. A. Brown, I. Walker, *Lancet Oncol.*, 5, 497 (2004).
22. G. Min, *Opt. Lett.*, 21, 988 (1996).
23. R. W. Boyd, *Nonlinear Optics* (Academic: San Diego, CA), Chapters 4 and 8 (1992).
24. A. Karotki, M. A. Drobizhev, M. Kruk, A. Rebane, E. Nickel, C. W. Spangler, *Proc. SPIE Int. Soc. Opt. Eng.*, 4612, 143 (2002).
25. S. J. Madsen, C. H. Sun, B. J. Tromberg, V. P. Wallace, H. Hirschberg, *Photochem. Photobiol.*, 72, 128 (2000).
26. P. K. Frederiksen, M. Jorgensen, P. R. Olgilby, *J. Am. Chem. Soc*., 123, 1215 (2001).
27. F. W. Fisher, *Photochem. Photobiol*., 66, 141 (1997).
28. T. D. Poulsen, *J. Phys. Chem*., 105, 11488 (2001).
29. D. Bhawalkar, N. D. Kumar, C. F. Zhao, P. N. Prasad, J. Clin., *Laser Med. Surg*., 15, 201 (1997).
30. E. M. Attas, M. G. Sowa, T. B. Posthumus, B. J. Schaktta, H. H. Mantsch, S. L. L. Zhang, *Biopolymers*, 67, 96 (2002).
31. D. Gao, R. R. Agayan, H. Xu, M. A. Philbert, R. Kopelman, *Nano Lett*., 6, 11, 2383 (2006).
32. S. Kim, T. Y. Ohulchanskyy, H. E. Pudavar, R. K. Pandey, P. N. Prasad, *J. Am. Chem. Soc*., 129, 2669 (2007).
33. H. Kano, S. Kawata, *Opt. Lett*., 21, 1848 (1996).
34. I. Cohanoschi, F. E. Hernàndez, *J. Phys. Chem. B*, 109, 30, 14506 (2005).
35. J. Turkevich, P. C. Stevenson, J. Hiller, *Discuss. Faraday Soc*., 11, 55 (1951).
36. M. Brust, M. Walker, D. Bethell, D. J. Schiffrin, R. Whyman, *J. Chem. Soc. Chem. Commun.*, 801 (1994).
37. M. Brust, J. Fink, D. Bethell, D. J. Schiffrin, C. Kiely, *J. Chem. Soc. Chem. Commun.*, 1655 (1995).
38. S. Roux, B. Garcia, J. -L. Bridot, M. Salomé, C. Marquette, L. Lemelle, P. Gillet, L. Blum, P. Perriat, O. Tillement, *Langmuir*, 21, 2526 (2005).
39. C. R. Mayer, E. Dumas, F. Miomandre, R. Méallet-Renault, F. Warmont, J. Vigneron, R. Pansu, A. Etcheberry, F. Sécheresse, *New. J. Chem*., 30, 1628 (2006).

40. M. E. Wieder, D. C. Hone, M. J. Cook, M. M. Handsley, J. Gavrilovic, D. A. Russell., *Photochem. Photobiol. Sci*., 5, 727 (2006).
41. M. Everts, V. Saini, J. L. Leddon, R. J. Kok, M. Stoff-Khalili, M. A. Preuss, C. Leigh Millican, G. Perkins, J. M. Brown, H. Bagaria, D. E. Nikles, D. T. Johnson, V. P. Zharov, D. T. Curiel, *Nano Lett.*, 6, 4, 587 (2006).
42. B. Julian-Lopez, C. Boissiere, C. Chaneac, D. Grosso, S. Vasseur, S. Miraux, E. Duguet, C. Sanchez, *J. Mater. Chem*., 17, 1563 (2007).

METHOD OF COMPETING IONS FOR SOL-GEL PROCESSING OF SORBENTS AND CATALYSTS IN AQUEOUS SOLUTIONS OF INORGANIC SALTS

VLADIMIR V. STRELKO*
Institute for Sorption and Endoecology Problems of National Academy of Sciences of Ukraine, General Naumov Str. 13, Kyiv-164

Abstract. An original method of competing ions has been proposed and experimentally tested permitting a sol-gel process to be conducted only with water solutions of simplest salts, alkalis and acids without using chelating reagents.

The data are also presented on the "oil-drop" and "air-drop" technologies for continuous sol-gel production of spherically granulated inorganic ion exchangers such as titanium and zirconium phosphates as well as solid high-porous acid catalysts based on sulfonated zirconium and titanium dioxide. The information is given about selective sorption of trace amounts of heavy metals, radionuclides, and uranium from a variety of technological solutions and drinking water on the prepared titanium and zirconium phosphates.

Keywords: Sol-gel processing, aqueous salt solutions, continuous granulation, inorganic ion exchangers, titanium and zirconium phosphates, titanium silicates, heavy metals, uranium and radionuclides, hard solid acids.

1. Introduction

Today the sol-gel approaches have realized their potentials in the preparation of a new generation of advanced materials: ceramic powders, membranes, glasses, fibers and monodisperse particles, coatings, biomaterials and sensors, electronic materials, and even untraditional sorbents and catalysts.[1]

*To whom correspondence should be addressed: Vladimir strelko; e-mail: vstrelko@ispe.org.ua

P. Innocenzi, Y. L. Zub and V. G. Kessler (eds.), *Sol-Gel Methods for Materials Processing*.

Two main sol-gel techniques are used nowadays. The first one involves aqueous solutions of salts as precursors and the second one is based on hydrolysis of metal-organic molecular precursors, such as metal alkoxides (mostly in alcohols as solvents).

The aqueous solutions of salt precursors free from any additives are employed only in sol-gel methods of processing silica gels and amorphous aluminosilicates (especially on industrial scale) using sodium silicate and aluminate as well as mineral acids. As regards water solutions of other polyvalent metal salts, the sol-gel process can be realized, as a rule, by chelating metal ions by organic ligands such as citrates or oxalates thus forming polymeric gel precursors.

The traditional method of sol-gel synthesis using polyvalent metal alkoxides may have a variety of modifications, for instance, the use of non-hydrolytic sol-gel techniques.

It should be, however, noted that in spite of many attractive prospects of using alkoxides in the sol-gel synthesis of materials (mild chemical conditions, easy miscibility of different metals, easily controlled homogeneous doping, high purity of products, use of functionalized precursors, etc.), this widespread method possesses a number of limitations. Indeed, alkoxides are not always available and easy to handle, and they are also quite expensive and volatile, sensitive to atmospheric moisture; moreover, application of usual organic solvents (e.g., alcohol) in the sol-gel method on an industrial scale is very dangerous due to their flammability.

In the above context, this paper presents the data on development of new continuous sol-gel methods for the synthesis of spherically granulated dispersed individual and mixed oxides (inorganic ion exchangers, solid catalysts, and catalyst supports) with controlled porosity and surface chemistry. An important feature of these sol-gel methods is the use of convenient and accessible water solutions of inorganic salts, alkalis (hydroxides), and acids as precursors without addition of chelating organic ligands.

In other words, the present study demonstrates possibility to realize the sol-gel process only with metal salt precursors using no alkoxides or organic chelating ligands. The emphasis will be on the description of an original method of sol-gel synthesis, mostly focusing on preparation of porous dispersed materials with spherical granulation, namely, inorganic ion exchangers and catalysts.

It is well known that the methods of wet chemistry (precipitation and co-precipitation, sol-gel synthesis from alkoxides, etc.) are widely practiced now for production of sorbents, catalysts, and catalyst supports. However, they have some grave drawbacks: the impossibility of continuous technological process, necessity of the granulation step (tableting, extrusion with a binder, etc.), and poor control of porometric characteristics.

A pivot concept of the approach stems from the fact that precipitation occurs always more rapidly than sol or gel formation in the course of dispersed oxide

preparation. Accordingly, the sol-gel process can be realized using water solutions of metal salts with the addition of organic ligands, as the chelation of metal ions slows down the solid phase formation (generation of sol particles and their coagulation to gels).

From our point of view, the slowing down of solid phase formation (sol-gel preparation from water solutions of metal salts) can also be caused by the competition of cations and anions added to one of starting precursors.

For experimental confirmation of the developed concepts, it is appropriate to consider the possibility of the occurrence of sol-gel processes in formation of classical inorganic ion exchangers, namely, acidic titanium phosphates (TiP) and zirconium phosphates (ZrP).[2,3] These materials are inorganic polymers consisting of individual or cross-linked chains as shown in the following scheme:

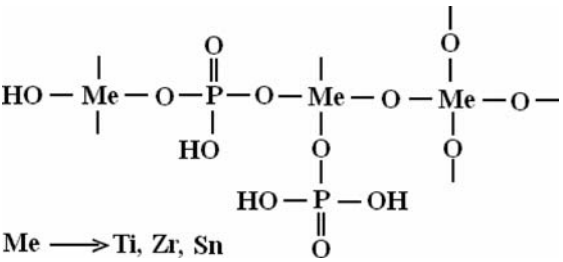

(1)

It is assumed that such polymer species are partially or entirely globule-folded preserving their ion-exchanging properties. As an example, Figure 1 shows the molecular structure of ZrP and the corresponding ^{31}P NMR spectrum which indicates the relative contents of the groups in the ion exchanger matrix and some amount of H_3PO_4 occluded in the synthesis.[4] TiP has a similar molecular structure.

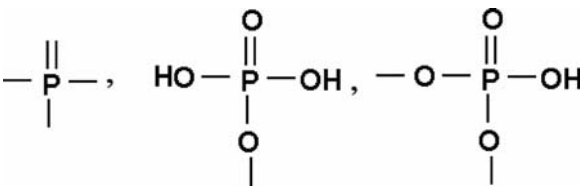

One can obtain such ion exchangers with much developed porosity; they are known for thermal, chemical, and radiation stability and manifest, due to surface complexing, high absorption selectivity even with respect to traces of heavy metals, radionuclides, and transuranium elements to be extracted from solutions of complex composition.[2,3]

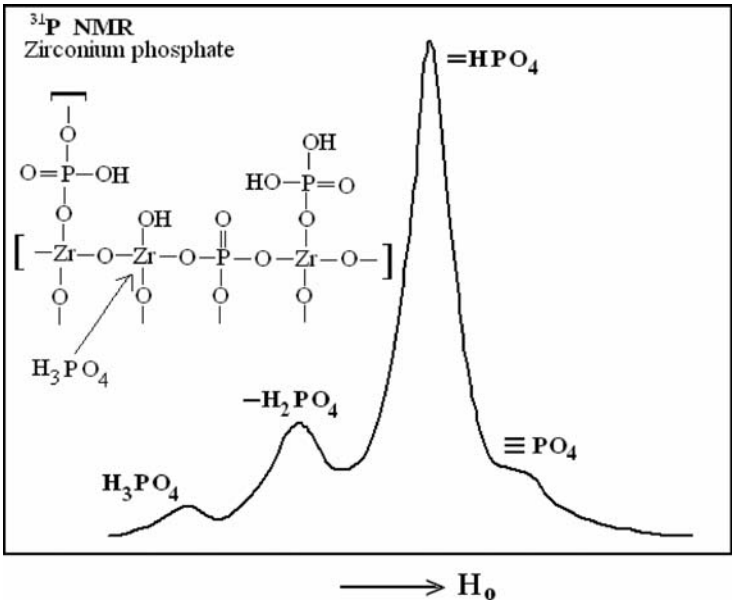

Figure 1. The suggested molecular structure and the ^{31}P NMR spectrum for a typical sample of zirconium phosphate.[4]

As a rule, these materials are obtained as precipitates, according to the equation:

$$TiCl_4(ZrOCl_2) + nH_3PO_4 \rightarrow \underset{\text{precipitates}}{Ti_x(HPO_4)_y{\cdot}nH_2O + Zr_v(HPO_4)_w{\cdot}nH_2O} + mHCl \quad (2)$$

By addition of Ti- and Zr-chelating organic ligands (e.g., urea or acetate and lactate anions) to the initial salt solution, we succeeded, under certain regimes, to obtain TiP and ZrP gels rather than precipitates, just as in the sol-gel preparation of Ti and Zr oxides when the metal complexes with the mentioned ligands are treated with ammonia.[5]

2. Competing ions as a Control Factor in the Sol-Gel Synthesis Based on Aqueous Salt Solutions

In our opinion, the solid phase generation in reaction (2) can also be slowed down by preliminary addition of some cations and anions to one of the components of the reaction medium; these ions are also capable of forming a solid phase (precipitate) or a stable soluble compound with Ti (Zr) or phosphoric acid. In this case, competing interaction should occur which can essentially

influence the formation of a solid phase (sol). As an example, the following reactions can proceed in the reaction system presented by (2) if SO_4^{2-} anions (competing with H_3PO_4) are introduced into it:

– The traditional reaction producing the TiP precipitate

$$TiCl_4 + H_3PO_4 + H_2O \rightarrow \underset{\text{precipitate}}{Ti_x(H_2PO_4)_y \cdot nH_2O} + HCl \quad (3)$$

– The competing reaction producing the stable soluble $TiOSO_4$ compound

$$TiCl_4 + H_2SO_4 + H_2O \rightarrow TiOSO_4 + 4HCl, \quad (4)$$

– TiP gelation induced by the addition of SO_4^{2-} anions:

$$TiCl_4 + H_3PO_4 + H_2SO_4 + H_2O \rightarrow \underset{\text{gel}}{Ti_x(H_2PO_4)_y \cdot (HSO_4)_z^*} + nHCl.$$

If SO_4^{2-} anions compete with phosphate anions in the reaction medium (5), the formation time of the solid phase (sol and gel) rises and grows almost linearly with the increasing SO_4^{2-} content in the system (Figure 2).

It is interesting to note that the variation of $SO_4/TiCl_4$ ratio in the reaction medium allows to regulate, in a certain range, the volume of sorption pores, V_s (measured by benzene vapor sorption), the specific surface area, S_{sp} (Figure 3), and the mesopore volumes distribution per radii of the corresponding xerogels (Figure 4).

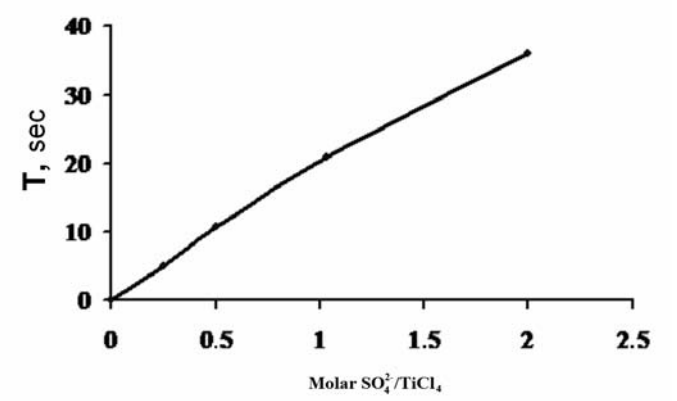

Figure 2. The effect of the $SO_4^{2-}/TiCl_4$ molar ratio in the reaction mixture on the TiP gelation time ($T = -10^0C$).

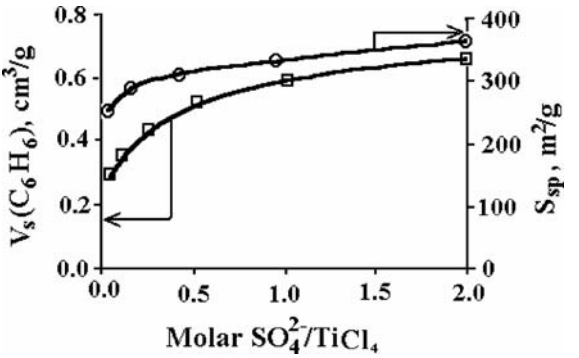

Figure 3. The effect of the $SO_4^{2-}/TiCl_4$ molar ratio in the reaction mixture on TiP xerogel porometric characteristics.

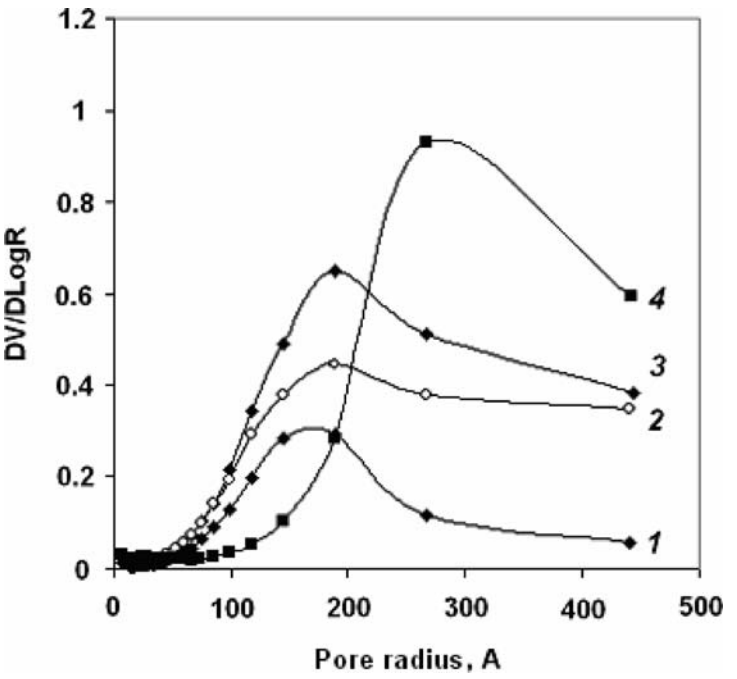

Figure 4. The distribution of pore volumes per radii for TiP samples synthesized from $TiCl_4$ solutions with different SO_4^{2-} ion contents: 1 – $SO_4^{2-}/Ti = 0.1$; 2 – $SO_4^{2-}/Ti = 0.5$; 3 – SO_4^{2-}/Ti –1.0; 4 – SO_4^{2-}/Ti – 2.0.

A special investigation has been carried out in order to confirm (5), i.e., to insure that the TiP solid phase can be generated, though more slowly, by the reaction of H_3PO_4 with $TiOSO_4$. Titanyl sulfate arises in process (5) as an intermediate in the reactions of the sol-gel formation of TiP. The affinity of Ti (IV) to the phosphate anion is likely to be higher than to the sulfate anion, which is evidenced by the fact that TiP does form in a system containing H_2SO_4.

In the following, we shall demonstrate that not only phosphate groups but also some amount of sulfonic $–SO_3H$ groups are chemically immobilized on the titanium phosphate surface at the presence of $SO_4^{2–}$ anions in the solution (5). For simplicity, this material is designated from here on as TiP.

In fact, the process occurs according to the following equation:

$$TiOSO_4 + H_3PO_4 \rightarrow \underset{\text{gel}}{Ti_x(H_2PO_4)_y(HSO_4)_n \cdot nH_2O}. \quad (6)$$

For this reaction, the temperature dependence of gelation time (Figure 5) and the time dependence of viscosity (Figure 6) were studied at varied P/Ti molar ratios. As it can be seen from Figure 6, the gelation time increases with the increasing $TiOSO_4$ content (the decreasing P/Ti molar ratio) in the system, thus corroborating the assumption represented by (5) and (6). Clearly exponential increase of viscosity in the system (Figure 6) results in formation of gel with various TiP content.

On the other hand, it is well known that Fe^{3+}, Al^{3+}, Cr^{3+}, Ti^{3+}, and other triple-charged cations, as well as Ti (IV), form insoluble phosphates in the reaction with phosphoric acid. That is why one would expect that the addition of these cations to the reaction medium presented by (2) can cause the competition between them and Ti, Zr(IV) for the interaction with phosphate anions

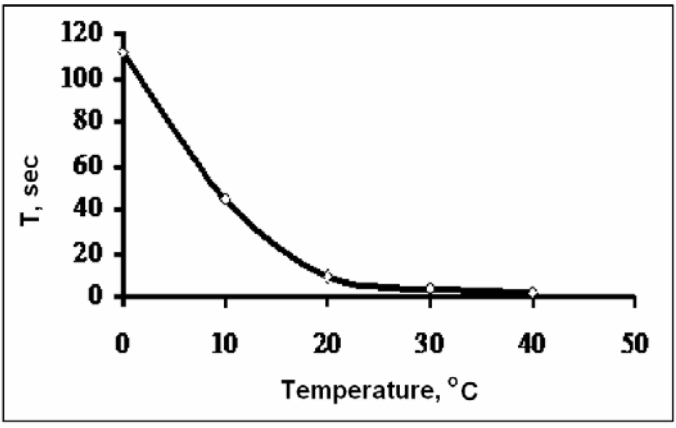

Figure 5. Gelation time of the synthesized TiP samples as a function of temperature (for the initial molar ratio P/Ti = 1).

(phosphoric acid). Finally, this should also slow down the process and hence may lead, under certain conditions, to the formation of the TiP sol and gel with the matrix containing the chemically bound triple-charged cations added in the synthesis.

In this case, it is apparent from general principles that the sequence of adding triple-charged cations (Fe^{3+} as an example) to the reagents can notably effect the course of the process. It is known that $FeCl_3$ addition to H_3PO_4 immediately

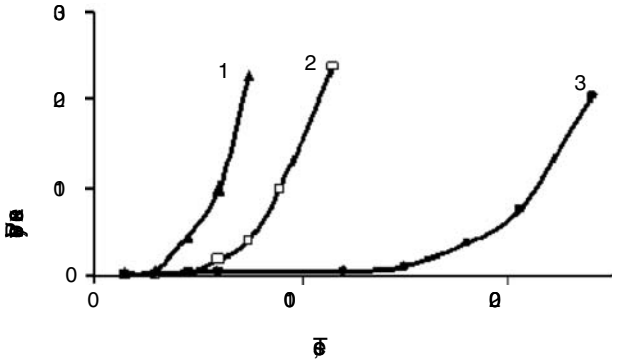

Figure 6. Effective viscosity plotted against reaction time for the TiP samples synthesized from $TiOSO_4$ at varied P/Ti molar ratios: 1 – 1.25; 2 – 1; 3 – 0.75.

$$[TiOSO_4 + FeCl_3] + H_3PO_4 \rightarrow \underline{TiP}\ (gel)\ (a)$$

$$TiOSO_4 + [\,FeCl_3 + H_3PO_4\,] \rightarrow \underline{TiP}\ (gel)\ (b)$$

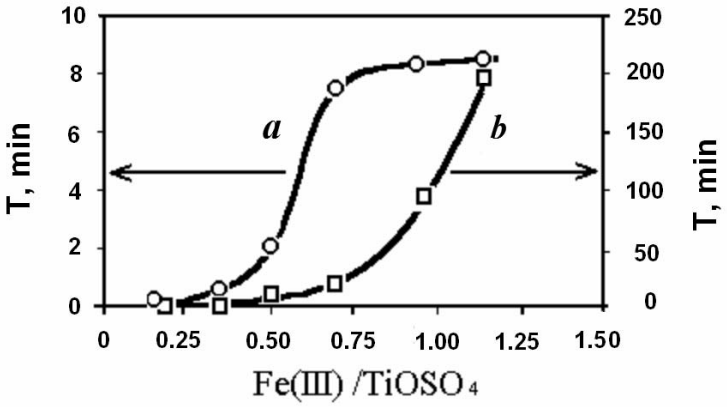

Figure 7. The effect of the sequence of the Fe(III) salt addition on the TiP gelation time at varied Fe(III)/$TiOSO_4$ molar ratios.

results in the soluble acidic phosphate, which should be destroyed in the reaction with $TiCl_4$. Indeed, we succeeded to demonstrate that adding Fe^{3+} to various precursors (a solution of $TiOSO_4$ or H_3PO_4) significantly changes the kinetic parameters of the process, as seen from the experimental data presented in Figure 7.

After drying the TiP hydrogels, the triple-charged cations involved in the sol-gel processing are almost completely removable from the ion exchanger matrix by washing with a mineral acid and then with water.

We have carried out an analogous study to assess the possibility that the ZrP sol-gel synthesis is induced by the addition of Al^{3+} ions competing with Zr(IV) to the starting precursors. The process occurs according the equation:

$$ZrOCl_2 + H_3PO_4 \xrightarrow{Al^{3+}} \underbrace{Al_x^{3+}Zr_y(H_2PO_4)_z \cdot nH_2O}_{\text{mixed AlZrP gel}} \xrightarrow{H^+} \underbrace{Zr(H_2PO_4)_2 \cdot nH_2O}_{\text{pure ZrP gel}} + Al^{3+} \quad (7)$$

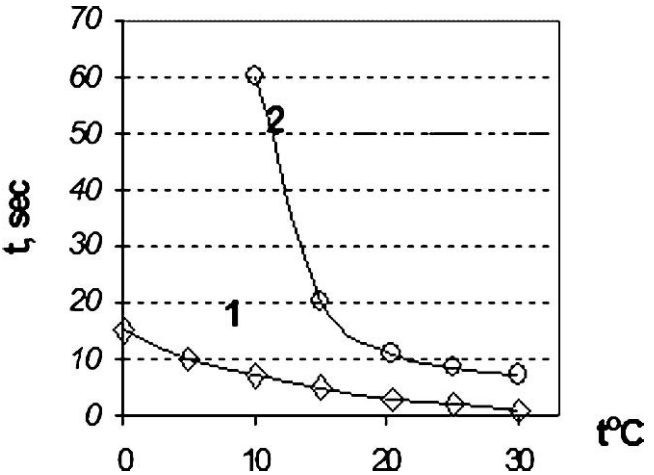

Figure 8. The temperature dependence of the ZrP gelation time at varied molar Al/Zr ratios: 1 – *0.5* and 2 – *1.0*.

Figure 8 shows the data testifying the essential influence of Al^{3+} ions on the ZrP gelation time at various temperatures.

We have been first to reveal not only the slowing-down effect of triply charged cations on TiP and ZrP gel synthesis but also their template action on the matrix of these materials. Indeed, the S_{sp} values of traditionally produced titanium and zirconium phosphates do not exceed 150–250 m^2/g. If they are prepared by the suggested procedure, i.e., by the sol-gel processing in the presence of triply charged cations, the S_{sp} values reach 300–700 m^2/g after desorption of these template cations from the matrix because they leave ultra-pores of comparable size (Figure 9):

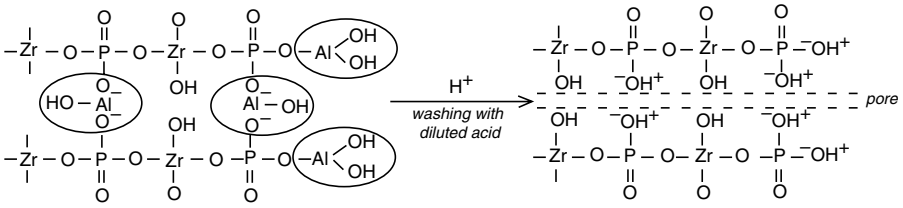

Figure 9. The scheme of the template action of Al^{3+} ions in the synthesis of ZrP cation exchangers.

It is essential that the TiP and ZrP samples synthesized in the presence of templating gel-forming cations (slowing down the process) exhibit much higher selectivity to d-metal cations. In the ZrP matrix, phosphate and hydroxyl groups oriented in the course of the synthesis and fixed in ultrapores (Figure 9) are spaced so that the coordination interaction with complexing cations is facilitated.

Figure 10 shows the isotherms of ion-exchange sorption for a series of d-metal cations. We notice from this figure that in the region of equilibrium near-zero concentrations, the isotherms start just at the ordinate axis, which unequivocally confirms high ion exchanger selectivity. Selectivity coefficients, K_d, for some cations have large values (10,000–20,000) and the selectivity series for ZrP is as follows:

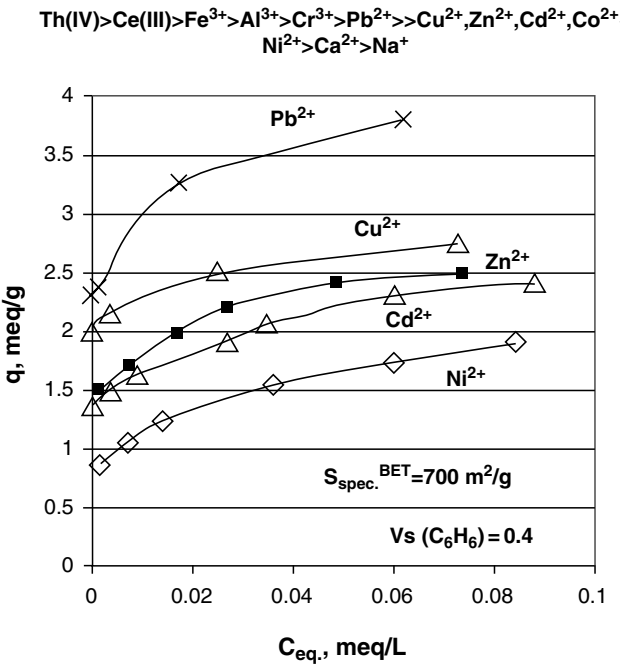

Figure 10. Typical isotherms of sorption of heavy metal cations onto the ZrP sample templated with Al^{3+} ions.

Summing up, it is appropriate to demonstrate (Figure 11) the appearance of solid transparent hydrogels containing various competing cations in the matrix; for comparison, gel-like precipitates (often misnamed gels) are also shown.

Figure 11. The appearance of gels and gel-like precipitates.

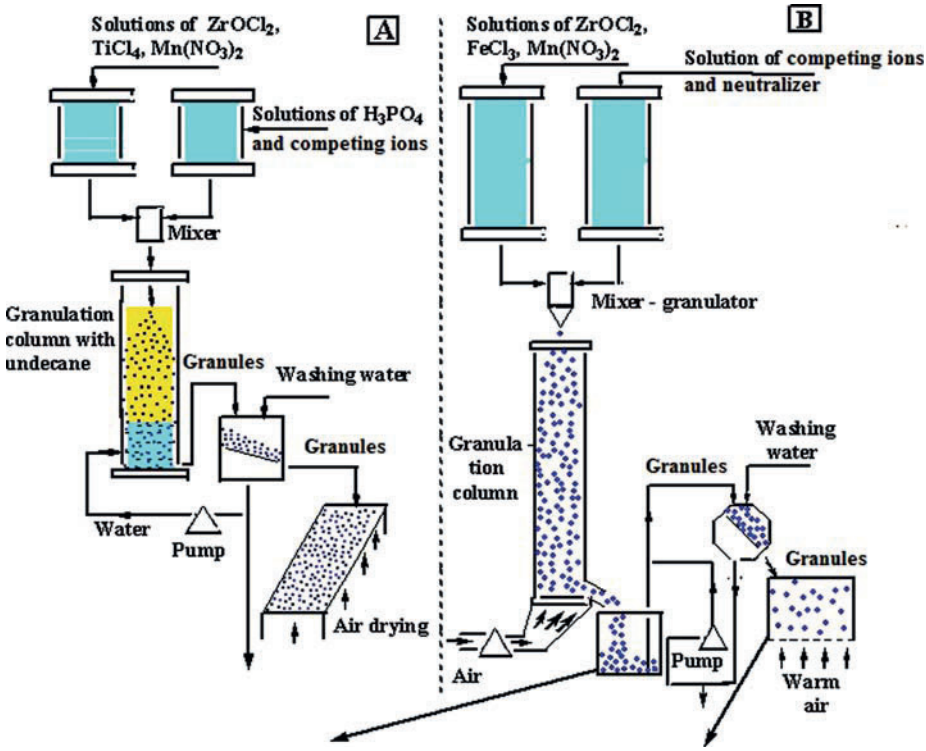

Figure 12. The schematic diagram of the "oil-drop" (A) and "air-drop" (B) sol-gel technologies to prepare spherically granulated hydrated oxides and phosphates of Ti and Zr by the method of competing ions.

By testing various reagent ratios, temperatures, pH values, and quantities of competing ions (mostly SO_4^{2-}), we managed to reduce the sol-gel conversion time to 3–5 sec. This allowed us to develop two semi-pilot technologies (the "oil-drop" and "air-drop" technologies) for the continuous preparation of individual and mixed hydrated oxides and phosphates of polyvalent metals (mostly Ti and Zr) obtained as highly porous spherical granules (Figure 12).

The "oil-drop" technology is based on fast injection of quickly mixed reagents into a column with oil or another water-immiscible liquid (like undecane). Entering the column, the reaction mixture stream is divided into spherical drops of controlled size which are transformed into hydrogel spherical granules within 3–5 sec during the slow movement through the organic liquid layer in the column.

The "air-drop" technology is organized in the same way; however, the drops of the reaction mixture enter the air stream (rather than organic liquid) blowing from the bottom of the column and controlling the air temperature and movement time of the hydrogel drops until they reach the flow of a washing solution or water.

The resulting spherical granules of hydrogels can be subjected to a number of different treatment schemes (washing with solutions of various pH values, substitution of intermicellar liquid, thermochemical and hydrothermal processing, etc.) which enable a wide-range variation of the porous structure and the surface chemistry of the materials obtained.

Figure 13 gives the appearance of the initial typical hydrogel produced by the continuous method and the corresponding dried xerogel with highly developed porosity and glass-like transparent granules of regular spherical shape.

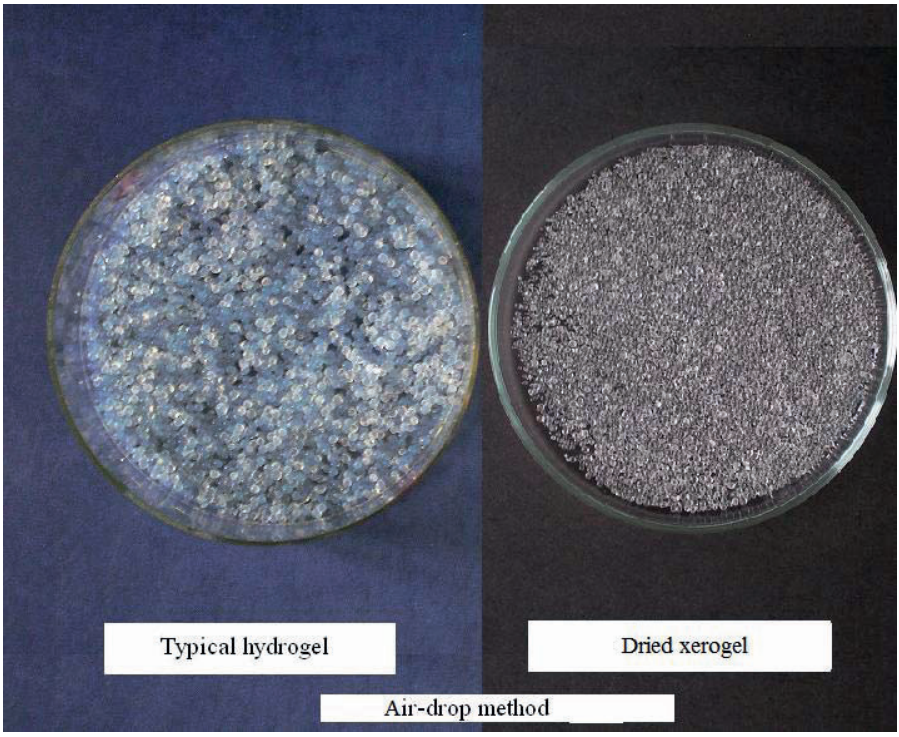

Figure 13. The appearance of the ZrP typical hydrogel and dried xerogel.

3. Porous Structure, Surface Chemistry, and Sorption Properties of Spherically Granulated TiP and ZrP Synthesized by the Sol-gel Method Using Competing Ions

Taking into account that $TiOSO_4$ is easier to handle and cheaper than $TiCl_4$, and also accessible as an industrial semi-product, we investigated thoroughly how the conditions of the sol-gel TiP synthesis with the $TiOSO_4$ precursor affect the physico-chemical properties of target materials.

This study addressed the effect caused by the P/Ti molar ratio in the synthesized ion exchanger on its porometric characteristics. Figure 14 demonstrates the N_2 adsorption-desorption isotherms for two TiP samples at -196^0C and the effective pore volumes distribution per radii. The mesoporous character of the samples with the P/Ti molar ratios 1 and 1.5 is evident from the figure.

It should be noted that the pore radius is ~120 Å, irrespective of the P/Ti molar ratio. The overall picture of how the P/Ti ratio affects the volume of sorption pores and $S_{sp.}$ values is judged from the data in Table 1. The Table lists also the corresponding data for the TiP sample obtained by the traditional

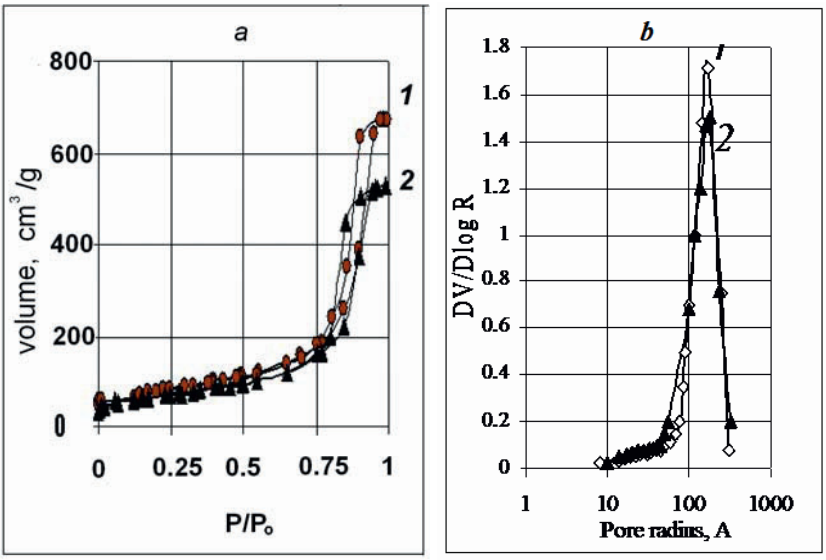

Figure 14. The N_2 adsorption-desoprtion isotherms (a) and pore volumes distribution per radii (b) for the TiP samples synthesized from $TiOSO_4$: TiP – 1.0 (1), TiP – 1.5 (2).

TABLE 1. Porometric characteristics of the synthesized TiP samples.

P/Ti ratios of TiP samples	Pore volume $V_s^{benzene}$ (cm^3/g)	Specific surface area S_{sp}^{Ar} (m^2/g)
0.75	0.89	295
1.00	0.72	280
1.25	0.84	285
1.50	0.66	240
1.65	0.65	255
2.00	0.42	210
2.50	0.46	185
TiP – $TiCl_4$	0.15	90

method based on $TiCl_4$. It is important to note that the porometric characteristics of this material are inferior to those of TiP produced from the $TiOSO_4$ precursor.

It is also worth noting that the TiP samples synthesized by the sol-gel method from the $TiSO_4$ precursor are characterized by a different kind of surface chemistry than ion exchangers produced on the $TiCl_4$ precursor. First and foremost, this can be deduced from the curves of potentiometric titration of the samples with a 0.01 M NaOH solution (Figure 15). As it can be seen, the TiP samples with different P/Ti ratios are very different from each other, especially on the initial portions of the curves (up to pH = 2.1). It can be assumed that the bending points on the curves occurring at pH ≈ 2 are caused by the presence of strongly acidic $–SO_3H$ surface groups which are fixed in the surface layer during the sol-gel synthesis. In this case, the contribution to sorption capacity from these groups rises, as the P/Ti ratio in ion exchangers decreases. Our supposition is supported by the fact that the bending point at pH ~ 2 is lacking on the titration curves of the TiP samples produced from $TiCl_4$. Thus, the molecular structure of the surface layer for the TiP samples synthe-sized by the sol-gel method from the $TiOSO_4$ precursor can be schematically represented as in Figure 16.

The thermal stability of functional phosphate and sulfate groups on the TiP surface is characterized by the data of Figure 17. It is seen that even after calination at 200°C, the ion-exchange capacity of the material does not decrease but even somewhat increases.

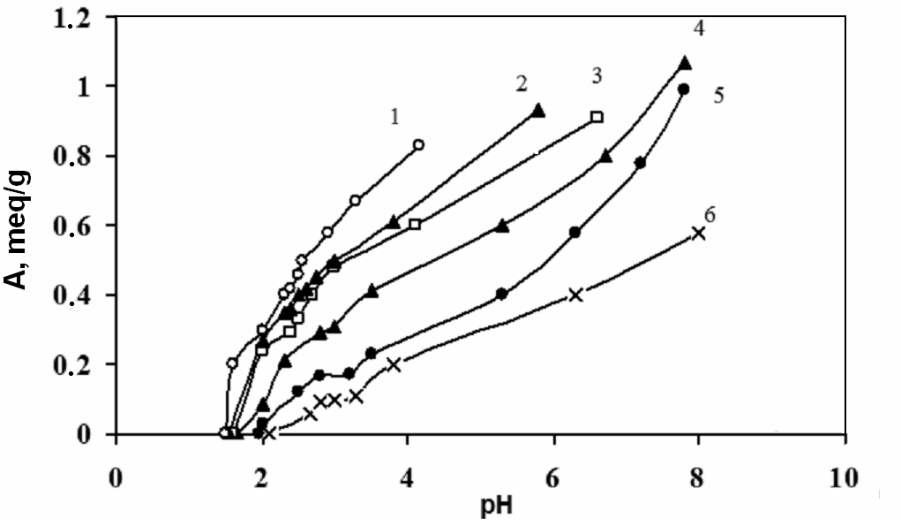

Figure 15. The pH-metric titration curves for the TiP samples synthesized from $TiOSO_4$ at different P/Ti ratios: P/Ti = 0.70 (1), 1.0 (1), 1.25 (3), 1.4 (4), 1.65 (5) and for the TiP sample synthesized from $TiCl_4$ at the molar ratio P/Ti = 1.5 (6).

With the above considerations, it makes sense to present the data demonstrating the peculiarities of the ion-exchange sorption on TiP and ZrP; in particular, it is appropriate to elucidate their sorption selectivity.[6] We have already noted that the isotherms of the ion-exchange sorption on templating ZrP (Figure 10) imply the high selectivity of this ion exchanger.

The same is evident from the data on TiP efficiency in the purification of water wastes containing a number of organic compounds and also Cd^{2+} ions (formed in the acetaldehyde production with the Cd catalyst) – see Table 2. On

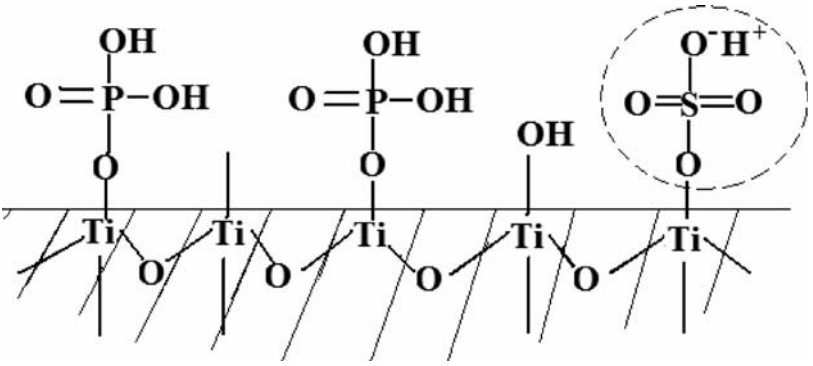

Figure 16. The molecular structure of the TiP surface synthesized from the $TiOSO_4$ precursor.

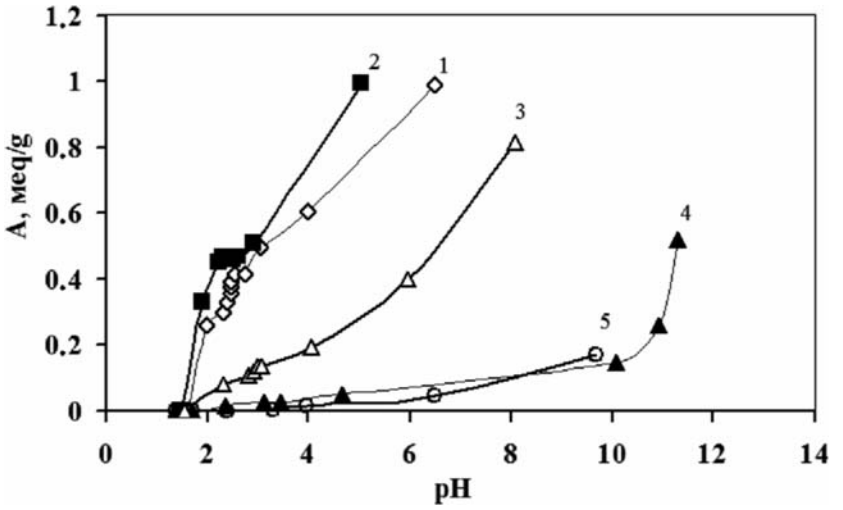

Figure 17. The pH-metric titration curves of the TiP samples calcinated at different temperatures: (1) before calcination; (2) 200°C; (3) 300°C; (4) 400°C; (5) 500°C.

purification, the content of toxic cadmium ions decreases from 0.05–10 to <0.002 mg/l.[7]

The data of the Table 2 (below) illustrate also the high efficiency of these ion exchangers in purification of some process solutions (concentrated salt solutions) which permits certain undesirable ion admixtures to be removed.

Finally, an essential advantage of TiP and ZrP is a potential possibility to use them in autonomous systems of drinking water purification.[8] In the known "Brita" system, the sorption column of the water-purifying unit contains a mixture of active carbon and carboxylic resin absorbing traces of heavy metals. In our system, spherically granulated TiP or ZrP are used instead of the synthetic resin.

TABLE 2. Application of TiP(ZrP) for deep purification of cadmium-containing wastes and some process solutions.

Technological process	Composition and content of undesirable admixture	
	Before purification	After purification
Cd removal from wastes of acetaldehyde production	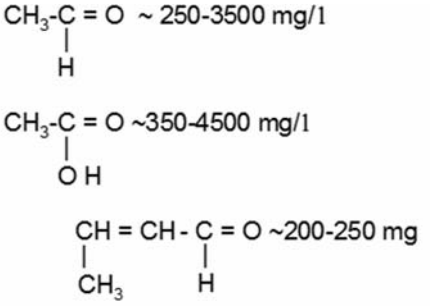 Cd ~ 0.05 – 10 mg/l	Cd < 0.002 mg/l
Fe removal from solution of mercury electrolysis	NaCl – saturated solution Fe – 5 mg/l	Fe < 0.02 mg/l
Cu^{2+} and Cd^{2+} removal from Zn-electrolyte	Zn^{2+} – 145 g/l Cu^{2+} – 2.0 g/l Cd^{2+} – 0.6 g/l	Cu^{2+} – 0.0005 g/l Cd^{2+} – 0.0015 g/l
Cu^{2+} removal from the electrolyte of nickelation	Ni^{2+} – 63 g/l Cu^{2+} – 0.1 g/l	Cu^{2+} – 0.0005 g/l

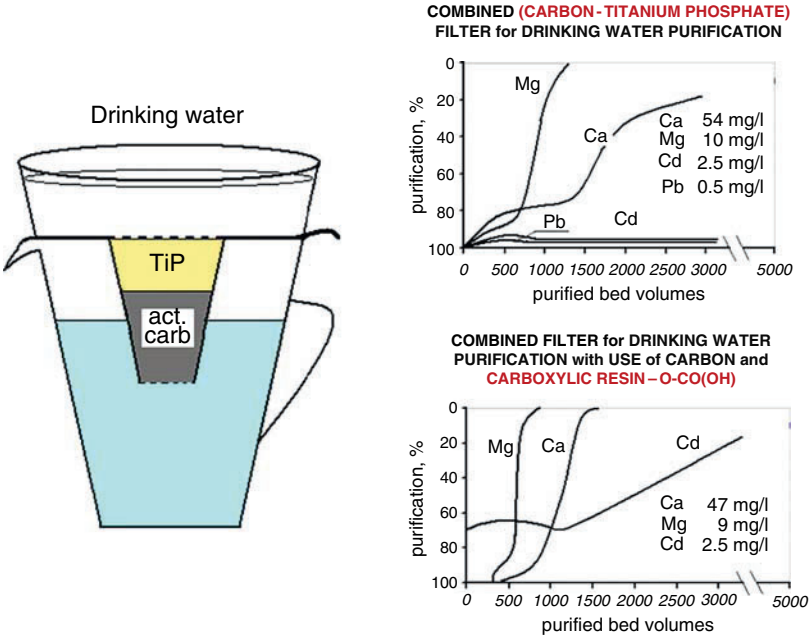

Figure 18. Sorption dynamics for Pb^{2+}, Cd^{2+}, Mg^{2+} and Ca^{2+} traces in drinking water purification on the combined sorption layers, viz., active carbon-titanium phosphate and active carbon-carboxylic resin.[8]

As Figure 18 suggests, it is possible to purify up to 5,000 column volumes of drinking water from lead and cadmium contaminants using combined sorption layer consisting of active carbon and titanium phosphate; at the same time, a breakthrough immediately occurs for biologically vital elements (such as Mg^{2+} and Ca^{2+} ions), i.e., they are not removed from drinking water. In contrast, in the case of the "Brita" system, the cadmium breakthrough is observed right after passing through the sorption layer, whereas Mg^{2+} and Ca^{2+} ions are completely absorbed in purification of the first 300–400 column volumes.

Of particular interest is the possibility to use inorganic ion exchangers for the absorption of uranium, cesium, and strontium radionuclides from liquid radioactive wastes, in particular, water solutions of complex composition. In a detailed study of this problem, we have revealed high sorption capacities (4–7 mg-eq/g) and unusually long times of sorption equilibration for most of TiP samples.

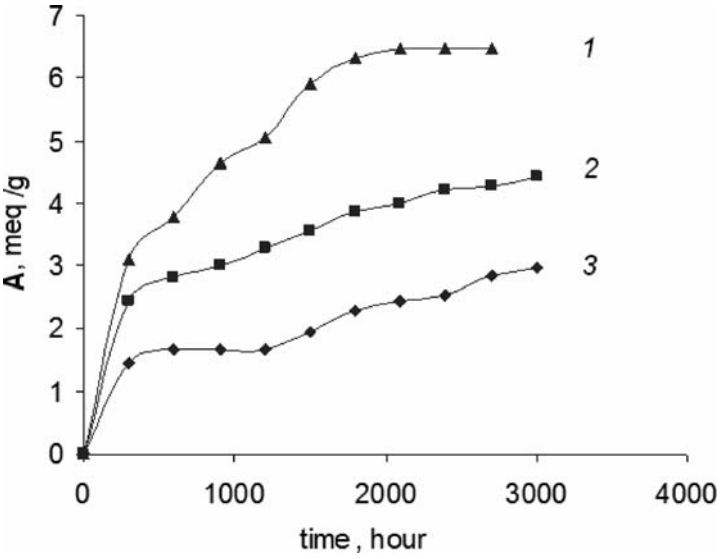

Figure 19. The kinetics of UO_2^{2+} sorption from a uranyl-acetate solution ($C_{in} = 1.5 \times 10^{-3}$ M) on TiP samples synthesized with different initial P/Ti molar ratios: 1 – 0.8; 2 – 1.0; 3 – 1.25.

As it is clear from Figure 19, the kinetic curves reach the plateau only within ~3,000 h, although their initial portions rather suggest fast saturation of some sorption centers.

Using the XPS method and X-ray analysis, it has been shown that the sorption process requiring such a long time to reach equilibrium is contributed not only by the ion exchange but also by formation of a new phase, $(UO_2)_3(PO_4)_2$. This phenomenon is probably due to the fact that the phosphate anion affinity to uranyl cations is higher than to Ti (IV).

In our opinion, the revealed features of uranium sorption on TiP make this sorbent also applicable in the so-called "capping method"[9] which implies binding of undesirable admixtures by placing a thin sorbent layer onto the ground sediments in cooling ponds or in natural reservoirs contaminated with uranium and transuranium elements. As a result, uranium and other radio-nuclides will be fixed on TiP in the bottom zone and its drainage into water horizons will be prevented.

As regards Cs-137 and Sr-90, the titanium silicate ion exchangers developed by us (produced by the sol-gel technique from the $TiOSO_4$ and Na_2SiO_3 precursors) appear to be most promising for selective adsorption of traces of these radionuclides. The synthesis of such ion exchangers can be generalized by the following equation:

$$TiOSO_4 + Na_2SiO_3 + NaOH \rightarrow \underset{\text{amorphous hydrogel}}{Na_2O \cdot TiO_2 \cdot SiO_2 \cdot nH_2O} \rightarrow \underset{\text{semicrystalline product}}{Na_2Ti_2O_3SiO_4 \cdot nH_2O} \quad (8)$$

As it is evident from the equation, this process permits preparation of ion exchangers in the semicrystalline form under mild conditions, contrary to the reported methods of hydrothermal action[10] leading to full material crystallization. At the same time, it has been found that the ion exchanger with the molar ratio Ti/Si = 1:1 is selective to Sr-90 and the material with Ti/Si = 2:1 is selective not only to Cs-137 but also to UO_2^{2+}. Selectivity coefficients being rather large: K_d(Cs-137) = 137,000; K_d(Sr-90) = 34,000, and $K_d(UO_2^{2+})$ = 310,000.

It is also significant that due to the small thermal expansion coefficient, this universal rationuclide absorber can be melted, after saturation with the Cs and Sr radioisotopes, as well as U, to chemically stable ceramics and then kept in special depositories.

4. Sulfated ZrO_2 and TiO_2 as Strong Solid Acid Catalysts

According to K. Tanabe et al.,[11] about 120 of 130 modern industrial processes are catalyzed by solid acids. Solid acid catalysts have many advantages over their liquid Broensted- and Lewis-acid counterparts, especially in liquid-phase processes: strong solid acids are non-corrosive and environmentally benign, create fewer disposal problems, are much easier in recycling and separation from liquid products, have a longer catalyst life, etc. In this context, solid catalysts are now regarded as most promising in view of the challenges of the green chemistry.

It should be noted that, along with solid acid catalysts of the zeolite type (mostly used in high-temperature large-scale processes like cracking or isomerization), much recent attention has also been paid to the solid acids derived from sulfated Zr, Ti, and Sn oxides.[12] The practical advantage of the latter catalyst type is exemplified by sulfated zirconia (ZrO_2/SO_4^{2-}) which is used as a solid acids catalyst in fine organic synthesis; it displays excellent activity and good selectivity for a variety of processes including those of commercial value. Among them are isomerization, hydration, dehydration, etherification and esterification (e.g. in the production of dibutyl and dioctylphthalate plasticizers, as well as numerous drugs and pharmaceuticals), the Friedel-Crafts alkylation of phenols with alkenes, alkanols, ethers and alkyl halides, etc.[13–15]

The synthesis of these new catalytical materials is rather simple and consists in covering the surface of porous oxides with 3–4% H_2SO_4 or $(NH_4)_2SO_4$, followed by drying and calcination at 500–700°C in the open air.

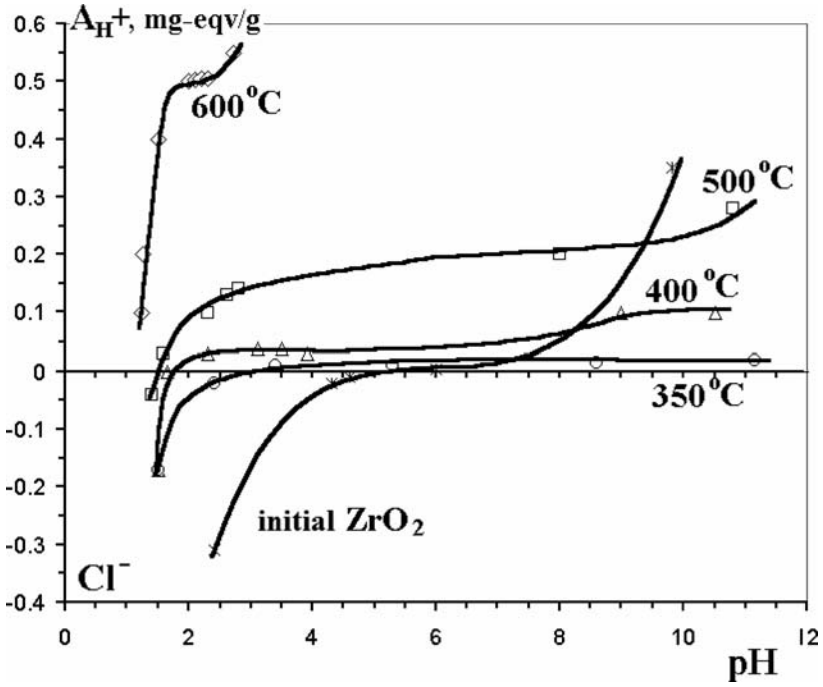

Figure 20. The curves of potentiometric titration for the initial ZrO_2 sample and for the samples treated with H_2SO_4 and calcinated at various temperatures .[16]

Previously we proposed a mechanism for strong-acid center formation resulting from the mentioned treatment.[16] Leaving aside the details of this mechanism, such centers arise during thermally induced recrystallization of the material

(Figure 20); they are represented by stable sulfate groups chemically immobilized in the surface layer. As already mentioned, such sulfate groups are also fixed in the surface layer of TiP synthesized from $TiOSO_4$, as evidenced by the potentiometric titration curves plotted in Figures 15 and 17. One can thus infer that TiP samples even with a small P/Ti molar ratio display properties of strongly acidic mesoporous catalysts. It is just mesoporous materials free of kinetic restrictions that are necessary for liquid-phase catalysis.

On the other hand, the above-described semi-pilot technologies (Figures 12, 13) for the continuous sol-gel synthesis of Ti and Zr phosphates and oxides (obtained as easy-to-handle spherical granules of a controlled diameter) can be used in large-scale production of high-quality solid acid catalysts.

To conclude, the wet sol-gel method of competing ions pioneered by us represents a convenient, easy-to-handle, safe, and cheap technological strategy. It provides great potentialities for large-scale production of sorbents, selective

inorganic ion exchangers and strong solid acid catalysts for fine organic synthesis. Moreover, a pronounced porosity and thermal stability of these materials make them applicable as stable catalyst supports.

5. Conclusions

- The original methods for sol-gel synthesis of hydrated oxides and phosphates of polyvalent metals have been proposed and experimentally tested. The methods are based on the use of simple salts, acids, and alkalis with the addition of competitive cations and anions affording the control of gelation time.
- Using the proposed method of competing ions, we have developed the "oil-drop" and "air-drop" semi-pilot technologies for the continuous production of spherically granulated sorbents derived from hydrated oxides and phosphates of polyvalent metals.
- The templating effect of competing M^{3+} cations in the sol-gel synthesis of TiP and ZrP has been discovered improving significantly the adsorption properties of inorganic cation exchangers.
- As demonstrated, inorganic ion exchangers synthesized by the sol-gel method remove efficiently the traces of radionuclides (including uranium) and heavy metals from waste and drinking water as well as from process solutions thus enabling their deep purification.
- It has been found that spherically granulated Ti and Zr oxides can be used in the preparation of strong solid acid catalysts with controlled porosity and surface chemistry.

Acknowledgements

The author is grateful to Drs. V. Kanibolotskii, I. Zhuravlev, A. Zaitseva, and O. Zakutevskyy for their efficient contribution to the experimental part of the study and valuable discussions. The fruitful help of Drs. V. Klymenko and O. Zakutevskyy in the preparation of the manuscript is also thankfully acknowledged.

References

1. S. Sakka (ed.), *Handbook of Sol-gel Science and Technology. Processing, Characterization and Applications*. Volume I: *Sol-gel Processing*, vol. ed. H. Kozuka (Kluwer, Boston, MA/Dordrecht, The Netherlands/London, 2004).
2. C.B. Amphlett, *Inorganic Ion Exchangers* (Elsevier, New York, 1964).
3. A. Clearfield (ed.), *Inorganic Ion Exchange Materials*(CRC Press, Boca Raton, Fl, 1982).

4. S.B. Randarevich, V.V. Strelko, V.N. Belyakov, V.Yu. Korovin, and A.I. Bortun, State of phosphorus in sorbents based on titanium and zirconium phosphates from ^{31}P NMR spectroscopic data, *Theor. Experim. Chem.* 24(5), 607–610 (1988).
5. A.I. Bortun and V.V. Strelko, Synthesis, sorptive properties and applications of spherically granulated titanium and zirconium hydroxophosphates, in: *Fundamentals of Adsorption: Proceedings of the Fourth International Conference of Funda-mentals of Adsorption*, Kyoto, May 17–22, 1992, edited by M. Suzuki (Tokyo, Kodansha, 1992), pp. 59–65.
6. V.V. Strelko, A.I. Bortun, and V.N. Belyakov, Regularities of sorption of d-metal cations by titanium and zirconium phosphates in dynamical regime, *Chem. Water Tech.* (Russian) 10(6), 487–490 (1988).
7. T.E. Mitchenko, V.V. Strelko, V.N. Belyakov, and L.E. Postolov, Cadmium removal from waste waters with sorbent based on titanium phosphate, *Chem. Water Tech.* (Russian) (5)5, 418–421 (1983).
8. A.I. Bortun, S.A. Khainakov, V.V. Strelko, and I.A. Farbun, in: *Ion Excange Deve-lopments and Applications*: *Proceedings*, edited by J.A. Greig (Cambridge, 1996), pp. 305–310.
9. X.Q. Wang, L.J. Thibodeaux, K.T. Valsaraj, and D.D. Reible, The efficience of capping contaminated sediments in situ. I. Lab-scale experiments of diffusion/ adsorption in the capping layer, *Environ. Sci. Technol.* 25(9), 1578–1584 (1991).
10. A. Clearfield, A. Tripathi, D. Medvedev, A.I. Celestian, and I.B. Parise, *In situ* type study of hydrothermally prepared titanates and silicotitanates, *J. Mater. Sci.* 41, 1325–1333 (2006).
11. K. Tanabe and W.F. Hölderich, Industrial application of solid acid-base catalysts, *Appl. Catal. A: General* 181(2), 399–434 (1999).
12. A. Corma, Inorganic solid acids and their use in acid-catalized hydrocarbon reactions, *Chem. Rev*. 95(3), 559–614 (1995).
13. S. Furuta, H. Matsuhashi, and K. Arota, Catalytic action of sulfated tin oxide for etherification and esterification in comparison with sulfated zirconia, *Appl. Catal. A :General* 269(1–2), 187–191 (2004).
14. B.M. Reddy, P.M. Sreekanth, and P. Lakshmann, Sulfated zirconia as an efficient catalyst for organic synthesis and transformation reactions, *J. Molec. Catal. A: Chemical* 237(1–2), 93–100 (2005).
15. G.D. Yadav and G.S. Pathre, Chemoselective catalysis by sulfated zirconia in O-alkylation of guaiacol with cyclohexene, *J. Molec. Catal. A: Chemical* 243(1), 77–84 (2006).
16. V.V. Strelko, Mechanism of the effect of thermal treatment on the formation of strong acid sites in the surface layers of sulfated metal oxides, *Kinet. Catal.* 44(6), 834–839 (2003).

ABOUT INTERACTIONS BETWEEN SOL-GEL DERIVED SILICA, TITANIA AND LIVING ORGANISMS

REETA VIITALA*, SAMI AREVA
Turku Biomaterials Centre, University of Turku, Itäinen Pitkäkatu 4 B, FI-20520 Turku, Finland

MIKA JOKINEN, MIKA KOSKINEN
DelSiTech Ltd, Itäinen Pitkäkatu 4 B, FI-20520 Turku, Finland

Abstract. Sol-gel derived silica and titania have a specific interaction with many biological molecules, microbes, algae, cells and living tissue. The specific interactions mean that they differ from common reactions between non-viable materials and biomolecules or living tissues and the interactions are mostly beneficial from the viewpoint of biotechnical applications. Pepetides and proteins may preserve their activity and bacteria, algae and cells may preserve their viability and viruses their infectivity as encapsulated in sol-gel derived silica. Silica and titania are known to form a direct bond with living tissue which can be utilized in the biomaterial applications. Other application areas of silica and titania are in biosensing, tissue engineering, gene therapy, controlled delivery of therapeutic agents and environmental protection.

Keywords: Sol-gel method, silica, titania, biomaterials, virus delivery, tissue bonding.

1. Introduction

Silica is one of the naturally occurring substance in living systems and it is found e.g. in diatoms, plants and in humans. Silica is also a potential candidate for biomaterial applications. Implantable biomaterials can be used for example to replace injured or damaged soft or hard tissue and in drug delivery applications. Silica is the main component in bioactive glass which was originally developed by Larry Hench. Bioactive glass is used as bone replacement material mainly in applications where load bearing properties are not needed.[1] It is known that bioactive glass has the ability to bond to bone which is a good example of the

*To whom correspondence should be addressed: Reeta Viitala, Turku Biomaterials Centre, University of Turku, Itäinen Pitkäkatu 4 B, FI-20520 Turku, Finland; e-mail: reeta.viitala@utu.fi

P. Innocenzi, Y. L. Zub and V. G. Kessler (eds.), *Sol-Gel Methods for Materials Processing*.

suitability of silica in biomaterials. On the other hand titanium metal, with naturally occurring titania thin film on the surface, is used as an implant material in load bearing applications. Titania films can be prepared also with sol-gel method and it has been shown that these films can bond directly to tissue. These two examples on bioactive glass and sol-gel derived titania coatings show that silica and titania are able to bond directly to the surrounding tissue and no capsule formation around the implant is observed after implantation. Typically if a foreign material is implanted in body a capsule layer forms around it, which prevents the higher interaction between the material and living tissue.

Generally biomaterials can be divided in four categories which are (i) toxic materials, which elicits a harmful response and thus causing the death of the host tissue, (ii) biologically inactive, nearly inert materials that are encapsulated by fibrous capsules, (iii) bioresorbable materials, which dissolve during the tissue and body fluid contact and (iv) bioactive materials that can be either bioresorbable or biostable. Furthermore, the bioactive materials can be classified as class A (osteopromotive i.e. material elicits both an intracellular and an extracellular response at its interface) and class B (osteoconductive i.e. material elicits only an extracellular response at its interface). The bioactive material can also be defined as: "a material that elicits a specific biological response at the interface of the material, which results in the formation of a bond between the tissues and the material".[2]

Sol-gel derived silica matrices, which are typically biodegradable, can be used in drug encapsulation and delivery applications. In the beginning of 1990s the interest on the delivery and/or encapsulation of different active agents (therapeutic or biologically active) started to grow for many reasons, one of them was the first biopharmaceuticals or biotechnically produced agents (e.g., therapeutic proteins) that reached the phase where the controlled delivery became a real issue. Choradin et al. have reviewed the use of sol-gel materials in medicinal science and they give many good examples on the encapsulation of proteins as well as DNA, cells, algae and bacteria in silica.[2] They discuss also organic modifications of silica and hybrids materials that further widen the possibilities to use silica-based materials in medical applications. Approximately at the same time in 1980s and to a larger extent in the beginning of 1990s, several groups started to encapsulate enzymes, other proteins and cells in the sol-gel derived silica, not to develop delivery device, but to use silica as a matrix material for, e.g., (bio)catalysis and sensors. Avnir et al., Gill et al. and Livage et al. have made excellent reviews on the topic.[3–6] These studies contain a lot of information on the silica sol-gel formulations as well as on the preservation of the activity of proteins encapsulated in silica.

Preparation of SiO_2 and TiO_2 by sol-gel processing is well studied and it is shown that the final structure of the material depends on the preparation parameters. This is advantageous also in biomaterial applications. Sol-gel technique makes it possible to prepare different formulations like monoliths, films, fibres or powders. Sol-gel processing also offers an alternative for the preparation of bioactive glasses with potential advantages over conventional melt processing, such as higher purity, lower processing temperature, and the possibility to modify pore structure, nanoscale topography, composition, adsorption capacity as well as dissolution rate.[7,8]

In this paper is described the suitability of sol-gel derived silica in encapsulation of viruses and the suitability of titania films in tissue bonding applications. Also the interaction between silica, titania and living tissue are discussed.

2. Silica in Living Tissue

The Nobel Price winner for chemistry, Professor Adolf Butenandt, provided that life can not exist without silica. According to his research conducted in 1972, silica is an essential nutrient and must be supplied continuously from food. Silica is also the most common substance in earth's crust. Silicon is found in the same element group on the periodic chart as carbon. In the past, this close family relationship to carbon has led many scientists to speculate that a realm of silicon chemistry awaited discovery, however silicon was not a replacement for carbon. However silica is an important element in many body functions like in bone and cartilage growth. Silica is also a natural constituent of blood and urine (<1 ppm). The average human body has about seven grams of silica. Since silica is so common in earth's crust and in living systems it has led to the situation that living systems have been adapted to the presence of silica very well.

Silica can be found in crystalline and amorphous forms. It has been reported that crystalline form of silica can cause fibrosis in lungs as inhaled, this is a serious illnesses called silicosis, which was called at the old times "coal workers disease". Crystalline silica has very low water solubility.9 Whereas the amorphous silica is water soluble and biocompatible. The solubility of amorphous silica in water at body fluid pH is most commonly determined to be 130–150 ppm (μg/ml). Amorphous silica is known to dissolve into body fluids as silicic acid and is removed through urine. No silica accumulation is observed in organs.

The interest on the delivery of large biologically active molecules such as proteins, peptides and polysaccharides is growing fast. However the direct administration of these new biotechnically produced drugs is difficult due to intestinal decomposition. The difficulties can be avoided by encapsulating the

administrated molecules into amorphous sol-gel derived silica matrices and by implanting or injection these systems locally into the desired tissue.[10] One parameter, which affects the drug release rate is the silica matrix degradation rate e.g. the release of proteins from silica matrix is totally controlled by the matrix degradation.[11]

During the material development, first the in vitro matrix degradation and drug release are studied and in the second stage the correlation between the in vitro and in vivo matrix degradation is studied. According to our experimental observations, the *in vitro-in vivo* correlation of the biodegradation rates for silica structures with high silanol amounts and more or less encapsulated water (processed at ≤40°C) is about 8–10. This means that already in vitro dissolution rate of few days will result in relatively slow *in vivo* degradation, i.e., several weeks. This correlation has been observed several times for sol-gel derived silica, mostly in subcutaneous implantation in recent studies[12,13] in mice and rats, but also in our studies in intraperitoneal implantation in mice. The same correlation has been observed for relatively different silica implants developed for drug delivery, i.e., for hydrogel implants with 90% (w/w) water in structure and for xerogels (drying up to constant weight at 40°C). Both silica hydrogels and xerogels contain a lot of silanol groups and both are quite porous, only larger difference is in the water amount. The in vitro biodegradation rates (dissolution rates in simulated body fluid or in corresponding medium buffered to pH = 7.4 at 37°C) in sink conditions varied from 2–3 days to 6–7 days, respectively. These resulted in 25–30 and 55–60 day's degradation *in vivo,* respectively. The difference between *in vitro* and *in vivo* degradation rate is suggested to depend on two main reasons, (1) the obvious difference in the fluid flows in vitro and in tissue and (2) the fibrous capsule formed on the silica implants, which may retard any transfer of matter between the implant, also the fluid flow.

3. Encapsulation of Viruses in Sol-Gel Derived Silica

Wet silica gels can be used to encapsulate proteins, cells and viruses. Livage et al. and Avnir et al. discussed the idea to use wet silica gels in the cell and protein encapsulation.[3,6] We have developed silica gel with high water content that preserved the activity of encapsulated adenoviruses that can be utilized in gene therapy or in cancer vaccines.[14] Such silica with encapsulated viruses can then be implanted and the viruses are released by silica dissolution in the living tissue so that the gene transfer occurs.[12]

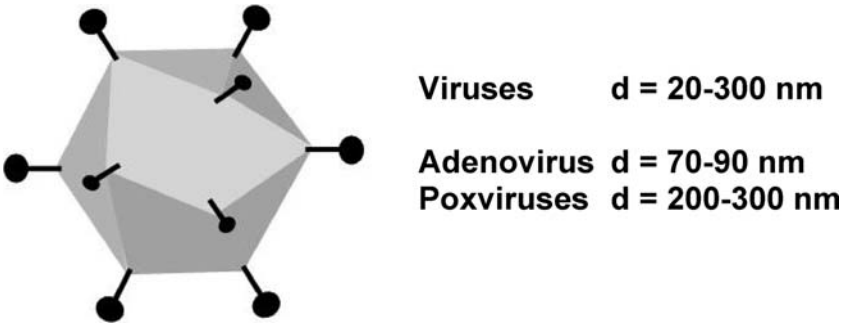

Figure 1. Schematic presentation of a virus and the typical sizes of the viruses.

In order to maintain the functional structure of viruses inside the silica gel, wet gels have to be used. These gels are called silica hydrogels. Water content in silica hydrogels is about 90% (w/w) and silica about 8–9%. Typical precursors in sol-gel process are silicon alkoxides (e.g. tetraethoxysilane, TEOS), acid, base and water. First the hydrolysis of TEOS is done at low pH (pH 1–3) and before adding the viruses into sol the pH of the sol is adjusted to higher level (pH 5–7). After adding the viruses the sol gelation occurs and hydrogel structure with encapsulated viruses is formed. The sols for these hydrogels are typically prepared at high water-to-alkoxide ratios ("R"), typical value of R is between 50–100. Ethanol is the by-product of the hydrolysis and condensation reaction of TEOS (Figure 3), but concentration of ethanol is quit low in the sol because high R-values are used and no harmful effects of ethanol on the viability of adenoviruses has been detected. The hydrolysis reaction of TEOS is closely to 100% because the remaining TEOS amounts in the hydrogels were near the detection limits giving at maximum 0.01 ppm (μg/ml) by GC/MS after extraction of the silica implants as such and as crushed in 5 ml of EtOH at 37–50°C for 3 days, i.e., TEOS content in the ready-made silica hydrogel implant was less than 0.001% (w/w). Ethanol content was maximally 0.5% (w/w). It is quite clear that silica structures that are full of water are also ready to dissolve in water. In addition, it is obvious that the pores are quite large and the porosity is high. The pore structure is difficult to measure directly due to high water amounts, but indirect measurements (dried structures) gave specific surface areas of several hundreds of square meters per gram. This kind of hydrogel silica structures dissolve in sink conditions (in body fluid mimicking water solutions buffered to pH 7.4 at 37°C) totally in 2–3 days.

3.1. STORAGE AND RELEASE

Sol-gel derived silica hydrogels are naturally structurally labile, the preservation of high water content (needed to keep the hydrogel structure virus-compatible) depends on the surrounding conditions, if the hydrogels are stored in dry environment silica matrix will dry and encapsulated viruses may lost their infectivity. This problem was solved by storing the hydrogels in silica-saturated water. We have showed that the labile water-containing silica structure could be stabilized from the viewpoint of virus infectivity by adding the silica implants in water that is saturated with respect to silicic acid or into water of which volume is so low that the slight degradation of the implant will saturate the solution and silica dissolution is terminated. At the same time, the aging of the silica structure in the water storage did not significantly change the dissolution rate of silica.[15] Due to the saturation the silica hydrogel implants do not dissolve in the liquid, but the aging of the silica structure proceeds. It was also observed that it is important to determine a proper aging of the gel prior to storage in silica-saturated water. Too early or too late immersion into water solution may break the implant during the storage. The structure develops during the water storage, dissolution rate decreases slightly within the first month after which it stays rather stable. The water content inside the silica structure may also decrease, but from the point of view of desired virus infectivity, the water storage has been found to be good, e.g., adenoviral vectors preserve their infectivity at least for several months. It is also important to note here that silica hydrogels are primarily developed for encapsulation of large biologically active agents, such as viruses and proteins and other large biomolecules that are not able to diffuse out from the silica structure, but are released by the silica matrix degradation.

In our previous studies where protein (BSA) was encapsulated into the silica matrix it was shown that the protein release was controlled by the matrix degradation. The protein release was studied in sink conditions where the free dissolution of the matrix was allowed and also in the SiO_2 saturated Tris buffer where no matrix degradation was possible. Results indicate that big molecules like proteins or even bigger viruses, cannot be released from the silica matrix without the matrix degradation. By storing the virus containing silica matrices in silica saturated solution viruses can be kept inside the matrix during the storage time and no matrix degradation occurs.[11]

4. Implant Fixation

Traditionally bioactive glasses and ceramics which are used as bone replacement materials are divided in two categories: class A and B. Class B materials are only osteoconductive, which means that the bone can grow onto the surface of

these materials with a passive process. Where as the class A materials are also osteopromotive which means that they are able to awoke a biological response where chemical signals induce bone formation which leads to direct bone growth and formation of the implant surface, bioactive glass belongs to this class.

4.1. MECHANICAL IMPLANT FIXATION

Metal implants are widely used in load-bearing orthopedic and dental applications. However, these materials are biologically inactive and they do not form a chemical bond with bone but are rather surrounded by a fibrous tissue capsule. In order to overcome the poor tissue bonding of the metal implant, the concept of mechanical implant fixation i.e. biological fixation by bone ingrowth through a metallic cage, is issued already in the early 1900s.[16] Mechanical fixation is still the most widely applied concept for ensuring implant fixation, which is frequently done by either controlling the materials pore size and interconnectivity or by surface roughening techniques such as mechanical grinding, sand-blasting and chemical etching. These techniques are also applicable to porous polymers.[16] The optimal pore size for bone ingrowth has been shown to be approximately 200–400 μm.[17,18] The surface roughening techniques are used to produce surfaces with less than 10 μm of micro-roughness.[19–22] Although improved mechanical interlock between the implants and bone have been achieved, metal implants do not attach to bone through chemical bonding.

4.2. CHEMICAL IMPLANT FIXATION BY SOL-GEL DERIVED COATINGS

Sol-gel derived TiO_2 coatings on metal surface enhance the bone bonding (class B bioactivity) of metel implants. This has been studied *in vitro* and *in vivo.* Based on the *in vitro* experiments in simulated body fluid (SBF) it has been shown that the bone bonding starts with the formation of negative charged surface which attract positively charged Ca^{2+} ions from the body fluid and after that adsorption of phosphate (HPO_4^{2-}/PO_4^{3-}) ions occurs. First the adsorbed layer will be amorphous calcium phosphate and will finally turn in to bone mineral-like hydroxyapatie (HA) through which the material bonds to bone. Thus the following general calcium phosphate formation mechanism on TiO_2 surfaces was suggested[23,24]:

Step 1. Formation of TiO^- groups on the surface. This is followed by a rapid accumulation and adsorption of Ca^{2+} and PO_4^{3-} ions on the surface due to electrostatic interactions.

Step 2. The formation of the initial calcium phosphate nuclei.

Step 3. Organization of the initially formed nuclei to a more stable and larger structure, which is influenced by the surface curvature.

Step 4. Once the nuclei has obtained a more stable structure and the critical size is achieved it will rapidly grow forming a poorly crystalline bone mineral-like hydroxyapatite layer on the surface via dissolution and reprecipitation processes, which is similar to the processes occurring on the surfaces of many bioceramics. This stage is delayed or inhibited in the presence of proteins.

TiO_2 is negatively charged at pH 7.4. In addition to the charge complementary of the negatively charged TiO_2 surface (at pH 7.4) and the firstly adsorbed Ca^{2+} ions, the nucleation property (or the lowering of the nucleation activation energy) is also dependent on the surface topography, which is one of the things that can be adjusted by the sol-gel method.

4.3. SURFACE MODIFICATIONS OF METAL IMPLANTS

Titanium (Ti) metal and its alloys are used in dental and orthopaedic applications. The biocompatibility of titanium metal is related to its surface oxide layer, which naturally occurs on the metal surface. In addition to biocompatibility, the bioactivity of the metal can be increased by introducing thicker titania coatings by different surface treatment techniques. One method is to use sol-gel technique to produce bioactive titania films on metal surface and an other method is to use simple chemical surface modification methods. Such methods were well known in conventional metallurgy, but their use for implant surface functionalization was novel. First the titanium metal was treated with mild H_2O_2 solutions as a chemical surface cleaning procedure leading to Ti-peroxide (TiO_2^{2-}) and Ti-superoxide (TiO_2^{-}) formation on their surface.[25–28] However it has been shown that H_2O_2 treatments using higher concentrations produce a thick titania gel layer with microporous structure on the surface of titanium implant enhancing the bioactivity and biocompatibility.[29–38] The most widely used and studied bioreactive metal implant of such type has been obtained by soaking of metal implant in either NaOH or H_2O_2 solutions with subsequent heat-treatments.

An other approach is to employ a bioceramic coating on the metal. Various bioceramic coatings have been used including calcium phosphates and hydroxyapatite coatings.[42–48] Techniques like sputtering and plasma spraying have been applied for preparation of these coatings on metal implants. Bioactive ceramic coatings have been widely applied to ensure direct chemical implant-bone contact and to reduce the time required for osseointegration. In this respect the plasma-sprayed calcium phosphate coatings are the most widely applied[33–35] although the composition, structure and the adhesion to the substrate are difficult

to control. One potential risk connected to the clinical use of any bioactive ceramic coatings is delamination or fragmentation. For example, recent studies have suggested that a breakdown at the metal-ceramic interface may occur[36,37]

Recent findings also suggest that bioactive surfaces (in terms of cell adhesion and activation) can also be obtained by controlling the surface roughness in the nanometer scale.[38–41] The surface nanoscale dimensions were shown to be important with respect to the interaction between the nanostructured surfaces and proteins as well as cells affecting the soft and hard tissue formation. Both nanostructured ceramics and polymeric surfaces showed similar enhanced cell adhesion and activation effects compared to conventional materials. These studies showed that there are specific dimensions between 1–100 nm that have a direct influence either on the adsorption of proteins (e.g., vitronectin) that are important with respect to adhesion and growth of bone tissue forming cells (osteoblast) or on the gene activation of soft-tissue forming cells, fibroblasts.

Surface dimensions between 1–100 nm can be achieved by sol-gel derived TiO_2 coatings that together with titanium metal provide a potential material for good tissue attachment.

4.4. SOL-GEL DERIVED TITANIA COATINGS

The sol-gel systems of TiO_2 can be adjusted to form versatile coatings structures and the applying techniques are quite simple. The sol-gel reactions are induced by polymerizing Ti-alkoxides via hydrolysis and condensation reactions (Figure 2). The polymerization stages can be described as, (i) polymerization of monomers to oligomers, (ii) condensation of polymers to primary particles, (iii) growth or agglomeration of primary particles to larger particles and (iv) linking of particles into chains followed by extension of their network eventually transforming into a gel.[7,9] In the preparation of sol-gel derived coatings by dip-coating, the substrates are immersed into a dilute sol and the gel-like coating is formed during substrate withdrawal.

$$\equiv\text{M-OR} + \text{H}_2\text{O} \leftrightarrow \equiv\text{M-OH} + \text{ROH}$$

Hydrolysis → ← Esterification

$$\equiv\text{M-OR} + \text{HO-M}\equiv \leftrightarrow \equiv\text{M-O-M}\equiv + \text{ROH}$$

Alcohol condensation → ← Alcoholysis

$$\equiv\text{M-OH} + \text{HO-M}\equiv \leftrightarrow \equiv\text{M-O-M}\equiv + \text{H}_2\text{O}$$

Water condensation → ← Hydrolysis

Figure 2. Hydrolysis and condensation reactions of (IV)-metal alkoxides. M=Ti or Si.

During film deposition, the structure of the film forms rapidly (as compared to bulk structures) and is influenced by several complex factors. The film thickness can be controlled, for example, by sol viscosity and withdrawing speed, where the increasing viscosity and/or increasing withdrawing speed increases film thickness. In addition to film thickness, the pore volume, pore size and surface area of the final film can be controlled by controlling the size and extent of branching of the reacted species in the sol prior to film deposition. Also the contribution of the competition between evaporation and continuing condensation reactions is crucial for the final film structure. If the rate of evaporation is significantly higher than the condensation, it results in a more compact film structure and vice versa. After the film deposition films are heat-treated, typically the heat-treatment temperature for sol-gel derived films is between 80–500˚C. Dip-coating can be done at room-temperature which allows the preparation of ceramic coatings at lower temperatures.

Since the ceramic coatings are deposited from colloidal sols, film thickness, surface area, porosity etc. can be controlled. In Figure 3 is schematically presented how the colloidal structure in the sol has an effect on the film surface topography. Furthermore, sol-gel dip-coating method is cost effective and technically simple giving the possibility to coat substrates with difficult geometries.

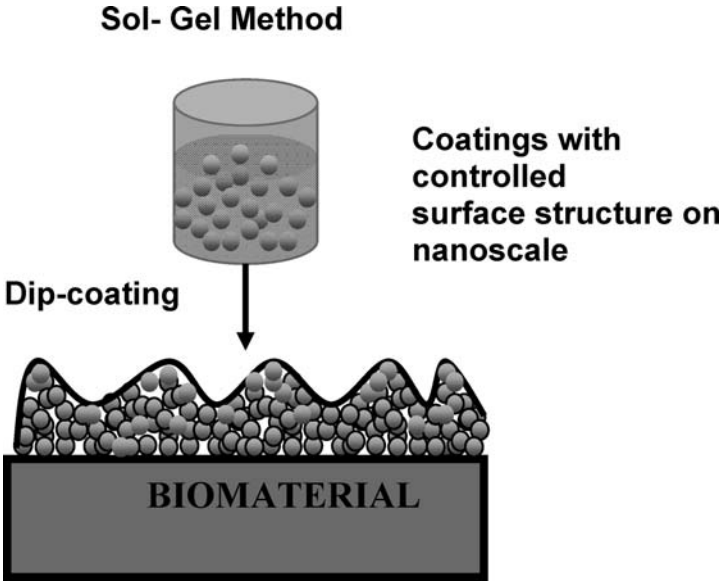

Figure 3. A schematic presentation of sol-gel dip-coating method.

It is now well established that the sol-gel derived titania coatings promote bone bonding (class B) via the formed bone mineral-like calcium phosphate on their surfaces *in vitro* and *in vivo*.[49–51] The use of sol-gel-derived titania coatings is also motivated by the fact that a nonresorbable, reactive coating might guarantee a direct and immediate contact between the implant and the tissues, whereas for resorbable reactive coatings, the underlying inert substrate might be exposed during long-term implantation. Although, titanium metal and metal alloy implants have been shown to leach metal ions during long-term implantation[52,53] the titania (TiO_2) is not degraded and it is thought to be stable in the body environment. Furthermore, coatings thinner than 1 μm are known to possess self-healing properties due to crack and dislocation annihilation, providing enhanced material toughness as for the whiskers and glass fibers, which get more elastic as they get thinner[54] Also the energy required for coating self-healing becomes smaller the thinner the coating. One of the attractive features of the application of TiO_2-sol-gel derived coatings lays in the possibility of local processing, for example with a focused CO_2-laser beam.

4.4.1. *Modification of Titania Coatings with Laser Processing*

Sol-gel derived TiO_2 coatings can be locally treated with CO_2 laser beam, achieving local modification of the bioactive properties of the surface.[56–58] The use of a CO_2 laser is based on the fact that the radiation on the 10.6 μm wavelength is absorbed by the titania film. Besides, CO_2 lasers are rather common and inexpensive devices. The output of the laser can be controlled to obtain the desired effect on the surface.[58–60] Unlike the traditional furnace firing direct laser densification of sol-gel derived TiO_2 coatings allows the selective treatment of the surface of the coating. Further, the surface is only heated locally in the proximity of its surface. This permits the manufacture of the coatings with different areas of the same coating having different properties and coatings of implant materials other than titanium, including those that do not withstand extensive heat-treatment. The CO_2 laser treatment on the sol-gel-derived TiO_2-coatings has been successfully applied in inducing *in vitro* calcium phosphate formation either as post treatment method or as direct densification after dip-coating.[55,56]

4.5. BIOACTIVE PROPERTIES OF SOL-GEL DERIVED TITANIA COATINGS

The heat-treatment of sol-gel derived TiO_2 coatings at different temperatures produces titanates with different structures i.e. amorphous, anatase or rutile (in the order of increasing calcination temperature). The amount of hydroxyl groups on the TiO_2 film depends also on the heat-treatment temperature, the higher the heat-treatment temperature less OH-groups will remain on the film.[61–64] It has

been shown that hydroxyl groups and the negatively charged surface at pH 7.4 are properties which enhance the chemical bonding of TiO_2 coatings to bone. In addition, there is also evidence of strong surface structural dependence to the calcium phosphate formation properties on these coatings. The surface topography at the nanometer level has been shown to influence the *in vitro* bioactivity. This phenomenon was related to the charge density and the topographical matching of the titania surface and calcium phosphate crystal size found in bone (i.e. not with the matching of the atomic distances in single crystals) as shown in Figure 4.[65–67] It was shown that the anatase structure favours bone minerallike hydroxyapatite formation compared to rutile when the rutile is produced by increased heat-treatment temperatures [70,71]. One possible reason could be that the crystallographic lattice match of anatase and hydroxyapatite (HA) is closer to each other than that of rutile and HA.[68,69]

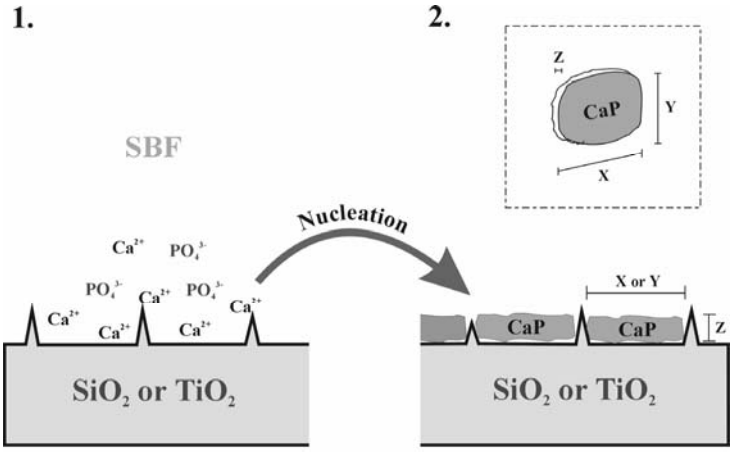

Figure 4. The most favourable dimensions on the titania surface for the formation of calcium phosphate match the natural size of calcium phosphate crystals in bone (plate-like calcium phosphate crystals, X = 20 nm, Z,Y = 3–7 nm).[73–74]

Calcium phosphate nucleation ability of TiO_2 coatings with different crystal structure is studied in simulated body fluid and it is shown that *in vitro* bioactivity was enhanced on the coatings with existence of surface OH-groups and anatase crystal phase. It was shown that the anatase structure favours bone minerallike hydroxyapatite formation compared to rutile when the rutile is produced by increased heat-treatment temperatures.[70,71] However, when the rutile phase on the coatings coatings were produced by the laser induced thermal "shock" treatment (i.e. the surface OH-groups are not removed by extensive heat-treatment) it was observed that the as prepared rutile phase favors the bone mineral-like hydroxyapatite formation compared to the anatase phase prepared by conventional heat treatment.[57] It should be noted that the bone mineral-like hydroxyapatite formation

experiments were done in a competing system where the coatings having anatase and rutile structures were in the same flask and these results are not interpreted so that the anatase coatings produced by laser treatment are not bioactive at all. These results indicate that the precise lattice matching of anatase and HA is not a crucial factor in the in vitro properties of TiO_2 based coatings.

A possible reason for the low bioactivity of amorphous TiO_2 may be that particle size on the film surface is smaller than what is required for the optimal topographical features. During the film densification (e.g. by heat- or laser-treatment) the deposited particles form particles and/or aggregates, and the final surface structure is formed. Furthermore, during densification the mechanical and chemical stability of the coating is enhanced. Following this reasoning bioactive amorphous TiO_2 coatings could be obtained if the initial deposited particles and/or aggregates are large enough although their mechanical properties and chemical stability probably remains too poor for practical application.

The influence of topography on calcium phosphate formation on sol-gel derived TiO_2 coatings is shown experimentally using AFM image analysis.[65,66] By controlling the particle size and particle size distribution in the dipping sol, the surface topography on the nanometer scale can be varied. It was concluded that the optimal topographical features of the outermost surface for calcium phosphate formation was in the range of 2–50 nm (as obtained from the line section analysis of the AFM images in vertical and lateral directions). It should be noted that also the highly bioactive rutile containing coatings exhibited such topographical features.[57] The aspect of topography on nucleation of inorganic solids has been well studied in the context of organic matrix-mediated biomineralization processes. It has been stated that "electrostatic accumulation of ions on organic surfaces is influenced by the localized clustering of ligands and their spatial charge distribution, which in turn depend on the surface structure and topography". For example, surfaces with concave-like topographical features give rise to a high spatial charge density and 3-D clustering of ions and are thus good nucleation sites.[72] This theory has been applied in one model of bone mineralization where the calcium phosphate nucleation is proposed to occur in regiospecific hole zones of collagen having a distinct size and topography.

A firm bond between the soft tissue and implant is also important for the performance of many medical devices like stents, canyls and dental implants. It is shown that the sol-gel derived titania coatings can bond also to soft tissue. A direct attachment between soft tissue and sol-gel derived titania coating was found in vivo after 2 days of implantation in rats, where as the titanium control implants showed no evidence of soft tissue attachment. The coated implants were in immediate contact with connective tissue, whereas the titanium controls formed a gap and a fibrous capsule on the implant-tissue interface. The good soft tissue attachment of titania coatings may result from their ability to initiate

calcium phosphate nucleation and growth on their surfaces in vitro, thus the formation of bone mineral-like calcium phosphate layer is not crucial for their integration in soft tissue.[73]

5. Conclusions

Both silica and titania based materials can be produced with sol-gel method and can be used as biomaterial in different applications. Sol-gel derived silica and titania are biocompatible and can be used in direct contact with different organisms e.g. microbes and living tissue. The main parameter controlling the beneficial interactions between silica and living organisms is nanoscale and molecular structure of sol-gel derived silica combined with a large amount water in structure during encapsulation in silica structure. Whereas the most important driving force for calcium phosphate nucleation on sol-gel derived TiO_2 coatings is the electrostatic accumulation of ions in the localized regions (grooves and/or pockets) of high spatial charge density. This can be achieved with the negatively charged TiO_2 surface at pH 7.4 and also the surface topography has to be suitable the calcium phosphate nucleation. It is shown that sol-gel derived titania films can bond to living bone and soft tissue.

Acknowledgement

This research is financially supported by Academy of Finland grant no: 114117.

References

1. L. Hench, R. J. Splinter, W. C. Allen and T.K. Greenlee, Bonding mechanisms at the interface of ceramic prosthetic materials, *J. Biomed. Mater. Res.* 2, 117–141 (1971).
2. L. L. Hench and J. Wilson, *Introduction to Bioceramics* (World Scientific, Singapore, 1993).
3. D. Avnir, S. Braun, O. Lev and M. Ottolenghi, Enzymes and other proteins entrapped in sol-gel materials, *Chem. Mater.* 6, 1605–1614 (1994).
4. I. Gill and A. Ballesteros, Bioencapsulation within synthetic polymers (Part 1): sol-gel encapsulated biologicals, *Trends Biotech.* 18, 282–196 (2000).
5. I. Gill, Bio-doped nanocomposite polymers: sol-gel bioencapsulates, *Chem. Mater.* 13, 3404–3421 (2001).
6. J. Livage, T. Choradin and C. Roux, Encapsulation of biomolecules in silica gels, *J. Phys. Condens. Matter*, 13, R673–R691 (2001).
7. C. J. Brinker and G. W. Scherer, *Sol-Gel Science: The Physics and Chemistry of Sol-Gel Processing* (Academic, San Diego, CA, 1990).
8. S. Sakka and H. Kozuka, *Sol-Gel Processing* (Kluwer, New York, 2005).

9. R. K. Iler, *The Chemistry of Silica: Solubility, Polymerization, Colloid and Surface Properties, and Biochemistry* (Wiley, New York, 1979).
10. R. Viitala, M. Jokinen, S. L. Maunu, H. Jalonen and J. B. Rosenholm, Chemical characterization of bioresorbable sol-gel derived SiO_2 matrices Prepared at Protein-Compatible pH, *J. Non-Cryst. Solid.*, 351, 3225–3234 (2005).
11. R. Viitala, M. Jokinen, J. B. Rosenholm, Mechanistic studies on release of large and small molecules from biodegradable SiO_2, *Int. J. Pharm.* 336, 382–390 (2007).
12. M. Koskinen, M. Toriseva, M. Jokinen, H. Jalonen, J. Salonen and V.-M. Kähäri, Silica gel in targeted and controlled viral gene therapy, *Mol. Ther.* 11, S422–S427 (2005).
13. P. Kortesuo, M. Ahola, S. Karlsson, I. Kangasniemi, A. Yli-Urpo and J. Kiesvaara, Silica xerogels as an implantable carrier for controlled drug delivery – evaluation of drug distribution and tissue effects after implantation, *Biomaterials*, 21, 193–198 (2000).
14. M. Koskinen, E. Säilynoja, M. Ahola, H. Jalonen, J. Salonen and V.-M. Kähäri, Biodegradable carrier and method for preparation thereof, *PCT Publication*, WO02/80977 (2002)
15. M. Jokinen, M. Koskinen and H. Jalonen, Method of storing silica-based material, package produced with the method and use of package for packing of silica-based products, *PCT Publication*, WO2007/135224 (2007).
16. H. Knienapfel, C. Sprey, A. Wilke and P. Griss, Implant fixation by bone ingrowth. *J. Arthoplasty*, 14, 355–368 (1999).
17. H. U. Cameron, R. M. Pilliar and I. Macnab, The rate of bone ingrowth into porous metal. *J. Biomed. Mater. Res.*, 10, 295–302 (1976).
18. J. D. Bodyn, R. M. Pilliar, H. U. Cameron and G. C. Weatherly, The optimum pore size for the fixation of porous-surfaced metal implants by the ingrowth of bone. *Clin. Orthop.*, 150, 263–270 (1980).
19. D. Buser, R. K. Schenk, S. Steinemann, J. P. Fiorellini, C. H. Fox and H. Stich, Influence of surface characteristics on bone integration of titanium implants. A histomorphometric study in miniature pigs. *J. Biomed. Mater. Res.*, 25, 889–902 (1991).
20. M. Wong, J. Eulenberger, R. Schenk and E. Hunziker, Effect of surface topology on the osseointegration of implant materials in trabecular bone. *J. Biomed. Mater. Res.*, 29, 1567–1575 (1995).
21. A. Wennerberg, T. Albrektsson, B. Andersson and J. J. Krol, A histomorphometric and removal torque study of screw-shaped titanium implants with three different surface topographies, *Clin. Oral. Impl. Res.*, 6, 24–30 (1995).
22. T. Hayakawa, M. Yoshinari, H. Kiba, H. Yamamoto, K. Nemoto and J. A. Jansen, Trabecular bone response to surface roughened and calcium phosphate (Ca-P) coated titanium implants, *Biomaterials*, 23, 1025–1031 (2002).
23. S. Areva, *Sol-Gel Derived Titania Based Ceramic Thin Films for Implant Coatings*, Ph.D. thesis, Åbo Akademi University (Åbo Akademi tryckeri, Turku, 2006).
24. H. M. Kim, T. Himeno, M. Kawashita, J. H. Lee, T. Kokubo and T. Nakamura, Surface potential change in bioactive titanium metal during the process of apatite formation in simulated body fluid, *J. Biomed. Mat. Res. Part A*, 67A, 1305–1309 (2003).
25. P. Tengvall, H. Elwing, L. Sjöqvist, I. Lundström and L. M. Bjursten, Interaction between hydrogen peroxide and titanium: A possible role in the biocompatibility of titanium, *Biomaterials*, 10, 118–120 (1989).
26. P. Tengvall, I. Lundström, L. Sjöqvist and H. Elwing, Titanium-hydrogen peroxide interaction: model studies of the influence of the inflammatory response on titanium implants, *Biomaterials*, 10, 166–175 (1989).
27. P. Tengvall and I. Lundström, Physico-chemical considerations of titanium as a biomaterial: Review paper. *Clin. Mater.*, 9, 115–134 (1992).

28. P. Tengvall, H. Elwing and I. Lundström, Titanium gel made from metallic titanium and hydrogen peroxide, *J. Colloid. Inter. Sci.*, 130, 405–413 (1989).
29. J.-M. Wu, S. Hayakawa, K. Tsuru and A. Osaka, Low-temperature preparation of anatase and rutile layers on titanium substrates and their ability to induce in vitro apatite deposition, *J. Am. Chem. Soc.*, 87, 1635–1642 (2004).
30. C. Ohtsuki, H. Iida, S. Hayakawa and A. Osaka, Bioactivity of titanium treated with hydrogen peroxide solution containing metal chlorides, *J. Biomed. Mater. Res.*, 35, 39–47 (1997).
31. X.-X. Wang, S. Hayakawa, K. Tsuru and A. Osaka, A comparative study of in vitro apatite deposition on heat-. H_2O_2-. and NaOH-treated titanium surfaces. *J. Biomed. Mater. Res.*, 54, 172–178 (2001).
32. J.-M. Wu, S. Hayakawa, K. Tsuru and A. Osaka, Porous titania films prepared from interactions of titanium with hydrogen peroxide solution, *Scripta Materialia*, 46, 101–106 (2002).
33. R. G. T. Geesink, K. de Groot and C. P. A. T. Klein, Chemical implant fixation using hydroxyl-apatite coatings, *Clin. Orthop.*, 225, 147–170 (1987).
34. K. de Groot, R. Geesing, C. P. A. T. Klein and P. Serekian, Plasma sprayed coatings of hydroxylapatite, *J. Biomed. Mater. Res.*, 21, 1375–1381 (1987).
35. M. Ogiso, M. Yamamura, P. T. Kuo, D. Borgese and T. Matsumoto, A comparative push-out test of dense HA implants and HA-coated implants: findings in a canine study, *J. Biomed. Mater. Res.*, 39, 364–372 (1998).
36. W. J. A. Dhert, C. P. A. T. Klein, J. G. C. Wolke, E. A. van der Velde, K. de Groot and P. M. Rozing, A mechanical investigation of fluorapatite, magnesiumwhitlockite, and hydroxylapatite plasma-sprayed coating on goats, *J. Biomed. Mater. Res.*, 25, 1183–1200 (1991).
37. E. C. Combe, F. J. T. Burke and W. H. Douglas, *Dental Biomaterials* (Kluwer, London, 1999).
38. T. J. Webster, C. Ergun, R. H. Doremus, R. W. Siegel and R. Bizios, Specific proteins mediate enhanced osteoblast adhesion on nanophase ceramics, *J. Biomed. Mater. Res.*, 51, 475–483 (2000).
39. T. J. Webster, C. Ergun, R. H. Doremus, R. W. Siegel and R. Bizios, Enhanced osteoclast-like cell functions on nanophase ceramics, *Biomaterials*, 22, 1327–1333 (2001).
40. M. J. Dalby, M. O. Richle, H. Johnstone, S. Affrossman and A. S. G. Curtis, In vitro reaction of endothelial cells to polymer demixed nanotopography, *Biomaterials*, 23, 2945–2954 (2002).
41. M. J. Dalby, M. O. Richle, D. S. Sutherland, H. Agheli and A. S. G. Curtis, Fibroblast response to a controlled nanoenvironment produced by colloidal lithography, *J. Biomed. Mater. Res.*, 69, 314–322 (2004).
42. T. Brendel, A. Engel and C. Russel, Hyrdoxyapatite coating by a polymeric route, *J. Mater. Sci. Mater. Med.*, 3, 175–179 (1992).
43. Q. Qiu, P. Vincent, B. Lowenberg, M. Sayer and J. E. Davies, Bone growth on sol-gel calcium phosphate thin films in vitro. *Cells Mat.*, 3, 351–360 (1993).
44. D. B. Haddow, P. E. James and R. van Noort, Characterization of sol-gel surfaces for biomedical applications, *J. Mater. Sci. Mater. Med.*, 7, 255–260 (1996).
45. W. Weng and J. L. Baptista, Sol-gel derived porous hydroxyapatite coatings, *J. Mater. Sci. Mater. Med.*, 9, 159–163 (1998).
46. K. A. Gross, C. S. Chai, G. S. K. Kannangara, B. Ben-Nissan and L. Hanley, Thin hydroxyapatite coatings via sol-gel synthesis, *J. Mater. Sci. Mater. Med.*, 9, 839–843 (1998).
47. D. M. Liu, Q. Yang and T. Troczynski, Sol-gel hydroxyapatite coatings on stainless steel substrates, *Biomaterials*, 23, 691–698 (2002).
48. L. Gan and R. Pilliar, Calcium phosphate sol-gel-derived thin films on porous-surfaced implants for enhanced osteoconductivity. Part I: Synthesis and characterization, *Biomaterials*, 25, 5302–5312 (2005).

49. P. Li and K. de Groot, Calcium phosphate formation within sol-gel prepared titania *in vitro* and *in vivo*, *J. Biomed. Mater. Res.*, 27, 1495–1500 (1993).
50. P. Li, K. de Groot and T. Kokubo, Bonelike hydroxyapatite induction by sol-gel derived titania coating on a titanium substrate, *J. Am. Ceram. Soc.*, 77, 1307–1315 (1994).
51. T. Peltola, M. Pätsi, H. Rahiala, I. Kangasniemi and A. Yli-Urpo, Calcium phosphate induction by sol-gel-derived titania coatings on titanium substrates in vitro, *J. Biomed. Mater. Res.*, 41, 504–510 (1998).
52. P. Lalor and P. Revell, T-lymphocytes and titanium aluminum vanadium (TiAlV) alloy: evidence for immunological events associated with debris deposition. *Clin. Mater.*, 12, 57–62 (1993).
53. H. P. von Schroeder, D. C. Smith, A. E. Gross, R. M. Pilliar, R. A. Kandel, R. Chernecky and S. J. Lugowski, Titanemia from total knee arthoplasty, *J. Arthoplasty*, 11, 620–625 (1996).
54. J. E. Gordon, *The New Science of Strong Materials or Why You Don't Fall Through the Floor* (Penguin Books, England, 1976).
55. N. Moritz, M. Jokinen, T. Peltola, S. Areva and A. Yli-Urpo, Local induction of calcium phosphate formation on TiO_2 coatings on titanium via surface treatment with a CO_2 laser, *J. Biomed. Mater. Res.*, 65, 9–16 (2003).
56. N. Moritz, E. Vedel, H. Ylänen, M. Jokinen, T. Peltola, S. Areva, M. Hupa and A. Yli-Urpo, Bioactive glass and sol-gel-derived TiO_2 coatings, *Mat. Tech. Adv. Perf. Mat.*, 1, 29–32 (2003).
57. N. Moritz, S. Areva, J. Wolk and T. Peltola, TF-XRD examination of surface reactive TiO_2 coatings produced by heat-treatment and CO_2-laser treatment, *Biomaterials*, 26, 4460–4467 (2005).
58. D. J. Taylor, D. P. Birnie and B. D. Fabes, Temperature calculations for laser irradiated sol-gel films on oxide substrate, *J. Mater. Res.*, 10, 1429–1434 (1995).
59. S. Pelli, G. C. Reghine, A. Scaglione, C. Ascoli, C. Frediani, A. Martucci and M. Guglielmi, Characterization of laser written sol-gel strip waveguides, *SPIE Proc.*, 2288, 573–590 (1994).
60. S. Pelli, G. C. Reghine, A. Scaglione, M. Guglielmi and A. Martucci, Direct writing of ridge optical waveguides on silica- titania glass sol-gel films, *J. Opt. Mater.*, 5, 119–126 (1996).
61. R. E. Day and G. D. Parfitt, Characterization of the surface of rutile by nitrogen and water vapour adsorption, *Trans. Faraday Soc.*, 63, 708–716 (1967).
62. K. E. Lewis and G. D. Parfitt, Infra-red study of the surface of rutile, *Trans Faraday Soc.*, 62, 204–214 (1965).
63. W. H. Wade and N. Hackerman, Heats of immersion in TiO_2-H_2O system-variations with particle sizes and outgassing temperature, *J. Phys. Chem.*, 65, 1681–1683 (1961).
64. C. Monterra, An infrared spectroscopic study of anatase properties. Part 6. Surface hydration and strong lewis acidity of pure and sulphate-doped preparations, *J. Chem. Soc. Faraday Trans.*, 1, 1617–1637 (1988).
65. M. Jokinen, M. Patsi, H. Rahiala, T. Peltola, M. Ritala and J. B. Rosenholm, Influence of sol and surface properties on in vitro bioactivity of sol-gel-derived TiO_2 and TiO_2-SiO_2 films deposited by dip-coating method, *J. Biomed. Mater. Res.*, 4, 295–302 (1998).
66. T. Peltola, M. Jokinen, H. Rahiala, M. Pätsi, J. Heikkilä, I. Kangasniemi and A. Yli-Urpo, Effect of aging time of sol on structure and in vitro calcium phosphate formation of sol-gel-derived titania films, *J. Biomed. Mater. Res.*, 51, 200–208 (2000).
67. T. Peltola, H. Paldan, N. Moritz, S. Areva, J. Korventausta, M. Jokine, T. Narhi, R. P. Happonen and A. Yli-Urpo, Methods to enhance biomimetic activity and ability to tissue bonding of sol-gel-derived nanoporous titania, *Key Eng. Mat.*, 218–220, 207–212 (2002).
68. M. Uchida, H. M. Kim, T. Kokubo and T. Nakamura, Structural dependence of apatite formation on titania gel in simulated body fluid, *J. Biomed. Mater. Res.*, 64, 164–170 (2003).

69. J.-M. Wu, S. Hayakawa, K. Tsuru and A. Osaka, Low-temperature preparation of anatase and rutile layers on titanium substrates and their ability to induce in vitro apatite deposition, *J. Am. Chem. Soc.*, 87, 1635–1642 (2004).
70. W. A. Ganong and A. Lange, *Medical Book: Review of Medical Physiology* (Lange Medical Publications, Los Altos, CA, 1987).
71. T. Peltola, *Nanoscale Dimensions and In Vitro Calcium Phosphate Formation: Studies on Sol-Gel Derived Materials and Bioactive Glass*, Ph.D. thesis, University of Turku (Typopress Oy, Turku, 2000).
72. S. Mann, *Biominerilization* (Oxford University Press, Oxford, 2001).
73. S. Areva, P. Paldan, T. Peltola, T. Närhi, M. Jokinen and M. Lindén, Use of sol-gel derived titania coating for direct soft tissue attachment, *J. Biomed. Mater. Res.*, 70A, 169–178 (2004).

MESOPOROUS SILICAS: MORPHOLOGY CONTROL AND TEMPLATE SYNTHESIS INSIDE LARGE PORES OF SILICA GEL

INNA S. BEREZOVSKA*, VIKTOR V. YANISHPOLSKII, VALENTIN A. TERTYKH
O.O. Chuiko Institute of Surface Chemistry of National Academy of Sciences of Ukraine 17 General Naumov Str., 03164 Kyiv, Ukraine

Abstract. The influence of pH, nature of alcohol and initial components concentrations in micellar solution on the structural-adsorption characteristics of spherical mesoporous silicas has been investigated. The peculiarities of template synthesis of mesoporous silicas inside large pores of silica gel were also studied. Synthesized silicas were characterized by low-temperature nitrogen adsorption-desorption, X-ray diffraction and scanning electronic microscopy.

Keywords: Mesoporous silica, template synthesis, spherical particles, MCM-41, nanoporous reactor.

1. Introduction

The use of supramolecular micellar templates for synthesis of ordered mesoporous materials is considered as one of the most important discoveries in the field of materials science. The ability of this approach to design nanoscale pore structure is being intensively investigated with the aim to create new type of catalysts and adsorbents.[1,2] Pore structure control and regulation of macroscopical shape of mesoporous silicas are the current trends in the template synthesis of ordered porous materials.[3–5] Besides, the improvement of MCM-41 silicas mechanical stability is a significant parameter for MCM-41 appli-cation. In the present paper the optimal conditions for synthesis of mesoporous silicas with spherical morphology of particles were determined. It was also proposed an approach for improvement of mechanical properties of the nano-materials by carrying out template synthesis of mesoporous silicas inside pore volume of silicas with more stable porous structure.

* To whom correspondence should be addressed: Berezovska I., Institute of Surface Chemistry, NAS of Ukraine, 17 General Naumov Str., 03164 Kyiv, Ukraine; e-mail: berinna2003@rambler.ru

P. Innocenzi, Y. L. Zub and V. G. Kessler (eds.), *Sol-Gel Methods for Materials Processing*.

2. Experimental

2.1. SYNTHESIS OF MESOPOROUS SILICAS WITH SPHERICAL MORPHOLOGY OF PARTICLES

Syntheses were carried out in the alcohol-ammonia media by the modified Stöber method[6] in ethanol and isopropanol using tetraethoxysilane (TEOS) as a silica precursor and cetyltrimethylammonium bromide (CTAB) as supramolecular template with the molar ratio of components 1TEOS: xCTAB: 11NH_3 : 144H_2O : 58ROH, where X = 0.1, 0.2 and 0.3. Synthesis in the acidic media was held using TEOS and CTAB with the molar ratio of components 1TEOS: 0.1CTAB: 0.45HCl: 100H_2O.

2.2. SYNTHESIS OF MESOPOROUS SILICAS IN NANOREACTORS BASED ON LARGE PORES OF SILICA GEL

Step-by-step incorporations of micellar solutions inside pore volume of silica gel with the surface area about 115 m^2/g and the average pore diameter about 24 nm were made. Micellar solution with molar ratio of components 1TEOS: 0.18CTAB: 5NH_3: 75H_2O was prepared according to procedure.[7]

After template elimination the synthesized materials were characterized by low-temperature adsorption-desorption of nitrogen (ASAP-2000) to estimate surface area (BET equation), pore size distribution (BJH method). Structure of samples was determined by X-ray diffraction at small angles. Scanning electronic microscopy was used to investigate particle size and morphology of the synthesized silica materials.

3. Results and Discussions

3.1. SYNTHESIS OF MESOPOROUS SILICAS WITH SPHERICAL MORPHOLOGY OF PARTICLES

Nitrogen adsorption-desorption isotherms for silicas synthesized in the alcohol-ammonia media using ethanol at different molar ratios to CTAB/TEOS are type IV in the IUPAC classification.8 In the interval of relative pressures p/po = 0.15–0.27 the range of capillary condensation with steep increase in the adsorbed nitrogen is observed. Surface areas of the synthesized silicas were 700–1,200 m^2/g, pore sizes determined by the BJH-method are 2.5–3.0 nm. Nitrogen adsorption-desorption isotherms for the silicas synthesized in the alkaline media with use of isopropanol with molar ratio of CTAB/TEOS = 0.2 and 0.3 are also the type IV in the IUPAC classification, surface areas of synthesized

samples are 400–500m^2/g. Nitrogen adsorption isotherm for silicas synthesized in acidic media is the type I in IUPAC classification, surface area of synthesized sample is 600m^2/g (Figure 1).

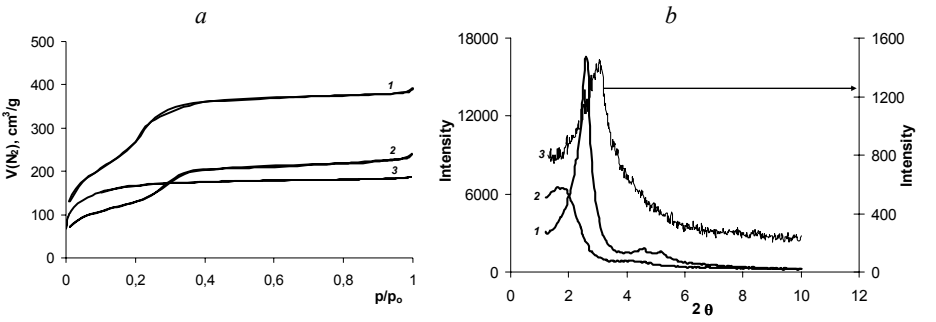

Figure 1. Nitrogen adsorption-desorption isotherms (a) and diffractograms (b) for silicas synthesized in the alkaline media using ethanol (1) or isopropanol (2) in acidic media (3).

X-ray powder patterns of silicas synthesized in ethanol with ratio of TEOS/CTAB = 0.3 and 0.2 show three Braggs peaks in the range of 2θ = 2.5–7.0 with (100), (110) and (200) indexes, characterizing the periodic structures with the hexagonal pore orientation. X-ray powder patterns of silicas synthesized in isopropanol with molar ratio of CTAB/TEOS = 0.2 and 0.3 have only one marked peak. Lattice parameter a_o (a distance between cylindrical pore centers) is estimated by $a_o = 2d_{100}/3^{0.5}$. Pore thickness is determined according to the formula $h = a_o - d_p$, where d_p – a pore diameter determined by the BJH-method; and the values of *h* are 1.4–2.0 nm that are typical for the MCM-41 silicas.[9] X-ray powder patterns of silicas synthesized in acidic media have only one peak characterizing a weakly ordered pore structure (Figure 2). Structural-adsorption characteristics of the materials synthesized in the alcohol-ammonia media are presented in the Table 1.

TABLE 1. Structural-adsorption characteristics of materials synthesized in the alcohol-ammonia media.

CTAB/TEOS molar ratio	Alcohol	Structure	a_o (nm)	d_p (nm)	Surface area (m^2/g)
0.1	Isopropanol	Disordered	–	3.4	166
0.2	Isopropanol	Disordered	–	3.0	505
0.3	Isopropanol	Disordered	–	3.1	458
0.1	Ethanol	Weakly ordered	5.2	3.0	701
0.2	Ethanol	Hexagonal ordered	4.0	2.7	1,227
0.3	Ethanol	Hexagonal ordered	3.9	2.5	946

Scanning electronic microscopy results for silicas synthesized with molar ratio of CTAB/TEOS = 0.3 testify the unimodal spherical particles of 0.5μ size. The silicas synthesized in hydrochloride acid, unlike the alkaline media samples, have larger particle diameter and SEM-photos show spherical particles of 10μ size (Figure 3). The final particles size depends on the rates of precursor silica hydrolysis and further polycondensation of hydrolysis products. In the alkaline media fast hydrolysis and polycondensation provide the formation spherical particles after two-hours stirring. On the contrary, slow condensation rate in the acidic media is favor for the larger size particles growth. Mesophase for-mation in the acidic media is possible due to halide anions coordination of positive charged micellar aggregates and silica surface. Such weak interactions are considered to provide the organization of weakly ordered pore structure. In the alkaline media pore structure formation is a result of direct interaction between silica macroanions and positive charged CTAB micelles. Thus, in the alcohol-ammonia media mesoporous silicas with the ordered hexagonal pore structure and high specific surface area have been synthesized.

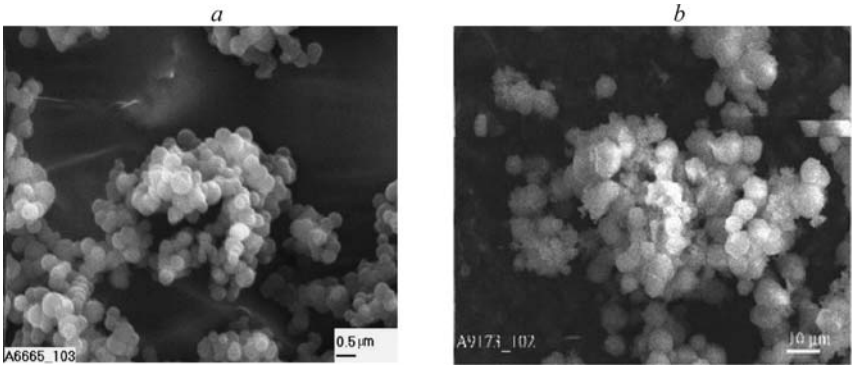

Figure 2. SEM-photos of silicas synthesized in the ethanol-ammonia media with molar ratio of CTAB/TEOS = 0.3 (a) and in the acidic media with molar ratio of CTAB/TEOS = 0.1 (b).

Particles of unimodal spherical granulation have been obtained in ethanol using molar ratio of CTAB/TEOS = 0.2 and 0.3. Porous silicas with weakly ordered pore structure and spherical particles of 10 μ size have been synthesized in the acidic media.

3.2. SYNTHESIS OF MESOPOROUS SILICAS INSIDE NANOREACTORS BASED ON LARGE PORES OF SILICA GEL

Nitrogen adsorption-desorption isotherm for silica gel is a type III in the IUPAC classification,[8] has a hysteresis loop at high relative pressure and reveals the existence of large pores in the sample. Nitrogen adsorption-desorption isotherms

of silica gel after template syntheses inside nanopores are characterized by appearance of capillary condensation ranges ($0.3 < p/p_o < 0.4$) and testify the mesopores presence. The sharpness of these sections was increased after each template synthesis and accompanied with decreasing of hysteresis loop that can be explained by filling of silica gel pore volume with mesoporous silicas.

Specific surface area of the initial silica gel is 115 m^2/g (by the BET-equation) and the BJH pore size distribution curve for silica gel has a broad peak in the range of pore size 30–50 nm (Figure 3, curve 1). Samples with incorporated mesoporous silicas are characterized by increase in specific surface area from 115 up to 377 m^2/g (Figure 3*a*). Pore size distributions curves exhibit the presence of peaks corresponding to pores of 2.5 nm size (Figure 3*c*).

Absence of any peaks in the X-ray powder patterns of initial silica gel confirms its amorphous nature (Figure 3*b*, curve 1). It is clear from X-ray diffraction patterns that introduction of micellar solution increases the reflections' intensity in the low-angle region (Figure 3b, curves 2–7). Broad low angle diffraction peak should result from the formation of wormlike pore structure and weak intensity of reflection can be explained by small quantity of incorporated silicas (20% of sample total weight after the sixth introduction of

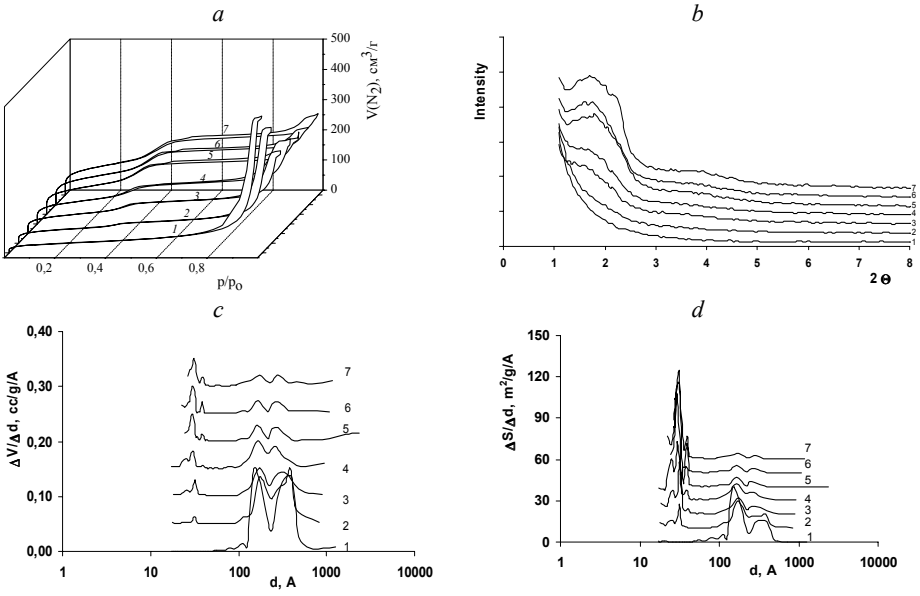

Figure 3. Nitrogen adsorption-desorption isotherms (a), diffractograms (b) and differential curves of dependence of pore size on pore volume (c) and surface area (d) for silicas synthesized inside large pores of silica gel: initial silica gel (1) and silica gels after the first (2), the second (3), the third (4), the fourth (5), the fifth (6), the sixth (7) introducing of MCM-41.

TABLE 2. Structural-adsorption characteristics of synthesized silicas (where S_{BET} – specific surface area by BET-equation; S_t – total surface area, S_{ex} – external surface area, S_p – pore surface area, V_p – pore volume, V_c – core volume and r_p – mesopore radius estimated by α_s-analysis).

N	Samples	S_{BET} (m^2/g)	α_s-analysis					
			S_t (m^2/g)	S_{ex} (m^2/g)	S_p (m^2/g)	V_p (cm^3/g)	V_c (cm^3/g)	r_p (nm)
1	Initial silica gel	115	116	–	–	0.615	–	–
2	Silica gel after the first introduction o f micellar solution	170	173	–	–	0.54	0.018	–
3	Silica gel after the second introduction of micellar solution	233	237	–	–	0.34	0.033	–
4	Silica gel after the third introduction of micellar solution	283	289	11.56	277	0.32	0.060	1.3
5	Silica gel after the fourth introduction of micellar solution	349	347	5.78	341	0.34	0.079	1.3
6	Silica gel after the fifth introduction of micellar solution	362	364	5.78	358	0.35	0.098	1.4
7	Silica gel after the sixth introduction of micellar solution	377	376	5.78	370	0.36	0.105	1.4

micellar solution). Structural-adsorption characteristics of synthesized silicas were estimated by α_s-analysis.[8,10]

Elaborated synthetic procedures are systematic combination of template synthesis and conventional sol-gel process. Syntheses were realized via two stages: at the first stage silica gel was impregnated with micellar solution and at the second stage ammonia was added in order to catalyze hydrolysis and condensation of TEOS to provide mesoporous silicas formation. The main condition for successful template synthesis inside pores of silica gel matrix was a high value of TEOS/H_2O molar ratio. Template synthesis of mesoporous silicas with pore diameter of 2.5 nm were carried out inside nanoreactors based on large pores of silica gel. Specific surface area of initial silica gel was 115 m^2/g and after micellar solution introducing the calcined samples had surface area about 377 m2/g.

References

1. Ciesla U., Schuth F., Ordered mesoporous materials, *Micropor. Mesopor. Mat.*, 27, 131–149 (1999).
2. Corma A., From microporous to mesoporous molecular sieve materials and their use in catalysis, *Chem. Rev.*, 97, 2373–2420 (1997).
3. Grun M., Unger K.K., Matsumoto A., Tsutsumi K., Novel pathways for the preparation of mesoporous MCM-41 materials: control of porosity and morphology, *Micropor. Mesopor. Mat.*, 27, 207–216 (1999).
4. Sierra L., Lopez B., Guth J.-L., Preparation of mesoporous silica particles with controlled morphology from sodium silicate solutions and a non-ionic surfactant at pH values between 2 and 6, *Micropor. Mesopor. Mat.*, 39, 519–527 (2000).
5. Yang H., Vovk G., Coombs N., Sokolov I., Ozin G.A., *J. Mater. Chem*., 8, 743 (1998).
6. Stöber W., Fink A., Bohn E., Controlled growth of monodisperse silica spheres in the micron size range, *J. Colloid Interface Sci.*, 26, 62–69 (1968).
7. Hakuman M., Naono H., A new method of calculating pore size distribution: analysis of adsorption isotherms of N_2 and CCl_4 for a series of MCM-41 mesoporous silicas, *J. Colloid Interface Sci*., 241, 127–141 (2001).
8. Parfitt G.D., Sing K.S.W., Characterization of powder surfaces, Academic, London (1976).
9. Wang X., Li W., Zhu G., Qiu S., Zhao D., Zhong B., Effects of ammonia/silica molar ratio on the synthesis and structure of bimodal mesopore silica xerogel, *Micropor. Mesopor. Mat.*, 71, 87–97 (2004).
10. Jaroniec M., Kruk M., Standard nitrogen adsorption data for characterization of nanoporous silicas, *Langmuir*, 15, 5410–5413 (1999).

HYBRID SILOXANE-POLYAMINOAMIDES FOR THE ABSORPTION OF HEPARIN FROM BLOOD

DANIELE CAUZZI*, ALESSANDRO STERCOLI, GIOVANNI PREDIERI
Dipartimento di Chimica Generale ed Inorganica, Chimica Analitica, Chimica Fisica,Università degli Studi di Parma, Viale Usberti 17/A, I-43100, Parma, Italia

Abstract. Heparin is an anticoagulant which is widely used during blood-dialysis. To now, there is not a commercial device able to "filter" heparin from blood after or during the medical treatment. Heparin can give, on life-long treatments, several health problems. We prepared siloxane-modified hybrid poly(aminoamides) which can be obtained from water solution. They shown good heparin absorption properties.

Keywords: Sol-gel, heparin, polymers.

1. Introduction

The use of an extracorporeal apparatus for the medical treatment of blood, implies the presence of anticoagulant substances such as heparin, in order to avoid the formation of blood-clots inside the artificial circuit. Haemodialysis is widely used to remove waste products form blood and often the patient undergoes life-long cares with a frequency of two-three times a week. Generally, heparin is used as an injectable preparation.

Heparin is a mucopolysaccharide acting on the antithrombin mechanism which inhibits the serine-proteases involved in the coagulation processes.

Heparin is a polymer with variable chain lengths having a molecular weight ranging from 3,500 to 35,000 Da. It is formed by different di-saccharide units and is acidic, due to the presence of a high content of sulphate ($HOSO_3$) groups. The most common disaccharide found in heparin is formed by 2-O-sulfated iduronic acid and 6-O-sulfated, N-sulfated glucosamine.

* To whom correspondence should be addressed: Daniele Cauzzi; e-mail: cauzzi@unipr.it

P. Innocenzi, Y. L. Zub and V. G. Kessler (eds.), *Sol-Gel Methods for Materials Processing*.

At the physiological pH, heparin is found in its poly-anionic form; the cations present in the medical preparations can be changed following the treatment needs; sodium and calcium are the most used. Heparin binds to the enzyme inhibitor antithrombin III (AT-III) causing a conformational change which results in its active site being exposed. The activated AT-III then inactivates thrombin and other proteases involved in blood clotting. The rate of inactivation of these proteases by AT-III increases 1,000-fold due to the binding of heparin .[1]

Heparin is normally absorbed and degraded in the human body with a half-life of about one hour, depending on its molecular weight. Sometimes heparin, mostly on life-long treatments, can give several problems like hemorrhage, hypersensitivity, bone decalcification. As far as we know, the only practically applied method of de-heparinization is a plasmapheresis system that uses polylysine cationic polymers.[2] Another approach that seems effective, is the use of poly (amido-amine)s (PAAs), polymers obtained by the reaction of bis-acrylamides and primary or bis-secondary amines. They were widely studied by the group of Ferruti.[3] It appears that hydrolysis and solubility of these polymers, even when organically crosslinked, is preventing them to be practically applied. PAAs can be easily prepared in water or alcohol as solvent and without the need of a catalyst through a Michael addition:

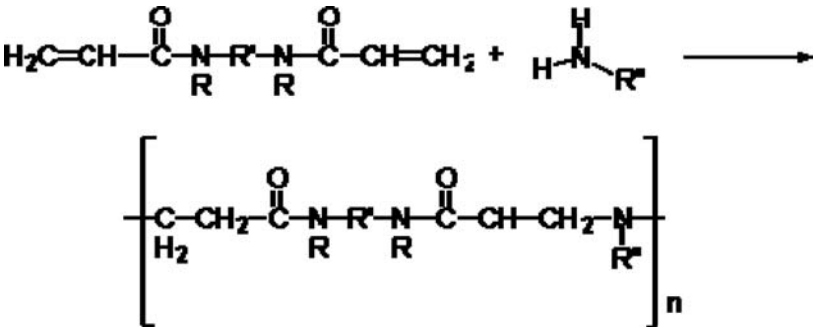

Every aminic hydrogen is a point of polymerization by reacting with an acrylamidic group. Primary amines and secondary diamines will yield linear polymers. Primary diamines, e.g. ethylenediamine, will produce branched polymers.

2. Results

Organic PAAs can be modified in order to be used for the preparation of hybrid materials by the sol-gel method.

In fact, the use of 3-aminopropyl-triethoxysilane (APTES), allows for the introduction of the $(EtO)_3Si$- group covalently bonded to the polymer chain.[4]

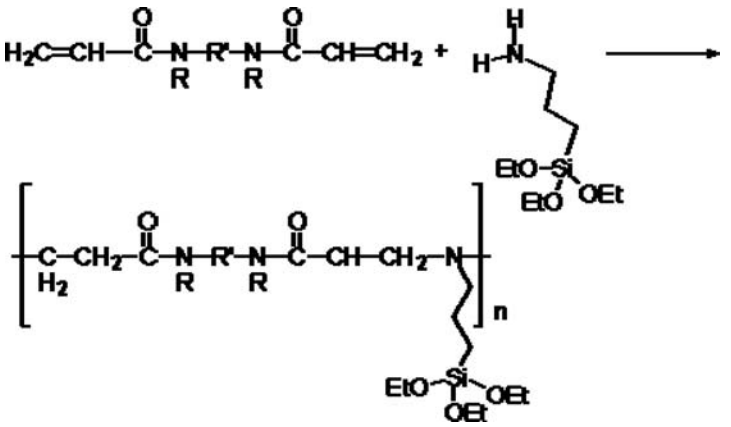

Different formulations have been tested, by changing the reaction components. The aim of the research was to find a formula able to yield a flexible polymer, to be used as a thick coating on the surface of biomedical PVC objects. The better composition was found to be a mixture of a bis-acrylamide, APTES or APMDES (3-aminopropyl-methyldiethoxysilane) and 1,6-dimethylaminohexane, a secondary diamine. The polymers obtained from water only are transparent, flexible and insoluble in water or any other solvent. They possess, as expected (Figure 1), an intermediate character with respect to the brittle and opaque TEOS xerogel (on the left in the figure) and the sticky an water soluble PAA polymer (on the right in the figure).

Figure 1. TEOS xerogel, hybrid siloxane-PAA, organic PAA.

Two bis-acrylamides were used, methylenebis-acrylamide (MBA) and bis-acryloylpiperazine (BAP).

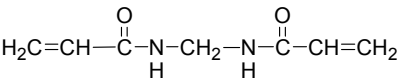

MBA

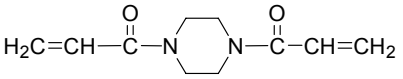

BAP

The choice was dictated by their low cost required in the case of real production. 1,6-dimethyl-diaminohexane was found to infer elastic properties to the polymer, together with a higher capacity to bind heparin.

Typical infrared and X-Ray powder diffraction are reported in Figure 2:

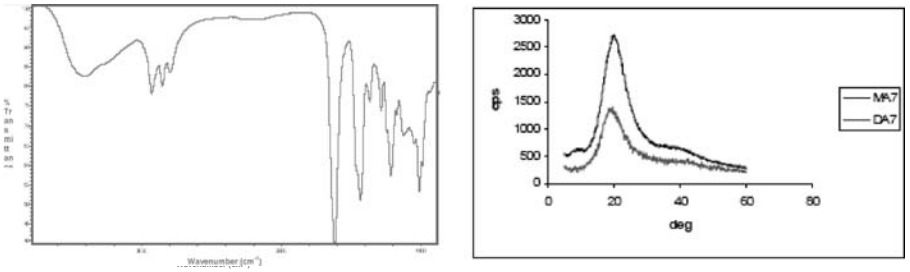

Figure 2. Infrared spectrum and XRD spectra of typical hybrid PAAs.

Absorption tests *in vitro* and on human blood

Heparin absorption *in-vitro* tests were performed on these materials using com-mercial heparin solutions (Sodium heparin, Liquemin Roche). Following the published literature, we decided that spectroscopic determination would be the quickest way to analyze many samples. Other methods, based on biological activity, could be used but were to complex for a quick screening of the best formulation. We then applied an indirect method,[5] which consists in measuring the lowering of the absorption bands of the dye O-Toluidine blue, due to the formation of a heparin-toluidine complex. Suitable PVC medical devices were coated using a water solution of the forming polymers. In order to produce more robust coatings, a PVC-SiO2 blend was also tested (Figure 3).

Surface heparin absorption values ranges from 250 to 750 mg/m^2, which are more than enough to absorb the heparin injected in one treatment. The highest values were found for polymers obtained from MBA with a high content of secondary diamine, and probably depends on the swelling ability of the coating.

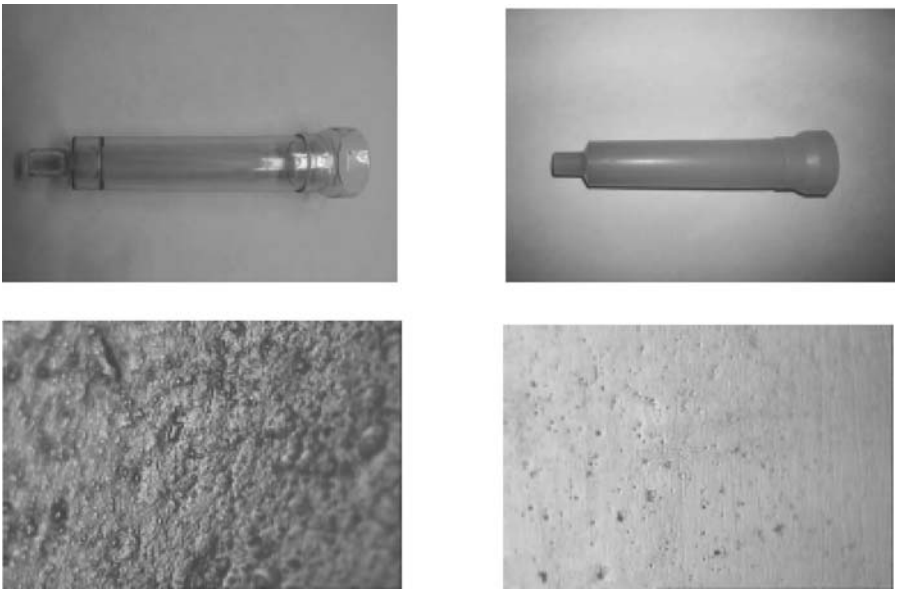

Figure 3. On the upper left, a PVC blood dropper, upper right a PVC/SiO_2 blood dropper; down left: the surface, washed with ethanol to remove the plastifier, of a PVC/SiO_2 dropper. down right; the same surface after coating with a hybrid polymer.

Tests performed on human blood were also very promising. Human blood contains a very high quantity of albumin which is in competition with heparin in the absorption process; polymers obtained from MBA resulted more selective towards heparin when in competition with albumin.

Acknowledgments

Heparin absorption tests on human blood were performed at the Hospital of Parma by the equipe of Professor Salvatore David, M.D.

References

1. W. Li, D. J. D. Johnson, C. T. Esmon, J. A. Huntington, *Nat. Struct. Mol. Biol.*, 11, 857 (2004); I. Bjork, U. Lindahl, *Mol. Cell. Biochem.*, 48, 161 (1982).
2. L. K. Von Segesser, T. Mihailevic, M. Toenz, B. Leskosek, A. Von Felten, M. Turina, *Asaio J.*, 40, M565 (1994); D. Jegger, H. T. Tevaerai, J. Horisberger, XM. Mueller, I. Seigneuil, N. Pierrel, Y. Boone, L. K. von Segesser, *Perfusion*, 15, 453 (2000); H. T.

Tevaearai, D. Jegger, XM. Mueller, J. Horisberger, L. K. von Segesser, *Thorac. Cardiov. Surg.*, 46, 303 (1998).

3. P. Ferruti, E. Ranucci, G. Di Silvestro, C. Yuan, N. Caronzolo, R. Donetti, M. Marchisio, *La Chimica e L'Industria*, 739 (1999); P. Ferruti, M. Marchisio, R. Duncan, *Macromol. Rapid Commun.*, 23, 332 (2002).
4. D. Cauzzi, G. Predieri, A. Stercoli, L. Balzano Patent (2004). "Composti xerogel polimerici reticolati inorganico-organici di poliammidoammine silossanizzate, loro metodo di preparazione e loro utilizzo come materiali eparino-assorbenti." MI2004A000503. C.O.M.E.F. S.r.l. Carpi (MO).
5. P. K. Smith, A. K. Mallia, G. T. Hermanson, *Anal. Biochem.*, 10, 466 (1980); M. S. Ahola et al., *Biomaterials*, 22, 2163 (2001).

SOL-GEL SILICA FILMS DOPED WITH CHROMIUM (III) ACETYLACETONATE ON ALUMINIUM SUBSTRATE

LYUDMYLA DAVYDENKO*, YURI PLYUTO
O.O. Chuiko Institute of Surface Chemistry, National Academy of Sciences of Ukraine, General Naumov Str. 17, 03164 Kiev, Ukraine

EVA MARIA MOSER
University of Applied Sciences of Geneva, 4, rue de la Prairie, CH-1202 Geneva, Switzerland

Abstract. Sol-gel silica films doped with $Cr(acac)_3$ and having *ca*. 100 nm thickness on aluminium substrate were synthesised by dip-coating from the precursor composition prepared by TEOS acidic hydrolysis. It has been found out the that the C = O groups of doping $Cr(acac)_3$ molecules are involved into interaction with silica network terminated with silanol groups. Upon thermal treatment of $Cr(acac)_3$-SiO_2 film in air, the ligand elimination from doping $Cr(acac)_3$ molecules took place, resulting in complete thermolysis at 613 K. The latter was accompanied by oxidation of Cr (III) to Cr (VI).

Keywords*:* Sol-gel silica films, TEOS acidic hydrolysis, chromium acetylacetonate.

1. Introduction

Presently, trivalent chromium Cr (III) anticorrosion pretreatments of metal substrates are of great interest as an alternative to toxic hexavalent chromium Cr (VI) corrosion-inhibiting formulations. Pretreatments based on Cr (III) were reported to improve corrosion resistance of aluminium and aluminium alloys.[1,2] Protection of aluminium was provided by seal coatings consisting of insoluble Cr (III) compounds.[1] The improving of the coating's protective action was achieved by combining Cr (III) with silica[3] or organically modified silica ORMOSIL.[4,5] Combustion chemical vapour deposition (CVD) of chromium (III) acetylacetonate and tetraethylorthosilicate (TEOS) was used for the development of multilayer chromia-silica coatings with increased corrosion resistance on aluminium substrate.[3]

*To whom correspondence should be addressed: L. Davydenko, O.O. Chuiko Institute of Surface Chemistry, 17 General Naumov Str., Kyiv 03164, Ukraine; e-mail: l.davydenko@yahoo.com

P. Innocenzi, Y. L. Zub and V. G. Kessler (eds.), *Sol-Gel Methods for Materials Processing*.

Acetylacetonate ligands undergo thermally activated elimination from metal acetylacetonates deposited on the surface of oxide supports that was studied in detail upon the synthesis of heterogeneous catalysts.[6,7] The resulting coordinatively unsaturated Cr (III) species may be attractive for the development of protective corrosion-inhibiting coatings. In addition, the environmentally benign by-products of thermal decomposition of acetylacetonate ligands (carbon dioxide and water) are acceptable for manufacturers with respect to environmental policies.

Sol-gel approach is a low-temperature alternative to a high-temperature CVD synthesis of SiO_2 films. The thickness of SiO_2 sol-gel film can be easily varied by the degree of condensation of primary siloxane oligomers and the withdrawal or spinning rate for a dip- or spin-coating, respectively. Introduction of organic or inorganic doping components to silica sol for the rational design of functional coatings enables a direct tailoring of their properties.

Interaction of metal acetylacetonates with a supporting matrix has a substantial influence on properties of the resulting surface species (degree of dispersion as well as chemical composition) formed upon thermal transformations. The high dispersion of supported species is ensured by hydrogen bonding (H-bonding) of metal acetylacetonates with surface groups or ligand substitution.[6] In contrast, the unbound metal acetylacetonates may transform to crystalline phase upon thermal activation or be eliminated in the case of volatile acetylacetonates. Therefore, information about the mechanism of anchoring of metal acetylacetonates in oxide matrixes is important for the rational design of the materials in which Cr (III) species play a critical role.

The objective of the present work was to study the state of chromium (III) acetylacetonate in sol-gel silica films deposited on aluminium substrate.

2. Experimental

Silica films of *ca*. 100 nm thickness on aluminium substrate were synthesised by sol-gel dip-coating method using TEOS precursor composition.

The as-received aluminium substrate made from bare 3003 H14 alloy (Type A test panels, Q-Panel Lab Products) was cleaned with acetone, etched in 0.01 M aqueous KOH for 10 min at 303 K, rinsed with deionised water and dried under the flow of air.

The TEOS precursor composition was prepared by $Si(OC_2H_5)_4$ (Aldrich, 98%) acidic hydrolysis[8] (the reactant molar ratio was 1.0 $Si(OC_2H_5)_4$: 0.05 HCl : 3.82 H_2O). For the synthesis of SiO_2 films by dip-coating, TEOS precursor composition was diluted with C_2H_5OH in the proportion 1:3 per volume. Silica films doped with $Cr(acac)_3$ (Aldrich, 97%), hereinafter denoted as $Cr(acac)_3$-SiO_2 films, were synthesised from the similar precursor composition diluted

with $Cr(acac)_3$ solution in C_2H_5OH in the proportion 1:3 per volume. To reach the highest loading of $Cr(acac)_3$ in silica film, the sutured solution of $Cr(acac)_3$ (c = 0.037 M) was used.

IR spectra in a reflectance mode were recorded within 400–4,000 cm^{-1} by Nexus Nikolet FTIR spectrometer (Thermo Scientific) equipped with a Smart Collector reflectance accessory. For recording the spectra of the as-synthesised films on aluminium substrate, the background correction was performed using the golden mirror as a reflectance standard. Powder of bulk $Cr(acac)_3$ was diluted with KBr (1:35) before IR spectrum recording and KBr was used for the background correction in this case.

UV-vis spectra were recorded within 190–1,100 nm using Lambda 35 UV-vis spectrometer (Perkin-Elmer) equipped with a Labsphere RSA-PE-20 diffuse reflectance and transmittance accessory with 8^o sample holder. Background correction was performed using a cleaned aluminium substrate as reflectance standard.

3. Results and Discussion

The formation of silica network in the presence of doping $Cr(acac)_3$ molecules in the films on aluminium substrate was proved by FTIR. The IR spectra of the initial aluminium substrate, air-dried SiO_2 and $Cr(acac)_3$-SiO_2 films dip-coated on aluminium substrate are shown in Figure 1. The presence of silica network in the case of air-dried SiO_2 and $Cr(acac)_3$-SiO_2 films is seen from Si-O-Si stretching bands[9,10] within 980–1,260 cm^{-1} (Figure 1, curves 2 and 3) which are absent in the spectrum of the initial substrate (Figure 1, curve 1).

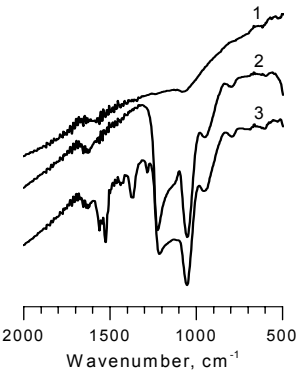

Figure 1. FTIR reflectance spectra of aluminium substrate (1) air-dried SiO_2 (2) and $Cr(acac)_3$-SiO_2 (3) films on aluminium substrate.

The presence of the vibration bands within 1,250–1,650 cm^{-1} characteristic for acetylacetonate ligands[11,12] in the IR spectrum of $Cr(acac)_3$-SiO_2 films (Figure 1, curve 3) indicates the presence of doping $Cr(acac)_3$ molecules. The doping of silica film with $Cr(acac)_3$ does not lead to the noticeable changes of the spectrum within Si-O-Si stretching bands. One can conclude that silica doping with $Cr(acac)_3$ does not have a significant influence on Si-O-Si bonds and thus insertion of the complex into siloxane chains does not occur. Nevertheless, $Cr(acac)_3$ appears to be localised within silica network.

In order to investigate the interaction of doping $Cr(acac)_3$ molecules with active sites of silica network, one should perform the analysis of IR spectra in the region of stretching vibrations of free and hydrogen-bonded silanol groups (3,000–3,800 cm^{-1}).[9,10] However, this approach can hardly be applied for silica sol-gel films because of superposition of the bands of free (3,740–3,748 cm^{-1})[9,10,13,14] and hydrogen-bonded (2,600–3,700 cm^{-1}) silanol groups [9,10,14] with hydroxyl groups in the molecules of the residual solvent and water (3,327–3,636 cm^{-1}).[15] Therefore, the alternative approach was applied.

The IR spectra of bulk $Cr(acac)_3$ and $Cr(acac)_3$-SiO_2 film in the region of 1,250–1,650 cm^{-1} are shown in Figure 2. The bulk $Cr(acac)_3$ exhibits the bands of acetylacetonate ligand vibrations at 1,278, 1,330–1,470, 1,521 and 1,577 cm^{-1}. In IR spectrum of the $Cr(acac)_3$-SiO_2 film the bands are observed at 1,283, 1,330–1,470, 1,527 and 1,562 cm^{-1}. The bands position and their assignments[11,12,16–18] are summarised in Table 1.

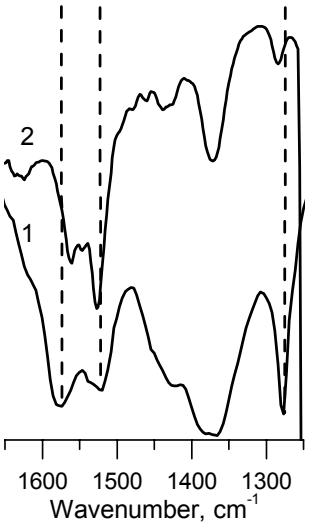

Figure 2. FTIR reflectance spectra of bulk $Cr(acac)_3$ (1) and air-dried $Cr(acac)_3$-SiO_2 film on aluminium substrate (2).

TABLE 1. The bands position and their assignments in IR spectra of bulk $Cr(acac)_3$ and $Cr(acac)_3$-SiO_2 film on aluminium substrate.

Band assignment	Band position (cm^{-1})	
	$Cr(acac)_3$	$Cr(acac)_3$-SiO_2
ν (C – O)	1,278	1,283
δ (C – H) + ν (C – C)	1,330–1,470	1,330–1,470
ν (C = C – C)	1,521	1,527
ν (C = O)	1,577	1,562

As one can see, the positions of the vibration bands of acetylacetonate ligands in the spectrum of $Cr(acac)_3$-SiO_2 film significantly differ from those in the spectrum of bulk $Cr(acac)_3$. The shift of C = O vibration band in the IR spectrum of the $Cr(acac)_3$-SiO_2 film to lower wavenumbers can mean the involvement of C = O groups of doping $Cr(acac)_3$ molecules in interaction with silica network terminated with silanol groups. The observed shift which reaches 15 cm^{-1} can be attributed to the formation of H-bond of the middle strength.[16] The slight shift to higher wavenumbers of the bands corresponding to C – O and C = C –C vibrations of acetylacetonate ligands can mean that H-bonding is strong enough to perturb the bonds which are not involved into this interaction.

The thermal treatment of $Cr(acac)_3$-SiO_2 film in air at 473 K resulted in slight decrease in the intensities of bands in IR spectrum (Figure 3, curve 2) while they retained their positions. This means that $Cr(acac)_3$ molecules in $Cr(acac)_3$-SiO_2 film after treatment at 473 K remained H-bonded with silanol groups of silica network. This is in good agreement with our earlier work[19] where H-bonding of $Cr(acac)_3$ molecules with silanol group of silica surface up to 463 K was observed. The complete disappearance of the vibration bands of acetylacetonate ligands in the IR spectrum of $Cr(acac)_3$-SiO_2 film is observed after thermal treatment at 613 K (Figure 3, curve 3) and confirms a complete thermolysis of the doping $Cr(acac)_3$ molecules.

UV-vis reflectance spectra of the air-dried $Cr(acac)_3$-SiO_2 film and $Cr(acac)_3$-SiO_2 films thermally treated at 473 and 613 K in air are shown in Figure 4. In the UV-vis spectrum of the air-dried $Cr(acac)_3$-SiO_2 film (Figure 4, curve 1), the intense bands at 214, 258 and 331 nm are observed. These bands correspond to Cr→O charge transfer transitions in $Cr(acac)_3$ molecule.[20] The intensity of these bands decreases after thermal treatment at 473 K (Figure 4, curve 2) that means the beginning of the thermolysis of doping $Cr(acac)_3$ molecules. This conclusion is in agreement with the data obtained by IR spectroscopic characterisation of $Cr(acac)_3$-SiO_2 film thermally treated at 473 K (Figure 3, curve 2).

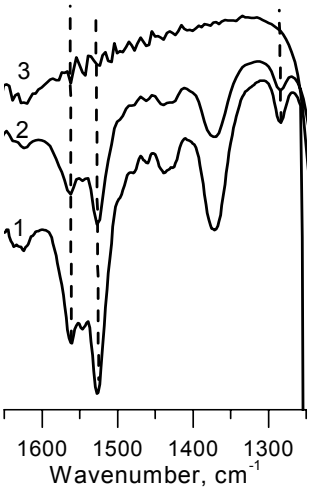

Figure 3. FTIR reflectance spectra of air-dried $Cr(acac)_3$-SiO_2 film (1) and after thermal treatment at 473 (2) and 613 K (3).

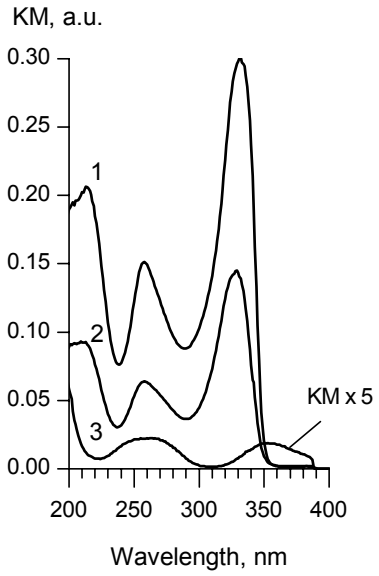

Figure 4. UV-vis reflectance spectra of air-dried $Cr(acac)_3$-SiO_2 film (1) and after thermal treatment at 473 (2) and 613 K (3).

$Cr(acac)_3$-SiO_2 film after thermal treatment at 613 K becomes yellow that results in appearance of the bands at 261 and 353 nm in UV-vis spectrum (Figure 4, curve 3). These bands have to be attributed to the Cr→O charge transfer transitions in Cr (VI) oxy-species.[21,22] The appearance of Cr (VI) species means the complete thermolysis of doping $Cr(acac)_3$ molecules that is accompanied by Cr (III) to Cr (VI) oxidation. This conclusion agrees with a complete disappearance of the vibration bands of acetylacetonate ligands in IR spectrum of the $Cr(acac)_3$-SiO_2 film after thermal treatment at 613 K (Figure 3, curve 3).

4. Conclusions

Sol-gel silica films doped with $Cr(acac)_3$ of *ca*. 100 nm thickness on aluminium substrate were synthesised by dip-coating from the precursor composition prepared by TEOS acidic hydrolysis. It has been found out that the observed C = O band at 1,577 cm^{-1} of acetylacetonate ligands in IR spectrum of bulk $Cr(acac)_3$ appeared to be shifted to 1,562 cm^{-1} in the case of $Cr(acac)_3$-SiO_2 film. This means the involvement of C = O groups of doping $Cr(acac)_3$ molecules into interaction with silica network terminated with silanol groups. Upon thermal treatment of $Cr(acac)_3$-SiO_2 film in air, the decrease of the intensities of IR bands of acetylacetonate ligands in the region of 1,250– 1,650 cm^{-1} was observed and resulted in the complete thermolysis of doping $Cr(acac)_3$ molecules at 613 K. This was accompanied by Cr (III) to Cr (VI) oxidation observed from the appearance of UV-vis bands at 261 and 353 nm characteristic for Cr→O charge transfer transitions in Cr (VI) oxy-species instead of the bands at 214, 258 and 331 nm corresponding to Cr→O charge transfer transitions in $Cr(acac)_3$ molecules.

Acknowledgements

The work was supported in the frame of SCOPES project IB7320-111146 of the Swiss National Science Foundation and the Programme of Fundamental Research "Nanosystems, Nanomaterials and Nanotechnologies" of the National Academy of Sciences of Ukraine.

References

1. F. Pearlstein and V.S. Agarwala, Trivalent chromium solution for sealing anodized aluminum, United States Patent No. 5,374,347, December 20 (1994).
2. C.A. Matzdorf, J.L. Green, and M.J. Kane, Pretreatment for aluminum and aluminum alloys, United States Patent No. 6,521,029 B1, February 18 (2003).

3. A.T. Hunt, T.J. Hwang, M.R. Hendrick, and H. Shao, J.R. Thomas, Corrosion-resistant multilayer coatings, United States Patent No. 6,214,473, April 10 (2001).
4. E. Stesikova, T.L. Metroke, P.L. Reed, V.S. Agarwala, and E.T. Knobbe, Impact of trivalent chromium conversion layers and hybrid silicate coatings on corrosion resistance of aluminum alloys, *Corrosion 2000*, Paper No. 00287 (NACE International, Conferences Division, 2000).
5. T.L. Metroke, E. Stesikova, O. Kachurina, and E.T. Knobbe, Organic-inorganic hybrid coatings as corrosion inhibiting surface treatments for aluminum alloys, *Corrosion 2001*, Paper No. 01550 (NACE International, Publications Division, 2001).
6. J.C. Kenvin, M.G. White, and M.B. Mitchell, Preparation and characterization of supported mononuclear metal complexes as model catalysts, *Langmuir* 7(6), 1198–1205 (1991).
7. S. Köhler, M. Reiche, C. Frobel, and M. Baerns, Preparation of catalysts by chemical vapor-phase deposition and decomposition on support materials in a fluidized-bed reactor, in: *Preparation of Catalysts VI Scientific Bases for Preparation of Heterogeneous Catalysts*, edited by G. Poncelet et al. (Elsevier Science, New York, 1995), pp. 1009–1016.
8. J. Widera, A.M. Kijak, D.V. Ca , G.E. Pacey, R.T. Taylor, H. Perfect, and J.A. Cox, The influence of the matrix structure on the oxidation of aniline in a silica sol-gel composite, *Electrochem. Acta* 50, 1703–1709 (2005).
9. R.L. White, and A. Nair, Diffuse reflectance infrared spectroscopic characterization of silica dehydroxylation, *Appl. Spect.* 44(1), 69–75 (1990).
10. A. Burneau, O. Barrès, J.P. Gallas, and J.C. Lavalley, Comparative study of the surface hydroxyl groups of fumed and precipitated silicas. 2. Characterization by infrared spectroscopy of the interactions with water, *Langmuir* 6, 1364–1372 (1990).
11. W.O. George, The infrared spectra of chromium (III) acetylacetonate and chromium (III) malondialdehyde, *Spectrochim. Acta* 27A, 265–269 (1971).
12. K. Nakamoto, *Infrared and Raman Spectra of Inorganic and Coordination Compounds* (4th ed., Wiley-Interscience, New York, 1986).
13. A.J. McFarlan, and B.A. Morrow, Infrared evidence of two isolated silanol species on activated silicas, *J. Phys. Chem.* 95, 5388–5390 (1991).
14. B.A. Morrow, and A.J. McFarlan, Surface vibrational modes of silanol groups on silica, *J. Phys. Chem.* 96, 1395–1400 (1992).
15. K.M. Davis, and M. Tomozawa, An infrared spectroscopic study of water-related species in silica glasses, *J. Non-Cryst. Solid.* 201, 177–198 (1996).
16. A.J. Gordon, and R.A. Ford, *The Chemist's Companion. A Handbook of Practical Data, Techniques and References* (Wiley-Interscience, New York, 1972).
17. J. Coates, Interpretation of infrared spectra, a practical approach, in: *Encyclopaedia of Analytical Chemistry*, edited by R.A. Meyers, pp. 10815–10837 (Wiley, Chichester, 2000).
18. D.R. Lide, *Handbook of Chemistry and Physics* (84th ed., CRC Press, Boca Raton, FL, 2003–2004).
19. I.V. Babich, Yu.V. Plyuto, P. Van Der Voort, and E.F. Vansant, Thermal transformations of chromium acetylacetonate on silica surface, *J. Coll. Int. Sci*. 189, 144–150 (1997).
20. A.Y. Ustinov, O.M. Ustinova, V.I. Vovna, and M.V. Kazachek, Electron absorption spectra and electronic structure of chromium tris-β-diketonates, *Russ. J. Coord. Chem.* 20(8), 600–603 (1994).
21. M.I. Zaki, N.E. Fouad, J. Leyrer, and H. Knözinger, Physicochemical investigation of calcined chromia-coated silica and alumina catalysts: characterization of chromium-oxygen species, *Appl. Cat.* 21, 359–377 (1986).
22. A.B. Gaspar, and L.C. Dieguez, The influence of Cr precursors in the ethylene polymerization on Cr/SiO_2 catalysts, *Appl. Cat. A* 227, 241–254 (2002).

SORPTION OF Hg^{2+} BY MESOPOROUS SILICAS WITH A FUNCTIONAL $\equiv Si(CH_2)_2NHP(S)(OC_2H_5)_2$ GROUP IN THE SURFACE LAYER

OKSANA A. DUDARKO*, VASYL' P. HONCHARYK, YURIY L. ZUB
O. O. Chuiko Institute of Surface Chemistry, National Academy of Sciences of Ukraine, 17 General Naumov Str., Kyiv 03164, Ukraine

Abstract. Polysiloxane materials containing residual thiophosphonic acid groups $\equiv Si(CH_2)_3NHP(S)(OC_2H_5)_2$ in the surface layer have been prepared by sol-gel template methods (S_{sp} = 240 – 670 m^2/g; V_s = 0.19 – 0.41 cm^3/g; d = 3.3 – 4.5 nm). It was supposed that synthesized silicas are able to adsorb mercury(II) ions from nitric acid solutions (their SSC can be close to 450 mg/g). It was shown that the complexes in 1:1 ratio were formed in the surface layer. The excessive sorption of metal ions was shown to be due to partial hydrolysis of ethoxy-groups attached to the phosphorus atom.

Keywords: Sol-gel method, polysiloxane xerogels, thiophosphonic acid functional groups, adsorption of mercury.

1. Introduction

Sorbents of organic and inorganic nature that contain a number of derivatives of phosphonic acids in a superficial layer, find broad application in adsorption, catalysis, ion-exchange processes, as carriers in chromatography, etc.[1,2] Use of inorganic carriers for creation of such sorbents has certain advantages compared to organic ones. Greater firmness of such materials in aggressive environments and under promoted radiation makes them more attractive. Earlier[3,4] we showed that it was possible to obtain mesoporous silicas with derivatives of phosphonic acids in a superficial layer using sol-gel and template methods.

*To whom correspondence should be addressed: O.A.Dudarko, O.O. Chuiko Institute of Surface Chemistry, NAS of Ukraine, 17 General Naumov Str., Kyiv 03164 Ukraine; e-mail: dudarko@ bigmir.net

P. Innocenzi, Y. L. Zub and V. G. Kessler (eds.), *Sol-Gel Methods for Materials Processing*.

Mesoporous silicas which contain thiophosphonic complexing groups (≡P=S) evoke special interest. It is known that such sorbents have affinity to ions of heavy and noble metals. Hence, the goal of the present work was to use the technique of synthesis of inorganic sorbents (similar to the above mentioned methods) with thiophosphonic acid groups $\equiv Si(CH_2)_3NHP(S)(OC_2H_5)_2$ in the surface layer. Furthermore the ability of these sorbents to extract cations of toxic metals from aqueous solutions was proved here, using the adsorption of Mercury(II) as an example.

2. Experimental

*Procedure for the synthesis of **MXI** and **MXII**:* 0.0075 mol $(C_2H_5O)_3Si(CH_2)_3NHP(S)(OC_2H_5)_2$ (DTPPA) (0.01 mol for the sample **MXII**) and 0.06 mol $Si(OC_2H_5)_4$ (TEOS) were dissolved separately in ethanol (10 ml). NH_4F (F^-/Si = 1/100) solution in water was added in small portions to the first solution. The resulting solution was agitated for 2 min, and the TEOS solution was gradually added. The obtained sol was agitated for 1 min and left to stand at room temperature. Already within 1 min, the gel with a marked opalescence was formed. After 24 h aging, the gel was ground and dried in vacuum for 1 h at room temperature, 1 h at 50°C, and 4 h at 105°C.

*Procedure for the synthesis of **MSIII** and **MSIV**:* 0.075 mol TEOS and 0.0075 (0.015 for **MSIV**) DTPPA were dissolved separately in ethanol (10 ml). NH_4F (F^-/Si = 1/100) solution in water was added in small portions to the second solution. Then 0.0225 mol of 1-dodecylamine, $CH_3(CH_2)_{11}NH_2$ (DDA) in a mixture with 40 cm^3 ethanol and 50 cm^3 water was added to previously mixed solutions of these alkoxysilanes on constant stirring. After 2 min, a white, bulk substance precipitated, and stirring was stopped. After 24 h, the precipitate was filtered off, washed with 50 cm^3 of ethanol, and air-dried for 24 h. The template was then removed with boiling methanol (30 cm^3 of methanol per gram of the sample) over a period of 3 h (this step was repeated three times). The resultant material was vacuum-dried at 100°C for 4 h.

The structure-related adsorption characteristics of the silicas were calculated from the isotherms of low temperature adsorption–desorption of nitrogen measured by a Kelvin-1042 instrument (Costech Microanalytical Ltd). Before measurements, the samples were degassed in flowing helium at 100°C for 2 h. The specific surface area of adsorbents was determined by BET measurements,[5] and the pore size distribution, by BJH measurements.[6]

The sorption of Hg(II) from acidic solutions by the obtained sorbents was studied in static conditions at 20°C. In all experiments the weight of sorbents

under study was 0.1 g, the volume of liquid phase – 20 cm^3, period of sorption – 3–5 days. The residual metal contents were determined in solution after sorption by standard, well-established techniques.[7,8] The value of adsorption (in mmol/g) was estimated on the basis of difference before and after sorption. The data obtained were used for construction of isotherms of metal ion sorption.

3. Results and Discussion

Polysiloxane xerogels containing residual thiophosphonic acid groups ≡ $Si(CH_2)_3NHP(S)(OC_2H_5)_2$ in the surface layer have been prepared by sol–gel method. The variation in the ratio (TEOS/DTPPA) – from 8:1 (**MXI**) to 6:1 (**MXII**) in an initial solution – allowed us to obtain porous sorbents with different contents of ligand groups (Table 1).

TABLE 1. Elemental analysis data and structural–adsorption characteristics of the samples obtained.

Sample	[a]$C_{f.gr.}$ (mmol/g)	$S_{sp.}$ (m^2/g)	$V_{s.}$ (cm^3/g)	$d_{ef.}$ (nm)	[b]*SSC* (mg/g)	[a]$C_{f.gr.}$ (mmol/m^2)	$C_{Hg}^{2+}/C_{f.gr.}$
MXI	1.2	470	0.41	3.8	360	0.0026	1.6/1
MXII	1.6	240	0.19	3.6	450	0.0067	1.3/1
MSIII	1.3	360	0.23	3.3	180	0.0033	0.6/1
MSIV	1.9	670	0.36	4.5	420	0.0028	1.1/1

[a]Calculated from the elemental analysis against phosphorus; [b]Static sorptive capacity

The second series of samples with the same functional groups in the surface layer was obtained using template method (template – DDA) (Table 1, **MSIII** and **MSIV**).

All the synthesized materials are pale yellow, loose, powdered substances (Figure 1a) with hydrophobic properties. The samples **MSIII** and **MSIV,** obtained by template method, consist of primary spherical particles which form agglomerates with a size up to 200 μm (Figure 1b, c).

As shown in Table 1 the xerogel **MXII** possesses maximal surface concentration of functional groups, expressed in mmol/m^2. This value was within quite a narrow range of 0.0026–0.0033 mmol/m^2 for the rest of samples.

In Figure 2 there are displayed the isotherms of sorption for mercury (II) by the sulfur-containing samples. All isotherms are characterized by rapid increase in the region of small-scale equilibrium concentrations of Hg^{2+} and emerged on the plateau at equilibrium concentrations of mercury(II) equal ~2 mmol/l in case of mesoporous silicas and 2.5–5.0 mmol/l – for xerogels. It confirms high affinity of sulfur-containing sorbents to Hg(II) ions.

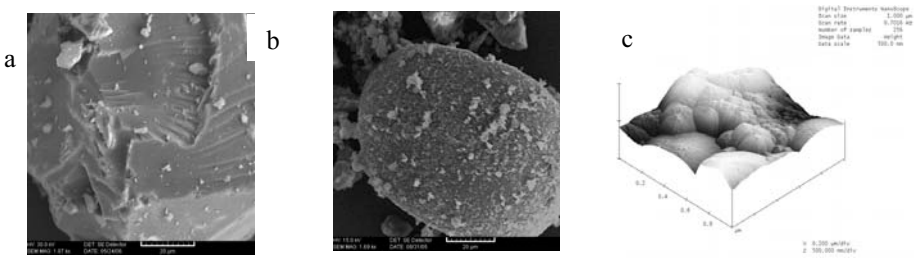

Figure 1. SEM micrographs of xerogels **MXII** (a), **MSIII** (b) and AFM graph of sample **MSIII** (c).

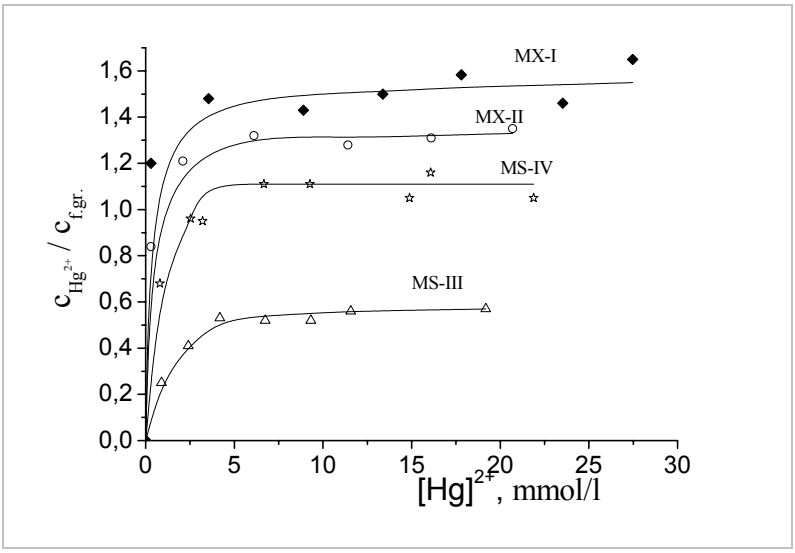

Figure 2. Isothems of Hg(II) sorption for the sulfur-containing samples.

The formation of surface complexes of 1:1 composition is observed for mesoporous silica **MSIV** with high value of specific surface area and relatively low surface concentration of functional groups. Obviously all thiophosphonic groups of this sample ($d_{ef} \approx 4.5$ nm) are available for Hg(II) ions.

Apparently, the functional groups are evenly distributed on the pore surface of this sorbent. According to calculations, the distance between them is ~7 Å. Under these conditions the formation of complexes of Hg(II) with two sulfur atoms in coordination sphere is unlikely, which is confirmed experimentally.

The surface concentration of functional groups for mesoporous silica **MSIII**, is close to that of the sample **MSIV** (Table 1), and the ratio of Hg^{2+} adsorbed to the concentration of functional groups equals to 0.6:1. It is difficult to imagine

that island station of functional groups for the sample **MSIII**, resulted in formation of surface complexes Hg(II) with a composition of 1:2. Most likely, the formation of surface complexes with a composition of 1:1 occurred during sorption. This implies that around half of the functional groups are inaccessible for metal ions, a possible scenario if there is a considerable structure disorder. This has been indeed unambiguously proved for this sample by its XRD pattern.[4]

For the mesoporous xerogels **MXI** and **MXII** the molar ratios of "adsorbed metal/functional group" are (1.6–1.3):1 (Table 1). It is obvious, that there exists, in addition to the thiophosphonic acid groups on the surface of xerogels (**MX)**, an additional type of sorption center of a different nature. Measured pH of aqueous suspensions of xerogel **MXI** was shown to be slightly acidic (pH = 4) – in contrast to the analogous sample **MSIII**, obtained by template method (pH of its suspensions equals to 6.9). It was observed[9] in the previous work that some of the phosphonic acid groups formed –(HO)(O)P–O–Si linkages during vacuum drying due to condensation of phosphonic-silanol groups for the same type of xerogels. Such linkage is hydrolytically unstable and it was hydrolysed during the contact with water, forming =P(O)(OH) groups. Indeed, as was proved by reverse titration of aqueous suspension, the xerogel **MXI** contained 0.7 mmol/g proton-donor groups. Consequently, it was supposed, that for the **MXI** sample the formation of –P(S)–OH groups occurs. The sorption of excessive amount of Hg^{2+} is connected with this. For this case the value of its limited sorption (Figure 2) is dependent on the content of functional groups.

4. Conclusions

Xerogels containing residues of amide derivatives of thiophosphonic acids, $Si(CH_2)_3NHP(S)(OC_2H_5)_2$ have been prepared by sol-gel and template methods. It was shown that parameters of porous structure of such sorbents – at given nature of reacting alkoxysilanes – depend on both the ratio of the last and on the method of synthesis. It is shown, that polysiloxane xerogels, and mesoporous silicas containing thiophosphonic ligand groups in the superficial layer, are able to adsorb the ions of mercury(II) from nitric acid solutions. Thus SSC of such sorbents can reach 450 mg/g. The obtained functionalised silicas can find application in environmental analytical chemistry and sorption technologies.

References

1. Yu.V. Kholin, V.N. Zaytsev, Complexes on the surface of chemical modified silicas, pp. 3, 136 (*Folio, Charkiv, 1997)* (in Russian).
2. Yu. L. Zub, A.A. Chuiko, Salient features of synthesis and structure of functional polysiloxane xerogels. Colloidal silica: fundamentals and applications. *Ed. by Bergna H.E. and Roberts W.O*., 397–424 (*CRC Press, Boca Raton, FL, 2006*).
3. O.A. Dudarko, V.Ya. Semenii, A. Dabrowski, Yu.L. Zub, The preparation of polysiloxane xerogels containing amide derivatives of phosphonic and thiophosphonic acids in the surface layer, *Kolloidn. Zh.* 69 (1), 72−80 (2007) (in Russian).
4. O.A. Dudarko, I.V. Melnyk, Yu.L. Zub, A. Dabrowski, Structure-adsorbtion charac-teristics of template-based mesoporous silicas containing residues of some phosphorus acids derivatives in their surface layer, *Stud. Surf. Sc. Catal.* 160, 479−486 (2006).
5. J.S. Brunauer, P.H. Emmet, E. Teller, Adsorption of gases in multimolecular layers, *J. Am. Chem. Soc.* 60, 309–319 (1938).
6. E.P. Barret, L.G. Joyner, P.P. Halenda, The determination of pore volume and area distributions in porous substances. I. Computations from nitrogen isotherms, *J. Am. Chem. Soc*. 73, 373–380 (1951).
7. G. Shwarzenbach, G. Flashka, Complexonometric titration (*Khimiya, Moscow, 1970*) 380 p. (in Russian).
8. V.P. Gladyshev, S.A. Levitskaya, L.M. Philipova, Analytical chemistry of Hydrargyrum, 227 p. (*Nauka, Moscow, 1974*) (in Russian).
9. A. Dabrowski, M. Barchak, O.A. Dudarko, Yu.L. Zub Preparation and characterisation of polysiloxane xerogels having covalently attached phosphonic asids groups, *Polish J. Chem.* 81, 475–483 (2007).

SOL-GEL PROCESS PREPARATION OF FUNCTIONAL SILICA MATERIALS AND THEIR APPLICATION

VLADIMIR E. GAISHUN*, YANINA A. KOSENOK, DMITRY L. KOVALENKO, ALINA V. SEMCHENKO
Advanced Materials Research Laboratory, F. Skorina Gomel State University, 104 Sovetskay Str., Gomel, 246019, Belarus

Abstract. The development of new high-performance materials for electronic, optical-mechanical and other industries is restrained by traditional mode of their production. It concerns materials technologies based on physical processes, for example, fusion and sintering, which require heat treatment and high pressure. The synthesis of materials with new properties is possible using chemical, colloid processes. In this respect the processes of transition of a sol into a gel, and further into a solid body with particular properties, is the basis of development of new sol-gel technologies.

Keywords: Sol-gel technology, silicon alkoxides, thin films, protection coatings, thick silica gel glasses, colloidal nanosized silica, aerogels.

1. Introduction

Sol-gel science and technology continues to interest researchers decades after its discovery. Although first discovered in the late 1800s and extensively studied since the early 1930s, it met a renewed interest[1,2] in the early 1970s, when monolithic inorganic gels were formed at low temperatures and converted to glasses without high temperature melting process.[3] Using this approach, homogeneous inorganic oxide materials with desirable properties of hardness, optical transparency, chemical durability, tailored porosity, and thermal resistance, can be produced at room temperatures, in contrast to much higher melting temperatures required in the production of conventional inorganic glasses.[3–5] The specific

*To whom correspondence should be addressed: V.E. Gaishun, Advanced Materials Research Laboratory, F. Skorina Gomel State University, 104 Sovetskay Str., Gomel, 246019, Belarus; e-mail: vgaishun@gsu.unibel.by

P. Innocenzi, Y. L. Zub and V. G. Kessler (eds.), *Sol-Gel Methods for Materials Processing*.

use of these sol-gel produced glasses and ceramics is derived from various material shapes generated in the gel state, i.e., monoliths, films, fibers, and monosized powders.

2. Experimental

The sol-gel process, as the name implies, involves evolution of inorganic networks through formation of a colloidal suspension (sol) and gelation of the sol to form a network in a continuous liquid phase (gel).[2] A precursors for synthesis of these colloids consists of a complex of metal or metalloid element with various reactive ligands. Metal alkoxides are most popular because they react readily with water. The most widely used metalloid alkoxides are the alkoxysilanes, such as tetramethoxysilane (TMOS) and tetraethoxysilane (TEOS). However, other metal alkoxides such as alkyl aluminates, titanates, or metalloid alkoxides such as alkyl borates are also commonly used in the sol-gel process, often mixed with TEOS.

The sol-gel coating process consists usually of four steps:

1. The desired colloidal particles are dispersed in a liquid to form a sol.
2. The deposition of sol solution produces coatings on the substrates by spraying, dipping or spinning.
3. The particles in sol are aggregated through the removal of the stabilizing components and produce a gel in a state of a continuous network.
4. The final heat treatment pyrolyzes the remaining organic or inorganic components and form an amorphous or crystalline coating.[3,6–8]

During hydrolysis, addition of water results in the replacement of [OR] group with [OH] group. Concerning the mechanisms of hydrolysis under different conditions, see.[9] Hydrolysis can be accelerated by adding a catalyst such as HCl and NH_3. Hydrolysis continues until all alkoxy groups are replaced by hydroxyl groups. Subsequent condensation involving silanol group (Si-OH) produced siloxane bonds (Si-O-Si) and alcohol and water.

Polymerization to form siloxane bond occurs by either a water or alcohol release. The condensation leads to formation of monomer, dimer, cyclic tetramer, and high order rings. The rate of hydrolysis is affected by pH, reagent concentration and H_2O/Si molar ratio (in case of silica gels). Also ageing and drying are important. By control of these factors, it is possible to vary the structure and properties of sol-gel derived inorganic networks.

As the number of siloxane bonds increases, the molecules aggregate in solution, where they form a network, a gel that can be reinforced by drying. The water and alcohol are driven off and the network shrinks. At pH of greater than 7, and

H_2O/Si ratio ranging from 7 to 5, spherical nano-particles are formed. Polymerization to form siloxane bonds by either an alcohol or water elimination occurs.

$$2\ HOSi\ (OR)_3 \rightarrow (OR)_3\ Si\ O\ Si\ (OR)_3 + H_2O$$
or
$$2\ HOSi\ (OR)_3 \rightarrow (OR)_2OH\ Si\ O\ Si\ (OR)_3 + ROH$$

Above pH of 7, silica is more soluble and silica particles grow in size. Growth stops when the difference in solubility between the smallest and largest particles becomes indistinguishable. Larger particles are formed at higher temperatures.

3. Results and Discussion

The applications of sol gel-derived products are numerous (Figure 1).

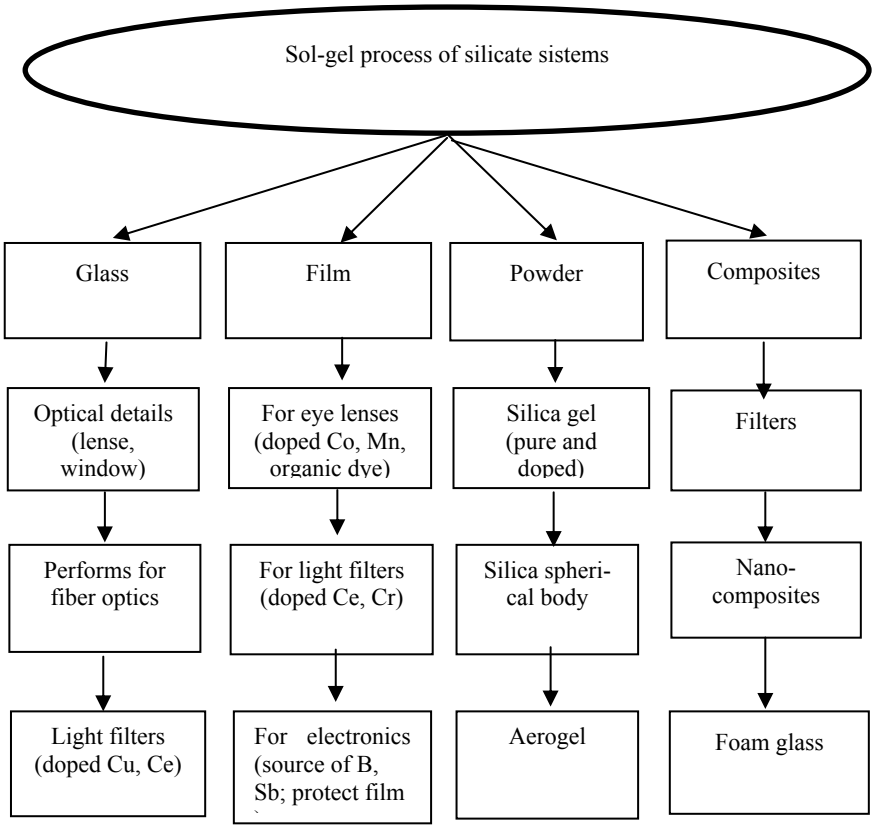

Figure 1. Applications of the sol-gel method.

One of the largest application areas is *thin films*, which can be produced on a substrate by spin-coating or dip-coating. Other methods include spraying, electrophoresis, inkjet printing or roll coating. Optical coatings, protective and decorative coatings, and electro-optic components can be applied to glass, metal and other types of substrates by these methods.

Sol-gel silica films for integrated circuits protection

1. Sol deposition onto circuits by spin-coating method
2. After heat treatment at 500^0C on a surface of circuits a homogenous transparent coating was formed
3. Thickness of the coating was 0.2–2 μm
4. Good adhesion to a surface of silicon, silicon dioxide, aluminum (aluminium distributings of a microcircuit)
5. Electric strength not less than 500 V/mm
6. Mechanical stability to a temperature cycling

Sol-gel silica films as source of B and Sb diffusion dopants in silicon electronic engineering

We developed a sol-gel technique for preparation of B and Sb doped glassy film on silicon wafers. The use of both types of dopants allowed fabrication of p-n layers in silicon. Homogeneous and transparent films of thickness in the range 0.2–2 μm were produced after the heat treatment at 500°C and 1,100°C in air with good adhesion to the surface of glasses and silicon wafers. Table 1 below demonstrates main characteristics of the sols for boron doping. Dielectric properties of the films were controlled within the operations used, and the final resistance of silicon was in the range 7–90 Ω/cm.

TABLE 1. Characteristics of the sols for boron doping.

Kinematic viscosity at 20°C (cSt)	Density at 20°C (g/cm^3)	Content of boron oxide (g/l)
2.2–5.0	0.84–0.86	7.0–9.0
2.3–5.0	0.84–0.86	14.0–18.0
2.3–5.0	0.84–0.86	22.0–26.0
1.4–1.6	0.85–0.88	51.0–61.0

Protection coatings

Technology for manufacturing of coatings by sol-gel method includes following steps: preparation of mixture (sol); sol aging for 1–2 weeks; filtration; application of a medium on the wafer by centrifugation method; thermal treatment in the controlled gas atmosphere.

Protective quartz coatings (Figure 2) have following characteristics:

- Homogeneous clear coating is formed after thermal treatment at temperatures 200–500°C
- Coating thickness is 1–3 μm
- Coating size: 1–11 cm in diameter
- Mechanical durability to temperature variation
- Humidity and corrosion resistance
- Dielectric capacitance coefficient: 10.5
- Initial charge on the board of silicon division: approximately 2*1,010 cm^{-2}
- Ion **Na, K, Li** charge: 1,012 atoms/cm^2

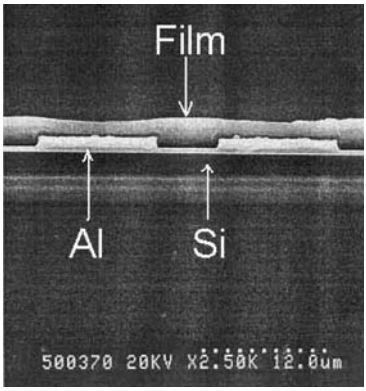

Figure 2. SEM-edge of protective sol-gel film.

Decorative coatings have following characteristics:

- Treatment temperature: 200–500°C
- Good adhesion to glass surface, plastics, silicon
- Coating thickness: 0.2 μm
- Humidity and corrosion resistance
- Ultraviolet radiation resistance (Figure 3)

Cast into a mold, and with further drying and heat-treatment, *dense ceramic* or *glass* articles with novel properties can be formed that cannot be created by any other method. Macroscopic optical elements and active optical components as well as large area hot mirrors, cold mirrors, lenses and beam splitters all with optimal geometry can be made quickly and at low cost via the sol-gel route.

Thick silica gel glasses

Thick silica gel glasses (Figure 4) can be applied in optics, quantum electronics, microelectronics, spectacles of different types, screens of TFT- displays, optical windows in devices, plates for a microwave microcircuit, etc.

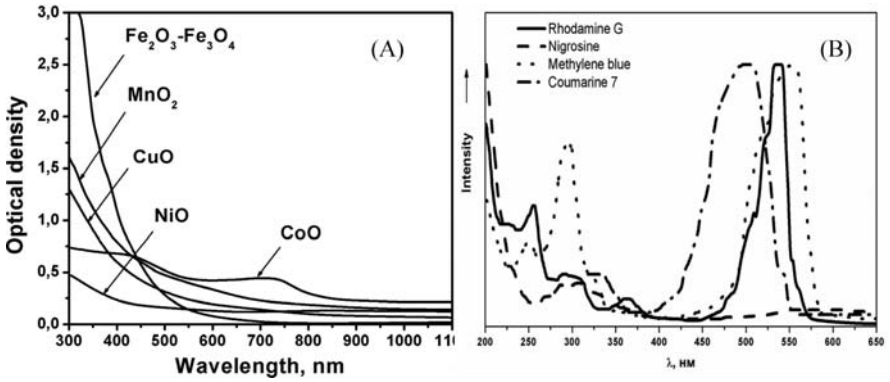

Figure 3. Colored sol-gel films doped by oxides of metals (A) and organic dyes (B).

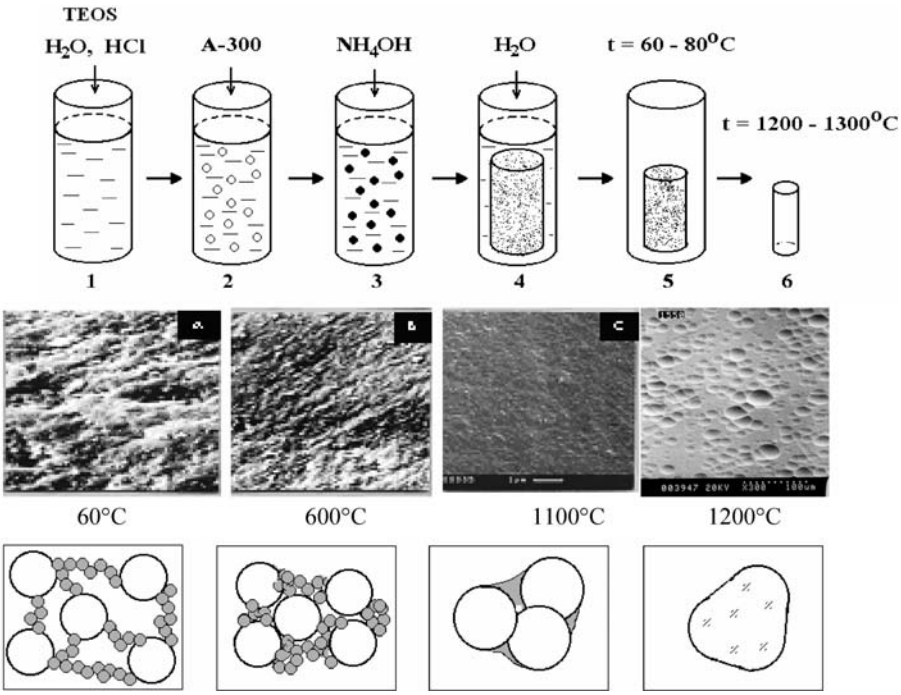

Figure 4. The steps of sol-gel glass synthesis.

With the viscosity of a sol adjusted into a proper range, both optical and refractory ceramic *fibers* can be drawn which are used for fiber optic sensors and thermal insulation, respectively.

Ultra-fine and uniform ceramic *powders* can be formed by precipitation. These powders of single- and multicomponent compositions can be made in submicrometre particle size for dental and biomedical applications. Composite

powders have been patented for use as agrochemicals and herbicides. Also powder abrasives, used in a variety of finishing operations, are made using a sol-gel type process.

Spherical particles

Silica spheres were prepared by hydrolysis and polycondensation of tetraethylorthosilicate in water solution with basic catalyst and continuous mixing. The silica spheres were dried at temperatures ~293 K. Spherical silica particles of 1–3 mm average diameter have been obtained (Figures 5, 6).

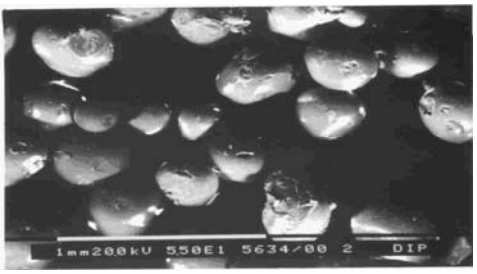

Figure 5. SEM micrograph of the spherical silica particles.

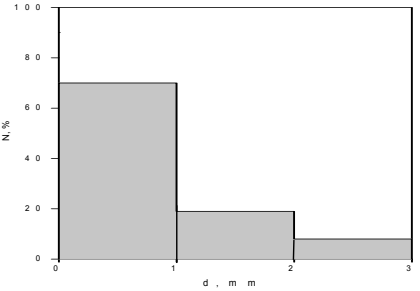

Figure 6. Distribution on the sizes of the sol-gel spherical silica particles.

Colloidal nanosized silica

We produced new ultra dispersed suspension on the basis of pyrogenic silicon dioxide (Figure 7). The obtained product has following characteristics:

– Density of suspension	1.09–1.10 г/см^3
– pH at 200^{0}C	5.5–7.0
– Contents SiO_2, wt%	13–17
– Size of fragments, nm	30–80.

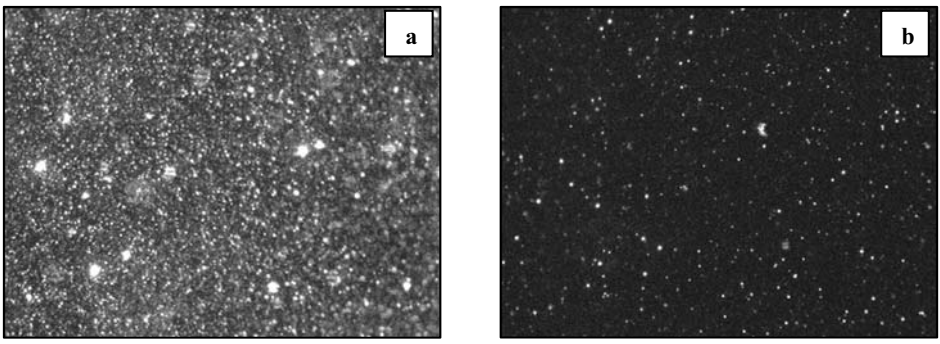

Figure 7. Micrographs of the colloidal nanosized silica (aerosil A-90): (a) – with NaOH, (b) – without stabilizer.

Colloidal nanosized silica is of huge interest for application in various branches of a science and industry: during production of paper, high-temperature wear-resistant ceramics, quartz glass by sol-gel method, polishing of semiconducting materials, manufacturing of cellophane et al.

Aerogels

If the liquid in a wet gel is removed under a supercritical conditions, a highly porous and extremely low density material called *aerogel* is obtained. Aerogels are a novel class of porous materials with wide range of applications. The unique properties include low density, high surface area, low thermal conductivity and low dielectric permittivity. They are highly porous solid materials with extremely low densities (bulk densities 0.004–0.500 g/cm^3), large, open pores, and high specific surface areas. Aerogels possess high thermal isolation ability – up to 800°C, acoustic isolation – speed of a sound through aerogel makes only 100 m/s. The refraction coefficient of aerogel is very small: – 1.0–1.05. One ounce (28,349 g) aerogel has a surface area equal to ten areas of a football field.

The most famous examples of inorganic gels are produced from silicon precursors (Figure 7). The most common of these are tetramethyl orthosilicate (TMOS, $Si(OCH_3)_4$), and tetraethylorthosilicate (TEOS, $Si(OCH_2CH_3)_4$. The balanced chemical equation for the formation of a silica gel from TEOS is:

$$Si(OCH_2CH_3)_4(l) + 2H_2O\ (l) \longrightarrow SiO_2\ (s) + 4\ HOCH_2CH_3 \qquad (l)$$

The physical-chemical properties of SiO_2 aerogels vary over a wide range because of the differences in the structure of the primary particles and network formation.

Drying the gel at low temperature (25–100^{0}C), it is possible to obtain porous solid matrices called *xerogels*.

One of the more important applications of sol-gel processing is to carry out *zeolite* synthesis. Other elements (metals, metal oxides) can be easily incorporated into the final product and the silicalite sol formed by this method is very stable.

Other products fabricated with this process include various *ceramic membranes* for microfiltration, ultrafiltration, nanofiltration, pervaporation and reverse osmosis.

4. Conclusions

The sol-gel method is known to produce materials from solutions either in bulk, coatings, films, fibers or powders. It is also known that this method makes

possible a low temperature processing of materials. This technology has dramatically grown in the last three decades. Concerning the microstructures, the sol-gel method applies to porous materials, dense materials like glasses and ceramics, organic-inorganic hybrids and nanocomposites.

Advantages of Sol-Gel Technique

1. Can produce thin bond-coating to provide excellent adhesion between the metallic substrate and the top coat
2. Can produce thick coating to provide corrosion protection performance
3. Can easily shape materials into complex geometries in a gel state
4. Can produce high purity products because the organo-metallic precursor of the desired ceramic oxides can be mixed, dissolved in a specified solvent and hydrolyzed into a sol, and subsequently a gel, the composition can be highly controllable
5. Can have low temperature sintering capability, usually 200–600°C
6. Can provide a simple, economic and effective method to produce high quality coatings

References

1. L.L. Hench and J.K. West Chem. Rev., 90, 35–40 (1990).
2. O. Lev et al., Anal. Chem. 67(1), 22A–30A (1995).
3. C.J. Brinker and G.W. Scherer, Sol-Gel Science: The Physics and Chemistry of Sol-Gel Processing (Academic, New York, 1990).
4. C.J. Brinker and G.W.J. Scherer, Non-Cryst. Solid. 70, 301–322 (1985).
5. K.D. Keefer, in: Silicon Based Polymer Science: A Comprehensive Resource; eds. J.M. Zeigler and F.W.G. Fearon, ACS Advances in Chemistry Ser. No. 224 (American Chemical Society, Washington, DC, 1990), pp. 227–240.
6. C.J. Brinker, A.J. Hurd, P.R. Schunk, C.S. Ashely, R.A. Cairncross, J. Samuel, K.S. Chen, C. Scotto and R.A. Schwartz, Sol-gel derived ceramic films–fundamentals and applications, in: K. Stern (Ed.), Metallurgical and Ceramic Protective Coatings (Chapman & Hall, London, 1996), pp. 112–151.
7. T. Troczynski and Q. Yang, Process for Making Chemically Bonded Sol-Gel Ceramics. U.S. Pat. No. 6,284,682, May 2001.
8. T. Olding, M. Sayer and D. Barrow, Ceramic sol-gel composite coatings for electrical insulation, Thin Solid Films 398–399, 581–586 (2001).
9. V.G. Kessler, G.I. Spijksma, G.A. Seisenbaeva, S. Håkansson, D.H.A. Blank and H.J.M. Bouwmeester, J. Sol-Gel Sci. Tech. 40, 163–179 (2006).

SOL-GEL DERIVED FILMS IN POROUS ANODIC ALUMINA

NIKOLAI V. GAPONENKO*
Laboratory of Nanophotonics, Belarusian State University of Informatics and Radioelectronics, Browki Str. 6, 220013 Minsk, Belarus

Abstract. The report summarizes peculiarities of synthesis and optical properties of the structures xerogel/porous anodic alumina doped with Er, Tb and Eu. Porous anodic alumina is considered as attractive material for sol-gel synthesis from viewpoint of luminescence properties of the structure xerogel/porous anodic alumina. Origin of strong luminescence of lanthanides from xerogels in mesoporous matrices is discussed.

Keywords: Sol-gel, xerogel, porous anodic alumina, photonic crystal, luminescence, erbium, terbium, europium.

1. Introduction

Interest in sol-gel synthesis arises from the relatively low cost and the approach allows the chemical content and concentration ratio of the elements of the sol-gel derived films to be tailored, with ready fabrication in a form of powder, thin films and bulk materials. Sol-gel derived materials could be prepared from a colloidal solution which is a dispersion of colloidal particles with diameter of 1–100 nm in a liquid.[1]

About a decade ago it was demonstrated that colloidal solutions deposited by spinning are able to penetrate through the channels of mesoporous matrices, enabling after heat treatment fabrication of a xerogel (dried gel) located within the porous layer of several micrometers thickness. Most of the experiments with this property of sol-gel synthesis have been done with mesoporous materials as porous silicon, porous anodic alumina and artificial opals.

*To whom correspondence should be addressed: Nikolai V. Gaponenko, Laboratory of Nanophotonics, Micro and Nanoelectronics Department, Belarusian State University of Informatics and Radioelectronics, Browki Str. 6, 220013 Minsk, Belarus; e-mail: nik@nano.bsuir.edu.by

P. Innocenzi, Y. L. Zub and V. G. Kessler (eds.), *Sol-Gel Methods for Materials Processing*.

Synthesis of sol-gel derived oxides in mesoporous materials was started from porous silicon, indeed, fabrication of porous silicon still remains one of the most simply method of synthesis porous material due to silicon ability to oxidize or dissolve.[2]

Type of porosity of this material depends on the doping level of silicon substrate, the current density and concentration of electrolyte, thus micro-, meso-, and macroporous silicon could be fabricated using the same electrochemical cell.[3] Although porous silicon had been investigated in microelectronics since 1950s,[4,5] a burst of interest to it occurred in 1990 when luminescent properties of porous Si has been reported.[6] Interest in fabrication of the structure xerogel/porous silicon was initiated in 1990s by a challenging problem of development light-emitting devices for visible and infrared emission on silicon basis. In the experiments micro-,[7] meso-[8–14] and macroporous[15] silicon was used for spin-on deposition of coatable sols containing erbium nitride dissolved in water and ethanol. Penetration of the sols of metalloorganic precursors through the channel of the pores was concluded from observation the components of xerogels with SIMS and SNMS,[9] TEM[13] and RBS[12] analyses in porous silicon 0.3,[13] 1.5[12] and 5[9] μm thick. However, wide size dispersion of the pores and their orientation hampers in reproducible synthesis of xerogels, that was concluded even from comparison of PL measurements from xerogels in micro-, meso- and macroporous silicon.[7,9,12]

2. Experimental

Furthermore, porous anodic alumina (PAA) is known to exhibit a regular pore morphology with pores at the center of approximately hexagonal cells, whose size can be tailored.[16,17] Illustration the possibility of tailoring the size of the cells by choosing the electrolyte and anodizing conditions is given by Figure 1, which bring together selected SEM-images of our PAA samples taken at the same magnification 40,000.

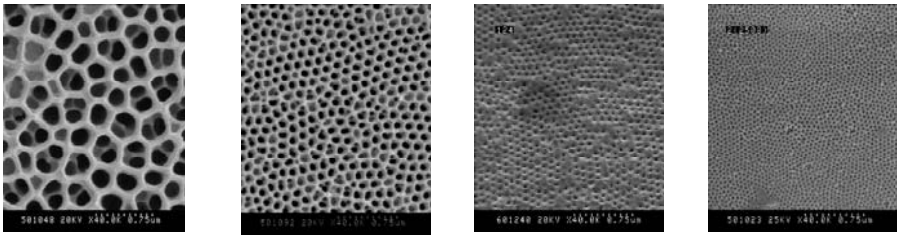

(a) (b) (c) (d)

Figure 1. SEM-images of porous anodic alumina films illustrating variation in size of the honeycomb cells and diameter of the pores. All images were selected for magnification 40,000. The samples were prepared at different electrolytes: (a) phosphoric acid 1.7%, (b) oxalic acid 3%, (c) sulphosalicylic acid 17%, (d) sulphuric acid 9%.

Transmission of porous anodic alumina film within the wide visible range could be greater then 90% at direction parallel to the pore channels and increases with perfection of the structure due to diminishing diffuse scattering caused by the defects of a sample. Transmission of porous anodic alumina film drastically reduces even with slight deviation the angle of incidence (registration) from direction parallel to the channels of the pores (Figure 2a). This feature is considered regarding anisotropy of the photonic density of states (DOS) in mesoscopic structures with periodically modulated refractive index in two dimensions – 2D photonic crystals 18. Anisotropy of DOS in porous anodic alumina is well-refined from the scattering measurement (Figure 2b). Three petals are always observed at scattering indicatrixes measured for different angles of incidence. The one side petal coincides with incident beam propagation, whereas orientation of the other side petal shows mirror symmetry to incident beam with respect to the pore axis. Significantly is appearance of the central petal along the channels of the pores regardless the angle of incidence. This central petal originates from diffuse scattering of light through the matrix with nonisotropic DOS like porous anodic alumina film. DOS has a maximum value in the direction along the pores of anodic alumina films and a minimum in the perpendicular directions.

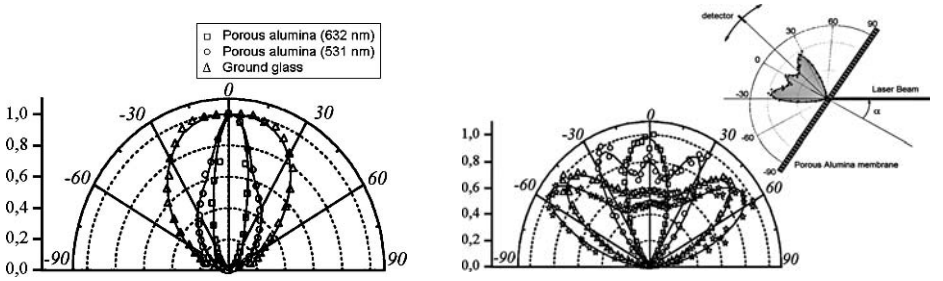

Figure 2. Angular diagrams of the porous anodic alumina membrane: (a) transmission angular diagram and diagram of glass given for comparison; (b) scattering indicatrixes for different angles of laser beam incidence. Inset of (b) depicts scheme of experimental setup. Laser beam wavelength 632 and 531 nm (a), 632 nm (b) (After ref.[18]).

High-transparency of anodic alumina oxide on the one hand and strong optical anisotropy on the other hand may be one of the reasons of growing interest to exploit this material as a cage for light-emitting species. Filling the channels of the pores of anodic alumina films with silica,[19–21] titania,[22–26] alumina[27–29] xerogels doped with lanthanide ions Er, Tb, Eu, organic dyes,[30] semi-conductor nanocrystals,[31,32] polymers[33,34] quantum dots[35,36] and biological samples[37] has been investigated, and strong luminescence of optically active species incurporated in voids of anodic alumina was reported.

To investigate the spatial distribution of xerogel deposited onto porous anodic alumina by spinning followed by thermal treatment, selected samples containing terbium-doped titania and – alumina xerogels were examined by SIMS, [21,23] TEM, SEM and EDX analyses.[22,24,28,38] After the first spin-on deposition of a sol followed by drying transmission electron micrographs revealed relatively dark, fine textured material of amorphous appearance at the base of the pore. Gel material towards the middle of the film appeared to be limited to a thin film on the surface of the cell material adjacent to the pores with the main parts of the pore volumes remaining unfilled. Further the base of the pore 30 μm thick is completely filled with the microporous alumina xerogel after five sequential spin-on depositions.

Technological methods of increase the PL intensity through electrochemistry and sol-gel synthesis is given in Figure 3. Er, Tb and Eu luminescence from xerogels fabricated by spinning on porous anodic alumina is much stronger then from the same xerogels fabricated on flat silicon substrate.[22,29] Because of the low efficiency of Er PL, fabrication of one spin-on layer is not sufficient for registration 1.54 μm light emission. Generally, PL of lanthanide from the structure xerogel/PAA increases with the thickness of porous anodic alumina, and for some excitation wavelength increases with the number of xerogel layers inside the pores,[39] and even with the chosen concentration of lanthanides in xerogels.[22,26,28,40] Concentration quenching of lanthanides in xerogels embedded in mesoporous matrices has not been detected.

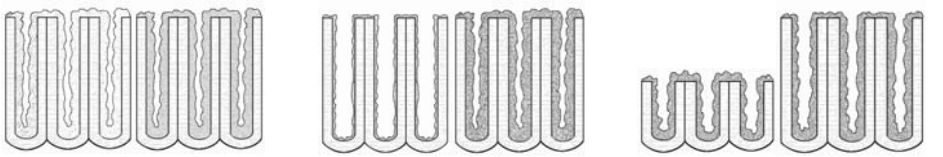

Figure 3. Technological factors towards increase in PL of lanthanides from xerogel/porous anodic alumina structure: (a) increase the concentration of lanthanides in xerogel (see for the details[22,26,28,40]); (b) increase the number of xerogel layers[22,23,25,28]; (c) increase the porous Al_2O_3 film thickness.[21,23,45]

Some porous anodic alumina samples fabricated in oxalic acid exhibit blue PL visible to the naked eye with a strong band at about 450 nm.[36,41–43] The origin of the blue PL from PAA grown in oxalic acid is associated with generation F-centres during anodizing of aluminium or excitation of residual chemical components absorbed from the electrolytes.

A method for the fabrication of luminescent visible images based on anodizing of aluminium, photolithography and sol-gel synthesis of Tb- and Eu-doped xerogels was recently proposed.[44,45] Development of multicolor luminescent images with the use of blue PL of porous anodic alumina, light emission of

quantum dots, lanthanides and also dye molecules[46,47] from xerogels in porous anodic alumina needs further experimental work.

In conclusion, penetration of sols containing lanthanide ions through mesoscopic channels of porous anodic alumina followed by thermal treatment promotes strong photoluminescence of lanthanides. One of the reasons of enhanced photoluminescence observed from porous anodic alumina is supposed to be the anisotropy of photonic density of states.

Acknowledgements

The samples described in the paper were prepared in Laboratory of Nanophotonics, BSUIR, by I.S. Molchan, O.V. Sergeev, E.A. Stepanova, G.K. Maliarevich, T.I. Orekhovskaja, D.A. Tsyrkunov.

References

1. V.E. Borisenko, S. Ossicini, *What Is What in the Nanoworld* (Wiley-VCH, Weinheim, 2004).
2. J.-C. Vial, J. Derrien (eds), *Porous Silicon Science and Technology* (*Springer-Verlag and Les Editions de Physique Les Ulis* 1995), 356 pp..
3. A.G. Cullis, L.T. Canham, P.D.J. Calcott, *J. Appl. Phys.* 82, 909 (1997).
4. A. Uhlir, *Bell Syst. Tech. J.* 35, 333 (1956).
5. D.R. Turner, *J. Electrochem. Soc.* 105, 402 (1958).
6. L.T. Canham, *Appl. Phys. Lett.* 57, 1046 (1990).
7. M. Stepikhova, L. Palmetshofer, W. Jantsch, H.J. von Bardeleben, N.V. Gaponenko, *Appl. Phys. Lett.* 74, 537 (1999).
8. A.M. Dorofeev, N.V. Gaponenko, V.P. Bondarenko, E.E. Bachilo, N.M. Kazuchits, A.A. Leshok, G.N. Troyanova, N.N. Vorozov, V.E. Borisenko, H. Gnaser, W. Bock, P. Becker, H. Oechsner, *J. Appl. Phys.* 77, 2679 (1995).
9. A.M. Dorofeev, E. Bachilo, V. Bondarenko, V. Borisenko, N. Gaponenko, N. Kazuchits, G. Troyanova, N. Vorosov, H. Gnaser, W. Bock, P. Becker, H. Oechsner, *Thin Solid Films* 276, 171 (1996).
10. S. Sen, J. Siejka, A. Savtchouk, J. Lagowski, *Appl. Phys. Lett.* 70, 2253 (1997).
11. N.V. Gaponenko, A.V. Mudryi, O.V. Sergeev, V.E. Borisenko, E.A. Stepanova, A.S. Baran, A.I. Rat'ko, J.C. Pivin, J.F. McGilp, *Phys. Stat. Sol. (a)* 165, 131 (1998).
12. W. Henley, Y. Koshka, J. Lagowski, J. Siejka, *J. Appl. Phys.* 87, 7848 (2000).
13. A. Moadhen, H. Elhouichet, S. Romdhane, M. Questati, J.A. Roger, H. Bouchriha, *Semi-cond. Sci. Technol.* 18, 703 (2003).
14. A. Moadhen, H. Elhouichet, C. Jardin, M. Questati, J.A. Roger, *Phys. Stat. Sol. (a)* 202, 1508 (2005).
15. N.V. Gaponenko, A.V. Mudryi, O.V. Sergeev, M. Stepikhova, L. Palmetshofer, W. Jantsch, J.C. Pivin, B. Hamilton, A.S. Baran, A.I. Rat'ko, *J. Luminescence* 80, 399 (1999).
16. G.E. Thompson, R.C. Furneaux, G.C. Wood, J.A. Richardson, J.S. Goode, *Nature* 272, 433 (1978).
17. G.E. Thompson, G.C. Wood, *Nature (London)* 290, 231 (1981).

18. A.A. Lutich, S.V. Gaponenko, N.V. Gaponenko, I.S. Molchan, V.A. Sokol, V. Parkhutik, *Nano Lett.* 4, 1755 (2004).
19. N.V. Gaponenko, V.M. Parkun, E.E. Bachilo, G.E. Malashkevich, V.E. Borisenko, in: *Physics, Chemistry and Application of Nanostructures: Reviews and Short Notes to NANOMEETING'95*, edited by V.E. Borisenko, A.B. Filonov, S.V. Gaponenko, V.S. Gurin (BSUIR, Minsk, 1995), 80 pp..
20. N.V. Gaponenko, A.V. Mudryi, V.M. Parkun, E.A. Stepanova, A.I. Ratko, V.E. Borisenko, *Inorg. Mater.* 33, 916 (1997).
21. N.V. Gaponenko, V.M. Parkun, O.S. Katernoga, V.E. Borisenko, A.V. Mudryi, E.A. Stepanova, A.I. Rat'ko, M. Cavanagh, B. O'Kelly, J.F. McGilp, *Thin Solid Films* 297, 202 (1997).
22. N.V. Gaponenko, J.A. Davidson, B. Hamilton, P. Skeldon, G.E. Thompson, X. Zhou, J.C. Pivin, *Appl. Phys. Lett.* 76, 1006 (2000).
23. N.V. Gaponenko, O.V. Sergeev, E.A. Stepanova, V.M. Parkun, A.V. Mudryi, H. Gnaser, J. Misiewicz, R. Heiderhoff, L.J. Balk, G.E. Thompson, *J. Electrochem. Soc.* 148, H13 (2001).
24. N.V. Gaponenko, I.S. Molchan, G.E. Thompson, P. Skeldon, A. Pakes, R. Kudrawiec, L. Bryja, J. Misiewicz, *Sensor. Actuator. A* 99, 71 (2002).
25. I.S. Molchan, N.V. Gaponenko, R. Kudrawiec, J. Misiewicz, G.E. Thompson, P. Skeldon, *J. Electrochem. Soc.* 151, H16 (2004).
26. Peng, E. Xie, C. Jia, R. Jiang, H. Lin, *Mater. Lett.* 59, 3866 (2005).
27. N.V. Gaponenko, A.V. Mudryi, O.V. Sergeev, V.E. Borisenko, E.A. Stepanova, A.S. Baran, A.I. Rat'ko, J.C. Pivin, J.F. McGilp, *Spectrochim. Acta A* 54, 2177 (1998).
28. N.V. Gaponenko, I.S. Molchan, O.V. Sergeev, G.E. Thompson, A. Pakes, P. Skeldon, R. Kudrawiec, L. Bryja, J. Misiewicz, J.C. Pivin, B. Hamilton, E.A. Stepanova, *J. Electrochem. Soc.* 149, H49 (2002).
29. R. Kudrawiec, A. Podhorodecki, N. Mirowska, J. Misiewicz, I. Molchan, N.V. Gaponenko, A.A. Lutich, S.V. Gaponenko, *Mat. Sci. Eng. B* 105, 53 (2003).
30. Moadhen, H. Elhouichet, L. Nosova, M. Oueslati, *J. Luminescence* 126, 789 (2007).
31. V.S. Dneprovski, E.A. Zhukov, O.A. Shalygina, V.L. Lyaskovski, E.A. Muljarov, S.A. Gavrilov, Y. Masumoto, *J. Exp. Theor. Phys.* 94, 1169 (2002).
32. A.I. Belogorokhov, S.A. Gavrilov, L.I. Belogorokhova, *Phys. Status Solidi A* 197, 204 (2003).
33. D. Qi, K. Kwong, K. Rademacher, M.O. Wolf, J.F. Young, *Nano Lett.* 3, 1265 (2003).
34. Y. Shen, R. Jia, H. Luo, X. Chen, D. Xue, Z. Hu, *Spectrochim. Acta Part A* 60, 1007 (2004).
35. J. Xu, J. Xia, J. Wang, J. Shinar, Z. Lin, *Appl. Phys. Lett.* 89, 133110 (2006).
36. N.V. Gaponenko, T.I. Orehovskaya, G.K. Maliarevich, D.A. Tsyrkunov, I.S. Molchan, G.E. Thompson, in: *Physics, Chemistry and Applications of Nanostructures: Reviews and Short Notes to NANOMEETING-2007*, edited by V.E. Borisenko, S.V. Gaponenko, V.S. Gurin (World Scientific, Singapore, 2007), p. 570.
37. V. Grasso, V. Lambertini, P. Ghisellini, F. Valerio, E. Stura, P. Perlo, C. Nicolini, *Nanotechnology* 17, 795 (2006).
38. I.S. Molchan, N.V. Gaponenko, R. Kudrawiec, J. Misiewicz, G.E. Thompson, *Mat. Sci. Eng. B* 105, 37–39 (2003).
39. N.V. Gaponenko, I.S. Molchan, D.A. Tsyrkunov, G.K. Maliarevich, M. Aegerter, J. Puetz, N. Al-Dahoudi, J. Misiewicz, R. Kudrawiec, V. Lambertini, N. Li Pira, P. Repetto, *Microelectron. Eng.* 81, 255 (2005).
40. I.S. Molchan, N.V. Gaponenko, R. Kudrawiec, J. Misiewicz, L. Bryja, G.E. Thompson, P. Skeldon, *J. Alloys Comp.* 341, 251 (2002).
41. G.H. Li, Y. Zhang, Y.C. Wu, L.D. Zhang, *J. Phys.-Condens. Mat.* 15, 8663 (2003).

42. W.L. Xu, M.J. Zheng, S. Wu, W.Z. Shen, *Appl. Phys. Lett.* 85, 4364 (2004).
43. G.H. Li, Y. Zhang, Y.C. Wu, L.D. Zhang, *Appl. Phys. A* 81, 627 (2005).
44. N.V. Gaponenko, I.S. Molchan, G.E. Thompson, V. Lambertini, P. Repetto, *J. SID* 11, 27 (2003).
45. N.V. Gaponenko, *Sol-Gel Derived Films in Mesoporous Matrices* (Belaruskaja Navuka, Minsk, 2003) – in Russian.
46. K. Maruszewski, D. Andrzejewski, W. Strek, *J. of Luminescence* 72–74, 226 (1997).
47. K. Maruszewski, M. Jasiorski, M. Salamon, W. Strek, *Chem. Phys. Lett.* 314, 83 (1999).

SOL-GEL SYNTHESIS OF MESOPOROUS TiO_2 FILMS FOR VISIBLE LIGHT SENSITIVE TiO_2/CdS HETEROSTRUCTURES

YURIY GNATYUK[1], MAXIM ZHUKOVSKYJ[1], NATALIA SMIRNOVA[1*], ANNA EREMENKO[1], ASTA GUOBIENE[2], SIGITAS TAMULEVIČIUS[2]

[1]*O. Chuiko Institute of Surface Chemistry, Ukrainian National Academy of Sciences, 17 General Naumov Str., Kyiv, 03164, Ukraine*

[2]*Institute of Physical Electronics of Kaunas University of Technology, Savanoriu 271, Kaunas LT-51368, Lithuania*

Abstract. Mesoporous TiO_2 films were prepared by template assisted sol-gel method and used as support for deposition of CdS particles on its surface to produce visible light sensitive nanocomposites. The influence of the surface morphology of mesoporous titania matrix onto the TiO_2/CdS heterostructure formation was investigated using UV-Vis, IR, low-angle XRD, SEM and AFM methods.

Keywords: Sol-gel, mesoporous TiO_2 films, TiO_2/CdS.

1. Introduction

Modified titania materials are good candidates to produce efficient photocatalysts, solar cell devices, self-cleaning surfaces, gas sensors, etc.[1,2] For most applications one would prefer to obtain visible light sensitive titanium dioxide with the developed porous structure and high surface area. A lot of ways have been explored to reach desired properties. Sol-gel synthesis for the preparation of modified oxides is usually used at the laboratory scale due to its low cost and possibility to perform different kind of modifications. Surfactant incorporation for synthesis of porous powders and films, metal ion introduction to control the phase composition, porosity, band gap and electronic structure could be easily

*To whom correspondence should be addressed: Dr. N. Smirnova; e-mail: smirnat@i.com.ua

P. Innocenzi, Y. L. Zub and V. G. Kessler (eds.), *Sol-Gel Methods for Materials Processing*.

achieved utilizing sol-gel technology.[3–5] Alternative route is modification of sol-gel synthesized mesoporous titanium dioxide films through adsorption or precipitation of semiconductor nanoparticles to produce coupled nanocomposites with increased efficiency.[6]

This study is devoted to investigation of the influence of surface morphology of sol-gel synthesized mesoporous TiO_2 films on the structure and spectral response of visible light sensitive TiO_2/CdS nanocomposites prepared via precipitation of CdS particles by bath method.

2. Experimental

Mesoporous TiO_2 thin films were synthesized by sol-gel method using titanium tetraisopropoxide as a metal source and three-block copolymer $(PEO)_{20}(PPO)_{70}(PEO)_{20}$ Pluronic P123 as a template in alcoholic medium. Concentrated hydrochloric acid and acetylaceton were added to the precursor as stabilizers for the resulting colloid. Molar ratio of the components in the sol for films deposition was as following: $Ti(O^iPr)_4$: P123 : acac : HCl : H_2O : C_2H_5OH = 1 : 0.05 : 0.5 : 4.6 : 10 : 41. To burn out organic residues and to form titania photocatalytically active phase, anatase, the films were heat treated at 300°C, 400°C and 500°C in air.

TiO_2/CdS heterostructures were prepared by chemical bath deposition method.[7] CdS particles were precipitated onto the surface of the mesoporous TiO_2 films under thiourea decomposition in alkaline medium (NH_4OH, 25%) in the presence of Cd^{2+} source ($CdSO_4 \cdot 2.5H_2O$ (AnalaR grade)).

Samples were characterized by UV-Vis, IR, low-angle XRD, SEM, AFM methods.

3. Results and Discussion

Template assisted sol-gel synthesis method of mesoporous TiO_2 films was chosen for the preparation of titania coatings with developed porous structure. Selection of amphiphilic three-block copolymer of ethylene and propylene oxides Pluronic P123 as the structure directing agent is based on its ability to interact with the polar fragments of titania/alkoxide network by means of hydrogen bonding and weak electrostatic interactions[8–9] and, thus, not to destroy mesostructure after template removal under moderate conditions (solvent extraction, slow heating, etc.). Concentrated hydrochloric acid and acetylacetone were added to the precursor to slow down the agglomeration of TiO_2 primary particles and to prevent immediate precipitation of oxide phase with poor porosity.[10] As-prepared TiO_2 films have a set of reflections in the low-angle XRD spectra (Figure 1) for which calculated *d* spacing values are 19.6, 10.9, 5.6, 3.7, 2.8 and

2.3 nm correspondingly. This set of reflections can be attributed to the formation of ordered lamellar mesophase[11] for organic/ inorganic hybrid films before calcination. After calcination at 300°C and 400°C, only one peak was preserved in the low-angle XRD spectra of the TiO_2 films (Figure 1, inset) due to the partial disordering of the mesoporous structure of the films as a result of organic residuals burnout/TiO_2 matrix crystallization. In addition, considerable shrinkage of the mesoporous structure of the films can be postulated taking into account *d* spacing values (300°C – 15.1 nm, 400°C – 14.9 nm) calculated for films after thermal treatment. Further increase of calcination temperature up to 500°C led to disappearance of the low-angle XRD reflections for the TiO_2 films as a result of loss of long-range meso-ordering in the films because of the high tendency of titanium dioxide to crystallize at temperatures higher than 400°C.

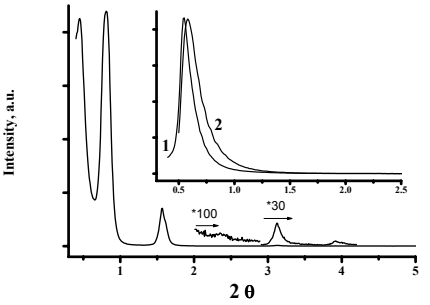

Figure 1. Low-angle XRD pattern for as-prepared TiO_2 film. Inset: low-angle XRD patterns for TiO_2 film heat treated at 300°C – 1and 400°C – 2.

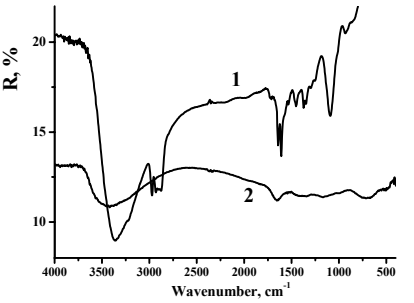

Figure 2. FT-IR spectra of the TiO_2 mesoporous films: 1 – as-prepared, 2 – heat treated at 500°C.

FT-IR spectra of the investigated TiO_2 films (Figure 2) deposited onto steel substrates indicate clearly that the organic part of the gel is burnt out after thermal treatment of the films up to 500°C.

Chemical deposition of the CdS particles onto the surface of the TiO_2 films was made by early-described bath method.[7] The deposition process is based on the slow release of Cd^{2+} and S^{2-} ions in the solution, which permits controlled crystal growth on the substrates that are suitably mounted in the solution. The slow release of Cd^{2+} ions is achieved by the dissociation of a complex species of cadmium $[Cd(NH_3)_4]^{2+}$. The S^{2-} ions are supplied by decomposition of thiourea.

The overall reaction for the process is given by.[7]

$$[Cd(NH_3)_4]^{2+} + SC(HN_2)_2 + 4OH^- \rightarrow CdS + 6NH_3 + CO_3^{2-} + H_2O$$

Cadmium sulphide precipitation on the surface of the mesoporous TiO_2 films was monitored by means of UV-Vis spectroscopy and characterized by SEM and AFM microscopy (*vide infra*).

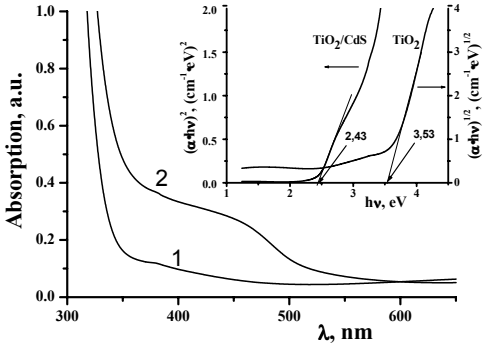

Figure 3. Optical absorption spectra of the TiO_2 – 1 and TiO_2/CdS – 2 films. Inset: $(\alpha h\nu)^{1/2} = f(h\nu)$ and $(\alpha h\nu)^2 = f(h\nu)$ dependences for TiO_2 and TiO_2/CdS films.

Synthesized TiO_2 films were optically transparent in the wide spectral range $350 < \lambda < 1{,}000$ nm (Figure 3, curve 1). Absorption onset for the TiO_2 films is observed near 350 nm and is shifted towards higher energy in comparison with bulk TiO_2 powders (380–400 nm). TiO_2/CdS composites were yellow colored, that is typical for cadmium sulphide, which has absorption band in the visible range of the spectrum with absorption onset at $\lambda = 517$ nm (Figure 3, curve 2). Band gap energy E_g values were calculated by extrapolation of the linear parts of the dependences $(\alpha h\nu)^{1/2} \sim f(h\nu)$ and $(\alpha h\nu)^2 \sim f(h\nu)$ to abscissa axis for TiO_2 and CdS nanocrystals (Figure 3, inset) assuming indirect and direct electronic transitions to prevail for above semiconductors,[12,13] correspondingly. E_g value of 3.5 eV was obtained for mesoporous TiO_2 films that is considerably higher than reported E_g for bulk titanium dioxide, 3–3.2 eV, and corresponds to the formation of nanosized crystallites of TiO_2 in our films.[12] E_g value for chemically deposited CdS does not exceed that one for bulk cadmium sulphide and is equal to 2.4 eV.

Surface morphology of the mesoporous TiO_2 films as well as TiO_2/CdS heterostructures was studied using AFM microscopy. Surface of the TiO_2 film heat treated at 400°C consists of ordered rows of formations with sizes of 600–800 nm and heights in the range of 220–800 nm (Figure 4a) that might be attributed to the structure directing action of the template agent. Root mean square roughness R_q of the film is 105.3 nm. As it was stated earlier, further increase of heat treatment temperature up to 500°C leads to the loss of long-range mesoordering of the films. Now this effect can be observed assuming AFM image

of surface of the film (Figure 4b), from which it can be seen that the surface is much smoother and composed of densely packed formations with sizes of 300–600 nm and heights of 5–32 nm compared to the surface of 400°C treated

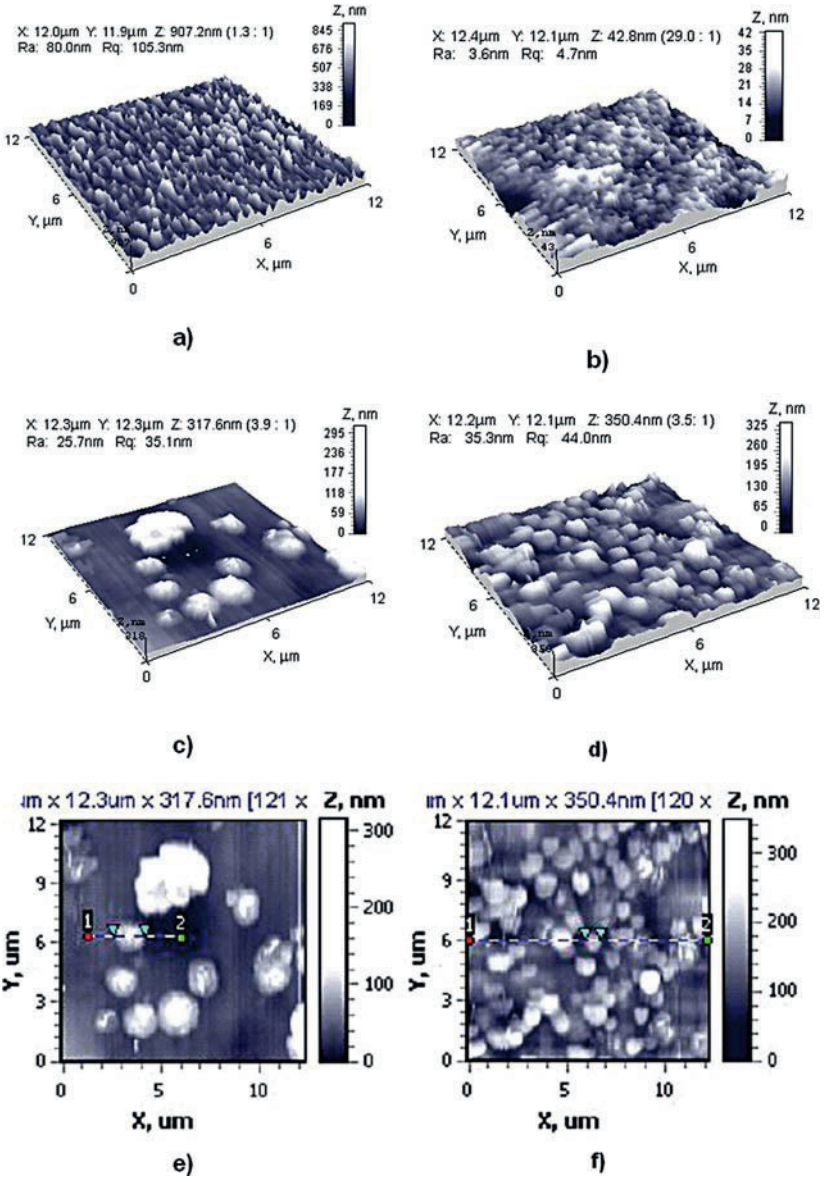

Figure 4. 3D and *2D* AFM images of the surface of TiO_2 and TiO_2/CdS films deposited onto glass substrates: (a) TiO_2 (400°C), (b) TiO_2 (500°C), (c), (e) TiO_2/CdS (400°C), (d), (f) TiO_2/CdS (500°C).

film.Substantial decrease of surface roughness R_q to 4.7 nm for the TiO_2 film treated at 500°C can be attributed to the crystallization of the titanium dioxide and possible compression of the structure. It was observed that size distribution of CdS particles over the TiO_2 support surface depends strongly on the substrate morphology. Large cadmium sulphide particles were formed on the surface of TiO_2 film calcined at 400°C with mean size in the range of 1.6–1.8 μm and heights of 5–170 nm (Figure 4c, e). Root mean square roughness R_q of the TiO_2(400°C)/CdS composite film is 35.1 nm. On the other hand, more homogeneous coverage with uniform CdS particles was observed for titanium dioxide film calcined at 500°C. As was evaluated from the AFM image, CdS particles with mean size of 0.8–1.0 μm and heights in the range of 65–265 nm (Figure 4d, f) homogeneously cover TiO_2 substrate surface treated at 500°C.

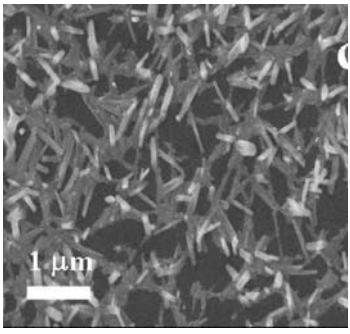

Figure 5. SEM image of TiO_2/CdS heterostructure.

Observed variations in the formed cadmium sulphide particles can be obviously attributed to the changes in the surface morphology and roughness of TiO_2 films' surface that in its turn is determined by heat treatment conditions. Homogeneous surface structure as well as low roughness of the mesoporous TiO_2 film calcined at 500°C favors the formation of great number of nuclei in crystallization of CdS particles with uniform growth rate in *z*-axis direction relative to the substrate. In opposite, in our opinion, highly rough surface of the TiO_2 film treated at 400°C has energetically not equivalent surface sites on which cadmium sulphide parti-cles nucleate during deposition process and thus, preferentially grow on them. Nevertheless high width to height ratio for formed CdS particles witnesses of high degree of coverage of TiO_2 surface by cadmium sulphide that was also proved by SEM microscopy of TiO_2 films surface after modification (Figure 5). As it was determined from SEM images, surface of mesoporous titanium dioxide films with pores in the range of 8–26 nm is homogeneously covered by CdS agglomerates that are aggregates of nanorod type formations with width of 50–70 nm and length in the range of micron.

4. Conclusions

Mesoporous TiO_2 films were synthesized using template assisted sol-gel method. Thermal treatment conditions determined the surface morphology and roughness of titanium dioxide films that in one's turn depends on degree of burnout of organic residuals and crystallization of oxide matrix.

Deposition of CdS particles onto the surface of mesoporous TiO_2 film can be proposed as a way of inorganic sensitization of titania film to visible light. Distribution of cadmium sulphide particles was highly sensitive to surface morphology and roughness of titanium dioxide films' surface.

References

1. A. Fujishima, T.N. Rao, D.A. Tryk, *J. Photochem. Photobiol. C: Photochem. Rev.* 1, 1–21 (2000).
2. M.R. Hoffmann, S.T. Martin, W. Choi, D.W. Bahnemann, *Chem. Rev.* 95, 69–96 (1995).
3. J. Wang, S. Uma, K.J. Klabunde, *Appl. Catal. B: Environ.* 48, 151–154 (2004).
4. J. Kim, K.C. Song, S. Foncillas, S.E. Pratsinis, *J. Europ. Ceram. Soc.* 21, 2863–2872 (2001).
5. C.T. Kresge, M.E. Leonowicz, W.J. Roh, J.S. Beck, *Nature* 359, 710–712 (1992).
6. M.G. Kang, H.-E. Han, K.-J. Kim, *J. Photochem. Photobiol. A: Chem.* 125, 119–125 (1999).
7. J.M. Dona, J. Herrero, *J. Electrochem. Soc.* 139, 2810–2814 (1992).
8. P. Yang, D. Zhao, D.I. Margolese, B.F. Chmelka, G.D. Stucky, *Nature* 396, 152–155 (1998).
9. G. Soler-Illia, C. Sanchez, *New J. Chem.* 24, 493–499 (2000).
10. V.G. Kessler, G.I. Spijksma, G.A. Seisenbaeva, S. Håkansson, D.H.A. Blank, H.J.M. Bouwmeester, *J. Sol-Gel Sci. Tech.* 40, 163–179 (2006).
11. P. Alberius, K. Frindell, R. Hayward, E. Kramer, G. Stucky, B. Chmelka, *Chem. Mater.* 14, 3284–3294 (2002).
12. B. Enright, D. Fitzmaurice, *J. Phys. Chem.* 100, 1027–1035 (1996).
13. D. Patidar, R. Sharma, N. Jain, T.P. Sharma, N.S. Saxena, *Bull. Mater. Sci.* 29, 21–24 (2006).

OBTAINING OF THE HYBRID SLICA-POLYMER SORBENTS FOR LIQUID CHROMATOGRAPHY

SERGEY S. HAYRAPETYAN, LILIT S. BANYAN,
LUSINE G. MANGASARYAN,
HAMBARDZUM G. KHACHATRYAN*
Yerevan State University, Department of Chemistry,
Chair of Analytical Chemistry,
1, Alek Manoukian Str., Yerevan, 375025 Armenia

Abstract. The obtaining of hybrid mineral-polymer sorbents, based on wide-porous microspherical silica gels (with 30 nm average pore diameter) and polymer components, has been discussed. The possibility to apply the obtained sorbents in reversed-phase high performance liquid chromatography has been studied. Introducing the polymer layer onto the surface of micro-spherical silica gel has been realized by means of "dry polymerization" of the corresponding monomers in the adsorbed layer of the porous matrix surface.

Keywords: Polymer-mineral packings, reversed-phase high performance liquid chromatography, poly-octadecylmetacrylate (Poly-ODMA), poly-octadecylmethcrylate-methylmethacrylate (Poly-ODMA-MMA), poly-octadecylmethacrylate-methylmethacrylate-divinylbenzene (Poly-ODMA-MMA-DVB), dry polymerization.

1. Introduction

The development of new methods for the synthesis of packing materials for chromatography aiming to improve their structure and chromatographic parameters always was and remains significant even today. Most often, researchers turn to different means of modification of the surface of already existing chromatographic systems. Reversed phase high performance liquid chromatography (RP-HPLC) is considered as the most popular HPLC technique. At present silica remains the most widely used packing material for HPLC.[1–4]

Problems with the modification of porous silica by organic compounds with different functional groups occupy the central place during the design of HPLC-packings.[5]

*To whom correspondence should be addressed: Hambardzum Khachatryan, Yerevan State University, Analytical Chemistry Chair, 1 Alek Manoukyan str., 375025 Yerevan, Armenia; e-mail: gold@ysu.am

P. Innocenzi, Y. L. Zub and V. G. Kessler (eds.), *Sol-Gel Methods for Materials Processing.*

Silanol groups play a key role during the modifying process of the silica gel surface by series of modifiers (in particular, alkylchlorosilanes).[6] It is important to mention that the presence of the silanol groups grafted to the surface of the obtained phases is mandatory. At the same time, this fact causes problems during the chromatography of basic compounds (peaks "tailing", restricted pH-stability range, etc.).[7,8] Different methods are used to avoid these disadvantages of the silica gel packings. In our opinion, among these methods the polymer modification (more exactly encapsulation of the silica surface) may be the most reliable. In this case not only silanol groups undergo screening but also an access of the aggressive environment to the silica surface may be completely excluded. This circumstance augments pH-stability of the sorbent.

The polymer-based chromatographic materials possess following disadvantages: they don't have hard structure, are less efficient, swell in the organic solvents.[3] The joining of positive properties of these components permits to obtain hybrid mineral-polymer (silica-polymer) packings deprived of disadvantages intrinsic to the silica and polymer materials.

The polymer modification of porous systems (particularly, silica gel) surface has the following advantages in comparison to alkylsilanes:

- The disadvantages of silica materials are eliminated (silanol groups are absent (screened), pH working range may be broadened).
- The quantity of the inserted phase is not restricted.
- It is possible to introduce simultaneously several functional groups (including the groups with inverse polarity).
- Such systems may be successfully applied in RP-HPLC.[9–12]

2. Experimental

2.1. INSTRUMENTATION AND RAW MATERIALS

Micro-spherical silica gel (MSG) with the following characteristics has been used as the initial porous silica: specific surface area $S_{sp.}$ = 80 m^2 g^{-1}; specific pore volume V_{sp} = 0.50; 0.57; 0.70 cm^3 g^{-1}; average pore diameter $d_{av.}$ = 30 nm, particle size $d_{p.}$ = 7.5 μm, obtained by hydrothermal treatment (T = 200°C; duration – 4 h, pH 8.0). The process was carried in the 0.5 l capacity autoclave; solid:liquid ratio (S:L) 1:14; autoclave loading level 0.8.

Monomers and polymerization initiator, dicumyl peroxide (DCP), were obtained from Aldrich.

The content of the polymer component was determined gravimetrically (from sorbent mass values before and after the baking at 800°C during 4 h).

2.2. "DRY POLYMERIZATION" ON THE SURFACE

2.2.1. *Coating of Silica Supports*

Silica beads were added to a solution of the monomer and DCP in *n*-pentane. The monomers composition and their quantities are given in the Table 1. DCP quantity consists 5.0% mass of the total monomer mass. Subsequently, the evaporation of the solvent was carried out in a rotary evaporator. Temperature was initially increased to 100°C over 1 h then kept for another hour at this temperature, then heated to 130°C over 1 h and then kept at this temperature for another 1 h. The sorbent thus obtained was rinsed with a hot mixture of dimethylformamide-toluene, further with ethanol then dried by acetone on a filter. The final drying of the samples was carried out in the drying oven at 120°C during 2 h.

2.3. CHROMATOGRAPHIC INVESTIGATIONS

Chromatographic investigations have been carried out on a Waters HPLC system (Waters 626 Pump, Waters 600 Controller, Waters 486 Tunable Absorbance Detector) using 150 × 4.6 mm columns. An acetonitrile-water (50/50) mixture was used as a mobile phase (pH 7.0; flow rate 1 ml/min). Absorbance was measured at UV 254 nm wavelength.

3. Results and Discussion

The chromatographic data for separation of uracil (1) – pyridine (2) – phenol (3) – toluene (4) test mixture (are presented in Table 1, line 1) was obtained with the column packed by the MSG modified by the ODMA homo-polymer. The toluene retention time in the given case is 5.04 min which is 1 min more than its retention time on the Si-300 C_{18} column. It is notable that the ODMA homo-polymer practically screens the silanol groups on the silica gel surface which is proved by the coincidence of the retention times for pyridine and phenol. Apparently the "methacrylate" part of the polymer "secures" the polymer encapsulation of the surface and the "octadecyl" part – provides the presence of the C_{18}-groups on it. 15.0 mass% polymer content on the surface provides about 10.0–12.0 mass% C_{18}-groups content, which exceeds two times the amount of the reversed phase obtained as a result of modification of the surface by octadecyltrichlorosilane ODS.[13] The increase of the toluene retention time from 3.70 to 5.04 min may be explained namely by this circumstance.

The increase of the toluene retention time depends on the increase of the polymer (ODMA-MMA co-polymer) quantity introduced into the silica gel surface. Conceivably, structuring of the polymer occurs and the influence of

this phenomenon becomes more appreciable with increase of the polymer quantity. Such assumption is based on the fact that the reverse picture must be observed with increase of the polymer quantity.

Namely, the retention time for the toluene must decrease as much as the surface area value of the porous material decreases when polymer content increases. This fact contradicts with the known equation connecting the retention factor with the specific surface area values:

$$k' = S / V_m \cdot K$$

where S is the surface area of the column, V_m the volume of the mobile phase in the column, and K is the distribution coefficient.

One can solve this problem only when assuming that the polymer introduced into the surface possesses its own porosity. Only in this case it becomes possible to involve more C_{18}-groups into the chromatography process. The introduction of the DVB to the co-polymer composition increases the porosity of the polymer cover (see Table 1, lines 5–7). This allows involving of higher number of C_{18}- and phenyl groups into the chromatographic process. The accessibility of the surface for modification by silanes is determined by porous characteristics of the sorbent. In case of polymer modification the situation looks a bit different. As the value of the specific surface area isn't the limiting factor for the quantity of the modifier (most likely pore volume, and average pore diameter in some level) in this case polymer coatings consisting of several layers may be obtained. In addition, mutual overlapping of functional groups takes place when increasing the quantity of the polymer introduced. Furthermore, as a result of the polymer layer structuring, it is not only the maximal participation of the whole amount of the C_{18}-groups that influences the toluene retention time. It is necessary to account for the influence of the phenyl groups of the DVB as well, because it is known that such groups are not inferior to C_{18}-groups by their hydrophobicity.

It is evident that the modification by the ODMA homo-polymer in 15.0 mass% quantity secures 11.5 mass% C_{18}-groups content and the toluene retention time is 5.04 min. When modifying by ODMA-MMA co-polymer, the toluene retention time increases with the increase of the introduced polymer quantity. When the polymer content is 33.33 mass%, the ODMA content equals 16.67 mass%, which corresponds to the 12.5 mass% C_{18}-groups content. The toluene retention time in this case is 6.10 min.

We can see from the dependence of the toluene retention time on the C_{18}-groups content for the ODMA-MMA systems, that the retention time values are somewhat higher as compared with ODMA homo-polymer (Sample 1). It is necessary to note that in the latter case the pore volume is lower than in the first case owing the presence of the MMA in the polymer composition.

TABLE 1. Hybrid mineral-polymer packing materials for the RP-HPLC.

The initial monomer content (% Of the total mass)			Column	Total polymer content (mass.%)	ODMA-groups content (mass%)	C_{18}-groups content (mass%)	Phenyl-groups content (from DVB) (mass%)	Peak retention time (min)		k
ODMA	MMA	DVB						Uracil	Toluene	
100	–	–	ODMA-15	15.0	15.00	11.25	–	1.47	5.07	2.44
50.0	50.0	–	ODMA-MMA	20.0	10.00	7.50	–	1.76	3.46	0.97
50.0	50.0	–	ODMA-MMA	27.3	13.65	10.24	–	1.36	4.60	2.29
50.0	50.0	–	ODMA-MMA	33.3	16.67	12.50	–	1.32	6.10	3.63
42.0	42.0	16.0	ODMA-MMA-DVB[a]	25.0	10.50	7.88	4.0	1.56	8.14	4.21
42.0	42.0	16.0	ODMA-MMA-DVB[b]	25.0	10.50	7.88	4.0	1.62	8.50	4.25
42.0	42.0	16.0	ODMA-MMA-DVB[c]	25.0	10.50	7.88	4.0	1.73	9.20	4.32

[a] – V_{sp} = 0.50 g· cm^{-3}; [b] – 0.57 g cm^{-3}; [c] – 0.70 g cm^{-3}.

According to the toluene retention time 5.50 min corresponds to the 11.25 mass% C_{18}-groups content. Actually it equals to 5.07 min. OIne can thus conclude that the polymer layer is more structured (more porous) in the ODMA-MMA system. We assume that some part of the C_{18}-groups in the pore spaces is inaccessible for chromatography process. The chromatograms of the systems modified by the ODMA-MMA-DVB co-polymer prove this fact. When the total content of C_{18}- and phenyl groups does not exceed 12.0 mass% (11.88 mass%), the calculated value of the toluene retention time must be 5.70 min while actually it equals 8.14–9.20 min, which is one and half times higher than for systems without DVB. The last three lines of the Table 1 correspond to the hybrid sorbent samples obtained on the base of the silica gels with pore volume V_{sp} = 0.50; 0.57; 0.70 g cm $^{-3}$ correspondingly. When pore volume increases from 0.50 to 0.70 g cm^{-3}, the toluene retention time increases from 8.14 to 9.20 min. So, it is more expedient to use silica gels with comparatively higher pore volume to prepare polymer-containing sorbents as the hybrid sorbents thus obtained possess higher capacity.

4. Conclusions

The polymers introduced onto the silica surface possess their own porosity. The porosity of the polymer layer increases in the poly-ODMA, poly-ODMA-MMA, poly-ODMA-MMA-DVB series. The increase of toluene retention time is observed when polymer layer composition is multi-component and the sewing agent (DVB) is introduced. This may be explained by the polymer layer porosity increase.

It is more expedient for polymer modification to use the silica gels with higher pore volume.

References

1. R.E. Majors, *LC-GC International April*, 7 (1998).
2. A.D. Rogers, J.G. Dorsey, *J. Chromatogr. A* 982 (1–2), 57–65 (2000).
3. U.D. Neue, HPLC Columns. Theory, Technology, and Practice. Wiley-VCH, New York, 1997, 395 p.
4. U.D. Neue "Silica and its Derivatization for Liquid Chromatography," in Meyers R.A. (ed). Encyclopedia of Analytical Chemistry, Wiley, Chichester, 11450 (2000).
5. J.W. Dolan, *LC-GC International May*, 292 (1998).
6. J. J. Nawrocky, *Chromatogr. A* 779 (1–2), 29–71 (1997).
7. D.V. McCalley, R.G. Brereton, *J. Chromatogr. A* 828 (1–2), 407–420 (1998).

8. S. Kobayashi, I. Tanaka, O. Shirota, *J. Chromatogr. A* 828 (1–2), 75–81 (1998).
9. M. Hanson, K.K. Unger, *TrAC* 11 (10), 368 (1992).
10. M. Hanson, K.K. Unger, G. Schomburg, *J. Chromatogr*. 517, 269 (1990).
11. M. Hanson, K.K. Unger, C.T. Mant, R.S. Hodges, *J. Chromatogr. A* 599, 65 (1992).
12. Y. Shen, X. Shao, K. Tanaka, K. O'Neill, *J. Chromatogr. A* 866, 1 (2000).
13. S.S. Hayrapetyan, H.G. Khachatryan, *Chromatographia* 61, 43–47 (2005).

BIMETALLIC Co-BASED CATALYSTS PREPARED BY SOL-GEL FOR METHANE REFORMING BY CARBON DIOXIDE

SHOLPAN S. ITKULOVA*, GAUKHAR D. ZAKUMBAEVA, ANATOLIY A. SHAPOVALOV, LARISSA V. KOMASHKO
D.V. Sokolsky Institute of Organic Catalysis and Electrochemistry; 142, Kunaev Str., Almaty, 050010, Republic of Kazakhstan

Abstract. The 5% Co-M/SiO_2 catalysts (M – VIII Group metal) prepared by sol-gel method have been tested in dry reforming of methane by carbon dioxide and in bi-reforming of methane by both carbon dioxide and water steam. The conditions for formation of stable bimetallic nano-sized particles have been determined. The activity and selectivity of catalysts depend on the nature of the second metal. Presence of water in initial $CO_2 + CH_4$ mixture causes a decrease in the catalyst activity.

Keywords: Co-containing catalysts, sol-gel method, dry reforming of methane, bire-forming of methane, syngas.

1. Introduction

CO_2 reforming of methane (1) attracted great attention during the last years, since it produces synthesis gas with high CO/H_2 ratio (1/1) suitable for the synthesis of higher hydrocarbons and oxygenates. Both CO_2 and CH_4 are greenhouse gases that stimulate additional interest in the processes of their utilisation, because of converting these gases into a valuable feedstock may significantly reduce the atmospheric emissions of CO_2 and CH_4.[1]

$$CH_4 + CO_2 \rightarrow 2CO + 2H_2 \quad 247 \text{ kJ/mol} \qquad (1)$$

Most of the group VIII metals are more-or-less catalytically active toward this reaction.[2] A major problem in the reaction is the deactivation of the catalyst

*To whom correspondence should be addressed: Sholpan S. Itkulova; D.V. Sokolsky Institute of Organic Catalysis and Electrochemistry; 142, Kunaev str., Almaty, 050010, Republic of Kazakhstan; e-mail: *itkulova@nursat.kz*

P. Innocenzi, Y. L. Zub and V. G. Kessler (eds.), *Sol-Gel Methods for Materials Processing.*

because of the deposition of carbon under reaction conditions (typically, 800–900°C). Although noble metals have proved to be very active and insensitive/or low sensitive to coking,[2] the expensive cost and restricted availability limit their large-scale commercial use. While the Ni- and Co-based catalysts are easily available, they are rapidly deactivated, when the conventional supports, such as Al_2O_3 or SiO_2, and conventional methods of preparation are used.[3,4]

To suppress carbon deposition, noble metals are better to use as an active promoting component. Also, the preparation method for catalysts has significant effect on catalytic activity and coking resistance for methane conversion to synthesis gas.[1,5] Among various approaches to catalyst preparation, the sol-gel method was proposed as a new flexible approach to preparation of supported metal catalysts with high dispersion, high thermal resistance to sintering, and low deactivation rate, compared to the conventional impregnated catalysts.[6]

At present, a significant number of works have been focused on the development of the Ni-based catalysts for this reaction, while the Co-containing catalysts are incomparably less studied.

The objective of this study was to in vestigate the performance of cobalt-based catalysts modified by platinum metals (M =Rh, Pd, and Pt) and supported on SiO_2, prepared by a sol–gel method, in CO_2 reforming of methane. Also, the effect of water steam has been studied.

2. Experimental

2.1. CATALYST PREPARATION

The Co-M/SiO_2 catalysts (M =Rh, Pd, and Pt) we re prepared by sol-gel method. For preparation of the catalysts, the tetraethyl orthosilicate (TEOS) – $Si(C_2H_5O)_4$ has been added to absolute alcohol. After 1 day, the aqueous solution of appropriate metal precursors ($Co(NO_3)_26H_2O$, and $RhCl_3nH_2O$, or $H_2PtCl_6nH_2O$, or $H_2PdCl_4nH_2O$) has been added with a suitable amount of nitric acid to avoid the reduction of metals and formation of metallic black. The final solution was left for 3 days for gelation. Drying of the samples was carried out in a vacuum drying oven at T =50 °C and P =0.5 atm. After complete drying, the samples were calcined at 400–600°C. The total content of metals was 5 wt% for all the catalysts. Weight ratio of Co:M (M =Rh, Pt, Pd) was 8:2.

2.2. CATALYST TESTING

The catalysts were tested in dry reforming of methane (interaction between carbon dioxide and methane), where the ratio of CH_4/CO_2/Ar was 1/1/8, and in

bi-reforming of methane (combining the dry reforming of methane (1) and steam reforming of methane (2), where the ratio of $CH_4/CO_2/H_2O/Ar$ was 1/1/0.1/8. The processes have been carried out in a quartz flow reactor at varying temperatures from 300°C to 880°C, P = 1 atm, and space velocity of 1,000 h^{-1}. The initial and final reaction products have been on-line analysed by the GC's.

$$CH_4 + H_2O \rightarrow CO + 3H_2 \quad (2)$$

The physico-chemical properties of catalysts were studied by electron microscopy (EM) and using BET surface area measurements.

3. Results and Discussion

3.1. PHYSICO-CHEMICAL PROPERTIES OF SOL-GEL 5% Co-M/SiO_2

The samples were studied at different stages of their preparation, treatment and exploitation.

After drying, the initial samples of the 5% Co-M/SiO_2 catalysts are rigid and have different colours depending on the nature of the second metal. Table 1 shows the physico-chemical characteristic of the initial samples before their treatment (calcination and reduction) and exploitation. As it is shown in Table 1, the initial samples possess high BET surface area lying in the range 550.5–747.9 m^2/g. The high support surface area is essential for reforming catalysts because it helps in the stabilization of metal dispersion. Mainly the nano-sized uniformly distributed metallic particles were observed by electron microscopy. Average size of metal particles for all the initial samples is varying within 2.5–7.0 nm depending on the nature of second metal (Table 1).

There is no significant growth of metal particle size and decrease in the BET surface after calcination and reduction under mild conditions (400°C, air and 300°C, H_2 respectively). Besides the amorphous nano-sized particles, the separate particles of noble metals with size varying within 2.0–7.0 nm in reduced and oxidized states are formed in calcined and reduced samples of catalysts.

TABLE 1. Physico-chemical properties of 5% sol-gel made Co-M/SiO_2[a]

Catalyst	Colour of catalysts	BET surface area of catalysts (m^2/g)	Average size of metallic particles (nm) estimated from EM
5% Co-Pt(8:2)/SiO_2	Orange	747.9	6.0–7.0
5% Co-Pd(8:2)/SiO_2	Dark-brown	557.9	2.5–3.0
5% Co-Rh(8:2)/SiO_2	Brown	550.5	3.0–5.0

[a]Initial samples

After calcination at higher temperature – 600°C, the agglomeration of metallic particles is occurred and the size of some particles is reaching 40 nm. The BET surface area is decreased to 170 m^2/g.

The electron microscopic study of the catalysts exploited in bi-reforming of methane (T =900 °C, $CO_2 + CH_4 + H_2O$) showed the improved uniform distribution of small metal particles over the support. At the same time, the large metal particles (up to 100 nm) are formed due to the agglomeration under severe conditions (T >800 °C).

3.2. DRY REFORMING OF METHANE OVER SOL-GEL 5% Co-M/SiO_2

All the sol-gel 5% Co-M/SiO_2 catalysts are more or less active in dry reforming of methane. The main reaction product is syngas. Also, insignificant amount of oxygenates and C_{2+} hydrocarbons are formed. In Table 2, the comparative data on behaviour of 5% Co-M/SiO_2 catalysts (M =Pt, Pd, Rh) in dry reforming of CH_4 are given.

Activity and selectivity of the sol-gel catalysts in reforming depend on the nature of second metal and process conditions. With increase in the process temperature, the conversion of both initial products and yield of reaction products are grown over all the catalysts and reached a maximum value at a certain temperature depending on the catalyst composition. The following raising temperature does not effect the conversion and selectivity. For instance, the maximum conversion of methane and carbon dioxide over the 5% Co-Pt (8:2)/SiO_2 is reached at temperature of about 450°C, while maximum selectivity to syngas is observed at higher temperature – 680°C. Both conversion and selec-tivity are not changed with temperature increase from 450°C and 680°C respectively to 900°C. For this reason, in Table 2 the results are given for temperatures, when maximum selectivity is observed.

The composition of syngas formed during dry reforming over the sol-gel made catalysts depends on the catalyst nature. While the high ratio of H_2/CO = 1.1 is observed over the Co-containing catalysts modified by Pd and Rh, the catalyst modified by Pt shows producing syngas with lower content of hydrogen (H_2/CO =0.75) (Table 2).

TABLE 2. Dry reforming of methane over the sol-gel 5% Co-M/SiO_2 catalysts (P =0.1 MPa, S.V. =1,000 h^{-1}, CO_2:CH_4 =1:1)

Catalyst	T (℃)	Conversion (%)		H_2/CO
		CH_4	CO_2	
5% Co-Pt (8:2)/SiO_2	680	45	48.9	0.75
5% Co-Pd(8:2)/SiO_2	885	40.9	14.8	1.1
5% Co-Rh(8:2)/SiO_2	660	80.2	57.9	1.1

The comparison of catalysts demonstrates that 5% co-rh(8:2)/sio$_2$ is the most effective catalyst in dry reforming of methane. maximum stable conversion is 80.2% and н$_2$/co = 1.1 at т = 660^{o}c.

3.3. BI-REFORMING OF METHANE OVER SOL-GEL 5% Co-M/SiO_2

Aiming to increase the content of hydrogen in syngas, water steam has been added to the initial reactants in amount of 10 vol%. Activity of all synthesized catalysts in bi-reforming of methane, representing the combination of dry reforming of methane and steam reforming of methane, is significantly less than in dry reforming (Table 3). Conversion of both methane and carbon dioxide is 12.1–33.2% and 10.0–14.9% respectively (Table 3).

Study of the effect of water showed that the yield of hydrogen and consequently the H_2/CO ratio are varied depending on nature of second metal. While H_2/CO ratio is increased from 0.75 to 1.2 and from 1.1 to 1.5 over 5% Co-Pt/SiO_2 and 5% Co-Pd/SiO_2 respectively, a non-significant decrease in hydrogen formation is observed over 5% Co-Rh/SiO_2 (Table 3).

Thus, water addition has no direct positive effect for reforming of methane over the sol-gel silica supported catalysts.

TABLE 3. Bi-reforming of methane over the sol-gel 5% Co-M/SiO_2 catalysts (P = 0.1 MPa, S.V. = 1,000 h^{-1}, CO_2:CH_4:H_2O = 1:1:0.1).

Catalyst	T (°C)	Conversion (%)		H_2/CO
		CH_4	CO_2	
5% Co-Pt (8:2)/SiO_2	680	12.1	12.5	1.2
5% Co-Pd(8:2)/SiO_2	650	33.2	10.0	1.5
5% Co-Rh(8:2)/SiO_2	760	28.5	14.9	1.0

4. Conclusions

The nano-sized 5% Co-containing silica supported catalysts modified by noble metals have been synthesized by sol-gel method. A size of metal particles is varied within 2–7 nm depending on nature of second metal.

It has been established that the sol-gel made 5% Co-M/SiO_2 catalysts possess the with a high BET surface area – 550–755 m^2/g

The formation of metal particles, their size and stability depend on a nature of the second metal, pH of medium and pretreatment conditions.

Depending on nature of the second metal, the Co-containing catalysts prepared by sol-gel show different activity in dry reforming of methane.

Stability, activity and selectivity of the sol-gel catalysts in reforming and bi-reforming of methane depend on the nature of the second metal and the process conditions.

Water effects negatively the conversion of $CH_4 + CO_2$ over all catalysts studied and has a different effect on ratio H_2/CO depending on the catalyst nature.

References

1. S. Wang and G. Q. (Max) Lu, Carbon dioxide reforming of methane to produce synthesis gas over metal-supported catalysts: state of the art, *Energy & Fuels* 10, 896–904 (1996).
2. F. Solymosi, Gy. Kutsan, and A. Erdohelyi, Catalytic reaction of methane with carbon dioxide over alumina supported platinum metals, *Catalysis Letters* 11 (2), 149–156 (1991).
3. E. Ruckenstein1 and H. Y. Wang, Carbon deposition and catalytic deactivation during CO_2 reforming of CH_4 over Co/Al_2O_3 catalysts, *Journal of Catalysis* 205, 289–293 (2002).
4. K. Tomishige, Y. Chen, and K. Fujmoto, Studies on carbon deposition in CO_2 reforming of CH_4 over nickel–magnesia solid solution catalysts, *Journal of Catalysis* 181**,** 91–103 (1999).
5. L. Ji, S. Tang, H. C. Zeng, J. Lin and K. L. Tan, CO_2 reforming of methane to synthesis gas over sol–gel-made Co/Al_2O_3 catalysts from organometallic precursors, *Applied Catalysis A: General* 207, 247–255 (2001).
6. K. Balakrishnan and R. D. Gonzalez, Preparation of Pt/alumina catalysts by the sol-gel method, *Journal of Catalysis* 144, 395–413 (1993).

EFFECT OF SODIUM DODECYLSULFATE AND CETYLPYRIDINIUM CHLORIDE ACT AS TEMPLATES AT DIFFERENT PH VALUES ON SORPTION AND TEXTURAL PROPERTIES OF MESOPOROUS SILICAS

TATYANA F. KOUZNETSOVA[1*], ANATOLY I. RATKO[1], VLADIMIR S. KOMAROV[1], SVETLANA I. EREMENKO[1], YURIY L. ZUB[2]

[1]*Institute of General and Inorganic Chemistry, NAS of Belarus 9/1, Surganova Str., Minsk 220072, Belarus*

[2]*O. O. Chuiko Institute of Surface Chemistry, NAS of Ukraine 17 General Naumov Str., Kyiv 03164, Ukraine*

Abstract. Cationic and anionic surfactants are used for structuring of the negatively charged silica species during the formation of ordered mesoporous silicas from stable dilute silica sols, obtained by ion-exchange method. Isotherms of nitrogen adsorption-desorption at 77 K on silicas, which are prepared by the thermal decomposition of silica hydrogels, obtained at different pH using sodium dodecylsulfate or cetylpyridinium chloride as surfactants, are measured. The shape of the capillary condensation hysteresis and the type of the sorption isotherms are identified using the IUPAC classification. It is found that the adsorption and textural properties of the si1ica gels depend on the concentration and the type of surfactant (SAA), and also on pH.

Keywords: Mesoporous silica gel, stable silica sol, templation, cationic and anionic surfactants, nitrogen adsorption-desorption isotherms, type of isotherms and shape of hysteresis loops, pore volume, surface area.

*To whom correspondence should be addressed: T.F. Kouznetsova, Ph.D., Institute of General and Inorganic Chemistry, NAS of Belarus, 9/1, Surganova Str., Minsk 220072, Belarus; e-mail: kouzn@igic.bas-net.by

P. Innocenzi, Y. L. Zub and V. G. Kessler (eds.), *Sol-Gel Methods for Materials Processing*.

1. Introduction

Amorphous and crystalline silicas are widely used as catalyst supports and adsorbents. Despite the outstanding progress made in preparing new silica materials with uniform pores in the mesoporous region, up to now, we are still uncertain whether very small initially formed particles of a silicon(IV) oxide hydroso1, being of 1.0–1.5 nm in size, grow by the coa1escence of primary particles[1,2] or due to the formation of c1usters.[3,4] In this work, by means of the c1uster model,[4] we studied the influence of cationic and anionic surfactants, used for structuring of the negatively charged silica species, on the change in the sorption and textural properties of silicas prepared from silica sol, which has been decationized by an ion-exchange method. Synthesis of silica ge1 from such a sol[5] ensures the presence of dense particles of silicon(IV) oxide up to the onset of ge1ation. At the same time, the adsorption properties of silica ge1 produced by the acidification of si1icate in an aqueous medium, depend on the conditions of the condensation-polymerization reaction fo11owed by the treatment of gel (washing, syneresis, drying, etc.).[3]

2. Experimental

The decationized silica sol with pH 3.5 containing 4 wt% of silicon (IV) oxide, was prepared by passing a dilute aqueous sodium metasilicate solution through a column with a KU-2 sulfonic cationite in the H-form.[5] The sol was then mixed with the aqueous solutions of cetylpyridinium chloride and sodium dodecylsulfate in various concentrations ranging from 0.1 to 5.0 wt%. An aqueous ammonia or hydrochloric acid solutions were added to the mixture to achieve the necessary pH, and the ge1 was precipitated. After syneresis and aging for 16 h, the gel was dried first in air at room temperature and then in a desiccator for 4 h at 393 K. The thermal decomposition of silica gels was carried out at 923 K. Adsorption-desorption isotherms of nitrogen were measured by volumetry at 77 K after preliminary evacuation of samples for 2 h at 523 K using Surface Area and Porosity Analyzer ASAP 2020 MP (Micromeritics, USA). The specific surface area was calcu1ated from the monolayer capacity using the Brunauer-Emmett-Teller (BET) equation. Adsorption cumulative volume of pores between 1.7 and 300.0 nm and adsorption average pore diameter were estimated by the Barrett, Joyner, and Halenda method (BJH), micropore volume – by t-plot method. The shape of pores was analyzed, according to the IUPAC recommendations.[6]

3. Results and Discussion

Isotherms for the obtained silicas belong to Type IV, Type I or Type (I + IV) isotherms of physical sorption. It is demonstrated that the silica gel synthesis with templates leads to changes in the shapes of hysteresis loops from H4 (samples 184, 188, 185, 146, 148) to H2 (samples 182, 183, 186, 195, 147, 149, 141, 143, 189, (H2 + H4) (samples 194, 150, 142, 144), (H2 + H1) (samples 145, 179) or H1 (sample 190), resulting from the original changes in the pore shape of the forming mesoporous adsorbents.

Almost all nitrogen sorption isotherms belong to type IV with the typical reversible part at low relative pressure p/p_0, the hysteresis at larger p/p_0 ratios that is associated with the capillary condensation in mesopores, and, finally, a small part of limiting adsorption at the largest p/p_0 ratios. The pattern of the hysteresis loop, as well as the reversible part of the isotherm, changes from sample to sample (Table 1). In general, the loops correspond to three types of hysteresis (H1, H2, H4). The observed forth type of hysteresis is, presumably, a combination of the H2 and H4 types of loops (samples 194, 150, 142, 144) and fifth type is a combination of the H2 and H1 types (samples 145, 179). Sorption isotherms 192, 146 belong to type I, and isotherm 148 – to the hybrid type (IV + I).

The obtained gels have a specific parity between concentration, and also a template sort, pH value, on the one hand, and pore volume and surface area, on the other hand. At templating by cetylpyridinium chloride the growth of silica pore volume and reduction of the particle size or increase of a BET surface area are observed (Table 1). The average pore diameter thus increases. It testifies that coefficient of spontaneously occurring coalescence between SiO_2 particles is higher for finer particles so that the resulting silica gel appears mechanically stronger and more stable in relation to shrinkage. The effect of compression forces arising from a superficial tension of water during its removal, at SAA presence is not essential even in narrow pores between very small silica particles.

At templating by sodium dodecylsulfate the increase in its concentration leads to the increase in the size of silica particles and also some increase of cumulative volume of the pore diameter from 1.7 up to 300.0 nm and average pore diameter. The micropores disappear. Unlike templating by cetylpyridinium chloride, the presence of anionic template leads to larger formations of primary particles strongly connected with each other, the so-called agglomerates (clusters), which then are reconstructed into a dense structure. These large structural elements communicate with each other relatively weakly, easily moving on drying, and are packed, or aggregated, more densely in comparison with smaller size primary particles, than in case of templating by cetylpyridinium.

TABLE 1. Effect of pH and SAA concentration on the textural and sorption properties of silicas.

Sample no.	SAA wt%	pH	Isotherm type	Hysteresis shape	BJH adsorption cumulative volume of pores between 1.7 and 300.0 nm (cm^3/g)	t-Plot micropore volume (cm^3/g)	BET surface area ($м^2/g$)	BJH adsorption average pore diameter (4 V/A) (nm)
192	abs	5.0	I	abs	0.0605	0.1142	584	3.3515
193	abs	7.0	IV	H2	0.3796	abs	692	3.3048
Cetylpyridinium chloride								
184	0.1	5.0	I + IV	H4	0.1686	abs	697	3.5052
188	0.3	5.0	I + IV	H4	0.3130	abs	776	3.6387
185	1.0	5.0	IV	H4	0.8323	abs	834	4.7891
182	2.0	5.0	IV	H2	1.1779	abs	918	4.8092
183	3.0	5.0	IV	H2	1.3171	abs	967	4.7882
186	5.0	5.0	IV	H2	1.5282	abs	1090	4.8122
194	0.1	8.0	IV	H2 + H4	0.3615	abs	672	3.4564
195	0.3	8.0	IV	H2	0.6072	abs	698	4.1299
190	5.0	8.0	IV	H1	2.4151	abs	968	9.5790
Sodium dodecylsulfate								
146	0.1	5.0	I	H4	0.0542	0.0644	413	3.2613
148	0.3	5.0	IV + I	H4	0.0796	0.0378	363	3.5612
150	2.0	5.0	IV	H2 + H4	0.1413	0.0023	205	4.6210
142	3.0	5.0	IV	H2 + H4	0.2045	abs	143	6.2489
144	5.0	5.0	IV	H2 + H4	0.1812	abs	160	5.6665
147	0.1	7.0	IV	H2	0.4835	abs	572	3.8058
149	0.3	7.0	IV	H2	0.4657	abs	558	3.7081
141	1.0	7.0	IV	H2	0.6215	abs	496	4.3652
143	3.0	7.0	IV	H2	0.6758	abs	481	4.7237
145	5.0	7.0	IV	H2 + H1	0.6626	abs	370	5.8040
189	1.0	8.0	IV	H2	0.5962	abs	543	4.1453
179	3.0	8.0	IV	H2 + H1	0.6920	abs	431	5.0644

pH Value, according to literature,[1] influences mainly the size of particles which is firmly established before the start of the gel formation. In spite of the fact that increase in pH causes normally an increase in the size of the primary particles, in the template synthesis of SiO_2 the pH together with silica concentration is only a secondary factor. It is due to the fact that mesopores at templating are developed according to the mechanism based on micellar self-assembly of SAA that forms a supramolecular structure of silicate anions.[7] The textures changes are observable at templating silica by cationic and anionic SAA at pH value 5.0, pH 7.0 and 8.0. However, A and V values increase always with increasing pH. The highest mesopore volume, equal to 2.4151 cm^3/g, and the

largest pore diameter, equal to 9.5790 nm, were obtained through silica templating by cetylpyridinium chloride at pH 8.0.

For the process of silica formation in the presence of cationic SAA in mother liquor and on drying it is characteristic that the particles, formed at the sol stage, keep their sizes in the structure of gel. Presence of cationic SAA, on one hand, suppresses the influence of pH on the size of the particles, firmly established before the start of gel formation, and also on their size distribution and density of packing, and, on the other hand, prevents a damp deposit of hydrogel from condensation on drying.

The silica structures prepared without compression during dehydration and constructed of very small primary particles (or their doublets and triplets) have high values of BET surface area and great pore volumes (samples 182–186, 190, 194, 195). The observed dependence between pH values and changes of A and V values of the samples obtained in the presence of cationic SAA, is caused by that adsorption SiO_2 on the surface of SAA micelles results from the general surface charge defined by the pH value. The increased pH there increases the negative SiO_2 charge, leading to its better adsorption on positively charged cetylpyridinium ions.

It is interesting to note that the increase in concentration of cetylpyridinium chloride decreases the particles size, while the micropores are, however, absent. Micropores appear only on silica templation by dodecylsulfate anion (samples 146, 148, 150). However, with increase of its concentration the micropores degenerate, and only the mesopore texture is formed. As pyridinium bases possess an ability to connect silicate-anions, their influence on processes of sol-gel transformation will, probably, result in precipitation of dissolved silica during drying and partial blocking of their microporous texture. In the presence of pyridinium bases aggregating around silicate-ions, the BET surface area increases with the increase of pH. In case of anionic SAA it is necessary to consider specificity of their orientation on interaction with silicate anionic centers on the surface of silica – an acidic sorbent.

Decrease in structuring action of sodium dodecylsulfate is caused by the competition between SAA micellar phase and SiO_2 phase, due to decrease in alkylsulfate adsorption on silica in comparison with cetylpyridinium chloride.

4. Conclusions

Ordered mesoporous silicas, possessing BET surface area ranging from 600 to 1,100 $м^2/g$, are obtained from decationized silica sols with cationic surfactant at pH in the range 5.0–8.0. Templation by anionic SAA leads to decrease in the BET surface area from 600 to 200 $м^2/g$, to some increase in the pore volume, and appearance of micropores. It is shown that the synthesis of silica leads to changes

in the shapes of hysteresis loops in the isotherms of nitrogen low-temperature adsorption-desorption.

The effect of SAA and pH is manifested mainly in the spatia1 rearrangement of the particles of silicon (IV) oxide into supramolecular structure in case of cationic SAA or into dense agglomerates in case of anionic SAA as far as there is an electrostatic interplay among negatively charged silica species and SAA ions.

Acknowledgements

The authors appreciate the financial support from the Belarus State Fund of Basic Research (Grant Ch07K-022) and the State Fund of Basic Research (Ministry of Education and Science of Ukraine).

References

1. Iler, R.K., The Chemistry of Silica: Solubility, Polymerization, Colloid and Surface Properties, and Biochemistry, New York: Interscience Publication, 1979, vol.2.
2. Okkerse, C.K., Porous Silica, in *Physical and Chemical Aspects of Adsorbents and Catalysts*, Linsen, B.G., Ed., London and New York: Academic Press, 1970, 213.
3. Kuznetsova, T.F., Eremenko, S.I., Adsorption properties of silica gel prepared from a decationized sol, *Colloud Journal*, 64, 451–456 (2002).
4. Barby, D., Silicas, in *Characterization of Powder Surfaces*, Parfitt, G.D. and Sing, K.S.W., Eds., London and New York: Academic Press, 1976, 353.
5. Bird, P.G., Colloidal solutions of inorganic oxides, *U.S. Patent 2244325*, 1941.
6. IUPAC, Reporting physisorption data for gas/solid systems with special reference to the determination of surface area and porosity, *Pure and Applied Chemistry*, 57, 603–619 (1985).
7. Corma, A., From microporous to mesoporous molecular sieve materials and their use in catalysis, *Chemical Reviews*, 97, 2373–2419 (1997).

FACTORS INFLUENCING THE ADSORPTION PROPERTIES OF SILICAS FUNCTIONALIZED BY MACROCYCLIC LIGANDS

OLGA V. KUCHMA*, YURIY L. ZUB
O.O. Chuiko Institute of Surface Chemistry, National Academy of Sciences of Ukraine, 17 General Naumov Str., Kyiv 03164, Ukraine

Abstract. The adsorbents (polysiloxane xerogel, silicagel Davisil, mesoporous silica SBA-15) containing macroligands, such as calix[4]arenes, diaminodibenzo-18-crown-6-ethers, α- and β-cyclodextrins, have been obtained by the sol-gel method and the surface modification method. The influence of the synthesis conditions, the nature of macrocyclic compounds and routes of their grafting on the structural-adsorption characteristics of the obtained polysiloxane materials and their sorption properties toward Cs^+ (^{137}Cs) and Na^+, K^+, Sr^{2+} (^{90}Sr), and organic compounds of different kind, has been investigated.

Keywords: Organosilicon sorption materials, calixarenes, cyclodexrins, crown-ethers, adsorption of alkali-earth, alkaline and organic compounds.

1. Introduction

The chemistry of macrocycles able to form "guest - host" complexes is a strongly developing direction of supramolecular chemistry.[1] Nowadays in chemistry of "guest - host" complexes a special attention is given to several groups of macrocyclic ligands, first of all, to calix[n]arenes,[2] crown-ethers[3] and cyclodextrins.[4] This is due to unique property of such compounds – to form selective "guest - host" complexes with some metal ions and organic compounds.

These properties explain wide practical application of macrocyclic compounds in the radiochemical industry for selective extraction of radionuclides, chromatography, capillary electrophoresis, atomic engineering, pharmaceutical industry as chiral selectors[5,6] etc. However, the high cost of complexing agents,

*To whom correspondence should be addressed: O.V. Kuchma, Ph.D., O.O. Chuiko Institute of Surface Chemistry, NAS of Ukraine, 17 General Naumov Str., Kyiv 03164, Ukraine; e-mail: kuchma_olga@mail.ru

P. Innocenzi, Y. L. Zub and V. G. Kessler (eds.), *Sol-Gel Methods for Materials Processing*.

their low stability to action of aggressive environments, high solubility in water and/or polar solvents reduce considerably the application areas of such macrocyclic compounds. Therefore the development of new highly effective adsorbents based on hybrid organic-inorganic materials is perspective.

In the literature, however, there is no systematic approach to the development of techniques for the synthesis of silica matrixes functionalized by macrocyclic ligands. Moreover, the influence of the route and conditions of synthesis of such materials on their adsorption properties integrally and, in particular, in relation to selectivity, has not yet been investigated. Taking into account the structure features of the macrocyclic compounds, causing their specific adsorption properties, it is often difficult to expect changes, which can occur to macrocycles during their grafting to a matrix. Though, these changes could essentially influence the ability of the grafted macrocycles to selective complexing. Therefore the aim of this study was to estimate the influence of some factors (synthesis conditions, the structure of a macrocycle, an approach to its grafting) on adsorption properties of such matrixes, for example, of silica matrixes, functionalized by calix[4]arenes, 18-crown-6-ethers, α-and β-cyclodextrins.

2. Experimental

The grafting of macroligands onto silicas surface has been carried out by two approaches.

A. Using the reaction of hydrolytic polycondensation the polysiloxane xerogels with embedded molecules of calix[4]arene (further THC, samples **AI-AIII**) and covalently bounded calix[4]aren-crown-6 (K18C6, samples **BI-BII**),[7,8] diaminodibenzo-18-crown-6 (DADB18C6 (**CI-CIII**)), α-cyclodextrin (α-CD, samples **DI-DII**) and β-cyclodextrin (β-CD, samples **EI-EII**)[9] groups have been obtained. The content of functional groups has been set by the concentration of the macrocycles in the initial solution. Xerogels with the content of functional groups of about 0.1, 0.5 and 1.0 mmol/g have been obtained.

B. The mesoporous silicas with supramolecular surface layer have been synthesized by the method of silica surface modification. Two types of mesoporous silicas have been chosen as carriers: commercially available silicagel Davisil, and mesoporous silica SBA-15, obtained by the template method.[10] Before modification, the surface of mesoporous silicas has been activated by HCl with subsequent water flushing and vacuum drying. After activation of SBA-15 (sample **A**) its surface has been modified by macrocyclic compounds from water-ethanol solution (by β-CDs, sample **B**), THF (by calix[4]arene-18-crown-6, sample **C**) and toluene solution (by calix[4]arenes, sample **D**). The surface of Davisil (sample **J**) after initial activation has been modified by DADB18C6 groups (from ethanol solution, sample **E**), β-CD groups (from water-ethanol solution, sample **F**) and calix[4]arene groups (from toluene solution, sample **G**).

In case of samples **D** and **G** has been used the technique described in[11], where the silica's surface has been previously treated by $SiCl_4$.

3. Results and Discussions

The adsorptions properties of the polysiloxane xerogels with embedded THC molecules (samples **AI**–**AIII**) and functionalized by DADB18C6 groups (**CI**–**CIII**) and also the mesoporous silica SBA-15 modified by calix[4]arene (sample **D**) and calix[4]arene-crown-6 (sample **C**) have been studied in relation to Cs^+ (1 M HNO_3, pH 0.1, static conditions). The obtained results are presented in Table 1. The data of Table 1 show that adsorption equilibrium in case of sample **AI** and **CII** is attained in 1 hour. In case of sample **D** this dependence has more complex character. The kinetic curve of Cs^+ adsorption for sample **D** has two-stage character. Apparently it is caused by participation in adsorption of several types of active centers. It should be noted that at selected adsorption conditions the surface layer in these samples is hydrolytically stable. It is confirmed by the data of elemental analysis and IR spectroscopy.

The data presented in Table 1 indicate that the quantity of adsorbed cesium cations increases with an increase in amount of embedded THC molecules in xerogels (samples **AI-AIII**) (the reference experiment shows that the xerogel without immobilized macrocycles does not extract cesium cations under similar conditions). However, only 40% functional groups take part in adsorption of cesium.

Furthermore, it should be noted that no relation between the structural-adsorption characteristics of the xerogels with embedded THC molecules and their adsorption ability towards cesium ions is observed. The data of Table 1 testifies that adsorption activity of the xerogels containing DADB18C6 groups (samples **CI – CIII**) essentially depends on its structural-adsorption characteristics. An increase in DADB18C6 groups in the xerogels (from 0.1 to 1.0 mmol/g) causes decrease in the value of specific surface area and the sorption volume leading to nonporous matrix in case of sample **CIII**. The data of Table 1 indicate that on the increase in crown-ether groups to 0.5 mmol/g in the xerogels (samples **CI** and **CII**) the cesium adsorption by these materials increases and maximum quantity of groups take part in adsorption that amounts to 90%. However, the adsorption ability of the nonporous xerogel **CIII**, con-taining maximum quantity of functional groups, decreases significantly.

The adsorption selectivity of the xerogels with crown-ether groups (samples **CI – CIII**) towards alkali metals (Na^+, K^+ and Cs^+) has been investigated. It has been established that these adsorbents develop selectivity towards K^+. It's caused by the closeness of the DADB18C6 cavity size (0.26–0.32 nm) to the diameter of a potassium ion (0.266 nm).[12]

TABLE 1. Structure-adsorption characteristics and sorption data of cesium ions from 1 M HNO_3 for the synthesized xerogels.

Sample	S_{sp} (m^2/g)	V_s (cm^3/g)	Maximum quantity of groups taking part in sorption (%)		SAC (mg/g)
			1 hour	24 hours	
AI	643	0.39	11	10	9
AII	531	0.41	18	20	12
AIII	381	0.24	41	40	53
CI	550	0.40	38	40	5
CII	291	0.20	77	90	62
CIII	<2	–	8	7	11
C	543	0.78	48	46	62
D	384	0.45	16	32 (48)	36

Adsorption properties of samples **AII**, **CI** and **D** have been studied towards 137-cesium and 90-strontium. The analysis of obtained data testifies that all materials show higher adsorption activity towards ^{90}Sr in comparison with ^{137}Cs. The maximum amount of isotopes extraction is typical for SBA-15 modified by calixarene groups (sample **D**). This adsorbent is able to adsorb equal quantity of both isotopes: 53% ^{137}Cs and 50% ^{90}Sr.

The adsorption of *p*-nitrophenol from buffer solution in static conditions (pH 7, $Na_2HPO_4 + NaH_2PO_4$) has been investigated for samples containing α- and β-CD groups. It has been determined that adsorption equilibrium is achieved in 2–3 hours. Moreover, the adsorption rate of *p*-nitrophenol by samples **DII** and **EII** with the content of α- and β-CD groups ~0.5 mmol/g is higher. Davisil modified by β-CD (sample **F**) is characterized by the optimal adsorption activity.

The adsorption activity of materials with α- and β-CD groups towards various classes of organic compounds has been investigated in dynamic conditions by gas chromatography method. It has been shown that bonding organic molecules with α- and β-CD active centers results from both the electrostatic interactions (dipole-dipole) and hydrogen bonds. The xerogel with the concentration of β-CD groups ~0.5 mmol/g (sample **EII**) corresponds to requirements to adsorbents applied as a stationary phase in gas chromatography and can find applications as selective adsorbents for cyclohexanone, cyclohexanol and phenol.[13]

4. Conclusions

The polysiloxane xerogels with embedded molecules of calix[4]arene and covalently bounded calix[4]arene-crown-6, DADB18C6, α- and β-cyclodextrin groups have been synthesized by the sol-gel method.

The approaches for obtaining mesoporous silicas as SBA-15 and Davisil with surface layers containing β-cyclodextrin, calix[4]arene, calix[4]arene-crown-6 and DADB18C6 have been proposed.

The adsorption properties of the synthesized materials towards Cs^+ have been studied. The structural-adsorption characteristics' impact on adsorption properties of samples with covalently grafted macrocyclic groups has been determined. Though in case of samples with embedded macrocycles an influence of these parameters has not been revealed.

The adsorption properties of xerogels with DADB18C6 towards Na^+, K^+ and Cs^+ have been studied. It has been established that synthesized adsorbents adsorb better K^+-cations.

The adsorption ability of the obtained materials towards cesium-137 and strontium-90 has been investigated. It has been shown that SBA-15 modified by calix[4]arene groups are characterized by sufficiently high adsorption activity towards both isotopes.

The adsorption properties of polysiloxane materials containing α- and β-cyclodextrin groups towards a number of different organic compounds have been studied in static and dynamic (gas chromatography method) conditions. It has been pointed out the adsorption properties of adsorbents with α-CD groups are higher toward to *p*-nitrophenol.

Gas chromatography investigations have shown that the synthesized materials are characterized by higher adsorption activity towards oxygen-containing organic compounds.

Acknowledgements

Authors thank the NATO programme «Science for Peace» (Grant 978006) for financial support of this work.

References

1. F. Vogtle, E. Weber, *Host Guest Complex Chemistry Macrocycle. Synthesis, Structures, Applications* (Mir, Moscow, 1988) (in Russian).
2. V. Bohmer, Calixarenes. Macrocycles with (almost) unlimited possibilities, *Angew. Chem.* 34, 713–745 (1995).
3. J.F. Dozol, M. Dozol, R.M. Macias, Extraction of strontium and cesium by dicer-bollides, crown ethers and functionalized calixarenes, *J. Incl. Phenom. Macroc. Chem.* 38, 1–22 (2000).
4. G. Wenz, Cyclodextrins as building blocks for supramoleculars structures and func-tional units, *Angew. Chem. Int. Ed. Engl.* 33, 803–822 (1994).
5. V.V. Makhlyarchuk, S.V. Zatonskii, Radiation chemistry of crown compounds, *Uspekhi Khimii* 61(5), 883–909 (1992) (in Russian).
6. R.A. Hedges, Industrial applications of cyclodextrins, *Chem. Rev.* 98, 2035–2044 (1998).
7. O.V. Kuchma, Yu. L. Zub, A. Dabrowski, New sorption materials based on poly-siloxane xerogels with incorporated calix[4]arene: synthesis and structure, *Colloid. J.* 68(6), 792–799 (2006) (in Russian).
8. O.V. Kuchma, Yu. L. Zub, Experimental approach to the synthesis of hybrid adsorbents on the basis of polysiloxane xerogels functionalized by calix[4]arenes and their deri-vatives, in: *Combined and Hybrid Adsorbents: Fundamental and Applications* edited by J.M. Loureiro and M.T. Kartel (Springer, 2006), pp. 49–54.
9. O.V. Kuchma, Yu. L. Zub, Silicas functionalized by macrocyclic compounds: synthesis, structure, application, in: *Physics and Chemistry of Nanomaterials and Supramolecular Structures*, edited by A.P. Shpak and P.P. Gorbyk (Naukova Dumka, Kyiv, 2007), pp. 291–317.
10. C. Yang, P. Liu, Y. Ho, C. Chiu, K. Chao, Highly dispersed metal nanoparticles in func-tionalized SBA-15, *Chem. Mater.* 15(1), 275–280 (2003).
11. A. Katz, P. Da Costa, A.C.P. Lam Notestein, The first single-step immobilization of a calix[4]arene onto the surface of silica, *Chem. Mater.* 14, 3364–3368 (2002).
12. M. Chiraoka, *Crown-Compounds: Properties and Applications* (Mir, Moscow, 1986).
13. O.V. Kuchma, Yu. L. Zub, V.I. Lyashenko Hybrid adsorbents based on the cyclodextrins as perspective adsorbents for analytical media monitoring, *Hegiene Popul. Area.* 47, 53–58 (2006) (in Ukraine).

SENSORS WITH BIORECOGNITION ELEMENTS ENTRAPPED INTO SILICA BASED POLYMERS

GABRIELA KUNCOVÁ*
Institute of Chemical Process Fundamentals ASCR v.v.i., Prague 6, Czech Republic

Abstract. The paper presents characteristics of biosensors with biorecognition elements entrapped in silica based polymers developed and tested in the Institute of Chemical Process Fundamentals ASCR, Prague (ICPF). Prepolymerized alkoxysilanes were used for preparing whole cell biosensors of phenol, naphthalene or salicylic acid intermediate, and polychlorinated biphenyls (PCB). Modifications of prepolymer composition and immobilization procedure could increase viability of entrapped cells but can also influence sensors properties. UV curable polymers with silica skeleton, ORMOCER®s, have been matrices of a sensitive element of optical sensor for the in-situ continuous monitoring of glucose in bioreactors. This enzymatic sensor, developed within the project MATINOES, displayed 3 week stability during fermentation in a laboratory bioreactor.

Keywords: Whole cell biosensor, silica based polymers, sol-gel method, immobilization, sensor of polychlorinated biphenyls, bioluminescent bioreporters, optical biosensor.

1. Introduction

Safeguarding human and environmental resources against harmful agents and monitoring of biotechnological processes require in situ real time sensors with biorecognition element encapsulated in a matrix that is strong enough to endure the rigour of the environment yet resilient enough to viably maintain enzymes and the fragile cells. Silica based polymers possess some of the most desirable properties for immobilization of biorecognition elements; biocompatibility, transparency, controlled porosity, and chemical, thermal and dimensional stability. In the Laboratory of immobilized biocatalyst and optical sensors of ICPF, silica

*To whom correspondence should be addressed: Gabriela Kuncová, Institute of Chemical Process Fundamentals ASCR v.v.i., Prague 6, Czech Republic; e-mail: kuncova@icpf.cas.cz

P. Innocenzi, Y. L. Zub and V. G. Kessler (eds.), *Sol-Gel Methods for Materials Processing*.

matrix was used for the construction of biosensors of phenol, PCBs, naphthalene, salicylate and other aromatic compounds. A sensitive element of glucose optical sensor (project MATINOES), which was tested in this laboratory, was immobilized in UV curable organic- inorganic polymer ORMOCER®.

2. Whole Cell Biosensors

Biorecognition elements of whole cell biosensors were living cells encapsulated into silica gel films. The films were prepared from mixtures of cells with a colloid solution of silica nanoparticles or prepolymerized alkoxysilanes (tretramethoxysilane, tetraethoxysilane). Sensitive elements of phenol sensors were thin films (2 μm) on nylon meshes[1] while in case of optical sensors of naphthalene, salicylate[2] and PCBs these were ~1 mm thick films on glass. Mixtures of cells with the colloid solution of silica and prepolymerized tetraethoxysilane were sufficiently stable to prepare thin films by dip coating. Due to fast gelation, reproducible formation of the films from prepolymerized tetramethoxysilane was possible only by dropping. During the time between gelation and the first immersion of the film, the cells suffer from the presence of evolved methanol and gel shrinkage. To maintain the cells alive, the films have to be immersed in water solution within few minutes after gelation.[3] We worked out some modifications, which made encapsulation into prepolymerized tetramethoxysilane less harmful[3]:

- Encapsulation of cells in the stage of stable growth phase
- Encapsulation into water diluted silica prepolymer
- Addition of nutrient rich media
- Addition of elastic, soft and cell-friendly polymers, such as alginate that ensures the viability of large and more fragile cells as yeasts and plant cells.

Nevertheless, biorecognition elements with these modified cell friendly matrices, can suffer from some side effects:

- Encapsulation of slowly proliferating or dormant cells could prolong sensor initiation.
- Bacteria, especially small and fast growing, escape from water rich, less mechanically stable matrix.
- Higher content of coimmobilized nutrients improves cell viability. However this often leads to the decrease in sensor sensitivity for organic pollution because cells preferably utilize nutrients.

2.1. PHENOL SENSOR

Phenolic compounds represent an important group of chemicals with environmental, industrial and toxicological significance. Metabolism of cells utilizing phenol derivatives as a sole carbon source consumes 2 mol O_2 per mol phenol. This high oxygen consumption was utilized for the measurement of phenol concentration by placing immobilized cells on oxygen electrode membrane.[4] We prepared biorecognition elements of phenol sensor by withdrawing a polyester mesh from a suspension of mixed bacterial consortium, in colloidal silica or prepolymerized tetraethoxysilane.[1,5] This mesh, with the cells encapsulated in 2 μm thick silica gel film, was placed on transducer, a tip of oxygen electrode. The encapsulation into colloidal silica was less stressful for microorganisms than in prepolymerized tetraethoxysilane. After encapsulation, three hour pre-conditioning was necessary to attain maximum signal response. The phenol concentration was proportional to oxygen consumption in the 2–10 mg/l range for both sensitive films, but the film with colloidal silica exhibited higher voltage response. Sensors performance was limited due to release of the cells from silica matrix for 1 week.

2.2. BIOLUMINESCENT SENSOR OF NAPHTALENE, SALICYLATE AND SOME OTHER AROMATIC DERIVATES

Biorecognition elements of optical sensors of naphthalene and/or salicylic acid intermediates and of their metabolisms have been living bacteria *Pseudomonas fluorescens* HK44 entrapped into prepolymerized tetramethoxysilane ~1 mm thick films.[2] *Pseudomonas fluorescens* HK44 is a genetically modified microorganism that harbors the pUTK21 plasmid which contains the *nah* genes coding for naphtalene degradation linked to the *luxCDABE* gene cassette from *Vibrio fisheri* coding for bioluminescence.[6] Induction of the *nah* genes by naphtalene and its degradation intermediates such as salicylic acid results in associated induction of the *luxCDABE* genes and subsequent bioluminescent light emission at 490 nm. Strain HK44 has been used to monitor the degradation of polyaromatic hydrocarbons by the direct measurement of emitted light[7] and monitoring of naphtalene in wastewater.[8] Bioluminescence of silica immobilized HK44 cells was first detected 50 min after the induction;. which is the higher value than 8–30 min published for the free and strontium alginate immobilized cells.[9] The reason was most likely the slower diffusion of the inducer, the medium and oxygen in the microporous (400 m^2/g) silica matrix compared to alginate (12 m^2/g). The silica gel films which performed 40 times induction of bioluminescence during 1 year, contained 15–20 g_{silica}/l_{film} and 10^7 cells/ml_{film}. The films with lower silica content or higher cell concentrations fall apart and in the

tougher films (with the higher content of silica) cells viability is lowered.[2] Limits of detection with the free and silica immobilized cells were identical: 0.05 $mg_{naphtalene}l^{-1}$ and 0.5 $mg_{salicylate}l^{-1}$, and the storage stability >3 months. From 72 compounds substituted naphtalenes, naphtalene-like compounds, substituted salicylic acids, salicylic acid-like compounds, oligocyclic aromates and intermediates of naphtalene metabolism, three – o-cresol, isochinoline and salicylamide induced bioluminescence significantly greater than naphtalene, 42 compounds induced bioluminescence lower than naphtalene and 27 of them showed no bioluminescent response.[2,10]

2.3. WHOLE CELL OPTICAL SENSOR OF POLYCHLORINATED BIPHENYLS

Aerobic bacteria, isolated from contaminated soil, co-metabolically transform PCBs to chlorobenzoic acids through the biphenyl catabolic pathway.[11] The third step of this catabolic pathway generates the corresponding chlorinated 2-hydroxy-6-oxo-6-phenylhexa-2,4-dienoic acid (HOPDA), a yellow *meta* ring-fission metabolite which absorbs light at 398 nm. The reusable whole cell biosensor (WCB) was prepared by immobilizing the cells of *Pseudomonas sp.* P2 in a silica matrix containing biphenyl.[12] WCBs were exposed to 17 individual PCB congeners, or to the commercial PCB mixture Delor103, toluene, xylene, naphthalene, 1-methylnaphthalene, anthracene, pyrene, phenanthrene or dibenzofuran. The results show that silica entrapped cells produce yellow, water soluble *meta* ring-fission products selectively in the presence of three PCB congeners: 2,3,4′-trichlorobiphenyl, 2,4,4′-trichlorobiphenyl and 2,5,4′-trichlorobiphenyl and also with the commercial mixture Delor103. PCBs detection was not influenced by anthracene, phenanthrene and pyrene. Naphthalene, toluene, 1-methylnaphthalene and xylene decreased the production of the yellow intermediates. Dibenzorufan was metabolized to an orange metabolite that interfered with PCBs detection. The WCB's detection limit was 0.5 $mg_{Delor\ 103}\ l^{-1}$ and 0.2 $mg_{2,4,4'CB}\ l^{-1}$, reproducibility ±10%, reusability four times and 2 week storage stability. The WCB is a successful example of encapsulation of viable *Pseudomonas sp.* P2 cells into prepolymerized tetramethoxysilane for constructing low cost sensors for environmental monitoring. Dissolution of biphenyl in tetramethoxysilane prior to prepolymerization ensures the accurate biphenyl dosage. This extends PCB detection based on monitoring of the yellow intermediates from qualitative to semiquantitative analytical method. The advantages of silica entrapped *Pseudomonas sp.* P2 cells in comparison with the cells physically adsorbed on porous glass[13] are: the shorter time for immobilization process, the accurate cometabolite dosage at the same time with the higher and the controlled cell concentration. Immobilisation into colloidal silica or modified, alcohol free sol-gel process[14] was not used because methanol released

from pre-polymerized TMOS during gelation neither negatively influenced *Pseudomonas sp.* P2 viability nor interfered sensing. In addition, the samples were dosed as methanol solutions.

3. Glucose Optical Sensor for Bioreactors

Biorecognition element of an enzyme based optical sensor for the in-situ continuous monitoring of glucose in bioreactors, developed within the project MATINOES, involved the combination of a fluorophore compound sensitive to oxygen with an enzymatic biotransducer within a rugged, permeable and transparent matrix ORMOCER® with a siloxane based network. The enzyme, glucose oxidase, catalyzes oxidization of glucose to gluconic acid by depleting oxygen. Oxygen consumption is determined by measuring the fluorescence lifetime of metal complex, which is quenched by oxygen. To protect the enzyme against harsh conditions during UV curing of ORMOCER®, the enzyme was pre-immobilized-stabilized via multipoint covalent attachment on pre-existing porous solids, sepabeads, before incorporation into inorganic-organic hybrid polymer ORMOCER®. Pre-immobilization prevented enzyme leakage and undesired interactions between the enzyme metal complex and the polymer. The biosensor survived in the bioreactor (yeast fermentation) up to 30 days and measured glucose concentration with an accuracy 0.1 mmol/l in the range of 0–30 mmol/l. Its storage stability was 2 months.[15,16]

4. Conclusions

The results of our research demonstrate the versatility of polymers with silica skeleton as matrices of biorecognition elements. These are silica gels with viably entrapped cells as well as rugged organo-silica polymers with firmly embedded enzymes. The applicability of developed sensors ranges from cheap screening tests of environmental pollution to the in situ sensors for on-line monitoring of glucose in bioreactors. Further improvement of characteristics of biorecognition elements such as the zero cell leakage and shorter response times, should bring encapsulations into nanostructured films.

Acknowledgements

The work was supported by Czech Science Foundation (grant no 104/05/2637), Ministry of Education, Youth and Sports of the Czech Republic (grant no OC121) and EU project GRD1-2001-40477 MATINOES.

References

1. T. Brányik et al., Application of bioencapsulation by sol-gel method for construction of biosensor, *Proceedings of International Workshop Bioencapsulation V*, Potsdam, Ger., Sept. 23–25 (1996).
2. J. Trögl et al., Selectivity of whole cell optical biosensor with immobilized bioreporter pseudomonas fluorescens HK44, *Sens. Actuators B* 107(1), 98–103 (2005).
3. G. Kuncová et al., Monitoring of the viability of cells immobilized by sol-gel process, *J. Sol-Gel Sci. Technol.* 31(1–3), 335–342 (2004).
4. J. Riedel et al., Microbial sensors for determination of aromatics and their chloroderivatives. Part III: Determination of chlorinated phenols using a biosensor containing *Trischoporon beigelii (cutaneum)*, *Appl. Microbiol. Biotechnol.* 43, 7–9 (1995).
5. T. Brányik et al., Changes in phenol oxidation rate of a mixed microbial culture caused by sol-gel immobilization, *Biotechnol. Lett.* 22(7), 555–560 (2000).
6. E.A. Meighen, Enzymes and genes from the *lux* operons of bioluminescent bacteria, *Ann. Rev. Microbiol.* 42, 151–176 (1988).
7. S. Ripp et al., Control field release of a bioluminescent genetically engineered micro-organism for bioremediation process monitoring and control, *Environ. Sci. Technol.* 34, 846–853 (2000).
8. E. Valdman et al., Naphtalene detection by a bioluminescence sensor applied to wastevate samples, *Sens. Actuators B: Chem* 103, 7–12 (2004).
9. A. Heitzer, et al., Optical biosensor for environmental on-line monitoring of naphthalene and salicylate with an immobilized bioluminescent catabolic reporter bacterium, *Appl. Environ. Microbiol.* 60, 1487–1494 (1994).
10. J. Trögl, et al., Response of the bioluminescent bioreporter *Pseudomonas fluorescens* HK44 to analogues of naphthalene and salicylic acid. *Folia Microbiol.* 52(1), 3–14 (2007).
11. B. Vrana et al., Aerobic biodegradation of polychlorinated biphenyls by bacteria, *Biologia* 53, 251–266. (1998).
12. P. Gavlasová et al., *Photon06: Abstract Book*, pp. 83–84 , Manchester, UK, 04–07 Sept. (2006).
13. G. Kuncova et al., Optical detection of polychlorinated biphenyls. *Proceeding of SPIE* 3853, 72–8 (1999).
14. D. Yu et al., Aqueous sol-gel encapsulation of genetically engineered *Moraxella spp*. cells for the detection of organophosphates, *Biosens. Bioelectron.* 20, 1433–1437 (2005).
15. P. Scully et al., Optical fibre biosensors using enzymatic transducers to monitor glucose, *Meas. Sci. Technol.* 18, 1–10 (2007).
16. ICPF (Report 2006) http://www.icpf.cas.cz/bio/matinoes.

SOL-GEL TEMPLATE-FREE AND TEMPLATE-STRUCTURED SILICA FILMS FUNCTIONALISATION WITH METHYLENE BLUE DYE AND Ag NANOPARTICLES

TETYANA LEVCHENKO* , YURI PLYUTO
O. O. Chuiko Institute of Surface Chemistry, National Academy of Sciences of Ukraine, 17 General Naumov Str., 03164 Kyiv, Ukraine
NINA KOVTYUKHOVA
The Pennsylvania State University, University Park, PA 16802, USA

Abstract. Sol-gel derived silica films are promising for application as working elements of sensors for environment control. The goal of the present work was to examine the difference in the post-synthesis functionalisation of nanometer-scale silica films prepared on glass substrates *via* template and template-free sol-gel routes. The films were prepared by dip-coating from TEOS sol-gel precursor in the absence or presence of CTAB template. It has been found out that the template-structured silica films can be functionalised with Ag nanoparti-cles *via* $[Ag(NH_3)_2]NO_3$ ion-exchange or with adsorbed Methylene Blue (MB) cationic dye due to the presence of the well-organised mesopores after template removal. In contrast, only the external geometric surface of the template-free silica films appeared to be accessible for modifier molecules.

Keywords: Sol-gel synthesis, silica film, post-synthesis functionalisation, methylene blue, Ag nanoparticles.

1. Introduction

Sol-gel derived silica films possess a number of attractive properties like sufficient adsorption capacity, favourable acid/base chemistry, high thermal stability that make them promising for analytical application as working elements of optical sensors or electrochemical detectors.[1,2] Besides, silica films can

*To whom correspondence should be addressed: Tetyana Levchenko, O. O. Chuiko Institute of Surface Chemistry, NAS of Ukraine, 17 General Naumov Str., 03164 Kyiv, Ukraine; e-mail: levchtat@i.com.ua

P. Innocenzi, Y. L. Zub and V. G. Kessler (eds.), *Sol-Gel Methods for Materials Processing*.

serve as host matrixes for immobilisation of different modifiers (post-synthesis functionalisation) that results in substantial extension of their applicability.

In the recent work of Walcarius et al.[3] the advantages of the template-structured mesoporous silica materials tailored with organic ligands and their application in electroanalysis was discussed in comparison with corresponding non-structured counterparts.

The goal of the present work was to examine the difference in ion-exchange and adsorption functionalisation of silica films prepared *via* template and template-free sol-gel routes.

2. Experimental

Template-free silica films on the pre-cleaned glass slides as model substrate were prepared by dip-coating technique (withdrawal rate 25 cm/min) using sol-gel precursor synthesised by acidic hydrolysis of $Si(OC_2H_5)_4$ (reagents molar composition was 1 $Si(OC_2H_5)_4$: 22 C_2H_5OH : 5 H_2O : 0.004 HCl) following the scheme published previously by Lu et al.[4]

Template-structured silica films were prepared in a similar way using the above-mentioned precursor solution to which the CTAB template [cetyltrimethyl-ammonium bromide, $CH_3(CH_2)_{15}N^+(CH_3)_3Br^-$] was added (reagents molar composition was 1 $Si(OC_2H_5)_4$: 22 C_2H_5OH : 5 H_2O : 0.004 HCl : 0.096 CTAB). The dip-coated silica films of both types were calcined in air at 400°C (heating rate 1.5°C/min) for 1 h to complete condensation of siloxane oligomers into silica framework and to remove the template molecules from the template-doped films. The surface morphology of the prepared silica films were determined by AFM technique using a Nanoscope IIIa (Digital Instruments, USA) in a tapping mode. For the film thickness measurements, special specimens were prepared by scratching the sections of the as-deposited films with sharp steel needle to the level of glass slide before calcination.

X-ray diffraction characterisation of silica films on glass slides were performed using a DRON-4-07 (LOMO, Russia).

UV-Vis absorption spectra of the initial and functionalised silica films were measured with a Perkin-Elmer Lambda 35 UV-Vis spectrometer.

For the adsorption functionalisation template-free and template-structured silica films on glass slides were contacted with 5×10^{-5} M aqueous Methylene Blue (MB) dye (pH 6.6) at room temperature for 20 min under permanent stirring, rinsed thoroughly with deionised water to remove non-adsorbed dye and dried in a flow of warm air.

For the ion-exchange functionalisation template-free and template-structured silica films on glass slides were contacted for 15 s with aqueous $[Ag(NH_3)_2]NO_3$ complex (pH 10.5) prepared by a dropwise addition of 24% aqueous NH_4OH to

5×10^{-2} M aqueous $AgNO_3$ up to formation of a clear colourless solution. The samples were immediately rinsed thoroughly with deionised water and dried in a flow of warm air. For the reduction of incorporated Ag^+ species, the as-synthesised samples were subjected to thermal treatment in hydrogen flow at 400°C (heating rate 5°C/min) for 1 h and cooled to room temperature.

3. Results and Discussion

The template-free and template-structured silica films on glass slides were prepared in a similar way in order to minimise a number of parameters which can influence their structure. The difference in applied sol-gel precursors concerned only the presence of CTAB template which was used upon the synthesis of the template-structured silica films. Both template-free and template-structured silica films were transparent and continuous of ca. 200 nm thickness.

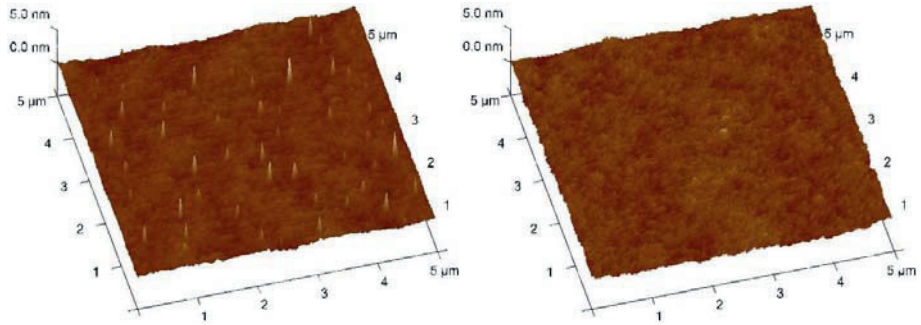

Figure 1. Surface morphology of the template-free (left) and template-structured (right) silica films.

AFM images of the template-free and template-structured silica films reveal a substantial difference of their surface morphology. The surface of the template-free film exhibits the irregularly located nanoscopic bumps of about 25 nm diameter and 2–3 nm height (Figure 1, *left*). In contrast, the template-structured silica film exhibits a relatively smooth and homogeneous surface morphology with no special surface features on a nanometer scale (Figure 1, *right*). We suppose that the difference in surface morphology of the template-free and template-structured silica films may be connected with the difference in their porosity. The bumps on the surface of the template-free silica film may originate from the explosive elimination of the residual ethanol solvent and water that evolves upon silanol group condensation and accumulates inside the film. In the case of template-structured silica film, the residual ethanol solvent and water can evolve through mesopores. As the result, the surface of the template-structured silica film appeared to be a defect-free.

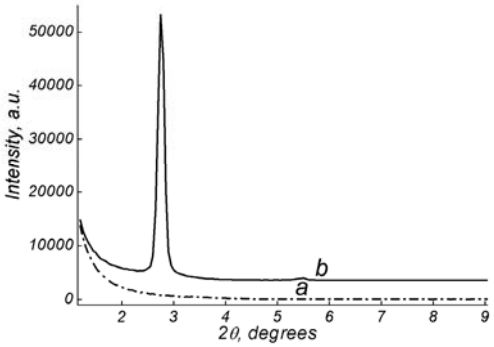

Figure 2. XRD patterns of the template-free (a) and template-structured (b) silica films.

For the template-free silica film (Figure 2*a*) no evidence of the formation of the arranged pore structure was detected in the low-angle XRD. In the case of the template-structured silica film, subjected to calcination at 400°C for the template removal (Figure 2*b*), the low-angle XRD pattern shows the peaks consistent with hexagonally arranged system of cylindrical pores.[4] The unit cell constant a_0 was calculated as 3.71 nm, the pore diameter of the prepared template-structured silica films the can be estimated as 2.7 nm.

Organic dyes of different nature immobilised on solid surfaces have a good potential for the detection of hazardous industrial substances such as hydrochloric acid, acetic acid and ammonia.[5, 6] Therefore, Methylene Blue (MB) cationic dye was selected as a model for functionalisation of the template-free and template-structured silica films since the MB molecules ($[RC_6H_3SNC_6H_3R]Cl$ where R = $N(CH_3)_2$) have extremely high molar absorption coefficient (ε reaches 9.5×10^4 M^{-1} cm^{-1} at λ = 664 nm)[7] and the ability to interact with silica surface *via* physical adsorption[8] or electrostatic interaction[9] mechanism.

It was revealed that contact of the template-structured silica films with aqueous solution of MB resulted in their intense colouring. In contrast, the template-free silica films remained almost uncoloured even after prolong (up to 24 h) immersion into MB aqueous solution. UV-Vis absorption spectra of the template-free and template-structured silica films contacted with MB aqueous solution are presented in Figure 3, *left*. For the template-structured silica film, the spectrum reveals the presence of the intense bands at 664 and 605 nm (Figure 3, *left*, *b*) which can be attributed to monomeric and dimeric MB molecules, respectively.[7] The intensity of corresponding bands in UV-Vis spectrum of the template-free silica film (Figure 3, *left*, *a*) is very low.

The differences in the behaviour of the template-free and template-structured silica films may be connected with their structure rather then with their surface

morphology. We suppose that the pore size of the template-structured silica film (2.7 nm as estimated from XRD) is large enough to accommodate the relatively small MB molecule with van der Waals size of 0.4 × 0.8 × 1.8 nm.[10] In the case of the template-free silica film MB molecules are located only at external geometric surface. To verify this supposition the experiments on functionalisation of silica films of both type were continued.

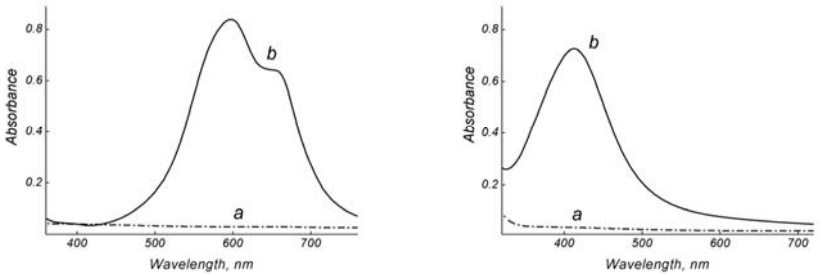

Figure 3. UV-Vis spectra of the template-free (a) and template-structured (b) silica films after contact with aqueous solution of MB (left) or ion-exchange in aqueous solution of $[Ag(NH_3)_2]NO_3$ complex followed by reduction in hydrogen (right).

For Ag nanoparticles, the presence of the intense optical absorption band, named as plasmon resonance peak, which depend both on the particle size and on the refractive index of the surrounding medium[11] is typical. The adsorbed molecules modify the dielectric properties of the surrounding medium and influence the optical absorption of Ag nanoparticles enabling to use this effect for the detection the nature and amount of the adsorbed substrates and its successful exploitation in chemical sensing.[12]

The ion-exchange route for functionalisation of the template-free and template-structured silica films with Ag nanoparticles[13] was selected. During the contact of silica films with aqueous solution of $[Ag(NH_3)_2]NO_3$ complex an incorporation of Ag^+ species into films due to deprotonation of hydroxy groups

$$\equiv Si–OH + Ag(NH_3)_2^+ \rightarrow \equiv Si–OAg(NH_3) + NH_4^+$$

on silica surface should occur. A subsequent reduction of Ag^+ species upon thermal treatment of the ion-exchanged films

$$\equiv Si–OAg(NH_3) + 1/2H_2 \rightarrow \equiv Si–OH + Ag + NH_3$$

should result in Ag nanoparticles exhibiting the intense peak at *ca.* 400–450 nm due to plasmon resonance absorption.

Both template-free and template-structured silica films were colourless after ion-exchange. The ion-exchanged template-free and template-structured silica films exhibited different behaviour upon subsequent thermal treatment in hydrogen at 400ºC. The template-free silica film remained colourless and no evidence of the formation of Ag nanoparticles was observed (Figure 3, *right*, *a*). In contrast, a yellowish colour appeared in the case of the template-structured silica film. The presence of the broad intense peak at 415 nm in the UV-Vis absorption spectrum (Figure 3, *right*, *b*) was due to the plasmon resonance of Ag nanoparticles.

The obtained results mean that the template-structured silica film can be easily doped with Ag nanoparticles using ion-exchange functionalision that can hardly be achieved in the case of the template-free silica film. In spite of the low thickness of the template-free silica film, only its external surface is accessible for doping with Ag^+ ions.

4. Conclusions

The template-free and template-structured silica films of ca. 200 nm thickness prepared on glass slides by dip-coating from TEOS sol-gel precursor in the absence or presence of CTAB template, respectively, differ in their surface morphology and in their ability to post-synthesis functionalisation. The template-structured silica films exhibit smooth surface morphology, whereas on the surface of the template-free film the irregular nanoscopic bumps were detected. It has been found out that the template-structured silica films can be doped with Ag nanoparticles *via* ion-exchange with $[Ag(NH_3)_2]NO_3$ complex or functionalised with the adsorbed Methylene Blue cationic dye due to the presence of the well-organised mesopores after template removal. In contrast, only the external geometric surface of the template-free silica films appeared to be accessible for modifier molecules.

Acknowledgements

The work was supported in part by the Programme of Fundamental Research of the National Academy of Sciences of Ukraine “Nanosystems, Nanomaterials, Nanotechnologies” and the INTAS 05-1000005-7726 grant.

References

1. M. M. Collinson, Sol-gel strategies for preparation of selective materials for chemical analysis, *Crit. Rev. Anal. Chem.* 29, 289–311 (1999).
2. D. K. Kambhampati, T. A. M. Jakob, J. W. Robertson, M. Cai, J. E. Pemberton, and W. Knoll, Novel silicon dioxide sol-gel films, *Langmuir* 17, 1169–1175 (2001).
3. A. Walcarius, M. Etienne, S. Sayen, and B. Lebeau, Grafted silicas in electroanalysis, *Electroanalysis* 15, 414–421 (2003).
4. Y. Lu, R. Ganguli, C. A. Drewien, M. T. Anderson, C. J. Brinker, W. Gong, Y. Guo, H. Soyez, B. Dunn, M. H. Huang, and J. I. Zink, Continuous formation of supported mesoporous films, *Nature* 389, 364–368 (1997).
5. L. Norena-Franco and F. Kvasnik, Chemically sensitive films for detection of hazardous substances, *Analyst* 123, 2185–2189 (1998).
6. E. Scorsone, S. Christie, K. C. Persaud, P. Simon, and F. Kvasnik, Fibre-optic evanescent sensing of gaseous ammonia, *Sens. Actuators B* 90, 37–45 (2003).
7. K. Bergmann and C. T. O'Konski, A spectroscopic study of Methylene Blue, *J. Phys. Chem.* 67, 2169–2177 (1963).
8. C. S. Brooks, Mechanism of methylene blue dye adsorption, *Coll. Polymer. Sci.* 199, 31–36 (1964).
9. I. Moriguchi, M. Honda, T. Ohkubo, Y. Mawatari, and Y. Teraoka, Adsorption and photocatalytic decomposition of Methylene Blue, *Catal. Today* 90, 297–303 (2004).
10. F. G. Lupashku, A. V. Mamchenko, and V. M. Ropot, Investigation of adsorption of water-soluble dyestuffs, *Koll. zhurn. (USSR)* 46, 364–368 (1984).
11. U. Kreibig and M. Vollmer, *Optical Properties of Metal Clusters* (Springer, Berlin, 1996).
12. H. Guo and S. Tao, Silver nanoparticles doped silica nanocomposites, *Sens. Actuators* 123, 578–582 (2007).
13. Y. Plyuto, J.-M. Berquier, C. Jacquiod, and C. Ricolleau, Ag nanoparticles synthesized in mesoporous silica films, *Chem. Comm.* 17, 1653–1654 (1999).

SYNTHESIS, STRUCTURE AND ADSORPTION PROPERTIES OF HEXAGONALLY ORDERED MESOPOROUS ORGANOSILICAS FUNCTIONALIZED WITH SULFUR-CONTAINING GROUPS

MARIUSZ BARCZAK*, ANDRZEJ DĄBROWSKI, STANISŁAW PIKUS
Faculty of Chemistry, Maria Curie-Sklodowska University, 20-031 Lublin, Poland

YURIY L. ZUB
Institute of Surface Chemistry, NAS of Ukraine, 17 General Naumov Str., 03-164 Kyiv, Ukraine

Abstract. SBA-15 mesoporous organosilicas with the *p6m* symmetry were synthesized by sol-gel co-condensation of tetraethyl orthosilicate with mercaptopropyltriethoxysilane, bis[3-(ethoxysilyl)propyl]ethane, bis[3-(ethoxy-silyl) propyl]disulfide, and bis[3-(ethoxysilyl)propyl]tetrasulfide. Final samples were characterized by X-ray diffraction and nitrogen sorption measurements. Depending on the monomers used, the resulted materials exhibit well or poorly ordered structures. All materials have a well-developed porous structure and high content of sulfur-containing moieties introduced by co-condensation.

Keywords: Hybrid materials, adsorbents, adsorption, SBA-15, sol-gel, porosity, thiol groups, functionalization.

1. Introduction

Ordered mesoporous silicas (OMS) are very attractive materials due to their high surface areas, large pore volumes, large, uniform and adjustable pore sizes, and diverse morphology making them interesting as potential catalysts and adsorbents.[1] The first successful attempt in these exciting field was done by resear-

* To whom correspondence should be addressed: Mariusz Barczak, Maria Curie-Sklodowska University, Maria Curie-Sklodowska Sq. 3, 20-031 Lublin, POLAND; e-mail: mbarczak@hermes.umcs.lublin.pl

P. Innocenzi, Y. L. Zub and V. G. Kessler (eds.), *Sol-Gel Methods for Materials Processing*.

chers from Mobil, when a family ordered mesoporous aluminosilicates, denoted as M41S materials, was obtained by supramolecular templating approach.[2,3]

The use of cationic surfactants as templates made it possible to obtain materials with the sizes of the pores in the range 2–7 nm. Sometimes, such pores are too small for catalytic or sorption application. Moreover M41S materials (particularly MCM-41 which is probably the most studied structure from the M41S family) had some unfavourable properties, such as for example low thermal and hydrothermal stability. Thus, a lot of efforts have been done to broad the accessible size of the pores and improve mechanical properties of OMS materials.

After discovery of M41S materials a broad spectrum of other mesoporous materials has been reported. The range of surfactants used as the structure directing agents has been gradually broadening from long-chain quaternary ammonium salts via anionic and neutral to nonionic polyethylene oxide (PEO).[4] In 1998 the use of a commercially available block copolymers resulted in obtaining a new family of mesoporous materials called SBA materials. These materials exhibited various types of ordered structure and large sizes of mesopores up to 30 nm.[5–7] Structure of SBA differs from M41S not only because of the size of the mesopores – in the case the network of ordered primary mesopores is additionally connected to each other by a network of micropores and smaller mesopores.[8] SBA materials have also thicker walls, which improves the thermal and hydrothermal stability.[9] The most studied structure from this group is hexagonally ordered SBA-15 structure with the *p6mm* symmetry.

Very important advantage connected with the sol-gel synthesis of SBA-15, as well as other materials, is the possibility of introduction of organic groups into the ordered structure during one-pot synthesis. In this way new organic-inorganic hybrids with desired optical, mechanical and electrical properties can be created, what make such materials attractive in adsorption, catalysis or sensing.[10] Functionalized materials are called ordered mesoporous organosilicas (OMOs) or periodic mesoporous organosilicas (PMOs) depending on the type of moieties incorporated (side-end groups sticking inside the pores in the case of the former or bridging groups incorporated in the mesopores walls in the case of the latter). Up to now dozens of organic moieties have been successively introduced into the framework of SBA-15 materials. A lot of attention is focused on the synthesis of sulfur-functionalized (particularly, but not only, thiol-functionalized) sorbents due to high affinity of such materials towards heavy metal ions, such as mercury, cadmium or lead.[10]

The main goal of this work is to take advantage of co-condensation method to introduce mercaptopropyl groups into the internal surface of the pores and ethylene, phenylene, disulfide and tetrasulfide bridges into the framework and study how structural-adsorption properties change with incorporation of these groups into the hexagonal structure of SBA-15 materials.

2. Experimental

2.1. REAGENTS

Initially the following compounds were used: tetraethoxysilane: (**TEOS**, 96%, ABCR), 1,2-bis(triethoxysilyl)ethane (**BTESE**, 96%, ABCR), 1,4-bis(triethoxysilyl)benzene (**BTESB**, 95%, Aldrich), bis[3-(triethoxysilyl)pro-pyl] disulfide (**BTESD**, 90%, ABCR), bis[3-(triethoxysilyl)propyl]tetrasulfide (**BTEST**, 95%, ABCR), 3-mercaptopropyltriethoxysilane (**MPTES**, 95%, ABCR), poly (ethylene oxide)-block-poly(propylene oxide)-block-poly(ethylene oxide) triblock copolymer Pluronic P123 (**P123**, BASF), hydrochloric acid (37%, POCH), ethanol (99.8%, POCH). All chemicals were used as received.

2.2. SYNTHESES OF THE SAMPLES

Syntheses of all channel-like mesoporous SBA-15 silicas were performed in the presence of P123 triblock copolymer by co-condensation of TEOS, MPTES and one of bridged monomers (BTESE, BTESB, BTESD or BTEST) to introduce the desired surface and framework functional groups. All materials were synthesized by one-pot route using by the similar synthesis procedure reported elsewhere.[10] In a model synthesis, 2 g of P123 was dissolved in 60 ml of 2 M HCl and 10 ml of deionized water under vigorous stirring at 40°C. After 6 h of stirring a specified volume of TEOS was added dropwise to this solution under vigorous mixing, and then the proper bridged silsesquioxane was pipetted after 10 min, and the MPTES after next 5 min. The resulting mixture was stirred for 24 h and aged at 100°C for 48 h. The white solid was thoroughly washed with deionized water, filtered and dried at 70°C. The template was removed by triple extraction with the acidic absolute ethanol (99.8%) at 70°C.

2.3. MEASUREMENTS

The content of the sulfur in the obtained samples was determined by XRF spectroscopy (Canberra). Nitrogen adsorption isotherms were measured at –196°C (ASAP 2405N sorptometer, Micromeritics) after degassing at 105°C. The BET surface area (S_{BET}) was evaluated in the 0.05–0.25 range of relative pressures. The total pore volume (V_p) was calculated by converting the amount adsorbed at a relative pressure about 0.99 to the volume of liquid adsorbate. The average pore size (d) was estimated using the BJH and KJS method.[11] Powder XRD measurements were recorded using a Carl Zeiss Jena HZG-4 diffractometer with Seifert RTG DRON-3 generator (Cu Kα radiation), 0.02° step size and 10 s step time over a range $0.5° < 2\theta < 5.0°$ at RT.

3. Results and discussion

Figure 1 presents the XRD patterns of the samples ***S1-S6***. In the case of samples ***S1-S3*** three well-resolved peaks are observed in the range of $2\theta \approx 0.8–2°$. The peaks can be indexed according to two-dimensional hexagonal *p6m* symmetry, indicating a well-defined SBA-15 mesostructure[6]: one sharp reflection at $2\theta \approx 0.8$ indexed as *100* and two minor but distinct reflections at $2\theta \approx 1.5$ and $2\theta \approx 1.8$, indexed as *110* and *200*, respectively. The samples ***S4-S6*** have less ordered structure confirmed by the lack of *110* and/or *200* signals on corresponding XRD patterns. An increase in the concentration of disulfide and tetrasulfide bridges affect meaningfully the XRD profiles, which is confirmed by deterioration of *100* signal of samples ***S4*** and ***S6*** in comparison with stronger *100* signal of samples ***S3*** and ***S5***, respectively. Moreover, XRD patterns of samples ***S4*** and ***S6*** possess only one very broad signal what testify to very poor mesostructural ordering. Thus, the increase of concentration of BTESD and BTEST in the initial mixture of monomers causes a deterioration of the mesostructural ordering.

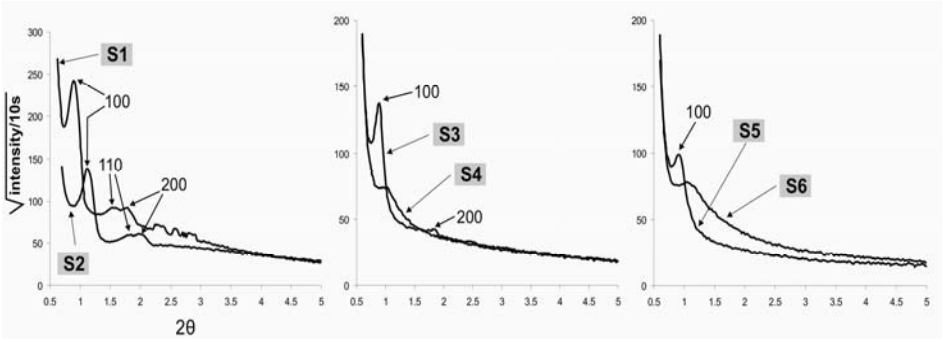

Figure 1. The XRD patterns of samples ***S1-S6***.

Nitrogen adsorption/desorption isotherms of the materials studied are shown in Figure 2. Hexagonally ordered ***S1-S3*** samples exhibit type IV adsorption-desorption isotherms. Isotherms of these samples have a sharp capillary condensation steps, reflecting capillary condensation of adsorbate in the uniform mesopores channels, and evaporation step related to the evacuation of adsorbate from the pores. Thus, it can be concluded that a framework of materials ***S1-S3*** has array of mesopores with the same diameter, what is also supported by XRD patterns (Figure 1). Samples ***S4-S6*** don't have sharp capillary condensation step, what testifies to deterioration of the structure's ordering.

All the materials have high values of S_{BET} in the range 568–820 m^2/g and pore volume in the range 0.52–1.02 cm^3/g. Values of pore volume are proportional to the degree of mesostructural ordering: highly ordered samples (***S1-S3***) have higher values of V_p (0.71–1.02 cm^3/g) while poorly ordered samples

(***S4-S6***) lower values of V_p (0.52–0.64 cm^3/g). KJS method was proved to be an elegant method for calculations of PSD of SBA-15 materials,[11] in opposite to often used BJH method which underestimates the pore size even by 50%. As can be seen from Table 1 the average pore sizes by BJH method (d_{BJH}) are lower than corresponding pores sizes obtained by KJS method (d_{KJS}).

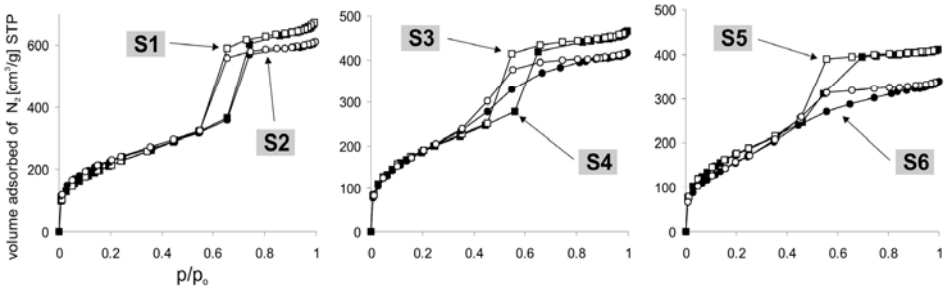

Figure 2. The nitrogen adsorption/desorption isotherms of samples ***S1-S6***.

We also testified a new method of determining average pore size directly from XRD data proposed recently by Pikus et al.[12] As it can be seen form the Table 1, the average pore sizes by this method (d_{XRD}) correspond very well with those obtained by KJS method.

The amounts of side-end thiol groups as well as disulfide and tetrasulfide bridges were estimated by elemental analysis and are presented in Table 1. The sulfur contents represent around 70–95% of the theoretical values estimated from the initial molar composition, indicating good incorporation efficiency.

TABLE 1. Properties of the materials ***S1-S6***.

No	Molar ratio of monomers	Content of sulfur (%)	Structural-adsorption characteristics				
			S_{BET} (m^2/g)	V_p (cm^3/g)	d_{KJS} (nm)	d_{XRD} (nm)	d_{BJH} (nm)
S1	TEOS/BTESE/MPTES 18:1:1	1.81	777	1.02	7.7	7.8	4.6
S2	TEOS/BTESB/MPTES 18:1:1	1.56	820	0.93	7.7	6.5	4.3
S3	TEOS/BTESD/MPTES 19:0.5:0.5	5.62	679	0.71	7.2	7.0	3.7
S4	TEOS/BTESD/MPTES 18:1:1	8.47	675	0.64	–	–	3.2
S5	TEOS/BTEST/MPTES 19:0.5:0.5	7.99	637	0.63	–	–	3.4
S6	TEOS/BTEST/MPTES 18:1:1	11.0	568	0.52	–	–	3.0

4. Conclusions

Mesoporous organosilicas with high content of thiol side-end groups and ethylene, phenylene disulfide and tetrasulfide bridges were obtained. Some of the materials have a highly ordered SBA-15 structure, other are disordered. The degree of ordering is dependent upon the type and amount of added organosilane monomers. The presence of ethylene and phenylene bridges leads to highly ordered structures, but mesostructural ordering decreases with the increase in the concentration of disulfide and tetrasulfide bridges. Values of average pore sizes by KJS method correlate very well with those determined by new method proposed by Pikus.[12] All materials have high loading of sulfur-containing moieties what make them attractive for adsorption applications.

References

1. E. B. Celer, M. Jaroniec, Temperature-programmed microwave-assisted synthesis of SBA-15 ordered mesoporous silica, *J. Am. Chem. Soc.* 128, 14408–14414 (2006).
2. C. T. Kresge et al., Ordered mesoporous molecular sieves synthesized by a liquid-crystal template mechanism, *Nature* 359(6397), 710–712 (1992).
3. J. S. Beck et al., A new family of mesoporous molecular sieves prepared with liquid crystal templates, *J. Am. Chem. Soc.* 114(27), 10834–10843 (1992).
4. C. Yu et al. in: *"Nanoporous Materials: Science and Engineering"* edited by G. Q. Lu and X. S. Zhao (Imperial College Press, London, 2004), pp. 14–48.
5. D. Y. Zhao et al., Triblock copolymer syntheses of mesoporous silica with periodic 50 to 300 angstrom pores, *Science* 279(5350), 548–552 (1998).
6. D. Y. Zhao et al., Nonionic triblock and star diblock copolymer and oligomeric surfactant syntheses of highly ordered, hydrothermally stable, mesoporous silica structures, *J. Am. Chem. Soc.* 1209(24), 6024–6036 (1998).
7. C. G. Goltner et al., Mesoporous silica from lyotropic liquid crystal polymer templates, *Angew. Chem. Int. Ed.* 37(5), 613–616 (1998).
8. R. Ryoo et al., Block-copolymer-templated ordered mesoporous silica: array of uniform mesopores or mesopore-micropore network? *J. Phys. Chem. B* 104(48), 11465–11471 (2000).
9. F. Zhang et al., Understanding effect of wall structure on the hydrothermal stability of mesostructured silica SBA-15, *J. Phys. Chem. B* 109(18) 8723–8732 (2005).
10. R. M. Grudzien, B. E. Grabicka, M. Jaroniec, Adsorption and structural properties of channel-like and cage-like organosilicas, *Adsorption* 12(5–6), 293–308 (2006).
11. M. Kruk, M. Jaroniec, A. Sayari, Application of large pore MCM-41 molecular sieves to improve pore size analysis using nitrogen adsorption measurements, *Langmuir* 13(23), 6267–6273 (1997).
12. S. Pikus, L. A. Solovyov, M. Kozak, M. Jaroniec, Comparative studies of p6m siliceous mesostructures by powder X-ray diffraction and nitrogen adsorption, *Appl. Surf. Sci.* 253(13), 5682–5687 (2007).

SOL-GEL ROUTE TO CARBON-SILICA MOLECULAR SIEVING ADSORBENTS

MAXIM S. MEL'GUNOV*, ALEKSEY N. VODENNIKOV, VLADIMIR B. FENELONOV
Boreskov Institute of Catalysis SB RAS, pr-kt Akad. Lavrentieva 5, Novosibirsk, 630090, Russian Federation

Abstract. Molecular sieve adsorbents have been prepared by the sol-gel route comprising simultaneous hydrolysis of tetraethylorthosilicate (TEOS) and polymerization of furfuryl alcohol (FA). The mixtures of TEOS (10%) and FA (90%) have been forced to interaction in the presence of small amounts of water (hydrolyzing agent) and sulfuric acid (polymerization catalyst) under ambient conditions, and successive carbonization at 923–1,023 K under argon. Adsorption of nitrogen at 77 K appears to be essentially non-equilibrium indicating activated character of diffusion. The ratio of CO_2/N_2 adsorption uptake at 1 bar changes from 9:1 for carbon, obtained without TEOS additives under other similar conditions, to 1:3 for carbon-silica composite, indicating the reciprocal change of the adsorption selectivity factor.

Keywords: Molecular sieve, adsorption selectivity, pressure swing adsorption.

1. Introduction

Molecular sieving adsorbents (MSA) are widely used for gas separation, drying and purification, as well as catalysts and catalyst supports. These materials show adsorption selectivity for molecules of various limiting sizes. Well known are alumo-silicates (zeolites), alumo-phosphates, carbon molecular sieves. New types of MSA are: metal-organic frameworks of MIL type, mesoporous silicates and carbons.

* To whom correspondence should be addressed: Maxim S. Mel'Gunov; e-mail: max@catalysis.ru

P. Innocenzi, Y. L. Zub and V. G. Kessler (eds.), *Sol-Gel Methods for Materials Processing*.

The main aim of this work was elaboration of carbonaceous molecular sieves, which are suitable for nitrogen, hydrogen or CO_2 purification from gaseous mixtures by means of pressure swing adsorption processes.

There are several known ways to prepare carbon molecular sieves. For example, natural precursors[1] such as lignin, cellulose, shells of various nuts are carbonized and partially burned-off to develop microporosity. This can be followed by carbon deposition in diffusion regime to tune the size of the microporous openings that provide molecular selectivity. The main disadvantage of this approach is application of natural precursors with technological characteristics that are too complex to be thoroughly controlled. Moreover, special additional procedures should be applied to give the resulting material a form suitable for particular separation process (film or membrane, granules of spherical form, or honeycombs). More technologically friendly is application of pure chemical liquid carbonaceous compounds (e.g. furfuryl alcohol (FA), phenol-formaldehyde resin, etc.) that can be polymerized and than carbonized under certain conditions.[2] During polymerization step the material changes its viscosity from very low to increasingly high, approaching the hard solid state. The forms with intermediate viscosity can be easily used to prepare materials of desirable form by extrusion and other related techniques. Known is also the way of impregnation of mineral molecular sieves (zeolites, for example, of Y-type) with carbonaceous liquid, carbonization and mineral template removal by dissolving in HF (for recent review one can consider[3]). The disadvantage of this way is its relatively high cost.

To enhance the separation properties of CMS one can apply functionalization of the carbon matrix with compounds that display high affinity to one of the permeating gas species. For example, addition of Ag nanoclusters increases the selectivity to O_2 over N_2 by a factor 1.6 compared to a nonfunctionalized CMS membrane prepared by the same pyrolysis procedure.[4] To increase hydrogen/methane permoselectivity copper(II) nitrate can be added (0–6 wt%) to cellulose–hemicellulose precursor followed by carbonization at 823, 923 K.[5]

"One pot" mixing of FA with tetraethyorthosilicate (TEOS), accompanied with successive polymerization and carbonization results in micro-mesoporous materials,[6] which even referred to as molecular sieves[7] with no exact example of molecular sieving effect. Polymerized FA + TEOS mixture was successfully applied for shapeless monoliths formation.[8] This is of real importance for gas separation techniques such as pressure swing adsorption, for which structured sieving adsorbents have strong advantage over granular adsorbents due to lower gasodynamic resistance and attrition.

In this work we present the results of the experiments on molecular sieving properties of carbon-silica adsorbents, synthesized from FA and TEOS mixture.

2. Experimental

2.1. MATERIALS PREPARATION

Furfuryl alcohol and tetraethylorthosilicate of 98+% grade were purchased from Alfa Aesar and Fluka, respectively, and used without additional purification. In typical synthesis 1 g of TEOS was mixed with 9 g of FA under ambient conditions, and 0.1 g of 0.03 M H_2SO_4 was added to the mixture under stirring. The mixture was heated up to 70°C for 5 min, and then cooled to 20°C in water thermostate and kept there until formation of solid composite. It is important to note that long exposition at 70°C results in rapid polymerization with high rate of gaseous ethyl alcohol formation. The reaction is exothermic and can result in flameless blowing of the mixture. After that the material was crashed to granules of 1–2 mm size and carbonized unde r argon at 923, 973, and 1,023 K. The corresponding samples are referred to as CSMS XXX, where CSMS means carbon-silica molecular sieve, and XXX is the temperature of activation. Blank experiment was also performed without TEOS addition other conditions being same. The material from pure FA was carbonized at 1,023 K and refereed to as FAC. NaX zeolite from UOP was also studied as reference.

2.2. CHARACTERIZATION

N_2 adsorption at 77 K, N_2 and CO_2 adsorption equilibrium and rate at 300 K were studied using ASAP-2020 instrument. Before the experiment the samples were degassed under dynamic vacuum of 10^{-4} torr for 15 h.

3. Results and Discussion

The result of nitrogen adsorption-desorption experiment under standard program suitable for microporous materials at 77 K is shown in Figure 1.

Such shape of the isotherm indicates that it is not adsorption-desorption equilibrium isotherm. The diffusion of N_2 molecules at 77 K has activation character. This is typical for the adsorbents (e.g. zeolites), which micropore size is close to the size of N_2 molecules. Since the measured isotherms are obviously non-equilibrium one can only estimate the specific surface area of 300 m^2/g and micropore volume of 0.05 cm^3/g.

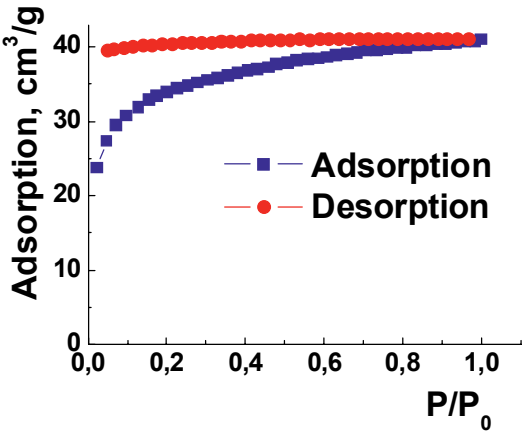

Figure 1. N_2 adsorption-desorption at 77 K for carbon-silica molecular sieve (CSMS 923) carbonized at 923 K.

Figure 2 shows N_2 and CO_2 adsorption-desorption isotherms for the studied materials at 300 K below atmospheric pressure. Noteworthy, nitrogen adsorption-desorption on CSMS 1023 and FAC has not absolutely equilibrium character. N_2 adsorption uptake has same order of magnitude for NaX, FAC and CSMS 1023, except only that the form of the adosprtion isotherm for NaX is closer to Henry type. Most probably, lower values of N_2 adsorption compared to FAC correspond to the presence of silicate in the CSMS sample, which does not add microporosity, but makes the material heavier, thus decreasing the values of specific adsorption (per gram). Decrease of the activation temperature

a) b)

Figure 2. Adsorption-desorption isotherms (300 K) of (a) N_2 and (b) CO_2. NaX is a commercial NaX zeolite, FAC is furfuryl alcohol carbon.

is also accompanied by decrease of N_2 adsorption uptake that can be explained by insufficient degree of carbonization and microporosity development. On the other hand, the adsorption of CO_2 on CSMSs does not significantly depend on the activation temperature, indicating that CO_2 adsorbs mainly on the external surface.

CO_2 adsorption isotherms at 300 K differ significantly from the isotherms for N_2. FAC sample has high values of CO_2 uptake comparing to that for N_2, which is typical for microporous carbon adsorbents due to usually higher values of adsorption heat for CO_2. Controversially, CO_2 uptake over CSMS samples is lower that that for N_2, indicating the reciprocal change of the adsorption selectivity factor. The values of the latter (ratio of N_2 to CO_2 adsorption) under 1 bar (experiment) and 10 bar (calculated from Langmuir extrapolation) are shown in Table 1.

TABLE 1. Adsorption selectivity factor for CO_2 and N_2.

Pressure (bar)	NaX	FAC	CSMS 923	CSMS 973	CSMS 1023
1	1.5	2.1	2.3	2.7	0.12
10[a]	5.6	3.4	3.7	4.5	0.10

[a]Calculated from Langmuir extrapolation to 10 bar from the measured isotherms.

The values of adsorption selectivity factor for CSMS samples are higher under 1 bar, and approach to that under 10 bar compared to NaX zeolite. Of course, extrapolation to 10 bar from the isotherms measured below 1 bar is rather rough, nevertheless, this extrapolation shows that selectivity of CSMS samples for N_2 and CO_2 is close to that for pure molecular sieve NaX. Reciprocal change of adsorption selectivity factor from preferable CO_2 adsorption for FAC to the preferable N_2 adsorption for CSMSs indicates changes of mesoporous structure of the material due to incorporation of silica most probably in a mono- or oligomolecular form.

Figure 3 shows the typical behavior of the rate of N_2 and CO_2 adsorption. The rate of adsorption for both gases and adsorbents starts from linear behavior in coordinates "adsorption vs time$^{-1/2}$" that is typical for microporous adsorbents. CO_2 adsorption goes faster compared to N_2 adsorption for both adsorbents. Simultaneously, adsorption of CO_2 over MSCS 923 is faster than that for FAC. Taking into account the dramatic change in CO_2 adsorption uptake between FAC and CSMS 923 one can assume, that decrease of CO_2 adsorption rate for FAC comparing to CSMS 923 is caused by slow diffusion in micropores, which are accessible for CO_2 in FAC and inaccessible in CSMS 923 at 300 K.

Figure 3. Typical rate of N_2 and CO_2 adsorption at 300 K for FAC and CSMS 923 samples.

4. Conclusions

One pot synthesis of carbon-silica adsorbents from furfuryl alcohol and tetraethylorthosilicate mixture catalyzed by sulfuric acid results in formation of materials that show adsorption selectivity towards N_2 in N_2-CO_2 system under ambient conditions. This is opposite to the properties of traditional activated carbons, can be refereed to as molecularly sieving effect, and can be applied for CO_2 purification from N_2.

References

1. W.M.A. Wan Dauda, M.A. Ahmad, Sep. Purif. Technol 57, 289–293 (2007) (and references therein).
2. A.F. Ismail, L.I.B. David, J. Membr. Sci. 193, 1–18 (2001); H. Wang, L. Zhang, G.R. Gavalas, J. Membr. Sci. 177, 25–31 (2000); W. Wei, G. Qin, H. Hu, L. You, G. Chen, J. Membr. Sci. 303, 80–85 (2007) (and references therein).
3. B. Sakintuna, Y. Yürüm, Ind. Eng. Chem. Res. 44, 2893–2902 (2005).
4. J.N. Barsema, J. Balster, V. Jordan, N.F.A. van der Vegt, M. Wessling, J. Membr. Sci. 219, 47–57 (2003).
5. D. Graingera, M.-B. Hägg, , J. Membr. Sci. 306, 307–317 (2007).
6. H. Müller, P. Rehak, C. Jager, J. Hartmann, N. Meyer, S. Spange, Adv. Mater. 12, 1671 (2000).
7. J. Liu, H. Wang, L. Zhang, Chem. Mater. 16, 4205–4207 (2004).
8. S. Grund, A. Seifert, G. Baumann, W. Baumann, G. Marx, M. Kehr, S. Spange, Micropor. Mesopor. Mater. 95, 206–212 (2006).

STUDY OF Hg^{2+} SORPTION FROM WATER SOLUTIONS BY MESOPOROUS SILICA WITH THIOUREA FUNCTIONAL GROUPS

INNA V. MELNYK*, OLENA I. GONA[1], LIDIA I. KOZHARA[1], YURIY L. ZUB[1], NEONILA A. YAROSHENKO[2], TATIANA F. KOUZNETSOVA[3], ANATOLIY I. RATKO[3]

[1] O.O.Chuiko Institute of Surface Chemistry, NAS of Ukraine, 17, General Naumov Str., Kyiv 03164 Ukraine

[2] Institute of Sorption and Endoecology Problems, NAS of Ukraine, 13, General Naumov Str., Kyiv 03164 Ukraine

[3] Institute of General and Inorganic Chemistry, NAS of Belarus, 9, Surganova Str., Minsk 220072 Belarus

Abstract. The mesoporous silicas with thiourea functional group $\equiv Si(CH_2)_3NHC(S)NHC_2H_5$ were synthesized using sol-gel and template methods (with cetylpyridinium chloride as template). It has been found that the sorption properties of these mesoporous silicas are influenced both by the functional group content and the character of the sorbent's porous structure. At low density of ligand groups all of them are accessible for Hg^{2+} sorption with formation, as a rule, of the simplest complexes (1:1 composition). The rising density of functional groups in the surface layer of sorbents results in the reduction of their accessibility and complicates the complex formation process. This, causes reducetion of static sorption capacity of such materials (from 357 to 46 mg/g). It was shown that mesoporous materials with thiourea groups synthesized by template method and possessing highly ordered structures have superior kinetic characteristics compared to xerogels with the same functional groups. is stable

Keywords: Sol-gel method, template method, mesoporous silica with thiourea groups, mercury(II) sorption.

*To whom correspondence should be addressed: Inna V. Melnyk, Ph.D., O.O. Chuiko Institute of Surface Chemistry, NAS of Ukraine, 17 General Naumov Str., Kyiv 03164 Ukraine; e-mail: inna_melnyk@mail.ru

P. Innocenzi, Y. L. Zub and V. G. Kessler (eds.), *Sol-Gel Methods for Materials Processing*.

1. Introduction

Silica is most frequently chosen as an initial matrix for production of highly effective and selective adsorbents. It does not swell in organic solvents and in a wide range of pH. Moreover, it can be provided with desirable textural characteristics. Sol-gel and template methods of synthesis are often used in this purpose to obtain materials functionalized with different organic groups. These synthetic approaches are based on the hydrolytic polycondensation reaction of silica alkoxy-derivatives[1–5]. The reaction mixture can be doped by various organic and inorganic substances, depending on the assigned target. This approach is, in particular, frequently used for the regulation, in broad limits, of structural and adsorption characteristics of silicas. The surfactants are therefore brought in during the hydrolytic polycondensation reaction, when the so-called template synthesis is carried out. In this case, the role of the surfactants is limited to formation of an organized phase with corresponding micelle packing and inclusion of these micelles into the matrix of the organo-silica anions. As a result of polycondensation and polymerization processes, a removable, instable framework of sorbent, a mesophase, is formed. Further hydrothermal and thermal processing of the materials results in formation of the inorganic framework of sorbent and surfactant removal which leads to the formation of mesoporous silicas, which pores are equal in form and size. Such approach enables to improve significantly the kinetic characteristics of the abovementioned sorbents. From this point of view, in this work there is made a comparison of structure and sorption properties of xerogels and mesoporous silicas, which contain the same functional group. The latter was the thiourea group possessing considerable potential for the sorption of heavy metal ions.[2,6]

2. Experimental

As sorbents, three xerogels and three mesoporous silicas which synthesis has been described earlier[7,8] were used (Table 1). The xerogels differed by the ratio between tetraethoxysilane (TEOS) and the trifunctional silane with thiourea group, which was used in the synthesis, and, as a result, by their structural-adsorption characteristics and functional groups content. Mesoporous silicas **M1** and **M2** differed also by the TEOS/trifunctional silane ratio. Furthermore, in their synthesis 1-dodecylamine (DDA)[7] and for the **M3** synthesis cetylpyridinium chloride (CPyCl)[8] were applied as a templating agents.

IR spectra of sorbents before and after mercury(II) sorption (in the latter case the samples were preliminary dried in air) were recorded using Nicolet NEXUX FTIR spectrometer in the region 4,000–400 cm^{-1} in reflection mode. The samples were initially mixed with calcined KBr (1:30).

TABLE 1. Functional groups content, parameters of porous structure and sorption characteristics of silicas with thiourea groups.

Sample	Ratio TEOS/ trifunctional silane during synthesis	$C_{gr.}$, mmol/g	$S_{sp.}$, m^2/g	$V_{s.}$, cm^3/g	$d_{ef.}$, nm	Ratio "Hg(II)/ functional group content" (in %) (in parentheses – sorption time, h)	Static Sorption Capacity (SSC), mg/g
X1	2:1	3.0	<1	–	–	8 (72)	46
X2	4:1	2.3	48	0.07	3.6	38 (72)	178
X3	8:1	1.4	180	0.53	10.4	127 (72)	357
M1	10:1	1.2	925	0.51	2.5	143 (24)	345
M2	10:2	1.8	400	0.21	3.6	58 (72)	211
M3	10:2	1.8	1,157	0.64	2.9	103 (3)	369

For the sorption studies (under static conditions) was used a mercury(II) nitrate solution of with concentration 0.049 mol/l in the 0.01 M nitric acid. The volume of mercury solution sample was 20 cm^3 and the sorbent weight 0.1 g (the xerogel fraction with particle size <0.063 mm was applied). Since the surface of resulting materials is hydrophobic, the sorbents were wetted in advance with 0.1 cm^3 ethanol. The distribution of metal was controlled through the aqueous phase by reverse titration with Trylon B and $MgSO_4$ solution. pH of working solutions was controlled by Universal EV74 Ionometer.

3. Results and Discussions

The Figure 1 shows sorption isotherms of mercury(II) ions by **X1, X2** and **X3** xerogels. The analysis of these isotherms leads to the following conclusions: in case of **X3** xerogel, which is characterized by the lowest density of functional groups (0.008 mmol/m^2) in its surface layer the mercury (II) complexes, apparently, are formed in 1:1 composition with thiourea groups. The somewhat elevated adsorbed metal content, in comparison with the number of functional groups, may be explained by the fixation of some amount of mercury(II) aqua complexes in the pores of this sorbent. The shape of mercury(II) ion sorption isotherm for the **X2** xerogel (density of functional groups is 0.048 mmol/m^2) is rather interesting, displaying two distinct plateaus (Figure 1). For the first one, the amount of adsorbed mercury is 0.45 mmol/g, for the second – 0.90 mmol/g. It may be assumed that in this case, on the surface of sorbent there exists a polymeric functional layer of specific structure. In addition, in the region of low equilibrium metal salt concentrations, only about 40% of thiourea groups take part in the sorption interaction and the formation of mercury(II) complexes with 1:2 composition occurs.

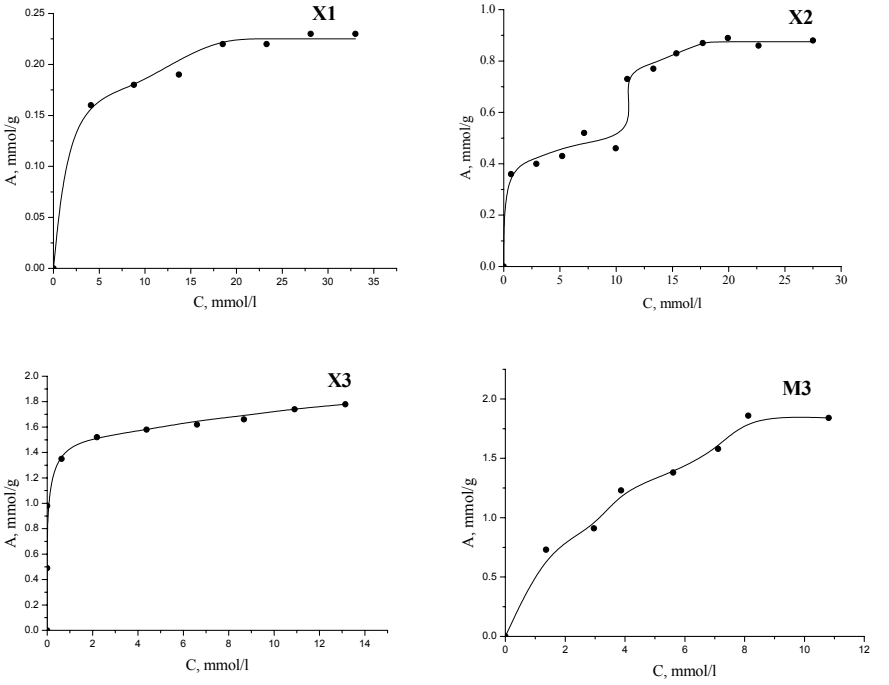

Figure 1. Isotherms of mercury adsorption by **X1**, **X2**, **X3** and **M3** samples.

Further increase in the equilibrium metal cation concentration stipulates the formation of complexes with simplified composition, with the 1:1 ratio (this assumption is confirmed by the fact that, in the second section of isotherm, the same amount of metal as in the first one is adsorbed). Consequently, 60% of the functional groups in the **X2** xerogel are inaccessible for metal ions under conditions of the experiment. In case of the **X1** xerogel a similar picture is observed, though it is not so clearly expressed (Figure 1). It is clear that the absence of porous structure in this xerogel with relatively high thiourea group content (3.0 mmol/g) should stipulate more pronouncedly the formation of a polymeric functional layer. In this connection, almost 80% of ligand groups become inaccessible for mercury(II) ion sorption. It may be concluded that the sorption properties of xerogels with thiourea groups are determined not only by the latter content but also by the chatacter of porous structure of the sorbents. In other words, the increase in functional group density stipulates increasingly their inaccessibility for metal ion sorption.

Comparing the sorption properties of mesoporous silica in relation to mercury(II) ions, the following conclusion may be made: in case of **M2** sample, even after 3 days of sorption, only about 50% of its functional groups participate

in binding the metal ions. The elevated mercury(II) sorption, in comparison with ligand group content, observed for **M1** sample is caused, apparently, by the incomplete removal of DDA (the presence in such samples of template has been previously acknowledged by solid NMR spectroscopy[9]). High sorption properties were observed for the **M3** sample obtained using CPyCl (Table 1). Thus, already during 3 h, the participation of all its thiourea groups in the complex formation was observed, the forming complexes being of 1:1 composition. This has been expected considering the density of functional groups in this sample (0.0016 mmol/m^2).

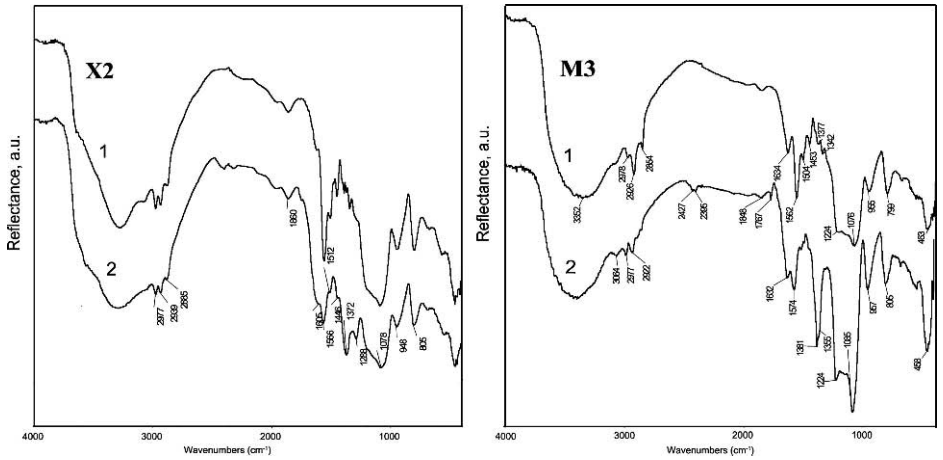

Figure 2. IR spectra of some samples 1-before Hg(II) sorption and 2-after Hg(II) sorption.

The Figure 2 shows IR spectra of some samples with adsorbed Hg^{2+} ions. On the basis of analysis of these spectra, the conclusion may be made that the intensive absorption band at 1,575 cm^{-1} (ν_{as} NCN) preserves practically its position in comparison with the IR spectra of the original sorption materials (1,562 cm^{-1}). However, it should be noted that its shape becomes structurally related. Moreover, in IR spectra of these samples, the appearance, as a shoulder, of a new low-intensity absorption band at above 1,610 cm^{-1} is indicated. It may be assumed that in the course of mercury(II) sorption the thion-thiol tautomerism is observed for a part of thiourea groups. The band in the region above 1,610 cm^{-1} in the examined IR spectra of xerogels may be attributed to the valence vibration of the forming azomethine group (–C=N–). The control measurements of pH during the experiment have shown that with the rise of metal ion equilibrium concentration in sorption series is associated with successive reduction of pH in the suspension: for **X1** – from ~2.0 to ~1.94; **X2**–

from ~2.0 to ~1.85; **X3** – from ~2.1 to ~1.8; **M1** – from ~1.96 to ~1.75; **M2** – from ~2.01 to ~1.86; **M3** – from ~2.01 to ~1.75. This is in agreement with the above assumption.

4. Conclusions

It has been found that the sorption properties of xerogels and mesoporous silicas containing thiourea groups in the surface layer are influenced by both the functional group content and the nature of the sorbent's porous structure. At low density of ligand groups (expressed in mmol/m^2), all of them are accessible for mercury(II) ions sorption with formation, as a rule, of simplest complexes with 1:1 composition. The rising density of functional groups in the surface layer of sorbents results in reduction of their accessibility and complicates the complex formation process. This, in its turn, causes reduction of SSC of such materials.

It has been found that mesoporous materials with thiourea groups in surface layer, synthesized by template method and possessing highly ordered structure, possess superior kinetic characteristics compared to xerogels with same functional groups.

On the basis of the obtained data, it can be concluded that the presence of thiourea functional groups in the surface layer of sorbents enables to use them for removal of heavy and noble metals including such dangerous for human organism ion as Hg^{2+} from solutions. The approaches proposed in this work for the synthesis of new materials permit, depending on the assigned task, to create sorbents with in advance designed characteristics.

Acknowledgements

This work was financed by State Fund of Basic Researches (Ministry of Education and Science of Ukraine) and Belarus State Fund of Basic Researches, for that authors express them the sincere gratitude.

References

1. *Handbook of Sol-Gel Science and Technology: Processing, Characterization, and Applications*, edited by S. Sakka (Kluwer, Dordrecht, The Netherlands, 1–3, 2005).
2. M.G. Voronkov, N.N. Vlasova, Yu.N. Pozhidaev, Organosilicon ion-exchange and complexing adsorbents, *Appl. Organometal. Chem*. 14, 287–303 (2000).
3. Yu.L. Zub, R.V. Parish, Functionalized polysiloxane sorbents: preparation, structure,

properties and use, *Adsorption on New and Modified Inorganic Sorbents,* Eds. A.Dabrowski and V.A.Tertykh (Elsevier, Amsterdam, 99, 1996).

4. Yu.L. Zub, I.V. Melnyk, A.A. Chuiko, D. Cauzzi, G. Predieri, Design of functionalized polysiloxanes: synthesis and investigation of sulfur-containing xerogels with mono- and bifunctional surface-layer, *Chem. Phys. Technol. Surf.* 7, 35–45 (2002).
5. I.V. Mel'nyk (Seredyuk), Yu.L. Zub, A.A. Chuiko, M. Jaroniec, S. Mann, Poly-functionalized silica adsorbents obtained by using dodecylamine as template, *Stud. Surf. Sci. Cat.* 141, 205–212 (2002).
6. I.V. Melnyk, V.Ya. Demchenko, Yu.L. Zub, and A.A. Chuiko, The sorption of Au(III) using polysiloxane xerogels functionalized by thiourea groups, *Chem. Phys. Technol. Surf.* 9, 31–36 (2003) (in Ukraine).
7. E.I. Gona, I.V. Melnyk, Yu.L. Zub, A. Dabrowski, New sorption materials containing in its surface layer functional groups $\equiv Si(CH_2)_3NHC(S)NHC_2H_5$, *Chem. Phys. Technol. Surf.* 15 (in press) (2008) (in Russian).
8. O.I. Gona, Yu.L. Zub, N.A. Yaroshenko, J. Goworek, Influence of synthetic conditions on the structure of mesoporous silicas containing thiourea functional group, *Polish J. Chem.* 82 (in press) (2008).
9. Yu.L. Zub, *Dr. Sc. Thesis*, Kiev, ISC of NASU (2003) (in Ukraine).

APPLICATION OF SOL-GEL METHOD FOR SYNTHESIS OF A BIOSENSITIVE POLYSILOXANE MATRIX

ROMAN P. POGORILYI*, VASYL P. HONCHARYK,
INNA V. MELNYK, YURIY L. ZUB
O.O. Chuiko, Institute of Surface Chemistry, National Academy of Sciences of Ukraine, 17 General Naumov Str., Kyiv 03164 Ukraine

Abstract. Sol-gel method was used to synthesize polysiloxane hydrogel with encapsulated urease (immobilization degree in the range of 79–88%) which preserved the enzymatic activity at the level of 56–84%. The nature of functional groups was shown to influence the pore structure parameters. Immobilization degree and preservation of adsorbed urease activity depend on the structural-adsorption characteristics of matrices. The possibility of "double immobilization" of urease on silica gel by sol-gel method and the opportunity of reuse of the synthesized formulations was investigated. Urease immobilization on the surface of magnetite ($FeO \cdot Fe_2O_3$) was also studied by adsorption method.

Keywords: Urease, immobilization, sol-gel method, magnetic nanoparticles, silica gel.

1. Introduction

Constant need in increasing control of environmental contamination, food quality, and increasing number of clinical studies require introduction of new analytical technologies. In particular, the application of high-sensitivity, selective, fast and economic biosensors is based on bio-sensitive membranes.[1,2] Such membranes are thin organic or inorganic films containing immobilized biopreparations.[3,4] Sol-gel method proposed in recent studies of enzymes immobilization was envisaged to produce thin polyorganosiloxane films with encapsulated enzymes.[8,9] It is possible also to synthesize such films on electrode surfaces.

*To whom correspondence should be addressed: Roman P. Pogorilyi, O.O. Chuiko Institute of Surface Chemistry, NAS of Ukraine, 17 General Naumov Str., Kyiv 03164 Ukraine; e-mail: roman_pogorilyi@rambler.ru

P. Innocenzi, Y. L. Zub and V. G. Kessler (eds.), *Sol-Gel Methods for Materials Processing*.

The opportunity of multicomponent systems application in such synthesis permits to obtain films with necessary properties and functions[11,12] In the present work the method of covalent and non-covalent urease immobilization using sol-gel approach is presented.

2. Experimental

For incorporation of urease in polysiloxane matrixes (PSM) after alkoxysilane hydrolysis, a water solution of urease in a phosphate buffer was introduced in the system. Hydrogels containing incorporated urease and without it were pounded and diluted with a buffer solution to the desired volume. Synthetic procedure included vacuum drying of obtained hydrogels without urease at 100–110°C, and with it at 20–25°C.[13]

To immobilize an enzyme, the xerogel (0.1 g) was impregnated with phosphate buffer containing urease solution (25 cm^3) and left overnight in a fridge. This method was used also to immobilize enzymes on silica hydrogel. For this propose a hydrogel suspension (1 cm^3), containing solid phase (0.04 g), was mixed with urease solution (10 mg) in a phosphate buffer (2 cm^3). In 12 hours the xerogel or hydrogel suspensions were centrifuged and the removed precipitates were washed five times by a phosphates buffer (5 cm^3).[14]

Double immobilization of urease on silica gel surface was realized by carrying out of hydrolytic polycondensation of alkoxysilanes, preliminary mixed in the chosen ratio, applying a catalyst (fluoride-ion), polyvinyl alcohol (PVA) and urease.[15] *Typical method of synthesis.* TEOS (0.15 cm^3), MTES (0.05 cm^3), DMDES (0.05 cm^3), solution of PVA (0.05 cm^3), NH_4F (0.01 cm^3, 10 mM/l), urease solution (0.75 cm^3, 17.5 mg urease in phosphate buffer, pH = 7), silica gel (0.25 g).

For urease immobolization was used magnetite and magnetite modified by silanol and 3-aminopropil groups. For this purpose a weighted portion of substrate (100 mg) was introduced in a phosphate buffer (3 cm^3) and left overnight in a fridge. The subsequent washing and determination of immobilized urease activity were carried out by standart technique described above.

Enzymatic activity of urease was determined by biochemistry methods. The unit of activity was transformation of 1 μmol of urea per minute of enzymatic reaction. The medium value of three parallel tests was used in all cases. The error in urease activity determinattion was not more than 10%.

Reservation of immobilized urease activity (%) was estimated by the formula:

$$A_{res.} = \frac{A_{imm.} \cdot 100}{35 \cdot m}$$

where:
$A_{res.}$– preservation of immobilized urease activity, %

$A_{imm.}$– activity of the immobilized urease, un/g
m – weight of the initial urease in 1 g of synthesized sample, mg

3. Results and Discussion

Immobilization of urease in hydrogels and xerogels was realized via two ways:

1. Inclusion of enzyme at the stage of the hydrogel synthesis with subsequent transformation of the hydrogel with immobilization of urease in a xerogel (one-stage process). In this way the immobilization of urease is influenced by the process of matrix structure formation.
2. Adsorption of urease on the hydrogel and xerogel with an already formed structure (two-stage process).

It was established that functionalization of polysiloxane hydrogel by 3-aminopropyl groups and 3-mercapthopropyl groups leads to almost complete bonding of enzyme in both ways of immobilization. Introduction of methyl groups in hydrogel provokes decrease in the extent of binding of the enzyme in the one-stage process and does not influence the extent of binding in the two-stage process.

Increasing the quantity of modifier for functonalization of hydrogel by 3-aminopropyl groups provides gradual reduction of preservation of urease activity from 80% to 50%. Functonalization of hydrogel by 3-mercapthopropyl and methyl groups doesn't influence significantly the preservation of urease activity both in one-stage and two-stage processes, and the value of urease activity preservation is 60–100%.

Hydrogels have high lability of polysiloxane skeleton. Possibly in such systems the influence of PSM on the urease structure (incorporated or absorbed) was insignificant, and diffusion obstacles for the substrate are practically absent. Therefore, in the experiment we observed high activity of enzyme (Figure 1).

Functionalization of PSM influences essentially the preservation of urease activity in time (see Figure 2). This figure shows that the urease immobilized on PSM with 3- mercaptgopropyl groups had the highest stability in time. In 300 days the activity of the enzyme immobilized on PMPSG decreased only by 30%.

Structural-adsorption characteristics of xerogels with and without urease are presented in Table 1.

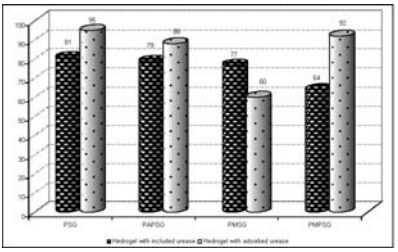

Figure 1. Dependence of size of preservation of activity urease from its way immobilization.

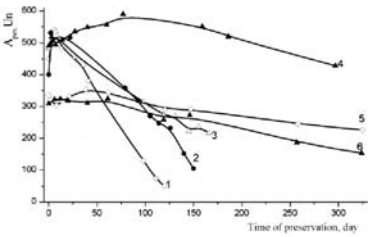

Figure 2. Preservation of activity urease, included in hydrogels, in time: 1 – PSG; 2 – PMSG; 3 – PAPSG; 4 – PMPSG; 5,6 – PMPSG.

TABLE 1. Parameters of the porous structure of the polysiloxane xerogel, prepared with urease (1) end without it (2).

Sample	PSG		PAPSG		PMSG		PMPSG	
	1	2	1	2	1	2	1	2
S_{sp}, m^2/g	230	570	–	130	280	280	140	230
V_s, cm^3/g	0.14	0,37	–	0.45	0.16	0.49	0.09	0.23
d, nm	2.3	2,6	–	14.0	2.3	6.9	2.6	4.0

(PSG – polysiloxane xerogel; PAPSG – poly(3-aminopropil)siloxan xerogel; PMSG – polymetylsiloxan xerogel; PMPSG – poly(3-mercaptopropil)siloxan xerogel).

Analysis of the results presented in Table 1 shows that the quantity of urease immobilized by adsorption was not determined by the value of specific surface area, but by the pore size of the xerogel. Therefore, enlargement of pore size increases the amount of immobilized urease.[13] It was known, that the diameter of urease macromolecule is approximately 5 nm.[15] It was possible to assume, that for PSX and PMPSX with pore diameters of less than 5 nm, urease can be adsorbed on the surface of the particles. For the samples PMSX and PAPSX with pore diameters of 6.9 and 14 nm, urease can be adsorbed both on surface of the particles, and in their pores.

Obtained samples with immobilized urease have some disadvantages. Such forms can't be reusable because it is difficult to separate hydrogels and powdery xerogels with immobilized urease from reaction solution. To avoid this defect we proposed a procedure of urease immobilization on silica gel by «double immobilization» method using sol-gel approach. Synthesis of biocatalysts in this case includes homogenous distribution of a solution, containing alcoxisilanes, and the enzyme on the surface of inorganic substrate.

Two systems have been used for coating: (a) tetraethoxysilane and methyltriethoxysilane, (b) tetraethoxysilane, methyltriethoxysilane and dimethyldiethoxysilane. Other components of systems were similar.

The analysis of the results presented in Table 2 allows assuming that preservation of activity of immobilized urease depends on the ratio of the volume of alcoxisilanes and the weight of the substrate. The influence of this factor was examined in details using two-component (TEOS/MTES) and tree-component (TEOS/MTES/DMDES) systems. The obtained results are presented in Figure 3.

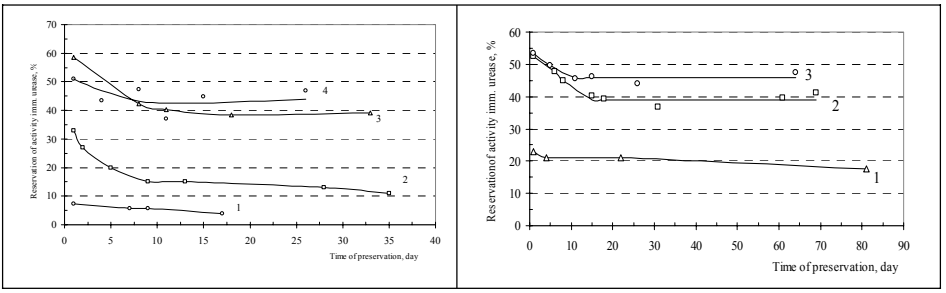

Figure 3. Change of activity of urease immobilized on silica gel in time: for TEOS/MTES/DMDES system (introduced alkoxysilanes, cm^3/g: 1.0 (1); 0.5 (2); 0.25 (3); 0.16 (4)); for TEOS/MTES system (introduced alkoxysilanes, cm^3/g: 0.4 (1); 0.2 (2); 0.13 (3)).

The possibility to reuse systems described above in practice (Figure 4) was demonstrated. The figure shows that double immobilization provides strong grafting of enzyme on a silica gel surface; the urease was not washed off and showed stable values of preserved activity.

A perspective direction in biotechnology is immobilization of enzymes on magnetic substrates. It could be explained by an advantage of using such formulations in practice. In particular, such substrate ensures fast separation of

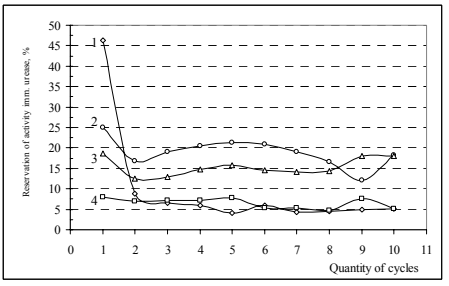

Figure 4. Influence of the number of cycles on the preservation of activity of urease, immobilized on silica gel by non-equilibrium adsorption (1) or sol-gel method (2–4; introduced alkoxysilanes, cm^3/g: 0.4 (2); 0.5 (3); 1.0 (4)).

immobilized enzyme from a reaction solution or its moving to the necessary point using an external magnetic field.

Data on adsorption of urease by magnetite and by modified magnetite are presented on Figure 5. As it can be seen from the figure, the highest level of enzyme binding was demonstrated for the magnetite modified by 3-aminopropil group resulting from ionic bonds formation between negatively charged groups of protein and ammonium cations on the magnetite surface. The highest preservation of activity of immobilized enzyme was observed for unmodified magnetite, which was connected with the accessibility of active centers. This effect can be explained by insignificant forces of enzyme bonding.[16]

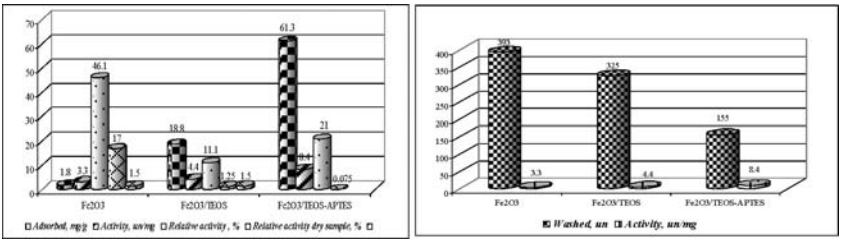

Figure 5. Influence of chemical modification of magnetite on adsorption and properties of immobilized urease.

4. Conclusions

Immobilization of urease by its inclusion in PSX in the process of hydrolytic polycondensation leads to encapsulation of enzyme and accordingly to loose of the enzyme activity. Urease immobilized by adsorption on xerogel keeps its activity at a level of 10%. The highest level of preservation of activity (≈80%) was observed for urease immobilized on hydrogels. The effective method of urease immobilization in a polysiloxane layer on silica gel surface is proposed with the use of sol-gel technology. Therefore enzyme showed stable activity (10–20%) at least after 10 cycles of reactions. For modified magnetite the extent of enzyme binding increases up to 61% compared to unmodified magnetite with only 2% of urease adsorbed. This fact can be explained by formation of additional chemical bonds between enzyme and the modified magnetic substrate.

Acknowledgements

The authors thank the State Fund of Basic Researches (Ministry of Education and Science of Ukraine) for the financial support.

References

1. N.F. Starodub, L.L. Fedorenko, V.M. Starodub, S.P. Dikij, S.V. Svetchnikov, Use of the silicon crystals photoluminescence to control immunocomplex formation, *Sensors & Actuators B*, N35–36, 44–47 (1996).
2. A.P. Soldatkin, V.N. Arkhypova, S.V. Dzyadevych, A.V. El'skaya, J.-M. Gravoueille, N. Jaffrezic-Renault, C. Martelet, Analysis of the potato glycoalkaloids by using of enzyme biosensor based on pH-ISFETs, *Talanta* 66, 28–33 (2005).
3. I. Gill, Bioencapsulated sol-gel polymer nanocomposites, in *Encyclopedia of Nanoscience and Nanotechnology*, Edited by. H.S. Nalwa, 1–24 (Amer. Sci. Publ., New York, 10, 2003).
4. V. Bisht, W. Takashima, K. Kaneto, An amperometric urea biosensor based on covalent immobilization of urease onto an electrochemically prepared copolymer poly (N-3-aminopropyl pyrrole-co-pyrrole) film Rajesh, *Biomaterials* 26, 3683–3690 (2005).
5. C.J. Brinker, G.W. Scherer, *Sol-Gel Science: The Physics and Chemistry of Sol-Gel Processing*. (Academic Press, San Diego, CA, 1990).
6. B.L. Cushing, V.L. Kolesnichenko, C.J. O'Connor, Recent advances in the liquid-phase syntheses of inorganic nanoparticles, *Chem. Rev.* 104, 3893–3946 (2004).
7. N.A. Shabanova, P.D. Sarkisov, Bases of sol-gel technology of nanodispersion silica (Akademkniga, Moscow, 2004) (in Russ.)
8. K. Ramanathan, B.R. Jönsson, B. Danielsson, Sol–gel based thermal biosensor for glucose, *Analytica Chimica Acta* 427, 1–10 (2001).
9. A. Kumara, R. Malhotra, B.D. Malhotra, S.K. Grover, Co-immobilization of cholesterol oxidase and horseradish peroxidase in a sol–gel film, *Anal. Chim. Acta* 414, 43–50 (2000).
10. H.C. Tsai, R.A. Doong, H.C. Chiang, K.T. Chen, Sol–gel derived urease-based optical biosensor for the rapid determination of heavy metals, *Anal. Chim. Acta* 481, 75–84 (2003).
11. Yu.L. Zub, A.A. Chuiko, Salient Features of Synthesis and Structure of Surface of Functionalized Polysiloxane Xerogels, in *Colloidal Silica: Fundamentals and Applications*, Edited by H.E. Bergna and W.O. Roberts., 397–424 (CRC Press, Boca Raton, FL, 2006).
12. A. Dabrowski M. Barczak, N.V. Stolyarchuk, I.V. Melnyk, Yu.L. Zub, Polysilsesquioxane xerogels functionalizated by amine– and thiol–groups: synthesis, structure, adsorption properties, *Adsorption* 11, 497–513 (2005).
13. R.P. Pogorilyi, Yu.L. Zub, V.P. Honcharyk, L.I. Kozhara, A.A. Chuiko, The comparative characteristic of activity urease, incorporation in polysiloxane hydrogels and xerogel, received sol-gel a method, *Ukr. Biochem. J.* 78, 1, 94–100 (2006) (Ukr.).
14. R.P. Pogorilyi, V.P. Honcharyk, L.I. Kozhara, G.R. Yurchenko, A.K. Matkovskiy, Yu.L. Zub, A.A. Chuiko, Immobilization urease on functionalized polysiloxane xerogels and the hydrogels, received sol-gel a method, *Questions of Chem. and Chem. Technol*. 6, 103–107 (2005) (Rus.).
15. R.P. Pogorilyi, E.Yu. Sileckaya, V.P. Honcharyk, L.I. Kozhara, G.R. Yurchenko, A.K. Matkovskiy, Yu.L. Zub, Immobilization urease on a surface silica gel by means of sol-gel of a method, *J. Appl. chem*. 80, 2, 331–335 (2006) (Rus.).
16. Krishna M.R. Kallury, W.E. Lee, M. Thompson, Enhancement of the thermal and storage stability of urease by covalent attachment to phospholipids-bound silica, *Anal. Chem.* 64, 1062–1088 (1992).

EPR STUDIES OF NEW MESOSTRUCTURED SILICA SYNTHESIS AND HEMOGLOBIN ENCAPSULATION

FEDERICA SARTORI[1,2*], PACO LAVEILLE[1], ANNE GALARNEAU[1], GILBERT RENARD[1], MICHELA CANGIOTTI[2], M. FRANCESCA OTTAVIANI[2] AND FRANCESCO DI RENZO[1]

[1]*Institut Charles Gerhardt, UMR 5253 CNRS-UM2-ENSCM-UM1, Matériaux Avancés pour la Catalyse et la Santé,ENSCM, 8 rue Ecole Normale, 34296 Montpellier, France;* [2]*Istituto di Scienze Chimiche, Università degli Studi di Urbino Carlo Bo, Piazza Rinascimento8, 61029 Urbino, Italy*

Abstract. Enzyme encapsulation in ordered porous silica has been modified by introducing a natural surfactant such as lecithin during the sol-gel process. β-lactose has been used as the enzyme protecting agent and tetraethoxysilane as the source of silica in an hydroalcoholic media. In the present study, the EPR spectroscopy of paramagnetic probes has allowed to monitor the formation of mesophases and the condensation of silica in an isotropic three-dimensional structure, named Sponge Mesoporous Silica, with a pore size of 6 nm and a specific surface area of 600 m^2/g. Different techniques of characterization (nitrogen sorption, XRD, TEM, SEM) have been used to study the influence of the different reactants on the structure of the materials. Hemoglobin has been encapsulated in the different materials and its catalytic pseudo peroxydase activity has been evaluated.

Keywords: Phospholipid, mesoporous materials, sponge phase, enzyme encapsulation, SMS.

1. Introduction

Supported enzymatic catalysts are powerful tools for the remediation of oil-polluted sites, especially as far as toxic compounds are concerned. Immobilized hemoproteins have been proposed for reducing the content of the highly toxic

* To whom correspondence should be addressed: Federica Sartori, Institut Charles Gerhardt-MACS, ENSCM, 8 rue Ecole Normale, 34296 Montpellier, France; e-mail: Federica.sartori@enscm.fr

P. Innocenzi, Y. L. Zub and V. G. Kessler (eds.), *Sol-Gel Methods for Materials Processing.*

polycyclic aromatic hydrocarbons (PAH) in a liquid medium, like as water from rainfall on petroleum refineries or leachate from polluted sites.[1]

Enzymes are powerful and environment-friendly oxidation catalysts but their fragility often hinders their application in technological processes.

A simple and economic method to stabilize enzymes against denaturation and to enable their separation from the reaction media can be realized by immobilizing the enzymes in an inorganic support such as silica gel.[2]

Hemoglobin has been encapsulated in different materials and its catalytic activity has been evaluate to determine the best structure for the encapsulation of the protein. Hemoglobin is a globular protein of 6 nm which pseudo-peroxidase activity is well known.[3] This protein is able to oxidize different substrates in presence of H_2O_2. The oxidation of ABTS in aqueous media was used as test reaction and catalysis results were followed by UV spectrophotometry.

Our group has recently developed a new method of enzyme encapsulation, which add a control of porosity to classical sol-gel synthesis by introducing natural surfactants, such as lecithin, during the sol-gel process.[4,5] β-lactose has been used as enzyme protecting agent and tetraethoxysilane as source of silica in an alcoholic/water media.

In the present study, we show, by introducing EPR probes into the system, that initial mixed micelles of dodecylamine and lecithin are formed and contribute to the formation of an isotropic tridimensional structure, named Sponge Mesoporous Silica (SMS), with a pore size of 6 nm and a specific surface area of 600 m^2/g. Different techniques of characterization (nitrogen sorption, XRD, TEM, SEM) have been used to study the influence of the different reactants on the structuration of the materials. The kinetic of synthesis of each materials has been followed by EPR by using radical probes dissolved into micellar systems. First results show that materials are formed following two steps, a rapid one in 100 minutes and a slower one which end after 5 hours. Addition of NaF accelerates the kinetics and change the structure of the materials.

2. Experimental

2.1. SYNTHESIS PROCEDURE

SMS synthesis was performed by using the following reactants: TEOS, Dodecylamine (in some syntheses), Lecithin from egg yolk, β-D-Lactose, NaF (in some syntheses, NaF/Si $1 \cdot 10^{-4}$ or $1 \cdot 10^{-3}$), see Figure 1. For the standard synthesis the molar ratio used was: 1/2 TEOS/0.055 Lecithin/0.05 Dodecylamine/8.5 EtOH/30 H_2O. The first solution of β-lactose, H_2O and NaF was prepared

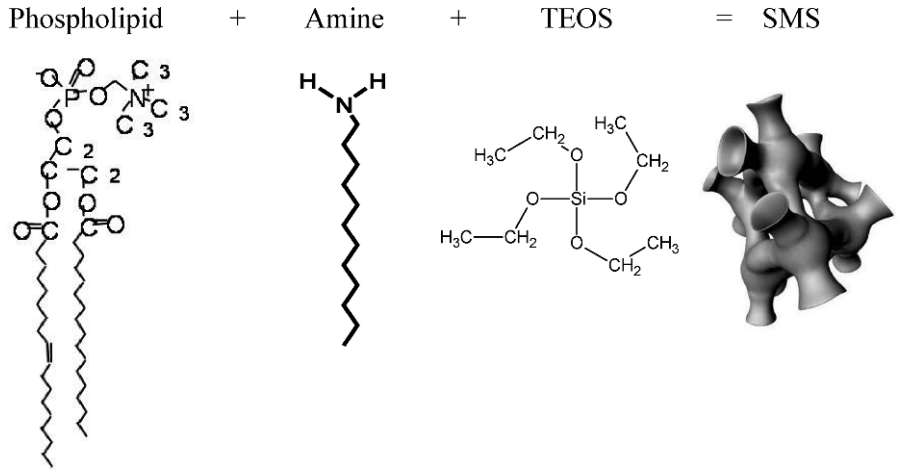

Figure 1. Reagents of SMS synthesis.

and added slowly under stirring to the second solution containing lecithin, dodecylamine and ethanol. Next, TEOS was added, while stirred at 37°C. The system was later left unstirred for 24 hours at the same temperature. In the end the material was dried under vacuum in the presence of P_2O_5.

3. Results and Discussions

3.1. CHARACTERIZATION OF THE MATERIALS

Nitrogen adsorption isotherms for calcined samples are type IV according to the IUPAC classification, indicating the presence of mesopores (Figure 2). The

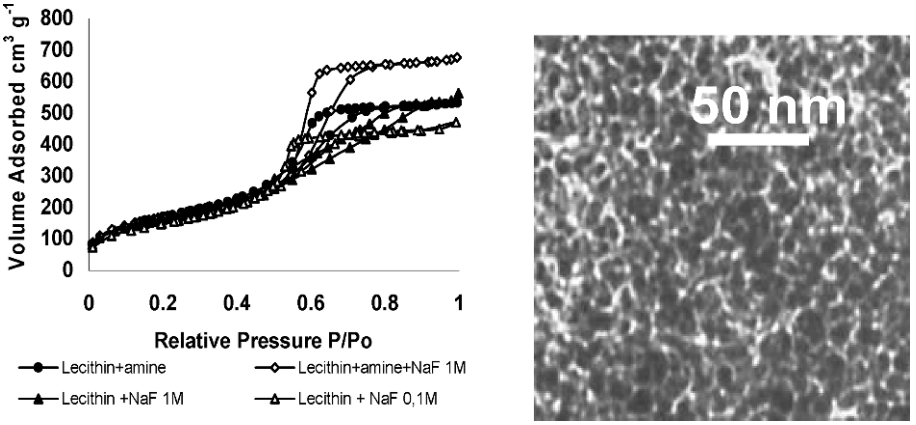

Figure 2. Adsorption isotherms and TEM micrograph of SMS.

size of the pores, calculated by the correlations of Broekhoff and de Boer, is centered around 6 nm. Mesoporous solids are formed both in the presence of amine and when NaF is used to condensate silica around the lecithin aggregates. The pore size distribution is broader for the solids formed in the absence of amine cosurfactant, with the exception of the solid formed at low NaF concentration.

Transmission electron microscopy of cross sections of the materials confirms the presence of 5–6 nm cavities in a sponge-like silica structure (Figure 2).

Powder X-ray diffractions (not shown) present a broad peak centered at 7 nm, indicating a non-ordered system with a periodicity corresponding to the average cage opening plus the thickness of the intermediate silica structures.

3.2. STUDY OF THE SYNTHESIS KINETICS BY EPR OF PROBE MOLECULES

The addition to the synthesis system of a small amount of a surfactant EPR probe (CAT16: 4-cetyldimethylammonium-2,2,6,6-tetramethyl-piperidine-N-oxide bromide) allows to monitor the state of lecithin and its interaction with the inorganic part of the composite material.

The evolution of the ratio between surfactant interacting with silica and free surfactant allows to follow the kinetics of condensation of the material (Figure 3).

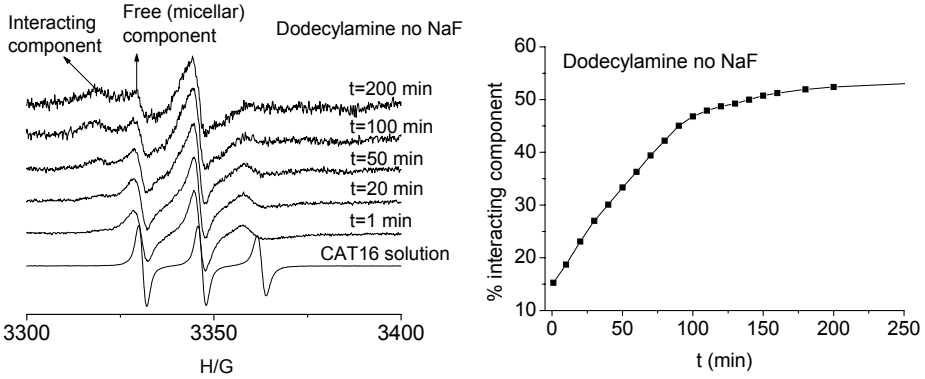

Figure 3. Kinetics of synthesis of a lecithin-dodecylamine templated SMS monitored by the evolution of the CAT16 EPR spectra (first derivative) and the evolution of the fraction of EPR probe interacting with silica.

By adding NaF, the synthesis is modified. The spectrum does not change over time, indicating that condensation of silica has been nearly instantaneous (Figure 4). However, after subtracting the free component, the interacting component is characterized by a much higher mobility than the interacting

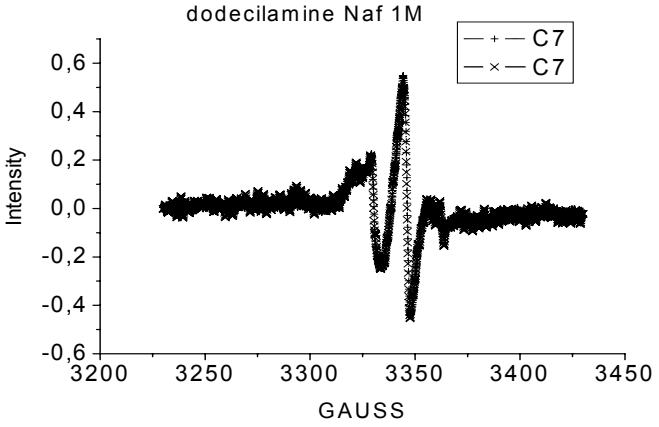

Figure 4. Superposed EPR spectra of CAT16 at 10 and 190 minutes of synthesis in the presence of lecithin, amine and NaF.

component without NaF. This means that NaF improves the polymerization of the solid, but the fast kinetics bring to the formation of a less ordered solid.

3.3. TEST OF CATALYTIC ACTIVITY

The catalytic activity of the biomaterial was measured through the transformation of ABTS (2,2'-azinobis-(3-ethylbenzothiazoline-6-sulfonic acid)) into its radical in the presence of H_2O_2.[6] The reaction was followed by spectrophotometry at 414 nm.

The highest specific activity is obtained for the biomaterial which has the highest quantity of hemoglobin (HB-2, see Table 1). However, the activity is not simply proportional to the amount of hemoglobin. Concentrated NaF decreases the activity. It may have a bad effect on the protein structure. Dodecylamine has a more negative effect on the activity. Indeed, materials 3-Hb and 4-Hb, which have a higher quantity of encapsulated hemoglobin than 1-Hb, show a lower

TABLE 1. Amount of hemoglobin incorporated in the biomaterials and initial rate of oxidation.

Sample	Amine/Si mol/mol	NaF/Si mol/mol	Hemoglobin mg g^{-1}	r° μmol s^{-1} $g(Hb)^{-1}$
1-Hb	No	$1 \cdot 10^{-3}$	65	0.057
2-Hb	No	$1 \cdot 10^{-4}$	150	0.117
3-Hb	Yes	$1 \cdot 10^{-3}$	130	0.018
4-Hb	Yes	0	85	0.032

activity. The simultaneous presence of NaF and dodecylamine has a more negative effect, because the material 3-Hb with a higher quantity of encapsulated hemoglobin has a lower activity than the 4-Hb. This indicates that 3-Hb contains a higher quantity of encapsulated hemoglobin in an inactive conformation than 4-Hb biomaterial.

4. Conclusions

A biological and biocompatible surfactant such as lecithin (phosphatidylcholine) has been used to template mesoporous silica materials with controlled pore size. The pore structure is isotropic and close to a disordered cubic phase. The addition of lactose in the synthesis mixture does not affect the pore structure but helps to maintain the catalytic activity of enzymes immobilized by this new SMS synthesis route. This new kind of material opens large perspectives for biomolecules processing for applications such as biocatalysis for green chemistry or remediation, biosensors or biofuel cells.

References

1. Jamrozik, C., Thomas, D., Pulvin, S., Bedel-Clouture, C., Galarneau, A., Renard, G., Fajula, F., Brunel, D., Langellier, C., Gilson, J.P., Method for degrading polycyclic aromatic hydrocarbons by using an immobilized hemoprotein, WO 2007/006925.
2. Reetz, M.T. , Tielmann, P., Wiesenhofer, W., Konen, W., Zonta, A., Second generation sol-gel encapsulated lipases: robust heterogeneous biocatalysts, Adv. Synth. Catal., 345 (6–7), 717–728 (2003).
3. Mieyal, J.J., Ackerman, R.S., Blumer, J.L., Freeman, L.S., Characterization of enzyme-like activity of human hemoglobin. Properties of hemoglobin-P-450 reductase-coupled aniline hydroxilase system, J. Biol. Chem., 255 (11), 3436–3441 (1976).
4. Galarneau, A., Renard, G., Fajula, F., Synthesizing mesoporous silica with simultaneous immobilization of protein, useful in enzymatic catalysis, French Patent 2, 879, 186 (2006).
5. Galarneau, A., Mureseanu, M., Atger, S., Renard, G., Fajula, F., Immobilization of lipase on silica. Relevance of textural and interfacial properties on activity and selectivity. New J. Chem., 30 (4), 562–571 (2006).
6. McCarthy, M.B., White, R.E., Functional differences between peroxidase compound-I and the cytochrome – P-450 reactive oxygen intermediate. J. Biol. Chem. 258 (15) 9153–9158 (1983).

MOLECULAR PRECURSORS OF MIXED OXIDE MATERIALS FOR SENSOR APPLICATIONS AND MOLECULAR IMAGING

GULAIM A. SEISENBAEVA*, SURESH GOHIL, VADIM G. KESSLER
Department of Chemistry, SLU, Box 7015, SE-75007, Uppsala, Sweden

Abstract. Cation-doped perovskite materials based on barium titanate, such as $(Ba,Sr)(Ti,Nb)O_3$, are of interest as transparent ceramic semiconductors with conductivity strongly dependent both on the cation and the oxygen stoichiometry. Development of precursor systems offering proper control over the cation stoichiometry and permitting to efficiently avoid residual carbon impurities is therefore an important problem. In the present communication we report the synthesis and structural characterization of a series of hetero-metallic precursors of these materials with the general formulae $M^{II}_2Ti_2(L)_4(OR)_8(ROH)_2$ and $M^{II}_2M^{V}_2(L)_2(OR)_{12}(ROH)_2$, where R = Et, ^{n}Pr; M^{II} = Ba, Sr; M^{V} = Nb, Ta; L = thd or R'OAcAc (R' = ^{t}Bu, ^{i}Pr). The compounds have been characterized by single crystal and power X-ray and by ^{1}H and ^{13}C NMR, vibration spectroscopy and mass-spectrometry. These species are very stable in solution and display even considerable gas phase stability. Solution microhydrolysis of the molecules in these series leads most often to oxo-aggregates with the cation stoichiometry rather close to 1:1, which additionally simplifies handling of solutions based on these precursors. The obtained precursors have been used for preparation of powders and films (on Si substrates), which were characterized by SEM-EDS and X-ray powder techniques.

Keywords: Perovskite materials, molecular precursors, barium titanate, strontium, niobium, tantalum, doping, rare earths, optical imaging, X-ray, nanoparticles.

*To whom correspondence should be addressed: Gulaim A. Seisenbaeva; e-mail: gulaim.seisenbaeva@kemi.slu.se

P. Innocenzi, Y. L. Zub and V. G. Kessler (eds.), *Sol-Gel Methods for Materials Processing*.

1. Introduction

The interest to mixed metal oxides in biological and environmental applications is due to their high potential as sensor materials and as contrasting agents in the medical diagnostics. The sensor properties, most commonly the variations in electric or optical characteristics, are originating from surface interactions with the molecules of targeted impurities and are exploited most commonly for such classes of compounds as transparent conductors, such as, for example, indium-tin oxide.[1–3] The objectives of medical imaging is to introduce chemically inert nanoparticles into the metabolic fluids and follow the major fluxes in them, indicating the enhanced biochemical activity associated commonly with the development of cancer tumors.[4,5] The characteristics, exploited in imaging can be the luminescent[6,7] or magnetic[8] properties and also high electron density for contrasting in electron microscopy.[9] It is necessary to mention that in spite of the inertness of the corresponding bulk materials, the related nanoparticles display often non-negligible biological activity and have even been applied in different bioassay studies.[10]

Perovskite materials based on barium titanate are good candidates for the role of sensor materials and nanoparticulate contrasting agents: they are highly chemical inert in bulk, which can be explained through their stable crystal structure ABO_3. The latter permits doping these materials with different cations. Doping can be made in two directions: in A-position they can be doped with Rare Earths to produce luminescent nanopowders and in B position they can be enriched with high-valent heavy metal cations, such as, for example, tantalum or tungsten, to achieve high electron concentration.

Development of the sol-gel approaches to the related perovskite materials, in particular $BaTiO_3$ and $SrZrO_3$, has attracted a lot of attention during the last two decades. Preparation of high purity dense coatings and narrow size distribution nanopowders of these phases requires application of highly solution stable single-source precursors.

2. Design and Synthesis of the Molecular Precursors

The development of approaches to design of the molecules of metal alkoxide complexes needs to exploit the occurrence of predominantly electrostatic bonding in their metal-oxygen cores.[11,12] The structures of bimetallic metal alkoxide molecules can be predicted following the principles of Goldschmidt's concept for design of ionic solids taking into account the complex shape of the alkoxide and other organic ligands. The Molecular Structure Design Concept we described in[13,14] is based on the choice of a proper molecular structure type and completing it with ligands providing the required number of donor atoms and

the necessary protection of the metal-oxygen core. The single-source precursors of perovskite materials have to contain the atoms of a heavy main-group cation together with an early transition metal cation in 1:1 ratio. The by far most common molecular structure type corresponding to this composition requirement is the $M_2M'_2O_{16+n}$ (n = 0, 2) – a fragment of dense hexagonal packing of metal and oxygen atoms following the CdI_2 motive common for the ionic solids. The approach to the complexes of this type has been originally developed for barium and strontium titanates: understanding that the sum of cation charges in this case (2 x 2 + 2 x 4 = 12) was in this case insufficient to provide the necessary number of donor atoms, we proposed to use four equivalents of bulky chelating ligands, for example, 2,2,6,6-tetramethyl-heptanedionate (thd) ones not forming insoluble salts with barium or strontium cations. The ionic nature of bonding in the precursor complexes made the preparation procedure extremely simple and efficient: the alkaline earth metal was dissolved in the parent alcohol and mixed (without any importance in the order of addition) with the stoichiometric amounts of the titanium alkoxide and chelating ligand in one pot. The products, $Ba_2Ti_2(thd)_4(OEt)_8(EtOH)_2$[15] and $Sr_2Ti_2(thd)_4(O^iPr)_8$[16] could be easily purified by re-crystallization. The sub-sequent study of solution stability for the related barium-zirconium and strontium-zirconium complexes, $Ba_2Zr_2(thd)_4(O^nPr)_8$ (^{n}PrOH)$_2$, $Ba_2Zr_2(thd)_4(O^nPr)_2(O^iPr)_6$ and $Sr_2Zr_2(thd)_4(O^iPr)_8$ has been reported in.[17] It has been notices at this point that the solution and especially gas phase stability was directly connected with the sterical requirements for the ligands and was granted by the application of the linear chain alkoxide moieties. While the n-propoxide strontium-zirconium complex, $Sr_2Zr_2(thd)_4(O^nPr)_8(^n$PrOH)$_2$, was perfectly stable in both hydrocarbon and parent alcohol media,[18] the corresponding isopropoxide, $Sr_2Zr_2(thd)_4(O^iPr)_8$, underwent solvolysis in the presence of the parent alcohol transforming into $Zr(O^iPr)(thd)_3$ and $Sr_2Zr(thd)_4(O^iPr)_4$ (^{i}PrOH)[19,20] (see Figure 1).

Following the same concept we proposed to approach the derivatives of alkaline earth and pentavalent metals, Nb and Ta. For the most common M_4O_{16} structure type in this case the sum of metal atom charges was giving 2 × 2 + 2 × 5 = 14, requiring only two additional donor atoms, i.e. application of two chelating ligands. For this role were chosen 2,2,6,6-tetramethylheptanedionate (thd) and isopropylacetoacetate (iPrAcAc) ligands, supporting solubility and improving the solution stability of alkaline earth metal complexes. Five new bimetallic complexes, $Sr_2Nb_2(thd)_2(OEt)_{12}(EtOH)_2$, $Sr_2Ta_2(thd)_2(OEt)_{12}(EtOH)_2$, and Ba_2Ta_2 (^{i}PrAcAc)$_2$(OEt)$_{12}$,[21] and also $Ba_2Nb_2(thd)_2(O^nPr)_{12}$ and $Sr_2Nb_2(thd)_2(O^nPr)_{12}$ have been successfully isolated in efficient one-batch syntheses. The solution stability of these species turned out to be very different.

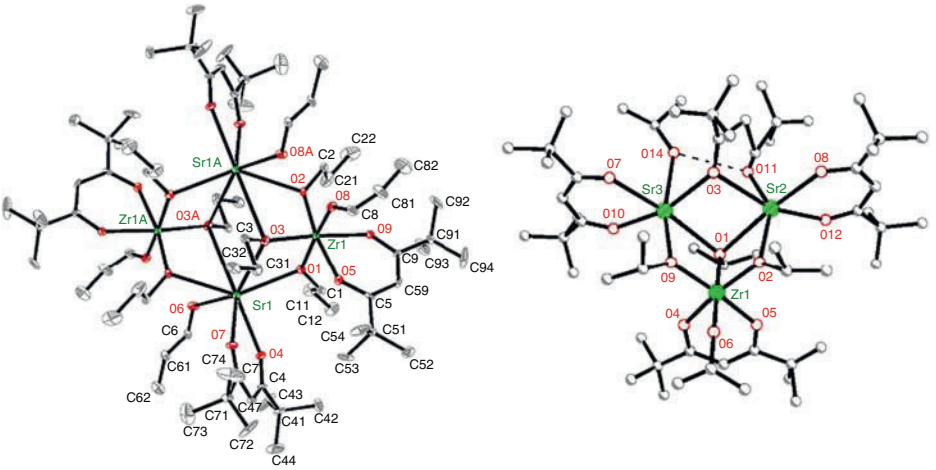

Figure 1. Molecular structures of $Sr_2Zr_2(thd)_4(O^nPr)_8(^nPrOH)_2$ and $Sr_2Zr(thd)_4(O^iPr)_4(^iPrOH)$.

$Sr_2Ta_2(thd)_2(OEt)_{12}(EtOH)_2$ re-crystallized as the initial individual complex even from solutions containing minor amounts of water. At the same time, the molecules displaying more structural tension, $Sr_2Nb_2(thd)_2(OEt)_{12}(EtOH)_2$ and $Sr_2Nb_2(thd)_2(O^nPr)_{12}$, transformed very easily on microhydrolysis into oxo-complexes with the same metal cation stoichiometry but higher content of chelating ligands, $Sr_2Nb_2O(thd)_3(OR)_9(ROH)_3$, R = Et, ^{n}Pr, showing in their turn the improved solution stability (see Figure 2).

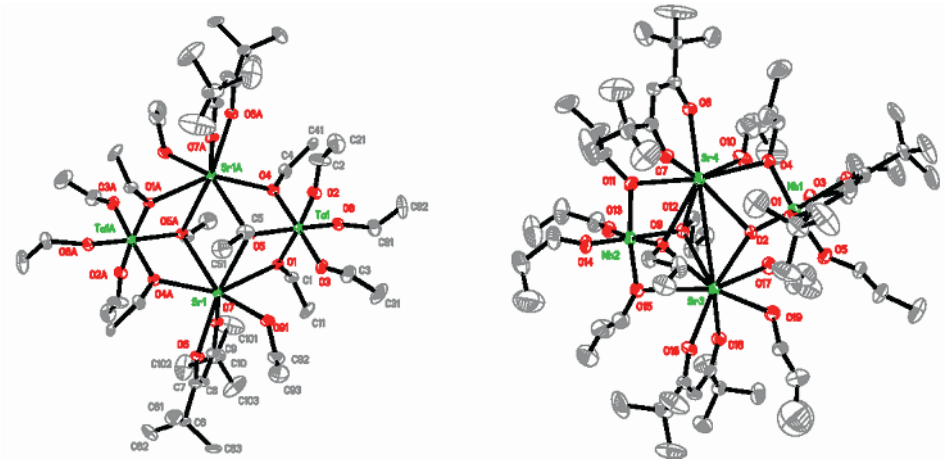

Figure 2. Molecular structures of $Sr_2Ta_2(thd)_2(OEt)_{12}(EtOH)_2$ and $Sr_2Nb_2O(thd)_3(O^nPr)_9(^nPrOH)_3$.

3. Transformations of The Molecular Precursors on Hydrolysis – Hierarchical Self-Assembled Structures

As it has recently been demonstrated, the hydrolysis in homogeneous media of metal alkoxides – highly reactive and kinetically unhindered species – leads to conditions of local thermodynamic equilibrium resulting in formation of self-assembled phase-separated nanoparticles, Micelles Templated by Self-Assembly of Ligands (MTSALs).[20] The size of MTSALs is normally of about 2–4 nm. If not crystalline, which is normally the case unless the hydrolysis is carried out under solvothermal conditions, they conserve a great deal of surface reactivity. The latter leads to their partial coalescence driven by the trend to minimization of the surface energy. The aggregates of partially coalesced particles develop the spherically shaped uniform outer shells, which can coalesce further providing next level aggregates. The resulting structures are not fractal polymer networks as it was earlier supposed in,[22] but hierarchical self-assembled structures. Our first observation of their formation in 2004[23] was recently followed by the analogous results from the groups of Mann,[24] Bao-Lian Su[25] and Guizard[26].

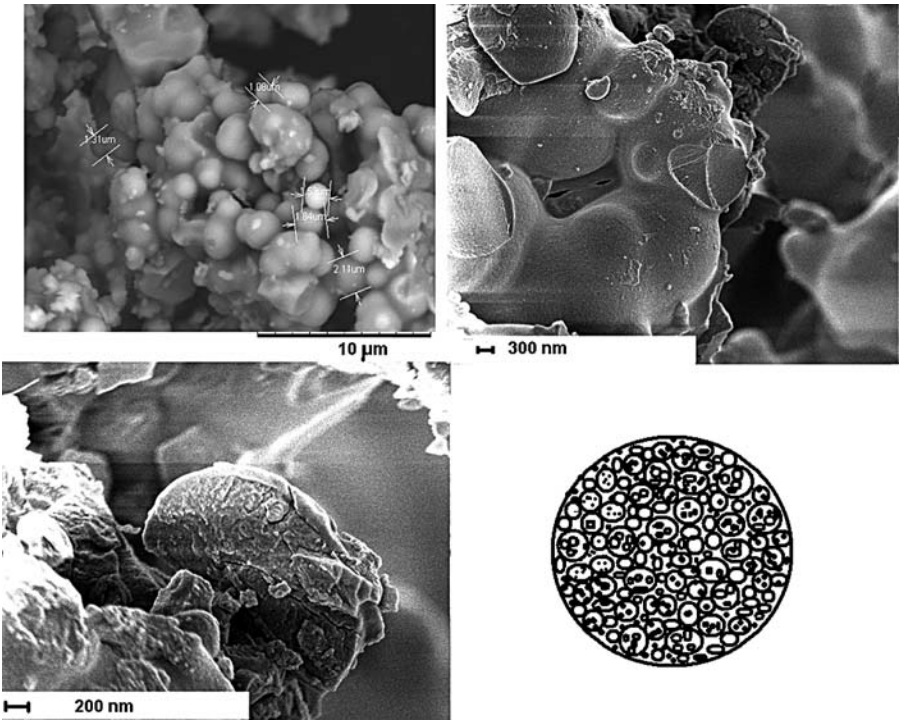

Figure 3. Hierarcical self-assembled structures from the gels derived from $Ba_2Ti_2(thd)_4(O^nPr)_8$ ($^nPrOH)_2$.

In fact the trends in materials formation in sol-gel process, applying single-source heteroleptic alkoxide precursors, were shown to follow the same mechanism. High-resolution SEM indicated clearly the formation of hierarchical self-assembled structures in the gel derived, for example, from $Ba_2Ti_2(thd)_4(O^nPr)_8(^nPrOH)_2$ (see Figure 3).[27]

The occurrence of the self-assembly process indicates possibility to obtain uniform dense coatings of perovskite materials for sensor application using low-polarity solvents, such as n-butanol or toluene and applying moist air as the source of water. Preparation of the uniform nanoparticles will present a challenge as it will require to provide much higher temperature for the formation of MTSALs. The results of this further work will be reported in the near future.

References

1. P. Knauth, H.L. Tuller, *J. Amer. Ceram. Soc*. 85, 1654 (2002).
2. M. Epiofani, R. Diaz, J. Arbiol, P. Siciliano, J.R. Morante, *Chem. Mater*. 18, 840 (2006).
3. J.W. Fergus, *Sensors & Actuators B – Chem*. 123, 1169 (2007).
4. D.B. Buxton, *Expert Rev. Mol. Diagn*. 7, 149 (2007).
5. D. Maysinger, *Org. Biomol. Chem*. 5, 2335 (2007).
6. T. Soukka, K. Kuningas, T. Rantanen, V. Haaslahti, T. Lövgren, *J. Fluoresc*. 15, 513 (2005).
7. Z. Ye, M. Tan, G. Wang, J. Yuan, *J. Fluoresc*. 15, 499 (2005).
8. J.H. Lee, Y.M. Huh, Y.W. Jun, J.W. Seo, J.T. Jang, H.T. Song, S. Kim, E.J. Cho, H.G. Yoon, J.S. Suh, J. Cheon, *Nature Medicine* 13, 95 (2007).
9. C. Destree, J. Ghijsen, J.B. Nagy, *Langmuir* 23, 1965 (2007).
10. A. Jääskeläinen, R.R. Harinen, U. Lamminamäki, T. Korpimäki, L.J. Pelliniemi, T. Soukka, M. Virta, *Small* 3, 1362 (2007).
11. G.A. Seisenbaeva, P. Werndrup, L. Kloo, V.G. Kessler, *Inorg. Chem*. 40, 3815 (2001).
12. G.A .Seisenbaeva, A.I. Baranov, P.A. Shcheglov, V.G. Kessler, *Inorg. Chim. Acta* 357, 468 (2004).
13. V.G. Kessler, *Chem. Comm*. 1213 (2003).
14. V.G. Kessler, *J. Sol-Gel Sci. Tech*. 32, 11 (2004).
15. V.G. Kessler, L.G. Hubert-Pfalzgraf, S. Daniele, A. Gleizes, *Chem. Mater*. 6, 2236 (1994).
16. L.G. Hubert-Pfalzgraf, S. Daniele, J.M. Decams, J. Vaissermann, *J. Sol-Gel Sci. Tech*. 8, 49 (1997).
17. G.A. Seisenbaeva, S. Gohil, V.G. Kessler, *J. Mater. Chem*. 14, 3177 (2004).
18. M. Andrieux, C. Gasqueres, C. Legros, I. Gallet, M. Herbst-Ghysel, M. Condat, V.G. Kessler, G.A. Seisenbaeva, O. Heintz, S. Poissonet, *Appl. Surf. Sci*. 253, 9091 (2007).
19. G.I. Spijksma, H.J.M. Bouwmeester, D.H.A. Blank, A. Fischer, M. Henry, V.G. Kessler, *Inorg. Chem*. 44, 9938 (2006).
20. V.G. Kessler, G.I. Spijksma, G.A. Seisenbaeva, S. Håkansson, D.H.A. Blank, H.J.M. Bouwmeester, *J. Sol-Gel Sci. Tech*. 40, 163 (2006).
21. V.G. Kessler, G.A. Seisenbaeva, S. Gohil, *Surf. Sci. Tech*. 201, 9082 (2007).
22. C. Sanchez, F. Ribot, P. Toledano, *Chem. Mater*. 3, 762 (1991).

23. P. Werndrup, M. Verdenelli, F. Chassagneux, S. Parola, V.G. Kessler, *J. Mater. Chem*. 14, 344 (2004).
24. S.R. Hall, V.M. Swinerd, F.N. Newby, A.M. Collins, S. Mann, *Chem. Mater*. 18, 598 (2006).
25. T.Z. Ren, Z.Y. Yuan, B.L. Su, *Colloid Surfaces A* 241, 67 (2004).
26. A. Hertz, S. Sarrade, C. Guizard, A. Julbe, *J. Eur. Ceram. Soc*. 26, 1195 (2006).
27. R. Pazik, D. Hreniak, W. Strek, V.G. Kessler, G.A. Seisenbaeva, *J. Alloys Comp*. 451, 557 (2008) doi:10.1016/j.jallcom.2007.04.232.

PROPERTIES OF MAGNETIC SILICA GEL FOR ENVIRONMENT MONITORING

ALINA V. SEMCHENKO*, VLADIMIR E. GAISHUN, VITALY V. SIDSKY, NATALYA A. STANKEVICH*, OLGA V. BAGHKO*, STANISLAV S. MECHKOVSKY*
Advanced Materials Research Laboratory, Gomel State University n. a. F. Skorina, 104 Sovetskay St., 246019 Gomel, Belarus

Abstract. Sol-gel method allows production of effective adsorbent systems from fine SiO_2 powder and magnetite. The protolytic exchange capacity of synthesized gels was studied within the pH range of 4–12. The main characteristics of the synthesized silica gel are: surface – 250–350 m^2/g; density – 0.9 g/cm^3; thermal stability – 900°C; sorbent capacity – 0.8–1.2 mmol-eq/g.

Synthesized silica gels have high sorption capacitance in relation to Pb^{2+} and Sr^{2+} ions and provide steep withdrawal of these ions from liquid environments. The isotherms of ion sorption on SiO_2–Fe_3O_4 as sorbent display two steps of sorption. The first step is responsible for the main contribution to capacitance of sorption, the second step provides complete extraction of metal from depletion at the maiden stage of solution.

With increase of the content of magnetite in the SiO_2–Fe_3O_4 sorbent, the sorption capacity of metals and depth of their withdrawal increases, indicating prospects to apply the data on such sorbents in geochemical research.

Keywords: Sol-gel process, silica gel, strontium, lead, selective sorption, sorption capacity, porosity.

1. Introduction

Silica gel is one of the most widespread solid sorbents because of its high thermal, chemical, and mechanical stability compared to other organic and inorganic substrates. Moreover, silica gel is characterized by a high rate of mass exchange,

*To whom correspondence should be addressed: A.V. Semchanko, BGU, Minsk 220050 pr .Nezavisimosty 4; *e-mail: semchenko@gsu.by*

P. Innocenzi, Y. L. Zub and V. G. Kessler (eds.), *Sol-Gel Methods for Materials Processing*.

limited swelling and has high hydrolytic stability in some cases. The structure characteristics of silica gel such as specific shape, pore size, and particle dimensions can be varied within quite wide ranges. This substrate is non-deficient and cheap. The surface of silica gel is covered by silanol groups reacting with metal ions rather weakly. The above advantages of silica gel explain the fact that numerous studies of sorbent modification have been carried out leading to different kinds of silica gel. To obtain a solid phase having certain selectivity, the silica gel surface is modified by various functional groups.

The composite sorbent materials synthesized on the basis of highly dispersive SiO_2 and Fe_3O_4 using colloidal sol-gel method,[1] can be referred to as a category of ions-exchangers with properties, typical for hydrated oxides with formula $M_XO_Z \times nH_2O$.[2–3] The sorption capacity of these materials is determined by chemical state of sorption centers and adsorbed components. According to,[2] for the description of the sorption act it is possible to dedicate some varieties of sorption centers. The molecules of water, located in the direct proximity, play a role of coordinated molecules and are capable to enter a dipole-dipole interaction with polar components of solution, determining thus power condition of sorption for the surface of solid fragments.

The hydroxyl groups of a solid phase can function as a "bridge"[2] towards hydrolyzed ions of metals, essentially influencing thus the protolytic properties of a system. The atoms of oxygen in a bridge position are capable to enter coordination interaction with metal ions, boosting thus the sorption last. The atoms of metals, which are included into a matrix of sorbent, can also interchange with ions of other metals located in liquid.

During formation of fragments of aqueous sorbents the empty space in the structure is filled by cations (including H_3O^+) or anions if possible. The empty space can include atoms possessing uncompensated electric charge or coordination unsaturation. In some cases the origin of a charge can be a change of an oxidation state of an atom included in the structure of the sorbent matrix. Isomorphous substitution of ions of the matrix with ions that differ in charge can also change the charge of the surface.

The metal cations participating in ion exchange or adsorption on a surface of solid fragments dependent on protolytic properties of the fluid phase and the sorbent can be present in one of the forms of the aquaacid: $M(H_2O)_n^{m+}$, $M(H_2O)_{n-1}OH^{(m-1)+}$, … $M(H_2O)_{n-m}OH_m^0$. These forms can pass into a solid phase due to exchange of protons or metal ions located in the empty space of the structure with subsequent compensation of the charge of atoms, which are included in the nearest environment. An exchange of metal ions of the matrix or affixture to oxygenated centers of sorbent (contact adsorption) owing to coordination unsaturation of oxygen atoms is also possible.

There is a possibility of joint occlusion by sorbent of both cations and anions. This can be connected with recharge of the sorbent matrix because of ion-exchange and occluding highly charged cations or anions of the opposite charge. The metabolic sorption of ion pairs of a type $M(OH)_n^{(m-n)+}$, $M(Cl)_n^{(m-n)+}$ or sorption of molecules MX_n (where $X - OH^-$, Cl^-, etc.) due to a coordination unsaturation of atoms of a matrix is also possible. There is also possibility of absorption of cations and anions by hydroxides of metals which are generatrix as a result of spurious processes in liquid or solid phase.

2. Experimental

The method of a frontal chromatography opens broad prospects in research of interphase concentration distribution of ions at high dilution.

The key feature of this method is that at given chemical quantity (n) of an adsorbed component is directly proportional to both the volume of a mobile phase, V, ml, and the concentration of the adsorbed substance according to a simple ratio:

$$m = C \cdot V \tag{1}$$

To sorption capacity (Z, mmol/g) at weight of sorbent m is set by a ratio:

$$Z = \frac{C \cdot V}{m} \tag{2}$$

The large role in this method is plaid by sensitivity and reproducibility of concentration measurements of the adsorbed metal in a mobile phase. For these purposes we used two methods: the chromatrimetricy method[6,7] and the atomic absorption spectrometry. Both methods give reliable outcomes up to minimum concentrations at a level 10^{-7} mol/l.

3. Results and Discussions

In Figure 1 the curves for ions Pb^{2+} and Sr^{2+} obtained using micropillars with 0.3 g of composite sorbents SiO_2-Fe_3O_4 at components ratio 9:1, 5:1 and 7:3 and constant initial concentrations ($3 \cdot 10^{-4}$ mol/l) of metal ions in mobile phase are displayed. The obtained curves have following general characteristics:

– "zero" concentrations of Pb^{2+} and Sr^{2+} in mobile phase, when leaving the pillar. This indicates capacity of sorbents for practically complete extraction of Pb^{2+} and Sr^{2+} ions from aqueous solution in dynamic conditions. Subject to the conditions of experiment (analysed by chromatrimetricy and atomic

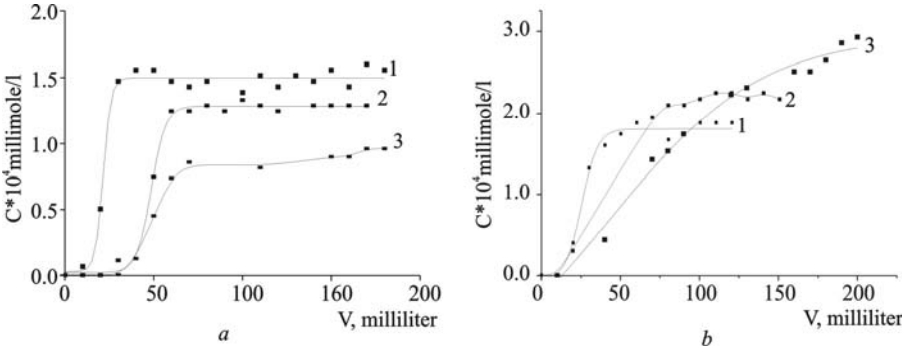

Figure 1. Sorption curve on composite sorbent SiO_2-Fe_3O_4 with SiO_2/Fe_3O_4 molar ratio: *1*. – 9:1; *2*. – 5:1; *3*. – 7:3. (a) For Pb^{2+} ions; (b) for Sr^{2+} ions.

absorption spectrometry) the residual concentration of metals does not exceed 10–7 mol/l. The latter testifies the capacity to provide steep cleaning of liquid environments from ions of heavy metals.

– With increasing of the content of magnetite in sorbent in case of Pb^{2+} ions the tendency to increase in the volume of a mobile phase is observed. For Sr^{2+} ions the opposite trend is observed. It is possible to explain this by essential influence on sorption of process of the formation of hydrooxo-complexes in liquid or on the phase border aqueous solution – solid phase. It is known,[7] that the tendency to formation of hydrooxocomplexes for ions of lead is much higher than for strontium ions.

– As relevant characteristics of the curves can be taken their slope values in the concentration area, close to the "center of gravity" of the curves. From this point of view it is possible to judge about the "force" of acid-base (on the Lewis) interactions between metal ions (acids) and adsorbent centers (bases). The large angle of leans are characteristic for Pb^{2+} ions at any Fe^3O_4 content in the adsorbent. Here the adsorption process can be explained as interaction between a strong acid and strong base. In case of Sr^{2+} ions the slopes of output curves decrease also much less with increase of the $Fe3O_4$ fraction. We can see that in case of lead the formation of hydroxocomplexes provides hard interaction with functional groups of the adsorbent, that, apparently, is contributing to lower hydration (coordination of water molecules) in comparison to free Sr^{2+} cations.

The isotherms of Pb^{2+} and Sr^{2+} sorption are displayed in a Figures 2, 3. It is possible to notice two features of the diagrams:

– Legibly expressed dome shape of initial segments of isotherms, that reflects the decreased influence of interphase distribution of lead and strontium ions

in the process because of their decreasing concentration in the mobile phase. This feature of isotherms determines depth of withdrawal of micro-components (in our case of metal ions) from the fluid phase.

– The bending (Figure 2), indicating sharp increase in sorption of metals after achievement of a distinct level in their concentration in the mobile phase are characteristic for the majority of reduced isotherms.

Such combination of two shapes of sorption isotherms reflects two steps of the process of interphase transfer for metal cations that can be considered as a positive factor. In this case the chromatographic system involves the greater part of sorbate (area of increased sorption capacity) at the maiden stage. At the second stage there is "after-purification" of the mobile phase, i.e. steep withdrawal from an already diluted solution to full development of the features of accumulative system.

It is important to mark that two steps of sorption are more characteristic for Pb^{2+} and less for Sr^{2+} (compare Figures 2 and 3). This is in agreement with the assumptions made about the role of formation of hydrooxocomplexes in the adsorption process.

It is important to notice the influence of the SiO_2 to Fe_3O_4 ratio in sorbent on the shape of Pb^{2+} and Sr^{2+}distribution isotherms. As it follows from the data

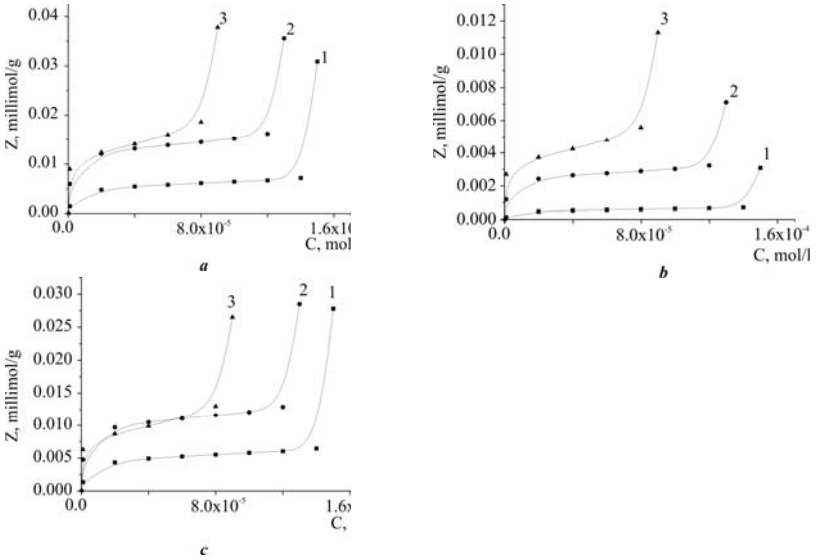

Figure 2. Pb^{2+} ions sorption isotherm on SiO_2-Fe_3O_4 composite sorbent with SiO_2/Fe_3O_4 molar ratio:*1*. – 9:1; *2*. – 5:1; *3*. – 7:3, (a) Z = m (SiO_2 + Fe_3O_4), (b) Z = m (Fe_3O_4), (c) Z = m (SiO_2).

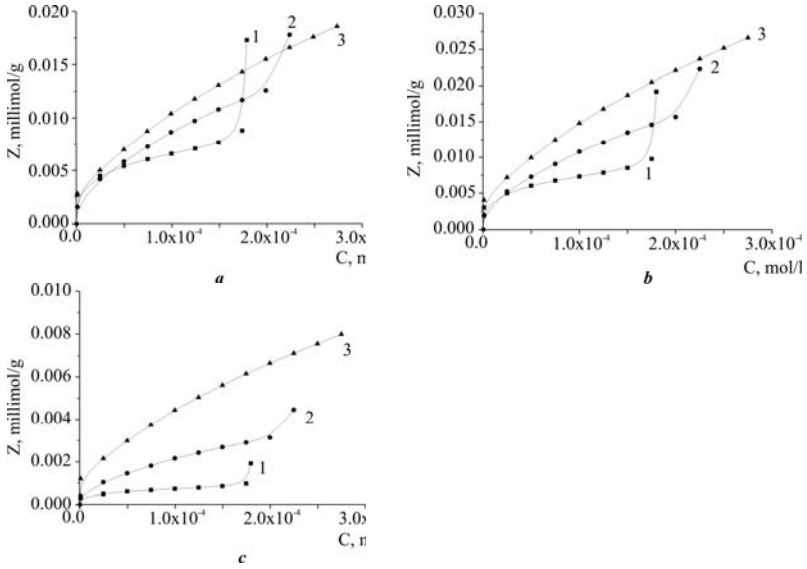

Figure 3. Sr^{2+} ions sorption isotherm on composite SiO_2-Fe_3O_4 sorbent with SiO_2/Fe_3O_4 molar ratio: *1*. – 9:1; *2*. – 5:1; *3*. – 7:3, (a) Z = m (SiO_2 + Fe_3O_4), (b) Z = m (Fe_3O_4), (c) Z = m (SiO_2).

of the Figure 3, gross-sorption (i.e. the sorbent capacity referred to the weight of composite sorbent as a whole) increases in all ranges of the studied concentrations with increased fraction of Fe_3O_4. It allows to give high estimation to the contribution of Fe_3O_4 to sorption. It is confirmed by the data of where the value of sorption is referred to the weight of SiO_2 in the sorbent, and also the data of showing values of adsorption capacity in relation to the weight of Fe_3O_4.

Thus, doping of silica gel by magnetite not only permits magnetic extraction of sorbent from the environment, but also essentially improves the sorption characteristics of the material.

3. Conclusions

Sol-gel method allows creation of effective sorbent systems with a particular mission. It is possible to use these systems for: (1) monitoring of sewages of industrial enterprises and public utilities, cleaning of liquid radioactive waste etc.; (2) monitoring of strongly contaminated sites of soils, bottom sediments, ash etc.

The main characteristics of the synthesized silica gel are: surface – 250–350 m^2/g; density – 0.9 g/cm^3; thermal stability – 900^0C; sorbent capacity – 0.8–1.2 mmol-eq/g.

Synthesized silica gels with magnetic properties have high sorption capacity in relation to Pb^{2+} and Sr^{2+} ions and provide steep withdrawal of these ions from liquid environments.

The isotherms of metal ions sorption on SiO_2-Fe_3O_4 as sorbent have stepwise appearance that reflects two steps in sorption. Thus the maiden stage introduces major contribution to capacity of sorption, the second stage provides complete extraction of metal from depletion at the maiden stage of solution.

With increase of the contents of magnetite in the SiO_2-Fe_3O_4 sorbent, the sorption capacity of metal cations and the depth of their withdrawal increase indicating prospects of application of the data concerning such sorbents in geochemical research.

References

1. E.N. Poddenezhny, A.A. Boiko, Sol - Gel synthesizing of the Optical Silica Glass, Gomel, 130–133 (2002).
2. A.P. Shuchko, V.M. Radovenchic, Optimum condition peelings of magnetite in processes clearing of water, *Chemistry and Technology of Water*, 16, 180–183 (1994).
3. A.V. Sandullyc, V.M. Karhov, A.P. Veshensky, On a ability is magneto sorption of radioactivity removal from radioactive waters, *Energy and Electrophysics*, 41–42 (1989).
4. K.C. Chen, T. Tsuchiya, J.D. Mackenzie, Sol-gel processing of silica, *Journal of Non-Crystalline Solids*, 81, 227–327 (1986).
5. L.L. Hehch, J.K. West, The sol-gel process, *Chemistry Review*, 90, 33–72 (1990).
6. A.B. Yroslavcev, V.V. Nikonenko, N.A. Sancevich, Ionic transportation in membranes and ion exchanges materials, *Chemistry's Results*, 72, 438–446 (2003).
7. S.A. Mechcovsky, O.V. Bochco, N.A. Sancevich, Accumulative indicator systems on the basis of highly dispersive sorption active materials, Sviridov Conf. Article Col. 74, 41–62 (2005).
8. Y. Incedy, Application of Complexes in Analytical Chemistry. M.: Mir., p. 376 (1979).

SOL-GEL SYNTHESIS OF FUNCTIONALIZED NANOCOMPOSITE SORBTIONAL MATERIAL WITH POLYMER-SILICA MATRIX

BAHODIR D. KABULOV[1], DILSHOD H. SHAKAROVA[2*], KAZIM A. AKHUNDJANOV[1], SAYIBJAN S. NEGMATOV[1], OLEG A. SHPIGUN
[1]*Tashkent State Technical University, Scientific-Technical Complex "Science and Progress"*
[2] *Moscow State university, Chemical Faculty, Moscow, Russia*

Abstract. Functionalized nanocomposite sorbtional material was prepared by sol-gel method based on of chitosan and polyethoxysilane oligomer. The resulting product was characterized by microscopy, FTIR-spectrometry, XRD and chromatography. XRD analysis has shown the suppression of crystallinity of chitosan included into silica network.

Keywords: Nanocomposite, chitosan/silica hybrid, sol-gel process, chromatography.

1. Introduction

Perspective direction of nanotechnology is the development of synthetic approaches to nanostructural polymer/silica nanocomposites possessing given porous morphology for application in sorption technologies.[1,2]

The general approach to preparation of such materials is synthesis based on sol-gel process in situ, in which the formation of reaction products occurs by assembly from components under conditions of certain stereochemical orientation of reagents.

The sol-gel technique including the polymers in hydrolysis process of alkoxysilane allowed to obtain the polymer/silica hybrid materials combining the hardness of silica gel and functional properties of polymers.[2–4] The sol-gel process comprises hydrolysis (1) and subsequent condensation reaction of alkoxy-or hydroxysilanes[5]:

[*]To whom correspondence should be addressed: D.SH. Shakarova, Ph.D. student, Tashkent State Techni-Technical University, Scientific-Technical Complex "Science and Progress," e-mail: dilshoda06@yahoo.com

P. Innocenzi, Y. L. Zub and V. G. Kessler (eds.), *Sol-Gel Methods for Materials Processing*.

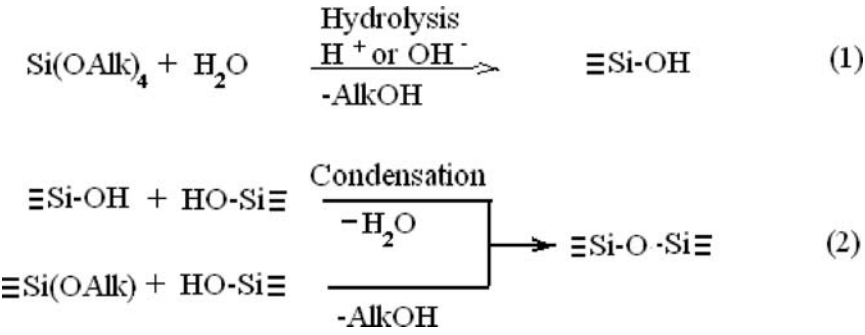

The Si-OH groups are formed by hydrolysis of alkoxy-groups and then, by condensation of hydroxyl-groups with alkoxy-groups, the ≡Si-O-Si≡ linkage(2) would be obtained. With further hydrolysis and condensation a siloxane network develops via cross-linking of the oligomers.

The peculiarity of forming silica gel is presence of residual Silanol groups.

Then functional organic polymers capable to interact with silica are available.

Experiments with polyethylene glycol,[6] polyacrylic acid and polystyrene sulfonic acid,[7] polybuthyl methacrylate,[8] poly-E-caprolactane,[9] polyacrylamide,[10] nylon-6[11] have shown that homogeneity between polymer and silica is achieved owing to formation of hydrogen bonds between silanol groups of silica and functional groups of polymer.

Of special interest are hybrid materials, in which the organic phase consists of polysaccharides (chitosan[12,13] and acetyl cellulose[13,14]). Chitosan possessing regular chain structure and forming true solutions in the dilute aqueous solutions of organic and inorganic acids permits to obtain hybrid materials using sol-gel process.

We have investigated a possibility to obtain microspheric chitosan/silica nanocomposite sorptional material by sol-gel technique. Polyethoxysoloxan oligomer was used as silica precursor.

2. Experimental

Materials: Tetracthoxsilan (TEOS)(Angarsk, Russia), acetic acid, aqueous ammonia and solvents were analytical grade. Polyethoxysiloxan (PES) oligomer was obtained from TEOS by method described in.[15] Chitosan (deacetylation degree ≈79%, average molecular weight ≈80 kDa) was prepared from chitin of silkworm *Bombyx mori* by method described in.[16] Gelling process in reaction mixture of PES oligomers with chitosan dissolved in acetic acid was studied using Reotest-2 rotary viscometer (VEB MLW, Germany). IR Spectra were registered in Specord 75-IR (Bruker, Ettlingen, Germany). The chromatographic

experiments were performed on a Shimadzu LC-10 Avp. Series equipped with a UV-Vis detector (Shimadzu, Kyoto, Japan). The chitosan/ silica sorbent (5 mm) was packed into stainless steel column (150 mm*4.6 mm i.d.). The volume of injected sample was 3 ml. The mixture of hexane and 2-propanol (49 + 1) as a mobile phase and o-, m-, p- nitroanilines were used as test compounds.

The mixture of 100 ml of 1% chitosan solution in 2% acetic acid and 10 ml of PES oligomer were stirred at 1,800 rpm at room temperature for 0.5 h, then the mixture was poured out into a flask, containing 200 ml of 3% ammonia solution, After 24 h the resulting precipitate was filtered, washed by water (up to neutrality), ethanol and hexane and dried first in air, and then on heating (at 80°C).

3. Results and Discussion

The formation of specific network structures forming on hydrolytic polycondensation of PES oligomer in combination with multifunctional molecules of polymer depends on its nature and ratio of elementary reaction speeds between various functional groups, determining the critical life time of the colloid system, answering for loss of fluidity and causing the structuration of sol (gelation). One of such polymers is chitosan, containing reactive hydroxyl, amine and acetamide groups.

We have studied the sol-gel process of hydrolytical polycondensation of PES oligomer in the presence of chitosan with ammonia as catalyst. The optimal conditions to precipitate the chitosan/silica nanocomposite sorbent, with 5% chitosan content in hybrid, such as reaction temperature (65–70°C) and concentration of the catalyst and process duration (0.5 h) were determined experimentally.

The resulting chitosan/silica hybrid was obtained as a porous powder consisting of microspherical particles. The micrograph of this product is shown in Figure 1. The analyses have shown that resulting samples of chitosan/silica sorbent revealed properties different from those of both the silica.(prepared from PES oligomers) and the chitosan. Thermogravimetric analyses were performed from room temperature to 600°C to test thermal stability of the samples. Exothermic effect in the temperature interval from 260°C to 360°C indicated as DTA peak characterized the chemical conversions connected with the weight loss up to 35–40% (Figure 2).

The X-ray diffraction analysis has shown that inclusion of chitosan into silica network leads to decreased crystallinity. Chitosan/silica hybrid is amorphous with no diffraction at $2\theta = 1623°$ (Figure 3(3)) in analogy with silica

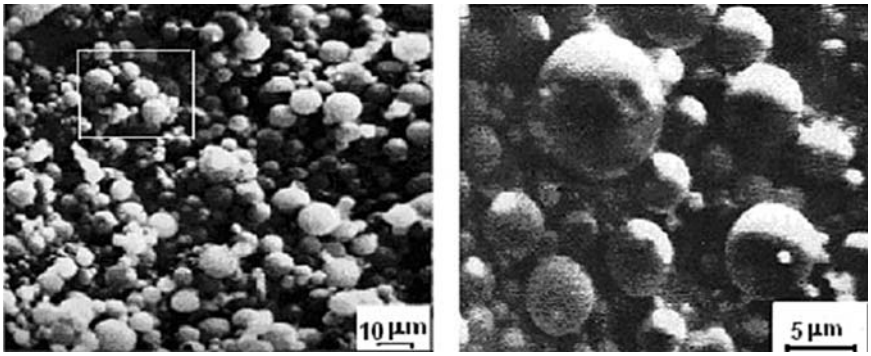

Figure 1. Micrographs of chitosan/silica hydride sorbents.

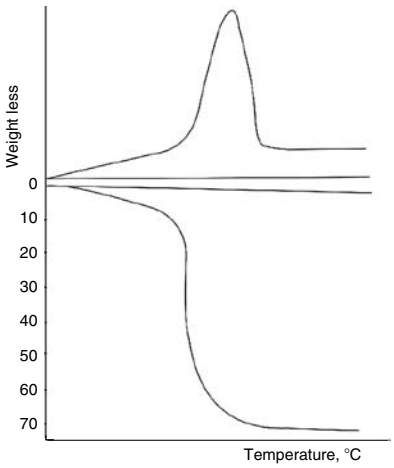

Figure 2. TGA curves for the chitosan/silica hybrid.

(Figure 3(1)), as compared to chitosan displaying an intensive reflex at 2θ = 22–23°C (Figure 3(2)). This difference suggests that strong hydrogen bonds are formed between silanol groups of silica network and functional groups of chitosan.

For the hybrid sample the broad absorption band at 3,440 cm^{-1} is assigned to hydrogen bonded ≡Si-OH groups, the increased frequency resulting from interaction between ≡Si-OH groups and the functional groups of chitosan. For the chitosan sample absorption bonds at 1,600 and 1,510 cm^{-1} are observed and assigned to stretching of amide groups, while for chitosan/silica hybrid the shift of these bands in the lower wave numbers (1,600 and 1,495 cm^{-1}) is observed, indicating the presence of hydrogen bonds between ≡Si-OH groups and C⊖ of amide groups of chitosan (see Figure 4).

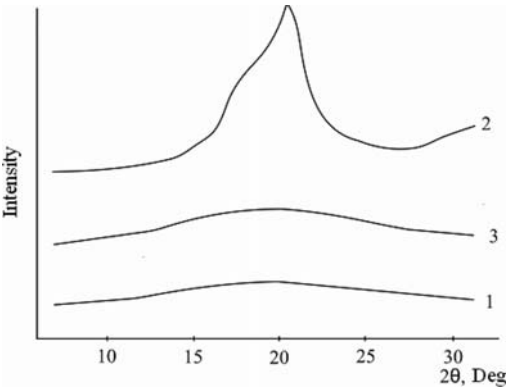

Figure 3. XRD patterns of silica gel (1), chitosan (2), and chitosan/silica hydride (3).

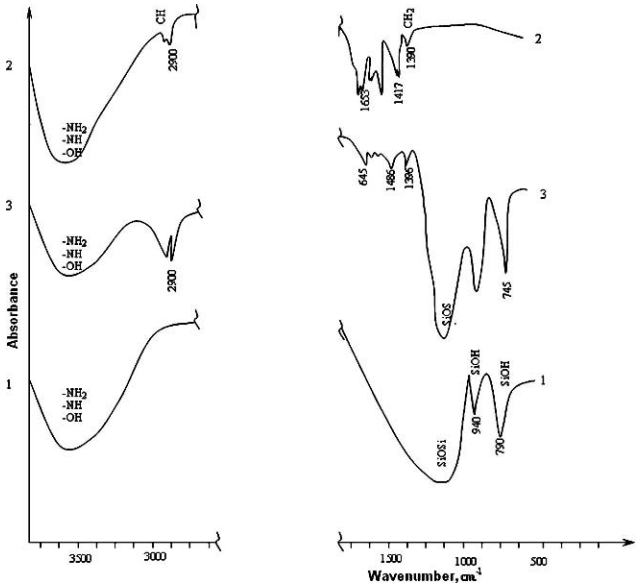

Figure 4. The IR-spectra of chitosan, silica and chitosan/silica hybrid.

Therefore, due to these interactions the decrease in adsorption ability for hybrid sorbent in comparison with silica can be expect, which is confirmed by HPTLS on testing a mixture of isomeric nitroanilines (Figure 5).

The results have shown well-defined separation of chromatographic peaks without tails in contrast to silica gel.

The possibility of application of chitosan/silica hybrid sorbent was also shown for separation by HTPLC of various organic compounds, such as carbohydrates, phenols, dyes and alkaloids.

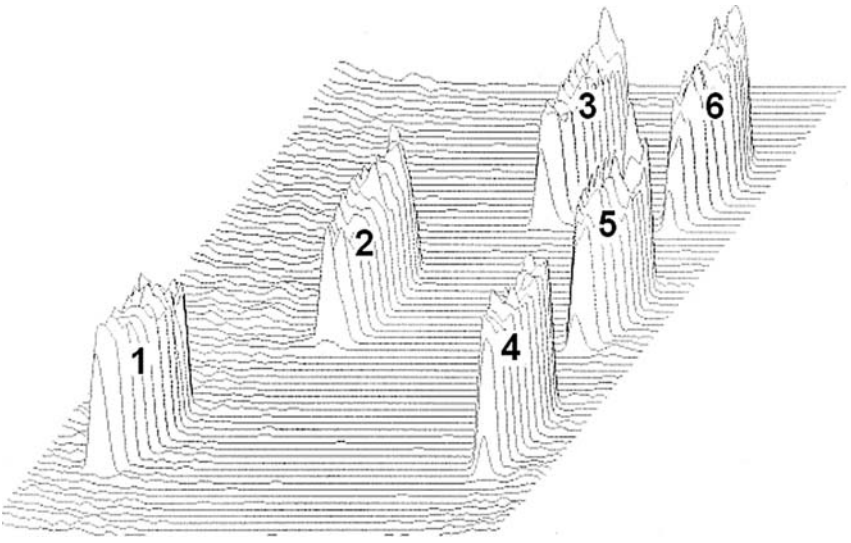

Figure 5. Resolution of test compounds on chitosan/silica hybride (1 – o-nitroaniline, 2 – m-nitroaniline, 3 – p-nitroaniline) and silica gel sorbent (4 – o-nitroaniline, 5 – m-nitroaniline, 6 – p-nitroaniline).

4. Conclusions

Chitosan/silica nanocomposite sorbent was prepared by sol-gel method. Effective separation of functional derivates of organic compounds results from formation of material via sol-gel reaction in situ from PES oligomer and chitosan resulting in new properties, different from silica, caused by interphase interacttions between chitosan molecules and silanol groups of silica network.

References

1. J.E. Mark, The sol-gel route to inorganic-organic composites, *Heterogeneous Chem. Rev.* 3, 307–326 (1996).
2. H. Sehmidt, G. Jonschker, S. Goedicke and M. Mennig, The sol-gel process as a basic Technology for nanoparticle-dispersed inorganic-organic composites, *J. Sol-Gel Sci. Tech.* 19, 39–51 (2000).

3. D. Avnir, L.C. Klein, D. Levy, U. Schubert and A.B. Wojcik, Organo-silica sol-gel materials, in: *The Chemistry of organic Silicon Compounds*, 2 (Wiley, New York), pp. 2317–2361 (1998).
4. C. Sanchez, B. Lebeau and F. Ribot In, Molecular design of sol-gel derived hybrid organic-inorganic nanocomposites, *J. Sol-Sel Sci. Tech*. 19, 31–38 (2000).
5. T. Saegusa, Organic-inorganic polymers hybrids, *Pure Appl. Chem*. 67, 12, 1965–1970 (1995).
6. P. Lesot, S. Chapuis, J.P. Bayle. J. Rault, E. Lafontaine, A. Campero and P. Judeinstein, Structural-dynamical relationship silica PEG hybrid gels, *J. Mater. Chem*. 8, 1, 147–151, (1998).
7. T. Ogoshi and Y. Chejo, Synthesis of anionic polymer-silica hybrids by controlling pH in an aqueous solution, *J. Mater. Chem*. 15, 315–322 (2005).
8. X. Tong, T. Tang, Q. Zhang, Z. Feng and B. Huang, Polymer/silica nanoscale hybrid through sol-gel method involving emulsion polymers, *J. Appl. Polym. Sci*. 83, 446–454 (2002).
9. D. Tian, S. Blacher and R, Jerome, Biodegradable and biocompatible inorganic-organic hybrid materials, *Polymer*, 40, 951–957, (1999).
10. J. Tang, H. Park, Formation and structure of polyacrylamide-silica nanocomposites by sol-gel process, *J. Appl. Polym. Sci*., 83, 1817–1823 (2002).
11. W.E. van Zyl, M. Garcia, B.A.G. Schrauwen, B.J. Kooi, J.Th.M. De Hosson and H. Veryweij, Hybrid polymide/silica nanocomposites: synthesis and mechanical testing, *Macromol. Mater. Eng*., 287, 2, 106–110, (2002).
12. W.M. Risen, J.S. Ti and X. Hu, Aerogel materials and detectors, liquid and gas absorbing objects and optical devices comprising same, *US Pat.* 6303046 (2001).
13. H. Kishi, C. Mihara, T. Takeda, Y. Kikuchi and T. Kobayashi, Method of manufacturing a suger inorganic hybrid composite, *US Pat.* 6830613 (2004).
14. R.A. Zoppi and M.C. Gonçalves, Hybrid of cellulose acetate and sol-gel silica: morphology, thermomechanical properties, water permeability and biodegradation evaluation, *J. Appl. Polym. Sci*., 84, 2196–2205 (2002).
15. K.K. Unger and B. Scharp, Controlled porosity silica supports from hydrolytic polycan-densation reaction of poly (ethoxy-siloxane), *J. Coll. Interface Sci*., 55, 377–380 (1976).
16. L.A. Nudga, E.A. Plisco and C.N. Danilov, *Russ. J. Gen. Chem.* (J. Obchsh Khim.) XLI(11), 2555–1558 (1971).

PHOTOCATALYTIC DEGRADATION OF CHLOROFORM USING A NEW TYPE OF PHOTO-REACTOR

MORTEN E. SIMONSEN*, ERIK G. SOEGAARD
Institute of Technology, Aalborg University, Esbjerg, Niels Bohrs Vej 8, 6700 Esbjerg, Denmark

Abstract. In the present study a new type of continuous photo-reactor is developed in which the TiO_2 catalyst is immobilized on the surface of quartz tubes surrounding the UV lamps. The paper presents the results of an initial investigation of the performance of a laboratory scale photo-reactor using chloroform as a model compound. The study showed that an initial chloroform concentration of 7 mg/l was degraded to under the detection limit in a period of 350 h. The half time $t_{½}$ for the photo-reactor was found to be 8 h.

Keywords: Photo-reactor, immobilized TiO_2, $CHCl_3$, photo-catalysis, trihalomethane.

1. Introduction

Swimming pools are disinfected in order to secure swimmers from getting infections caused by microbial pathogens. Chlorine is the most common disinfectant used in water disinfection practice due to its high efficiency and low cost.[1] However, the use of chlorine has been reported to produce various halogenated organic compounds.[1] These compounds are formed by reaction between chlorine and organic material (perspiration, urine, mucus, skin particles, hair, lotion, etc.). The two key disinfection by-products in swimming pools originating from chlorination are trihalomethanes (THM) and chloramines, whose health impacts have been subject to much study over the last years.[2,3] The presence of these disinfection by-products in even small amounts are a potential health issue. Chloroform, which is the primary component of THM, has been identified as possible carcinogenic.[4] The maximum allowed THM concentration in swimming pool water is 0.1 mg/l.[5]

* To whom correspondence should be addressed: Morten E. Simonsen; e-mail: mes@aaue.dk

P. Innocenzi, Y. L. Zub and V. G. Kessler (eds.), *Sol-Gel Methods for Materials Processing*.

In the present work the removal of THM using heterogeneous photo-catalysis will be investigated. Heterogeneous photo-catalysis is an advanced oxidation process that couples low-energy UV light with TiO_2 acting as a photo-catalysts. In this process completely destruction of organic pollutants is achieved.[6]

In order to incorporate photo-catalysis into the water treatment unit of swimming pool water a flow reactor has to be developed. Generally two types of photocatalytic reactors exist, slurry reactors applying TiO_2 in suspension or photo-reactors where the TiO_2 is immobilized.

There have been made numerous attempts to study the photocatalytic degradation of chloroform and other chlorinated compounds using a TiO_2 suspension.[7–9] The reaction stoichiometry proposed for the photocatalytic degradation of chloroform is shown in (1).

$$2CHCl_3 + 2H_2O + O_2 \xrightarrow{hv, TiO_2} 2CO_2 + 6HCl \quad (1)$$

The use of TiO_2 in suspension is efficient due to large surface area of the catalyst available for reaction. However, the use of suspensions requires an additional separation step, where the TiO_2 particles are removed after reaction. This is both time consuming and expensive.[10]

In order to avoid the separation step attention has been directed towards photo-reactors in which the TiO_2 catalyst is immobilized. There have been made several attempts to immobilize TiO_2 on different substrates in order to maximize the surface area of the catalyst.[6,11] However many of the proposed photo-reactor in literature suffer from non-uniform UV irradiation where only some of the TiO_2 is activated.[10]

In the present study a new type of continuous photo-reactor in which the TiO_2 catalyst is immobilized on the surface of quartz tubes surrounding the UV lamps has been developed. Immobilizing of the TiO_2 directly on the quartz tubes surrounding the UV lamps will remove the shielding effect in the reactor. The design also eliminates the loss of UV intensity due to absorption of UV light by the different chemical species in the water. The paper presents the results of an initial investigation of the performance of a laboratory scale photo-reactor using chloroform as a model compound.

2. Materials and Methods

The immobilized TiO_2 film was prepared from a modified sol-gel method initially described by Barbe et al. and Mills et al.[12,13] The sol-gel method produces a TiO_2 paste which can be coated onto different substrates. The TiO_2 paste was prepared by adding 5 ml titanium (IV) tetraisopropoxide to 1.1 ml glacial acetic acid which was mixing 30 ml 0.1 M nitric acid solution. The

solution was placed in a microwave system for 4 h at 220°C and a pressure of 60 bar. The particles were redispersed using ultra sound. The solution was rotary evaporated until the TiO_2 content was 10 wt%.

The TiO_2 coated quartz tube was prepared by spinning the quartz tubes in a TiO_2 paste which produced a homogeneous non scattering TiO_2 film. The coated quartz tubes were calcinated at 450°C for 1 h in order to achieve good mechanical stability.

The developed photoreactor was designed to allow insertion of four 16 W UV low pressure mercury lamps (254 nm) immersed in TiO_2 coated quartz tubes. The intensity of the emitted UV light was measured using a UV meter to 40 W/m^2 at the surface of the quarts tubes before coating. The quartz tubes were coated with a layer of TiO_2 with a thickness of approximately 1 μm.

The flow system used in the experiments is shown in Figure 1. The polluted water was pumped from a 66 l storage tank equipped with stirring into the photocatalytic reactor. The reactor volume was 9 l which makes the recycled volume 75 l. The flow system was equipped with sampling ports at the inlet and outlet of the reactor allowing measurement of the degradation of chloroform over the photo-reactor. The recycling flow rate in the experiments was 11 l/h. The experiment was conducted using oxygen saturated distilled water with a chloroform concentration of 7 mg/l. The degradation of chloroform was followed using a gas chromatograph.

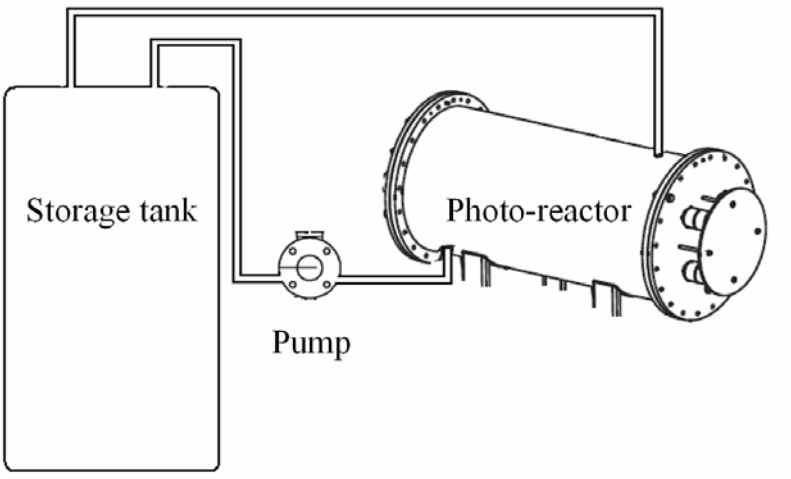

Figure 1. Flow system used in the experiments.

3. Result and Discussion

The photocatalytic degradation of chloroform in the developed photo-reactor is shown in Figure 2. It is seen from the degradation profile that the concentration

of chloroform is below the detection limit of the GC-ECD method after 350 h. Blank experiments showed that only negligible amount of chloroform were lost during experiments. Further analysis has shown that no hazardous by-products were formed during the photocatalytic degradation of chloroform.

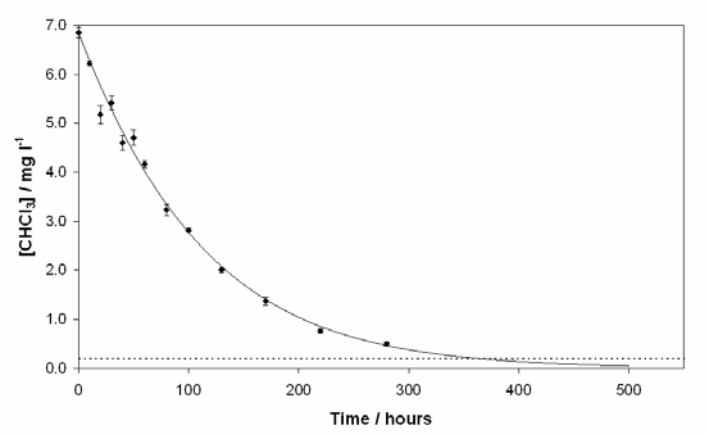

Figure 2. Degradation of chloroform as a function of time in the photo-reactor. The curve is a fit to the experimental data using Langmuir-Hinshelwood kinetics. The dotted line indicates the detection limit of the GC-ECD method.

Investigations of several photocatalytic reactions in batch reactors using a TiO_2 suspension have shown the existence of a linear relation between the rate of reaction and the level of substance adsorbed on the surface of the catalyst. In these cases the Langmuir adsorption isotherm has been proposed.[6,11]

In this investigation the system is assumed to perform as a batch or semi batch reactor since the polluted water is recycled. The Langmuir isotherm has been reported to be valid in flow systems, however the rate constant has been found to depend on the flow rate, indicating a mass transfer dependence not found in batch reactors.[6]

The Langmuir-Hinshelwood kinetic model proposed in this work for the degradation of chloroform is shown in (2).

$$\frac{dC_{CHCl_3}}{dt} = -r = -\frac{k_r K[CHCl_3]}{1 + K[CHCl_3]} \tag{2}$$

where k_r is the rate constant and K is the adsorption constant. The L-H model is fitted to the experimental data using a non linear least square method. The result of the approximation of the L-H model to the data is shown in Figure 2. The results show that there is a very good correlation between the fitted curve and

the experimental data. This result suggests that it is possible to apply the L-H model to describe the photocatalytic degradation of chloroform in the applied photoreactor. The rate constant and adsorption constant in the L-H model is estimated to 0.3262 mg l^{-1} min^{-1} and 0.0317 l mg^{-1} respectively. It is difficult to compare the fitted rate and adsorption constant to constants obtained by applying different photoreactors as the constants depends not only on the applied UV intensity but also on the reactor geometry.

From the stoichiometry of the photocatalytic degradation of chloroform in (1) it is clear that the concentration of Cl^- and H^+ in the system increase by a factor of 3 compared to the rate at which chloroform is degraded. The degradation profile in Figure 3 shows that there is a good correlation between the decrease in the chloroform concentration and the increase in the Cl^- and H^+ concentrations indicating that no major long lived intermediates are formed during the degradation.

The efficiency of the photo-reactor was analyzed from the ratio between the chloroform concentration at the inlet and outlet of the photo-reactor. The efficiency of the photo-reactor was found to be 15–20 % independent of the concentration of chloroform in the investigated concentration interval. The half time $t_{½}$ for the photocatalytic degradation of chloroform in the system can be calculated to 68.3 h. However, as the reactor volume is 9 l and the recycled volume is 75 l only about 1/8 of the polluted water is in the photo-rector at any given time. Therefore, the $t_{½}$ for the photo-reactor can be assumed to be about 8 h.

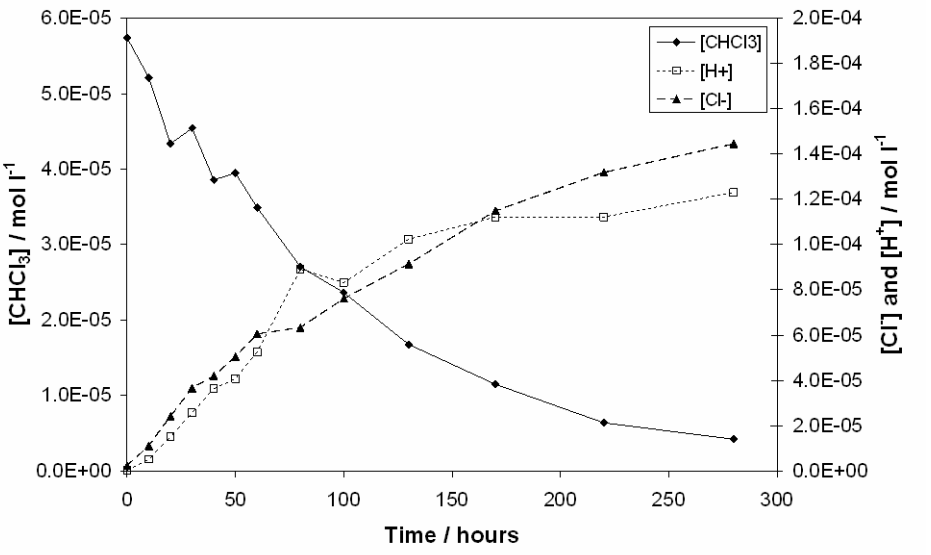

Figure 3. Relationship between the [$CHCl^3$], [Cl^-] and [H^+].

4. Conclusion

The conducted investigations showed that chloroform was degraded using the developed photo-reactor. The study showed that an initial chloroform concentration of 7 mg/l was degraded to under the detection limit of the GC method in a period of 350 h. Furthermore the half time $t_{½}$ for the photo-reactor was found to be 8 h.

Based on the conducted investigations photo-catalysis appears to be an interesting alternative which in time could be implemented in the water treatment of swimming pool water.

References

1. Judd, S. J., and Black, S. H., Disinfection by-product formation in swimming pool waters: A simple mass balance, *Water Res.* 34, 1611–1619 (2000).
2. Aggazzotti, G. et al., Blood and breath analyses as biological indicators of exposure to trihalomethanes in indoor swimming pools, *Sci. Total Environ.* 217, 155–163 (1998).
3. Judd, S. J., and Bullock, G., The fate of chlorine and organic materials in swimming pools, *Chemosphere* 51, 869–879 (2003).
4. Bekendtgørelse nr. 439, *Listen over farlige stoffer*. Miljøministeriet, Denmark (2002).
5. Kristensen, K. K., *Miljøprojekt nr. 80, Svømmebade og sygdomsrisici*. Miljøstyrelsen, Denmark (1986).
6. Mills, A., and Hunte, S. L., An overview of semiconductor photocatalysis, *J. Photochem. Photobiol. A: Chem.* 108, 1–35 (1997).
7. Choi, W., and Hoffmann, M. R., Novel photocatalytic mechanisms for $CHCl_3$, $CHBr_3$, and $CCl_3CO_2^-$ degradation and the fate of photogenerated trihalomethyl radicals on TiO_2, *Environ. Sci. Technol.* 31, 89–95 (1997).
8. Cassano, A. E. et al., Photocatalytic reactors. 3. Kinetics of the decomposition of chloroform including absorbed radiation effects, *Environ. Sci. Technol.* 30, 2355–2236 (1996).
9. Ollis, D. F., and Pruden, A. L., Degradation of chloroform by photoassisted heterogeneous catalysis in dilute aqueous suspensions of titanium dioxide, *Environ. Sci. Technol.* 17, 628–631 (1983).
10. Mukherjee, P. S., and Ray, A. K., Major challenges in the design of a large-scale photocatalytic reactor for water treatment, *Chem. Eng. Technol.* 22, 253–260 (1999).
11. Carp, O. et al., Photoinduced reactivity of titanium dioxide, *Prog. Solid State Chem.* 32, 33–177 (2004).
12. Barbé, C. J. et al., Nanocrystalline titanium oxide electrodes for photovoltaic applications, *J. Am. Ceram. Soc.* 80, 3157–3171 (1997).
13. Mills, A. et al., Preparation and characterisation of novel thick sol-gel titania film photocatalysts, *Photochem. Photobiol. Sci.* 2, 591–596 (2003).

MESOPOROUS TiO_2 AND TiO_2/ZnO/Ag FILMS: SOL-GEL SYNTHESIS, PHOTOELECTROCHEMICAL AND PHOTOCATALYTIC PROPERTIES

EUGENE MANUJLOV[1], YURIY GNATYUK[1], VERA VOROBETS[2], GENNADIY KOLBASOV[2], NATALIA SMIRNOVA[1*], ANNA EREMENKO[1], ASTA GUOBIENÉ[3], SIGITAS TAMULEVIČIUS[3]

[1]*Institute of Surface Chemistry, National Academy of Sciences, Ukraine 03164 Kyiv, General Naumov Str., 17.*

[2] *Institute of General & Inorganic Chemistry, Ukrainian National Academy of Sciences, 32/34 Palladin Str., Kyiv, 03680, Ukraine*

[3]*Institute of Physical Electronics of Kaunas University of Technology, Savanorių pr. 271. LT-50131, Kaunas, Lituania*

Abstract. TiO_2 and TiO_2/ZnO films with silver nanoparticles (Ag NPš) distributed in the matrix and on the surface were characterized by TEM, AFM and UV-Vis spectroscopy. Direct photoelectrochemical investigations of the TiO_2/Ag and TiO_2/ZnO/Ag heterojunctions showed the cathodic shift of the flat-band potential position and the increase of photocurrent quantum yield in comparison with unmodified TiO_2 electrodes. Photocatalytic activity of Ag/TiO_2 and Ag/TiO_2/ZnO films estimated in the process of Rhodamine B dye degradation is coincides with photoelectrochemical data.

Keywords: Mesoporous titania films, silver nanoparticles photodeposition, flat band potential, photocatalysis.

1. Introduction

In the past years the problems related to the elimination of toxic and hazardous chemical substances from air and wastewaters with the focus on titanium dioxide photocatalyst application have emerged as a high international priority.[1–3] Many of these processes require the semiconductor films with developed porous structure and high surface area.[3–5] The preparation of nanocomposites of oxide

* To whom correspondence should be addressed Dr. Natalia Smirnova; e-mail: smirnat@i.com.ua

P. Innocenzi, Y. L. Zub and V. G. Kessler (eds.), *Sol-Gel Methods for Materials Processing*.

films containing nanosized semiconductor or metal particles leads to the system with peculiar optical (third order nonlinear optical effects, selective optical absorption and reflection), electrical and photocatalytic properties. The addition of noble metals to the semiconductor enhanced the charge separation and improved their photocatalytic activity in important environmental redox processes.[6–9] This work is devoted to thermo- and photochemical deposition of Ag NPs onto mesoporous Ti O_2 and TiO_2/ZnO (1% ZnO) films, prepared via templated sol-gel route, and investigation of Ag doping effect on the photoelectrochemical properties and photocatalytic efficiency in xantene dye – Rhodamine B photodecomposition.

2. Experimental

Mesoporous TiO_2 and TiO_2/ZnO films were obtained as it was described earlier in[10,11] using titanium tetra-isopropoxide and zinc acetate as metal sources and Pluronic P123 triblock copolymer as the templating agent. Ag-modified films have been prepared via two techniques: (1) thermoinduced reduction of Ag^+ ions, added to the precursor as $AgNO_3$ 10^{-3}M aqueous solution, by calcination at 500°C; (2) photoreduction of Ag^+ ions deposited on mesoporous TiO_2 and ZnO/TiO_2 (1 at% ZnO) films from aqueous solution of $[Ag(NH_3)_2]NO_3$ under UV-irradiation followed by heat treatment at 20–550°C. TEM measurements were performed with films scratched from glass substrate and coated onto a carbon-coated copper grid. The samples were imaged by the JEOL 200C electron microscope. Atomic force microscopy (AFM) was carried out using a Digital Nanoscope (Nanoscope IIIa). UV-Vis optical absorption spectra were recorded by a Perkin-Elmer Lambda Bio-40 spectrophotometer.

The photoelectrochemical characteristics of the TiO_2/ZnO, Ag/TiO_2 and Ag/TiO_2/ZnO electrodes were estimated using the spectral dependence of the photoelectrochemical current (i_{ph}) as reported previously.[5] The i_{ph} spectra were expressed in units of quantum efficiency (electron/photon). Photocatalytic activity of synthesized films was checked in the process of xantene dye Rhodamine B photodegradation (C_M = 5·10^{-5}) as described previously.[8]

3. Results and Discussion

3.1. THERMOINDUCED REDUCTION OF Ag^+ IONS IN TiO_2 MATRIX

The bright-field TEM image of TiO_2/Ag film prepared via thermoinduced reduction of Ag^+ ions that were added to the precursor at the step of film formation is shown in the Figure 1a and confirms the samples mesoporosity but with

an overall reduction in the long-range order. The formation of Ag nanoparticles (Ag NPs) is clearly observed. The mean diameter of the particles was calculated to be 4–20 nm. This coincides with the results of electron spectroscopy (Figure 1b) and literature data.[11,12] Electron diffraction experiments (Figure 1a, inset) show the pattern of rings corresponding to the anatase phase of TiO_2 and cubic Ag crystals. Figure 1b (curves 1–4) shows the optical absorption spectra of the TiO_2/Ag films in comparison with undoped TiO_2 (curve 5). The maximum observed at around 400 nm can be assigned to the surface plasmon resonance (SPR) peak of spatially confined electrons in Ag NPs [11] and confirms the thermoinduced reduction of Ag^+ ions to the Ag^0 state. The easy reduction of Ag^+ to Ag^0 through removal of an electron from the organic moieties under thermal treatment conditions can be expected in the view of high value of the standard electrode potentials for the Ag^+ to Ag^0 couple (-1.8 V) in aqueous solutions.[14]

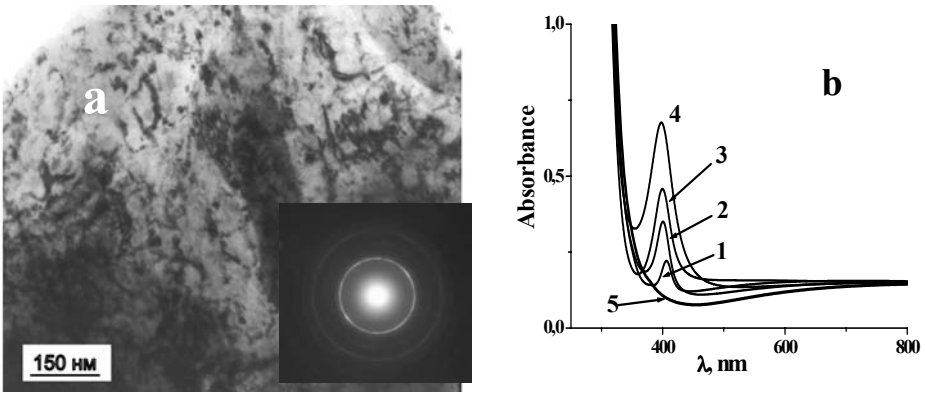

Figure 1. TEM image of the TiO_2/5 at% Ag film (a) and absorption spectra (b) of TiO_2/Ag films with different Ag contents: 1% – 1; 3% – 2; 5% – 3; 10% – 4; 0% – 5. Inset in Figure 1a, electron diffraction.

3.2. PHOTOINDUCED REDUCTION OF Ag^+ IONS ON THE SURFACE OF MESOPOROUS TiO_2 AND TiO_2/ZnO FILMS

Another method of Ag nanoparticles deposition on mesoporous TiO_2 and ZnO/TiO_2 films is a two-step procedure adopted from Ref.[9,13] The TiO_2 films were dipped in 10^{-3} M aqueous solution of $[Ag(NH_3)_2]NO_3$ (pH = 10), washed with ultra pure water and dried at 20°C. The following irradiation by UV – light at 254 nm was performed to reduce the deposited Ag^+ ions to Ag^0 nanoparticles. Available Ag^+ concentration was adjusted by repetition of the dipping procedure. During contact of ZnO/TiO_2 films with basic $[Ag(NH_3)_2]NO_3$ solution partial

dissolution of ZnO followed by exchange of Zn^{2+} ions in the film with Ag^{+} took place. This resulted in more homogeneous distribution of silver and stabilization of Ag NP's formed on the surface.[9] Surface morphology of mesoporous TiO_2/ZnO/Ag films with photodeposited Ag nanoparticles before as well as after thermal treatment at 500°C was studied using AFM microscopy (Fig. 2). Surface of as-prepared TiO_2/ZnO/Ag films consisted of agglomerates of the silver nanoparticles with sizes of app. 1.1 μm and heights in the range of 10–160 nm (maximum at 70 nm). Root mean square roughness of the film is 21.3 nm. After heat treatment at 500°C the surface of TiO_2/ZnO/Ag films is much smoother (roughness of the film is 15.3 nm) with rows of smaller Ag particles (height 10–95 nm with maximum app. 45 nm) oriented along one direction that follows mesoporous TiO_2 film topology.

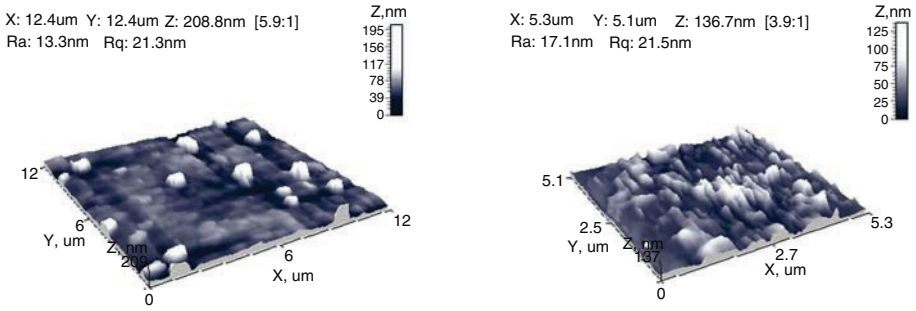

Figure 2. 3D AFM images of the surface of TiO_2/ZnO/Ag films deposited onto glass substrate: (a) – the film with as-deposited Ag particles; (b) – film treated at 500°C.

AFM data correlate with the absorption spectra of Ag/TiO_2/ZnO films (Figure 3): as-prepared films show a broad band in absorption spectra with maximum at 450 nm, indicating inhomogeneous distribution of Ag NPs on the surface; after heat treatment the smaller particles oriented along one direction were obtained (b) that gives bright yellow color and intensive plasmon resonance peak at 400 nm characteristic for particles with narrow size distribution. Only wide band in the visible region was seen in the absorption spectra of TiO_2/Ag films prepared for comparison via the same procedure that could be attributed to the formation of larger silver particles and/or silver oxide.[15] Subsequent thermal treatment leads to the decrease of absorption in visible range of spectra and discoloration of the films. We suggest that the heat treatment leads to the melting of Ag NPs a nd formation of extremely small (less than 2 nm) particles which do not possess the characteristic SPR spectrum.

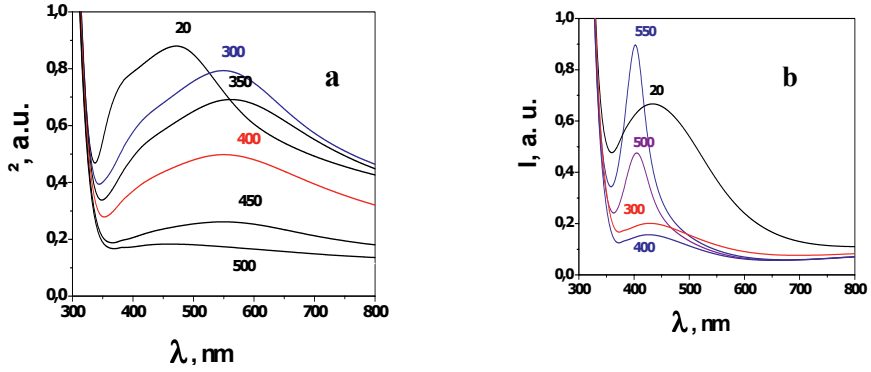

Figure 3. Absorption spectra of the TiO_2 – (a) and TiO_2/ZnO films – (b) with photodeposited silver nanoparticles as-prepared (20°C) and after thermal treatment at different temperatures up to 550°C.

3.3. PHOTOELECTROCHEMICAL PROPERTIES AND PHOTOCATALYTIC ACTIVITY OF Ag-MODIFIED TiO_2 AND TiO_2/ZnO COATINGS IN RHODAMINE B PHOTODEGRADATION

The position of the flatband potential (U_{fb}) of titania and Ag modified TiO_2 and TiO_2/ZnO films coated on the titanium substrates was estimated from the extrapolation of the photocurrent (i_{ph}) dependences on the applied potential. Flat-band potential values of the mesoporous TiO_2 and TiO_2/ZnO samples (Table 1) differ insignificantly from each other and are comparable with the value of –(0.47–0.49) V obtained at pH ≈ 7 for nitrogen-doped titanium dioxide[16] and U_{fb}=–0.58 V measured for anatase single crystal. [17] The charge distribution between semiconductor and Ag NPs causes th e flatband potential shift (see Table 1) to more negative values. The shift is minor (0.11, 0.2 V) for TiO_2 films containing thermoreduced and photodeposited Ag NPs and much more prominent (0.9 V) for Ag/TiO_2/ZnO films (before as well after thermal treatment at 500°C). This strong effect is attributable to stabilization of numerous small Ag NPs on the TiO_2 surface under the conditions of ion-exchange process,[9] followed by photoreduction of Ag^+. It is well known[6,7,18] that the more negative flat band potential resulted in better ability of semiconductor film to faciliate the charge separation.

TiO_2 and TiO_2/ZnO films modification with Ag NPs causes an increase in photocurrent quantum yields (Figure 4) for the nanocomposites with Ag NPs homogeneously distributed in the bulk or deposited on the surface (prepared by the thermo- or by the photoreduction method). The enhancement in the photo-current generation efficiency is indicative of the fact that the deposition of Ag

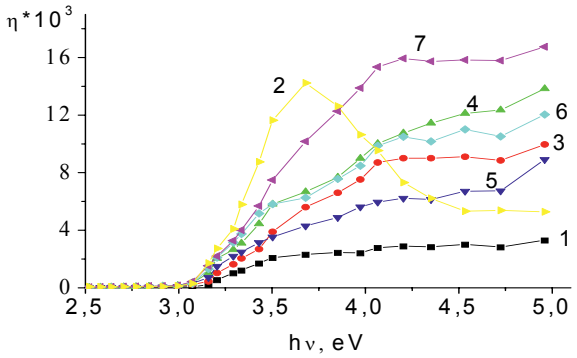

Figure 4. Quantum yields of photocurrent for TiO_2 – (1), TiO_2/Ag thermoreduced (2), TiO_2/Ag – photodeposited – before (3) and after (4) calcination at 500°C; TiO_2/ZnO – 5, TiO_2/ZnO/Ag – photodeposited – before (6) and after (7) calcination at 500°C.

NPs is beneficial for promoting the ch arge separation within the nanostructured TiO_2 film as well as improving the interfacial charge transfer process.[7,8]

The decrease of photocurrent quantum yield in the short-wave region is observed only for Ag/TiO_2 samples prepared via thermo-induced reduction. This effect can be explained by the appearance (due to heat treatment of film containing high amounts of organic residuals) of additional defect centers on the surface participating in cathodic photoreactions and contribution of the cathodic photocurrent to the whole process.[19] The activity of the samples in photooxidation processes was estimated in xantene dye Rhodamine B decomposition. For comparison of the Ag modified films photoactivity the samples with equal intensity of SPR were chosen. Rates of photooxidation were calculated in pseudo first order reaction approach under equal conditions (Table 1).

TABLE 1. The values of flat-band potential and photocatalytic efficiency for TiO_2 and TiO_2/ZnO films modified by Ag NPs.

Sample	E_{fb},[V, NHE]	Photocatalytic efficiency k, min^{-1}
TiO_2 (six layers on Ti)	–0.51	4,10E-03
TiO_2 Ag Thermo	–0.62	15,1 E-03
TiO_2 Ag Photo	–0.71	10,1E-03
TiO_2 Ag Photo + 500°C	–1.41	3,98E-03
1% ZnO/TiO_2	–0.71	4,50E-03
1% ZnO/TiO_2 Ag Photo	–1.41	12,4 E-03
1% ZnO/TiO_2 Ag Photo + 500°C	–1.41	15,5 E-03

Silver modified samples prepared via thermoreduction as well as photo-deposition procedure show the enhanced activity (in –three to four times) toward the undoped TiO_2 and ZnO/TiO_2 coatings that coincides with high efficiency of photocurrent generation and negative shift in flat band potential position.

4. Conclusions

Optically transparent, mesoporous TiO_2 and ZnO/TiO_2 thin film photocatalysts with homogeneously distributed in bulk Ag nanoparticles have been prepared via thermoinduced reduction. Photoreduction allows to stabilise of Ag^0 particles on the surface.

Direct photoelectrochemical investigation of the TiO_2/Ag heterojunctions showed cathodic shift in the position of the flat-band potential in comparison to the unmodified TiO_2 electrodes. TiO_2 modification with silver particles causes the increase of photocurrent quantum yield and photocatalytic activity of Ag/TiO_2 and Ag/ZnO/TiO_2 films in Rhodamine B decomposition.

Acknowledgment

The authors thank Glasunova V.A for the TEM measurements.

References

1. M. Hoffmann, S. Martin, W. Choi, and D. Bahnemann, Chem. Rev., 95, 69–96(1995).
2. T. Wu, G. Liu, J. Zhao, H. Hidaka, and N. Serpone, J. Phys. Chem. B, 102, 5845–5851 (1998).
3. Yu. Gnatyuk, N. Smirnova, A. Eremenko, and V. Iljin, Ads. Sci. Technol, 23, 497–508 (2005).
4. M.E. Zorn, D.T. Tompkins, W.A. Zelter, and M.A. Anderson, Environ. Sci. Technol., 34, 5206–5210 (2000).
5. N. Smirnova, Yu. Gnatyuk, A. Eremenko, G.Ya. Kolbasov, V. Vorobets, I. Kolbasova, and O. Linucheva, Int. J. Photoenergy, 2006, 1–6 (2006).
6. A. Dawson and P.V. Kamat, J. Phys. Chem. B, 105, 960–966 (2001).
7. V. Subramanian, E. Wolf, and P.V. Kamat, J. Phys. Chem. B, 105, 11439–11446 (2001).
8. Yu. Gnatyuk, E. Manujlov, N. Smirnova, A. Eremenko NATO Science Series II Functional properties of nanostructured materials, R. Kassing et al. (eds.), Vol. 223, 485–490 (Springer, The Netherlands, 2006).
9. C. He, Y. Yu, X. Hu, and A. Larbot, Appl. Surf. Sci. 200, 239–247 (2002)
10. T. Ptashko, N. Smirnova, A. Eremenko, E. Oranska, and W. Huang, Ads. Sci. Technol., 25, 35–43 (2006).
11. J. He, I. Ichinose, T. Kunitake, and A. Nakao, Langmuir, 18, 10005–10010 (2002).
12. K.L. Kelly, E. Coronado, L.L. Zhao, and G.C. Schatz, J. Phys. Chem. B, 107, 668–677 (2003).

13. I.M. Arabatis, T. Stergiopoulos, D. Andreeva, S. Kitova, S.G. Neophytides, and P. Falaras, J. Catal. 220, 127–135 (2003).
14. A. Henglein, Chem. Mater. 10, 444–450 (1998).
15. M. Epifani, C. Giannini, L. Tapfer, and L. Vasanelli, J. Am. Ceram. Soc. 88, 2385–2393 (2000).
16. S. Sakthivel and H. Kish, Chem. Phys. 4, 487–490 (2003).
17. M. Grätzel, S.E. Gilbert, C. Klemenz, and H.J. Scheel, J. Am. Chem. Soc. 118, 6716–6723 (1996).
18. M. Jakob, H. Levanon, and P. Kamat, Nano Lett. 3, 353–358 (2003).
19. L.G. Shcherbakova, D.B. Dan'ko, V.B. Muratov, I.A. Kossko, Yu. M. Solonin, G. Ya. Kolbasov, and I.A. Rusetskii, NATO Science Series II Hydrogen Materials Science and Chemistry of Carbon Nanomaterials, T.N. Veziroglu et al. (eds.), Vol. 172, 699–706 (Springer, The Netherlands, 2007).

POSSIBILITIES AND LIMITS OF TEXTURE PROPERTIES CHARACTERIZATION

OLGA ŠOLCOVÁ[1], LENKA MATĚJOVÁ[1*], PAVOL HUDEC[2] AND PETR SCHNEIDER[1]
[1]*Institute of Chemical Process Fundamentals, Academy of Sciences of the Czech Republic, v.v.i, Rozvojová 135, 165 02 Prague 6-Suchdol, Czech*
[2]*Department of Petroleum Technology and Petrochemistry, Faculty of Chemical and Food Technology, Slovak University of Technology, 812 37 Bratislava, Slovak Republic*

Abstract. A series of microporous-mesoporous mechanical mixtures of zeolite NaY and γ-alumina was used for testing the applicability of the modified (three-parameter) BET isotherm equation. Nitrogen adsorption isotherms (77 K) of NaY+ γ-alumina samples were analyzed by this equation and the results compared with the independent textural information obtained from t-plots (with the standard isotherm of nonporous α-alumina and the standard isotherms of Lecloux-Pirard). It appeared that the use of the modified BET equation as same as the standard t-plot method provided good micropore volumes and mesopore surface areas contrary to the incorrect results of the classic BET equation.

Keywords: Adsorption isotherm, microporous-mesoporous samples, modified BET equation, t-plots.

1. Introduction

The attention to microporous-mesoporous solids increased recently tremendously due to appearance of a couple of new materials (e.g. sol-gel materials etc.). This makes the textural analysis based on transformation of physical adsorption isotherms of inert gases (nitrogen, argon, krypton) much less straightforward than in case of porous solids with mesopores only. The simple BET analysis[1] is,

[*]To whom correspondence should be addressed: L. Matějová, Institute of Chemical Process Fundamentals, Academy of Sciences of the Czech Republic, v.v.i, Rozvojová 135, 165 02 Prague 6-Suchdol, Czech Republic; e-mail: solcova@icpf.cas.cz

P. Innocenzi, Y. L. Zub and V. G. Kessler (eds.), *Sol-Gel Methods for Materials Processing*.

nevertheless, usually (and incorrectly) performed. The reason is that the simple BET isotherm was developed explicitly for non-microporous solids and in the relative pressure range, x_{BET}, which guarantees the absence of capillary condensation in mesopores (e.g. $0.25 > x_{BET} > 0.05$). The correct way is to use the comparative plots (t-plots, α-plots) which can supply the micropore volume, a_μ, as well as the mesopore surface area, S_m. The complication with comparative plots arises from the requirement to know the adsorption isotherm for a non-porous solid with same chemical character as the analyzed porous sample (standard isotherm).[2] We have suggested[3] to use the modified BET (1) (three-parameter BET), which when applied to the analyzed sample gives the micropore volume, monolayer capacity as well as the correct parameter C.

$$a = a_\mu + \frac{a_m C x}{(1+x)\left[1+(C-1)x\right]} \tag{1}$$

Here a is the adsorbed amount at relative pressure x ($x = p/p_o$ with p the adsorbate pressure and p_o the saturation adsorbate pressure at the measurement temperature), a_μ the adsorbate amount corresponding to complete filling of micropores and C is a constant proportional to adsorption equilibrium constant in the first adsorbed layer. The mesopore surface area, S_m, is obtained from the monolayer capacity a_m as

$$S_m = a_m A \sigma \tag{2}$$

with the Avogadro constant, A, and the area covered by one adsorbate atom/molecule, σ. For nitrogen at normal boiling point (77 K) $\sigma = 0.162$ nm^2 is usually taken. Thus, the modified (three-parameter) BET equation differs from the classic (two-parameter) BET equation by the presence of the a_μ term, only.

2. Experimental

As microporous-mesoporous materials mechanical mixtures of microporous zeolite, NaY (batch No. NaY-091087V3 with Si/Al = 2.24), and mesoporous γ-alumina (laboratory prepared carrier for reforming catalysts from boehmite) with γ-alumina weight fractions, f, varying between 0 and 1 were used.

Adsorption measurements were performed with the ASAP2400 instrument (Micromeritics, USA). Prior to measurement the samples were degassed overnight at 350°C and 2 Pa.

Nitrogen adsorption isotherms at 77 K of the pure NaY zeolite and γ-alumina are shown in Figure 1 and for mixed NaY+ γ-alumina samples in Figure 2. Textural properties of pure samples are summarized in Table 1.

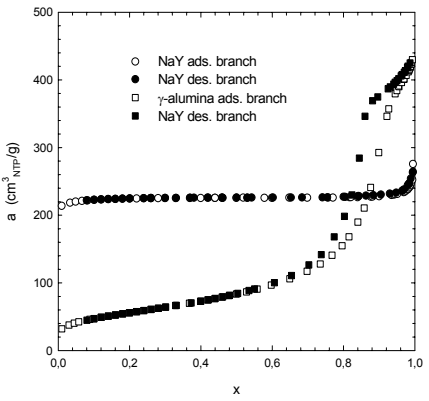

Figure 1. Nitrogen adsorption isotherms (77 K) of NaY and γ–alumina.

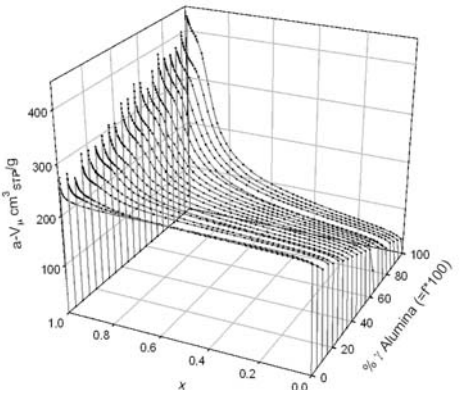

Figure 2. Adsorption branches of isotherms of NaY/γ-alumina mixtures.

TABLE 1. Textural properties of pure NaY and γ-alumina.

	NaY	γ-alumina
Monolayer capacity, a_m (mm^3_{liq}/g)[a]	11.7	71.2
Mesopore surface area, S_m (m^2/g)[a]	32.9	199.7
Micropore volume, a_μ (mm^3/g)[a]	335	0
C[a]	22.6	95.2
Most frequent pore radius (nm)[b]	–	5.1,[c] 6.9[d]

[a]From (1), for recalculation of adsorbed amounts in cm^3_{NTP}/g to mm^3_{liq}/g multiplication by the factor 1.4568 was used; [b]from Barrett-Joyner Halenda,[4] pore-size distribution with α–alumina standard isotherm[5]; [c]from adsorption isotherm branch; [d]from desorption isotherm branch

3. Results and Discussion

First, a thorough analysis of mixed sample isotherms by the use of the modified BET (1) was performed. Figure 3 summarizes the micropore volumes, a_μ, and mesopore surface areas, S_m, obtained by fitting of experimental mixed sample a(x) data to (1) with the C parameter fixed at the value for parent γ-alumina sample (C = 95.2 see Table 1). The non- linear data fitting was performed with use of simplex algorithm.

As can be seen the micropore volumes, a_μ, and mesopore surface areas, S_m, depend linearly on the amount of NaY (or γ-alumina) in the sample. The

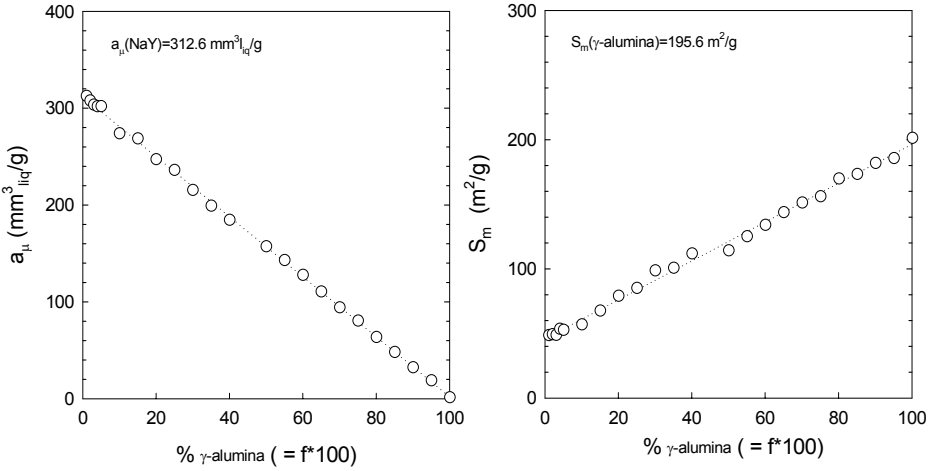

Figure 3. Micropore volumes, a_μ, and mesopore surface areas, S_m, for mixed samples determined by the modified BET equation.

micropore volume of NaY, a_μ, obtained by extrapolation of the linear dependence a_μ – f to f→0 (i.e. a_μ (NaY)=0.313 cm ^{3}$_{liq}$/g) and the specific surface area of γ-alumina, S_m, from extrapolation of S_m – f dependence to f→1 (S_m(γ- alumina) =196 m ^{2}/g agree with values of the pure samples (Table 1)These linear dependences make possible to determine the mesopore surface area of γ-alumina, S_m(γ-alumina), and the micropore volume of NaY, a_μ(NaY), from a_μ and S_m of mixed samples also as a_μ(NaY) =a $_\mu$/(1-f) and S_m(γ-alumina) =S $_m$/f. The obtainned numbers do not exceed the 3% deviation of results for pure samples.

The comparative t-plots were constructed in the usual way. Standard isotherm of nonporous α-alumina was used as the source of film thicknesses[5]. Figure 4 summarizes the t-plots for individual mixed samples and the resulting micropore volumes, a_μ. As can be seen a_μ decreases linearly with the fraction of γ-alumina in the sample, f. The micropore volume extrapolated to f=0 (i.e. pure NaY), a_μ =0.312 cm ^{3}$_{liq}$/g differs only slightly from the value of parent NaY (Table 1).

Figure 5 compares micropore volumes, a_μ, obtained from the modified BET equation with C =95.2 and t-plot analys is with the standard isotherm of nonporous α-alumina.[5] It can be seen that values of micropore volumes obtained by both independent methods differ only slightly. The general agreement of the modified BET equation and t-plot results prove the applicability of these equations for analysis of microporous- mesoporous samples.

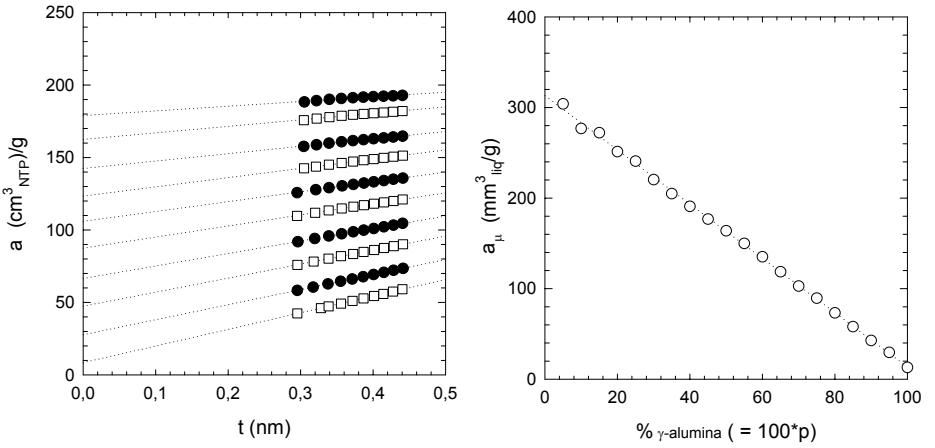

Figure 4. t-plots for mixed samples (standard isotherm: non-porous α-alumina) and the corresponding micropore volumes.

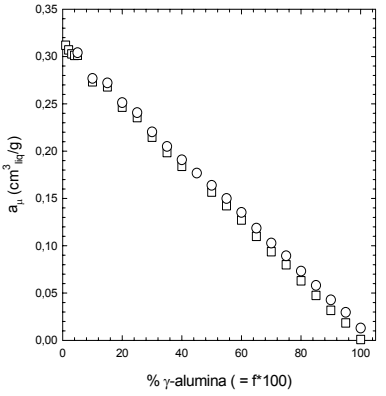

Figure 5. Comparison of micropore volumes, a_μ, obtained from the modified BET equation–o and t-plots analyses.

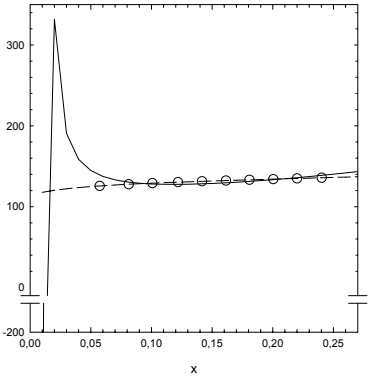

Figure 6. Experimental adsorption points and isotherms calculated with parameters of the classic (solid line) and modified BET (dashed lines).

Figure 6 compares the application of the classic and modified BET equations to microporous-mesoporous mixed samples. For illustration, adsorption points from the BET region ($0.05 < x_{BET} < 0.25$), for the sample with 50% γ-alumina and 50% NaY, were chosen. It can be seen that the isotherm calculated with use of parameters from the classic BET equation (solid line) deviates significantly from experimental points. Quite the opposite is true when parameters from the modified BET equation were used (dashed line). Also the physically incorrect value of the C constant obtained from the classic BET equation

(C =–71) points to the inappropriateness of application of the classic BET equation for isotherms of microporous-mesoporous samples.

4. Conclusions

The textural characteristics of mixed sample isotherms obtained directly from the modified BET equation agree very closely with independent results based on t-plots. This proves the suitability of the modified BET equation for analysis of adsorption isotherms of microporous-mesoporous samples. For illustration, the failure of classic (two-parameter) BET equation usually (and incorrectly) performed for samples of this type was clearly demonstrated.

Acknowledgement

The financial support of the Czech Academy of Sciences, Program Nano-technology for Society (KAN400720701) is gratefully acknowledged.

References

1. Brunauer S., Emmett P.H., Teller E., Adsorption of Gases in Multimolecular Layers, *J. Am. Chem. Soc*., 60, 309 (1938).
2. Lecloux A., Pirard J.P., The importance of standard isotherms in the analysis of adsorption isotherms for determining the porous texture of solids, *J. Coll. Interface Sci*., 70, 265 (1979).
3. Schneider P.: Adsorption isotherms of microporous-mesoporous solids revisited. *Appl. Catal*. A 129(2), 157–165 (1995).
4. Barrett E.P., Joyner L.G., Halenda P.P., The Determination of Pore Volume and Area Distributions in Porous Substances. I. Computations from Nitrogen Isotherms, *J. Am. Chem. Soc*., 73, 373 (1951).
5. Matějová L., Schneider P., Šolcová O., Standard (master) Isotherms of Alumina, Magnesia, Titania and Controlled-pore Glass, *Micropor. Mesopor. Mater.*, 107, 227 (2008).

PREPARATION AND CHARACTERIZATION OF THIN NANOCRYSTALLINE TIO_2 LAYERS

OLGA ŠOLCOVÁ[1*], LENKA MATĚJOVÁ[1], PETR KLUSOŇ[2], ZDENÌK MATĚJ[3], ZDENÌK STRÝHAL[4], JAROSLAV PAVLÍK[4] AND TOMÁ¹ CAJTHAML[5]

[1]*Institute of Chemical Process Fundamentals, Academy of Sciences of the Czech Republic, v.v.i, Rozvojová 135, 165 02 Prague 6-Suchdol, Czech*

[2]*Faculty of Chemical Technology, Institute of Chemical Technology Prague, Technická 5, 166 28 Prague 6-Dejvice, Czech Republic*

[3]*Faculty of Mathematics and Physics, Charles University in Prague, Ke Karlovu 3, 121 16 Prague 2, Czech Republic*

[4] *Faculty of Science, Department of Physics, University J.E. Purkyně in Ústí nad Labem, Ceske mladeze 8, 400 96 Ústí nad Labem, Czech Republic*

[5]*Institute of Microbiology of the Academy of Sciences of the Czech Republic, v.v.i*

Abstract. Thin nanolayers of titania prepared by repeated dip-coating of silica glass into transparent homogeneous sol from nonionic surfactants with various number of oxyethylene units were studied. Calcination in the air flow and/or extraction by supercritical CO_2, subcritical H_2O and subcritical CH_3OH were used to convert transparent gel layers into anatase layers. The influence of individual surfactants on the surface morphology, roughness, structural and textural properties was evaluated.

Keywords: Sol-gel method, thin films, texture, nanostructure, AFM, XRD, nitrogen adsorption.

1. Introduction

Recently, a huge research interest to nanoporous titania with special attention to its photocatalytic properties, significantly widening their promising application

* To whom correspondence should be addressed: O. Šolcová, Institute of Chemical Process Fundamentals, Academy of Sciences of the Czech Republic, v.v.i, Rozvojová 135, 165 02 Prague 6-Suchdol, Czech Republic; e-mail: solcova@icpf.cas.cz

P. Innocenzi, Y. L. Zub and V. G. Kessler (eds.), *Sol-Gel Methods for Materials Processing*.

potential, was noticed.[1–5] Nowadays, titania is prepared in various forms such as nanotubes, powder particles and transparent thin layers deposited on carriers[6–9] to optimize its photochemical efficiency. To achieve high photo-catalytic activity it is necessary to prepare crystalline anatase with suitable grain size, purity and textural morphology. Thin titania layers deposited on suitable carriers seem to be an optimal solution for industrial applications of the photo-catalytic reactions. For optimization of the photocatalytic activity the knowledge of structural and textural properties of titania layers is indispensable. Unfortunately, such studies appear only rarely.[10] Therefore our study was focused on preparation of a set of various titania layers by dip-coating via sol-gel method controlled in inverse micellar environment with tailoring textural and structural properties for photoactivity.

2. Experimental

2.1. SOL PREPARATION AND LAYER DEPOSITION

Nano-TiO_2 was synthesized by sol-gel process. Titanium (IV) isopropoxide ($Ti(OCH(CH_3)_2)_4$, Aldrich, 99.999%) was added into formed inverse micellar solution of cyclohexane (Aldrich, 99.9+%, HPLC grade), nonionic surfactant Triton X-(Aldrich) and water. The molar ratio of cyclohexane/Triton X-/water/ $Ti(OC_3H_7)_4$ was kept at 11/1/1/1.[7]

Firstly, the solution of cyclohexane, Triton X and water was intensively stirred for 15 min for homogenization and formation of inverse micelles. Then, the titanium isopropoxide was regularly dropped into the micellar solution under continued stirring. After the addition of the isopropoxide the sol was stirred for additional 10 min and then left for 2 h for stabilization. In this way the sol for dip-coating was prepared.

Ultrasonicly cleaned glasses were dipped into the sol with velocity 6 cm/min and kept in the sol for 10 s. After 4 h of stabilization the rigid gel layer was formed. The organic content was then reduced by calcination in air stream and/or extraction by supercritic CO_2, subcritical H_2O and subcritical CH_3OH. After this treatment the transparent nanoporous titania thin layer was obtained. To guarantee the homogeneity of the titania layer surface this procedure was repeated at least three times.

To explain the influence of the number of oxyethylene units in Triton X on the textural and structural layer characteristics, five different Triton X (102, 100, 114, 45 and 15) were used for layer preparation. Their characteristics are summarized in Table 1 and for better imagination the structural formula of Triton X is shown in Figure 1.

TABLE 1. Characteristics of used Triton X.

Type of Triton	Triton X-102	Triton X-100	Triton X-114	Triton X-45	Triton X-15
Molecular formula	$C_{39}H_{72}O_{13.5}$	$C_{33}H_{60}O_{10.5}$	$C_{29}H_{52}O_{8.5}$	$C_{23}H_{40}O_{5.5}$	$C_{17}H_{28}O_{2.5}$
Number of oxyethylene units	12.5	9.5	7.5	4.5	1.5

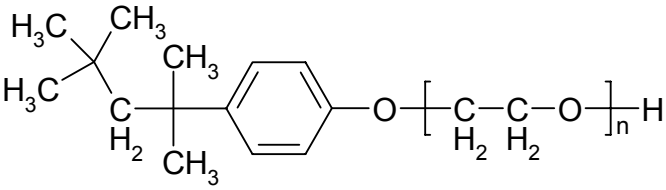

Figure 1. Structural formula of the surfactant Triton X molecule.

2.2. TREATMENT OF PREPARED GEL LAYERS

The samples were purified by calcination and three different extraction techniques and/or their combination: (a) supercritical fluid extraction (SFE), (b) subcritical water extraction (SWE) and (c) pressured solvent extraction (PFE).

Samples were calcined at 400°C for 4 h with temperature ramp 1°C/min in an air flow.

SFE was performed with a PrepMaster extractor (Suprex, USA) equipped with VaryFlow restrictor operating at 40°C. Carbon dioxide of SFE/SFC purity was used as extraction medium. The samples were placed in a 10 ml stainless steel extraction vessel and purified at 400 bar and 100°C with a CO_2 flow rate 1.5 ml/min for 500 min.

SWE and PFE were performed with the same system: a common HPLC pump (Varian, Series 200) equipped with a GC oven and Valco needle valve as a back pressure restrictor. Ultra pure water or methanol (gradient grade, Merck) was used for extraction at 5 ml/min flow rate; samples were purified in a 100 ml extraction vessel for 200 min.

2.3. SAMPLE CHARACTERIZATION

Textural properties of the samples were evaluated from nitrogen physical adsorption-desorption isotherms at 77 K obtained with the ASAP2020M (Micromeritics, USA).

Surface topography and roughness were measured by the Atomic Force Microscopy (AFM – Metris – 2001A – NC, Burleigh Instruments Inc.). A commercially available silicon probe was used. All AFM measurements were carried

out in the non-contact mode under ambient atmosphere and at room temperature. The scan area varied from 1.2 × 1.2 μm to 25 × 25 μm. Scans were made with 256 × 256 pixels resolution.

The sample crystallinity was characterized by X-ray diffraction (XRD). For all samples the Seifert-FMP or the Panalytical-MPD laboratory diffractometer with a Cu anode in the conventional focusing Bragg-Brentano experimental arrangement was used.

3. Results and Discussions

By dissolving the initial metal alkoxide in reverse micelles (of Triton X) the hydrolysis with a controlled amount of water, contained inside the micelle, takes place. At low water/surfactant molar ratio the generation of uniform spherical nanoparticles is expected. Micelles become entrapped in the forming inorganic matrix as an ordered liquid-crystalline phase that after treatment should be transformed into rigid nanocrystals essential for photocatalytic activity.

The surface topography and roughness of calcined layers for all used Triton X are shown in Figure 2. It is clearly seen that the surface layer prepared from Triton X15 and X45 surfactants are nearly smooth without presence of crystallites. Surfaces layers from Triton X114, X100 and X102 are somewhat rough with the size of crystallites in the range 6–10 nm. This is confirmed by XRD analysis (see Figure 3), where the shapes of curves for Triton X15 and 45 are similar to pure glass and do not indicate any crystalline phase; the curves for layers from Triton X114, 110 and 102 demonstrate clearly the presence of a crystalline phase. The phase analysis confirmed the presence of nearly pure anatase with a small amount of brookite.

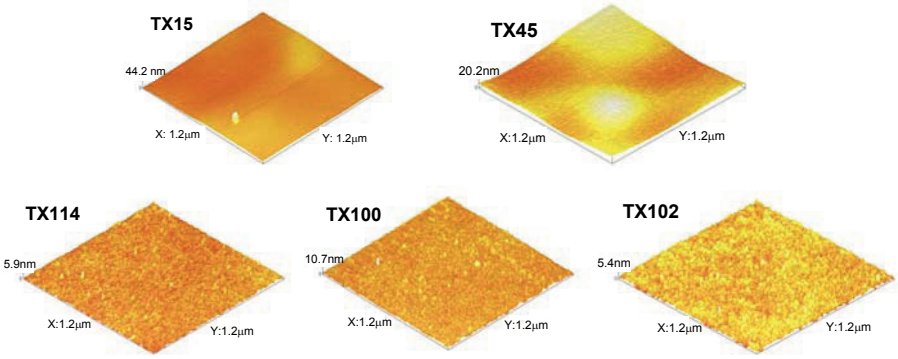

Figure 2. Photographs of calcined layers from AFM analysis.

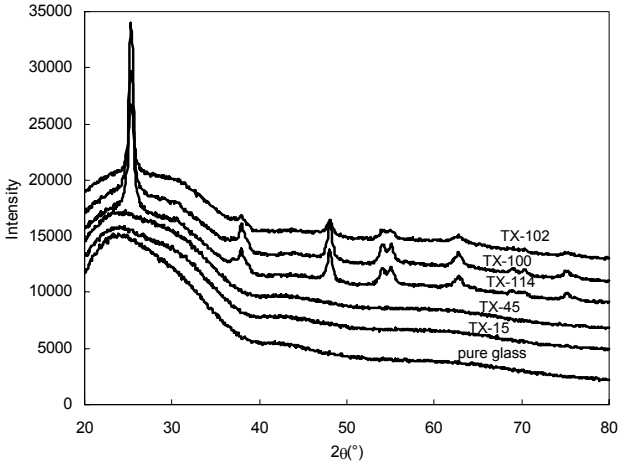

Figure 3. XRD patterns of pure glass and calcined films deposited on glass.

The influence of the treatment for removal of organic matter is shown in Table 2. Obviously, an ideal removal of the organic matter should preserve the order of the template structure. The common thermal treatment may result in the collapse of the forming structure and cause a significant decrease of surface area. This is noticed in Table 2, where the BET surface areas for all surfactants and calcination and extraction are summarized. The specific surface area of extracted samples is three to four times higher than for samples treated by calcination.

TABLE 2. Specific surface areas of calcined and extracted layers.

	Calcination	SFE	SWE+PFE
		$S_{BET}[m^2/g]$	
TX-15	28.3	–	–
TX-45	70.2	292.6	250.4
TX-114	80.1	281.3	233.6
TX-100	77.5	278.7	246.3
TX-102	74.3	310.4	248.2

4. Conclusions

The influence of various surfactants used for preparation of titania thin layers on the surface morphology, roughness, structural and textural properties was studied. It was confirmed that thermal treatment causes an important decrease of specific surface area as compared to the organic matter removal by extraction, which results in approximately three times higher surface areas. It was

determined that the number of oxyethylene units in surfactant influences the morphology of the layer surface; more than 7 units leads to a crystalline phase and less than 4.5 units leads to an amorphous phase.

Acknowledgement

The financial support of the Czech Academy of Sciences, Program Nanotechnology for Society (KAN400720701) is gratefully acknowledged.

References

1. Maira A.J., Yeung K.L., Soria J., Coronado J.M., Belver C., Lee C.Y., Augugliaro V., Gas-phase photo-oxidation of toluene using nanometer-size TiO_2 catalysts, Applied Catalysis B 29, 327–336 (2001).
2. Neppolian B., Jung H., Choi H., Photocatalytic degradation of 4-chlorphenol using TiO_2 and Pt-TiO_2 nanoparticles prepared by sol-gel method, Journal of Advanced Oxidation Technologies 10 (2), 369–374 (2007).
3. De la Fourniere E.M., Leyva A.G., Gautier E.A., Litter M.I., Treatment of phenylmercury salts by heterogenous photocatalysis over TiO_2, Chemosphere 69 (5), 682–688 (2007).
4. Evans P., Sheel D.W., Photoactive and antibacterial TiO_2 thin films on stainless steel, Surface and Coatings Technology 201 (22–23 Special issue), 9319–9324 (2007).
5. Yang L., Liu Z., Shi J., Hu H., Shangguan W., Design consideration of photocatalytic oxiadation reactors using TiO_2-coated foam nickels for degrading indoor gaseous formaldehyde, Catalysis Today 126 (3–4 Special issue), 359–368 (2007).
6. Sheng Q., Yuan S., Zhang J., Chen F., Synthesis of mesoporous titania with high photocatalytic activity by nanocrystalline particle assembly, Microporous And Mesoporous Materials 87, 177–184 (2006).
7. Kluson P., Luskova H., Cajthaml T., Solcova O., Non thermal preparation of photoactive titanium (IV) oxide thin layers, Thin Solid Films 495, 18–23 (2006).
8. Addamo M., Augugliaro V., Di Paola A., Garcia-Lopez E., Loddo V., Marci G., Palmisano L., Preparation and photoactivity of nanostructured TiO_2 particles obtained by hydrolysis of $TiCl_4$, Colloids and Surfaces A 265, 23–31 (2005).
9. Kluson P., Luskova H., Cerveny L., Klisakova J., Cajthaml T., Partial photocatalytic oxidation of cyclopentene over titanium (IV) oxide, Journal of Molecular Catalysis A 242, 62–67 (2005).
10. Černigoj U., Lavrenčič Štangar U., Trebše P., Opara Krašovec U., Gross S., Photo-catalytically active TiO_2 thin films produced by surfactant-assisted sol-gel processing, Thin Solid Films 495, 327–332 (2006).

SOL- GEL APPROACH FOR DEVELOPMENT OF THEMESOPOROUS STRUCTURES FOR CREATION OF THE SENSORS AND DISPOSAL OF LOW MOLECULAR WEIGHT TOXIC SUBSTANCES FROM ENVIRONMENTAL OBJECTS

NIKOLAI F. STARODUB[1*], GERMAN M. TELBIZ[2]
[1]*Palladin Institute of Biochemistry of National Academy of Sciences of Ukraine, 9 Leontovicha Str., 01601 Kiev, Ukraine*
[2]*Pisarzhevsky Institute of Physical Chemistry of National Academy of Sciences of Ukraine, 31 Nauki av., Kiev, Ukraine*

Abstract. Mesoporous sol-gel materials are among the ideal host matrixes for immobilizing enzymes because of their large pore volumes and controllable pore sizes appropriate for inclusion compounds. Although indirect enzyme immobilization in mesoporous materials has been achieved by impregnating of the MCM41 matrix with an enzyme, there are only few reports on one-step direct immobilization of bioactive species in surfactant-templated mesoporous sol-gel materials. We demonstrate here the principle by immobilization of 2,4D herbicide and mycotoxins T2 as model system. With that goal in view, various silica matrices with miscellaneous structural parameters were prepared and characterized.

Keywords: Sol-gel materials, mesopous matrix, structure, immobilization, horseradish peroxidise, 2,4D herbicide.

1. Introduction

Inorganic supports with surfaces favourable for the immobilization resulting in high sensor activity have been highly sought.[1,2] However, formation of the channels and the pores of the sol–gel matrix are not controlled, and various sizes of pores and channels are formed, ranging from 0.1 to 50 nm in size. Often interconnected micropores and channels are formed, allowing only the smallest of the substrates to penetrate, while the bigger substrates block the channels,

* To whom correspondence should be addressed: Nickolai F. Starodub, Palladin Institute of Biochemistry of NA S of Ukraine, 9 Leontovicha Str., 01601 Kiev, Ukraine; e-mail: nikstarodub@yahoo.com

P. Innocenzi, Y. L. Zub and V. G. Kessler (eds.), *Sol-Gel Methods for Materials Processing*.

slowing the reactions. The hexagonal mesoporous silicas have great potential for high organic molecules loading, provided that pore size is sufficiently large for anchoring some organic molecules (enzyme, pesticide, toxin, biomolecules) and also for permitting substrates to access and diffuse easily through a pore channel, while appropriate functional groups provide high affinity for various biomolecules.[3,4] Self-organized materials with high surface area and 3–25 nm pore size were produced using templation and co-assembly. The highly porous nature of the ordered structure combined with low adsorption and emission in the visible area of spectrum and facile diffusion make them good candidate for optical and chemical sensor applications and provide new avenues for encapsulation/immobilization processes. We have shown that such mesoporous silica materials with variable pore sizes and surface susceptible for functionalization, can be utilized as good separation devices and immobilization hosts for biomolecules. The latter can be sequestered and released depending on their size and charge within the channels. Mesoporous silicas with large-pore-size structures are best suited for this purpose, since more molecules can be immobilized and the large porosity of the materials provide better access for the substrates to the immobilized molecules. The mechanism of bimolecular adsorption in the mesopore channels was suggested to be ionic interaction. On the first step on the way to creation of chemical sensors on the basis of functionalized mesoporous silica materials for selective determination of herbicide in an environment the study of sorption activity number of such materials in relation to 2,4-D was conducted.

Various morphologies can be achieved for mesoporous silica using either the templation method or the phase transformation approach. These usually involve ordering or shaping on the micron scale. In addition to the normal particulate form, there are obtained fibres and ropes, gyroids and discoids, hollow and solid spheres, films, tubular, and pillar-within-spheres.[5]

Organic-inorganic composites may combine the unique properties of both components.[6] Due to own microstructures they would greatly improve their performances, such as better mechanical properties, chemical and thermal stability, higher sensitivity, etc. We could have focused on three sorts of organic–inorganic nanocomposites from mesoporous and mesostructured materials – organic substances molecularly dispersed in the frameworks, functional organic molecules or groups in the internal pore channels, and polymer materials encapsulated in the pore channels. The discovery of meso-structured silica formed by the cooperative self-assembly of silicates and surfactants has opened up a new range of possibilities for chemical sensors. The highly porous nature of these materials makes them excellent hosts for sensing molecules, since the species to be

sensed can easily diffuse towards the sensing centre.[7,8] Principally, the requirements of fast response and negligible leaching can be fulfilled advantageously in large-pore mesoporous materials by covalently anchoring the active sensor dye during synthesis and low-temperature removal of the structure directing agent afterwards.

2. Results and Discussion

In order to control the morphology of the pore structure, doped mesostructured silicas should be carefully investigated for development of new materials with excellent sensor properties. In the present work we have explored further application of mesoporous silicas for direct immobilization of biomolecules. We demonstrated the principle by immobilization of horseradish peroxidase (HRP) and 2,4 D herbicide as model enzyme system. To achieve this aim, various silica matrices with miscellaneous structural parameters were prepared by sol-gel synthesis and characterized (Table 1). The release was dependent on the size and charge distribution within the channels.

TABLE 1. Structural characteristics of the monitored mesoporous materials.

Sample	Symmetry	D, nm	V, cm^3/g	S,m^2/g
MCM-41	Hexagonal	3.0	0.67	989
MCM-48	Cubic	2.5	1.29	1,690
KBT-22	Hexagonal	3.3	0.6	834
SBA-15	Hexagonal	10.7	1.02	375
SBA-15	Hexagonal	10.7	1.13	420
MCF-1	Spherical	8.1	1.74	770
MCF-2	Spherical	11.9	1.9	790
MCF-3	Spheric	13.9	2.1	840

The sample KBT-22 presents amino modified form of the MCM-41 structure (first in the Table 1). The apparent activity of HRP/2,4D conjugate was studied in order to monitor the influence of the matrix on the level of selectivity towards binding of conjugate in various mesoporous materials (Table 1). Results

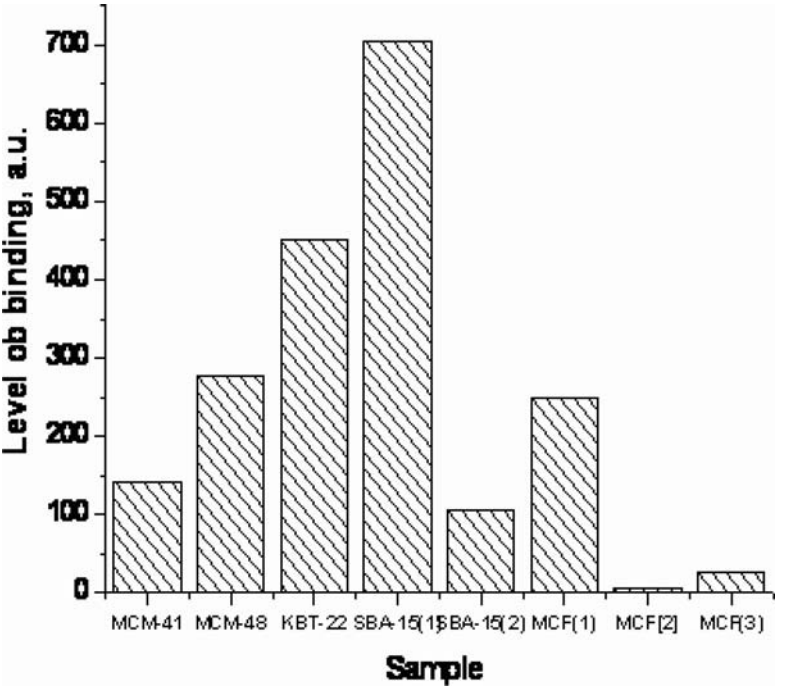

Figure 1. Level of selective binding of HRP in the various mesoporous materials.

obtained with the help of enzyme immunoassay (ELISYS 2 HUMAN), are shown in Figure 1.

The above results testify that none of the explored structural parameters of matrix can be considered negligible in relation to the efficiency of binding of biomolecules (see Figure 2).

Optimum there appears to be the SBA-15 matrix to the type SBA-15, that has the relatively small area of specific surface area (420 cm^2/m), diameter of channels a 10.7 nm and pore volume of 1.13 cm^3/g.

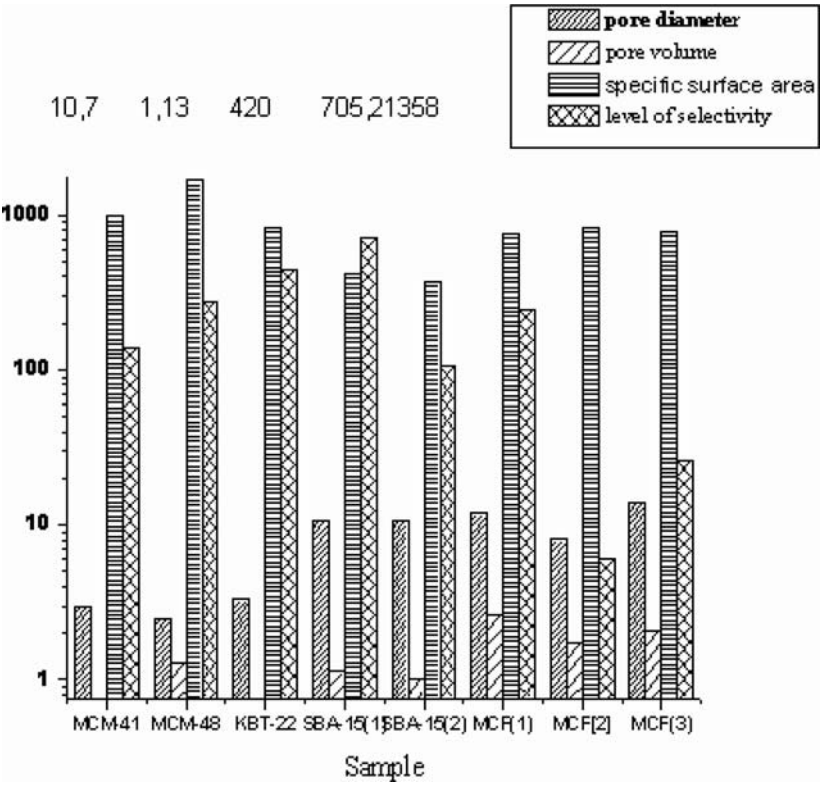

Figure 2. Factors influencing the level of the selective binding (from above resulted parameters of matrix which has the greatest level [705, 2,138] pore diameter, the pore volume and specific surface area).

3. Conclusions

Mesoporous materials can function as biological molecules separation devices, where we can isolate a desired biomolecule and perspective especially for potential applications at the creation of sensitive element of new biosensors, such as effective substances for the decontamination of environmental objects from low molecular weight toxic elements presented in form of pesticides and mycotoxins.

References

1. J. Castillo et al. Biosensors for life quality: Design, development and applications, *Sensor Actuator B*, 102, 179–194 (2004).
2. O. S. Wolfbeis, Fiber-optic chemical sensors and biosensors, *Anal. Chem.*, 72, 81R–89R (2000).
3. T. Kresge, M. E. Leonowicz, W. J. Roth, J. C. Vartuli, J. S. Beck. Ordered mesoporous molecular sieve synthesized by a LCT mechanism. *Nature*, 359, 710–713 (1992).
4. J. S. Beck, J. C. Vartuli, W. J. Roth, M. E. Leonowicz, C. T. Kresge, K. D. Schmitt, C. T.-W. Chu, H. Olson, E. W. Sheppard, S. B. Higgins, J. L. Schlenker. A new family of mesoporous sieves prepared with liquid crystal templates*, Am. Chem. Soc.*, 114, 10834–10843 (1992).
5. H. Yang, G. Vovk, N. Coombs, I. Sokolov, G. A. Ozin. Synthesis of mesoporous silica spheres under quiescent aqueous acidic conditions*, Mater. Chem.* 8, 743–750 (1997).
6. A. Stein, B. J. Melde, R. C. Schroden, Hybrid inorganic-organic mesoporous silicates - nanoscopic reactors coming of age, *Adv. Mater.*, 12, 19 , 1403–1419 (2000).
7. G. Wirnsberger, P. Yang, B. J. Scott, B. F. Chmelka, G. D. Stucky, Mesostructured materials for optical applications: from Low-k dielectrics to sensors and lasers, *Spectrochim Acta*. 57A, 2049–2060 (2001).
8. G. Wirnsberger, B. J. Scott, G. D. Stucky, pH Sensing with mesoporous thin films, *Chem. Commun*., 119, 120 (2001).

PHOTOREDUCTION OF NITRATE IONS OVER Ag/TiO_2 SYSTEM

MIKHAIL SYCHEV[1*], ALEXANDR LOZOVSKI[1], ROMAN PRIHOD'KO[1], KRZYSZTOF ERDMANN[2], VLADISLAV GONCHARUK[1]

[1]*Dumanski Institute of Colloid and Water Chemistry, National Academy of Sciences of Ukraine, Vernadski blv. 42, Kiev 03142, Ukraine*

[2]*Faculty of Chemistry, Nicolaus Copernicus University, Gagarin Str. 7, 87-100 Torun, Poland*

Abstract. The Ag/TiO_2 materials synthesised by a pH-controlled photocatalytic process and triblock copolymer-induced reduction of the $[Ag(NH_3)_2]^+$ ions under ambient light illumination appeared to be active and selective catalysts for the photocatalytic reduction of the nitrate ions in water. High efficiency of such Ag/TiO_2 catalysts was attributed to the presence of both the highly dispersed silver nanoclusters on the surface of titania and the hetero-junctions in the TiO_2 support. The influence of the structural features and the phase composition of the titania support on catalytic properties of the Ag/TiO_2 materials is discussed.

Keywords: Photocatalysis, titania, silver, photoreduction, nitrate ions.

1. Introduction

Abundance of nitrate ions in ground water, which is the main source for drinking water, has strongly increased during the last years throughout the world as a result of intensive agricultural activities, mainly due to the overuse of man-made fertilisers. In some regions, the nitrate concentration in the ground water can be as high as 50 mg/l (calculated by the nitrogen weight).[1] Too high concentration of the NO_3^- ions may be fatal to infants in the bodies of whom they are reduced to nitrites that combine with hae-moglobin to form methaemoglobin. This results in methaemo-globinemia, commonly known as "blue baby syndrome". Moreover, the nitrate ions can be converted into nitrosoamine causing hypertension or cancer. Thus, to reduce the nitrate content in water is presently an imperative task.

[*]To whom correspondence should be addressed: Dr. M.V. Sychev, Leading researcher of Dumanski Institute of Colloid and Water Chemistry, National Academy of Sciences of Ukraine, Vernadski blv. 42, Kiev Ukraine; e-mail: m.v.sychev@icccw.kiev.ua

P. Innocenzi, Y. L. Zub and V. G. Kessler (eds.), *Sol-Gel Methods for Materials Processing*.

Direct conversion of the nitrate ions into nitrogen via their liquid-phase hydrogenation is an interesting and challenging subject, which is expected to be more economical and to have ecological advantages.

During the last two decades, the photocatalytic water denitrification over metal-loaded semiconductors was also extensively investigated.[1,2] Titania was considered to be the carrier material with a great potential for this purpose, due to its unique optical and electronic properties, chemical stability, and non-toxicity.[1,2] The nature of metal, its loading, and presence in the reacting medium of hole scavengers play a key role in the efficient photo-reduction of the NO_3^- ions. Recently, the Ag/TiO_2 catalysts synthesised by a pH-controlled photocatalytic process[3] were used in the photocatalytic nitrate reduction. It was reported that their performance was better than that of the Pd/Cu-based hydrogenation systems. It was suggested that silver nanoparticles enhanced the photocatalytic activity of TiO_2 while stimulating formation of the Schottky barrier at every Ag/TiO_2 contact surface.[1] Thus, they promote the charge separation and inhibition of the electron-hole pairs recombination, whereas the hole scavengers are essential for the reduction of the target ions.

In this study, we evaluated the significance of both the preparation procedure and the potentially controlling photocatalytic behaviour of the Ag/TiO_2 system towards its performance in the water denitrification. The influence of the structural features and phase composition of a titania support on the catalytic properties of the Ag/TiO_2 materials was investigated as well.

2. Experimental

Nanocrystalline TiO_2 anatase (NTi) has been prepared by the sol-gel method described by Gnanasekar et al.[4] Ordered macroporous titania (OMT) was synthesised, in accordance with the method reported in the literature,[5] by the dropwise addition of the above-mentioned titanium alkoxide to ammonia.

The Ag/TiO_2 catalysts, denoted as AT, were synthesised by a pH-controlled photocatalytic process[3] with $AgNO_3$ as the source of silver, whereas the materials designated as PAT were prepared by reduction of $[Ag(NH_3)_2]^+$ in ethanol, induced by the P123 triblock copolymer ($PEO_{20}PPO_{70}PEO_{20}$).[6,7] All the catalysts were characterised by means of the UV-Vis and IR spectroscopies, transmission electron microscopy (TEM), N_2 adsorption, and X-ray photoelectron spectroscopy (XPS). The photocatalytic reaction was carried out in a double-walled quartz cell cooled with water, using a 125-W high pressure Hg lamp (main wavelength around 365 nm) as a light source. The initial concentration of the nitrate anions was 100 mgN/l (calculated by the nitrogen weight). No treatment was performed to remove the dissolved oxygen. The residual concentrations of the nitrate, nitrite, and ammonium ions in supernatant were determined with the ion-exchange chromatography.

3. Results and Discussions

As reported by Gnanasekar et al.,[4] the TiO_2 sol obtained by hydrolysis of titanium isopropoxide in excess of 2-propanol and subsequently heated in water at 85°C exhibits, indeed, the anatase structure. This points to an important role of the 2-propanol excess in the hindering of an agglomeration process, which promotes the titania sol transformation directly to the nanocrystalline TiO_2 particles affected by the heat treatment of the reacting mixture. The heating of the material obtained in the presence of the 2-propanol excess at 400–410°C could not significantly affect the width of the XRD peaks, which points to the absence of the intense growth of the anatase grains. Similarly to the reported results,[4] our TiO_2 material contains a small fraction of the brookite phase. The BET surface area of the titania precipitate obtained in excess of isopropanol and then dried at 85°C is about 240 m^2/g, being much larger than that of the P-25 titania. As expected, the drop-wise addition of titanium isopropoxide to a 5-wt% ammonia solution leads to formation of the ordered macroporous titania (OMT). This material is arranged by millimetre-sized, irregularly shaped TiO_2 grains that are fragments of larger particles with heterogeneous channel dimensions (5–8 mm, SEM). Under heating, the air-dried precipitates transform to a mixture of crystalline anatase and rutile, with a complete or partial retention of the macroporous architecture. The ratio between those two phases depends on the calcination temperature. The BET surface area of the air-dried precipitates was as high as 350 m^2/g. After calcination, this value decreased to 80–90 m^2/g, most likely due to sintering of the titania particles in the channel walls.[5]

The AT catalysts synthesised by a pH-controlled photocatalytic process contain silver particles with diameter of ca. 2 nm (TEM), homogeneously dispersed on the surface of TiO_2. Based on the binding energy of silver in the XPS spectra (around 367.0 eV), the coated silver on those catalysts is expected to be in the metal state. All these data agree very well with those previously published by Zhang et al.[3] Upon preparation of the PAT catalysts, the reduction of $[Ag(NH_3)_2]^+$ under ambient light in the P123-ethanol solution led to the formation of highly dispersed silver nanoclusters (the average size of ca. 2 nm) on the surface of titania (TEM and HRTEM). Most likely, the surfactant micelles and TiO_2 nanoparticles prevent aggregation of the silver clusters, as suggested by Zhang and Yu.[6] The silver in the silver-coated TiO_2 is of a metallic nature, as evidenced by the presence of the UV-Vis absorption band at 480 nm, attributed to the surface plasmon resonance of metallic silver. However, the atomic ratios of Ag/Ti in the PAT catalysts noticeably differ in relation to the amount of the $[Ag(NH_3)_2]^+$ solution used for their preparation. One of possible reasons for that could be incomplete reduction of the $[Ag(NH_3)_2]^+$ ions during 1-h ambient light illumination.[6]

In order to enable comparison with the literature data,[1] the catalytic experiments were performed using formic acid as the hole scavenger in the amount of 0.04 mol/l. It was found that, when the P-25 titania was utilised as a carrier for silver nanoparticles, the Ag/TiO_2 catalysts prepared by the two applied methods exhibited a similar denitrification efficiency. Hence, further study was conducted while applying the P123 triblock copolymer for inducing the reduction of $[Ag(NH_3)_2]^+$ in ethanol. The dependence of catalytic activity on the silver content in the synthesised catalysts is of a volcano-type shape (Figure 1) that has commonly been detected for a number of photocatalytic systems.

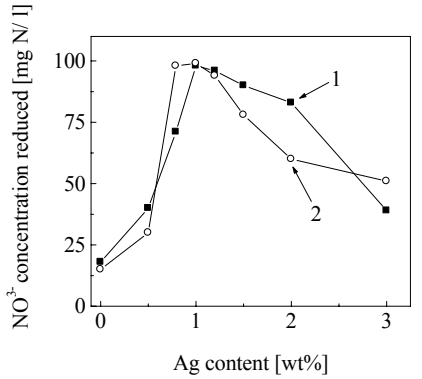

Figure 1. Influence of Ag loading on activity of differently prepared Ag/TiO_2(P-25) catalysts: (1) pH-controlled route, (2) ambient light reduction.

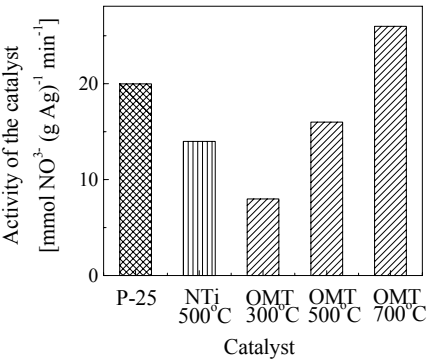

Figure 2. Influence of the TiO_2 origination on photocatalytic activity of Ag/TiO_2 catalysts.

To explain this feature, we have considered some optional hypotheses. It is well known that noble metal clusters can efficiently trap the photoinduced electrons.[1] At the same time, metal coating can reduce the photocatalytic ability due to the decreasing photoinduction efficiency of the semiconductor or because of formation of new recombination centres of photogenerated electrons and holes, when metal particles are too large. In the catalysts containing ca. 1% of silver, dispersion and/or size of coated Ag nanoparticles, most likely, provide in an optimum way prolongation of the lifetime of photogenerated electrons responsible for reduction of the nitrate ions, as manifested by the highest activity of these samples. Preliminary calcination of the NTi titania significantly improves activity of the Ag/TiO_2 catalyst prepared on its basis (Figure 2). Although the anatase structure of this material was already formed at 85°C, such a result indicates importance of the TiO_2 crystallinity, which increased upon heating, in the creation of a phocatalytic function of the Ag/TiO_2 system. The NTi-based catalyst exhibits a significantly larger surface area as compared to that of the P-25 titania; however, it shows somewhat lower activity. One option explaining

this finding is that this material contains a noticeable amount of micropores (as reflected in the shape of the N_2 adsorption isotherm) in which transfer of the formic acid molecules and/or nitrate ions to the active sites can be hindered. It cannot be excluded that the presence of the rutile phase in the P-25 titania can also favourably affect the photocatalytic activity of the resulting Ag/TiO_2 catalyst. This suggestion is supported by the results obtained using the catalysts prepared from the ordered macroporous titania, OMT (Figure 2). Under heating, OMT transforms to a mixture of crystalline anatase and rutile, the ratio of which depends on the temperature. Since such TiO_2, pre-calcined at 700°C, contains about 15–19% of the rutile phase (XRD), its photocatalytic behaviour can be compared with that of P-25.

It is interesting that the denitrification activity of the catalysts prepared using OMT pre-calcined at 700°C is higher than that of the materials synthesised from the P-25 titania. This can be attributed to the fact that hetero-junctions, such as anatase/rutile, Ag/anatase, and Ag/rutile, existing in the Ag/TiO2 multi-phase, can promote activity of those composite catalysts towards deni-trification. Also the macroporous architecture of the Ag/TiO_2 catalyst based on OMT could provide better mass transfer of the reacting hole scavenger molecules and nitrate ions and, thus, enhancement of the activity of the resulting catalysts. The preparation mode and origin of the titania support do not influence selectivity towards nitrogen formation of all the Ag/TiO_2 catalysts containing ca. 1 wt% of silver. Using the materials prepared from P-25 and OMT, it was possible to achieve the denitrification activity of about 20 and 25-26 mmol NO_3^- $(g\ Ag)^{-1}$ min^{-1}, respectively, with the selectivity to N_2 of ca. 100% after a 30-min illumination with UV.

4. Conclusions

The Ag/TiO_2 catalysts synthesised by both the pH-controlled photocatalytic process and the triblock copolymer-induced reduction of the $[Ag(NH_3)_2]^+$ ions under ambient light illumination are active and selective catalysts for the photocatalytic reduction of the nitrate ions in water. These differently prepared materials exhibit comparable catalytic behaviour although the same titania support was used. Nevertheless, the latter method is more preferable since it does not require use of the UV irradiation nor an energy-consuming thermal treatment process. The presence of hetero-junctions in the TiO_2 support enhances catalytic activity of the resulting Ag/TiO_2 catalysts. The ordered macroporous titania prepared by the drop-wise addition of titanium isopropoxide to ammonia seems to be a promising material for the synthesis of advanced photocatalysts for reduction of the nitrate ions in a water medium.

References

1. F. Zhang, R. Jin, J. Chen, C. Shao, W. Gao, L. Li, N. Guan, High photocatalytic activity and selectivity for nitrogen in nitrate reduction on Ag/TiO_2 catalyst with fine silver clusters, *J. Catal*. 232, 424–431(2005).
2. W. Gao, R. Jin., X. Guan, H. Zeng, F. Zhang, N. Guan, Titania-supported bimitallic catalysts for photocatalytic reduction of nitrate, *Catal. Today* 90, 331–336 (2004).
3. F. Zhang, N. Guan, Y. Li, X. Zhang, J. Chen, H. Zeng, Control of morphology of silver clusters coated on titanium dioxide during photocatalysis, *Langmuir* 19, 8230–8234 (2003).
4. K.I. Gnanasekar, V. Subramanian, J. Robinson, Direct conversion of TiO_2 sol to nanocrystalline anatase at 85°C, *J. Mater. Res.* 17(6), 1507–1512 (2002).
5. A. Collins, D. Carriazo, S.A. Davis, S. Mann, Spontaneous template-free assembly of ordered macroporous titania, *Chem. Commun.* 568–569 (2004).
6. L. Zhang, J.C. Yu, H.Y. Yip, Q. Li, K.W. Kwong, A.-W. Xu, P.K. Wong, Ambient light reduction strategy to synthesize silver nanoparticles and silver-coated TiO2 with enhanced photocatalytic and bactericidal activities, *Langmuir 19*, 10372–10380 (2003).
7. L. Zhang, J.C. Yu, A simple approach to reactivate silver-coated titanium dioxide photocatalyst, *Catal. Commun.* 6, 684–687 (2005).

SOL-GEL TEMPLATE SYNTHESIS OF THE ORIENTED MESOPOROUS THIN OXIDE FILMS AND NANOSTRUCTURES

GERMAN M. TELBIZ*, VICTORIA GONCHARUK, PETRO MANORYK
Institute of Physical Chemistry NASU, Pr. Nauky 31, Kyiv 03039, Ukraine

OKSANA LYTVYN
Institute of Semiconductor Physics NASU, Pr. Nauky 31, Kyiv 03039, Ukraine

CHRISTOPHER DEFRANOUX, ANTONIO MORENO,
SOPRA S.A., 26 rue Pierre Joigneaux, 92270 Bois Colombes, France

Abstract. In this communication, a different approach to the preparation of mesoporous SiO_2 and TiO_2 thin films and nanocomposites has been adopted, aimed at preparation of oriented mesoporous thin films with highly stable roughness of the film surface and controlled pore dimension. We describe the preparation and compositional analysis of thin film coatings prepared using sol-gel techniques (thickness 50–500 nm, roughness ± 0.5 nm with pore distribution 2.4–8 nm for silica oxide and up to 300 nm for titanium oxide and porosity 30–50%). Analyses of these systems were based on XRD, AFM, FTIR, and elipsometry porosimetry data. The structural evolution of the film during thermal treatment was observed by FTIR spectroscopy and XRD.

Keywords: Mesopous oxide film, spin coating, silica oxide, Titanium oxide, AFM/elipsometry porosimetry, structural evolution, nanocomposites.

* To whom correspondence should be addressed:. German Telbiz , Physic-Inorganic Chemistry Department Institute of Physical Chemistry, Nuke av., 31, 03028, Kyiv, Ukraine; e-mail: g_telbiz@yahoo.com

P. Innocenzi, Y. L. Zub and V. G. Kessler (eds.), *Sol-Gel Methods for Materials Processing*.

1. Introduction

In the recent years, a substantial progress in the synthesis and performance characterization of SiO_2 and TiO_2 based materials has been achieved. First, there has been an interest in the development of mesoporous dioxide thin films. The preparation procedures usually combine the use of structure directing agents in non-aqueous or highly acidic solutions for organizing the network forming dioxide species and the dip-coating technique. Thin mesoporous films of silicon and titanium oxide have extensive applications in many fields such as photoelectric devices, optical components, materials for analytical sensing and separations of environmental contaminates and enhanced environmental measurements.[1,2] In this communication, a different approach to the preparation of mesoporous SiO_2 and TiO_2 thin films and nanocomposites has been adopted, namely the preparation of oriented mesoporous thin films with highly stable roughness of the film surface and controlled pore dimension is aimed at.[3] The latter property is of utmost importance for the above mentioned materials for separations of environmental contaminates and enhanced environmental measurements such as photo catalytic degradation of organic compounds highly diluted in water for titanium surface, which is, as mentioned above, unfortunately further enhanced due to the illumination, precludes efficient adsorption of organic compounds on the photo-catalyst surface and their effective degradation.[4]

2. Experimental

Silica and titania mesostructured films have been produced using evaporation induced self-assembling processing via spin-coating. Ionic and non-ionic surfactants as structure–directing agents such as cetyltrimethylammonium bromide (CTAB), block copolymer (Pluronic F-123) and 18-Crown-6 and have been removed from the films by calcinations (350–500°C). A source of silica and titania was tetraethylortosilicate (TEOS) and titanium tetraisopropoxide (TIP). The stock and templating solution was finally stirred at room temperature and subsequently aged with stirring before the films were spin-coated onto glass slides, cleaned by "piranha" solution, at various speed for silica and titania in the range of 2,000–5,000 min^{-1}. Then the films were aged overnight, calcined by heating at a rate of 5°C/min to 350–500°C (depending on the template) and held for 4 h to remove the organic species.

The templated films have been characterized as function of the temperature of calcination by FTIR (Fourier Transform Infrared Spectroscopy) to obtain compositional information and allow checked degree of structural evolution of the films during thermal treatment. Spectra had been recorded in the 4,000–400 cm^{-1} range. Low angle X-Ray diffraction (XRD) was used to provide structural characterization. Texture parameters (Porosity and Pore Size Distribution) are

calculated from the isotherm of adsorption using the Kelvin equation by Elipsometry Porosimetry method using water as the adsorptive. The parameters were measured and then modeled using a dispersion law in order to determine its exact refractive index.[5] Once determined, the optical parameters of the substrate were then implemented in the sample model. All starting values were determined for the first measurement which had been performed for a relative humidity (RH) of 0% before any adsorption took place. Morphological parameters of the films were obtained by combining several techniques. The surface relief of the films was revealed by atomic force microscopy (AFM) using NanoScope D 300 (Digital instrument) .The details of the surface texture were provided by transmission and scanning electron microscopy (TEM, SEM), using a Hitachi S-900 apparatus.

3. Results and Discussion

Mesostructured films were obtained via evaporation-induced self-assembly, a deposition process, which is driven by the preferential evaporation of the solvent. Thin films of surfactant-templated mesoporous silica and titania have been prepared by a spin-coating method. In this method an oligomeric solution of silica or titanium was prepared prior to the addition of surfactant. Using the spin-coating method, the pore diameter could be controlled by surfactant chain-length as in bulk materials. In films with lamellar ordering, silica (titanium)/surfactant ratio value was found to control the wall thickness of the silica. Macroscopic cracks, which were observed in the films prepared by spin-coating, could be prevented by pre-treatment of the glass support with piranha solution: it was suggested that the pre-treatment invokes covalent bonds between the film and the substrate, and thus improves their adhesion.

The progress of mesostructure formation of the materials in the as-synthesized films was monitored by powder X-ray diffraction.[4] The as-synthesized and calcined silica films showed good optical quality, with thicknesses in the range of 30–700 nm. The XRD patterns of the films, in comparison with an as-deposited film, have shown decrease in *d*-spacing (equivalent to the increase in Bragg angle) suggesting that a contraction of the framework structure occurred in a direction perpendicular to the substrates, which resulted from the removal of the template as well as additional condensation of silanol (Si-OH) species.

The TiO_2 films calcined at temperature up to 300°C were amorphous by XRD. On the other side, diffraction peaks atlow Θ were found for the as dried film with template. Similarly these peaks disappeared after calcination at 300°C for Plutonic 123 film and 450°C for 18-Crown-6 template film. Diffraction peaks of crystalline TiO_2 (anatase) were found for samples calcined at 500°C. This result shows that surfactant was removed by heating in range 300–500°C. The XRD patterns hardly changed with the type and concentration of template. The

relatively wide width of the peaks indicates small crystallite size, which was estimated to be approximately 9 nm using Scherrer's equation from the XRD peak broadening analysis at (101).[26] For the Crown templated TiO_2 film the crystallite size was more uniform and was estimate as 10 nm. It is worth to note that the crystallite size was in the range of 8–10 nm, which is known to be optimum for high catalytic activity. For the Crown templated TiO_2 film the crystallite size was more uniform and was estimated as 10 nm.

The microstructural evolution of the films during thermal treatment, up to a complete removal of the organic phase, was observed by FTIR Spectroscopy. Spectra had been recorded in the 4,000–400 cm^{-1} range. The absorption band related to C-H mode vibration of the surfactant was detected in wave number range 2,700–3,000 cm^{-1}. For example, for the sample containing Pluronic as template, this band was complete absent after the 350°C thermal treatment. At 3,000–3,750 cm^{-1}, instead, there was the band of –OH groups, at 1,640 cm^{-1} the absorption of molecular water and finally at 500–1300 cm^{-1} the band related to the silica polymerization. In the 3,800–3,700 cm^{-1} spectral region two overlapped regions of vibrational modes can clearly be distinguished. The first one in the lower wave number range, due to absorption of organic groups in Pluronic F127, can be taken as a signature of the presence of the block co-polymer within the material, and next one at higher wavenumber due to hydroxyl's absorption. This broad band appears as composed of several overlapping bands assigned to different types of O-H vibrational modes. In particular, at the low wave number side three overlapped vibrational modes at 3,743, 3,676 and 3,635 cm^{-1} are appeared. According to literature data this bands are assigned as: free single silanol groups; pairs of silanols mutually hydrogen bonded where only one oxygen is participating in the hydrogen bonding and the same pairs of silanols where hydrogen atoms form H-bonds with an oxygen atom of an adjacent silanol respectively. These bands appear only after calcination at over 150°C.

Similar results can be obtained for samples synthesized using other surfactant. After calcination at 350°C, the templating agents were removed (the block copolymer bands disappeared) whilst the –OH concentration increased in intensity in comparison with the non-mesoporous silica film (broad band in the 3,750–2,800 cm^{-1} range). For a film synthesized with CTAB and 18-Crown-6 as templating agent the surfactant (bands at 2,950 and 2,860 cm^{-1} was removed upon thermal calcination between 500°C and 550°C. FTIR study of short-range and local order in silica films was used for the crystallization analysis of the structure in situ. Correlation was found between shift maximum of Si-O-Si bands and the crystallization of the SiO_2 film structure. The finished spectra show that film is considered as a mixture of four- and six-fold rings of SiO_4 tetrahedra.

The Elipsometric Porosimetry investigations data are presented in Figure 1 by isotherms of water-adsorption-desorption for all prepared films. These isotherms are reported in terms of volume percent of water adsorbed at relative

pressure of water applied at the film atmosphere. The first information is the porosity of each film that corresponds to the maximal volume of water adsorbed at high pressure. The maximal porosity is measured to be 47% at room temperature for calcined films. The second part of very useful information is a possibility to extract from isotherms the type of pore distribution and inter-connection between them. All plotted isotherms show stiff adsorption and desorption sloops at different relative pressures.

They revealed that pores do grow in diameter 2.5–4 nm for STAB and from 5–7 nm for Pluronic 127 surfactant. In case of titanium oxide film we observes the pore do grow from 4 up to 100 nm in case of 18-Crown-6 as template.

Surface topographies of SiO_2 and TiO_2 mesoporous film have been revealed by AFM. Figure 2 compares the AFM images of typical mesoporous titania films obtained using of different template. Indeed a more regular topography is observed for the Pluronic-127 template derived films. Figure 2 shows that the

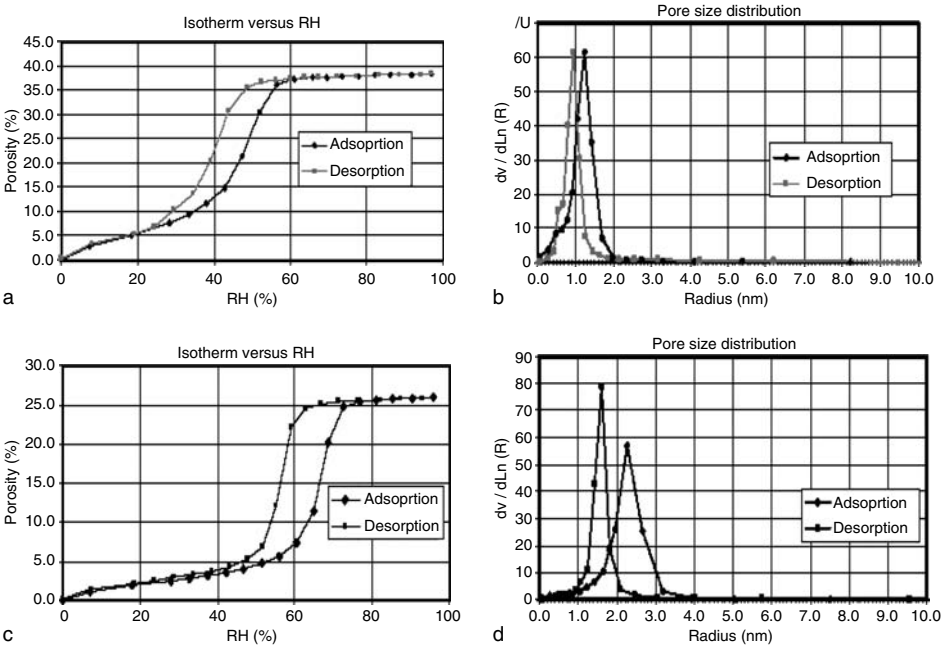

Figure 1. Adsorption-desorption isotherms (a, c) and pore size distribution from branches of isotherms (c, d) plotted for silica films templated by STAB (a, b) and triblock sopolimer (c, d).

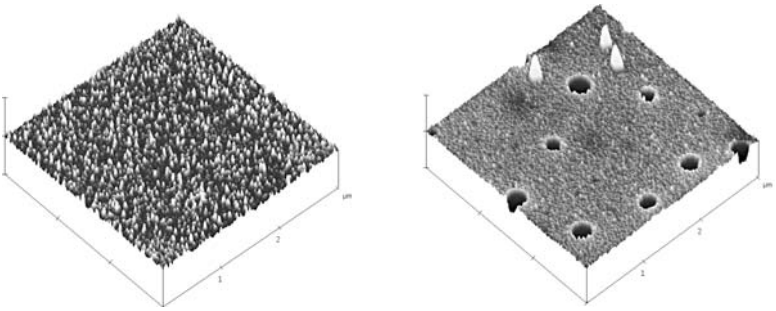

Figure 2. AFM image of calcined TiO2 films template by triblock copolimer (a) and 18-Crown-6 (b).

surface morphology of the 18-Crown-6 template film is rougher than that of the triblock copolymer films. The high roughness structure observed by AFM for 18-Crown-6 template attributed to the another mechanism of crystallisation of films when 18-Crown-6 template used. The STAB films presented morphologies with a surface roughness between 0.5 and 0.6 nm, Pluronic are 2–3 nm and for 18-Crown-6 up to 40 nm with quasi regular pores approximately 100 nm.

4. Conclusions

Macrostructure silica and titania films have been prepared by sol-gel method using different surfactants as template by a spin-coating method. We describe the preparation and compositional analysis of thin film coatings prepared using sol-gel techniques (thickness 50–500 nm, roughness ±0.5 nm with pore distribution 2.4–8 nm for silica oxide and up to 300 nm for titanium oxide and porosity 30–50%). Furthermore, the morphology and microstructure is strongly affected by organic template. Finally we have evaluated their possible applications as matrix for various nanostructures (semiconductor, dyes, and polymer) nanocasting such as sensing membranes for chemical sensor devices.

References

1. N. Kitazawa, H. Namba, M. Aono, Y. Watanabe, Sol–gel derived mesoporous silica films using amphiphilic triblock copolymers. Journal of Non-Crystalline Solids, **332**, 199–206 (2003)
2. H. Choi, E. Stathatos, D. Dionysiou, Synthesis of nanocrystalline photocatalytic TiO_2 thin films and particles using sol–gel method modified with nonionic surfactants. Thin Solid Films, **510**, 1–2, 107–114 (2006)

3. K. Chao, P. Liu, K. Huang, Thin films of mesoporous silica: characterisation and application. C. R. Chimie, **8**, 727–739 (2005)
4. H. Choi, E. Stathatos, D. Dionysiou, Sol–gel preparation of mesoporous photocatalytic TiO_2 films and TiO2/Al2O3 composite membranes for environmental applications Applied Catalysis B: Environmental, **63**, 60–67 (2006)
5. M. Losurdo, M. Hiangregorio, G. Bruno, F. Poli, L. Armelao, E. Tondello. Porosity of mesoporous silica thin films: kinetics of the template removal process by ellipsometry Sensors and Actuators B: Chemical, **126**, 1, 168–173 (2007)

MODIFICATION OF NATURAL ALUMOSILICATES SUSPENSIONS BY CATION-ACTIVE ORGANIC COMPOUNDS AND STUDY OF STRUCTURAL-SORPTION PROPERTIES OF THUS PREPARED SORBENTS

MARYNA YU. TRYFONOVA, SVETLANA V. BONDARENKO, SVETLANA A. DOLENKO, ZINAIDA G. IVANOVA, YURI I. TARASEVICH*

Institute of Colloid Chemistry and Chemistry of Water, Ukrainian National Academy of Sciences, 42 Vernadsky Avenue, Kyiv 03680, Ukraine

Abstract. The modification by cationic surfactants of sorbents based on hydromica and kaolinite – layered silicates with rigid structural cell – was performed by a modified sol-gel method. It was shown that the modification leads to sharp decrease of the minerals hydrophilicity, and to the increase of their affinity to the molecules of anionic and non-ionic surfactants. Significant increase of the sorption capacity of modified minerals with respect to non-ionic surfactants was ascribed to the formation of bulk associates of cationic and non-ionic surfactants.

Keywords: Modification, clay minerals, adsorption, surface, hydrophilicity, cationic surfactant, anionic surfactant, nonionic surfactant.

1. Introduction

The modification of clay minerals from aqueous dispersions by substitution of natural cations in their exchange complex by organic cations from the solution, and the properties of thus obtained sorbents were studied quite extensively.[1,2] However, these works have dealt mainly with the mineral sorbents with swelling structural cell (montmorillonite, vermiculite), while the similar studies

* To whom correspondence should be addressed: Yuri I. Tarasevich, Institute of Colloid Chemistry and Chemistry of Water, Ukrainian National Academy of Sciences, 42 Vernadsky Avenue, Kyiv 03680, Ukraine; e-mail: yuitaras@thomascat.kiev.ua

P. Innocenzi, Y. L. Zub and V. G. Kessler (eds.), *Sol-Gel Methods for Materials Processing*.

of layered alumosilicates with rigid structural cell (especially hydromica) are quite scarce. In particular, almost no attention was devoted to comprehensive studies regarding the structural-sorption properties of organoderivatives of hydromica and structurally imperfect kaolinite. At the same time, the structural features of these minerals make it possible to obtain surfaces with necessary hydrophobicity using much lower amount of modifier. It is to be noted also that the hydromica from Cherkasy deposit (Ukraine) is promising for industrial applications: it possesses high dispersity and, therefore, quite high specific surface area, which essentially determines the adsorption capacity of the sorbent.

In view of the considerations presented above, we performed a comprehensive study of structural-sorption properties of sorbents prepared by modification of these natural alumosilicates with rigid structural cell by cationic surfactant (cetyl pyridinium bromide) from their aqueous dispersions with subsequent isolation of the disperse phase by centrifugation (modified sol-gel technology method).

2. Experimental

All impurities and inclusions visible by an unaided eye were eliminated in advance from studied samples of natural minerals. The enrichment of the samples was performed then by wet elutriation according to.[3] The cation exchange capacity of the samples was determined by inverse conductometric titration[4] of the Ba-forms of the minerals obtained earlier.[5]

The modification process was as follows. The elutriated natural mineral in the form of suspension was brought into contact with cetyl pyridinium bromide; the sorbent concentration was 3.5–3.8 g/dm^3, and the amount of the cationic surfactant was by a factor of 1.3 larger than the cation exchange capacity of the corresponding mineral. The duration of the contact between the clay dispersion and the surfactant solution was 3 days; the stirring was applied periodically. The settled solution was decanted; the precipitate was washed out three times by distilled water, and then compacted by centrifugation (2,000 rpm) in 5 minutes. Then the physically bound modifier was washed out from the sorbent by seven-fold processing by water/alcohol (1:1) solution with intensive stirring and centrifugation (2,000 rpm) in 5 minutes and, subsequently, by four-fold processing by distilled water. Thus prepared sorbent was dried at 60°C. The amount of modifier adsorbed on the clay surface was determined by combustion technique.[6]

The low-temperature adsorption/desorption of nitrogen vapours on natural and modified minerals was studied using the NOVA 2200e device (Quantachrome, USA). The natural and modified samples were preliminary evacuated at 150°C

and 110°C, respectively. The BET values of specific surface area with respect to nitrogen $S(N_2)$, limiting adsorption volumes V_S and the plots of pore volume distribution of the sorbents with respect to pore radius were obtained using the device software.

The adsorption/desorption isotherms were recorded using the vacuum adsorption device with the McBain quartz spring balance at 26°C and 24°C for n-hexane and water, respectively; the preliminary evacuation temperature of the samples was 110°C. From the adsorption/desorption isotherms of n-hexane and water, the values of specific surface area, arbitrary monolayer capacity, the energy constant C and the area per one water molecule were calculated via the BET equation; the pore volume distribution of the sorbents with respect to the effective pore radius were determined using the Kelvin-Thomson equation. The specific surface areas of the sorbents with respect to hexane were calculated assuming its molecular area to be equal to 0.5 nm^2.

To determine the integral heat of wetting of the sorbents by water Q, the samples were loaded into glass sample tubes and evacuated during 6 hours at 150°C and 110°C for natural and modified samples, respectively. Then the sample tubes were sealed in vacuum and placed into the microcalorimeter. The integral heat of wetting was measured as described in.[7] The specific heat of wetting was calculated as $q = Q/S(N_2)$.

To study the adsorption of various types of organic substances from the solutions, an anionic surfactant, sodium dodecyl sulphate (DDSNa), and the non-ionic surfactant APh_9-10, which contains 10 oxyethyl groups and a C_9 hydrocarbon chain were chosen. To obtain the adsorption isotherms, the weighted amounts (0.1 g) of fine fraction (<0.2 mm) of the sorbents were immersed into 50 cm^3 of adsorbate solutions with concentrations of 0.02– 5.6 g/dm^3 (DDSNa) and 0.06–12.11g/dm^3 (APh_9-10). The adsorption equilibrium was established via continuous shaking during 6 hours at 24°C (DDSNa adsorption), 19°C and 16°C (APh_9-10 adsorption on natural and modified kaolinite, respectively). The spectrophotometric measurements of the surfactants concentration in the equilibrium solutions was performed using the SF-26 device: for DDSNa – from extraction-photometric method[8]; for APh_9-10 – from the intrinsic adsorption of the fugate (8,000 rpm, 60–90 minutes); for the modified sorbent the two-wave spectrophotometry[9] was used.

3. Results and Discussion

It can be seen from Table 1 that the amounts of the sorbed modifier were approximately equal to the cation exchange capacities of the studied minerals, indicating that the modifier, which remained on the samples surface was adsorbed due to the ion-exchange mechanism.

TABLE 1. Cation exchange capacity of sorbents and amount of the modifier sorbed thereon.

Adsorbent	Cation exchange capacity, mg-eq/100 g	Amount of modifier, mg-eq/100 g
Kaolinite	25	30
Hydromica	27.5	27

TABLE 2. Structural-sorption characteristics of studied sorbents.

Adsorbent	Adsorbate									q, mJ/m^2
	N_2			C_6H_{14}				H_2O		
	S, m^2/g	V_S, cm^3/g	r, nm	S, m^2/g	r, nm	C (BET)	a_m, mmol/g	a_m, mmol/g	ω, nm^2	
Kaolinite natural	69	0.13	2.0; 4.7	69	2.0–2.2; 5.9–7.4	15.0	0.23	1.39	0.08	661
Kaolinite modified	39	0.08	2.2; 3.9; 6.2	57	2.2; 3.5; 7.8	6.7	0.19	0.49	0.19	258
Hydromica natural	160	0.26	2.0; 6.3–8.8	161	1.2; 6.6–7.2	31.4	0.54	2.55	0.10	450
Hydromica modified	69	0.14	2.2; 4.8–6.1	92	2.3; 4.9–6.8	6.2	0.31	0.85	0.13	361

Table 2 summarises the structural-sorption characteristics of the studied sorbents obtained from the analysis of data for the adsorption from vapour phase; also the values of specific heat of wetting are listed. It can be seen that both the natural and modified sorbents are mesoporous materials. The modification leads to the decrease of the specific surface area with respect to the nitrogen and hexane due to the aggregation of the sorbent particles caused by the influence of cationic surfactant. The data of water adsorption and specific heat of wetting indicate that the modification results in the hydrophobisation of the sorbents.

Adsorption isotherms of anionic surfactant on natural and modified sorbents are shown in Figure 1; the results are illustrated also by Table 3. It can be seen that the shape of the isotherms in the initial coverage range for the modified sorbents is essentially different from that for the natural ones. In particular, the degree of extraction of anionic surfactant from water for modified samples in the initial coverage range is more than by a factor of two higher than that for the natural samples.

The APh_9-10 adsorption isotherms on natural and modified kaolinite are shown in Figure 2. It can be seen that the modification results in a essential increase of the sorption capacity of kaolinite with respect to the non-ionic surfactant.

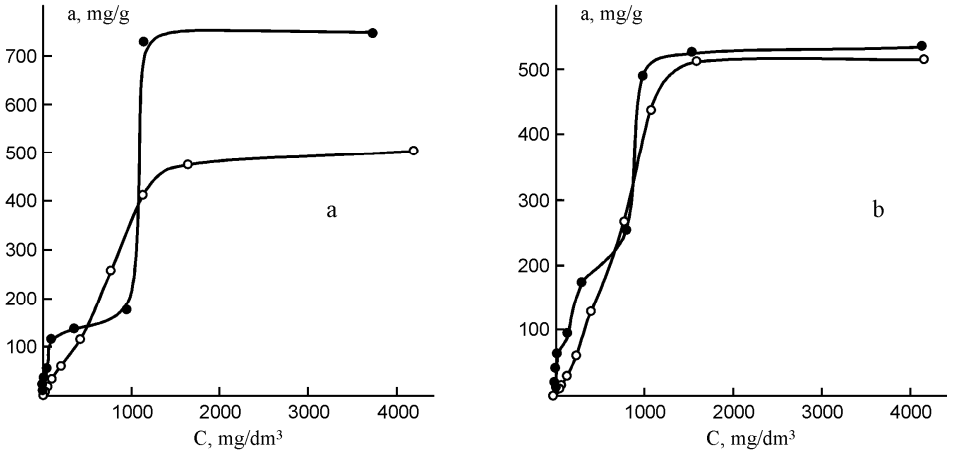

Figure 1. Sodium dodecyl sulphate adsorption isotherms on (a) hydromica and (b) kaolinite at 24°C; adsorption on: ○ natural, and ● modified samples.

TABLE 3. Equilibrium concentrations C_{eq}, adsorption a and extraction degree R of DDSNa from aqueous solutions with initial concentration C_0 = 81.25 mg/dm^3 by natural and modified sorbents.

Adsorbent	C_{eq}, mg/dm^3	a, mg/g	R, %
Kaolinite natural	49.50	15.88	39.08
Kaolinite modified	0.01	40.54	99.99
Hydromica natural	45.40	17.93	44.12
Hydromica modified	7.50	36.84	90.77

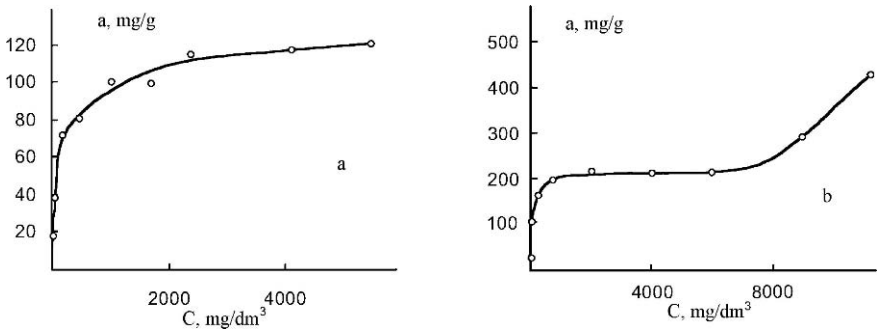

Figure 2. APh_9-10 adsorption isotherm on kaolinite: (a) natural at 19°C and (b) modified at 16°C.

The degree of the non-ionic surfactant extraction at the initial solution concentration $C_0 \sim 5.5$ g/dm^3 is 90%. This behaviour of the modified sorbent with respect to the non-ionic surfactant is due to the formation of bulk associates of

cationic and non-ionic surfactants. Our preliminary data indicate similar behaviour for the modified hydromica.

4. Conclusions

It is shown that the studied sorbents possess inhomogeneous porous structure in which mesopores prevail. The modification results in significant decrease of the hydrophilicity of natural sorbents, and sharp increase of the adsorption and the extent of the anionic surfactant extraction in the low sorbent surface coverage range. The sorption capacity of modified sorbents increases by dozens of times with respect to non-ionic surfactants.

References

1. B.K.G. Theng, *The Chemistry of Clay-organic Reactions* (Wiley, New York/Toronto, 1974).
2. E.V. Sharkina, *Structure and Properties of Organomineral Compounds* (Naukova Dumka, Kyiv, 1976) (in Russian).
3. Yu.I. Tarasevich, F.D. Ovcharenko, *Adsorption sur des Minéraux Argileux* (Institut Français du Pétrole, Rueil Malmaison, 1980).
4. N.G. Vasiliev, L.V. Golovko, F.D. Ovcharenko, A.G. Savkin, Study of cation exchange capacity of kaolinite with various degree of crystallinity, *Colloid Journal (USSR)* 38, 847–852 (1976) (in Russian).
5. V.E. Polyakov, Yu.I. Tarasevich, O.L. Alekseev, Preparation of cation-substituted forms of clay minerals, *Ukrainian Chemical Journal* 34, 526–528 (1988) (in Russian).
6. E.V. Arinushkina, *Manual for Chemical Analysis of Soils* (Moscow University, Moscow, 1961) (in Russian).
7. V.E. Polyakov, I.G. Polyakova, Yu.I. Tarasevich, Peculiarities of the determination of heats of wetting of disperse minerals with low specific surface area, *Colloid Journal (USSR)* 38, 188–191 (1976) (in Russian).
8. Yu.Yu. Lourier, *Analytical Chemistry of Industrial Waste Waters* (Khimiya, Moscow, 1984) (in Russian).
9. I.Ya. Bershtein, Yu.L. Kaminskiy, *Spectrophotometrical Analysis in Organic Chemistry* (Khimiya, Leningrad, 1975) (in Russian).

OPTICAL SPECTRA AND MORPHOLOGY OF PHOTOCHEMICALLY PRODUCED Ag/Au BIMETALLIC CLUSTERS

HALYNA YASHAN[1], ANNA EREMENKO[1*], NATALIA SMIRNOVA[1], GALINA KRYLOVA[2], WENYU HUANG[2], CHRISTOPHER TABOR[2]
[1]*Institute of Surface Chemistry, Ukrainian National Academy of Sciences, 17 General Naumov Str., Kyiv 03164, Ukraine*
[2]*Laser Dynamic Laboratory, School of Chemistry and Biochemistry, Georgia Institute of Technology, Atlanta, GA 30332, USA*

Abstract. The Ag-Au alloy and core-shell bimetallic nanoparticles (BMNP) in colloids can be successfully prepared by photoinduced reduction of corresponding salts in the presence of SiO_2/BP_{ads} (silica film with adsorbed Benzophenone) photocatalyst in water-IPA solution as a source of ketyl radicals and BP anion-radicals as the reductive agents, and CTAB as a stabilizer. Generation of BMNP during the photochemical process happens right away of UV-irradiation. The ageing of bimetallic colloids related with formation and stabilization of the alloy–to–core-shell structure occurs with time (from hours to days) and depends on the order of metal ions photoreduction, viz simultaneous or successive UV irradiation of silver and gold ions in solution, and varying of Ag/Au mole ratio. Ageing of photoproduced colloid nanocomposites accompanied by the change of structure from alloy to core-shell what is proved with UV-vis absorption spectra. Optical spectra demonstrate formation of core-shell structures, where the shell is enriched with the core atoms. For now, first conclusion should be that BMNP Ag:Au 1:1 in colloids are formed mainly with Au NP's in the shell. Photochemically produced and stabilized within pores of silica film Ag/Au BMNPs are formed as separate Ag and Au NP's, together with the big aggregates.

Keywords: Photoinduced reduction, silver, gold, bimetallic nanoparticles, core-shell, alloy, UV-spectra, TEM, SEM.

[*] To whom Correspondence should be addressed Professor Anna Eremenko, e-mail: annaerem@ukr.net

P. Innocenzi, Y. L. Zub and V. G. Kessler (eds.), *Sol-Gel Methods for Materials Processing*.

1. Introduction

One of the recent research targets in the field of new and advanced materials is the synthesis of composite nanoparticles, in which two or more metals coexist and enhance the tailored properties, i.e. catalytic, bactericide, optical etc. Bimetallic nanoparticles can exhibit electronic, optical and catalytic properties that are distinct from those of mono-metal particles, prompting numerous preparations of layered core-shell, alloys, nanorods, gold-coated silver particles, nanorattles, nanotubes etc.[1–12] Ag-Au bimetallic nanoparticles receive significant attention because of their optical and electrochemical properties. There are four basic concepts for BMNP behaviour manipulation: size and shape control, regulation of counterparts' concentration, production of layered structures and nanocrystal ordering. A variety of preparation methods have been used, such as photoreduction,[13] chemical reduction in aqueous medium with stabilizing polymers[14] and in reverse micelles[15] or thermal decomposition.[16] Chemical and thermal reduction ways demand either expensive reagents or require much more energy and time to produce metal nanoparticles, than the photochemical way, which is energy and time conserving.[17,18]

In this work, the photochemical preparation of Ag-Au bimetallic nanopaticles in colloid form and embedded in silica films in the presence of a photocatalytic element SiO_2/BP (benzophenone) developed by us[17,18] has been studied. Porous sol-gel produced silica films and powders modified with adsorbed benzophenone (BP) molecules have been found to be effective in photoreductive formation of nanosized silver and gold nanoparticles in colloids and solids.[17,18] Bimetallic Ag/Au compositions have been prepared by simultaneous photoinduced coreduction of silver and gold ions or successive reduction of one metal over the nuclei of another in presence of silica/BP systems. UV-vis, DRS, TEM and SEM techniques have been used for the characterization of the compositions under investigation.

2. Experimental

2.1. REAGENTS

The following chemicals: Silica gel (SG-150Å Davisil) with specific surface area of 300 m^2/g (Aldrich), $AgNO_3$, $HAuCl_4$, CTAB, Pluronic P123 and tetraethoxysilane 98% (TEOS) (Aldrich) were used as received. Benzophenone (BP, Fluka) was purified by double recrystallization from ethanol. Isopropyl alcohol (IPA) (Fluka) and hexane (Fluka) were purified by repeated distillation.

2.2. SILICA FILM PREPARATION

The mesoporous silica films have been prepared by the sol-gel method using template nonionic tri-block copolymer Pluronic $EO_{20}PO_{70}EO_{20}$ (P123, Aldrich) by the technique described in literature.[19,20] The precursor sol was prepared by hydrolysis of TEOS in a mixture of distilled water, ethanol (Fluka), and 1 M HNO_3 solution. After 24 h of prolonged hydrolysis, an ethanol solution of P123 was added. The total molar ratio of the precursor was 1 TEOS: 0.008 P123: 0.16 HNO_3: 15 H_2O: 15 C_2H_5OH. The coatings were deposited onto clean glass substrates by dip-coating technique. The films were dried for 12 h at ambient temperature, followed by heat treatment at 400°C with a rate of 1°C/min and held at 400°C for 6 h. The films have been used as the base to be modified with BP as well as the carrier of Ag/Au composites.

2.3. MODIFICATION OF SILICA FILMS AND POWDERS WITH BP VIA ADSORPTION

The adsorption of BP on the silica gel powders and SiO_2 films thermally pre-treated at 250°C was carried out from hexane solution. To measure the adsorption isotherm, the samples of silica gel were placed in the BP hexane solution with the initial concentration in the range of 10^{-5} to 10^{-3} M for 24 h until the adsorption equilibrium was achieved. The amount of adsorbed BP molecules was monitored by the measurement of the optical density of BP-hexane solution at 355 nm before and after adsorption using a Lambda UV-Vis spectrophotometer (Perkin Elmer). Special experiments defined that optimal amount of BP to initiate photoreduction of Ag and Au salts in solution is 8% of monolayer covering of silica surface.[21,22] In this case BP is strongly immobilized on the hydroxylated silica surface via H-bonding and no desorption of BP into solution from silica surface during UV-irradiation of Ag-Au salts occurred.

2.4. PHOTOREDUCTION EXPERIMENT

Porous silica powders and SiO_2 films with adsorbed BP (SiO_2/BPads) have been used as catalysts in the photochemical reduction of both silver and gold ions in water-alcohol solvent under mercury lamp irradiation. The catalyst was removed immediately after irradiation and the absorption spectra of the irradiated solutions were measured. A monochromatic 1,000-W high-pressure mercury lamp was used as an irradiation source for 253.7 nm light. The reaction cell was a cylindrical quartz vessel having a volume of 25 ml. Incident photon intensity (as determined by a tris(oxalato)ferrate(III)actinometer[17]) was determined at 253.7 nm to be $2 * 10^{17}$ cm^{-2} s^{-1}. Irradiation of the solution was carried out while bubbling argon through it at room temperature. The absorption spectra of the Ag-Au salt solutions before and after irradiation were measured with a Lambda

UV-Vis spectrophotometer (Perkin Elmer) in a rectangular 1 cm thick quartz cell. Diffusion reflectance spectra of SiO_2-BP films and SiO_2-BP powders were also measured with this spectrophotometer. For the TEM measurements of silver nanoparticle solutions, a drop of solution was allowed to dry overnight on a carbon coated copper TEM grid (Ted Pella) and imaged using an accelerating voltage of 100 kV in the JOEL JEM-100C transmission electron microscope (TEM). A scanning electron microscope (SEM) (LEO 1530) was used to probe the SiO_2-Ag film.

The formation of Ag-Au nanoparticles within the thin silica film has been achieved by introducing their ions in the SiO_2 porous matrix on the basis of 10 wt% Ag + Au NP's and the subsequent irradiation in the BP-IPA medium.

3. Results and discussion

3.1. Ag/Au BMNP IN COLLOID SOLUTIONS

We investigated the morphological, structural, compositional and spectral changes of Ag-Au BMNP photochemically produced in water-IPA (40:1) solution in presence of SiO_2/BP film or powder as photosensitizer and CTAB as stabilizer of NP's.

Principal scheme of photoreductive process is shown in.[18,19] The proposed reaction mechanism includes formation of triplet state of adsorbed BP followed by hydrogen atom abstraction by BP triplet from i-propanol and formation of two ketyl radicals, then protolytic dissociation of ketyl radicals and reduction of silver ions by the BP anion radicals leading to metal nanoparticles formation. Changes in the absorption spectra of colloidal solution during BMNP formation (after photolysis in presence of SiO_2/BP film) are presented in Figures 1 and 2. Corresponding changes in particles' size distribution and morphological changes monitored by TEM are shown in these figures too.

By simultaneous photochemical co-reduction of silver and gold ions with Ag:Au molar ratio 1:1, right away of irradiation, the intensive absorption band with maximum at 463 nm belonging to the Ag-Au alloy and located between SPR spectra of gold (520 nm) and silver(420 nm) appeared (Figure 1). After 60 min of irradiation the optical density of the absorption band remains constant. In dark storage, bimetallic alloy absorption spectrum of BMNP composition is changed, the maximum being shifted to the one typical for Au NP position. Intensity of light absorption decreases in time during 10 days, later not changing for months. Optical spectra and TEM image of this composition are evidence of the de-alloying of Ag/Au alloy and its transfer to core-shell structure with facing Au NP (Figure 1). TEM image of this composition corresponds to the core-shell structure. Besides, TEM image encloses another particles corresponding to the NP aggregates, probably alloy particles. Average diameter of NP corresponds to 2–10 nm.

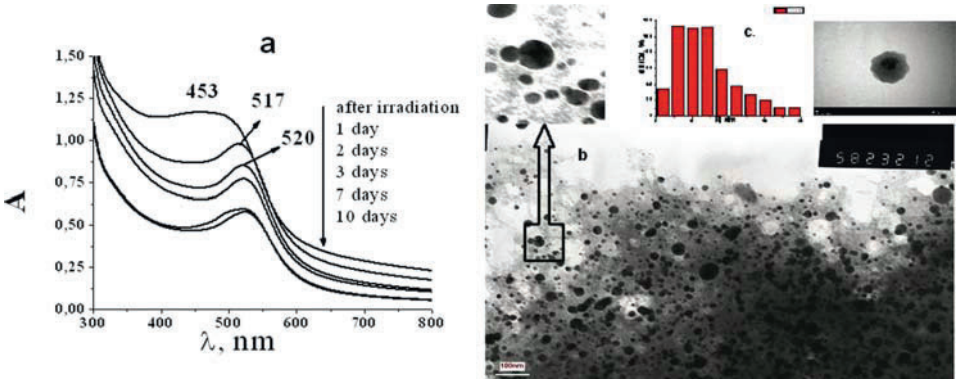

Figure 1. Optical spectra of Ag/Au BMNP prepared under 60 min UV-irradiation (1) of Ag and Au salts (1:1) in presence of SiO_2/BP as a sensitizer in the water – IPA – CTAB solution under Ar bubbling and 1–10 days-ageing (2–6) (a). TEM images of core-shell structure and aggregates formed in 24 h. Scale bar 100 nm (b). BMNP size distribution (c).

Ag/Au core-shell structure was photochemically formed also under successive reduction of gold over the nuclei of silver atoms. Spectral evolution of the plasmon band of the Ag core coated with Au NP's at different times of irradiation is shown in Figure 2. Ag NP's alone have been formed as first step of the BMNP photoreduction. SPR spectrum of silver NP's is formed in 20 min of irradiation with maximum at 415 nm. After that, $HAuCl_4$ solution has been added under continuous irradiation. Optical spectrum changed dramatically in 1 min demonstrating appearance of Ag/Au alloy (max 466 nm) and Au nanoparticles

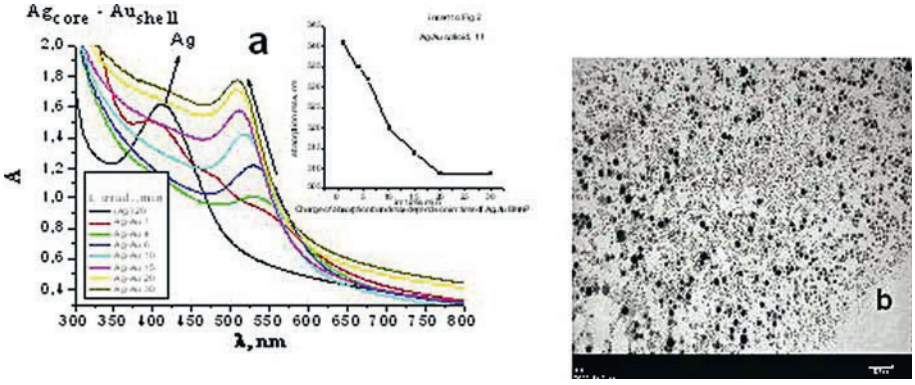

Figure 2. Kinetics of Ag/Au BMNP photoproduction. Kinetics of Ag/Au BMNP photoproduction in colloid solution by sequential irradiation AgNO3 ($7.5 \cdot 10^{-8}$ M) 30 min, whereupon $HAuCl_4$ ($7.5 \cdot 10^{-8}$ M) was added and irradiated, CTAB = $4.5 \cdot 10^{-4}$ M, SiO_2/BP, Ar bubbling (a). TEM image of the particles, scale bar 100 nm (b).

(max 536 nm) as the transient states of formation of photo-reduction products. This state is non-stable. During next 30 min of UV-irradiation the position of max absorption band of AuNP shifted from 536 to 507 nm. Absorption band is not symmetrical, rising in the Ag NPs area (Figure 2). The shape of the NP's is shown in the TEM image. It seems that in this case the Ag core/Au shell NP's enriched in the outer layer with Ag have been formed. The Ag atoms interdiffuse in Au shell. The spectral max positions at 509 nm is stabilized after 20–30 min of irradiation (Figure 2), and formation of core-shell structure is probably completed within this time.

The formation rate of Au nanoparticles is faster than that of Ag nano-particles. Depending on sequence of introduction of Ag(Au) ions in the irradiated solution, we have gained two type of core-shell structures, with Ag or Au shell. When Ag is positioned on the shell, we observed two distinct bands (Figure 3a). The spectra simulations confirm the existence of separate Ag and Au NP's (Figure 3b).

Dependence of the SPR maxima on Ag/Au ratio is linear till 30–35% of gold in the binary (Figure 4), excess of gold results in the Au NP's accu-mulation in the shell of particles.

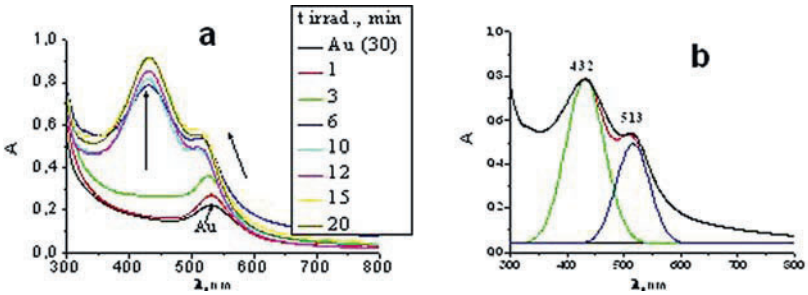

Figure 3. Kinetics of Ag/Au BMNP photoproduction in colloid solution by sequential irradiation $HAuCl_4$ ($7.5 \cdot 10^{-8}$ M) 30 min, whereupon AgNO3($7.5 \cdot 10^{-8}$ M) was added and irradiated, CTAB = $4.5 \cdot 10^{-4}$ M, SiO_2/BP , Ar bubbling (a). Simulation of optical spectrum obtained after 20 min of irradiation (b).

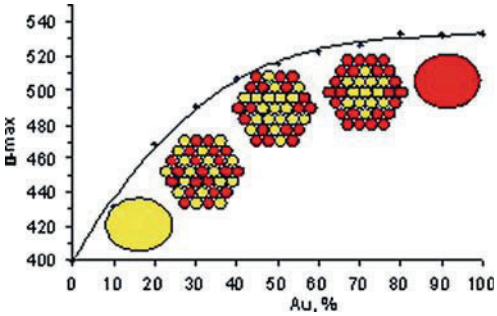

Figure 4. Dependence of SPR spectral maxima on Ag:Au ratio in BMNP colloids.

3.2. Ag/Au BMNP WITHIN SILICA FILM PORES

Kinetics of photochemical production of 10 wt% Ag and Au NP's (Ag:Au 1:1) within porous silica films is shown in Figure 5. Intensity of the SPR increased monotonously with time of irradiation and in 60 min was completed. Position of Au SPR spectrum is stable during irradiation (shift from 551 to 547 nm), maximum position of Ag NP's wide band at 435 nm transformed to the shoulder with max approx. 424 nm (Figure 5). Intensity of absorption bands increased under irradiation concurrently. The simulation of the spectra brings three separate absorption bands belonging to Ag NP's, Au NP's and big aggregates with absorption maximum at 840–940 nm. We suggest that in this case silver and gold NP's have been formed as separate particles in the porous silica matrix. Photoproduced BMNP in colloid form and being adsorbed on dispersive silica revealed good bactericide activity. This part of study is in progress.

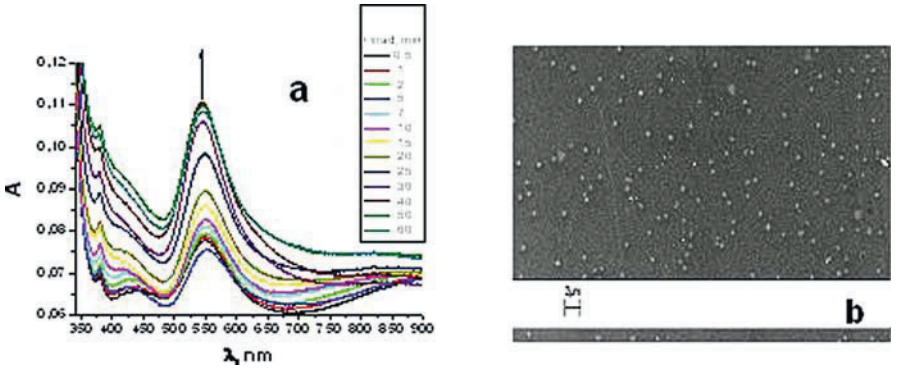

Figure 5. (a) Kinetics of accumulation of Ag/Au NPs within silica film pores under UV-irradiation of adsorbed Ag and Au ions with Ag:Au ratio 1:1 in presence of SiO_2/BP as photosensitizer. (b) TEM image shows the formation of Ag spheres and Au triangles within silica film.

4. Conclusions

Thus, the Ag-Au alloy and core-shell nanoparticles in colloids can be successfully prepared by photoreduction of corresponding salts in presence of SiO_2/BP photocatalyst in water-IPA solution as a source of ketyl radicals and BP anion-radicals, and CTAB as stabilizer. Formation of alloy or core-shell structures depends on the order of photoreduction – simultaneous (Ag + Au salts) or successive (Ag or Au salt is photoreduced one after another) adding in the solution under UV irradiation, and varying of Ag/Au mole fraction. Ageing of the photoproduced colloid nanocomposites occurred with the change of structure from alloy to core-shell. Photoinduced production of Ag/Au NP's adsorbed in silica pores resulted in the separate silver and gold particles formation.

References

1. J.H. Hodak, A. Henglein, G.V. Hartland, *J. Phys. Chem.* 104, 9954–9965 (2000).
2. S. Kundu, M. Mandal, S.K. Ghosh, T. Pal, *J. Coll. Interface Sci.* 272, 134–144 (2004).
3. T. Siebrands, M. Giersig, P. Mulvaney, Ch.-H. Fischer, *Langmuir* 9, 2297–2300 (1993).
4. P.V. Kamat, *J. Phys. Chem. B* 106, 7729–7744 (2002).
5. S. Link, Z.L. Wang, M.A. El-Sayed, *J. Phys. Chem. B* 103, 3529–3533 (1999). I.H. El-Sayed, X. Huang, M.A. El-Sayed, *Nano Lett*. 5, 829–834 (2005).
6. P. Mulvaney, M. Giershig, A. Henglein, *J. Phys. Chem*. 97, 7061 (1993).
7. H.M. Chen, R.S. Liu, L.-Y. Jang, J.-F. Lee, S.F. Hu, *Chem. Phys. Lett.* 421, 118–123 (2006).
8. L.M. Liz-Marzan, A. Philipse, *J. Phys. Chem*. 99, 15120 (1995).
9. S. Devarajan, B. Vimalan, S. Sampath, *J. Coll. Interface Sci*. 278, 126–132 (2004).
10. M.J. Hostetler, Ch.-J. Zhong, B.K.H. Yen, J. Anderegg, S.M. Gross, N.D. Evans, M. Porter, R.W. Murray, *J. Am. Chem. Soc*. 120, 9396–9397 (1998).
11. E. Hutter, J. H. Fendler, *Chem. Comm.* 378–379 (2002).
12. S.X. Liu, Z.P. Qu, X.W. Han, C.L. Sun, *Catal. Today* 93–95, 877–884 (2004).
13. N. Kometani, H. Doi, K. Asami, Y. Yonezawa., *Phys. Chem. Chem. Phys.* 101, 5142–5147 (2002).
14. L. Longenberger, G. Mills, *J. Phys. Chem.* 99, 475–478 (1995).
15. M. Mandal, S. Kundu, S.K. Ghosh, T. Pal, *J. Photochem. Photobiol. A: Chem*. 167, 17–22 (2004).
16. G. Mattei, C. Maurizio, C. Sada, P. Mazzoldi, C. de Julian Fernandez, E. Cattaruzza, G. Battaglin, *J. Non-Cryst. Solids* 345–346, 667–670 (2004).
17. S. Eustis, G. Krylova, A. Eremenko, N. Smirnova, A.W. Shill, M. El-Sayed, *Photochem. Photobiol. Sci.* 4(1), 154–159 (2005).
18. S. Eustis, G. Krylova, A. Eremenko, N. Smirnova, C. Tabor, W. Huang, M. El-Sayed, *J. Photochem. Photobiol. A: Chem.* 181, 385–393 (2006).
19. T. Yamada, K. Asai, A. Endo, H.S. Zhou, I. Honma, *J. Mater. Sci. Lett.* 19, 2167–2169 (2000).
20. N. Smirnova, A. Eremenko, O. Rusina, W. Hopp, L. Spanhel, *J. Sol-Gel Sci. Tech.* 21, 109–113(2001)
21. G. Krylova, A. Eremenko, N. Smirnova, S. Eustis, *Int. J. Photoenergy* 7(41), 193–198 (2005).
22. G. Krylova, A. Eremenko, N. Smirnova, S. Eustis, *Theor. Exp. Chem.* 41(6), 348–353 (2005).

SOL-GEL TECHNOLOGY OF THE MESOPOROUS METHYLSILICIC ACID HYDROGEL: MEDICINE ASPECTS OF GLOBULAR POROUS ORGANOSILICON MATERIALS APPLICATION

NATALIA I. YASHINA*, ELENA P. PLYGAN, VLADIMIR G. SEMENOV, ALEXANDR M. MARTYNENKO AND OKSANA V. GLUSHCHENKO
JSC "Ecologoprotective Firm" "KREOMA-PHARM", 3, Radishcheva Str., Kyiv 03680 Ukraine

Abstract. Determination of the chemical mechanisms and the influence of solvation-desolvation phenomena on the gel formation in methylsilicic acid sol-gel processing, based on theoretical modeling and modern physicochemical investigation techniques, led to creation of a new industrial technology for direct synthesis of materials and formulations for industrial and medicinal use. An industrial technology of synthesis of stable pastes characterized by selective adsorption properties has been developed. Medical aspects of application of «Enterosgel» developed on the basis of methylsilicic acid hydrogels, a new effective and safe medical formulation for organism detoxication have been presented.

Keywords: Sol-gel technology, mesoporous methylsilicic acid hydrogel, enterosgel, paste-like medicinal formulation, drug.

1. Introduction

Organosilicon adsorbents with the porous globular structure of matrices have been obtained first in the middle of 1960s and were rather well studied by the team of Prof. I.B. Slinyakova[1] until the end of 1980s. In contrast to the well-known organosilicon polymers[2,3] these compounds are characterized by such structural-adsorption characteristics as high specific surface area, specific pore radius and volume, and have high adsorption capacity. The most widespread became the polymethylsiloxanes (PMS), prepared via two major approaches: through formation of methylsilicic acids lyogel in a water-organic medium or

*To whom correspondence should be addressed: N.I. Yashina, Ph.D., JSC "Ecologoprotective Firm" "KREOMA-PHARM", 3, Radishcheva Str., Kyiv 03680 Ukraine; e-mail: kreoma@nbi.com.ua

P. Innocenzi, Y. L. Zub and V. G. Kessler (eds.), *Sol-Gel Methods for Materials Processing*.

through hydrogel precipitation from an aqueous alkaline solution of sodium methylsiliconate.

The xerogel of methylsilicic acid – a solid porous adsorbent – has been synthesized by desolvation of the hydrogel and accordingly the lyogel of methylsilicic acid at 120°C:

$$(CH_3SiO_{1,5} \cdot n\ Solv)_\infty \longrightarrow (CH_3SiO_{1,5})\infty + n\ Solv$$

where Solv is H_2O, CH_3CH_2OH or other organic solvent.

The composition of a sol of methylsilicic acid has been studied in paper[4] using the quantum-chemical methods, and modern physicochemical methods, such as FTIR, inelastic neutron dispersion spectroscopy, and ^{29}Si CP/MAS NMR. The chemical mechanism and reasons of globule formation have been established. The influence of the solvation-desolvation processes on gelation has been also investigated. It has been shown that globules form in these solutions via cross-linking of the pentameric cyclic structural units composed by siloxane bonds ≡Si-O-Si≡ and connected to each other via strong hydrogen bonds ≡Si-O···HO-Si≡. Due to the presence of high (-0.4) ÷ (-0.6) e negative charge on the methyl groups, they are solvated by the solvent. At reduced alkalinity of the medium the globules are coalescing and forming a porous gel structure – the hydrogel of methylsilicic acid.

Dependent on the nature of the solvent, the interaction of solvated particles with the globule surface, producing a double electric layer, can occur either due to electrostatic forces (a dipole-dipole interaction), through hydrogen bonds, or due to hydrophobic interactions, see Figure 1:

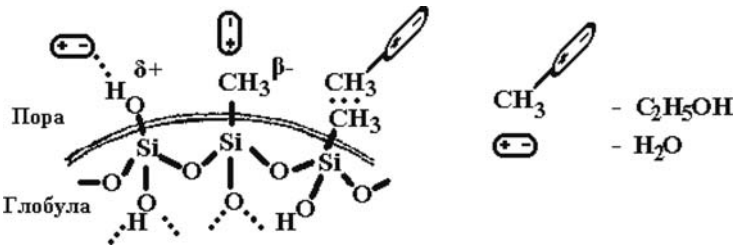

Figure 1. Interaction of solution particles with the globule surface.

At certain alkalinity of the colloid solution, the globules aggregate through formation of siloxane bridges and form pores with the following structure displayed below in Figure 2.

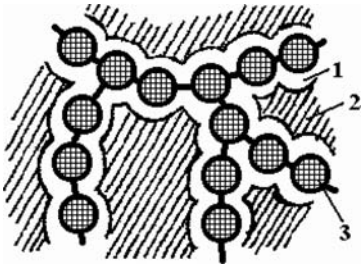

Figure 2. The structure of globule aggregates: 1 – first solvent shell, 2 – solvent in the pores, 3 – an individual globule.

These ideas have been applied for the development of industrial technology for directed synthesis of materials and formulations for industrial use and the medicine, characterized by selective adsorption properties, because the size and the chemistry of the globules' surface determine the porous structure of the formed organosilicon adsorbent.

2. Experimental

On implementation of the paste obtaining technology product properties were judged by the bulk weight (g/100 ml), indirectly characterizing the paste whip; by its colloid stability according to GOST 29188.3-91 (the quantity of liquid separated after centrifugation at 600 rev/min), and also by brightness, determined by leukometer on reflectance of luminous flux, comparing it with a standard, having in visible region a reflectance coefficient of 0.85.

The degree of dispersion of HGMSA was estimated using KRUSS MDL 2100 microscope, for suspensions of pastes (HGMSA) in a solution of Congo red dye. The linear size of particles has been measured from the maximal distance between most distant points counting particles manually in the groups below 5; 5–10; 10–20; 20–30 …, etc. to 250 μm and particles over 250 μm. Percentage of particles of the set size X has been determined as the relation of the number of particles with the size X to the total number of particles, multiplied by 100.

Structural-adsorption characteristics (the specific surface area, adsorption pore volume, average pore radius, pore size distribution) of the paste xerogels obtained under various dispersion conditions were evaluated by the BET method from low-temperature nitrogen adsorption using Quantachrome Nova Win 2 instrument (Institute of sorption and problem of ecology NAS of Ukraine).

3. Results and Discussion

At JSC "Ecoprotective Firm" "KREOMA-PHARM" the hydrogel of methylsilicic acid (HGMSA) has been developed for the first time and certified as a formulation with adsorption-detoxication effect for medical applications (formulation "Enterosgel"), having the formula:

$$\mathbf{(CH_3SiO_{1,5}\cdot n\ H_2O)_\infty,\ where\ n = 44\text{-}49.}$$

The compound is characterized by high selectivity towards medium molecular weight toxic metabolites (m.w. from 100 to 1,000 a.u.), high compatibility to biological tissues, blood, lymph, and body fluids. The adsorption properties of the formulation are similar (in the ratio 3.2 ÷ 4.5 μmol/g) towards two colorants: Congo red (a marker of toxic metabolites for liver diseases), methyl orange (a marker of toxic metabolites for nephritic insufficiency).

The porous structure of the corresponding xerogel has the following characteristics:

Specific surface area	S_{sp}	from 400	to	650	m^2/g
Adsorption pore volume	V_s	from 1.0	to	1.3	cm^3/g
Average pore radius	r_{av}	from 45	to	100	nm

HGMSA forms with water a stable suspension of a different consistence – from paste (water content 5–10%), viscous suspensions (water content up to 70 %), and stable liquid suspensions.

At JSC "Ecoprotective Firm" "KREOMA-PHARM" the industrial technology for obtaining a paste on the basis of hydrogel of the methylsilicic acid in a mixture with water has been developed by the dispersion-homogenization technique in a AP-3000 reactor (developed by the Institute of thermal physics, NAS of Ukraine). The new medical formulation of «Enterosgel-pasta» has been produced taking into account the influence of the following parameters on the stability of the HGMSA – water system: the affinity of HGMSA to water, the concentration of components, the dispersity of HGMSA.

In the view of significant affinity of HGMSA to water, it was considered that the crucial conditions for obtaining a stable colloid system HGMSA-water are concentrations of the components and degree of dispersion of HGMSA. On the basis of homogenization experiments we have found out that a paste with satisfactory consumer properties can be obtained at the HGMSA: water ratio of 70:30. The homogenizer rotation speed and homogenization duration were chosen to avoid segregation of the paste on both the centrifugation and also on long-term storage.

It is interesting to note that the initial HGMSA and the paste obtained from it, and also xerogels, obtained by drying of HGMSA and pasta at 185°C are identical with relation to the particle size distribution criterion (see Figure 3). The HGMSA xerogels and Enterosgel-pasta are characterized by identical total pore volume by benzene sorption (1.0–0.9 cm^3/g). It is determined in the course of synthesis of HGMSA during transformations in the sol-gel process as the stable polymethylsiloxane structure is formed, and changing practically not at all on mechanical dispersion and homogenization, and under action of moderate temperatures.

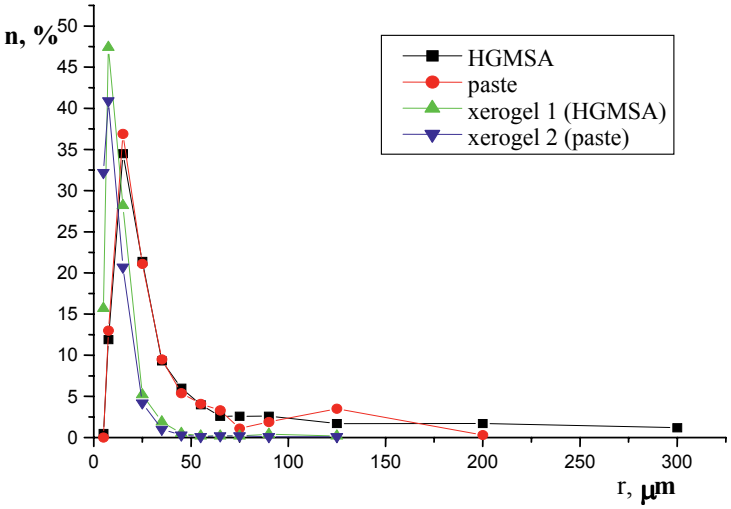

Figure 3. PSD for HGMSA, paste and xerogels.

The influence of the high-energy dispersion on colloid stability of formed pastes was also studied. It has been established, that significant changes of the porous structure of the initial adsorbent (HGMSA) are possible at long term and high-energy dispersive treatment. Thus within the first three days the external characteristics of the obtained paste remained satisfactory (it had the cream consistence), and then the paste segregated releasing huge amounts of water. Figure 4 illustrates the structural-adsorption characteristics and curves of pore size distribution by radius for the xerogels obtained from pastes after dispersing the mixture of HGMSA : H_2O with 70:30 ratio during 10 min (a) and 25 min (b). Structural-adsorption characteristics of the initial HGMSA completely coincide with those of the sample (a).

It is well known[5] that stability of the colloid systems towards aggregation depends on thermodynamic and kinetic factors. Their aggregative instability is caused by an excess of surface energy and the trend to increased enthropy. The

loss of stability to aggregation can be associated with increase in size for the particles in the dispersed phase, the coagulation in our case. Dependent on the system nature and the concentration of the dispersed phase, this process can result in either precipitation or structuring.

The measure of the kinetic stability towards aggregation is the coagulation rate constant, which depends on the viscosity of the medium, temperature, steric factors and interaction energy (potential barrier) for the particles. At considerable potential barrier the system can enter a state, where the aggregation rate for the particles is equal to the disaggregation rate and the system becomes stable to coagulation. All these factors have been taken into consideration for the development of technological parameters for the synthesis of dispersed systems such as pastes of the methylsilicic acid hydrogel.

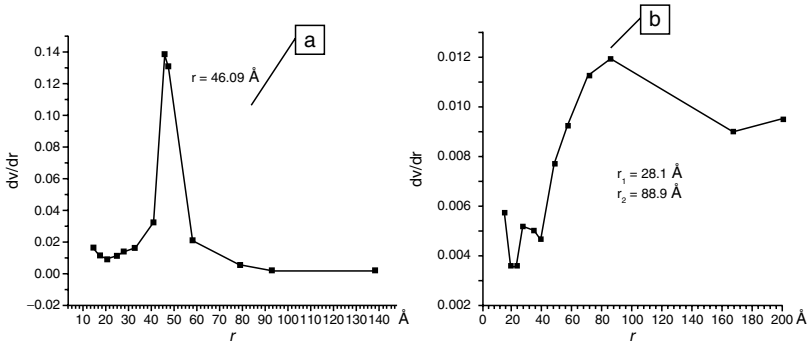

Figure 4. Curves of the distribution porous radius of the xerogel: (a) paste was obtained by dispergation during 10 min; ratio HGMSA: water = 70:30. Surface area = 590 $м^2/г$, volume of pores V_S = 1,0 $г/см^3$; (b) paste was obtained by dispergation during more then 25 min; ratio HGMSA: water = 70:30; surface area 32.4 $м^2/г$, volume of pores V_S = 0.45 g/cm^3.

4. Medicinal Aspects

During the short period that passed after the introduction of the detoxicator Enterosgel into the market it has gained trust from both medical personal – doctors of various specialties and pharmacists, and also from patients. This formulation adsorbs selectively the medium molecular weight toxic metabolites from the intestinal contents and blood (through the capillaries membrane of mucous tunic). Enterosgel interacts selectively with intestinal microflora. It binds and removes (adhesive interaction) only pathogenic microorganisms. Thus, 1 g of this formulation can bind up to 10^{14} pathogenic microbes. At the same time it does not oppress the normal microflora and promotes its distribution in the intestines. Enterosgel adsorbs actively various viruses – rotavirus, A hepatitis

virus and others. At 20–30 mg/ml concentration the formulation is able to bind 10^9 (to 98%) virus particles from a liquid medium.

Enterosgel is safe drug since it has no contraindications or side effects. It does not damage the mucous membrane of intestines, envelops and defends against erosive processes. Enterosgel does not adsorb in blood, is not accumulated in the organism, and removes quickly with the collected slags. Enterosgel acts as an additional eliminative organ and indirectly optimizes functions of vital organs and systems, normalizes the exchange processes in an organism. Thus, Enterosgel has a general and local detoxication effect, it normalizes the intestinal microflora, restores the hemato-intestinal barrier, reduces the cholesterol and lipid levels in blood, improves digestion, reduces expressiveness of the inflammatory reactions, actively binds bacterial endotoxins and reduces the antigenic loading on immune cells that promotes indemnification of a secondary immunodeficiency. In general, the Enterosgel application in the complex therapy of various diseases prevents serious complications and development of chronic pathological process. Enterosgel can be used in a complex therapy with any other formulations (if Enterosgel and other drugs are introduced separately). At the same time, Enterosgel prevents and eliminates side effects of other drug (infringement of a liver function, kidneys, an intestinal dysbacteriosis etc.). It allows the use of Enterosgel in a complex treatment of helycobacter infections, nonspecific ulcerous colitis, tuberculosis and HIV-infection. The latter can appear even more interesting, taking into account numerous testimonies of the leading role played by intestinal inflammatory syndrome in the progress of AIDS.

Enterosgel can be applied for treatment of wide variety of diseases in adults and children: virus and microbial infections; various intoxications, including mushrooms and alcohol poisoning; toxic and virus hepatite, enterocolitis, colitis, dysbacteriosis of intestines, diarrhea, kidney diseases (pyelonephritis, glomerulonephritis and others); especially with chronic renal impairment, toxicosis during pregnancy, skin diseases (neurodermatitis, diathesis, psoriasis and others); allergic reactions, bronchial asthma, diabetes, purulent-septic processes, autoimmune and oncological diseases. Enterosgel is able also to extract the embedded radionuclides. The therapeutic effect of a two-week course of enteroadsorption by Enterosgel drug is comparable with the instrumental detoxication methods, but much easier and cheaper than the latter. It is not associated with any contraindications and complications.

Enterosgel is also used for preventive health care and pre-time aging. Such preventive courses are recommended to be carried out during two weeks, better in spring and in autumn.

The high efficiency of Enterosgel, its adsorption selectivity, safety and usability, absence of contraindications and an opportunity of combination with other medical products in the treatment of a wide range of diseases allow a

physician to individualize medical tactics, to avoid side effects of therapy and to realize a more efficient treatment with shorter duration.

5. Conclusions

1. The industrial sol-gel technology for the synthesis of mesoporous hydrogel of methylsilicic acids (HGMSA), through precipitation from water-alkaline solution, has been developed.
2. The industrial technology for production of a new medicinal form of an adsorbent based on a HGMSA paste with high colloid stability has been developed. The obtained paste is characterized by similar structural-adsorption characteristics as the initial gel.
3. HGMSA and the paste obtained from it are characterized by developed specific surface area with prevalence of mesopores that causes selective adsorption of medium molecular weight toxins from an organism.
4. Enterosgel is a drug based on HGMSA and has selective sorption properties. Formulation adsorbs only toxic products of metabolism and it binds and extracts (adhesive reaction) pathogenic microorganisms and viruses – rotavirus, virus hepatitis A and other. The formulation neither adsorbs nor depresses the normal microflora, but aids to its dissemination in the colon. Enterosgel is absolutely harmless.

References

1. I.B. Slinyakova, T.I. Denisova, *Organosilicon Adsorbents: Preparation and Properties* (Naukova Dumka, Kiev, 1988) (in Russian).
2. K.A. Andrianov, *Methods for Elementorganic Chemistry of Silicon* (Nauka, Moscow, 1968) (in Russian).
3. M.G. Voronkov, E.A. Maletina, V.K. Roman, *Heteropolysiloxanes* (Nauka, Novosibirsk, 1984) (in Russian).
4. Yu.N. Shevchenko, B.M. Dushanin, N.I. Yashina, New Silicon Compounds – Porous Organosilicon Matrices for Technology and Medicinw, in: *Silicon for the Chemical Industry III* (Norway, Institute for Materials Technology, Trondheim, June 18–20, 1999).
5. R.K. Iler, *Colloid Chemistry of Silicas and Silicates* (Gosstroiizdat, Moscow, 1959) (in Russian).

SOL-GEL SYNTHESIS OF MODIFIED SILICA ANTI-REFLECTING COATINGS

ARTURAS ZALGA*, IVAN KAZADOJEV, ALDONA BEGANSKIENE, AND AIVARAS KAREIVA
Department of General and Inorganic Chemistry, Vilnius University, LT-03225 Vilnius, Lithuania

Abstract. The thickness of the modified silica coatings and their transparency at specified wavelength were easily controled by changing sol concentration and the parameters of the spin-coating formation process. It was demonstrated that the modification of sols changes the maximum of the transmittance for the certain range of wavelength. Using modification process of the sols in the technology of preparation of transparent coatings, their hydrophobic properties and resistance to humidity increased. The transmittance spectra of the 3% SiO_2 coatings, which were applied on different glass substrates, showed that the usage of suitable sol and coating program will result a formation of films which possess antireflective properties

Keywords: Sol-gel method, silica coating, anti-reflecting coating, colloidal silica.

1. Introduction

Anti-reflection (AR) coatings are often used for optical components in order to reduce optical losses.[1] The residual reflectivity for a given wavelength and angle of incidence is often of the order of 0.2%, or less (in a limited bandwidth) with careful optimization. For application on prescription glasses, the achievable suppression of reflections is significantly lower, since the coating must operate in a wide wavelength range and for a wide range of incidence angles. AR coatings are also used on laser crystals and nonlinear crystals.

AR and protective coatings are usually applied on the substrates via sol-gel technique.[2–4] This chemistry produces a variety of inorganic networks from silicon or metal alkoxide monomer precursors. Through this process, homogeneous inorganic oxide materials with desirable properties of hardness, optical

*To whom correspondence should be addressed: Arturas Zalga; e-mail: Arturas.Zalga@chf.vu.lt

P. Innocenzi, Y. L. Zub and V. G. Kessler (eds.), *Sol-Gel Methods for Materials Processing*.

transparency, chemical durability, tailored porosity, and thermal resistance, can be produced at room temperatures. The specific uses of these sol-gel produced glasses and ceramics are derived from the various material shapes generated in the gel state, i.e., monoliths, films, fibers, and monosized powders. Many specific applications include optics, protective and porous films, optical coatings, window insulators, dielectric and electronic coatings, high temperature superconductors, reinforcement fibers, fillers, and catalysts.[5–7] Colloidal silica sols are created by the hydrolysis and condensation of silicon alkoxides in alcohol solvents in the presence of a base (e.g., NH_3) and H_2O. Controlling the amount of NH_3, it is possible to synthesize colloidal particles of different sizes.[8] In order to create an amorphous colloidal SiO_2 optical film - silica nanoparticles are used with variation in size from 20 to 35 nm. The refractive index of such films is somewhat about 1.23 and the porosity of the films is about 50–60%.[9] Though these films have a lack in being hydrophobic, they absorb molecules of water from the air on the surface of the film. This problem can be fixed by changing the properties of the nanoparticles or by modifying the surface of the film changing the from hydrophilic to hydro-phobic. Various reagents are used for the modification of silica particles and films, such as: heksamethyldisilo-zane (HMDS), methyltrietoxisilane (MTES) and methyldietoxisilane (DDS), etc.[10–16] The main aim of this study was investigation of sol-gel derived and modified silica coatings on different substrates.

2. Experimental

Colloidal silica oxide films were applied on different substrates, such as "Menzel–Glaser" (76 × 26 mm), BK-7 optical glass, quartz and KDP crystals. The coatings were formed either by dip-coating technique using "KSV Instruments Ltd. KSV D™" device, or by spin-coating technique using "Cookson electronics company SCS P-6708" device. The parameters for dip-coating were as follows: withd-rawal speed 40 mm/min, immersion time 20 s. The parameters for spin-coating were 2,000–3,000 rounds per min. Contact angle measurements were done by "KSV instruments CAM – 100" device. A drop of 0.0125 ml was introduced on the surface of the film. Coating transmittance and reflectance of normally incident light was measured using UV-VIS spectrophotometers (Perkin-Elmer Spectrum Lamda 19 and LOMO) over the spectral range of 350–1,000 nm. The particle size was determined from the micrographs obtained from TEM measurements.

Reagents used: tetraethylorthosilicate ($Si(OC_2H_5)_4$, 99–99.9%), ammonium hydroxide (33%), heksamethyldisilozane ($C_{19}H_{19}NSi_2$, 98%), anhydrous ethanol, 2-propanol, decane. Different sol-gel solutions SiO_2 (2%, 3%, 5%) and modified SiO_2 (3%, 5%) with HMDS (hexamethyldisilazane) were used for preparation silica coatings. Sol-gel synthesis of colloidal SiO_2 (2%, 3%, 5%) nanoparticles

was performed in non-aqueous system of TEOS. The precursor of SiO_2 colloidal sol was prepared by the base catalyzed hydrolysis of tetraethylorthosilicate by the following method of preparation of Stöber et al.[17] colloidal silica. The alkaline solution was added to the solution of TEOS in ethanol with continuous stirring at room temperature. The solutions with final silica concentration of 2%, 3%, 5% SiO_2 were prepared. The molar ratio of ammonium hydroxide to TEOS was 0.2 mol, to water – 0.4 mol, to ethanol – 39, 38 and 25 mol respectively. The obtained reaction mixtures were stored for 14 days at room temperature to allow hydrolysis as much as possible. The final product consisted of colloidal suspension of SiO_2 nanoparticles in an anhydrous solvent was used for preparation of the sol-gel coatings. The modified solutions were prepared by adding HMDS to stirred colloidal 3%, 5% SiO_2 suspensions. The molar ratio of HMDS to colloidal silica was from 0.05 to 1.5 parts per volume. The modified sol solution was stored for 1 day, after dilution three times with anhydrous ethanol was applied for sol-gel coatings at room temperature.

3. Results and Discussion

As was already mentioned, the main goal of this work was to prepare the modified sol-gel AR coatings on different substrates. For that reason several colloidal SiO_2 sols (2%, 3%, 5%) were synthesized. The morphology of colloidal silica was analyzed using transmitting electron microscope (TEM). Pictures of particles from 2%, 3%, 5% and modified SiO_2 sols are presented in Figures 1 and 2.

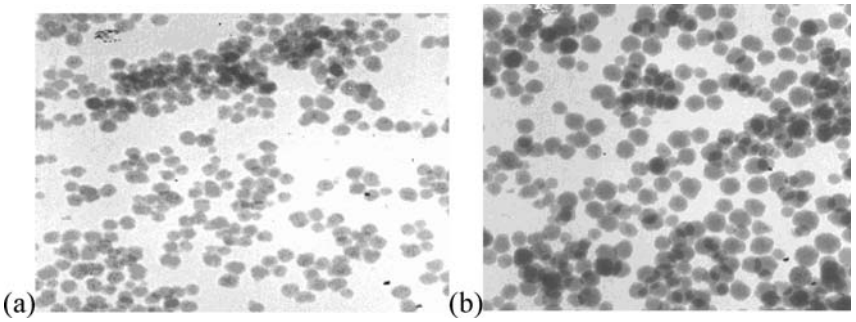

Figure 1. TEM pictures of colloidal silica particles: (a) SiO_2 (2%) (~20–35 nm) and (b) SiO_2 (3%) (~30–45 nm).

The change in the concentration affects the size of the particles, which means that the refractive index and the thickness of the coating will also change. Different amount of HMDS were mixed with SiO_2 sols and after applying them on the glass substrates via "dip-coating" technique, a number of permeability and contact angle analysis were done. The best result in this case was reached using modified sol, when the concentration of HMDS was 0.5 (p.p.v). Heating

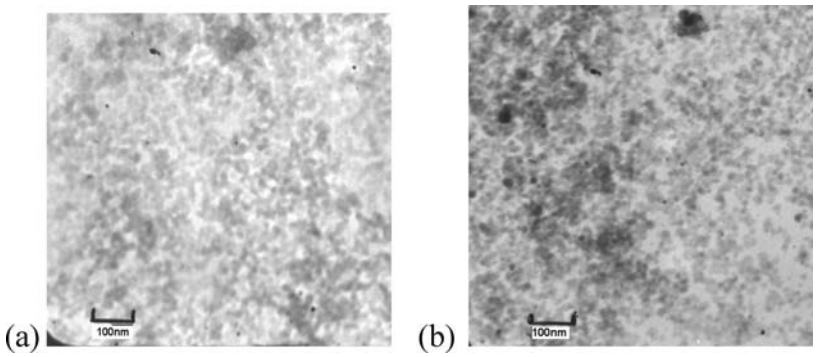

Figure 2. TEM pictures of colloidal silica particles: (a) SiO_2 (5%) sol and modified with HMDS (b) sol SiO_2 (5%) : HMDS (1:1.5).

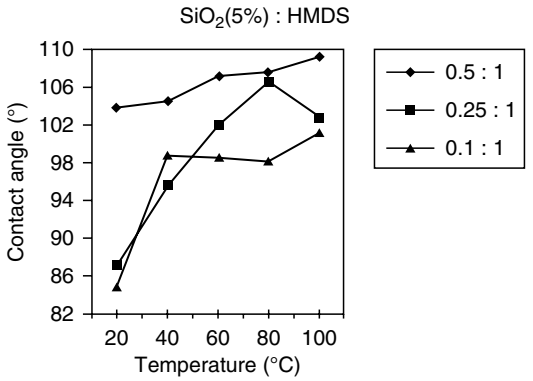

Figure 3. SiO_2(5%) : HMDS contact angle dependence on temperature of drying.

the substrates until 100°C also generates changes in contact angles of water drops on the coatings. The contact angle measurements are plot-ted in Figure 3.

The transparency of the coatings, made from SiO_2 (5%):HMDS (1:1.5 p.p.v.) reaches 97.37% in the interval of wavelength from 516.18 to 598.91 nm. The value of contact angle increases both with concentration of HMDS and in time (Figure 4).

The highest value of contact angle was obtained when the concentration of HMDS is 1.5 p.p.v, is 137.35°, after 40 days this value is changed and the contact angle of the applied coating is ~164°. There are several types of coatings, basing on the value of contact angle, hydrophilic (<60°), hydrophobic (60°–150°), superhydrophobic (>150°). Figure 5 shows us how the surface properties of our coatings are changed from hydrophilic SiO_2 (5%) – 15.73°, to superhydrophobic SiO_2 (5%):HMDS (1:1.5 p.p.v.) after 40 days – 164.98°.

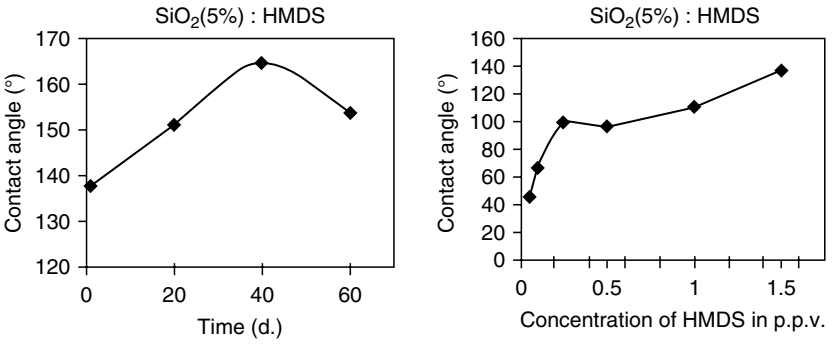

Figure 4. Contact angle of SiO_2 (5%):HMDS (1:1.5 p.p.v.) coating dependence on (a) time, (b) concentration.

The optical transparency is more likely to be dependent on the formation process of the coating, especially on the first stage of rotation. The best result is achieved using first program during the employment of SiO_2 (5%) sol, on the substrate, transparency of the coating reaches ~93%, thought it is not the best result in seeking for high optical properties. The transparency spectra of the samples are shown in Figure 6.

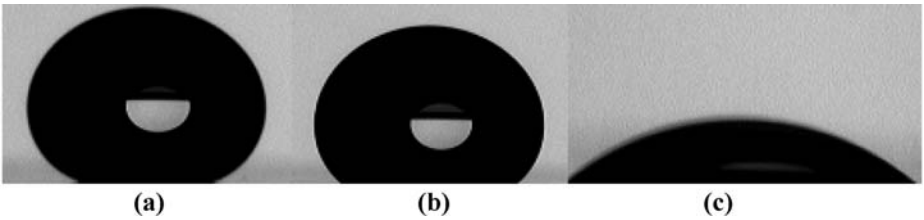

Figure 5. Pictures of water drops on the coatings made from: (a) SiO_2 (5%):HMDS (1:1.5 p.p.v.) after 40 days – 164.98°, (b) SiO_2 (5%):HMDS (1:1.5 p.p.v.) after 1 day. – 137.35°, (c) non-modified SiO_2 (5%) – 15.73°.

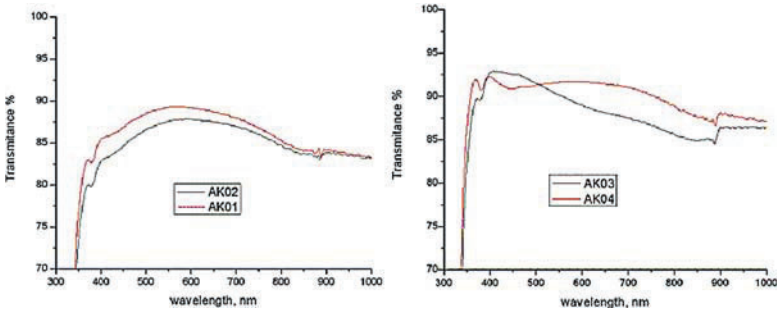

Figure 6. Transmission spectra of samples coated with: 5% SiO_2 HMDS (left) and 5% SiO_2 (right).

Nonetheless, modification of sols changes the maximum of the transmittance for the certain range of wavelength, this fact is really important in describing optical properties of the coatings. Coatings were also applied on different substrates, in order to investigate their optical properties. Lime glass, BK-7 (borosilicate glass) and quartz were coated using spin-coating technique. Glass substrates were coated with SiO_2 sols of different concentration (2%, 3%, 5%). This spectral analysis showed us, that the best transparency is ascribed to the coating which was formed using 5% SiO_2 sol. Afterwards we took 3% SiO_2 sol and applied coatings on simple glass, BK-7 glass and quartz using program No. 2. Transparency spectra are shown in Figure 7.

Analyzing the obtained data, we see that the transparency of a simple glass increased from 90.6% to 94.24% when the value of wavelength is 528 nm, BK-7 from 91.3% to 94.7% when the value of wavelength is 410 nm, quartz from 92.3% to 95.3% – 452 nm, so it is obvious that formed coatings possess antireflective properties.

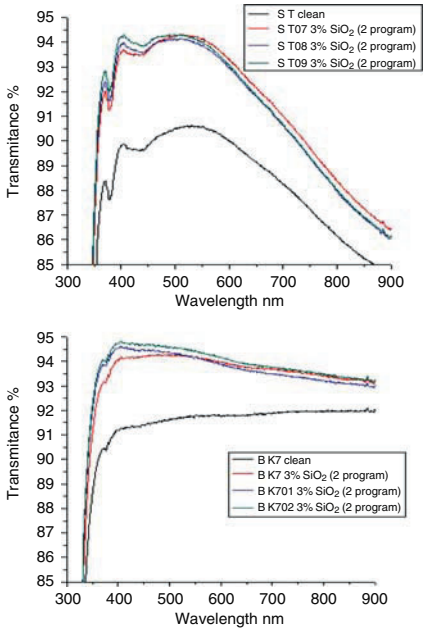

Figure 7. Transmission data for coated Lime and BK-7 glass substrates with 3% SiO_2 sol: Lime glass (top) and BK-7 glass (bottom).

4. Conclusions

Thickness and transparency of the coating depends on the first stage of the program due to the fact that viscosity of the sol solutions is small and evaporation

rate of the ethanol is quite high. Modification of sols changes the maximum of the transmittance for the certain range of wavelength, the refractive index of the coating and the amount of air in it decreases, this fact is really important in describing optical properties of the coatings. Using modi-fication process of the sols in the technology of creating transparent coatings increases their hydrophobic properties and resistance to humidity. Trans-mittance spectra of the 3% SiO_2 coatings, which were applied on different glass substrates, showed that the usage of suitable sol and coating program will result a formation of films which possess antireflective properties. Simple glass 94.24% at 528 nm, BK-7 94.7% at 410 nm, quartz 95.3% at 452 nm.

References

1. A. Melninkaitis, K. Juskevicius, M. Maciulevicius, V. Sirutkaitis, A. Beganskiene, I. Kazadojev, A. Kareiva, D. Perednis, *Proc. SPIE (Laser-Induced Damage in Optical Materials/Ed. G. J. Exarhos et al.)*, 6403, C/1 (2007).
2. T. Hubert, J. Schwarz and B. Oertel, *J. Sol-Gel Sci. Technol.*, 38, 179 (2006).
3. W. Hu, C. Yang, W. Zhang, G. Liu and D. Dong, *J. Sol-Gel Sci. Technol.*, 39, 293 (2006).
4. J. D. Mackenzie and E. P. Bescher, *Acc. Chem. Res.*, to be published (2007).
5. S. Smitha, P. Shajesh, P. Mukundan and K. G. K. Warrier, *J. Sol-Gel Sci. Technol.*, 42, 157 (2007).
6. Y. Xu, D. Wu, Y. Sun, H. Gao, H. Yuan and F. Deng, *J. Sol-Gel Sci. Technol.*, 42, 13, (2007).
7. J. Abdallah, M. Silver, S. A. B. Allen and P. A. Kohl, *J. Mater. Chem.*, 17, 873 (2007).
8. S. Sakka and K. Kamiya, *J. Non-Cryst. Solids*, 42, 40 (1980).
9. E. K.Wheeler, J. T. McWhirter, P. K. Whitman, C. Thorsness, J. De Yoreo, I. Thomas and M. Hester, *Proc. SPIE (Annu. Symp. Opt. Mater. High Power Lasers)*, 3902, 451 (1999).
10. W. Hertl and M. L. Hair, *J. Phys. Chem.*, 75, 2181 (1971).
11. C. Zettlemoyer and H. H. Hsing, *J. Coll. Interface Sci.*, 58, 263 (1977).
12. B. Boddenberg, R. Grosse and U. Breuninger, *Surf. Sci.*, 173, 655 (1986).
13. V. V. Brei, *J. Appl. Spectrosc.*, 56, 205 (1992).
14. S. Hauuka, E. L. Lakomaa and T. Suntola, *Appl. Surf. Sci.*, 82/83, 548 (1994).
15. A. Kytokivi and S. Haukka, *J. Phys. Chem.*, 101, 10365 (1997).
16. T. I. Suratwala, M. L. Hanna, E. L. Miller, P. K. Whitman, I. M. Thomas, P. R. Ehrmann, R. S. Maxwell and A. K. Burnham, *J. Non-Cryst. Solids*, 316, 349 (2003).
17. W. Stober, A. Fink and E. Bohn, *J. Coll. Interface Sci.*, 26, 62 (1968).

LIST OF PARTICIPANTS

Key Speakers

1. **BABONNEAU, Florence –** Professor, Laboratoire de Chimie de la Matière Condensée de Paris, Université Pierre et Marie Curie-Paris 6 – CNRS, 4 place Jussieu, F-75005 Paris, FRANCE;
Tel.: +33-1-44.27.40.75; Fax: +33-1-44.27.47.69;
e-mail: fb@ccr.jussieu.fr

2. **BONEKAMP, Ben C. –** Dr., Energy Research Centre of the Netherlands, Box 1, 1755 ZG Petten, The NETHERLANDS;
Tel.: +31-224-56.45.40; Fax: +31-224-56.86.15;
e-mail: bonekamp@ecl.nl

3. **DIONYSIOU, Dionysios D. –** Dr., Department of Civil and Environmental Engineering, University of Cincinnati, Cincinnati, OH 45221-0071 USA;
Tel.: +1-513-556.07.24; Fax: +1-513-556.25.99;
e-mail: dionysios.d.dionisiou@uc.edu

4. **EFREMENKO**, **Elena –** Dr., Chemical Enzymology Department, Chemical Faculty, M.V. Lomonosov Moscow State University, Lenin's Hills, 1/11, Moscow 11999, RUSSIA;
Tel.: +7-495-939.31.70; Fax: +7-495-939.54.17;
e-mail: efremenko@enz.chem.msu.ru

5. **HÜSING, Nicola –** Professor, Inorganic Chemistry I, Ulm University, Albert-Einstein-Allee 11, 89081 Ulm, GERMANY;
Tel.: +49-731-502.27.30; Fax: +49-731-502.27.33;
e-mail: nicola.huesing@uni-ulm.de

6. **INNOCENZI**, **Plinio –** Professor, D.A.P., Laboratory of Materials Science and Nanotechnology, University of Sassari, CR-INSTM and Nanoworld Institute, Palazzo Pou Salit, Piazza Duomo 6, 07041 Alghero (SS), ITALY;
Tel.: +39-079-972.04.08; Fax: +39-079-972.04.20;
e-mail: plinio@uniss.it

7. **JASIORSKI**, **Marek –** Dr., Wroclaw University of Technology, Institute of Materials Science and Applied Mechanics, Smoluchowskiego 25, 50-370 Wroclaw, POLAND;
Tel.: +48-71-320.32.21; Fax: +48-71-321.12.35;
e-mail: marek.jasiorski@pwr.wroc.pl

8. **KESSLER, Vadim G. –** Professor, Department of Chemistry, SLU, Box 7015, 75007 Uppsala, SWEDEN;
Tel.: +46-18-67.15.41; Fax: +44-18-67.33.92;
e-mail: vadim.kessler@kemi.slu.se

9. **LEV, Ovadia –** Professor, The Casali Institute of Applied Chemistry, The Chemistry Institute, The Hebrew University of Jerusalem, Jerusalem, 91904, ISRAEL;
Tel.: +972-2-658.41.91; Fax: +972-2-658.61.55;
e-mail: ovadia@vms.huji.ac.il

10. **MACQUARRIE, Duncan J. –** Professor, Centre of Excellence in Green Chemistry, University of York, Heslington, York YO10 5DD, UK;
Tel.: +0190-443.45.33; Fax: +0190-443.27.05;
e-mail: djm13@york.ac.uk

11. **NEDELEC, Jean-Marie –** Dr., Laboratoire des Matériux Inorganiques CNRS UMR 6002, TransChiMiC, Université Blaise Pascal & Ecole Nationale Supérieure de Chimie de Clermont-Ferrand, 24 Avenue des Landais, 63177 Aubière, FRANCE;
Tel.: +33-473-40.71.05; Fax: +33-473-40.71.08;
e-mail: j-marie.nedelec@univ-bpclermont.fr

12. **PAROLA**, **Stephane –** Professor, Laboratoire des Multimatériaux et Interfaces UMR CNRS 5615 University Lyon, FRANCE;
Tel.: +33(0)472-44.81.67; Fax: +33(0)472-43.15.68;
e-mail: stephane.parola@univ-lyon1.fr

13. **STRELKO**, **Volodymyr V. –** Professor, Institute for Sorption and Problems of Endoecology, NAS of Ukraine; 13, General Naumov Str., Kyiv 03164, UKRAINE;
Tel./Fax: +38-044-452.93.27;
e-mail: vstrelko@ispe.kiev.ua

14. **VIITALA, Reeta –** Dr., Turku Biomaterials Centre, Itäinen Pitkäkatu 4 B, PharmaCity, FI-20520, Turku, FINLAND;
Tel.: +358-2-333.85.30; Fax: +358-2-333.87.50;
e-mail: reevii@utu.fi

15. **ZUB**, **Yuriy L. –** Dr., O.O.Chuiko Institute of Surface Chemistry, NAS of Ukraine; 17, General Naumov Str., Kyiv 03164, UKRAINE;
Tel.: +38-044-422.96.30; Fax: +38-044-424.35.67;
e-mail: yuriyzub@voliacable.com

Participants

1. **BACCILE, Niki –** Dr., Max-Planck Institute for Colloids and Interfaces Colloid Departement, Research Campus Golm, Am Muhlenberg 1 14476 Golm, GERMANY;
Tel.: +49(0)331-567-9508; Fax: +49(0)331-567-9502
e-mail: niki.baccile@mpikg.mpg.de

2. **BARCZAK, Mariusz –** Ph.D. student, Faculty of Chemistry, Maria Curie-Sklodowska University, Maria Curie-Sklodowska Sq. 3, 20-031 Lublin, POLAND;
Tel.: +48-81-537.57.88; Fax: +48-81-533.33.48;
e-mail: mariuszbarczak@yahoo.co.uk

3. **BEREZOVSKA, Inna S. –** Ph.D. student, O.O. Chuiko Institute of Surface Chemistry, NAS of Ukraine; 17, General Naumov Str., Kyiv 03164 UKRAINE;
Tel.: +38-044-424.94.68; Fax: +38-044-424.35.67;
e-mail: berinna2003@rambler.ru

4. **CAUZZI, Daniele –** Dr., Dipartimento di Chimica Generale e Inorganica, Chimica Analitica, Chimica Fisica, Università di Parma, Viale Usberti 17/A, 43100 Parma, ITALY;
Tel.: +39-0521-90.54.25; Fax: +39-0521-90.55.57;
e-mail: cauzzi@unipr.it

5. **DUDARKO, Oksana A. –** Ph.D. student, O.O. Chuiko Institute of Surface Chemistry, NAS of Ukraine; 17, General Naumov Str., Kyiv 03164 UKRAINE;
Tel.: +38-044-422.96.30; Fax: +38-044-424.35.67;
e-mail: dudarko@bigmir.net

6. **EREMENKO, Anna –** Professor, O.O. Chuiko Institute of Surface Chemistry, NAS of Ukraine; 17, General Naumov Str., Kyiv 03164 UKRAINE;
Tel.: +38-044-422.96.98; Fax: +38-044-424.35.67;
e-mail: annaerem@voliacable.com

7. **GAISHUN, Vladimir E. –** Dr., Advanced Materials Research Laboratory, F. Skorina Gomel State University, 104 Sovetskay St., Gomel 246019 BELARUS;
Tel.: +375-232-57.64.36; Fax: +375-232-57.63.57;
e-mail: vgaishun@gsu.unibel.by

8. **GAPONENKO, Nikolai V. –** Professor, Head of the Laboratory of Nanophotonics, Belarusian State University of Informatics and Radioelectronics, P. Browka Str. 6, 220013 Minsk, BELARUS,
Tel.: +375 –172.93.88.69; Fax: +375-172. 93.23.33;
e-mail: nik@nano.bsuir.edu.by

9. **GNATYUK, Yuriy –** Ph.D. student, O.O. Chuiko Institute of Surface Chemistry, NAS of Ukraine; 17, General Naumov Str., Kyiv 03164 UKRAINE;
Tel.: +38-044-422.96.98; Fax: +38-044-424.35.67;
e-mail: yuriy_gnatyuk@yahoo.com

10. **HAYRAPETYAN, Sergey S. –** Dr., Analytical Chemistry Chair, Department of Chemistry, Yerevan State University, 1, Alek Manoukian Str., 375025 Yerevan, ARMENIA;
Tel./Fax: 37-410-57.06.63;
e-mail: gold@ysu.am or hayser@ysu.am

11. **ITKULOVA, Sholpan S. –** Dr., V. Sokolsky Institute of Organic Catalysis and Electrochemistry, 142 Kunaev Str., Almaty, 050010, REPUBLIC OF KAZAKHSTAN,
Tel.: + 7-327-991.68.26; Fax: +7-327-291.57.22;
e-mail: itkulova@nursat.kz

12. **KALENCHUK, Valentyna G. –** Researcher, Institute for Sorption and Problems of Endoecology, NAS of Ukraine; 13, General Naumov Str., Kyiv 03164, UKRAINE;
Tel.: +38-044-452.93.29; Fax: +38_044_452.93.27;
e-mail: melesh@ispe.kiev.ua

13. **KOUZNETSOVA, Tatyana F. –** Dr., Institute of General and Inorganic Chemistry, NAS of Belarus, 9/1, Surganova Str., Minsk 220072 BELARUS;
Tel.: +375-17-284.27.49; Fax: +375-17-284.27.03;
e-mail: kouzn@igic.bas-net.by

14. **KUCHMA, Olga V. –** Ph.D. student, O.O. Chuiko Institute of Surface Chemistry, NAS of Ukraine; 17, General Naumov Str., Kyiv 03164 UKRAINE;
Tel.: +38-044-422.96.98; Fax: +38-044-424.35.67;
e-mail: kuchma_olga@mail.ru

15. **KUNCOVA, Gabriela –** Dr., Institute of Chemical Process Fundamentals, Academy of Sciences of the Czech Republic, Rozvojová 135, 165 02 Prague 6-Suchdol, CZECH REPUBLIC;
Tel.: +420-220-39.02.43; Fax: +420-220-92.06.61;
e-mail: kuncova@icpf.cas.cz

16. **LEVCHENKO, Tetyana –** Ph.D. student, O.O. Chuiko Institute of Surface Chemistry, NAS of Ukraine; 17, General Naumov Str., Kyiv 03164 UKRAINE;
Tel.: +38-044-422.96.53; Fax: +38-044-424.35.67;
e-mail: levchtat@i.com.ua

17. **LOBNIK, Aleksandra –** Professor, Centre of Sensor Technology, Faculty of Mechanical Engineering, University of Maribor, Smetanova 17, 2000, Maribor, SLOVENIA;
Tel.: +386-2-220.79.12; Fax: +386-2-220.79.90;
e-mail: aleksandra.lobnik@uni-mb.si

18. **MALFATTI, Luca –** Dr., D.A.P., Laboratory of Materials Science and Nanotechnology, University of Sassari, CR-INSTM and Nanoworld Institute, Palazzo Pou Salit, Piazza Duomo 6, 07041 Alghero (SS), ITALY;
Tel.: +39-079-998630; Fax: +39-079-972.04.20;
e-mail: luca.malfatti@uniss.it

19. **MEL'GUNOV, Maxim S. –** Dr., Boreskov Institute of Catalysis SB RAS, pr-kt. Akad. Lavrentieva 5, Novosibirsk 630090 RUSSIA;
Tel.: +7-383-330.92.55; Fax: +7-383-330.80.56;
e-mail: max@catalysis.ru

20. **MELNYK, Inna V. –** Dr., O.O. Chuiko Institute of Surface Chemistry, NAS of Ukraine; 17, General Naumov Str., Kyiv 03164 UKRAINE;
Tel.: +38-044-422.96.98; Fax: +38-044-424.35.67;
e-mail: inna_melnyk@mail.ru

21. **PLYUTO, Yuri –** Dr., O.O. Chuiko Institute of Surface Chemistry, NAS of Ukraine; 17, General Naumov Str., Kyiv 03164 UKRAINE;
Tel.: +38-044-422.96.53; Fax: +38-044-424.35.67;
e-mail: plyuto@ukr.net

22. **POGORILYI, Roman P. –** Ph.D. student, O.O. Chuiko Institute of Surface Chemistry, NAS of Ukraine; 17, General Naumov Str., Kyiv 03164 UKRAINE;
Tel.: +38-044-422.96.30; Fax: +38-044-424.35.67;
e-mail: roman_pogorilyi@rambler.ru

23. **PRIKHODCHENKO, Petr –** Dr., Institute of General and Inorganic Chemistry, RAS, 31, Leninskii Prospekt, 119991, Moscow, RUSSIA;
Tel.: +7-495-153.15.00; Fax: +7-495-955.48.50;
e-mail: prikhman@gmail.com

24. **SARTORI, Federica –** Ph.D. student, Institut Charles Gerhardt (UMR 5253 CNRS/UM2/ENSCM/UM1), Equipe « Matériaux Avancées pour la Catalyse et la santé», ENSCM, 8, rue de l'Ecole Normale, 34296 Montpellier, Cedex 5, FRANCE,
Tel.: + 33-467-16.34.62; Fax: +33-467-16.34.70;
e-mail: federica.sartori@enscm.fr

25. **SEISENBAEVA, Gulaim A. –** Associate Professor, Ph.D., Department of Chemistry, SLU, Box 7015, 75007 Uppsala, SWEDEN;
Tel.: +44-18-67.15.41; Fax: +44-1273-67.93.33;
e-mail: gulaim.seisenbaeva@kemi.slu.se

26. **SEMCHENKO, Alina V. –** Ph.D. student, Advanced Materials Research Laboratory, F. Skorina Gomel State University, 104 Sovetskay St., Gomel 246019 BELARUS;
Tel.: +375-232-57.63.67; Fax: +375-232-57.63.57;
e-mail: semchenko@gsu.unibel.by

27. **SHAKAROVA, Dilshod Sh. –** Ph.D. student, Scientific and Technical Complex «Science and Progress», Tashkent State Technical University, UZBEKISTAN;
Tel.: +998-71-246.83.71; Fax: +998-71-393.12.73;
e-mail: dilshoda06@yahoo.com

28. **SIMONSEN, Morten E. –** Ph.D. student, Aalborg University , Esbjerg Institute of Technology, Niels Bohrs Vej 8, 6700 Esbjerg, DENMARK,
Tel.: + 45-79.12.76.22 Fax: +45-75.45.36.43;
e-mail: mes@aaue.dk

29. **SMIRNOVA, Natalia –** Dr., O.O. Chuiko Institute of Surface Chemistry, NAS of Ukraine; 17, General Naumov Str., Kyiv 03164 UKRAINE;
Tel.: +38-044-422.96.98; Fax: +38-044-424.35.67;
e-mail: smirnat@i.com.ua

30. **ŠOLCOVÁ, Olga –** Dr., Institute of Chemical Process Fundamentals, Academy of Sciences of the Czech Republic, Rozvojová 135, 165 02 Prague 6-Suchdol, CZECH REPUBLIC;
Tel.: +420-220-39.02.79; Fax: +420-220-92.06.61;
e-mail: Solcova@icpf.cas.cz

31. **SYCHEV, Mikhail V. –** Dr., Dumanski Institute of Colloid and Water Chemistry, NAS of Ukraine, 42 , Blv.Vernadskogo, Kyiv 03680 UKRAINE;
Tel.: +38-044-424.21.04; Fax: +38-044-423.82.24;
e-mail: m.v.sychev@icccw.kiev.ua

32. **WONG CHI MAN, Michel –** Professor, Laboratoire Architectures Moléculaires et Matériaux Nanostructurés (ICGM UMR CNRS 5253), Ecole Nationale Supérieure de Chimie de Montpellier, 8, rue de l'Ecole Normale, 34296 Montpellier, FRANCE ;
Tel.: +33-467-14.72.19; Fax: +33-467-14.43.53;
e-mail: michel.wong-chi-man@enscm.fr

33. **ZALGA, Arturas –** Ph.D. student; Department of General and Inorganic Chemistry, Vilnius University, Naugarduko 24, LT-03225 Vilnius, LITHUANIA;
Tel.: +370-5-219.31.08; Fax: +370-5-233.09.87;
e-mail: arturas.zalga@chf.vu.lt

Local Participants

1. **DAVYDENKO, Lyudmyla –** Researcher, O.O. Chuiko Institute of Surface Chemistry, NAS of Ukraine; 17, General Naumov Str., Kyiv 03164 UKRAINE;
Tel.: +38-044-422.96.53; Fax: +38-044-424.35.67;
e-mail: l.davydenko@yahoo.com

2. **LOZOVSKI, Alex –** Dr., Dumanski Institute of Colloid and Water Chemistry, NAS of Ukraine, 42 , Blv.Vernadskogo, Kyiv 03680 UKRAINE;
Tel.: +38-044-424.21.04; Fax: +38-044-423.82.24;
e-mail: avatar@online.com.ua

3. **MARTYNENKO, Olexandr –** Researcher, JSC "Ecologoprotective firm "KREOMA-PHARM", Radyscheva Str., 3, Kyiv 03680 UKRAINE;
Tel.: +38-044-206.21.59; Fax: +38-044-497.95.45;
e-mail: kreoma@nbi.com.ua

4. **MUTOVKIN, Petro –** Dr., PPG Industrie, Inc., Box 9, 4325 Rosanna Drive, Allison Park, PA 15101, USA;
Tel.: +8-050-514.04.94; Fax: +8-044-258.12.36;
e-mail: pmutovkin@ppg.com

5. **NASIEDKIN, Dmytro –** Ph.D. student, O.O. Chuiko Institute of Surface Chemistry, NAS of Ukraine; 17, General Naumov Str., Kyiv 03164 UKRAINE;
Tel.: +38-044-422.96.53; Fax: +38-044-424.35.67;
e-mail: nasiedkin@email.ua

6. **PRIKHOD'KO, Roman V. –** Researcher, Dumanski Institute of Colloid and Water Chemistry, NAS of Ukraine, 42 , Blv.Vernadskogo, Kyiv 03680 UKRAINE;
Tel.: +38-044-424.21.04; Fax: +38-044-423.82.24;
e-mail: r.v.prihodko@icccw.kiev.ua

7. **SHARANDA, Lyudmyla –** Researcher, O.O. Chuiko Institute of Surface Chemistry, NAS of Ukraine; 17, General Naumov Str., Kyiv 03164 UKRAINE;
Tel.: +38-044-422.96.53; Fax: +38-044-424.35.67;
e-mail: lyusharanda@yahoo.com

8. **STARODUB, Nikolai F. –** Professor, Palladin Institute of Biochemistry, NAS of Ukraine, 9 Leontovicha Str., Kyiv 01601 UKRAINE;
Tel.: +38-044-279.47.43; Fax: +38-044-279.63.65;
e-mail: nikstarodub@yahoo.com

9. **TELBIZ, German M. –** Dr., Institute of Physical Chemistry NASU, 31, Pr. Nauky, Kyiv 03039 UKRAINE;
Tel.: +38-067-500.07.61; Fax: +38-044-525.61.16;
e-mail: g_telbiz@yahoo.com

10. **TERTYKH, Valentyn A. –** Professor, O.O. Chuiko Institute of Surface Chemistry, NAS of Ukraine; 17, General Naumov Str., Kyiv 03164 UKRAINE;
Tel.: +38-044-422.96.73; Fax: +38-044-424.35.67;
e-mail: tertykh@public.ua.net

11. **TRIFONOVA, Msrina Yu. –** Ph.D. student, Dumanski Institute of Colloid and Water Chemistry, NAS of Ukraine, 42 , Blv.Vernadskogo, Kyiv 03680 UKRAINE;
Tel.: +38-044-424.80.79; Fax: +38-044-423.82.24;
e-mail: yuitaras@thomascat.kiev.ua

12. **VITYUK, Nadezhda –** Ph.D. student, O.O. Chuiko Institute of Surface Chemistry, NAS of Ukraine; 17, General Naumov Str., Kyiv 03164 UKRAINE;
Tel.: +38-044-422.96.98; Fax: +38-044-424.35.67;
e-mail: vityuk@univ.kiev.ua

13. **YASHINA, Natalia I. –** Dr., JSC "Ecologoprotective firm "KREOMA-PHARM", Radyscheva Str., 3, Kyiv 03680 UKRAINE;
Tel.: +38-044-206.21.58; Fax: +38-044-497.95.45;
e-mail: kreoma@nbi.com.ua

14. **YASHAN, Halyna –** Ph.D. student, O.O. Chuiko Institute of Surface Chemistry, NAS of Ukraine; 17, General Naumov Str., Kyiv 03164 UKRAINE;
Tel.: +38-044-422.96.98; Fax: +38-044-424.35.67;
e-mail: annaerem@voliacable.com

15. **ZHUKOVSKIY, Maxim –** Ph.D. student, O.O. Chuiko Institute of Surface Chemistry, NAS of Ukraine; 17, General Naumov Str., Kyiv 03164 UKRAINE;
Tel.: +38-044-422.96.98; Fax: +38-044-424.35.67;
e-mail: yuriy_gnatyuk@yahoo.com